ENGINEERING CORYNEBACTERIUM GLUTAMICUM CHASSIS FOR SYNTHETIC BIOLOGY, BIOMANUFACTURING, AND BIOREMEDIATION

EDITED BY: Akihiko Kondo, Yu Wang, Volker F. Wendisch, Christoph Wittmann, Zheng-Hong Xu and Ping Zheng

PUBLISHED IN: Frontiers in Bioengineering and Biotechnology and Frontiers in Microbiology

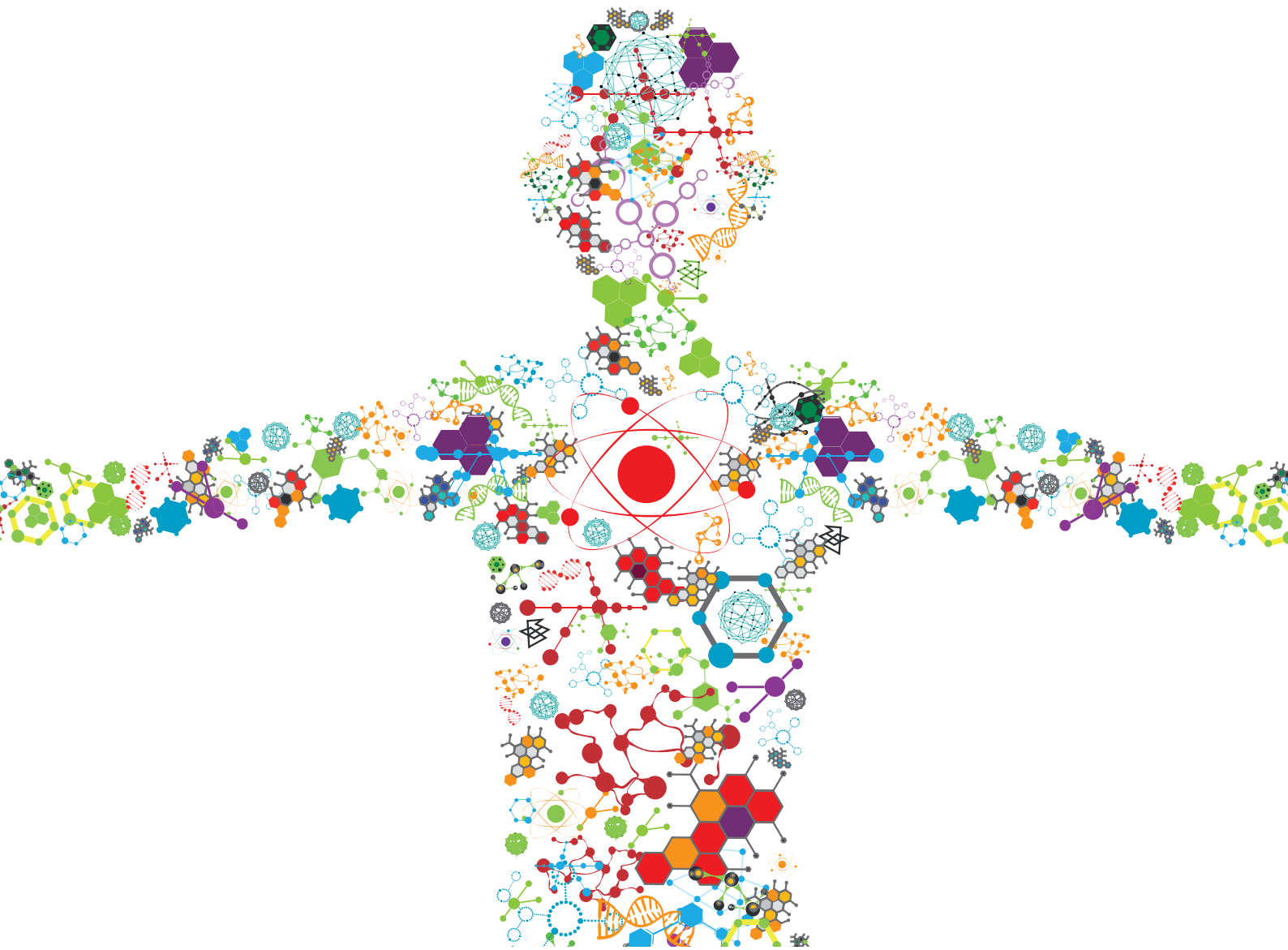

frontiers Research Topics

frontiers

ISSN 1664-8714
ISBN 978-2-88976-484-6
DOI 10.3389/978-2-88976-484-6

About Frontiers

Frontiers is more than just an open-access publisher of scholarly articles: it is a pioneering approach to the world of academia, radically improving the way scholarly research is managed. The grand vision of Frontiers is a world where all people have an equal opportunity to seek, share and generate knowledge. Frontiers provides immediate and permanent online open access to all its publications, but this alone is not enough to realize our grand goals.

Frontiers Journal Series

The Frontiers Journal Series is a multi-tier and interdisciplinary set of open-access, online journals, promising a paradigm shift from the current review, selection and dissemination processes in academic publishing. All Frontiers journals are driven by researchers for researchers; therefore, they constitute a service to the scholarly community. At the same time, the Frontiers Journal Series operates on a revolutionary invention, the tiered publishing system, initially addressing specific communities of scholars, and gradually climbing up to broader public understanding, thus serving the interests of the lay society, too.

Dedication to Quality

Each Frontiers article is a landmark of the highest quality, thanks to genuinely collaborative interactions between authors and review editors, who include some of the world's best academicians. Research must be certified by peers before entering a stream of knowledge that may eventually reach the public - and shape society; therefore, Frontiers only applies the most rigorous and unbiased reviews.
Frontiers revolutionizes research publishing by freely delivering the most outstanding research, evaluated with no bias from both the academic and social point of view. By applying the most advanced information technologies, Frontiers is catapulting scholarly publishing into a new generation.

What are Frontiers Research Topics?

Frontiers Research Topics are very popular trademarks of the Frontiers Journals Series: they are collections of at least ten articles, all centered on a particular subject. With their unique mix of varied contributions from Original Research to Review Articles, Frontiers Research Topics unify the most influential researchers, the latest key findings and historical advances in a hot research area! Find out more on how to host your own Frontiers Research Topic or contribute to one as an author by contacting the Frontiers Editorial Office: frontiersin.org/about/contact

ENGINEERING CORYNEBACTERIUM GLUTAMICUM CHASSIS FOR SYNTHETIC BIOLOGY, BIOMANUFACTURING, AND BIOREMEDIATION

Topic Editors:
Akihiko Kondo, Kobe University, Japan
Yu Wang, Tianjin Institute of Industrial Biotechnology, Chinese Academy of Sciences (CAS), China
Volker F. Wendisch, Bielefeld University, Germany
Christoph Wittmann, Saarland University, Germany
Zheng-Hong Xu, Jiangnan University, China
Ping Zheng, Tianjin Institute of Industrial Biotechnology, Chinese Academy of Sciences (CAS), China

Citation: Kondo, A., Wang, Y., Wendisch, V. F., Wittmann, C., Xu, Z.-H., Zheng, P., eds. (2022). Engineering Corynebacterium Glutamicum Chassis for Synthetic Biology, Biomanufacturing, and Bioremediation. Lausanne: Frontiers Media SA. doi: 10.3389/978-2-88976-484-6

Table of Contents

frontiers | Frontiers in Bioengineering and Biotechnology

EDITORIAL
published: 08 June 2022
doi: 10.3389/fbioe.2022.923145

Editorial: Engineering *Corynebacterium glutamicum* Chassis for Synthetic Biology, Biomanufacturing, and Bioremediation

Yu Wang[1], *Ping Zheng*[1]*, *Zhenghong Xu*[2], *Akihiko Kondo*[3], *Christoph Wittmann*[4] *and Volker F. Wendisch*[5]*

[1]Key Laboratory of Systems Microbial Biotechnology, Tianjin Institute of Industrial Biotechnology, Chinese Academy of Sciences, Tianjin, China, [2]The Key Laboratory of Industrial Biotechnology, Ministry of Education, School of Biotechnology, Jiangnan University, Wuxi, China, [3]Department of Chemical and Engineering, Graduate School of Engineering, Kobe University, Kobe, Japan, [4]Institute of Systems Biotechnology, Saarland University, Saarbrücken, Germany, [5]Genetics of Prokaryotes, Faculty of Biology and CeBiTec, Bielefeld University, Bielefeld, Germany

Keywords: ***Corynebacterium glutamicum*, synthetic biology, biomanufacturing, biochemicals, omics technology, gene regulation**

OPEN ACCESS

Edited and reviewed by:
Jean Marie François,
Institut Biotechnologique de Toulouse (INSA), France

***Correspondence:**
Ping Zheng
zheng_p@tib.cas.cn
Volker F. Wendisch
volker.wendisch@uni-bielefeld.de

Specialty section:
This article was submitted to Synthetic Biology, a section of the journal Frontiers in Bioengineering and Biotechnology

Received: *19 April 2022*
Accepted: *02 May 2022*
Published: *08 June 2022*

Citation:
Wang Y, Zheng P, Xu Z, Kondo A, Wittmann C and Wendisch VF (2022) Editorial: Engineering Corynebacterium glutamicum Chassis for Synthetic Biology, Biomanufacturing, and Bioremediation. Front. Bioeng. Biotechnol. 10:923145. doi: 10.3389/fbioe.2022.923145

Editorial on the Research Topic

Engineering *Corynebacterium glutamicum* Chassis for Synthetic Biology, Biomanufacturing, and Bioremediation

The Gram-positive soil bacterium *Corynebacterium glutamicum* was discovered about 60 years ago as an L-glutamate producer and has become a leading workhorse in industrial biotechnology. It is now used for the industrial production of over 6 million tons of amino acids (such as L-lysine and L-glutamate) per year and shows great potential for producing many more compounds ranging from alcohols and organic acids to plant secondary metabolites (Wolf et al., 2021). Several characteristics of *C. glutamicum* make it particularly interesting for industrial biotechnology, such as the GRAS (generally regarded as safe) status of its products, fast growth with relatively few nutrient requirements, and capability of utilizing sugars, sugar alcohols, organic acids, and aromatic compounds. With the development of CRISPR-based genome editing methods and synthetic and systems biology tools, the ability to understand and engineer the metabolism and regulation of *C. glutamicum* has been extensively enhanced (Liu et al., 2022). However, over 40% of genes of the type strain ATCC 13032 have not been experimentally characterized for their biological functions and the metabolic and regulatory mechanisms underlying the superior industrial performance of *C. glutamicum* have not been fully deciphered. Research on metabolic modeling, chassis engineering, multi-omics understanding, genome mining, etc., is expected to further realize the potential of this bacterium in biomanufacturing of chemicals and proteins and bioremediation of pollutants.

A Research Topic of articles including 18 original research articles and 1 mini review article specialized in *C. glutamicum* research from the leading groups in this field is presented. Each article provides a state-of-the-art view of the metabolic engineering efforts, systems biology analyses, and/or technical advances. The Research Topic focuses on the development of enabling technologies, mining of functional components, and engineering of *C. glutamicum* as microbial cell factories for bioconversion of renewable feedstocks to useful chemicals and proteins (**Figure 1**).

It is great to see that a significant part of the Research Topic presents modern enabling technologies and their practical application in *C. glutamicum*. In the design-build-test-learn biological engineering cycle, genome-scale metabolic models (GEMs) are considered fundamental

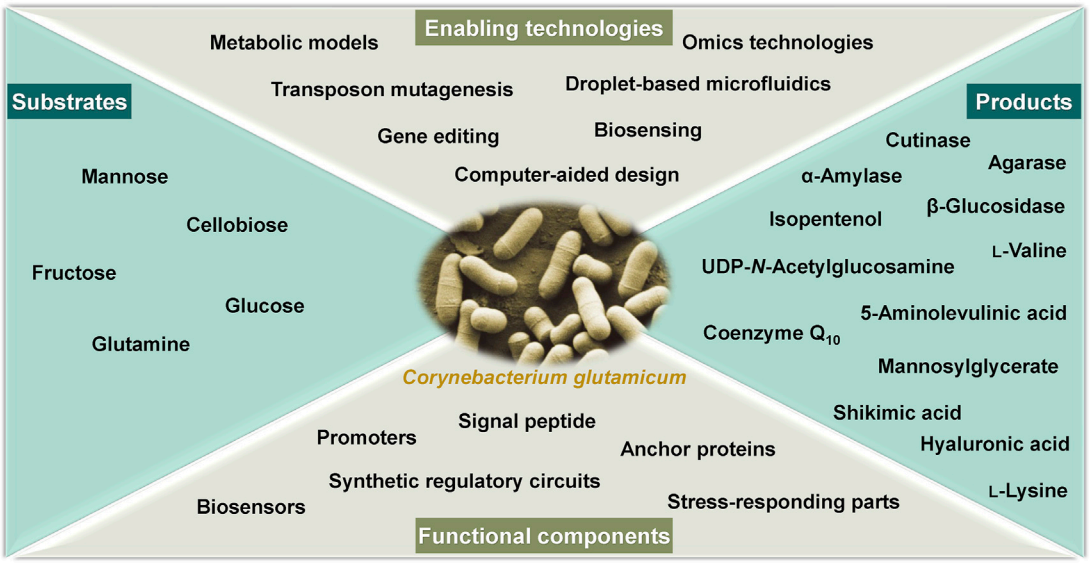

FIGURE 1 | A general categorization of the keywords of the articles collected in this Research Topic.

tools. Feierabend et al. presented an updated and unified GEM of *C. glutamicum* ATCC 13032 (iCGB21FR) with high quality regarding comprehensiveness and data standards. The *in silico* analysis may provide numerous designs for strain engineering. To bring these designs to life, computer-aided design tools and robotic system-assisted genome editing technologies will certainly help. Yang et al. developed a free online tool called GEDpm-cg for the design of genomic point mutations in *C. glutamicum*. Primers required for tool plasmid assembly and sequencing verification were quickly designed and provided, which would be useful for large-scale mutation analysis. As summarized by Wang et al., versatile genome editing tools including those based on the CRIPSR systems have been developed for *C. glutamicum*. Tailored design tools for not only point mutation but also large-scale genome engineering are still needed. In the test and learn parts, many high-throughput and systematic technologies including genome-scale transposon mutagenesis (Linder et al.), droplet-based microfluidics (Balasubramanian et al.), biosensing (Bakkes et al.), and multi-omics analyses (Kappelmann et al. and Banerjee et al.) have been used. Kappelmann et al. performed a comprehensive analysis of single or double deletion mutants in the anaplerosis of *C. glutamicum* under defined glucose conditions. Valuable information regarding the genotype-phenotype relationships in these mutants was unraveled by combining untargeted proteomics, quantitative metabolomics, and whole-genome sequencing. Banerjee et al. conducted genome and RNA sequencing of an engineered isopentenol-producing *C. glutamicum* strain under industrially relevant conditions including scale transition and ionic liquid stress. This omics information clarified the cell response of a *C. glutamicum* strain engineered to produce isopentenol.

The advances of enabling technologies considerably accelerate the running of the design-build-test-learn cycle and promote the engineering of *C. glutamicum* chassis, development of new components and circuits, and construction of microbial cell factories. To engineer a chassis that can efficiently metabolize fructose and channel the carbon flux to the oxidative pentose phosphate pathway for NADHP generation, Krahn et al. engineered and evolved fructose-utilizing mutants. Crucial mutations in the glucose phosphotransferase system enzymes were identified to explain the altered fructose uptake. A *C. glutamicum* chassis named CR101 with the removal of prophages and all insertion sequence (IS) elements was constructed by Linder et al. This chassis CR101 shows growth characteristics identical to the wild-type and increased transformability and could serve as an optimal host for basic research and biotechnology including genome-scale transposon mutagenesis.

Several articles collected in this Research Topic describe new functional components for engineering of *C. glutamicum*. To provide more available anchoring motifs for the display of recombinant proteins on the surfaces of *C. glutamicum* cells, Lin et al. predicted and screened 14 potential anchor proteins and identified 3 new anchoring proteins that performed better than the commonly used ones. Inducible gene expression systems are always important for reprogramming the metabolism and regulation of microorganisms. Three sets of gene regulation systems induced by myo-inositol, hyperosmotic stress, and phenolic compounds such as ferulic acid were developed and applied for dynamic control of gene expression. Lu et al. constructed a *myo*-inositol-inducible expression vector pMI-4 using the $iolR^q$ cassette and the *myo*-inositol-inducible promoter P_{iolT1}, which was used for gene overexpression for 5-aminolevulinic acid production. Huang et al. characterized the promoters controlled by the two-component signal transduction system MtrA/MtrB responding to hyperosmotic stress. The promoter of *NCgl1418* that exhibited a high inducibility was further engineered and used to develop a CRISRPi system induced by hyperosmotic stress. Siebert et al. utilized the VanR/

P_{vanABK}* regulatory system responding to phenolic compounds ferulic acid, vanillin, and vanillic acid to develop a timed off-switch for dynamic control of gene expression. With the depletion of exogenous phenolic compounds, genes controlled by P_{vanABK}* were efficiently turned off, allowing the control of gene expression in *C. glutamicum* in a timed manner.

Finally, a substantial part of this article Research Topic reports bioproduction of chemicals and proteins by *C. glutamicum*. Sato et al. engineered a *C. glutamicum* strain with β-glucosidase secreting ability for production of shikimate from both glucose and cellobiose. The shikimate pathway is a common route for the biosynthesis of a range of aromatic compounds, which also provides precursors for the biosynthesis of coenzyme Q10, an electron carrier in aerobic respiration and an antioxidant in medical treatment. Burgardt et al. metabolically engineered *C. glutamicum* for *de novo* biosynthesis of coenzyme Q10, which to the best of our knowledge is the first report of coenzyme Q10 production in a non-ubiquinone-containing bacterium. Uridine diphosphate-*N*-acetylglucosamine (UDP-GlcNAc) is an acetylated amino sugar nucleotide that can serve as a sugar donor for synthesis of many pharmaceutically relevant oligosaccharides, polysaccharides, and glycoproteins. Gauttam et al. constructed a series of recombinant *C. glutamicum* strains by engineering the UDP-GlcNAc biosynthetic pathway and the highest level of microbial production of UDP-GlcNAc was obtained. Different from most metabolic engineering strategies directly targeting the biosynthetic pathway, Du et al. applied indirect metabolic engineering strategies targeting the substrate uptake, membrane composition, oxygen transfer, and nitrogen metabolism for enhanced biosynthesis of hyaluronic acid. Metabolic engineering approaches have also been combined with process engineering approaches by Schwentner et al. to develop a *C. glutamicum* strain for the production of compatible solute mannosylglycerate and an easy product separation process to extract mannosylglycerate from cytosol by cold water shock.

In addition to bioproduction of chemicals, secretory production of recombinant proteins using *C. glutamicum* also attracts great attention. Lee et al. found that mutations to increase the iron and carbon consumption were responsible for the enhanced production of recombinant protein in an evolved fast-growing *C. glutamicum* strain. Balasubramanian et al. screened *C. glutamicum* mutants with enhanced enzyme secretion capacity by using a droplet-based microfluidic high-throughput screening method and analyzed the single nucleotide variants in these mutants. Bakkes et al. used a fluorescence-based biosensor for Sec-dependent protein secretion to evolve the Sec signal peptides from *Bacillus subtilis* and optimize the secretion of heterologous enzyme cutinase. These findings are expected to promote the application of *C. glutamicum* in protein production.

Overall, *C. glutamicum,* that was initially used as an L-glutamate producer, is now becoming a versatile chassis for bioproduction of various amino acids, chemicals, and proteins from renewable feedstocks. The importance of *C. glutamicum* in industrial biotechnology drives the development of advanced synthetic and systems biology technologies such as *in silico* metabolic modeling, multiplex gene editing, multi-omics analyses, and high-throughput functional genomics methods. It is believed that the series of articles collected in this Research Topic provide contemporary and valuable information that can help to fully unlock the potential of *C. glutamicum* in industrial biotechnology.

AUTHOR CONTRIBUTIONS

YW wrote a draft of the manuscript and PZ, ZX, AK, CW, and VW edited and finalized the manuscript. All authors approved the final version of the manuscript.

FUNDING

YW is supported by the National Key R&D Program of China (2018YFA0900300), the Youth Innovation Promotion Association of Chinese Academy of Sciences (2021177), and the Tianjin "Project + Team" Key Training Program (XC202038).

ACKNOWLEDGMENTS

The guest editors thank all the authors contributing to this Research Topic. The guest editors also thank editors Dr. Jens O. Krömer, Dr. Pablo Ivan Nikel, and Dr. Xiao-Jun Ji and all the reviewers for their kind support.

REFERENCES

Liu, J., Liu, M., Shi, T., Sun, G., Gao, N., Zhao, X., et al. (2022). CRISPR-assisted Rational Flux-Tuning and Arrayed CRISPRi Screening of an L-Proline Exporter for L-Proline Hyperproduction. *Nat. Commun.* 13 (1), 891. doi:10.1038/s41467-022-28501-7

Wolf, S., Becker, J., Tsuge, Y., Kawaguchi, H., Kondo, A., Marienhagen, J., et al. (2021). Advances in Metabolic Engineering of *Corynebacterium glutamicum* to Produce High-Value Active Ingredients for Food, Feed, Human Health, and Well-Being. *Essays Biochem.* 65 (2), 197–212. doi:10.1042/ebc20200134

Conflict of Interest: The authors declare that the research was conducted in the absence of any commercial or financial relationships that could be construed as a potential conflict of interest.

frontiers in Bioengineering and Biotechnology

ORIGINAL RESEARCH
published: 10 September 2020
doi: 10.3389/fbioe.2020.569406

Metabolic Engineering of Shikimic Acid-Producing *Corynebacterium glutamicum* From Glucose and Cellobiose Retaining Its Phosphotransferase System Function and Pyruvate Kinase Activities

*Naoki Sato, Mayumi Kishida, Mariko Nakano, Yuuki Hirata and Tsutomu Tanaka**

Department of Chemical Science and Engineering, Graduate School of Engineering, Kobe University, Kobe, Japan

OPEN ACCESS

Edited by:
Yu Wang,
Tianjin Institute of Industrial Biotechnology (CAS), China

Reviewed by:
Jian-Zhong Liu,
Sun Yat-sen University, China
Ralf Takors,
University of Stuttgart, Germany

***Correspondence:**
Tsutomu Tanaka
tanaka@kitty.kobe-u.ac.jp

Specialty section:
This article was submitted to Synthetic Biology, a section of the journal Frontiers in Bioengineering and Biotechnology

Received: *04 June 2020*
Accepted: *19 August 2020*
Published: *10 September 2020*

Citation:
Sato N, Kishida M, Nakano M, Hirata Y and Tanaka T (2020) Metabolic Engineering of Shikimic Acid-Producing Corynebacterium glutamicum From Glucose and Cellobiose Retaining Its Phosphotransferase System Function and Pyruvate Kinase Activities. Front. Bioeng. Biotechnol. 8:569406. doi: 10.3389/fbioe.2020.569406

The production of aromatic compounds by microbial production is a promising and sustainable approach for producing biomolecules for various applications. We describe the metabolic engineering of *Corynebacterium glutamicum* to increase its production of shikimic acid. Shikimic acid and its precursor-consuming pathways were blocked by the deletion of the shikimate kinase, 3-dehydroshikimate dehydratase, shikimate dehydratase, and dihydroxyacetone phosphate phosphatase genes. Plasmid-based expression of shikimate pathway genes revealed that 3-deoxy-D-arabino-heptulosonate 7-phosphate (DAHP) synthase, encoded by *aroG*, and DHQ synthase, encoded by *aroB*, are key enzymes for shikimic acid production in *C. glutamicum*. We constructed a *C. glutamicum* strain with *aroG, aroB* and *aroE3* integrated. This strain produced 13.1 g/L of shikimic acid from 50 g/L of glucose, a yield of 0.26 g-shikimic acid/g-glucose, and retained both its phosphotransferase system and its pyruvate kinase activity. We also endowed β-glucosidase secreting ability to this strain. When cellobiose was used as a carbon source, the strain produced shikimic acid at 13.8 g/L with the yield of 0.25 g-shikimic acid/g-glucose (1 g of cellobiose corresponds to 1.1 g of glucose). These results demonstrate the feasibility of producing shikimic acid and its derivatives using an engineered *C. glutamicum* strain from cellobiose as well as glucose.

Keywords: shikimic acid, shikimate pathway, *Corynebacterium glutamicum*, metabolic engineering, beta-glucosidase, cellobiose

INTRODUCTION

Shikimic acid is a valuable hydroaromatic compound. It is a key metabolic intermediate in the shikimate pathway, a common route for the biosynthesis of a range of aromatic compounds. Shikimic acid possesses a highly functionalized six-carbon ring with three asymmetric centers, and is therefore, a useful precursor for the synthesis of products such as pharmaceuticals, antibiotics,

antithrombotic agents, and vitamins (Rawat et al., 2013; Martinez et al., 2015; Candeias et al., 2018; Kogure and Inui, 2018). This compound has been used as a starting material for the industrial synthesis of oseltamivir phosphate, otherwise known as the anti-influenza drug Tamiflu (Díaz Quiroz et al., 2014). Shikimic acid is also an important starting material for the synthesis of anticancer drugs such as (+)-zeylenone (Liu et al., 2004). Current industrial production of shikimic acid primarily involves its extraction from the seeds of the Chinese star anise plant (almost 80% or more), *Illicium verum*, and subsequent chemical synthesis (Bochkov et al., 2012; Ghosh et al., 2012; Rawat et al., 2013). However, these processes are complex and incur problems such as limitations of raw material and high costs.

The production of biomolecules using microorganisms has recently attracted considerable attention because of the potential for relatively rapid, cost-effective, low-pollution production of industrially important compounds. Shikimic acid is of particular interest due to its importance in a range of industrial applications (Rawat et al., 2013; Martinez et al., 2015; Noda and Kondo, 2017). Microbial production of shikimic acid has several advantages: low-cost renewable feedstocks are readily available in large quantities; the system is environmentally friendly; and high yields can be obtained. Shikimic acid is produced via the shikimate pathway, which is ubiquitous in bacteria, plants, and fungi. This pathway begins with the condensation of phosphoenolpyruvate (PEP) and D-erythrose 4-phosphate (E4P), catalyzed by 3-deoxy-D-arabino-heptulosonate-7-phosphate (DAHP) synthetase. DAHP is converted to 3-dehydroquinate (DHQ) by DHQ synthase. DHS synthase catalyzes the next step to produce 3-dehydroshikimate (DHS), which is then converted to shikimic acid by shikimate dehydrogenase. Metabolic engineering for the production of useful compounds derived from the shikimate pathway, including shikimic acid, has been extensively studied (Jiang and Zhang, 2016; Lee and Wendisch, 2017; Noda and Kondo, 2017; Averesch and Krömer, 2018; Huccetogullari et al., 2019; Braga and Faria, 2020), primarily using *Escherichia coli* as the host strain. A typical strategy for shikimic acid production involves the elimination of the carbon flow from shikimate to chorismite by deletion of the shikimate kinase gene and the reinforcing of carbon flux from glycolysis into the shikimate pathway by overexpression of the shikimate pathway enzymes, including a feedback-resistant DAHP synthase (Gu et al., 2017). Improvement of PEP and E4P availability is another key issue for shikimic acid production. Deletion of pyruvate kinase, inactivation of the phosphotransferase system (PTS) and the redirection of carbon flux from pyruvate to PEP by PEP synthase expression have all been utilized (Chandran et al., 2003). Combining these metabolic approaches, Rodriguez et al. (2013) engineered a shikimic acid-producing *E. coli* strain, which achieved production of 43 g/L of shikimic acid at a yield of 43% (mol/mol) from glucose in a batch fermenter. However, the inactivation of PTS or pyruvate kinase often causes growth defects, and a laboratory-based adaptive evolution process is required to recover cell growth (Flores et al., 2005, 2007). Introduction of alternative glucose transporter Glf from *Zymomonas mobilis* with an additional copy of glucokinase from *Z. mobilis* could recover cell growth without applying an adaptive evolution experiment (Chandran et al., 2003). Another concern about pyruvate kinase and/or PTS deletion is the shortage of pyruvate supply. For the synthesis of various plant polyphenols such as flavonoids and stilbenoids, pyruvate and acetyl-CoA are important precursor as well as chorismic acid followed by shikimic acid synthesis (Kogure and Inui, 2018).

Corynebacterium glutamicum is a Gram-positive non-pathogenic bacterium, which is already widely used for the industrial production of amino acids such as L-glutamate and L-lysine (Hirasawa and Wachi, 2017; Ikeda, 2017; Baritugo et al., 2018; Becker et al., 2018; Cheng et al., 2018; D'Este et al., 2018; Pérez-García and Wendisch, 2018; Wendisch et al., 2018), and aromatic amino acids such as L-phenylalanine and L-tyrosine (Ikeda, 2006; Zhang C. et al., 2015). This microbe is one of the most promising microbial chassis for the bioproduction of a range of chemicals and fuels, including alcohols, diamines, and organic acids. Kogure et al. (2016) achieved a production of 141 g/L of shikimic acid from glucose using the *C. glutamicum* R strain using growth-arrested cell reactions in fed-batch fermentation. These researchers induced the expression of a heterologous gene encoding a feedback-resistant form of DAHP from *E. coli* (Ger et al., 1994), as well as shikimate pathway-related genes. In the engineered strain, PTS and the PEP-independent glucose uptake system were also inactivated. Another study described the production of an engineered *C. glutamicum* strain derived from strain ATCC13032 using CRISPRi system-mediated transcriptional control. This strain produced 7.76 g/L shikimic acid from sucrose in flask cultivation (Zhang et al., 2016). Zhang et al. constructed an engineered strain using ribosome binding site libraries (Zhang C. et al., 2015; Zhao et al., 2020) or the introduction of the archaeal shikimate pathway (Zhang et al., 2015a). The strains produced shikimic acid at 11.3 and 23.8 g/L, respectively, using sucrose as a carbon source.

Lignocellulosic biomass has attracted much attentions as a promising feedstock because it is renewable, inexpensive and abundant (Bhatia et al., 2020; Zhao et al., 2020). Bio-fuels and chemicals produced from lignocellulosic biomass has a potential to develop the sustainable economic growth. However, most microorganisms cannot directly utilize lignocellulosic biomass, and degradation of this material requires expensive and complex steps. To convert cellulose into monomeric sugars such as glucose, enzymetic saccharification procedures involving endoglucanase, exglucanase and beta-glucosidase (BGL) have been required (Khare et al., 2015). After cleaving the cellulose chain in the middle by endoglucanase, then cellobiohydrolases release cellobiose units from the end of the cleaved cellulose. Finally, BGL hydrolyze cellobiose and cello-oligosaccharides to glucose (Davies et al., 2005). The cellobiose and glucose causes product inhibition of BGL activity. To overcome this problem, excess amount of BGL is added to cellulase mediated hydrolysis (Van Dyk and Pletschke, 2012) or simultaneous saccharification and fermentation (SSF) processes (Liu et al., 2019). Other inhibitors such as tannic, gallic, vanillin were able to cause 20–80% BGL inhibition (Ximenes et al., 2011). It was found that amounts of disaccharides existed in the hydrolyzate,

such as cellobiose (Li et al., 2010). Although shikimic acid production from the mixture of glucose, xylose and arabinose were carried out (Kogure et al., 2016), shikimic acid production using cellobiose or cello-oligosaccharides as a carbon source have not yet been used.

In this study, we constructed a high-producing shikimic acid *C. glutamicum* strain by rational metabolic engineering approaches without PTS inactivation, pyruvate kinase disruption, or the introduction of feedback-resistant variants of DAHP synthase. We simply disrupted shikimic acid and its precursor-consuming genes and introduced only endogenous genes related to the shikimate pathway. Our engineered strain produced 13.8 g/L of shikimic acid, a yield of 0.25 (g-shikimic acid/g-glucose). Further, we demonstrated successful shikimic acid production using cellobiose as the sole carbon source. The titer of shikimic acid production was 13.8 g/L with the same yield of glucose.

MATERIALS AND METHODS

Bacterial Strains, Media, and Cultivation Conditions

All bacterial strains and plasmids used in this study are listed in **Table 1**. *C. glutamicum* ATCC13032 and its recombinants were cultivated aerobically at 30°C in Brain Heart Infusion (BHI) medium or defined CGXII minimal medium containing 50 g/L of glucose or cellobiose and 100 mg/L of aromatic amino acids. CGXIIY medium (CGXII medium containing 4 g/L of yeast extract) was used for shikimic acid production. *E. coli* NovaBlue, which was used for recombinant DNA experiments, was routinely cultivated in Luria–Bertani medium (10 g/L peptone, 5 g/L yeast extract, and 10 g/L NaCl) at 37°C. Kanamycin (25 μg/mL for *C. glutamicum* strains and 50 μg/mL for *E. coli*) was added when required.

Construction of Plasmids and Strains

The strains and plasmids used in this study are summarized in **Table 1**. All DNA oligonucleotides used in this study are listed in **Supplementary Table S1**. Gene deletion or substitution plasmids were constructed as follows.

For the *aroK* deletion, the upstream and downstream regions were amplified from *C. glutamicum* strain ATCC 13032 by PCR using the primer pairs ΔaroK_up_fw/ΔaroK_up_rv, and ΔaroK_down_fw/ΔaroK_down_rv, respectively. The two fragments were conjugated by overlap PCR using the primer pair ΔaroK_up_fw/ΔaroK_down_rv, and the resulting fragment was ligated into pK18mobsacB digested using *Eco*RI/*Hin*dIII. Other plasmids for gene deletion (Δ*qsuD*, Δ*qsuB*, Δ*nagD*, and Δ*cg2392*) and for point mutation (gnd S361F) were constructed similarly.

We constructed an *aroG*-expressing plasmid under the control of the H36 promoter as follows. A gene fragment encoding *aroG* was amplified by PCR from *C. glutamicum* ATCC13032 using the primer pairs H36_aroG_fw and AroG_re. The fragment was ligated into plasmid pCC-H36-ldcC digested with *Bam*HI/*Xho*I. The resultant plasmid was named pCC-H36-aroG. Other plasmids expressing *aroB, qsuC, aroE1* and *aroE3* were constructed similarly.

For *aroG* integration into the Δ*aroK* region, the upstream and downstream regions of Δ*aroK* were amplified by PCR using the primer pairs aroK up fw/aroK up rv and aroK down fw/aroK down rv. An *aroG*-expressing cassette with the H36 promoter and rrnB T1T2 terminator was amplified by PCR using pCC-H36-aroG as a template with the primer pairs aroK-H36_fw/aroK_term_re. The three fragments were conjugated by overlap PCR using the primer pair aroK up fw and aroK down rv, and the resulting fragment was ligated into pK18mobsacB digested with *Eco*RI/*Bam*HI. Other plasmids for genome integration (Δ*aroK*:*aroB*, Δ*pta*:*aroG*,Δ*ldh*:*aroE1 and*Δ*ldh*:*aroE3*) were constructed similarly.

All gene deletions, mutations, and integrations of the *C. glutamicum* genome were introduced by homologous recombination and two-step selection using kanamycin resistance to select for plasmid integration and the *sacB* system to counterselect for plasmid excision.

Transformation of *C. glutamicum*

C. glutamicum was cultured overnight in 5 mL of BHI medium at 30°C. A further 400 μL of seed culture was inoculated into 50 mL of BHI medium. After incubation at 30°C until OD_{600} reached 0.5, the cell suspension was centrifuged at 4,000 g for 5 min and washed three times with 5mL of 15% (v/v) glycerol before resuspension in 0.5 mL of 15% glycerol. Transformation of *C. glutamicum* was performed by electroporation with a 2.5-kV, 200-Ω, 25-μF electric pulse in a 0.2-cm cuvette using a Gene Pulser (Bio-Rad Laboratories, Hercules, CA).

Conditions for Shikimic Acid Production by *C. glutamicum*

A single colony was used as the inoculum for preculture (5 mL BHI medium in test tubes) and was incubated overnight at 30°C with shaking at 220 rpm. Cells were collected by centrifugation at 4,000 g for 2 min and resuspended in 1 mL of CGXII medium supplemented with 100 mg/L of L-phenylalanine, 100 mg/L of L-tyrosine, 100 mg/L of L-tryptophan, and 100 mg/L of p-aminobenzoate. The suspension (400 μL) was inoculated into 5 ml of CGXII medium or CGXIIY medium containing 50 g/L of glucose and incubated at 30°C with shaking at 220 rpm 72 h.

Analysis of Substrates and Products

Cell growth was determined by measuring the OD600 nm on a UVmini-1240 spectrophotometer (Shimadzu Corporation, Kyoto, Japan). Glucose concentration was analyzed using a Prominence high-performance liquid chromatography (HPLC) system (Shimadzu) equipped with a Shodex SUGAR KS-801 column (6 μm, 300 × 8.0 mm L × I.D., Shodex). The column was maintained at 50°C, and water was used as the mobile

phase at a flow rate of 0.8 ml/min. The HPLC profile was monitored using a refractive index detector. The concentration of shikimic acid was determined using HPLC equipped with COSMOSIL PBr column (5 μm, 4.6 mm × 250 mm, I.D. × L, Nacalai Tesque). A 98:2 mixture of 0.2% phosphoric acid and methanol was used as the mobile phase at a flow rate of 1.0 ml/min, and the column was maintained at 40°C. The HPLC profile was monitored using a UV-VIS detector at 240 nm.

Quantification of NADPH/NADP and NADH/NAD Ratio

Preparation of samples for the analysis of NADPH and NADH was conducted as follows. Precultured *C. glutamicum* was

TABLE 1 | Bacterial strains and plasmids used in this study.

Strains or plasmids	Genotype	Source or reference
Escherichia coli		
Nova Blue	*endA1 hsdR17(rK12-mK12$^+$) supE44 thi-I gyrA96 relA1 lac recA1/F' [proAB$^+$ laclq Z ΔM15:Tn10(Tet r)];* used for gene cloning.	Novagen
SCS110	*rpsL (Str1) thr leu endA thi-I lacY galK galT ara tonA tsx dam dcm supE44 Δ(lac-proAB) [F' traD36 proAB laclqZ ΔM15]*	STRATAGENE
Corynebacterium glutamicum		
ATCC13032	Wild-type strain	ATCC
SA-1	ATCC13032 + ΔcglMRR (cg1996-cg1998), *ΔqsuD, ΔqsuB, ΔnagD, ΔaroK*	This study
SA-2	SA-1 + *gnd^{S361F}*	This study
SA-3	SA-2 + *aroK:P$_{H36}$-aroG*	This study
SA-4	SA-2 + *aroK:P$_{H36}$-aroB*	This study
SA-5	SA-2 + *aroG$^{gtg\rightarrow atg}$*, *Δcg2392*	This study
SA-6	SA-5 + *aroK:P$_{H36}$-aroB*	This study
SA-7	SA-5 + *aroK:P$_{H36}$-aroB, pta:P$_{H36}$-aroG*	This study
SA-8	SA-7 + *Δldh*	This study
SA-9	SA-7 + *ldh:P$_{H36}$-aroE1*	This study
SA-10	SA-7 + *ldh:P$_{H36}$-aroE3*	This study
Plasmids		
pCCS	*E. coli–C. glutamicum shuttle vector for control, KmR*	Matsuura et al., 2019
pCC-H36-cgR0949-Tfu0937	pCCS derivative carrying sequences encoding the CgR0949 secretion signal fused to *T. fusca* Tfu0937 under the control of the H36 promoter	Matsuura et al., 2019
pCC-P$_{H36}$-aroG	pCCS containing *aroG* under the control of the H36 promoter	This study
pCC-P$_{H36}$-aroB	pCCS containing *aroB* under the control of the H36 promoter	This study
pCC-P$_{H36}$-qsuC	pCCS containing *qsuC* under the control of the H36 promoter	This study
pCC-P$_{H36}$-aroE1	pCCS containing *aroE1* under the control of the H36 promoter	This study
pCC-P$_{H36}$-aroE3	pCCS containing *aroE3* under the control of the H36 promoter	This study
pCC-P$_{H36}$-tal-tkt	pCCS containing *tal* and *tkt* (cg1774-cg1776, NCgl1512-NCgl1513) under the control of the H36 promoter	This study
pCC-P$_{H36}$-pck	pCCS containing *pck* under the control of the H36 promoter	This study
pK18mobsacB	sacB, lacZ, Km^R, MCS, mobilizable vector, enables selection/counter-selection for integration/excision in *C. glutamicum*	ATCC
pK18-gnd^{S361F}	pK18mobsacB derivative for substitution of *gnd^{S361F}*	This study
pK18-ΔqsuD	pK18mobsacB derivative for *qsuD* deletion	This study
pK18-ΔqsuB	pK18mobsacB derivative for *qsuB* deletion	This study
pK18-ΔnagD	pK18mobsacB derivative for *nagD* deletion	This study
pK18-ΔaroK	pK18mobsacB derivative for *aroK* deletion	This study
pK18-Δldh	pK18mobsacB derivative for *ldh* deletion	This study
pK18-ΔaroK-P$_{H36}$aroB	pK18mobsacB derivative for insertion of *aroB* expression cassette under the control of H36 promoter into *aroK* locus	This study
pK18-Δpta-P$_{H36}$aroG	pK18mobsacB derivative for insertion of *aroG* expression cassette under the control of H36 promoter into *pta* locus	This study
pK18-Δldh-P$_{H36}$aroE1	pK18mobsacB derivative for insertion of *aroE1* expression cassette under the control of H36 promoter into *ldh* locus	This study
pK18-Δldh-P$_{H36}$aroE3	pK18mobsacB derivative for insertion of *aroE3* expression cassette under the control of H36 promoter into *ldh* locus	This study

inoculated into 5 ml of CGXIIY medium containing 50 g/L of glucose and incubated at 30°C with shaking at 220 rpm for 24 h. The extraction buffer (methanol: chloroform = 7:3) was added to cells and incubated at 1,000 rpm at 4°C overnight. The supernatant was centrifuged at 13,000 g for 5 min and evaporated. The evaporated samples were analyzed using the Enzychrom NADP + /NADPH Assay Kit ECNP-100 (BioAssay Systems, Hayward, United States) and Enzychrom NAD + /NADH Assay Kit E2ND-100 (BioAssay Systems, Hayward, United States) according to the manufacturer's procedures.

Quantification of the Transcriptional Level of mRNA Using Real-Time qPCR

The transcriptional expression of *aroB*, *aroG*, and *ldh* in SA-2, SA-5, and SA-7 was quantified using real-time qPCR. Total RNA was isolated after 24 h of cultivation in CGXIIY medium using a NucleoSpin RNA column (Takara Bio, Shiga, Japan) according to the manufacturer's protocol.

Quantitative real-time qPCR was performed using a LightCycler® 96 System (Roche Molecular Systems, Inc., CA, United States) with RNA-direct™ Real-time PCR Master Mix (TOYOBO). The primer pairs used are listed in **Supplementary Table 1**. The normalized transcriptional level of each mRNA was calculated using the relative quantification method using the cg3177 (Ncgl2772) gene as the housekeeping gene.

Statistical Analysis

Analysis of variance (ANOVA) was conducted with Honestly Significant Difference (HSD) test by EZR software (Kanda, 2013). The data of shikimic acid are average of 3 biological replicates with error bars representing standard deviation and asterisk indicates significant difference ($p < 0.05$) from control strain.

RESULTS AND DISCUSSION

Construction of Shikimic Acid-Producing *C. glutamicum*

We used ATCC13032 ΔMRR (a partially prophage-free variant) as the parent strain for constructing shikimic acid-producing *C. glutamicum* (Bott et al., 2013). We disrupted four genes encoding shikimate kinase *aroK* (cg1828, NCgl1560); DHS dehydratase *qsuB* (cg0502, NCgl0407); QA/SA dehydratase *qsuD* (cg0504, NCgl0409); and DHAP phosphatase *nagD* (cg2474, NCgl2175), leading to the accumulation of shikimic acid (**Figure 1**). The strain, called SA-1 (D*aroK*, D*qsuB*, D*qsuD*, and *DnagD*), exhibited auxotrophy for aromatic amino acids and p-aminobenzoate. Therefore, small amounts of L-phenylalanine, L-tyrosine, L-tryptophan, and p-aminobenzoate (100 mg/L) had to be added to the minimal medium for the strain to grow. No shikimic acid was detected in the parental strain, but SA-1 produced 1.3 ± 0.04 g/L of shikimic acid in CGXII medium containing 50 g/L of glucose after 72 h of cultivation (**Figure 2A**). Ohnishi et al. reported that the point mutation Ser361Phe of the 6-phosphogluconate dehydrogenase gene (gnd; cg1643, NCgl1396) increased L-lysine production due to enhancement of NADPH supply (Ohnishi et al., 2005). Shikimate dehydrogenase *aroE* requires NADPH as a cofactor for its enzymatic activity, so we introduced this point mutation into SA-1 by allelic replacement. The resulting strain SA-2 produced 1.9 ± 0.23 g/L of shikimic acid after 72 h, an increase of approximately 40% over that of SA-1 (**Figure 2A**).

Overexpression of Shikimate Pathway Genes in Strain SA-2 Using a Plasmid-Based Expression Method

To improve shikimic acid production, each gene of the shikimate pathway was overexpressed under the control of the strong synthetic constitutive promoter P_{H36} (Yim et al., 2013). This promoter has been used to produce recombinant single-chain variable fragment (Yim et al., 2014), gamma-aminobutyrate (Choi et al., 2015), and 1,5-diaminopentane (Matsuura et al., 2019; Kim et al., 2020). Key genes located on the *C. glutamicum* chromosome are DAHP synthase, encoded by *aroG* (cg2391, NCgl2098); DHQ synthase, encoded by *aroB* (cg1827, NCgl1559); DHS synthase, encoded by *qsuC* (cg0503, NCgl0408); shikimate dehydrogenase, encoded by *aroE1* (cg1283, NCgl1087); and *aroE3* (cg1835, NCgl1567). Although *C. glutamicum* carries the DAHP synthase encoded by *aroF*, its contribution to the shikimate pathway is less than that of *aroG* (Liu et al., 2008), and we did not select it as a candidate. Individual plasmids were created for the overexpression of *aroG*, *aroB*, *qsuC*, *aroE1*, and *aroE3*, under the control of the strong constitutive promoter P_{H36}. Each plasmid was introduced into the SA-2 strain, and the strains were cultivated in CGXII medium containing 50 g/L of glucose. **Figure 2B** shows shikimate production after 72 h of cultivation. SA-2 overexpressing *aroG* gene (SA-2/aroG) produced 5.4 ± 0.65 g/L of shikimate, 2.8-times higher than SA-2 (**Figure 2A**). Overexpression of aroB (SA-2/aroB) also slightly increased shikimate production (2.3 ± 0.23 g/L after 72 h). Overexpression of *qsuC, aroE1*, and *aroE3* did not increase shikimic acid production.

Construction of *C. glutamicum* Strains With Integrated Shikimate Pathway Genes, and Introduction of Additional Shikimate Pathway Genes Using Plasmid-Based Expression

As shown in **Figure 2B**, the enhancement of *aroG* or *aroB* gene expression contributed to the increased production of shikimic acid. We therefore integrated an extra copy of *aroG* or *aroB* under the control of the promoter P_{H36} into the *aroK* locus of the SA-2 genome. The resulting strains were named SA-3 (SA-2/aroK:P_{H36}-aroG) and SA-4 (SA-2/aroK:P_{H36}-aroB), respectively. To enhance the expression of *aroG*, we changed the start codon of *aroG* from "gtg" to "atg" ($aroG^{gtg\rightarrow atg}$) with an in-frame deletion of *cg2392* (NCgl2099) in SA-2 (**Figure 3D**). The resulting strain was named SA-5 (SA-2/Δcg2392, $aroG^{gtg\rightarrow atg}$). Changing the translational start codon of the gene increased its expression (Vogt et al., 2016; Jorge et al., 2017). The *aroG* gene is located downstream of *cg2392*, a predicted exonuclease,

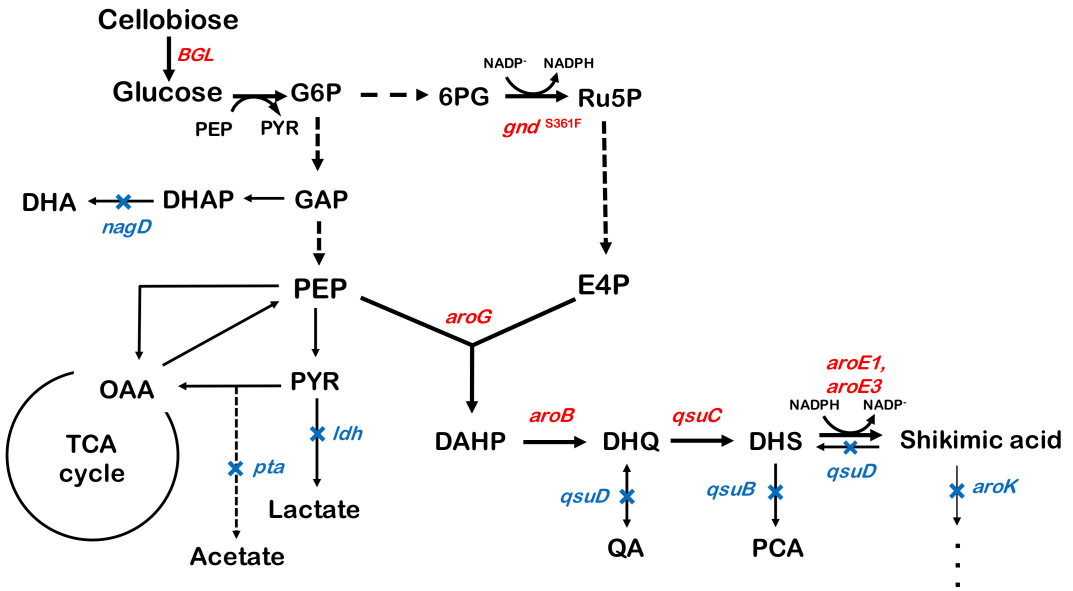

FIGURE 1 | Metabolic engineering of *Corynebacterium glutamicum* for shikimic acid production. The blue X indicates deletion of the *nagD, qsuD, qsuB, qsuD, aroK*, and *pta* genes. Genes involving shikimic acid synthesis pathways are indicated in red. G6P, glucose-6-phosphate; GAP, glyceraldehyde-3-phosphate; DHAP, 1,3-dihydroxyacetone phosphate; DHA, 1,3-dihydroxyacetone; PEP, phosphoenolpyruvate; PYR, pyruvate; OAA, oxaloacetate; Ru5P, ribulose-5-phosphate; E4P, erythrose 4-phosphate; DAHP, 3-deoxy-D-arabinoheptulosonate-7-phosphate; DHQ, 3-de-hydroquinate; DHS, 3-dehydroshikimate; PCA, protocatechuate; *aroG*, DAHP synthase; *aroB*, DHQ synthase; *aroD*, DHQ dehydratase; *aroE1*, *aroE3*, shikimate dehydrogenase; *aroK*, shikimate kinase; *qsuB*, DHS dehydratase; *qsuD*, QA/shikimate dehydrogenase; *gnd,* 6-phosphogluconate dehydrogenase; *BGL*, beta-glucosidase from *Thermobifida fusca* YX.

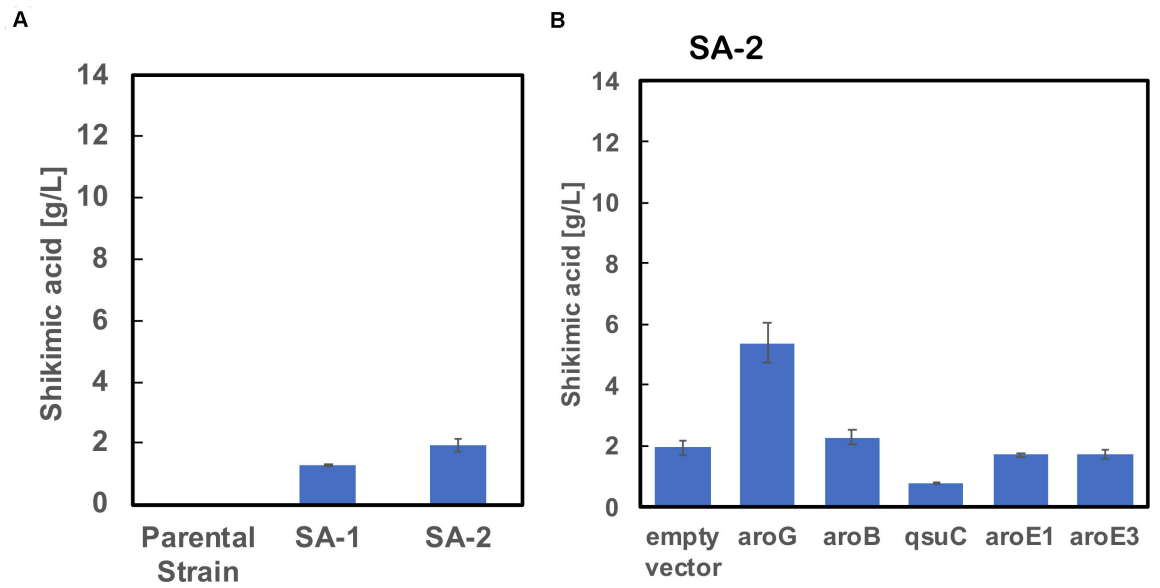

FIGURE 2 | (A) Shikimic acid production titer in strains SA-1 and SA-2 harboring empty vectors. **(B)** SA production titer in SA-2 harboring each individual shikimate pathway gene expression plasmid. CGXII medium containing 50 g/L of glucose was used as the sole carbon source. The data are presented as the average of three independent experiments, and error bars indicate the standard deviation.

and they constitute an operon. In-frame deletion of *cg2392* and replacement of *aroG* downstream from the native promoter should increase *aroG* expression. To evaluate the shikimic acid production of SA-3, SA-4, and SA-5, we introduced an empty plasmid and cultivated the strains. **Figures 3A–C** (left bars of each panel) shows the shikimic acid production of SA-3, SA-4, and SA-5. Using CGXII medium containing 50 g/L of glucose, SA-3, SA-4, and SA-5 strains produced 1.7 ± 0.30 g/L, 3.0 ± 0.09 g/L, and 2.4 ± 0.15 g/L of shikimic acid, respectively. Statistical analysis revealed that significant difference was observed between SA-2

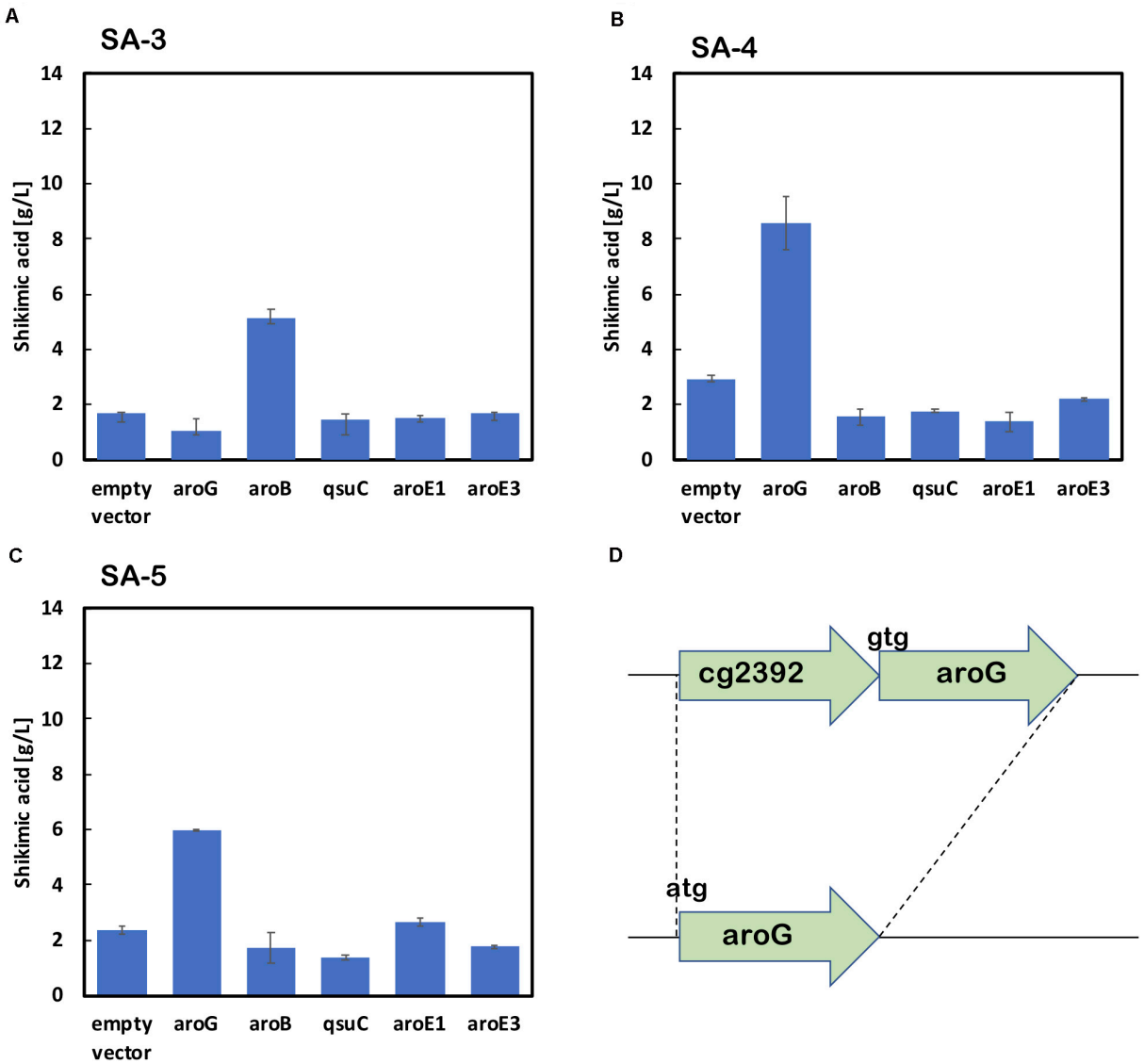

FIGURE 3 | Shikimic acid production titer in strains **(A)** SA-3, **(B)** SA-4, and **(C)** SA-5 harboring each shikimate pathway gene expression plasmid. CGXII medium containing 50 g/L of glucose was used as the sole carbon source. Panel **(D)** illustrates a gene cg2392 deletion and replacement of the start codon in the SA-5 strain. The data are presented as the average of three independent experiments, and error bars indicate the standard deviation.

and SA-5, SA-3, and SA-5 (**Supporting Figure S1**). Glucose was consumed all strains, and the yield were 0.035 mol/mol (SA-3), 0.062 mol/mol (SA-4), 0.03550 mol/mol (SA-5), respectively. Unlike plasmid-based expression systems (**Figure 2B**), the integration of aroB increased shikimic acid production 1.5-fold over SA-2. In contrast, the integration of *aroG* into strain SA-2 decreased the production of shikimic acid. The SA-5 strain with the modified start codon had increased shikimic acid production by 26% compared with SA-2. These results suggest that *aroG* expression from the integrated *aroG* expression cassette was insufficient for shikimic acid production. In the case of *aroB*, a single integration of the *aroB* gene increased the shikimic acid titer over that of the plasmid-based overexpression system (SA-2/aroB; **Figure 2B**). Although we used medium copy number plasmid (about 30; Tauch, 2005), these results suggest that the production of large amounts of shikimic acid seems to depend on the plasmid copy number (Hashiro et al., 2019).

Using SA-3, SA-4, and SA-5 as host cells, each shikimate pathway gene *aroG*, *aroB*, *qsuD*, *aroE1*, and *aroE3* were introduced using a plasmid-based expression system. **Figures 3A–C** shows shikimic acid production after 72 h of cultivation. In the case of SA-3 (an *aroG*-integrated strain), additional plasmid-based *aroB* gene overexpression (SA-3/aroB) produced 5.1 ± 0.65 g/L of shikimic acid production, three-fold higher than SA-3. In strain SA-4 (an *aroB*-integrated strain), additional overexpression of *aroG* (SA-4/aroG) resulted in the highest shikimic acid production, up to 8.6 ± 0.96 g/L in CGXII minimal media containing 50 g/L of glucose. Overexpression of

other genes did not improve shikimate production in either SA-3 or SA-4. The SA-5 strain expressing *aroG* (SA-5/aroG) increased the shikimate titer up to 6.0 ± 0.05 g/L, slightly higher than that of SA-2/aroG (5.4 ± 0.65 g/L; **Figure 2B**).

Construction of *C. glutamicum* Strains With Integrated *aroG* and *aroB* Genes and Cultivation in Nutrient-Rich Media

As shown in **Figure 3**, *aroG* and *aroB* are key genes for high shikimic acid production. Zhang et al. reported that high-level expression of aroG and medium-level expression of aroB using plasmids having different ribosome binding sites were suitable for shikimic acid production (Zhang et al., 2015b). In the engineered strain series developed by Kogure's group, all of the genes of the shikimate pathway were expressed using a plasmid (Kogure et al., 2016). In this study, we introduced an *aroB* expression cassette into the *aroK* locus of the SA-5 strain. The resulting SA-6 strain produced 3.3 ± 0.29 g/L of shikimic acid (data not shown), which was slightly higher than the production of SA-5. We constructed strain SA-7 (SA-2/Δ*pta*:*aroG*, Δ*aroK*:*aroB*, Δ*cg2392*, $aroG^{gtg \rightarrow atg}$) by introducing an extra copy of the *aroG* gene chromosomally into the *pta* region of SA-6. The *pta* locus, encoding phosphate acetyltransferase, was selected for *aroG* integration to minimize any tendency for the formation of acetate as a byproduct. After cultivation, the SA-7 strain produced 5.7 ± 0.36 g/L of shikimic acid in CGXII medium containing 50 g/L of glucose (**Figure 4**, left blue bar), which was three-fold higher than SA-3 and 1.9-fold higher than SA-4. We additionally introduced each shikimate pathway gene into SA-7. SA-7 overexpressing *aroG* (SA-7/aroG) produced 8.7 ± 0.23 g/L of shikimic acid (**Figure 4**), almost the same as SA-4/aroG. SA-7 overexpressing *aroB* (SA-7/aroB) produced 5.0 ± 0.46 g/L of shikimic acid (**Figure 4**), almost the same as SA-4/aroB. These results suggest that a combination of plasmid-based aroG expression and single integration of *aroB* are valuable for high shikimic acid production. We measured the shikimic acid production of SA-7 transformants in nutrient-rich CGXIIY medium (CGXII medium containing 4 g/L of yeast extract and 50 g/L of glucose). Strain SA-7 carrying an empty plasmid produced 10.9 ± 0.92 g/L of shikimic acid (**Figure 4**, orange bar) with a yield of 0.22 g shikimate/g-glucose, about two-fold higher than SA-7 cultivated in CGXII minimal medium. Graf et al. reported that ATP and NADPH generation was enhanced in nutrient-rich medium (Graf et al., 2018), contributing to increased shikimic acid production. SA-7 overexpressing *aroG* and *aroB* strains produced 10.9 ± 0.38 g/L and 10.6 ± 0.36 g/L of shikimic acid in CGXIIY medium (**Figure 4**, orange bars), respectively, almost the same as SA-7 carrying an empty vector. Alternatively, SA-7 carrying plasmids containing *qsuC*, *aroE1*, or *aroE3* had slightly increased shikimic acid titers of up to 11.3 ± 0.31, 12.0 ± 1.70, and 13.5 ± 0.50 g/L, respectively. The one-way ANOVA analysis on the titer of shikimic acid production in CGXIIY medium revealed a statistically significant between empty vector and aroE3. These results indicate *aroE3* would be a rate-limiting step.

Feedback inhibition is another concern for shikimic acid production. In *E. coli*, AroG is specifically feedback regulated by L-phenylalanine, AroF and AroH are feedback regulated by L-tyrosine and L-tryptophan, respectively (Martinez et al., 2015).

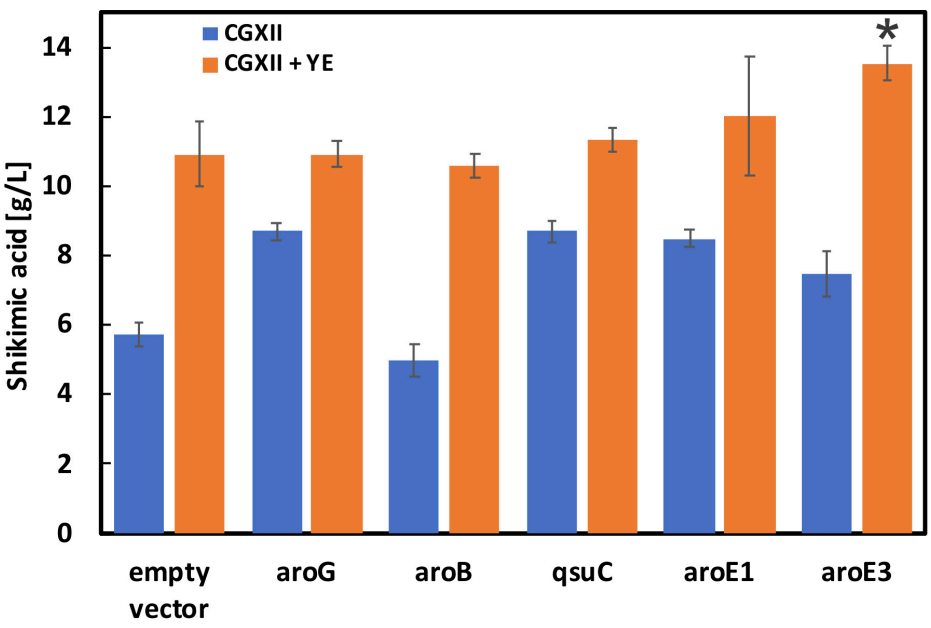

FIGURE 4 | Shikimic acid production titer in SA-7 strains harboring each shikimate pathway gene expression plasmid. Blue bars indicate SA production when the CGXII medium containing 50 g/L of glucose was used as the sole carbon source. Orange bars indicate the CGXIIY medium used. The data are presented as the average of three independent experiments, and error bars indicate the standard deviation. *P* values were computed using the two-tailed Student's *t*-test (*$P < 0.05$; **$P < 0.01$).

In the case of *C. glutamicum*, AroG activity was decreased only a 10 to 15% under 5 mM of L-phenylalanine and L-tyrosine concentrations (Liu et al., 2008). We also evaluated shikimic acid production CGXIIY medium including 100-fold higher (10 g/L) concentration of L-phenylalanine, L-tyrosine and L-tryptophan. The shikimic acid titer after 72 h was 6.6 ± 0.12 g/L (data not shown), about 40% decrease. These results suggest that the feedback inhibition of shikimic acid production with 100 mg/L (about 5–6 mM) of these amino acids was a small impact.

The time courses of each strain carrying an empty vector in CGXIIY medium containing 50 g/L of glucose are shown in **Figure 5**. SA-7 produced the highest amount of shikimic acid (10.9 ± 0.92 g/L), followed by SA-4, with 8.4 ± 0.19 g/L. The amount of shikimic acid produced by SA-4 in nutrient-rich CGXIIY medium was 2.8-fold higher than in CGXII minimum medium (**Figure 3B**, left bar). SA-2, SA-3, and SA-4 produced shikimic acid at 2.9 ± 0.24 g/L, 2.9 ± 0.04 g/L, and 4.0 ± 0.36 g/L, respectively, after 72 h in CGXIIY medium. The cell growth of SA-2 and SA-3 was higher than that of SA-7 and SA-4, suggesting that the carbon flux in SA-2 and SA-3 is distributed toward cell growth rather than shikimic acid synthesis. All strains except SA-3 consumed glucose for 48 h. Lactic acid was observed to be a major byproduct (**Figure 4D**). The SA-4 and SA-7 strains accumulated lactic acid at 6.9 ± 0.85 g/L and 8.3 ± 0.70 g/L,

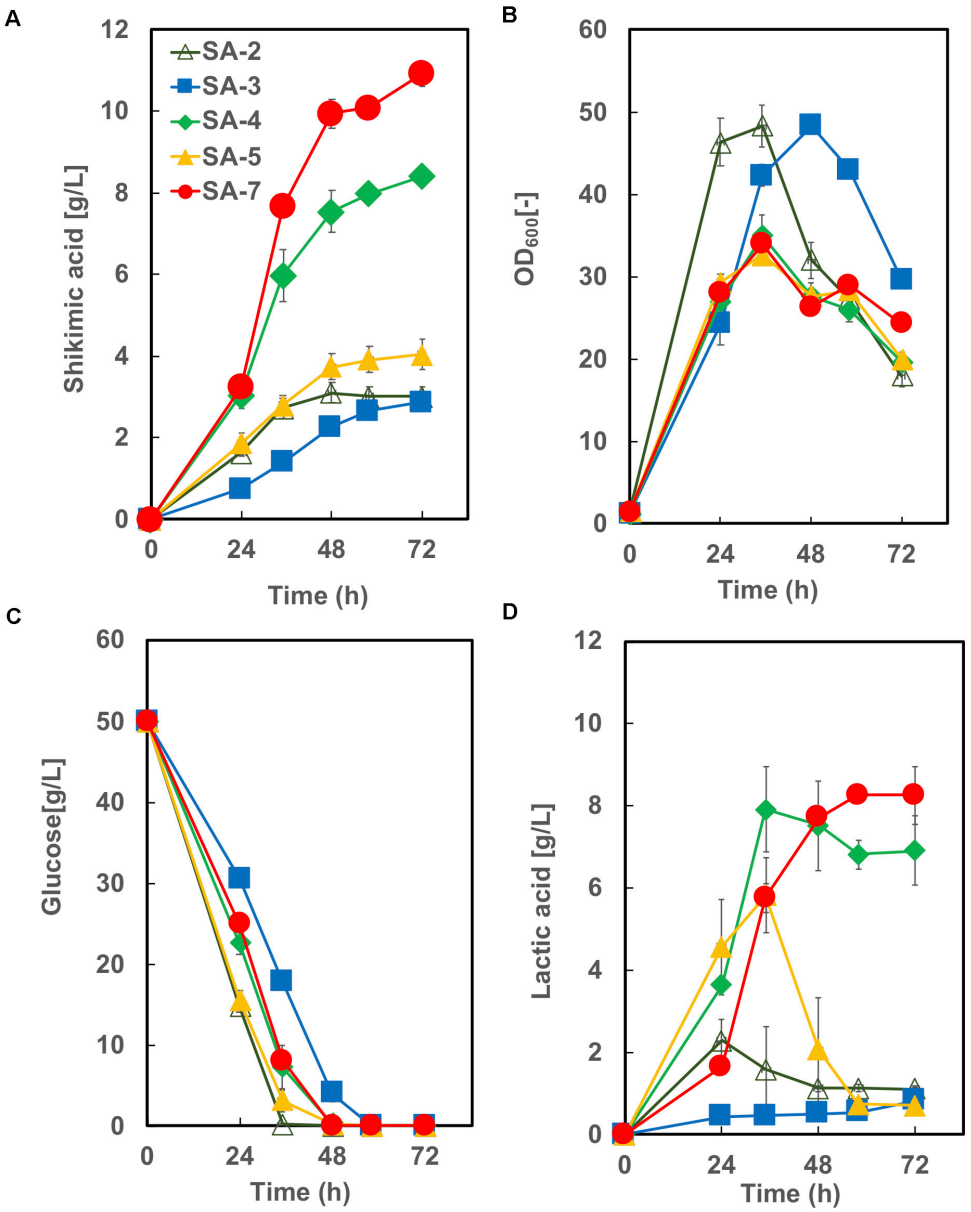

FIGURE 5 | Culture profiles of SA-7 and its derived strains. **(A)** Shikimic acid production, **(B)** cell growth, **(C)** glucose consumption, and **(D)** lactic acid accumulation. The data are presented as the average of three independent experiments, and error bars indicate the standard deviation.

respectively. When these strains were cultivated in the CGXIIY medium without glucose, shikimic acid production was less than 0.5 g/L (data not shown). Acetic acid was not detected during cultivation in SA-7 or other strains. 3-dehydroshikimate, reported as a major precursor, was not detected in any strain.

Evaluation of Cofactor Balance and Transcription Levels of the Lactate Dehydrogenase Gene in SA-6

As shown in **Figure 5D**, lactic acid accumulation was a major metabolic byproduct. **Figures 6A,B** show intracellular NADPH/NADP + and NADH/NAD + ratios after 24 h of cultivation in CGXIIY medium. In spite of lactic acid formation, as shown in **Figure 5D**, the NADH/NAD + ratio was almost the same among the parental strains SA-2 and SA-7. The NADPH/NADP + ratio of SA-7 was decreased relative to SA-2 due to the final reaction of shikimic acid synthesis, which is catalyzed by shikimate dehydrogenase, *aroE*. These results are consistent with previous reports (Kogure et al., 2016).

The transcription levels of *aroG*, *aroB*, and lactate dehydrogenase gene *ldh* were evaluated using real-time qPCR after 24 h of cultivation. The *aroG* levels of the SA-5 strain were slightly increased compared with those of SA-2 (**Figure 6C**), suggesting that a gene *cg2391* deletion had little influence on aroG transcription level (**Figure 4D**). Alternatively, in the case of the SA-7 strain, in which *aroG* and *aroB* are integrated under the control of the P_{H36} promoter, the transcription levels of *aroG* and *aroB* were significantly increased, up to 64.3- and 40.0-fold higher than those of the parental strain, contributing to improved shikimic acid production. The transcription levels of *ldh* were increased in all strains other than the parental strain. We disrupted the *ldh* gene (cg3219, NCgl2810) in SA-7. The resulting strain, SA-8, produced 9.9 ± 0.78 g/L of shikimic acid and accumulated 8.1 ± 0.18 g/L of lactic acid (**Supplementary Figure S2**), almost the same as SA-7. *C. glutamicum* has another putative lactate dehydrogenase gene (cg3227, NCgl2817), which might contribute lacate accumulation. A gene *lldD* (cg3227, NCgl2817) encoding quinone-dependent L-lactate dehydrogenase has the ability to utilize lactate as a carbon source (Stansen et al., 2005), however, activation of lactate re-assimilation pathway required a full oxygen supply (Käß et al., 2014). A limited-oxygen condition after glucose depletion in the test tube was another factor for lactate accumulation.

Construction of *C. glutamicum* Strains With Integrated *aroG*, *aroB*, and *aroE3* Genes and Shikimic Acid Production Using Cellobiose as a Carbon Source

Based on the results from **Figure 5**, we constructed strain SA-9 (SA-7/Δ*ldh:aroE1*) and SA-10 (SA-7/Δ*ldh:aroE3)* by introducing an extra copy of the *aroE1* or *aroE3* gene chromosomally into the *ldh* region of SA-7, respectively. After 72 h cultivation, the SA-9 strain produced 8.5 ± 0.46 g/L of shikimic acid in CGXIIY medium containing 50 g/L of glucose (**Figure 7A**). Alternatively, SA-10 produced 13.1 ± 0.25 g/L of shikimic acid with the yield of 0.26 g-shikimic acid/g-glucose (**Figure 7A**), which was almost same level of SA-7 harboring aroE3 expressing plasmid (**Figure 4**). We then focused on improving the availability of the shikimate pathway precursors PEP and E4P. To increase the supply of E4P, we constructed a plasmid for the overexpression of the endogenous transketolase (*tkt*) and transaldolase (*tal*) genes (cg1774-cg1776, NCgl1512-NCgl1513) and introduced into SA-10. Alternatively, to increase the availability of PEP, a plasmid for overexpression of endogenous phosphoenolpyruvate carboxykinase gene (*pck*; cg3169, NCgl2765) was introduced into SA-10. The resulting strain produced shikimic acid at 11.2 ± 0.71 g/L and 12.3 ± 0.25 g/L, respectively (**Figure 7B**).

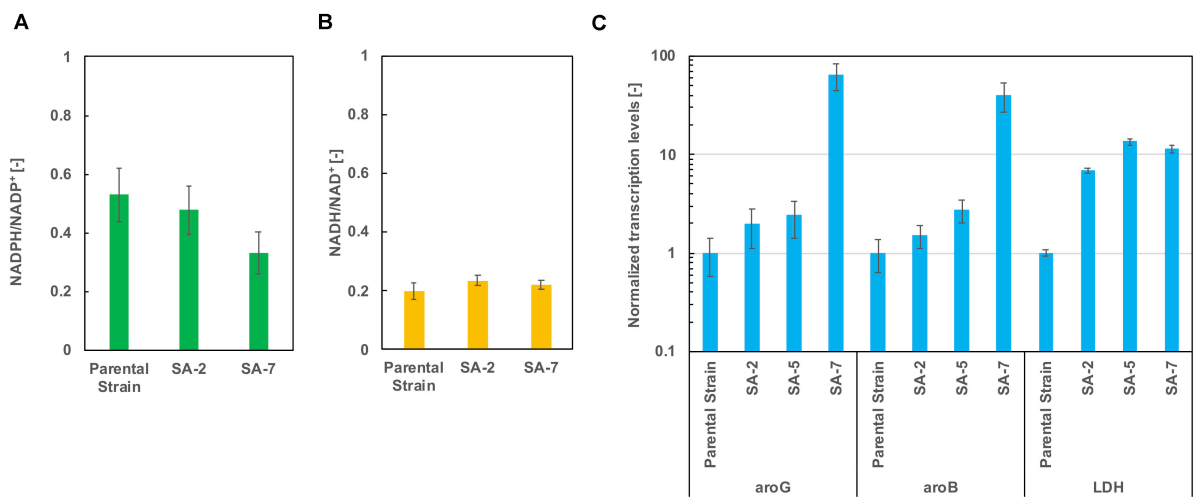

FIGURE 6 | The ratio of **(A)** NADPH/NADP + and **(B)** NADH/NAD + after 24 h cultivation in CGXIIY medium. Panel **(C)** shows the transcription levels of *aroG*, *aroB*, and *ldh* after 24 h of cultivation. The data are presented as the average of three independent experiments, and error bars indicate the standard deviation.

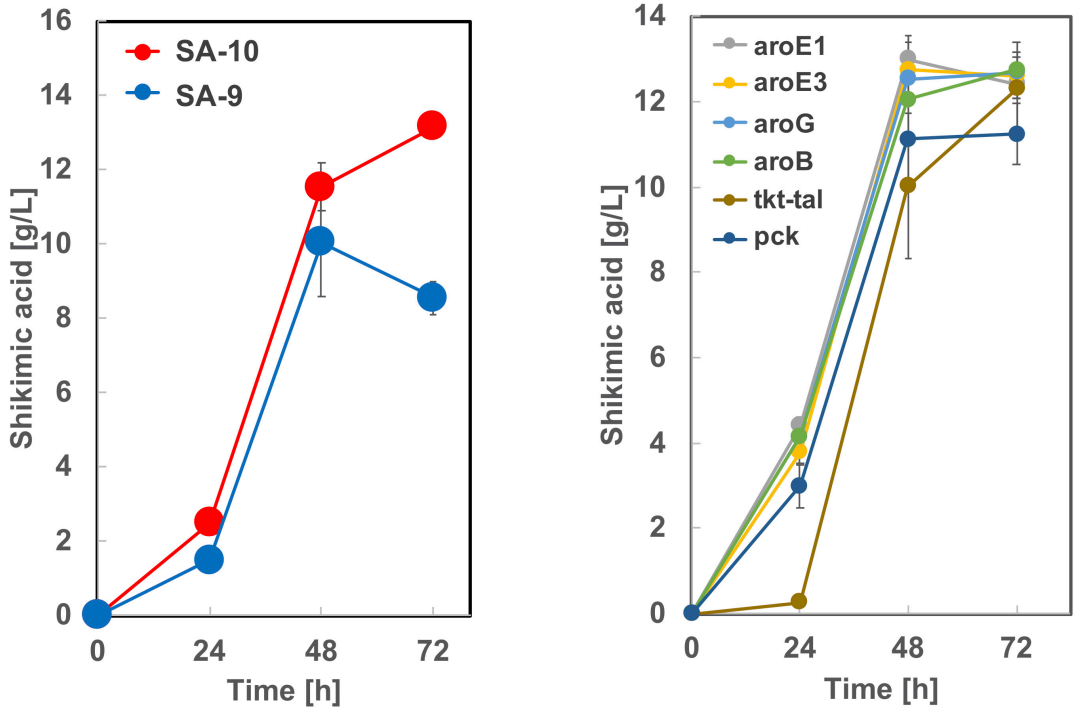

FIGURE 7 | Shikimic acid production titer in **(A)** SA-9, SA-10 and **(B)** its derived strains. CGXII medium containing 50 g/L of glucose was used as the sole carbon source. The data are presented as the average of three independent experiments, and error bars indicate the standard deviation.

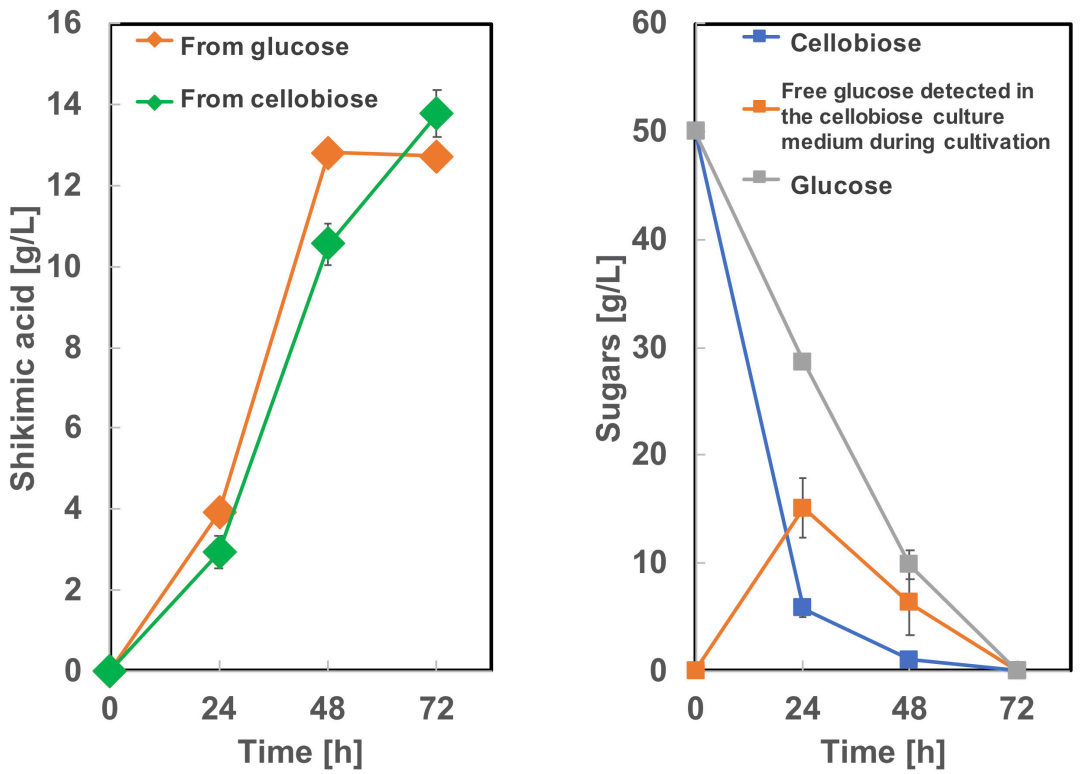

FIGURE 8 | Culture profiles of BGL expressing SA-10 strain. **(A)** Shikimic acid production, **(B)** cellobiose and glucose consumption. The data are presented as the average of three independent experiments, and error bars indicate the standard deviation.

We also introduced *aroB*, *aroG*, *aroE1,* and *aroE3* expression plasmid into SA-10 strain. Each strain produced shikimic acid at 12.8 ± 0.11 g/L, 12.7 ± 0.37 g/L, 12.4 ± 0.34 g/L and 12.6 ± 0.55 g/L, respectively (**Figure 7B**).

To produce shikimic acid from cellobiose as a carbon source, we used BGL Tfu0937 from *Thermobifida fusca* YX, which has been shown to exhibit high BGL activity in *E. coli* (Tanaka et al., 2011) and *C. glutamicum* (Matsuura et al., 2019). A plasmid secretory expressing BGL (Matsuura et al., 2019) was introduced into SA-10 and cultivated in CGXIIY medium containing 50 g/L of glucose or cellobiose as a carbon source. As shown in **Figure 8**, this BGL-secreting SA-10 strain produced 13.8 ± 0.56 g/L of shikimic acid from cellobiose as well as 12.7 ± 0.19 g/L of shikimic acid from glucose. The yield from cellobiose is 0.25 g-shikimic acid/g-glucose (1 g of cellobiose corresponds to 1.1 g of glucose), which was almost same as that from glucose (0.25 g-shikimic acid/g-glucose). These results show BGL expression did not affect shikimic acid production, which are corresponding to previous report (Matsuura et al., 2019). Cellobiose was completely consumed by 72h. However, free glucose was observed in the culture medium at 24 and 48 h cultivation. indicating the conversion of cellobiose into glucose by BGL was sufficient and improvement of glucose uptake might enhance shikimic acid production.

Microbial shikimic acid production has been reported by many groups. An engineered *E. coli* strain reported by Chandran et al. (2003) produced 87 g/L of shikimic acid from glucose with a yield of 0.36 (mol/mol) in fed-batch fermentation. Rodriguez et al. (2013) reported a metabolically engineered *E. coli* strain and the strain produced 43 g/L of shikimic acid with the yield of 0.43 (mol/mol) in batch culture. In the case of *C. glutamicum*, Kogure et al. (2016) reported 141 g/L of shikimic acid production using growth-arrested cell reaction with the yield of 0.51 (mol/mol). In our study, although shikimic acid titer (13.1 g/L) and yield (0.27 mol/mol) were less than those reports, we developed high shikimic acid producing *C. glutamicum* ATCC13032 strain without loss of PTS function and pyk activity. It should be useful property for the synthesis of plant polyphenols. In addition, we demonstrated direct shikimic acid production from cellobiose, which has the possibility of the reduction of the production cost.

CONCLUSION

In conclusion, The *C. glutamicum* strain SA-10 was metabolically engineered for enhanced shikimic acid production from glucose by optimizing its metabolic pathway, retaining the PTS system and *pyk* activity. Genomic integration of the *aroB, aroG* and *aroE3* genes improved shikimic acid production up to 13.1 g/L with a yield of 0.26 g-shikimic acid/g-glucose. Moreover, BGL-expressing SA-10 strain produced shikimic acid from cellobiose with almost same titer and yield from glucose. This study is an important step in developing an economically feasible and sustainable process for shikimic acid production.

DATA AVAILABILITY STATEMENT

The datasets presented in this study can be found in online repositories. The names of the repository/repositories and accession number(s) can be found in the article/ **Supplementary Material**.

AUTHOR CONTRIBUTIONS

NS and TT proposed the idea, designed the experiments, and wrote the manuscript. NS, MK, MN, YH, and TT performed the experiments. All authors read and approved the final manuscript.

FUNDING

This work was supported by the JST-Mirai Program (Grant Number JPMJMI17EI), Japan to TT, the Japan Society for the Promotion of Science (JSPS) Grant-in-Aid for Scientific Research (B) (Grant Number 19H02526), Japan to TT.

ACKNOWLEDGMENTS

The authors would like to thank Enago (www.enago.jp) for the English language review.

SUPPLEMENTARY MATERIAL

The Supplementary Material for this article can be found online at: https://www.frontiersin.org/articles/10.3389/fbioe.2020.569406/full#supplementary-material

FIGURE S1 | Culture profiles of strain SA-2, SA-3 and SA-5. The data are presented as the average of three independent experiments, and error bars indicate the standard deviation. *P* values were computed using the two-tailed Student's *t*-test (*, $P < 0.05$).

FIGURE S2 | Culture profiles of strain SA-8. **(A)** Shikimic acid production, **(B)** cell growth, **(C)** glucose consumption, **(D)** lactic acid accumulation. The data are presented as the average of three independent experiments, and error bars indicate the standard deviation.

TABLE S1 | Oligonucleotide primers used in this study.

REFERENCES

Averesch, N. J. H., and Krömer, J. O. (2018). Metabolic engineering of the shikimate pathway for production of aromatics and derived compounds - present and future strain construction strategies. *Front. Bioeng. Biotechnol.* 6:32. doi: 10.3389/fbioe.2018.00032

Baritugo, K. A., Kim, H. T., David, Y., Choi, J. I., Hong, S. H., Jeong, K. J., et al. (2018). Metabolic engineering of *Corynebacterium glutamicum* for fermentative production of chemicals in biorefinery. *Appl. Microbiol. Biotechnol.* 102, 3915–3937. doi: 10.1007/s00253-018-8896-6

Becker, J., Rohles, C. M., and Wittmann, C. (2018). Metabolically engineered *Corynebacterium glutamicum* for bio-based production of chemicals, fuels,

materials, and healthcare products. *Metab. Eng.* 50, 122–141. doi: 10.1016/j.ymben.2018.07.008

Bhatia, S. K., Jagtap, S. S., Bedekar, A. A., Bhatia, R. K., Patel, A. K., Pant, D., et al. (2020). Recent developments in pretreatment technologies on lignocellulosic biomass: effect of key parameters, technological improvements, and challenges. *Bioresour. Technol.* 300:122724. doi: 10.1016/j.biortech.2019.122724

Bochkov, D. V., Sysolyatin, S. V., Kalashnikov, A. I., and Surmacheva, I. A. (2012). Shikimic acid: review of its analytical, isolation, and purification techniques from plant and microbial sources. *J. Chem. Biol.* 5, 5–17. doi: 10.1007/s12154-011-0064-8

Bott, M., Noack, S., and Frunzke, J. (2013). Construction of a prophage-free variant of *Corynebacterium glutamicum* ATCC 13032 for use as a platform strain for basic research and industrial biotechnology. *Appl. Environ. Microbiol.* 79, 6006–6015. doi: 10.1128/AEM.01634-13

Braga, A., and Faria, N. (2020). Bioprocess optimization for the production of aromatic compounds with metabolically engineered hosts: recent developments and future challenges. *Front. Bioeng. Biotechnol.* 8:96.

Candeias, N. R., Assoah, B., and Simeonov, S. P. (2018). Production and synthetic modifications of shikimic acid. *Chem Rev.* 118, 10458–10550. doi: 10.1021/acs.chemrev.8b00350

Chandran, S. S., Yi, J., Draths, K. M., von Daeniken, R., Weber, W., and Frost, J. W. (2003). Phosphoenolpyruvate availability and the biosynthesis of shikimic acid. *Biotechnol. Prog.* 19, 808–814. doi: 10.1021/bp025769p

Cheng, J., Chen, P., Song, A., Wang, D., and Wang, Q. (2018). Expanding lysine industry: industrial biomanufacturing of lysine and its derivatives. *J. Ind. Microbiol. Biotechnol.* 45, 719–734. doi: 10.1007/s10295-018-2030-8

Choi, J. W., Yim, S. S., Lee, S. H., Kang, T. J., Park, S. J., and Jeong, K. J. (2015). Enhanced production of gamma-aminobutyrate (GABA) in recombinant *Corynebacterium glutamicum* by expressing glutamate decarboxylase active in expanded pH range. *Microb. Cell Fact* 14:21. doi: 10.1186/s12934-015-0205-9

Davies, G. J., Gloster, T. M., and Henrissat, B. (2005). Recent structural insights into the expanding world of carbohydrate-active enzymes. *Curr. Opin. Struct. Biol.* 15, 637–645. doi: 10.1016/j.sbi.2005.10.008

D'Este, M., Alvarado-Morales, M., and Angelidaki, I. (2018). Amino acids production focusing on fermentation technologies - A review. *Biotechnol. Adv.* 36, 14–25. doi: 10.1016/j.biotechadv.2017.09.001

Díaz Quiroz, D. C., Carmona, S. B., Bolívar, F., and Escalante, A. (2014). Current perspectives on applications of shikimic acid aminoshikimic acids in pharmaceutical chemistry. *Res. Rep. Med. Chem.* 4, 35–46. doi: 10.2147/RRMC.S46560

Flores, N., Flores, S., Escalante, A., De Anda, R., Leal, L., Malpica, R., et al. (2005). Adaptation for fast growth on glucose by differential expression of central carbon metabolism and gal regulon genes in an *Escherichia coli* strain lacking the phosphoenolpyruvate:carbohydrate phosphotransferase system. *Metab. Eng.* 7, 70–87. doi: 10.1016/j.ymben.2004.10.002

Flores, N., Leal, L., Sigala, J. C., De Anda, R., Escalante, A., Martínez, A., et al. (2007). Growth recovery on glucose under aerobic conditions of an *Escherichia coli* strain carrying a phosphoenolpyruvate: carbohydrate phosphotransferase system deletion by inactivating *arcA* and overexpressing the genes coding for glucokinase and galactose permease. *J. Mol. Microbiol. Biotechnol.* 13, 105–116. doi: 10.1159/000103602

Ger, Y. M., Chen, S. L., Chiang, H. J., and Shiuan, D. (1994). A single Ser-180 mutation desensitizes feedback inhibition of the phenylalanine-sensitive 3-deoxy-D-arabino-heptulosonate 7-phosphate (DAHP) synthetase in *Escherichia coli*. *J. Biochem.* 116, 986–990. doi: 10.1093/oxfordjournals.jbchem.a124657

Ghosh, S., Chisti, Y., and Banerjee, U. C. (2012). Production of shikimic acid. *Biotechnol. Adv.* 30, 1425–1431. doi: 10.1016/j.biotechadv.2012.03.001

Graf, M., Zieringer, J., Haas, T., Nieß, A., Blombach, B., and Takors, R. (2018). Physiological response of *Corynebacterium glutamicum* to increasingly nutrient-rich growth conditions. *Front. Microbiol.* 9:2058. doi: 10.3389/fmicb.2018.02058

Gu, P., Fan, X., Liang, Q., Qi, Q., and Li, Q. (2017). Novel technologies combined with traditional metabolic engineering strategies facilitate the construction of shikimate-producing *Escherichia coli*. *Microb. Cell Fact* 16:167. doi: 10.1186/s12934-017-0773-y

Hashiro, S., Mitsuhashi, M., and Yasueda, H. (2019). High copy number mutants derived from *Corynebacterium glutamicu*m cryptic plasmid pAM330 and copy number control. *J. Biosci. Bioeng.* 127, 529–538. doi: 10.1016/j.jbiosc.2018.10.012

Hirasawa, T., and Wachi, M. (2017). Glutamate fermentation-2: mechanism of L-Glutamate overproduction in *Corynebacterium glutamicum*. *Adv. Biochem. Eng. Biotechnol.* 159, 57–72. doi: 10.1007/10_2016_26

Huccetogullari, D., Luo, Z. W., and Lee, S. Y. (2019). Metabolic engineering of microorganisms for production of aromatic compounds. *Microb. Cell Fact* 18:41. doi: 10.1186/s12934-019-1090-4

Ikeda, M. (2006). Towards bacterial strains overproducing L-tryptophan and other aromatics by metabolic engineering. *Appl. Microbiol. Biotechnol.* 69, 615–626. doi: 10.1007/s00253-005-0252-y

Ikeda, M. (2017). Lysine fermentation: history and genome breeding. *Adv. Biochem. Eng. Biotechnol.* 159, 73–102. doi: 10.1007/10_2016_27

Jiang, M., and Zhang, H. (2016). Engineering the shikimate pathway for biosynthesis of molecules with pharmaceutical activities in *E. coli*. *Curr. Opin. Biotechnol.* 42, 1–6. doi: 10.1016/j.copbio.2016.01.016

Jorge, J. M., Nguyen, A. Q., Pérez-García, F., Kind, S., and Wendisch, V. F. (2017). Improved fermentative production of gamma-aminobutyric acid via the putrescine route: Systems metabolic engineering for production from glucose, amino sugars, and xylose. *Biotechnol. Bioeng.* 114, 862–873. doi: 10.1002/bit.26211

Kanda, Y. (2013). Investigation of the freely available easy-to-use software 'EZR' for medical statistics. *Bone Marrow Transplant.* 48, 452–458. doi: 10.1038/bmt.2012.244

Käß, F., Junne, S., Neubauer, P., Wiechert, W., and Oldiges, M. (2014). Process inhomogeneity leads to rapid side product turnover in cultivation of *Corynebacterium glutamicum*. *Microb. Cell. Fact* 13:6. doi: 10.1186/1475-2859-13-6

Khare, S. K., Pandey, A., and Larroche, C. (2015). Current perspectives in enzymatic saccharification of lignocellulosic biomass. *Biochem. Eng. J.* 102, 38–44. doi: 10.1016/j.bej.2015.02.033

Kim, H. T., Baritugo, K., Hyun, S. M., Khang, T. U., Sohn, Y. J., Kang, K. H., et al. (2020). Development of metabolically engineered *Corynebacterium glutamicum* for enhanced production of cadaverine and its use for the synthesis of bio-polyamide 510. *ACS Sus. Chem. Eng.* 8, 129–138. doi: 10.1021/acssuschemeng.9b04693

Kogure, T., and Inui, M. (2018). Recent advances in metabolic engineering of *Corynebacterium glutamicum* for bioproduction of value-added aromatic chemicals and natural products. *Appl. Microbiol. Biotechnol.* 102, 8685–8705. doi: 10.1007/s00253-018-9289-6

Kogure, T., Kubota, T., Suda, M., Hiraga, K., and Inui, M. (2016). Metabolic engineering of *Corynebacterium glutamicum* for shikimate overproduction by growth-arrested cell reaction. *Metab. Eng.* 38, 204–216. doi: 10.1016/j.ymben.2016.08.005

Lee, J. H., and Wendisch, V. F. (2017). Biotechnological production of aromatic compounds of the extended shikimate pathway from renewable biomass. *J. Biotechnol.* 257, 211–221. doi: 10.1016/j.jbiotec.2016.11.016

Li, Q., Yang, M. H., Wang, D., Li, W. L., Wu, Y., Zhang, Y. J., et al. (2010). Efficient conversion of crop stalk wastes into succinic acid production by A*ctinobacillus succinogenes*. *Bioresour. Technol.* 101, 3292–3294. doi: 10.1016/j.biortech.2009.12.064

Liu, A., Liu, Z. Z., Zou, Z. M., Chen, S. Z., Xu, L. Z., and Yang, S. L. (2004). Synthesis of (+)-zeylenone from shikimic acid. *Tetrahedron* 60, 3689–3694. doi: 10.1016/j.tet.2004.02.066

Liu, C. G., Xiao, Y., Xia, X. X., Zhao, X. Q., Peng, L., Srinophakun, P., et al. (2019). Cellulosic ethanol production: progress, challenges and strategies for solutions. *Biotechnol. Adv.* 37, 491–504. doi: 10.1016/j.biotechadv.2019.03.002

Liu, Y. J., Li, P. P., Zhao, K. X., Wang, B. J., Jiang, C. Y., Drake, H. L., et al. (2008). *Corynebacterium glutamicum* contains 3-deoxy-D-arabino-heptulosonate 7-phosphate synthases that display novel biochemical features. *Appl. Environ. Microbiol.* 74, 5497–5503. doi: 10.1128/AEM.00262-08

Martinez, J. A., Bolivar, F., and Escalante, A. (2015). Shikimic acid production in *Escherichia coli*: from classical metabolic engineering strategies to omics applied to improve its production. *Front. Bioeng. Biotechnol.* 3:145. doi: 10.3389/fbioe.2015.00145

Matsuura, R., Kishida, M., Konishi, R., Hirata, Y., Adachi, N., Segawa, S., et al. (2019). Metabolic engineering to improve 1,5-diaminopentane production from cellobiose using β-glucosidase-secreting *Corynebacterium glutamicum*. *Biotechnol. Bioeng.* 116, 2640–2651. doi: 10.1002/bit.27082

Noda, S., and Kondo, A. (2017). Recent advances in microbial production of aromatic chemicals and derivatives. *Trends Biotechnol.* 35, 785–796. doi: 10.1016/j.tibtech.2017.05.006

Ohnishi, J., Katahira, R., Mitsuhashi, S., Kakita, S., and Ikeda, M. (2005). A novel gnd mutation leading to increased L-lysine production in *Corynebacterium glutamicum*. *FEMS Microbiol Lett.* 242, 265–274. doi: 10.1016/j.femsle.2004.11.014

Pérez-García, F., and Wendisch, V. F. (2018). Transport and metabolic engineering of the cell factory *Corynebacterium glutamicum*. *FEMS Microbiol. Lett.* 365:fny166. doi: 10.1093/femsle/fny166

Rawat, G., Tripathi, P., and Saxena, R. K. (2013). Expanding horizons of shikimic acid. Recent progresses in production and its endless frontiers in application and market trends. *Appl. Microbiol. Biotechnol.* 97, 4277–4287. doi: 10.1007/s00253-013-4840-y

Rodriguez, A., Martínez, J. A., Báez-Viveros, J. L., Flores, N., Hernández-Chávez, G., Ramírez, O. T., et al. (2013). Constitutive expression of selected genes from the pentose phosphate and aromatic pathways increases the shikimic acid yield in high-glucose batch cultures of an *Escherichia coli* strain lacking PTS and pykF. *Microb. Cell Fact* 12:86. doi: 10.1186/1475-2859-12-86

Stansen, C., Uy, D., Delaunay, S., Eggeling, L., Goergen, J. L., and Wendisch, V. F. (2005). Characterization of a *Corynebacterium glutamicum* lactate utilization operon induced during temperature-triggered glutamate production. *Appl. Environ. Microbiol.* 71, 5920–5928. doi: 10.1128/AEM.71.10.5920-5928.2005

Tanaka, T., Kawabata, H., Ogino, C., and Kondo, A. (2011). Creation of a cellooligosaccharide-assimilating *Escherichia coli* strain by displaying active beta-glucosidase on the cell surface via a novel anchor protein. *Appl. Environ. Microbiol.* 77, 6265–6270. doi: 10.1128/AEM.00459-11

Tauch, A. (2005). "Native plasmids of amino acid-producing *Corynebacteria*," in *Handbook of Corynebacterium glutamicum*, eds L. Eggeling and M. Bott (Boca Raton, FL: CRC Press), 57–75. doi: 10.1201/9781420039696.ch4

Van Dyk, J., and Pletschke, B. (2012). A review of lignocellulose bioconversion using enzymatic hydrolysis and synergistic cooperation between enzymes—factors affecting enzymes, conversion and synergy. *Biotechnol. Adv.* 30, 1458–1480. doi: 10.1016/j.biotechadv.2012.03.002

Vogt, M., Brüsseler, C., Ooyen, J. V., Bott, M., and Marienhagen, J. (2016). Production of 2-methyl-1-butanol and 3-methyl-1-butanol in engineered *Corynebacterium glutamicum*. *Metab. Eng.* 38, 436–445. doi: 10.1016/j.ymben.2016.10.00

Wendisch, V. F., Mindt, M., and Pérez-García, F. (2018). Biotechnological production of mono- and diamines using bacteria: recent progress, applications, and perspectives. *Appl. Microbiol. Biotechnol.* 102, 3583–3594. doi: 10.1007/s00253-018-8890-z

Ximenes, E., Kim, Y., Mosier, N., Dien, B., and Ladisch, M. (2011). Deactivation of cellulases by phenols. *Enz. Microb. Technol.* 48, 54–60. doi: 10.1016/j.enzmictec.2010.09.006

Yim, S. S., An, S. J., Choi, J. W., Ryu, A. J., and Jeong, K. J. (2014). High-level secretory production of recombinant single-chain variable fragment (scFv) in *Corynebacterium glutamicum*. *Appl. Microbiol. Biotechnol.* 98, 273–284. doi: 10.1007/s00253-013-5315-x

Yim, S. S., An, S. J., Kang, M., Lee, J., and Jeong, K. J. (2013). Isolation of fully synthetic promoters for high-level gene expression in *Corynebacterium glutamicum*. *Biotechnol. Bioeng.* 110, 2959–2969. doi: 10.1002/bit.24954

Zhang, B., Liu, Z. Q., Liu, C., and Zheng, Y. G. (2016). Application of CRISPRi in *Corynebacterium glutamicum* for shikimic acid production. *Biotechnol. Lett.* 38, 2153–2161. doi: 10.1007/s10529-016-2207-

Zhang, B., Jiang, C. Y., Liu, Y. M., Liu, C., and Liu, S. J. (2015a). Engineering of a hybrid route to enhance shikimic acid production in *Corynebacterium glutamicum*. *Biotechnol. Lett.* 37, 1861–1868. doi: 10.1007/s10529-015-1852-y

Zhang, B., Zhou, N., Liu, Y. M., Liu, C., Lou, C. B., Jiang, C. Y., et al. (2015b). Ribosome binding site libraries and pathway modules for shikimic acid synthesis with *Corynebacterium glutamicum*. *Microb. Cell Fact* 14:71. doi: 10.1186/s12934-015-0254-

Zhang, C., Zhang, J., Kang, Z., Du, G., and Chen, J. (2015). Rational engineering of multiple module pathways for the production of L-phenylalanine in *Corynebacterium glutamicum*. *J. Ind. Microbiol. Biotechnol.* 42, 787–797. doi: 10.1007/s10295-015-1593-x

Zhao, X., Zheng, Z., Cai, Y., Zhao, Y., Zhang, Y., Gao, Y., et al. (2020). Accelerated biomethane production from lignocellulosic biomass: pretreated by mixed enzymes secreted by *Trichoderma viride* and *Aspergillus* sp. *Bioresour. Technol.* 309:123378. doi: 10.1016/j.biortech.2020.123378

Conflict of Interest: The authors declare that the research was conducted in the absence of any commercial or financial relationships that could be construed as a potential conflict of interest.

frontiers in Bioengineering and Biotechnology

ORIGINAL RESEARCH
published: 09 December 2020
doi: 10.3389/fbioe.2020.588070

Reverse Engineering Targets for Recombinant Protein Production in *Corynebacterium glutamicum* Inspired by a Fast-Growing Evolved Descendant

*Min Ju Lee[1], Jihoon Park[1†], Kyunghoon Park[1], Jihyun F. Kim[2] and Pil Kim[1]**

[1] Department of Biotechnology, The Catholic University of Korea, Gyeonggi, South Korea, [2] Department of Systems Biology, Division of Life Sciences, and Institute for Life Science and Biotechnology, Yonsei University, Seoul, South Korea

OPEN ACCESS

Edited by:
Yu Wang,
Tianjin Institute of Industrial Biotechnology, Chinese Academy of Sciences, China

Reviewed by:
Zhi-Gang Jeff Qian,
Shanghai Jiao Tong University, China
Dae-Hee Lee,
Korea Research Institute of Bioscience and Biotechnology (KRIBB), South Korea

***Correspondence:**
Pil Kim
kimp@catholic.ac.kr

†Present address:
Jihoon Park,
Durae Corporation, Gangwon, South Korea

Specialty section:
This article was submitted to Synthetic Biology, a section of the journal Frontiers in Bioengineering and Biotechnology

Received: *28 July 2020*
Accepted: *09 November 2020*
Published: *09 December 2020*

Citation:
Lee MJ, Park J, Park K, Kim JF and Kim P (2020) Reverse Engineering Targets for Recombinant Protein Production in Corynebacterium glutamicum Inspired by a Fast-Growing Evolved Descendant. Front. Bioeng. Biotechnol. 8:588070. doi: 10.3389/fbioe.2020.588070

We previously reported a *Corynebacterium glutamicum* JH41 strain with a 58% faster growth rate through application of adaptive laboratory evolution. To verify that the fast-reproducing strain was useful as a host for recombinant protein expression, we introduced a plasmid responsible for the secretory production of a recombinant protein. The JH41 strain harboring the plasmid indeed produced the secretory recombinant protein at a 2.7-fold greater rate than its ancestral strain. To provide the reverse engineering targets responsible for boosting recombinant protein production and cell reproduction, we compared the genome sequence of the JH41 strain with its ancestral strain. Among the 15 genomic variations, a point mutation was confirmed in the 14 bases upstream of NCgl1959 (encoding a presumed siderophore-binding protein). This mutation allowed derepression of NCgl1959, thereby increasing iron consumption and ATP generation. A point mutation in the structural gene *ramA* (A239G), a LuxR-type global transcription regulator involved in central metabolism, allowed an increase in glucose consumption. Therefore, mutations to increase the iron and carbon consumption were concluded as being responsible for the enhanced production of recombinant protein and cell reproduction in the evolved host.

Keywords: *Corynebacterium glutamicum*, host for recombinant protein, iron consumption, cellular energy, glucose consumption, ribosome

INTRODUCTION

Many attempts through microbial metabolic engineering have been made to overproduce metabolites by (1) improving the substrate uptake rate, (2) reducing the flux to undesired by-products, (3) introducing heterologous pathways and optimizing the activity of the enzyme, and (4) balancing product formation in cells, such as secretion of product to the extracellular medium (Yadav et al., 2012). However, the metabolic manipulation of microorganisms can cause flux imbalance due to the lack of understanding of the complex regulatory mechanisms essential for operation (Yadav et al., 2012). Adaptive laboratory evolution (ALE) is a reasonable approach because it not only copes with the physical defects of strains caused by genetic manipulation but also improves the productivity of cell factories (Sandberg et al., 2019; Lee and Kim, 2020). In addition, the commercialization of next-generation sequencing (NGS) technology and the

development of omics tools have enabled reverse engineering by helping us better understand mechanisms of microbial regulation (Stella et al., 2019). Besides, genetically modified organism (GMO)-related issues in the food industry have increased the demand for non-GMO strains derived from ALE.

Growth rate is a significant parameter in evaluating the compatibility of industrial strains. It is generally recognized that fast growth rates can achieve high cell densities and high productivity (Feist et al., 2010). Genomic analyses of fast-growing mutant strains have revealed previously unknown metabolic engineering targets and methods to improve production hosts. Rugbjerg et al. (2018) reported that the introduction of the *rpoB* mutation into *Escherichia coli* increased the growth rate by 13% while also increasing the production rate of mevalonate, a building block of terpenoid products such as fragrances and bioplastics, by 71%. In addition, Wang et al. reported that the introduction of *gntR1* and *ramA* mutations into *Corynebacterium glutamicum* increased the growth rate by 37% and the productivity of lysine by 100% (Wang et al., 2018).

Recently, we reported a fast-reproducing *C. glutamicum* JH41 strain, obtained through the application of ALE (Park et al., 2020). The transcriptome pattern of the evolved JH41 strain revealed that the upregulation of genes in the tricarboxylic acid cycle (TCA) cycle and respiratory chain, and oxidative stress responses allowed the growth promotion. Since *C. glutamicum* is a useful host for recombinant protein expression (Lee and Kim, 2018), it was proposed that the fast-reproducing JH41 strain might be an improved host for recombinant protein production and may also provide hidden genetic targets for reverse engineering of *C. glutamicum* hosts. In this report, the fast-reproducing JH41 was indeed verified as an improved host for recombinant protein production. Genomic analysis of the evolved strain was therefore performed to explain the reasons for the increased growth rate and recombinant protein production.

MATERIALS AND METHODS

Strains and Plasmids

Corynebacterium glutamicum PT strain (ancestor of JH41) and a fast-reproducing JH41 strain (descendant of PT) were used as hosts for recombinant protein production and genomic analysis (Park et al., 2020). DNA manipulation followed the method described by Sambrook et al. using *E. coli* DH10B (Invitrogen Inc., Carlsbad, CA, United States) (Sambrook and Russell, 2001). The strains and plasmids are listed in **Table 1** and the primers in **Supplementary Table 1**. Target gene-disrupted or gene-substituted *C. glutamicum* strains were prepared by double crossover using the pK*mobsacB*-based plasmids. Homologous arms of the target genes were constructed by connecting two fragments amplified from genomic DNA using overlap extension PCR (Ho et al., 1989). Oligonucleotide synthesis and plasmid sequence confirmation were performed at a facility of Bionics Inc., (Seoul, South Korea). *pfu* polymerase was purchased from Solgent Inc., (Daejeon, South Korea) and restriction enzymes and T4-ligase from New England Biolabs Inc., (Ipswich, MA, United States).

Media and Batch Cultures

As for the preculture for DNA manipulations, lysogeny broth (LB) complex medium was used for *E. coli*, and brain heart infusion (BHI) medium was used for *C. glutamicum*. *C. glutamicum* was incubated at 30°C and 200 rpm in a shaking incubator, and *E. coli* was incubated at 37°C and 220 rpm. For batch cultures of *C. glutamicum* strains, a modified MCGC minimal medium [0.9% glucose, 6 g Na_2HPO_4, 4 g $(NH4)_2SO_4$, 3 g KH_2PO_4, 1 g sodium citrate dehydrate, 1 g NaCl, 0.1 g $MgSO_4$–$7H_2O$, 20 mg $FeSO_4$–$7H_2O$, 2 mg $MnSO_4$–H_2O, 2 mg $FeCl_3$, 1 mg thiamine–HCl, 200 μg biotin, 35 μg $CaCl_2$, 0.5 μg $ZnSO_4$–$7H_2O$, 0.2 μg $Na_2B_4O_7$–$10H_2O$, 0.2 μg $CuCl_2$–$2H_2O$, 0.1 μg $(NH_4)_6Mo_7O_{24}$–$4H_2O$ per liter] was used (Osten et al., 1989). A 500-ml baffled flask containing 50 ml of the modified MCGC medium was used for efficient oxygen transfer. The initial cell mass was adjusted to OD_{600} = 0.1. Biomass was estimated by measuring optical density (OD) at 600 nm every hour and converting into g_{-DCW}/L unit by the coefficient of 0.25.

Secretory Production of Recombinant Protein

To confirm the recombinant protein production of the hosts, pCG-H36A-agarase encoding a strong autonomous promoter and TAT-secretion signal sequence with the agarase gene from *Streptomyces coelicolor* was further transformed into the PT and JH41 strains (Yim et al., 2016). After incubating for 24 and 48 h in a 500-ml baffled flask containing 50 ml of MCGC media, 50 ml of the culture broth was centrifuged (12,000 × g, 4°C, 5 min). The supernatant containing the secreted protein was concentrated 50-fold using a centrifugal filter (Amicon® Ultra-15 10K, Merck Millipore, Burlington, MA, United States), and then, the buffer was changed with 50 mM Tris–HCl (pH 7.0). The prepared protein samples were diluted to final OD_{600} values and then loaded on a 12% sodium dodecyl sulfate–polyacrylamide gel electrophoresis (SDS-PAGE) gel. The photograph of the gel was captured using a chemical fluorescence image analyzer (Chemi Doc MP System, Bio-Rad Laboratories, Inc., Hercules, CA, United States), and the intensity of the target band was compared using the ImageJ program.

Genome Sequencing

For genome sequencing, genomic DNAs of *C. glutamicum* PT and JH41 were isolated using a gDNA prep kit (Solgent Inc., Daejeon, South Korea) according to the manufacturer's instructions. The genome sequence was determined using the PacBio RS II (Pacific Biosciences Inc., Menlo Park, CA, United States) at a DNA sequencing facility (ChunLab Inc.). Raw sequences were assembled with PacBio SMRT Analysis ver. 2.0 software (Pacific Biosciences Inc., Menlo Park, CA, United States). Gene prediction was performed using Glimmer 3 (Delcher et al., 2007), and annotations were performed by a homology search against the SEED database, Universal Protein Resource (UniProt) database, and eggNOG database (Disz et al., 2010). Genome sequences of the PT and JH41 strains were compared using EzGenome (http://ezgenome.ezbiocloud.net/ezg_browse) and CLgenomics program (ChunLab). Analysis

TABLE 1 | Strains and plasmids used in this study.

Strains and plasmids	Description	References
Strains *E. coli*		
DH10B	F$^-$ *mcrA* Δ(*mrr-hsd*RMS-*mcrBC*) Φ80*lacZ*ΔM15 Δ*lacX74 recA1 endA1 araD139*Δ(*ara leu*)7697 *galU galK rpsL nupG* λ$^-$	Invitrogen
BL21(DE3)	*E. coli* F$^-$*ompT gal dcm lon hsdS*$_B$ r$_B$$^-$ m$_B$$^-$; *E. coli* B strain), with λDE3	Novagen
C. glutamicum PT	Home stock of *C. glutamicum* wild-type, Biotin auxotroph, derived from KCTC No. 1445	Kim et al., 2016
JH41	A descendant of *C. glutamicum* PT, selected after 600 generation, 58% faster reproduction than PT	Park et al., 2020
PT NCgl0774:35-bp	PT harboring genomic NCgl0774, putative siderophore- binding lipoprotein A, inserting the 35-bp sequence	This study
PT NCgl1159^{C-108T}	PT harboring genomic NCgl1159, F_0F_1-ATP synthase subunit A, substituting the 108th upstream sequence of NCgl1159 from C to T	This study
PT Δ*ripA*	PT derivative, Δ*ripA* (0.8-kb deletion)	This study
PT Δ*dtxR*	PT derivative, Δ*dtxR* (0.9-kb deletion)	This study
PT *ramA*^{A239G}	PT harboring genomic *ramA*, transcriptional regulator MalT, substituting to A239G	This study
PT SBP B^{C-14G}	PT harboring genomic SBP B (NCgl1959), putative siderophore-binding lipoprotein, substituting the 14^h upstream sequence of SBP from C to G	This study
PT S + R	PT harboring genomic mutation of PT *ramA*^{A239G} and PT SBP B^{C-14G}	This study
Plasmids		
pET24a	*E. coli* expression vector, P_{T7}, Km^R	Novagen
pET24a-DtxR	pET24a harboring DtxR (NCgl1845) of *C. glutamicum*	This study
pSL360	*E. coli* and *C. glutamicum* shuttle vector, Km^R	Park et al., 2004
pCG-H36A	*C. glutamicum* vector, TAT-signal sequence of cg1514 (start codon is changed to ATG), a strong synthetic H36 promoter	Yim et al., 2016
pCG-H36A-agarase	pCG-H36A derivative, harboring *S. coelicolor* agarase	Yim et al., 2016
pCG-H36A(-SS)	pCG-H36A derivative, signal peptide deleted vector, H36 promoter	This study
pCG-H36A(-SS)-GFP	pCG-H36A(-SS) derivative, harboring eGFP	This study
pCG-H36A-*porD*	pCG-H36A derivative, TAT-signal sequence of *porD*, H36 promoter	This study
pCG-H36A-*porD*-GFP	pCG-H36A-*porD* derivative, harboring eGFP	This study
pK19*mobsacB*	Suicide vector for double recombination, Km^R, *sacB* of *Bacillus subtilis*	Schafer et al., 1994
pSL360-SBP B	pSL360 harboring putative siderophore-binding lipoprotein, SBP B (NCgl1959) of *C. glutamicum*	This study
pK19*mobsacB* -NCgl0774:35-bp	pK19*mobsacB* harboring homologous arm for insertion of NCgl0774:35-bp	This study
pK19*mobsacB* -Δ*ripA*	pK19*mobsacB* harboring homologous arm for deletion of Δ*ripA*	This study
pK19*mobsacB* -Δ*dtxR*	pK19*mobsacB* harboring homologous arm for deletion of Δ*dtxR*	This study

of single-nucleotide polymorphisms (SNPs) and gap was performed using the MAUVE (Darling et al., 2004) and MegaX (Kumar et al., 2018) programs.

Analyses of ATP, Iron, and Glucose Concentrations

Cells were harvested from batch cultures (1 ml) at 5 h by centrifugation (8,000 × *g*, 4°C, 5 min) and washed twice with sterile distilled water. The cell suspension (0.8 ml) was mixed with 0.2 g of glass beads (212–300 μm) in a screw-capped tube followed by homogenization for 30 s using a bead beater (Model 607, BioSpec Inc., Bartlesville, OK, United States). After chilling in an ice bath for 1 min, homogenization was repeated five more times. Cell debris was removed by centrifugation (8,000 × *g*, 4°C, 5 min), and the supernatant was used for measuring intracellular ATP.

ATP concentration was estimated using an ENLITEN ATP Assay System Bioluminescence Detection Kit (#FF2000, Promega Inc., Madison, WI, United States). Light intensity was detected by a luminometer (GloMax®-96 Microplate Luminometer, Promega Inc., Madison, WI, United States) after a luciferase-driven reaction (Na et al., 2015).

Iron consumption was estimated by measuring the remaining free iron concentration using the *o*-phenanthroline colorimetric method (Serra et al., 2015) after cell removal. Culture broth (1 ml) was centrifuged (12,000 × *g*, 4°C, 5 min), and the supernatant (100 μl) was mixed with 20 μl of bromophenol blue (0.4 g/L). After pH adjustment to 3.5 by adding 0.2% H_2SO_4, a further 10 μl of hydroquinone (1 g/L), 20 μl of *o*-phenanthroline (2.5 g/L), and distilled water (up to 250 μl) were added to the mixture. After 1 h of color development at room temperature, absorbance was measured at 510 nm. The analyses of ATP and iron concentrations were determined at least three times with three biological replicates.

To analyze the glucose consumption of JH41 and PT *ramA*^{A239G}, the glucose concentration in the medium was measured by a reducing sugar quantification method using a 3,5-dinitrosalicylic acid (DNS) reagent (Deshavath et al., 2020). After cell removal, 150 μl of supernatant and 150 μl of DNS reagent were mixed and heated at 100°C for 5 min. After standing to cool for 10 min at room temperature, 200 μl of the mixture was

dispensed into 96-well plates to measure absorbance at 540 nm. D-Glucose reagent was used as a standard.

Determination of DtxR Affinity on the Mutated Promoter Sequence

The affinity of negative regulator diphtheria toxin repressor (DtxR) on the mutated promoter region was determined by an electrophoresis mobility shift assay using the purified DtxR protein and the PCR-amplified DNA fragment. The *dtxR* gene from *C. glutamicum* was cloned and expressed in *E. coli* BL21 (DE3) with an additional 12 × His tag in the expression plasmid (pET24b-*dtxR*, **Table 1**). The protein was further purified using Ni^{2+} chelate affinity chromatography, as described previously (Wennerhold et al., 2005). To test the binding of DtxR to the putative target promoter DNA, the purified DtxR protein (0–350 ng, dimeric form) was dissolved with PCR-amplified DNA fragments (399 bp, 200 ng) in a 10-μl binding buffer [50 mM Tris–HCl (pH 7.5), 5 mM $MgCl_2$, 40 mM KCl, 5% (v/v) glycerol, 1 mM dithiothreitol (DTT), and 150 μM $MnCl_2$]. The reaction mixture was loaded onto a 15% native polyacrylamide gel containing 1 mM DTT and 150 μM $MnCl_2$ after incubation for 30 min at room temperature. Electrophoresis was performed at room temperature and 170 V using 1 × TB (89 mM Tris base, 89 mM boric acid) supplemented with 1 mM DTT and 150 μM $MnCl_2$ as an electrophoresis buffer. The gel was then stained with a fluorescent dye (SYBR Green I EMSA Kit, Invitrogen Inc., Carlsbad, CA, United States) according to the manufacturer's instructions. The photograph of the gel was captured using a chemical fluorescence image analyzer (Chemi Doc MP System, Bio-Rad Laboratories, Inc., Hercules, CA, United States).

Transcription Quantification of rRNAs

The ribosomal RNAs (rRNAs) transcription level determination method was followed as described (Kwon et al., 2015). Total RNA was extracted from actively growing *C. glutamicum* strains using TRIzol1 reagent (Invitrogen, Carlsbad, CA, United States) and NucleoSpin1 RNA II Kit (Macherey-Nagel, Düren, Germany) after cell disruption using a Mini-Beadbeater-16 (BioSpec, Bartlesville, PA, United States) with glass beads (acid washed, 212–300 mm, Sigma-Aldrich, MO, United States). The 50 ng of total RNAs was used for complementary DNA (cDNA) synthesis using ReverTra Ace-α-1 (Toyobo, Osaka, Japan) according to the manufacturer's instructions. THUNDERBIRD SYBR1 qPCR Mix (Toyobo, Osaka, Japan) and the Step-One Plus Real-Time PCR System (Applied Biosystems, Foster City, CA, United States) were used for the gene expression analysis. Step-One Plus Software ver. 2.0 (Applied Biosystems, Foster City, CA, United States) was used to quantify the relative transcription. *gapA* [glyceraldehyde 3-phosphate dehydrogenase (GAPDH)] and *leuA* (2-isopropyl malate synthase) genes were used as internal references. The relative expression of rRNAs with the reference genes was determined using the $2^{-\Delta\ \Delta\ CT}$ (Livak) method. Primers for identifying transcription levels are shown in **Supplementary Table 1**.

RESULTS

Effect of Fast-Growing JH41 Host on the Secretory Production of Recombinant Protein

Because protein is the major macromolecule in cells, the rapidly reproducing JH41 strain was supposed to be able to produce a protein at an enhanced rate. The fact that no extracellular protease activity or economical purification of secretory protein was found in *C. glutamicum* host (Lee and Kim, 2018) further encouraged us to hypothesize that the rapidly reproducing JH41 strain would become an improved *C. glutamicum* host for secretory protein production. To verify this hypothesis, a plasmid designed to secrete foreign agarase (pCG-H36A-agarase) was introduced into JH41 and PT strains. The secretory recombinant protein (agarase, 34 kDa) showed a major band in the SDS-PAGE (**Figure 1A**). The band intensities of the recombinant protein from the JH41 host were 7,490 AU at 24 h and 17,231 AU at 48 h, while those from the PT host were 4,780 AU at 24 h and 6,212 AU at 48 h (**Figure 1B**). The JH41 host produced the secretory recombinant protein (56% at 24 h and 177% at 48 h) at a greater rate than the PT host. In order to confirm the production effect of other proteins in the JH41 host, a plasmid expressing green fluorescent protein (GFP) in cytoplasm (pCG-H36A[-SS]-GFP, no signal sequence) and a plasmid secreting GFP by a TAT-signal sequence (pCG-H36A-*porD*-GFP) were introduced into the JH41 host (**Supplementary Figure 1**). The productions of cytoplasmic GFP and secreted GFP from the JH41 host were greater than those from the PT host by 5–16% and 13–116%, respectively. Therefore, the rapid-reproducing JH41 strain was an enhanced host for the production of recombinant proteins.

Genome Analysis of the JH41 Host

To understand the reasons for enhanced cell reproduction and to provide reverse engineering targets responsible for the improved recombinant protein production, the JH41 genome was resequenced and deposited [National Center for Biotechnology Information (NCBI) accession number PRJNA554987]. A total 15 genomic mutations were found to be accumulated in JH41 compared to its ancestral PT (**Table 2**). Among them, four were found in the non-coding region, including an internal transcribed spacer (ITS) mutation, and 11 in the coding region. Genomic mutations were categorized into the clusters of orthologous groups of proteins (COG) as four to the function unknown group (S), two to the transcription group (K), two to the inorganic ion transport and metabolism group (P), one to the defense mechanism (V), one to the signal transduction mechanism (T), and one to the energy production and conversion group (C). The remaining three mutations did not show protein function or were not protein-encoding regions. A 35-bp repeated mutation in the structural gene encoding a putative siderophore-binding lipoprotein A (SBP A, NCgl0774) and a substitution mutation (C→G) at the 14 bases upstream of the start codon of the gene encoding a putative siderophore-binding lipoprotein B (SBP B, NCgl1959) were identified. A condensed mutation was also found in one of the operons encoding rRNA primary

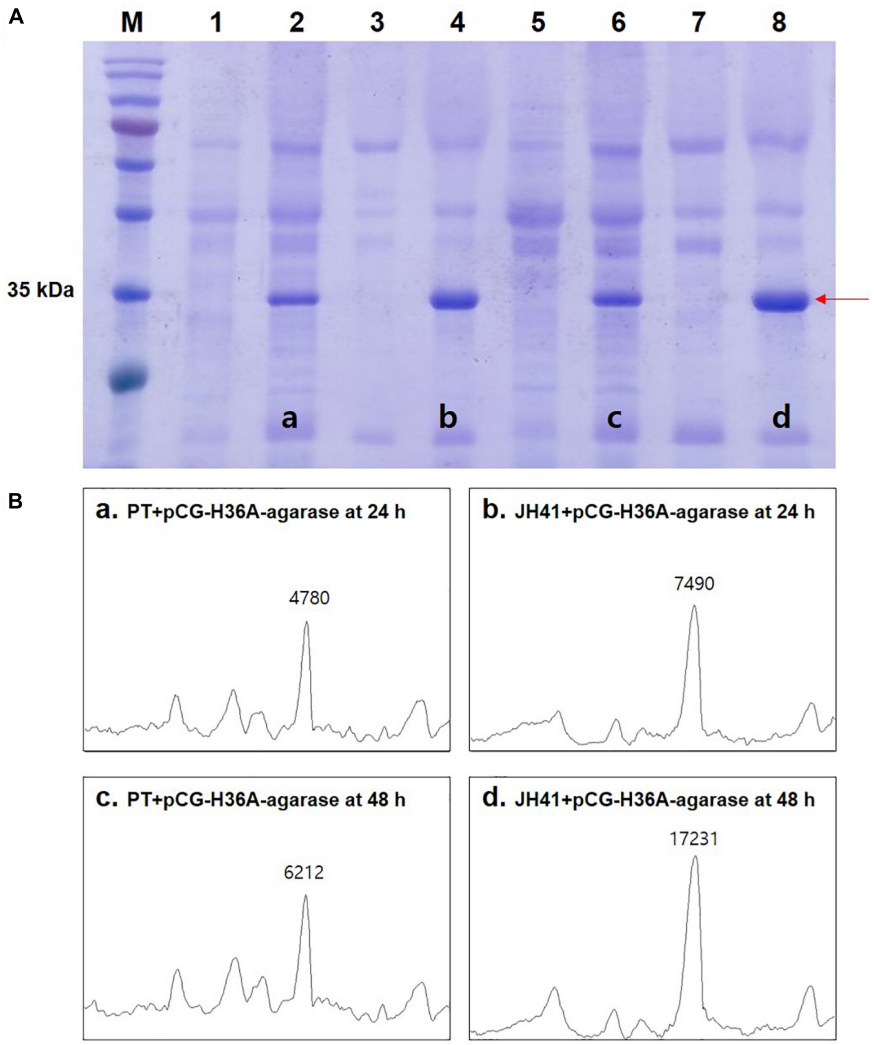

FIGURE 1 | Effects of host on the secretory production of recombinant protein. **(A)** Image of sodium dodecyl sulfate–polyacrylamide gel electrophoresis (SDS-PAGE). Lane 1, PT + pCG-H36A (empty vector) at 24 h; lane 2, PT + pCG-H36A-agarase at 24 h; lane 3, JH41 + pCG-H36A (empty vector) at 24 h; lane 4, JH41 + pCG-H36A-agarase at 24 h; lane 5, PT + pCG-H36A (empty vector) at 48 h; lane 6, PT + pCG-H36A-agarase at 48 h; lane 7, JH41 + pCG-H36A (empty vector) at 48 h; lane 8, JH41 + pCG-H36A-agarase at 48 h. Arrow indicates the secreted agarase band (34 kDa). The image is from the representative experiment from three independent experiments. **(B)** Band density estimation of the SDS-PAGE image using ImageJ software. a: lane 2; b: lane 4; c: lane 6; d: lane 8.

transcript. One mutation was found in the 16S rRNA structural gene, and another 23-point mutations were densely observed between the 16S and 23S rRNA sequences, which are called 16S–23S internal transcribed spacer (ITS) (Osorio et al., 2005).

Mutation Effect on Iron Consumption

The mutations observed in two presumed siderophore-binding lipoproteins (NCgl0774: 35-bp repeated mutation; NCgl1959: point substitution mutation at -14 bp) suggested their possible role in the rapid reproduction of JH41. To explore the functional significance of these putative iron-importing systems (Ribeiro and Simões, 2019), the iron consumption of JH41 was profiled (**Figure 2B**). Iron concentration in the medium decreased more rapidly in the JH41 strain. Since iron is an essential element for bacteria and acts as a redox center for several cytochromes and iron–sulfur proteins in the electron transfer chain (Hider and Kong, 2010), it was assumed that the rapidly reproducing JH41 might harbor greater energy than its ancestor. To validate this, ATP concentrations of the fast-growing JH41 and ancestral PT were analyzed. Indeed, the intracellular ATP concentrations of JH41 were greater than those of the PT strain with a range of 19–35% during the active growing phase (**Figure 2C**).

To assess which of the putative siderophore-binding lipoproteins affected iron consumption, a PT strain harboring the genomic NCgl0774 gene with the precise 35-bp repeated sequence (PT NCgl0774:35-bp) was constructed for complementation tests. The constructed PT NCgl0774:35-bp strain showed no differences compared with the PT strain in the growth profile (**Supplementary Figure 2**). This result indicated

TABLE 2 | Genomic mutations of the JH41 host over ancestral host.

PT position[a]	JH41 position[a]	COG functional category[b]	Locus tag	Mutation region	Variants	Function (gene name)	mRNA fold based on transcriptome[c)]
80,225	1,076,088	S	NCgl2726	Non-coding (-57 bp of NCgl2726)	Substitution (G→A)	Tripartite tricarboxylate transporter substrate binding protein	3.05
461,943	1,457,809	-	-	16S rRNA coding region	Substitution (A→G)	Bacterial small subunit ribosomal RNA; 16S ribosomal RNA	–
462,350	1,458,217			Non-coding (16S-23S ITS of 1st rRNA operon)	Similar to 16S–23S ITS of 5th rRNA operon	rRNA operon 16S-23S ITS (internal transcribed spacer)	–
1,191,984	2,187,859	T	NCgl0722	Coding (372 bp)	Insertion (C)	Histidine protein kinase (*mtrB*)	1.27
1,251,401	2,247,312	P	NCgl0774	Coding (15 bp)	Repeat (35 bp, AAAACTCTCCTCCGCA CTGATCGTGCTTCTCG CAG)	ABC transporter system; A putative Fe^{3+}-siderophore-binding lipoprotein	0.03
1,660,001	2,655,914	C	NCgl1159	Non-coding (-108 bp of NCgl1159)	Substitution (C→T)	ATP synthase F_0F_1 subunit A	0.27
1,968,380	2,964,295	K	NCgl1435	Coding (201 bp)	Substitution (A→G)	Transcriptional regulator	1.17
2,004,381	3,000,298	–	–	Coding (67 bp)	Substitution (G→A)	Hypothetical protein	–
2,326,488	217,999	P	NCgl1959	Non-coding (-14 bp of NCgl1959)	Substitution (C→G)	ABC transporter system; a putative Fe^{3+}-siderophore-binding lipoprotein	5.1
2,521,778	413,291	S	NCgl2129	Coding (110 bp)	Substitution (A→T)	Uncharacterized protein, cell membrane; membrane; signal; transmembrane; transmembrane helix.	1.43
2,589,950	481,463	S	NCgl0891	Coding (709 bp)	Substitution (T→G)	HNH endonucleases	1.08
2,589,952	481,465	S	NCgl0891	Coding (711 bp)	Substitution (G→T)	HNH endonucleases	1.08
2,708,045	599,558	K	NCgl2298	Coding (757 bp)	Substitution (G→A)	HTH-type transcriptional repressor (*osrR*)	1.27
2,743,443	634,956	V	NCgl2331	Coding (610 bp)	Substitution (G→A)	Penicillin binding protein	0.53
2,899,770	791,283	K	NCgl2472	Coding (239 bp)	Substitution (T→C)	Transcriptional regulator MalT (*ramA*)	1.17

[a]Genome sequence data NCBI bioproject number: PRJNA554987. [b]COG functional categories (M, cell wall/membrane/envelope biogenesis; T, signal transduction mechanisms; V, defense mechanisms; K, transcription; L, replication, recombination and repair; C, energy production and conversion; E, amino acid transport and metabolism; P, inorganic ion transport and metabolism; S, function unknown). [c]Data adopted from the transcriptome (NCBI bioproject number: PRJNA556334) (Park et al., 2020).

that the 35-bp repeat mutation on the putative siderophore-binding protein A was not a prominent factor contributing to the rapid reproduction of JH41.

Another point mutation found in the JH41 strain was located at -14 bp of the start codon of NCgl1959 encoding a putative siderophore-binding lipoprotein B, in the

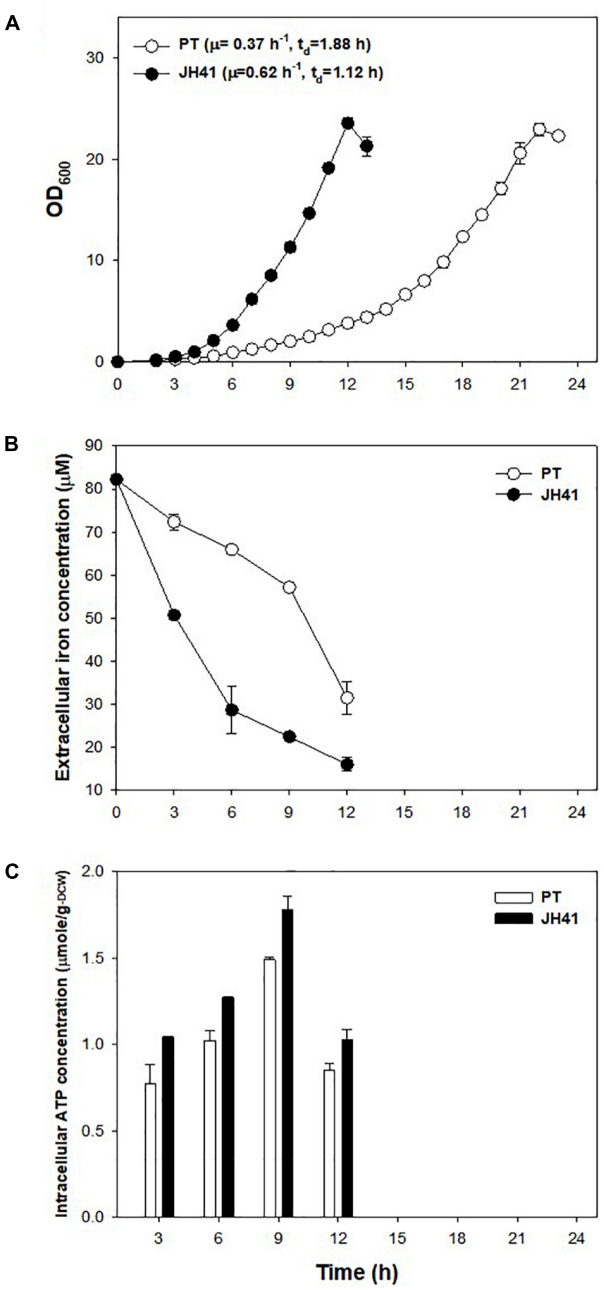

FIGURE 2 | Profiles of growth, iron consumption, and intracellular ATP concentration of the JH41 host. **(A)** Batch culture growth profiles of PT and JH41 hosts. Cultures were in a 500-ml baffled flask containing 50 ml of modified MCGC medium. Each data point represents the mean ± SD; *n* = 3 biologically independent samples. (PT: white; JH41: black). **(B)** Iron consumption in PT and JH41 hosts. Samples were taken from the batch cultures (500-ml baffled flask containing 50 ml of modified MCGC medium). Iron concentration of the medium was measured by the *o*-phenanthroline colorimetric method. Error bars show a statistical mean ± SD; *n* = 3 biologically independent samples. (PT: white; JH41: black). **(C)** Intracellular ATP concentrations in PT and JH41 strains. Samples were taken from the batch cultures (500-ml baffled flask containing 50 ml of modified MCGC medium). Intracellular ATP was measured by the luciferin–luciferase reaction immediately after disrupting cells. Error bars show a statistical mean ± SD; *n* = 3 biologically independent samples (PT: white; JH41: black).

middle of the consensus sequence of the DtxR binding site (**TTAGGCAAGGCTACCTTTTTGCCTATG**; bold: DtxR binding consensus sequence; underline: mutation C→G; italic: start codon), where DtxR is a repressor of the genes responsible for iron uptake and protection against free radical damage (Wennerhold and Bott, 2006). The mutation on the DtxR binding sequence was assumed to derepress the downstream NCgl1959. To this end, we also found that the transcriptome data show a 5.1-fold upregulation of NCgl1959 in JH41 [**Table 2**; messenger RNA (mRNA) fold based on transcriptome column]. To verify the hypothesis, the binding affinity between the NCgl1959 regulatory region and DtxR was investigated by gel shift assay (**Figure 3A**). The binding affinity of the His-tag purified DtxR protein on the DNA fragment carrying the point mutation was only 40% of the affinity of the original sequence, which suggested that the mutation would have caused the derepression of NCgl1959 by reducing affinity to the transcription repressor, DtxR. Further, complementation studies were performed by constitutively expressing NCgl1959, the putative siderophore-binding lipoprotein B, on a plasmid in the PT strain. The PT strain expressing NCgl1959 (PT + pSL360-SBP B) showed more rapid reproduction (75% increase) (**Figure 3B**), greater iron consumption (**Figure 3C**), and higher ATP concentrations (**Figure 3D**) than the parental PT strain. Therefore, the derepression or overexpression of the putative siderophore-binding protein (NCgl1959) enabled *C. glutamicum* to consume more iron and further increase intracellular ATP concentration.

The point mutation found at the -108 region of the NCgl1159 (subunit A of F_0F_1-ATP synthase) might be involved in ATP generation (**Table 2**). The growth profile of the PT host containing the genomic mutation at the -108 region of the NCgl1159 (PT NCgl1159^{C-108T}), however, was not different from that of the PT host (**Supplementary Figure 3**).

Investigating further, known regulators related to iron metabolism were found to be disrupted in the PT genome. Along with DtxR, the repressor of the putative siderophore-binding lipoprotein B expression, RipA, which is known to be a gene-enhancing regulator for iron-consuming proteins and is repressed by DtxR (Wennerhold et al., 2005), were chosen as the disruption targets. Part of the coding sequences of DtxR (1.9→1.0 kb) and RipA (1.7→0.9 kb) were removed from the genome of PT strain using a double crossover method. The PT Δ*dtxR* strain showed a 34% faster growth rate and the PT Δ*ripA* (47% slower growth rate) compared with PT strain (**Figure 4**). The disruption of RipA (leading downregulation of iron-consuming genes) led the cell to double more slowly, and the disruption of DtxR (leading to overexpression of iron-importing genes) resulted in the faster doubling.

Mutation Effect on Glucose Consumption

Another notable mutation in JH41 was on the NCgl2472 gene (A239G), encoding the LuxR-type global transcription

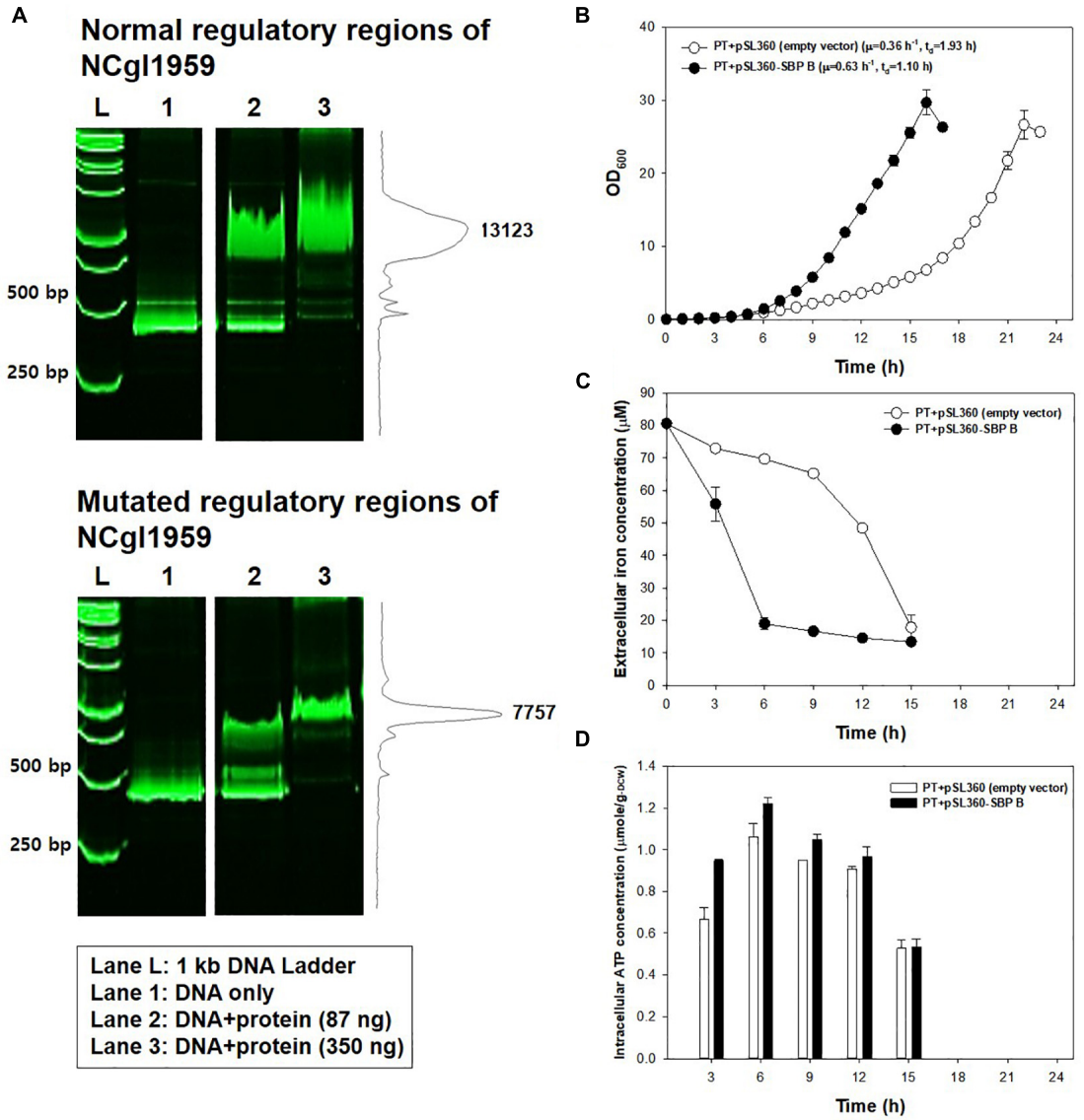

FIGURE 3 | Effects of the mutation at 14 bases upstream of NCgl1959. **(A)** Native polyacrylamide gel image showing the affinity of DtxR protein to the normal DNA fragment (up) and to the mutated DNA fragment (down). L: size marker; lane 1: DNA only; lane 2: DNA + DtxR (87 ng); lane 3: DNA + DtxR (350 ng). The DNA fragments were stained with SYBR Green. The chromatogram on the right side represents the intensity of bands by ImageJ software. The image is from the representative experiment from three independent experiments. **(B)** Growth profile of PT strain harboring plasmid constitutively expressing NCgl1959. Each data point is the mean ± SD; *n* = 3 biologically independent samples. (PT + empty vector: white; PT + pSL360-SBP B: black). **(C)** Iron consumption in PT strain harboring plasmid constitutively expressing NCgl1959. The iron concentration in the medium was measured by the *o*-phenanthroline colorimetric method. All strains were cultured in a 500-ml baffled flask containing 50 ml of modified MCGC medium. Bar heights and error bars show a statistical mean ± SD; *n* = 3 biologically independent samples (PT + empty vector: white; PT + pSL360-SBP B: black). **(D)** Intracellular ATP concentrations in PT strain harboring plasmid constitutively expressing NCgl1959. The intracellular ATP luciferin–luciferase reaction was measured immediately after harvest during the actively growing phase. Point and error bars show a statistical mean ± SD; *n* = 3 biologically independent samples (PT + empty vector: white; PT + pSL360-SBP B: black).

regulator RamA protein, which controls the expression of genes involved in sugar uptake, glycolysis, acetate, and many other metabolic pathways (Auchter et al., 2011). Wang et al. and Graf et al. reported a *ramA* mutation found in another fast-growing strain of *C. glutamicum*, and the mutation was described as a key mutation because it enabled substrate uptake and increased metabolic flux (Wang et al., 2018; Graf et al., 2019). To verify that the $ramA^{A239G}$ mutation in the JH41 strain also contributed to the enhanced cell division, the genomic point mutation was introduced to PT strain by homologous recombination to construct PT $ramA^{A239G}$ strain. Indeed, the PT $ramA^{A239G}$ strain consumed glucose at 0.89 ± 0.03 $g_{-glucose}/g_{-DCW}\cdot h$, whereas PT and JH41 consumed it at 0.64 ± 0.04 and 1.11 ± 0.01 $g_{-glucose}/g_{-DCW}\cdot h$, respectively

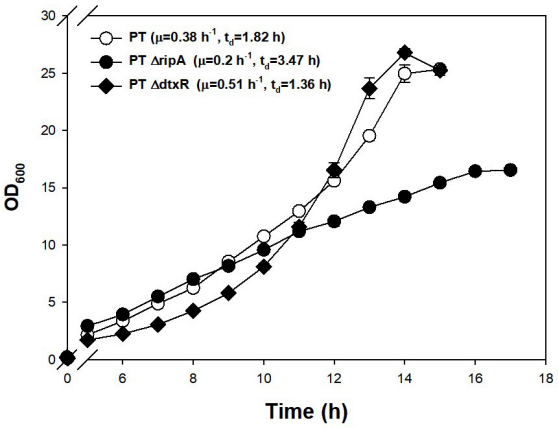

FIGURE 4 | Effect of genomic disruptions of iron-relevant regulator genes (*ripA, dtxR*) on the growth of PT strain. The PT Δ*ripA* and PT Δ*dtxR* strains were incubated at 30°C, 200 rpm in a shaking incubator. A 500-ml baffled flask containing 50 ml of the modified MCGC media was used for efficient oxygen transfer. The exponential growth rate (μ) in batch culture was determined by linear regression of log biomass concentrations over each process time. Each data point is the mean ± SD; *n* = 3 biologically independent samples (PT: white circle; PT Δ*ripA*: black circle; PT Δ*dtxR*: black rhombus).

(**Figure 5**). Therefore, the *ramA*^{A239G} mutation led the PT strain to increase the rates of glucose consumption by 39% and growth by 40%. The increase in glucose uptake would have provided the increased precursor metabolites and energy to *C. glutamicum* cells.

Mutation Effect on Ribosome Components

The ITS mutation (condensed 23 point mutations, **Table 2**) located in the non-coding region of rRNA primary transcript in the genome of JH41 was assumed to influence the maturation of rRNA from its pre-transcript, and this might contribute to the increased number of ribosomes. To confirm this hypothesis, concentrations of the mature 5S, 16S, and 23S rRNAs in the JH41 strain were compared with those in the PT strain by quantitative PCR (**Table 3**). The fast-growing JH41 strain harbored higher concentrations of mature rRNAs (45% more 16S rRNA, 72% more 23S rRNA, 37% more 5S rRNA) compared to the PT strain. Along with increases in the three rRNAs, our previous paper also reported that most of the mRNAs encoding ribosomal proteins were upregulated (**Supplementary Table 2**) (Park et al., 2020). These results enabled us to conclude the ITS mutation in rRNA primary transcript supported the fast growth of JH41 by increases in matured rRNAs and ribosomal proteins, and therefore, the increase in ribosome components might be a reverse engineering target to enhance the production of recombinant protein even though the genomic introduction of the multiple mutations in the one ITS region among the 6 rRNA operons would be technically difficult.

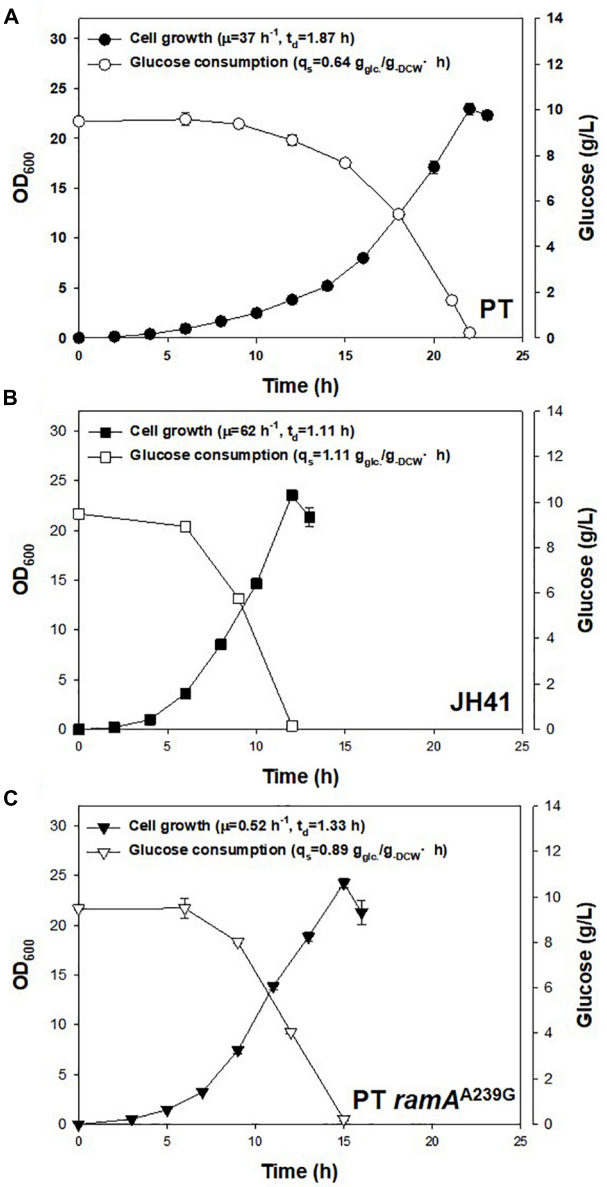

FIGURE 5 | Effects of genomic *ramA*^{A239G} mutation in PT strain on growth rate and glucose consumption. The growth rate and glucose consumption profiles of **(A)** PT, **(B)** JH41, and **(C)** PT *ramA*^{A239G}. Batch cultures were performed in a 500-ml baffled flask containing 50 ml of 0.9% glucose modified MCGC medium. Cell densities of *C. glutamicum* PT, JH41, and PT *ramA*^{A239G} were measured every 2 h. Glucose consumption was measured by 3,5-dinitrosalicylic acid (DNS) reduction sugar quantification method. Each data point represents mean ± SD; *n* = 3 biologically independent samples. (biomass: black; glucose concentration: white).

Combinatorial Effect of SBP B and RamA Mutations on Recombinant Protein

In the above results, the mutations on the SBP B upregulation (SBP B^{C-14G}) and the glucose-uptake regulator (*ramA*^{A239G}) were the clear genetic factors affecting the growth rate of JH41. To evaluate the combinatorial effect of the two mutations on

TABLE 3 | Levels of intracellular rRNAs in JH41.

Reference gene	Target gene	Fold difference ($2^{-\Delta\Delta CT}$)[a]
gapA	16S rRNA	1.45 ± 0.37
	23S rRNA	1.72 ± 0.64
	5S rRNA	1.37 ± 0.42
leuA	16S rRNA	1.47 ± 0.07
	23S rRNA	1.30 ± 0.10
	5S rRNA	1.18 ± 0.15

[a] *(rRNA ratio in JH41)/(rRNA ratio in PT). Values represent the statistical mean ± SD; n = 3 biologically independent samples.*

the growth profile and recombinant protein production, the genome of the PT host was mutated to have either the SBP B^{C-14G} mutation (PT SBP B^{C-14G} host) or the *ramA*^{A239G} mutation (PT *ramA*^{A239G} host) or to have both mutations (PT SBP B^{C-14G} *ramA*^{A239G}, in short, PT S + R). The growth rate of the SBP B genome-edited host (PT SBP B^{C-14G}) was 0.56 h^{-1} (t_D = 1.23 h) and that of the RamA genome-edited host (PT *ramA*^{A239G}) was 0.52 h^{-1} (t_D = 1.33 h), which were 51 and 41% faster doubling, respectively, than that of PT host (growth rate = 0.37 h^{-1}, t_D = 1.87 h). The double mutant of *ramA*^{A239G} and SBP B^{C-14G} host (PT S + R) showed the fasted growth rate of 0.66 h^{-1} (t_D = 1.05 h), which was 78% higher than that of PT and even faster than that of the evolved JH41 host (0.61 h^{-1}, t_D = 1.13 h) (**Figure 6A**).

The secretory protein productions in the PT SBP B^{C-14G} and the PT *ramA*^{A239G} hosts are also shown to be greater than that from the PT host (**Figures 6B,C**). The SDS-PAGE band intensity of the secretory recombinant proteins from the PT SBP B^{C-14G} and the PT *ramA*^{A239G} hosts were 8,149 and 6,146 AU, respectively, where those from PT host was 4,130 AU. The fastest growing PT S + R hosts, however, secreted the recombinant protein at only 4,064 AU, which is even lower than that of the PT host. Therefore, the mutations in *ramA*^{A239G} and SBP B^{C-14G}, respectively, resulted in the increased growth rates and protein production. Meanwhile, the combination of the two genes showed a remarkable increase in the growth rate but was found to have a negative effect on protein production. The iron metabolism regulator-deleted strains (PT Δ*dtxR* and PT Δ*ripA*) also decreased the recombinant agarase production by 34 and 37%, respectively, than that from PT host (**Supplementary Figure 4**).

DISCUSSION

The evolved *C. glutamicum* JH41 strain with increased growth rate was able to produce 2.7-fold greater secretory recombinant protein than PT host (**Figure 1**). The confirmed genetic factors that contributed to the increased growth rates and became the reverse engineering targets to enhance production of recombinant proteins were (1) SBP B^{C-14G} that enhanced iron transport leading the increase of intracellular energy and (2) *ramA*^{A239G} that enhanced glucose uptake leading to the increase in energy and metabolite pool. High levels of intracellular ATP have been known to improve target products by improving substrate uptake, cell growth, biosynthesis, and resistance to toxic compounds (Hara and Kondo, 2015). The authors also reported that the productions of recombinant proteins (green fluorescence protein and alkaline protease) were increased in the highly energized *E. coli* host by the overexpression of phosphoenolpyruvate carboxykinase (Pck) (Kim et al., 2012). A high level of intracellular energy can provide favorable conditions for energy-consuming reactions such as charging amino acids to transfer RNA (tRNA), translational elongation, folding, and secretion. In addition, a high intracellular energy state can upregulate the genes involved in the biosynthetic pathways for amino acid supply (Kwon et al., 2008).

The point substitution mutation in the regulatory region of NCgl1959 in JH41 strain, resulted in the increase in iron consumption by derepressing the cognate genes (**Figure 3**). Although the function of NCgl1959 protein in *C. glutamicum* has not yet been clearly identified, the NCgl1959 protein was estimated to have a similar 3D structure with the known siderophore-binding lipoproteins (*E. coli* FhuD and *Bacillus cereus* YfiY) (Clarke et al., 2000; Zawadzka et al., 2009) (**Supplementary Figure 5**). One might speculate that NCgl1959 would play the role of iron complex uptake. The imported iron could be used for the assembly of electron transfer chain components (i.e., iron–sulfur reaction center for NADH dehydrogenase; heme–iron for cytochrome *c* oxidase and cytochromes) and redox-containing proteins (i.e., heme-dependent catalase and peroxidase) (Park et al., 2020), and therefore, it is considered that the enhanced iron consumption in JH41 strain would contribute to generating more energy to the respiratory chain, along with a simultaneous increase in defense capability against oxidative stress.

In particular, RamA has been shown to act as a positive regulator of the TCA cycle genes, *sdhCAB* (succinate dehydrogenase operon) and *acn* (aconitase) (Bussmann et al., 2009; Teramoto et al., 2011). The point mutation *ramA*^{A239G} (corresponding to RamA^{Y80C}) of JH41 strain was located at the GAF-2 domain (amino acid positions 8 and 146), the same domain of the reports from Graf et al. and Wang et al. (Wang et al., 2018; Graf et al., 2019), and the GAF domain has been found in the cyclic nucleotide phosphodiesterase superfamily in other species (Fawcett et al., 2000; Schultz, 2009). Therefore, we considered that the *ramA*^{A239G} would have enabled the JH41 strain to increase glucose consumption by altering the cyclic nucleotide-mediated signals, thereby resulting in increased substrate uptake. The increase in carbon source in the JH41 host would have been favorable cellular conditions for the recombinant protein production by providing enhanced pools of precursor metabolites, along with more energy.

We do not understand why the combination of the two mutations of *ramA*^{A239G} and SBP B^{C-14G} showed a faster growth rate exceeding JH41 and less production of recombinant protein (**Figure 6**). The H36 promoter for the recombinant protein production was one of the most powerful synthetic promoter known in *C. glutamicum* (Yim et al., 2013), and it was able to promote the secretory production of agarase from the PT *ramA*^{A239G} and the PT SBP B^{C-14G}

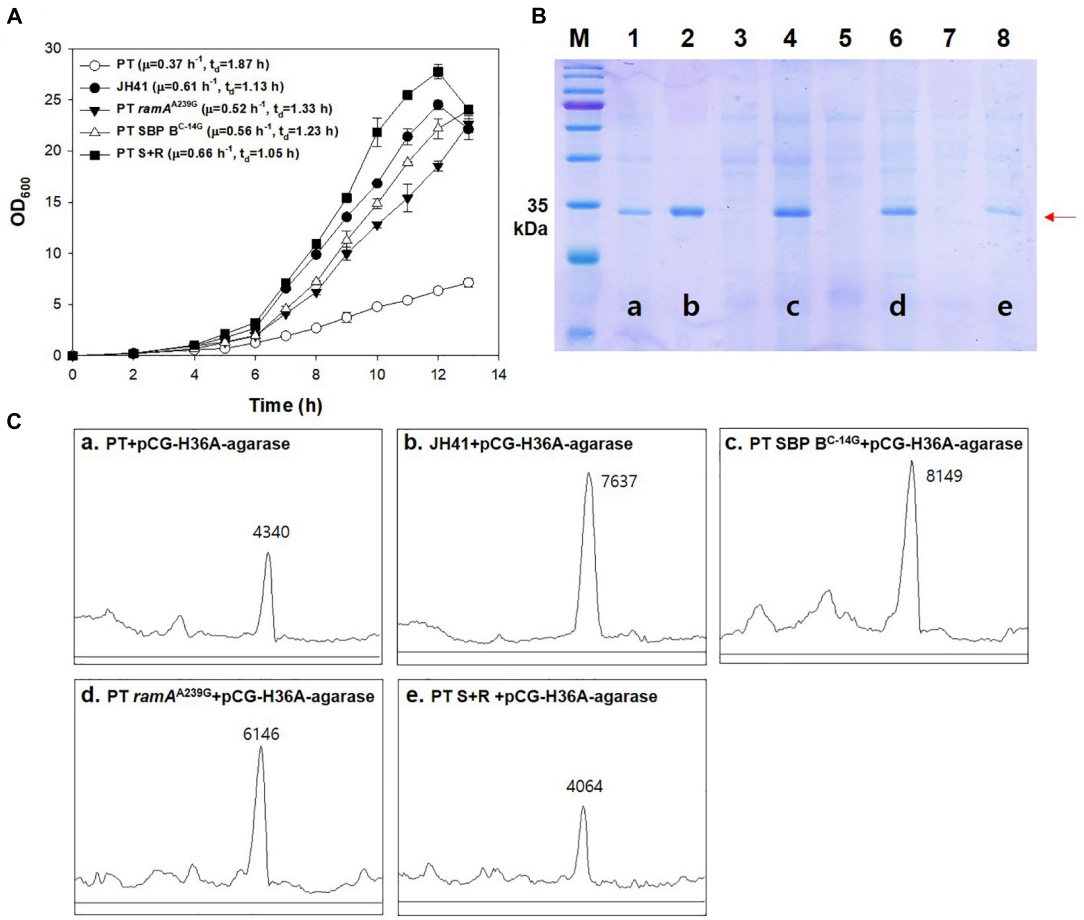

FIGURE 6 | Effects of genomic *ramA*^{A239G} and SBP B^{C-14G} mutation in PT strain on growth rate and the secretory production of recombinant protein. **(A)** Batch culture growth profiles of PT and JH41 strains. The growth rate profiles of PT, JH41, PT *ramA*^{A239G}, PT SBP B^{C-14G}, and PT S + R. Batch cultures were performed in a 500-ml baffled flask containing 50 ml of 0.9% glucose modified MCGC medium. Cell densities of *C. glutamicum* PT, JH41, PT *ramA*^{A239G}, PT SBP B^{C-14G}, and PT S + R were measured every 1 h. Each data point represents mean ± SD; *n* = 3 biologically independent samples. (PT: white circle; JH41: black circle; PT *ramA*^{A239G}: black triangle; PT SBP B^{C-14G}: white triangle; PT S + R: Black square). **(B)** Image of sodium dodecyl sulfate–polyacrylamide gel electrophoresis (SDS-PAGE). Lane 1, PT + pCG-H36A (empty vector); lane 2, JH41 + pCG-H36A-agarase; lane 3, PT SBP B^{C-14G} + pCG-H36A (empty vector); lane 4, PT SBP B^{C-14G} + pCG-H36A-agarase; lane 5, PT *ramA*^{A239G} + pCG-H36A (empty vector); lane 6, PT *ramA*^{A239G} + pCG-H36A-agarase; lane 7, PT S + R + pCG-H36A (empty vector); lane 8, PT S + R + pCG-H36A-agarase. Agarase production was confirmed after 24 h cultivation. Arrow indicates the secreted agarase band (34 kDa). The image is from the representative experiment from three independent experiments. **(C)** Band density estimation of the SDS-PAGE image using ImageJ software. a: lane 1; b: lane 2; c: lane 4; d: lane 6; e: lane 8.

along with the JH41 hosts. There might be unknown factor responsible for this mismatch between fast growth and less protein production (Nordholt et al., 2017). Further basic studies on cellular physiology are required to understand this unexpected phenomenon.

The condensed 23 point mutations occurred in the ITS region of the first rRNA operon among the six rRNA operons of *C. glutamicum* JH41. The multimutated first ITS sequence was similar to the sequence of the ITS in the fifth rRNA operon. A tRNA gene is located between 16S rRNA and 23S rRNA in *E. coli* rRNA pretranscript, while *C. glutamicum* does not contain tRNA in this sequence region. Although the processing mechanism of the rRNA pretranscript in *C. glutamicum* remains unknown, the ITS mutation in JH41 might have facilitated RNase processing, as in the case of *E. coli*. Therefore, the processing of the polycistronic primary transcript might have been increased to form mature ribosomes by the ITS mutation, having observed the increases in rRNAs and ribosomal proteins. The increase in mature ribosome components would contribute to the enhancement of recombinant protein productions, as observed in JH41.

Additional genetic factors enhancing growth and recombinant protein production remain veiled. It is worth mentioning another complementation on the genomic mutation on the coding region of NCgl2298 (*osrR*, G757A = D253N), an HTH-type transcription regulator known to upregulate the tolerance genes against oxidative stress and heat stress (Hong et al., 2016). The mutation on the *osrR* was expected to release the stress tension that was provoked by the enhanced iron and carbon uptakes.

The growth of the PT NCgl2298^{G757A} was, however, no better than that of the PT strain (**Supplementary Figure 6A**). The combination of mutations (i.e., the mutations on *ramA* + *osrR*) would be required for further understanding.

Besides, a mutation in the -109 region of NCgl1159 (F_0F_1-ATP synthase subunit A), which was expected to affect cell growth by altering ATP generation, did not increase the growth rate (**Supplementary Figure 3**). The transcription levels of ATP synthase components in JH41 were only half those in our previous paper (Park et al., 2020), so the half-expressed ATP synthase might have been somehow balanced for the enhanced energy generation under the increased iron and carbon uptake conditions. Another possible mutation to consider is NCgl2331, a penicillin-binding protein involved in cell defense. Substituting A for the 610th G of the NCgl2331 gene in the PT strain resulted in marginal increase (14%) in growth rate (**Supplementary Figure 6B**). Penicillin-binding proteins are membrane-associated macromolecules and are expected to play a key role in cell biosynthesis and cell division (Macheboeuf et al., 2006).

In this respect, our discovery offers essential cues for the construction of an efficient cell factory for the production of recombinant proteins and expands the biological knowledge base. Studies on the reverse engineering of the other mutations including the ITS condensed mutations might lead us to further improvement on *C. glutamicum* host.

DATA AVAILABILITY STATEMENT

The JH41 genome was resequenced and deposited in NCBI accession number: PRJNA554987.

AUTHOR CONTRIBUTIONS

ML, JP, and KP performed the experiments. ML and PK designed the experiments. JK and PK raised grant and supervised. ML and PK wrote the manuscript. All authors contributed to the article and approved the submitted version.

FUNDING

This work was financially supported by the grants from the National Research Foundation of Korea (2016R1E1A1A01943552).

SUPPLEMENTARY MATERIAL

The Supplementary Material for this article can be found online at: https://www.frontiersin.org/articles/10.3389/fbioe.2020.588070/full#supplementary-material

REFERENCES

Auchter, M., Cramer, A., Huser, A., Ruckert, C., Emer, D., Schwarz, P., et al. (2011). RamA and RamB are global transcriptional regulators in *Corynebacterium glutamicum* and control genes for enzymes of the central metabolism. *J. Biotechnol.* 154, 126–139. doi: 10.1016/j.jbiotec.2010.07.001

Bussmann, M., Emer, D., Hasenbein, S., Degraf, S., Eikmanns, B. J., and Bott, M. (2009). Transcriptional control of the succinate dehydrogenase operon sdhCAB of *Corynebacterium glutamicum* by the cAMP-dependent regulator GlxR and the LuxR-type regulator RamA. *J. Biotechnol.* 143, 173–182. doi: 10.1016/j.jbiotec.2009.06.025

Clarke, T. E., Ku, S. Y., Dougan, D. R., Vogel, H. J., and Tari, L. W. (2000). The structure of the ferric siderophore binding protein FhuD complexed with gallichrome. *Nat. Struct. Biol.* 7, 287–291. doi: 10.1038/74048

Darling, A. C., Mau, B., Blattner, F. R., and Perna, N. T. (2004). Mauve: multiple alignment of conserved genomic sequence with rearrangements. *Genome Res.* 14, 1394–1403. doi: 10.1101/gr.2289704

Delcher, A. L., Bratke, K. A., Powers, E. C., and Salzberg, S. L. (2007). Identifying bacterial genes and endosymbiont DNA with Glimmer. *Bioinformatics* 23, 673–679. doi: 10.1093/bioinformatics/btm009

Deshavath, N. N., Mukherjee, G., Goud, V. V., Veeranki, V. D., and Sastri, C. V. (2020). Pitfalls in the 3, 5-dinitrosalicylic acid (DNS) assay for the reducing sugars: interference of furfural and 5-hydroxymethylfurfural. *Int. J. Biol. Macromol.* 156, 180–185. doi: 10.1016/j.ijbiomac.2020.04.045

Disz, T., Akhter, S., Cuevas, D., Olson, R., Overbeek, R., Vonstein, V., et al. (2010). Accessing the SEED genome databases via Web services API: tools for programmers. *BMC Bioinformatics* 11:319. doi: 10.1186/1471-2105-11-319

Fawcett, L., Baxendale, R., Stacey, P., McGrouther, C., Harrow, I., Soderling, S., et al. (2000). Molecular cloning and characterization of a distinct human phosphodiesterase gene family: PDE11A. *Proc. Natl. Acad. Sci. U.S.A.* 97, 3702–3707. doi: 10.1073/pnas.050585197

Feist, A. M., Zielinski, D. C., Orth, J. D., Schellenberger, J., Herrgard, M. J., and Palsson, B. O. (2010). Model-driven evaluation of the production potential for growth-coupled products of *Escherichia coli*. *Metab. Eng.* 12, 173–186. doi: 10.1016/j.ymben.2009.10.003

Graf, M., Haas, T., Müller, F., Buchmann, A., Harm-Bekbenbetova, J., Freund, A., et al. (2019). Continuous adaptive evolution of a fast-growing *Corynebacterium glutamicum* strain independent of protocatechuate. *Front. Microbiol.* 10:1648. doi: 10.3389/fmicb.2019.01648

Hara, K. Y., and Kondo, A. (2015). ATP regulation in bioproduction. *Microb. Cell. Fact.* 14:198. doi: 10.1186/s12934-015-0390-6

Hider, R. C., and Kong, X. (2010). Chemistry and biology of siderophores. *Nat. Prod. Rep.* 27, 637–657. doi: 10.1039/b906679a

Ho, S. N., Hunt, H. D., Horton, R. M., Pullen, J. K., and Pease, L. R. (1989). Site-directed mutagenesis by overlap extension using the polymerase chain reaction. *Gene* 77, 51–59. doi: 10.1016/0378-1119(89)90358-2

Hong, E. J., Kim, P., Kim, E. S., Kim, Y., and Lee, H. S. (2016). Involvement of the osrR gene in the hydrogen peroxide-mediated stress response of *Corynebacterium glutamicum*. *Res. Microbiol.* 167, 20–28. doi: 10.1016/j.resmic.2015.09.005

Kim, H. J., Kwon, Y. D., Lee, S. Y., and Kim, P. (2012). An engineered *Escherichia coli* having a high intracellular level of ATP and enhanced recombinant protein production. *Appl. Microbiol. Biotechnol.* 94, 1079–1086. doi: 10.1007/s00253-011-3779-0

Kim, S. H., Kim, M. S., Lee, B. Y., and Lee, P. C. (2016). Generation of structurally novel short carotenoids and study of their biological activity. *Sci. Rep.* 6:21987. doi: 10.1038/srep21987

Kumar, S., Stecher, G., Li, M., Knyaz, C., and Tamura, K. (2018). MEGA X: molecular evolutionary genetics analysis across computing platforms. *Mol. Biol. Evol.* 35, 1547–1549. doi: 10.1093/molbev/msy096

Kwon, S. K., Kim, S. K., Lee, D. H., and Kim, J. F. (2015). Comparative genomics and experimental evolution of *Escherichia coli* BL21(DE3) strains reveal the landscape of toxicity escape from membrane protein overproduction. *Sci. Rep.* 5:16076. doi: 10.1038/srep16076

Kwon, Y. D., Lee, S. Y., and Kim, P. (2008). A physiology study of *Escherichia coli* overexpressing phosphoenolpyruvate carboxykinase. *Biosci. Biotechnol. Biochem.* 72, 1138–1141. doi: 10.1271/bbb.70831

Lee, M. J., and Kim, P. (2018). Recombinant protein expression system in *Corynebacterium glutamicum* and its application. *Front. Microbiol.* 9:2523. doi: 10.3389/fmicb.2018.02523

Lee, S., and Kim, P. (2020). Current status and applications of adaptive laboratory evolution in industrial microorganisms. *J. Microbiol. Biotechnol.* 30, 793–803. doi: 10.4014/jmb.2003.03072

Macheboeuf, P., Contreras-Martel, C., Job, V., Dideberg, O., and Dessen, A. (2006). Penicillin binding proteins: key players in bacterial cell cycle and drug resistance processes. *FEMS Microbiol. Rev.* 30, 673–691. doi: 10.1111/j.1574-6976.2006.00024.x

Na, Y. A., Lee, J. Y., Bang, W. J., Lee, H. J., Choi, S. I., Kwon, S. K., et al. (2015). Growth retardation of *Escherichia coli* by artificial increase of intracellular ATP. *J. Ind. Microbiol. Biotechnol.* 42, 915–924. doi: 10.1007/s10295-015-1609-6

Nordholt, N., van Heerden, J., Kort, R., and Bruggeman, F. J. (2017). Effects of growth rate and promoter activity on single-cell protein expression. *Sci. Rep.* 7:6299. doi: 10.1038/s41598-017-05871-3

Osorio, C. R., Collins, M. D., Romalde, J. L., and Toranzo, A. E. (2005). Variation in 16S-23S rRNA intergenic spacer regions in Photobacterium damselae: a mosaic-like structure. *Appl. Environ. Microbiol.* 71, 636–645. doi: 10.1128/AEM.71.2.636-645.2005

Osten, C. H. V. D., Gioannetti, C., and Sinskey, A. J. (1989). Design of a defined medium for growth of *Corynebacterium glutamicum* in which citrate facilitates iron uptake. *Biotechnol. Lett.* 11, 11–16. doi: 10.1007/bf01026778

Park, J., Lee, S., Lee, M. J., Park, K., Lee, S., Kim, J. F., et al. (2020). Accelerated growth of *Corynebacterium glutamicum* by up-regulating stress-responsive genes based on transcriptome analysis of a fast-doubling evolved strain. *J. Microbiol. Biotechnol.* 30, 1420–1429. doi: 10.4014/jmb.2006.06035

Park, S. D., Lee, S. N., Park, I. H., Choi, J. S., and Jeong, W. K. (2004). Isolation and characterization of transcriptional elements from *Corynebacterium glutamicum*. *Microbiol. Biotechnol.* 14, 789–795.

Ribeiro, M., and Simões, M. (2019). Advances in the antimicrobial and therapeutic potential of siderophores. *Environ. Chem. Lett.* 17, 1485–1494. doi: 10.1007/s10311-019-00887-889

Rugbjerg, P., Feist, A. M., and Sommer, M. O. A. (2018). Enhanced metabolite productivity of *Escherichia coli* adapted to glucose M9 minimal medium. *Front. Bioeng. Biotechnol.* 6:166. doi: 10.3389/fbioe.2018.00166

Sambrook, J., and Russell, D. W. (2001). *Molecular Cloning : A Laboratory Manual*. Cold Spring Harbor, NY: Cold Spring Harbor Laboratory Press.

Sandberg, T. E., Salazar, M. J., Weng, L. L., Palsson, B. O., and Feist, A. M. (2019). The emergence of adaptive laboratory evolution as an efficient tool for biological discovery and industrial biotechnology. *Metab. Eng.* 56, 1–16. doi: 10.1016/j.ymben.2019.08.004

Schafer, A., Tauch, A., Jager, W., Kalinowski, J., Thierbach, G., and Puhler, A. (1994). Small mobilizable multi-purpose cloning vectors derived from the *Escherichia coli* plasmids pK18 and pK19: selection of defined deletions in the chromosome of *Corynebacterium glutamicum*. *Gene* 145, 69–73. doi: 10.1016/0378-1119(94)90324-7

Schultz, J. E. (2009). Structural and biochemical aspects of tandem GAF domains. *Handb. Exp. Pharmacol.* 191, 93–109. doi: 10.1007/978-3-540-68964-5_6

Serra, P., Moliner-Martínez, Y., Herráez-Hernández, R., Verdú-Andrés, J., and Campíns-Falcó, P. (2015). Simplifying iron determination with o-phenanthroline in food ashes using 2-nitrophenol as an acid-base indicator. *Food Anal. Methods* 9, 1150–1154. doi: 10.1007/s12161-015-0294-4

Stella, R. G., Wiechert, J., Noack, S., and Frunzke, J. (2019). Evolutionary engineering of *Corynebacterium glutamicum*. *Biotechnol. J.* 14:e1800444. doi: 10.1002/biot.201800444

Teramoto, H., Inui, M., and Yukawa, H. (2011). Transcriptional regulators of multiple genes involved in carbon metabolism in *Corynebacterium glutamicum*. *J. Biotechnol.* 154, 114–125. doi: 10.1016/j.jbiotec.2011.01.016

Wang, Z., Liu, J., Chen, L., Zeng, A. P., Solem, C., and Jensen, P. R. (2018). Alterations in the transcription factors GntR1 and RamA enhance the growth and central metabolism of *Corynebacterium glutamicum*. *Metab. Eng.* 48, 1–12. doi: 10.1016/j.ymben.2018.05.004

Wennerhold, J., and Bott, M. (2006). The DtxR regulon of *Corynebacterium glutamicum*. *J. Bacteriol.* 188, 2907–2918. doi: 10.1128/JB.188.8.2907-2918.2006

Wennerhold, J., Krug, A., and Bott, M. (2005). The AraC-type regulator RipA represses aconitase and other iron proteins from *Corynebacterium* under iron limitation and is itself repressed by DtxR. *J. Biol. Chem.* 280, 40500–40508. doi: 10.1074/jbc.M508693200

Yadav, V. G., De Mey, M., Lim, C. G., Ajikumar, P. K., and Stephanopoulos, G. (2012). The future of metabolic engineering and synthetic biology: towards a systematic practice. *Metab. Eng.* 14, 233–241. doi: 10.1016/j.ymben.2012.02.001

Yim, S. S., An, S. J., Kang, M., Lee, J., and Jeong, K. J. (2013). Isolation of fully synthetic promoters for high-level gene expression in *Corynebacterium glutamicum*. *Biotechnol. Bioeng.* 110, 2959–2969. doi: 10.1002/bit.24954

Yim, S. S., Choi, J. W., Lee, R. J., Lee, Y. J., Lee, S. H., Kim, S. Y., et al. (2016). Development of a new platform for secretory production of recombinant proteins in *Corynebacterium glutamicum*. *Biotechnol. Bioeng.* 113, 163–172. doi: 10.1002/bit.25692

Zawadzka, A. M., Abergel, R. J., Nichiporuk, R., Andersen, U. N., and Raymond, K. N. (2009). Siderophore-mediated iron acquisition systems in *Bacillus cereus*: identification of receptors for anthrax virulence-associated petrobactin. *Biochemistry* 48, 3645–3657. doi: 10.1021/bi8018674

Conflict of Interest: The authors declare that the research was conducted in the absence of any commercial or financial relationships that could be construed as a potential conflict of interest.

frontiers in Bioengineering and Biotechnology

ORIGINAL RESEARCH
published: 20 January 2021
doi: 10.3389/fbioe.2020.602936

Comprehensive Analysis of *C. glutamicum* Anaplerotic Deletion Mutants Under Defined D-Glucose Conditions

*Jannick Kappelmann[1], Bianca Klein[1], Mathias Papenfuß[2], Julian Lange[3], Bastian Blombach[4], Ralf Takors[3], Wolfgang Wiechert[1], Tino Polen[1] and Stephan Noack[1]**

[1] Institute of Bio- and Geosciences 1, IBG-1: Biotechnology, Forschungszentrum Jülich GmbH, Jülich, Germany, [2] Institute of Biochemical Engineering, Braunschweig University of Technology, Braunschweig, Germany, [3] Institute of Biochemical Engineering, University of Stuttgart, Stuttgart, Germany, [4] Microbial Biotechnology, Campus Straubing for Biotechnology and Sustainability, Technical University of Munich, Straubing, Germany

OPEN ACCESS

Edited by:
Yu Wang,
Chinese Academy of Sciences, China

Reviewed by:
Guoqiang Xu,
Jiangnan University, China
Chen Yang,
Chinese Academy of Sciences (CAS), China

***Correspondence:**
Stephan Noack
s.noack@fz-juelich.de

Specialty section:
This article was submitted to Synthetic Biology, a section of the journal Frontiers in Bioengineering and Biotechnology

Received: *04 September 2020*
Accepted: *17 December 2020*
Published: *20 January 2021*

Citation:
Kappelmann J, Klein B, Papenfuß M, Lange J, Blombach B, Takors R, Wiechert W, Polen T and Noack S (2021) Comprehensive Analysis of C. glutamicum Anaplerotic Deletion Mutants Under Defined D-Glucose Conditions. Front. Bioeng. Biotechnol. 8:602936. doi: 10.3389/fbioe.2020.602936

Wild-type *C. glutamicum* ATCC 13032 is known to possess two enzymes with anaplerotic (C4-directed) carboxylation activity, namely phosphoenolpyruvate carboxylase (PEPCx) and pyruvate carboxylase (PCx). On the other hand, C3-directed decarboxylation can be catalyzed by the three enzymes phosphoenolpyruvate carboxykinase (PEPCk), oxaloacetate decarboxylase (ODx), and malic enzyme (ME). The resulting high metabolic flexibility at the anaplerotic node compromises the unambigous determination of its carbon and energy flux in *C. glutamicum* wild type. To circumvent this problem we performed a comprehensive analysis of selected single or double deletion mutants in the anaplerosis of wild-type *C. glutamicum* under defined D-glucose conditions. By applying well-controlled lab-scale bioreactor experiments in combination with untargeted proteomics, quantitative metabolomics and whole-genome sequencing hitherto unknown, and sometimes counter-intuitive, genotype-phenotype relationships in these mutants could be unraveled. In comparison to the wild type the four mutants *C. glutamiucm* Δ*pyc*, *C. glutamiucm* Δ*pyc* Δ*odx*, *C. glutamiucm* Δ*ppc* Δ*pyc*, and *C. glutamiucm* Δ*pck* showed lowered specific growth rates and D-glucose uptake rates, underlining the importance of PCx and PEPCk activity for a balanced carbon and energy flux at the anaplerotic node. Most interestingly, the strain *C. glutamiucm* Δ*ppc* Δ*pyc* could be evolved to grow on D-glucose as the only source of carbon and energy, whereas this combination was previously considered lethal. The prevented anaplerotic carboxylation activity of PEPCx and PCx was found in the evolved strain to be compensated by an up-regulation of the glyoxylate shunt, potentially in combination with the 2-methylcitrate cycle.

Keywords: *Corynebacterium glutamicum*, anaplerosis, phosphoenolpyruvate carboxylase, pyruvate carboxylase, phosphoenolpyruvate carboxykinase, oxaloacetate decarboxylase, malic enzyme, methylcitrate cycle

INTRODUCTION

C. glutamicum is one of the most important organisms for industrial biotechnology and the current product spectrum that is accessible with this host comprises proteinogenic as well as non-proteinogenic amino acids, organic acids, diamines, vitamins, aromates, and alcohols (Becker et al., 2018; Kogure and Inui, 2018). Most production strains have been generated by classical mutagenesis and selection, as well as by targeted and evolutionary metabolic engineering approaches (Lee and Wendisch, 2017; Stella et al., 2019). With the aim to enhance predictability of cellular functions and to reduce interference with heterologous pathways new chassis strains were introduced (Baumgart et al., 2013, 2018; Unthan et al., 2015). Several targeted and untargeted proteomics methods were developed, enabling relative, and absolute quantification of cytosolic as well as membrane-bound proteins (Fränzel et al., 2009; Voges and Noack, 2012; Trötschel et al., 2013; Küberl et al., 2014; Voges et al., 2015; Noack et al., 2017).

At the phosphoenolpyruvate-pyruvate-oxaloacetate node *C. glutamicum* ATCC 13032 (wild type) is known to possess two enzymes with anaplerotic (C4-directed) carboxylation activity, namely phosphoenolpyruvate carboxylase (PEPCx) and pyruvate carboxylase (PCx). On the other hand, C3-directed decarboxylation can be catalyzed by the three enzymes phosphoenolpyruvate carboxykinase (PEPCk), oxaloacetate decarboxylase (ODx), and malic enzyme (ME). While all enzymes show *in vitro* activity in cells grown in defined D-glucose media (Cocaign-Bousquet et al., 1996; Uy et al., 1999; Klaffl and Eikmanns, 2010; Blombach et al., 2013), only PEPCx and PCx are currently considered as dependent essential anaplerotic enzymes under these conditions (**Figure 1**).

Recently, the anaplerotic node of *C. glutamicum*, which represents a very flexible knot for diverting the carbon and energy flux introduced by different potential substrates, has again attracted our attention. Following detailed mathematical modeling and computational analyses, we could prove that only certain anaplerotic deletion mutants allow to uniquely determine the anaplerotic fluxes (Kappelmann et al., 2016).

Following shake flask experiments, it was shown that a single inactivation of either PEPCx, PCx, ODx or ME in wild-type *C. glutamicum* has no effect on biomass growth (Peters-Wendisch et al., 1993, 1998; Gourdon et al., 2000; Klaffl and Eikmanns, 2010). The only exception was found for PEPCk, whose inactivation resulted in a lower growth rate (Riedel et al., 2001). In contrast, the combined removal of PEPCx and PCx is thought to be lethal for *C. glutamicum* when grown under glycolytic conditions as no other carboxylation reaction enables replenishment of tricarboxylic acid intermediates (Peters-Wendisch et al., 1998). Recently, Schwentner et al. were able to evolve *C. glutamicum* Δ*ppc* Δ*pyc* to grow on CGXII medium with 20 g L^{-1} D-glucose and 1 g L^{-1} yeast extract (or alternatively 1 mM L-glutamate) (Schwentner et al., 2018). Comparative whole-genome sequencing revealed isocitrate dehydrogenase (ICD) as consistent target and the identified mutations could be linked to diminished ICD activities as well as increased activities of the glyoxylate shunt enzymes isocitrate lyase (ICL) and malate synthase (MS). Operation of the glyoxylate shunt can substitute for the missing carboxylation reactions to replenish oxaloacetate required for growth. Interestingly, on pure D-glucose media this evolution failed in the study reported (Schwentner et al., 2018).

In our study, we performed a comprehensive analysis of selected single or double deletion mutants in the anaplerosis of wild-type *C. glutamicum* under defined D-glucose conditions without other carbon supplements. By applying well-controlled lab-scale bioreactor experiments in combination with untargeted proteomics, quantitative metabolomics and whole-genome sequencing hitherto unknown genotype-phenotype relationships in these mutants could be unraveled and these are discussed in detail with regard to published data.

MATERIALS AND METHODS

Bacterial Strains

All strains, plasmids and oligonucleotids used in this study are listed in **Table 1**. The *C. glutamicum* WT as well as the single deletion mutants Δ*pyc*, Δ*malE*, Δ*pck* are from Blombach et al. (2013). The double deletion mutant Δ*ppc* Δ*pyc* is described in Schwentner et al. (2018). The three remaining double deletion mutants Δ*pyc* Δ*odx*, Δ*ppc* Δ*malE* and Δ*pck* Δ*malE* were constructed by chromosomal inactivation of the ODx gene *odx* in *C. glutamicum* Δ*pyc*, as well as the ME gene *malE* in *C. glutamicum* Δ*pck* and *C. glutamicum* Δ*ppc* using the plasmids pK19mobsacB-Δ*odx* and pK19mobsacB-Δ*malE*. Isolation of plasmids from *Escherichia coli* was performed as described elsewhere (Eikmanns et al., 1994). Plasmid DNA transfer into *C. glutamicum* was carried out by electroporation and recombinant strains were selected on Luria–Bertani Brain Heart Infusion agar plates containing appropriate concentrations of kanamycin (50 μg mL^{-1}) (Van Der Rest et al., 1999). The replacement at the chromosomal locus was verified by colony-PCR using primers odxfow/odxrev and Co-malE1/Co-malE1, respectively (Klaffl and Eikmanns, 2010; Blombach et al., 2011). Subsequently, shaking flasks with CGXII preculture medium containing 1% D-glucose (w v^{-1}) were inoculated with the corresponding strains (Unthan et al., 2014). Each culture was harvested during the late exponential phase following centrifugation at 4,500 rpm for 10 min, resuspension in sterile saline and finally in 20% (v v^{-1}) glycerol solution in sterile 0.9% (w v^{-1}) NaCl in distilled water. From this solution cryo stocks were prepared and immediately stored at −80°C. The Δ*ppc* Δ*pyc* mutant was able to grow on acetate, from which a corresponding cryo-culture was produced.

Evolution and Whole-Genome Sequencing of *C. glutamicum* Δ*ppc* Δ*pyc*

C. glutamicum Δ*ppc* Δ*pyc* was grown in microtiter plates in a BioLector parallel cultivation system (m2p-labs). Flowerplates with optodes for optical pH and dissolved oxygen (DO) measurements were employed. A cryo-culture for inoculation was washed once with sterile saline and resuspended in D-glucose-free CGXII medium. From this inoculum 50 μL were transferred into each well containing 950 μL 1% D-glucose

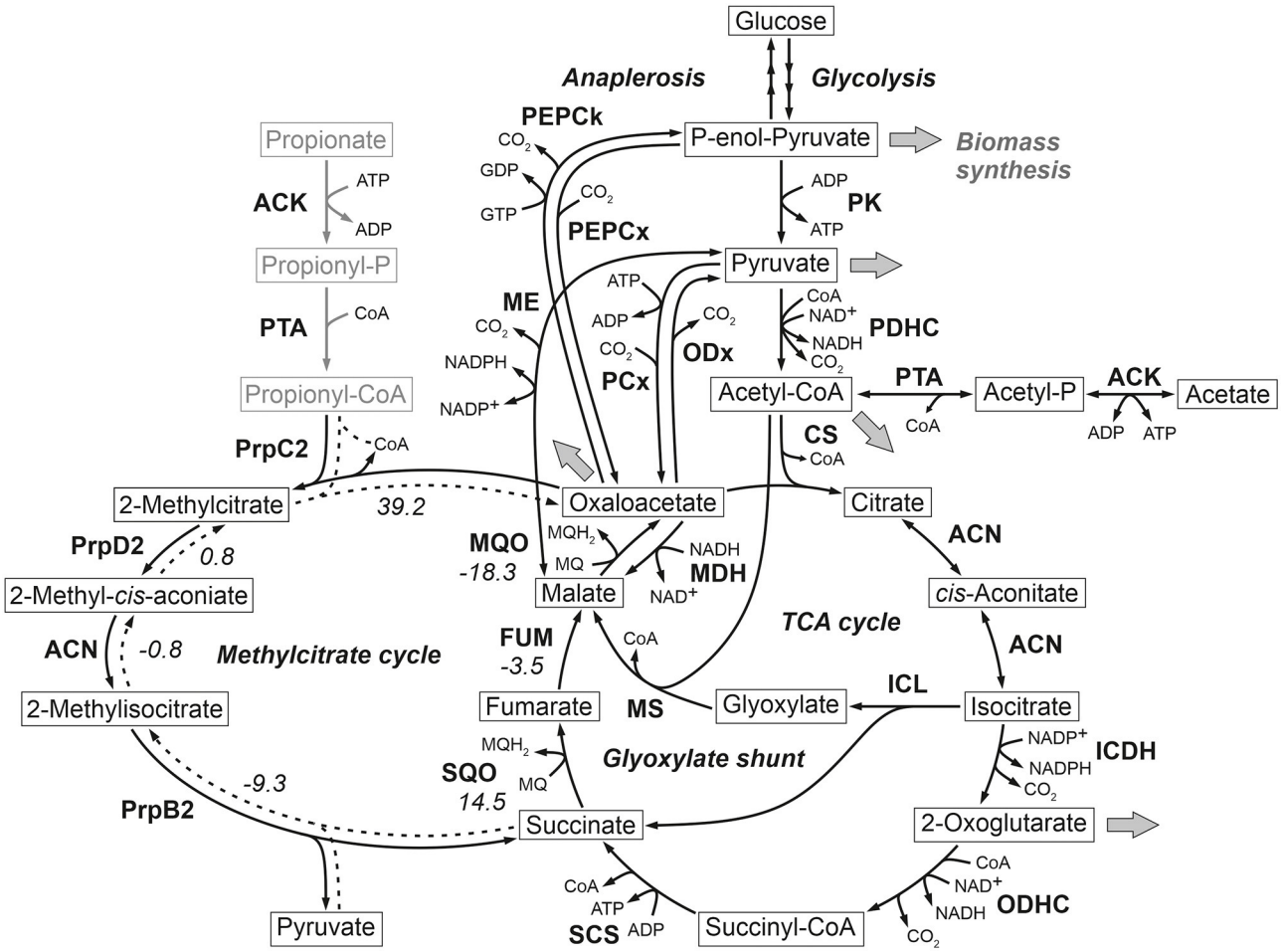

FIGURE 1 | Reactions comprising the anaplerotic node, TCA cycle, glyoxylate shunt and methylcitrate cycle in *C. glutamicum* ATCC 13032. Precursor effluxes into biomass are depicted by gray arrows. For some reactions the standard Gibbs energy of reaction in kJ/mol are shown, which were estimated using the eQuilibrator tool (Flamholz et al., 2012). The values for the methylcitrate cycle refer to the assumed reverse reaction direction represented by broken lines. ACN, aconitase; ACK, acetate kinase; CS, citrate synthase; FUM, fumarase; ICDH, isocitrate dehydrogenase; ICL, isocitrate lyase; MDH, malate dehydrogenase; ME, malic enzyme; MQO, malate: quinone oxidoreductase; MS, malate synthase; ODHC, 2-oxoglutarate dehydrogenase complex; ODx, oxaloacetate decarboxylase; PCx, pyruvate carboxylase; PDHC, pyruvate dehydrogenase complex; PEPCk, phosphoenolpyruvate carboxykinase; PEPCx, phosphoenolpyruvate carboxylase; PPS, phosphoenolpyruvate synthetase; PK, pyruvate kinase; PQO, pyruvate: quinone oxidoreductase; PrpB2, 2-methylcitrate lyase; PrpC2, 2-methylcitrate synthase; PrpD2, 2-methylcitrate dehydratase; PTA, phosphotransacetylase; SCS, succinyl-CoA-synthetase; SQO, succinate: quinone oxidoreductase.

medium. The plates were sterilely sealed and incubated at 30°C at 1,300 rpm.

For whole-genome sequencing, 200 µL of a well-inoculated at $OD_{init} = 1$ (see **Supplementary Figure 1**) and after growth has ceased was used to inoculate a subsequent shaking flask culture, from which a cryo-culture was produced. From this cryo-culture a sample was generated for whole-genome sequencing using the Illumina platform followed by sequence analysis as described elsewhere (Kranz et al., 2017).

Bioreactor Cultivations

C. glutamicum deletion strains were cultivated in a DASGIP parallel fermentation system (Eppendorf). Bioreactor cultivations of *C. glutamicum* strains were carried out with defined CGXII medium containing 1% D-glucose and 0.1% undiluted Antifoam 204 but no 3-(N-Morpholino)propanesulfonic acid (MOPS) buffer (Unthan et al., 2014). Bioreactors were inoculated from a preculture in CGXII medium buffered with 42 g L^{-1} MOPS at pH 7 which was inoculated directly from a cryo-culture of each strain in 80% 0.9% NaCl/20% glycerol (v v^{-1}) stored at −80°C. During bioreactor cultivations DO levels were maintained above 30% by adjusting stirrer speed and oxygen content of the inlet air. The gassing rate was set to 1 vvm and the pH was maintained at pH 7 by feeding either 4 M NaOH or 4 M HCl. The cultivation temperature was 30°C.

For quantitative metabolomics, samples from bioreactor cultivations were drawn into a syringe in technical duplicate at two time points yielding a total of four technical replicates per strain. These time points correspond to target BV

TABLE 1 | Strains, plasmids, and oligonucleotides used in this study.

Strains	Relevant characteristic(s) or sequence	Source/reference or purpose
C. glutamicum WT	wild type (WT) strain ATCC 13032, biotin-auxotrophic	American Type Culture Collection
C. glutamicum Δ*pyc*	*C. glutamicum* WT with deletion of the *pyc* gene encoding pyruvate carboxylase	Blombach et al., 2013
C. glutamicum Δ*malE*	*C. glutamicum* WT with deletion of the *malE* gene encoding malic enzyme	Blombach et al., 2013
C. glutamicum Δ*pck*	*C. glutamicum* WT with deletion of the *pck* gene encoding phosphoenolpyruvate carboxykinase	Blombach et al., 2013
C. glutamicum Δ*ppc* Δ*pyc*	*C. glutamicum* WT with deletion of the *ppc* and *pyc* gene encoding phosphoenolpyruvate carboxylase and pyruvate carboxylase, respectively	Schwentner et al., 2018
C. glutamicum Δ*pck* Δ*malE*	*C. glutamicum* WT with deletion of the *pck* and *malE* gene encoding phosphoenolpyruvate carboxykinase and malic enzyme, respectively	This work
C. glutamicum Δ*pyc* Δ*odx*	*C. glutamicum* WT with deletion of the *pyc* and *odx* gene encoding pyruvate carboxylase and oxaloacetate decarboxylase, respectively	This work
C. glutamicum Δ*ppc* Δ*malE*	*C. glutamicum* WT with deletion of the *ppc* and *malE* gene encoding phosphoenolpyruvate carboxylase and malic enzyme, respectively	This work
Plasmids		
pK19*mobsacB*-Δ*malE*	pK19*mobsacB* carrying a truncated *malE* gene	Blombach et al., 2011
pK19*mobsacB*-Δ*odx*	pK19*mobsacB* carrying the *odx* gene with internal 679-bp deletion	Klaffl and Eikmanns, 2010
Oligonucleotides		
odxfow	5′-ACCGGCATCAAATTGTGTC-3′	Primer to verify deletion of *odx*
odxrev	5′-TTGCCTTGAGCACAATGTC-3′	Primer to verify deletion of *odx*
Co-malE1	5′- CTTCCAGACACGGAATCAGAG-3′	Primer to verify deletion of *malE* (Blombach et al., 2011)
Co-malE2	5′- GTGATCCTTCCGAGCGTTCC-3′	Primer to verify deletion of *malE* (Blombach et al., 2011)

concentrations of 5 μL mL^{-1} (OD_{600} = 6.3) and 10 μL mL^{-1} (OD_{600} = 12.5), covering the mid-exponential phase (cmp. **Supplementary Figure 2**). The actual BV concentration in each sample was measured after sampling and used to calculate the extraction volume.

For untargeted proteomics, sampling was performed directly after all quenching samples for the metabolome analysis had been taken. From each reactor samples were drawn in technical quintuplicate by centrifuging 10 mL of culture broth for each replicate (10 min, 4500 rpm, GS-15R Centrifuge, Beckman Coulter). After the supernatant was decanted, the biomass pellets were immediately placed in aluminum racks at −20°C.

For biovolume (BV) measurements, cultivation samples were diluted 1:200 or 1:2,000 depending on the biomass concentration in 10 mL CASYton buffer (OMNI Life Science GmbH). The size distribution of the sample was determined by the MultiSizer3 Coulter Counter (Beckman Coulter) and the biovolume was computed by calculating the first moment of the distribution, assuming a spherical shape of the measured cells. Cell dry weight (CDW) was determined by centrifuging 2 mL of a bioreactor sample in a pre-dried and pre-weighted Eppendorf tube at 13,000 rpm for 7 min. The cells were washed in 1 mL 0.9% (w v^{-1}) NaCl by resuspension and renewed centrifugation. After decanting the supernatant, the pellets were dried for at least 2 days at 80°C.

A correlation between BV in μL mL^{-1} and CDW in g L^{-1} was derived for the Δ*pyc* Δ*odx*, Δ*ppc* Δ*malE* and WT strain (see **Supplementary Figure 3**) and then applied to calculate the CDW for all cultivations assuming a standard deviation of 5%.

Estimation of Extracellular Rates

Specific rates for biomass growth (μ) and D-glucose uptake (π_{GLC}) were estimated using a model-based approach and process data from the exponential phases of corresponding batch cultivations. In short, the remaining D-glucose concentration $c_{GLC}(t)$ at any given time point t is the integral over the volumetric uptake rate $\pi_{GLC,vol}(t)$ given in mmol L^{-1} h^{-1}:

$$c_{GLC}(t) = c_{GLC,0} - \int_{t_0}^{t} \pi_{GLC,vol}(t)dt \quad (1)$$

Assuming a constant D-glucose uptake from exponentially growing cells, it holds:

$$\pi_{GLC,vol}(t) = \pi_{GLC} \cdot X(t) \tag{2}$$

where $X(t) = X_0 \cdot e^{\mu \cdot t}$ denotes the biomass concentration in µL mL^{-1} or g L^{-1}, depending on whether the biomass signal is BV or CDW. Inserting Equations (2) into (1) and carrying out the integration yields:

$$c_{GLC}(t) = C - \frac{\pi_{GLC}}{\mu} \cdot X_0 \cdot e^{\mu \cdot t} \tag{3}$$

with model parameters X_0, μ, π_{GLC}, and C, where the latter absorbs the integration constant and the initial substrate concentration. Equations (2) and (3) were jointly fitted to the experimentally observed time courses of biomass and substrate concentration, respectively. The end of the exponential phase was judged by the peak in CO_2 volume fraction in the exhaust gas stream (see **Supplementary Figure 2**).

The fitting procedure was carried out using a sequential quadratic programming optimization routine from MATLAB (Mathworks Inc., R2019b). The estimation of confidence intervals was based on a parametric Monte Carlo bootstrapping approach from literature (Dalman et al., 2013). In short, every available measurement was perturbed independently within the normal distribution described by the measurement value and its standard deviation of the respective measurement. The perturbation operation consisted in sampling from the normal distribution of each measurement point and inserting the sample as measurements. The above-described variance-weighted least-square fit was then re-performed. The sample was generated as a Latin-Hypercube sample using the lhs-function of MATLAB and comprised 1,000 samples if not otherwise stated. The upper and lower confidence bounds were then derived as the α-th and (1-α)-th percentile of the parameter sample obtained from 1000 least-squared fits. If not otherwise stated α is set to 0.25, the confidence interval being the Interquartile Range (IQR).

The total CO_2 formation rate $\pi_{CO2,tot}(t)$ given in mol h^{-1} was calculated from balancing the gas phase of the bioreactor as:

$$\pi_{CO_2,tot}(t) = \frac{F \cdot p}{R \cdot T}\left[\frac{100 - \Phi^{\alpha}_{O_2} - \Phi^{\alpha}_{CO_2}}{100 - \Phi^{\omega}_{O_2}(t) - \Phi^{\omega}_{CO_2}(t)} \cdot \frac{\Phi^{\omega}_{CO_2}(t)}{100} - \frac{\Phi^{\alpha}_{CO_2}}{100}\right] \tag{4}$$

where Φ denotes the volume fraction of the gas species in question in vol% and the superscripts α and ω denote the inlet and outlet concentrations, respectively. F denotes the inlet air flow in m^3 h^{-1}. The biomass-specific carbon dioxide formation rate $\pi_{CO_2}(t)$ given in mmol g^{-1}_{CDW} h^{-1} or mmol mL^{-1}_{BV} h^{-1}, respectively, was obtained by dividing $\pi_{CO_2,tot}(t)$ by $X(t)$ at time point t.

The complete set of extracellular rate estimates for all independent bioreactor cultivation experiments can be found in **Supplementary Table 1**.

Quantitative Metabolomics

The metabolome samples of all strains were spiked with identical internal standard and were measured in one acquisition batch on the LC-ESI-QqQ MS system. Organic acids and unstable sugar phosphates were measured within 24 h from the extraction of samples. Quenching, cell separation, cell extraction, isotope dilution mass spectrometry and metabolite leakage correction were performed according to previous protocols (Paczia et al., 2012; Tillack et al., 2012).

For quantification of organic acids, samples were separated using a synergy hydro C18 reversed phase column (Phenomenex) on an Agilent 1200 chromatography system (Agilent Technologies). The HPLC column outlet was coupled to a QqQ MS device (API 4000, AB Sciex) equipped with a TurboSpray ion source in negative ionization mode. The elution was isocratic at 84% buffer A and 16% buffer B at a flowrate of 0.45 mL min^{-1} at 20°C. The eluents were as follows: Buffer A: 10 mM tributylamine, 15 mM acetic acid, pH 4.95; Buffer B: methanol. MS parameters were as follows: CAD (collision gas pressure): 5, CUR (curtain gas flow): 30, GS1 (nebulizer gas flow): 70, GS2 (turbo heater gas flow): 70, IS (electrospray voltage): −4,500 V, TEM (heater gas temperature): 650°C, entrance potential: −10 eV. Injection volume was 10 µL.

For quantification of amino acids, samples were separated using Luna SCX cation exchange column at 60°C on a JASCO HPLC system. The following buffers were employed: Buffer A: 5% acetic acid, B: 15 mM ammonium acetate. The applied elution gradient can be found in **Supplementary Table 2**. Injection volume was 10 µL.

For quantification of sugar and nucleoside phosphates, samples were separated on a synergy hydro C18 reversed phase column at 40°C. Eluent were Buffer A: 10 mM tributylamine, 15 mM acetic acid, pH 4.95 and Buffer B: methanol. The HPLC system, the QqQ MS device and its MS parameter settings were the same as for the LC-MS/MS method for organic acids. For quantification the gradient of **Supplementary Table 3** was applied. Injection volume was 10 µL.

Generation of Ion Libraries for Proteomics

To populate our *C. glutamicum* ion library, separate IDA acquisitions of samples of *C. glutamicum* WT cultivated as described above but with different carbon sources were performed. In each cultivation the carbon source was either 55 mM D-glucose, 111 mM sodium pyruvate, 83 mM disodium-L-malate, 55 mM sodium citrate or 48 mM sodium benzoate. Each sample was lysed and 100 µg protein thereof digested and processed as described elsewhere (Voges and Noack, 2012).

These samples were separated on a Agilent 1260 Infinity HPLC system (Agilent Technologies) equipped with a 150 * 2.1 mm Ascentis Express Peptide ES-C18 column with 2.7 µm particle size and an appropriate 5 * 0.3 mm Acclaim PepMap Trap Cartridge (Thermo Scientific) which were both maintained at 25°C and a flow rate of 200 µL min^{-1}. For LC separation 0.1% formic acid in LC-MS grade water (v v^{-1}) was used as buffer A, whereas buffer B was 0.1% formic acid in LC-MS grade acetonitrile (v v^{-1}). Before each injection, the column was equilibrated for 12 min at 97% A. After 20 µL were injected, the

gradient of **Supplementary Table 4** was applied. The LC-eluent was coupled to an ESI-QqTOF MS (TripleTOF 6600, AB Sciex) equipped with an DuoSpray ion source. The data acquisition was performed using Analyst TF 1.8 (AB Sciex). An information-dependent acquisition was performed on each injection during which all ions with $m/z > 300$, charge state 2–4 and above intensity of 150 were selected for fragmentation.

The acquired MS2 spectra of the *C. glutamicum* digests were searched against a FASTA database of *C. glutamicum* ATCC 13032 (GenBank assembly accession: GCA_000196335.1) using ProteinPilot software 5.0 (AB Sciex) employing default probabilities for biological modifications. The confidently identified peptides of each injection were assembled into a library covering 1727 ORFs. This library incorporates the peptide confidence after identification, peptide (precursor) intensity in the MS1 scan from the IDA acquisition, fragment ion intensities and the observed peptide retention time.

SWATH Acquisition

Starting from an IDA acquisition of each organism variable SWATH windows were calculated using the SWATH Variable Window Calculator 1.0 (AB Sciex). Using these windows, a SWATH acquisition method was set up, which employed the same chromatographic gradient and ion source setting as the IDA acquisition. The window width and CE ramp parameters can be found in **Supplementary Table 5**. For SWATH acquisition a digest of each sample was prepared according to the protocol of Voges and Noack, which involves mixing 50 µg unlabeled sample protein and 50 µg internal standard from a separate cultivation of *C. glutamicum* with $(^{15}NH_4)_2SO_4$ (Voges and Noack, 2012). Ten microliter of each sample was injected.

SWATH MS Data Processing

SWATH data processing was performed using the MS/MS^{all} SWATH Acquisition MicroApp in PeakView 2.2 (AB Sciex). The ion library from above was imported from ProteinPilot into this app by excluding shared peptides but not modified ones. From the imported ion library the ten most intense peptides were selected for quantification provided they had a peptide confidence of >96%. The intensity selection is based on the MS1 survey scan intensity of each peptide in the IDA runs used to build the ion library. If <10 peptides fulfilled the above criterion for a protein, only the available peptides were quantified.

For each peptide group the 12 most intense fragment ion traces were chosen by the SWATH processing algorithm. This algorithm favors the most intense fragment ion traces from the library spectrum whose m/z value lies above the Q1 window of their precursor ion. For each fragment ion, within 5 min around the expected retention time, an unlabeled mass trace was extracted from the SWATH spectra within ±15 ppm of its monoisotopic mass, whereas the labeled mass trace was extracted within ±15 ppm of its fully ^{15}N-labeled isotopologue. All transitions of one peptide were assembled into a so called peak group which was scored for congruency with the ion library. The false discovery rate was set to 0.1%. The finished processing session was saved as MarkerView file (.mrkvw extension), which was opened in MarkerView 1.3.1 (AB Sciex) for estimation of fold-changes (ratio of means) of protein levels between mutant and control.

Elemental Analysis of Biomass

The concentration of carbon, nitrogen and sulfur in biomass were determined at the central Analytical core facility of Forschungszentrum Jülich (ZEA-3). Biomass samples from the early stationary phase were processed following the same procedure as for CDW content determination. The dried biomass pellet was ground to a fine powder in a pre-dried mortar using a pre-dried pestle and sent in a sealed container to ZEA-3.

RESULTS AND DISCUSSION

Growth Phenotyping of Anaplerotic Deletions Mutants Under Defined D-Glucose Conditions

In our previous flux identifiability analysis focusing on the anaplerotic node in *C. glutamicum* those metabolic network structures were identified that are structurally identifiable under defined D-glucose conditions (Kappelmann et al., 2016). These structures are based on deletions of specific genes encoding for anaplerotic reactions. In this study, we comprehensively analyzed a set of mutant strains for which a unique solution using ^{13}C-MFA theoretically exists as well as mutants that are non-flux-identifiable strains.

All selected deletion mutants were able to grow on defined CGXII medium with D-glucose as sole carbon and energy source, except for strain *C. glutamicum* Δ*ppc* Δ*pyc* that is deficient in PEPCx and PCx activity (**Table 1**). While this mutant was able to grow on acetate without lag-phase no biomass formation could be monitored within 48 h cultivation on D-glucose and this observation is concordant with Peters-Wendisch et al. (1998). However, prolonged incubation of *C. glutamicum* Δ*ppc* Δ*pyc* under defined D-glucose conditions in a microbioreactor setup and at different inoculum sizes always resulted in the onset of growth after 75 h or later, mainly after 100 h (**Supplementary Figure 1**).

The whole mutant library was then cultivated under controlled bioreactor conditions on defined CGXII medium with 1% D-glucose. Specific growth and substrate uptake rates were estimated using a model-based approach (see Materials and Methods section). The D-glucose uptake rate of 4.82 mmol $g_{CDW}^{-1}h^{-1}$ and the specific growth rate of 0.45 h^{-1} for *C. glutamicum* WT agree well with literature (Buchholz et al., 2014). Based on the determined confidence intervals discernible growth phenotypes can be identified among the set of deletion mutants (**Figure 2A** and **Table 2**).

First, the *C. glutamicum* Δ*pck* mutant showed a lower growth rate although PEPCk catalyzes a gluconeogenetic reaction, not needed under glycolytic conditions to supply biomass precursors. However, the observed growth defect clearly indicates its activity under glycolytic conditions. This result was also obtained in the study of Riedel et al. with the comparable genotype (**Table 2**) and in the study of Petersen et al. (2001), who inferred PEPCk activity in a *C. glutamicum* L-lysine producer from ^{13}C-labeling data.

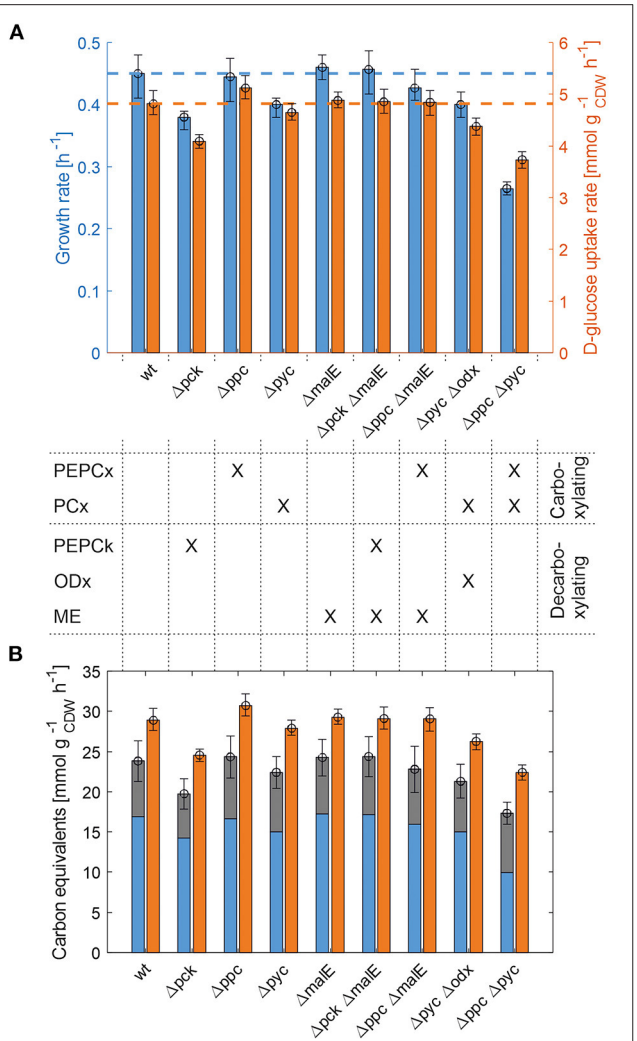

FIGURE 2 | Growth phenotyping of anaplerotic deletions mutants under defined D-glucose conditions. **(A)** Estimated specific growth and D-glucose uptake rates. Mean values of rate estimates are from biological duplicate or triplicate cultivations. Error estimates are given as the minimum of the lower bound and the maximum of the upper bound of each parameter over all replicate cultivations of the mutant in question (see **Supplementary Table 1**). **(B)** Carbon equivalents of the specific growth rate (blue), CO_2-formation rate (gray) and the substrate uptake rate (orange). The error bar on the stacked bars is the error on the sum of both rates, which was estimated according to Gaussian error propagation.

Since the carbon flow catalyzed by PEPCk is of opposite direction compared to the overall carbon flow under glycolytic conditions, its catalytic effect must be of indirect nature. Strangely, the double deletion mutant *C. glutamicum* Δ*pck* Δ*malE* showed a restored growth phenotype, with a growth rate equivalent to the WT.

Deletion mutants comprising a deletion in PEPCx do not show a significantly altered growth phenotype as long as PCx is still active (**Figure 2A** and **Table 2**). The stoichiometry of the reaction catalyzed by PEPCx is identical to the reaction sequence of pyruvate kinase (PK) and PCx, which apparently fully compensates for the missing carboxylation activity of PEPCx. On the other hand, mutant strains *C. glutamicum* Δ*pyc* and *C. glutamicum* Δ*pyc* Δ*odx* do exhibit a growth phenotype. This finding underscores the role of PCx as most important anaplerotic reaction under aerobic conditions and suggests that its catalyzed flux is most likely greater than that of PEPCx in the WT under standard D-glucose conditions. Noteworthy, a *C. glutamicum* mutant with single deletion of the *odx* gene was shown to grow equally well as the wild type (Klaffl and Eikmanns, 2010).

The evolved *C. glutamicum* Δ*ppc* Δ*pyc* strain, missing both carboxylation activities shows a greatly reduced growth rate of 0.27 h^{-1} (**Figure 2A** and **Table 2**). In the absence of both PEPCx and PCx, three other and different anaplerotic activities can possibly substitute the anaplerotic activity of PEPCx and PCx: First, ME may catalyze the carboxylation of pyruvate to malate in an NADPH-dependent manner. This appears plausible since ME was found to catalyze this reaction sequence in *in vitro* assays (Cocaign-Bousquet et al., 1996; Gourdon et al., 2000). Moreover, it could be experimentally shown that a NADPH-dependent ME from *E. coli* can act as sole anaplerotic enzyme in *Saccharomyces cerevisiae* sustaining a growth rate of 0.06 h^{-1} (Zelle et al., 2011). Second, PEPCk may act in reverse direction from phosphoenolpyruvate to oxaloacetate. This hypothesis is rather unlikely as this reaction directionality would couple anaplerotic carboxylation to the substrate level phosphorylation, generating one GTP molecule. Since the reaction from oxaloacetate to phosphoenolpyruvate is coupled to the hydrolysis of one GTP molecule, it can be expected to be favored. A third alternative represents the glyoxylate shunt, which exclusively fulfills the anaplerotic function in *C. glutamicum* under growth on acetate (Wendisch et al., 1997).

A Closer Look Into Carbon Balancing

Interestingly, the *C. glutamicum* Δ*ppc* Δ*pyc* mutant also showed an altered ratio of specific glucose uptake and growth rate in comparison to other mutants and the WT (**Figure 2A**). The observation that less biomass was formed per unit uptake rate raised the question as to where the excess carbon atoms end up. To answer this question, a carbon balance was performed. Contrary to the conventional carbon balancing approach, consisting in the quantification of the total carbon recovery in biomass and exhaust gas by the time all substrate has been consumed (Buchholz et al., 2014), we calculated the instantaneous carbon balance Θ as:

$$\Theta = \frac{\frac{\mu \cdot \omega_C}{M_C} + \pi_{CO_2}}{\pi_{GLC} \cdot 6} \tag{5}$$

where μ denotes the specific growth rate given in h^{-1} (here assumed to be constant for the considered exponentially growing cells), ω_C denotes the mass fraction of carbon in the biomass in $g_C\ g_{CDW}^{-1}$, M_C denotes the molecular weight of carbon in g $mmol^{-1}$, and π_{GLC} as well as π_{CO_2} denote the specific D-glucose uptake and carbon dioxide formation rates as derived from Equations (2) to (4).

Equation (5) balances the specific rates of carbon uptake and carbon flow into sinks at any given time. Here biomass and

TABLE 2 | Estimated specific growth rates (μ), D-glucose consumption rates (π_{GLC}), CO_2 formation rates (π_{CO2}), and instantaneous carbon balance (θ) for anaplerotic deletion mutants during exponential growth.

Strain	μ [h^{-1}]	π_{GLC} [mmol g_{CDW}^{-1} h^{-1}]	π_{CO2} [mmol g_{CDW}^{-1} h^{-1}]	θ [–]	Conditions	References
C. glutamicum ATCC 13032	0.44	–	–	–	Shake flask	Riedel et al., 2001
	0.40[a]	–	–	–	Bioreactor	Blombach et al., 2013
	0.45 ± 0.04	4.82 ± 0.25	6.94 ± 0.71	0.82 ± 0.089	Bioreactor	This work
C. glutamicum Δ*pck*	0.40	–	–	–	Shake flask	Riedel et al., 2001
	0.30[a]	–	–	–	Bioreactor	Blombach et al., 2013
	0.38 ± 0.02	4.10 ± 0.14	5.51 ± 0.53	0.81 ± 0.077	Bioreactor	This work
C. glutamicum Δ*ppc*	Equal to WT	–	–	–	Shake flask	Peters-Wendisch et al., 1993, 1996
	0.34[a]	–	–	–	Bioreactor	Blombach et al., 2013
	0.45 ± 0.04	5.12 ± 0.24	7.64 ± 1.09	0.79 ± 0.083	Bioreactor	This work
C. glutamicum Δ*pyc*	Nearly WT	–	–	–	Shake flask	Peters-Wendisch et al., 1998
	0.30[a]	–	–	–	Bioreactor	Blombach et al., 2013
	0.40 ± 0.02	4.65 ± 0.17	7.43 ± 0.76	0.80 ± 0.072	Bioreactor	This work
C. glutamicum Δ*malE*	Equal to WT	–	–	–	Shake flask	Gourdon et al., 2000
	0.34[a]	–	–	–	Bioreactor	Blombach et al., 2013
	0.46 ± 0.02	4.88 ± 0.17	7.00 ± 1.00	0.84 ± 0.080	Bioreactor	This work
C. glutamicum Δ*pck* Δ*malE*	0.46 ± 0.04	4.85 ± 0.24	7.27 ± 0.83	0.83 ± 0.087	Bioreactor	This work
C. glutamicum Δ*ppc* Δ*malE*	0.43 ± 0.03	4.84 ± 0.25	6.79 ± 1.92	0.79 ± 0.088	Bioreactor	This work
C. glutamicum Δ*pyc* Δ*odx*	0.40 ± 0.02	4.38 ± 0.17	6.31 ± 0.99	0.81 ± 0.078	Bioreactor	This work
C. glutamicum Δ*ppc* Δ*pyc*[b]	No growth	–	–	–	Shake flask	Peters-Wendisch et al., 1998
	0.27 ± 0.01	3.74 ± 0.16	7.40 ± 0.68	0.78 ± 0.070	Bioreactor	This work

Comparison of own data with available literature data for cultivation experiments with the specified strains on defined CGXII media and D-glucose as sole carbon and energy source. Data from C. glutamicum ATCC 13032 (WT) was only included from studies with corresponding deletion mutants. In case no quantitative data was available a qualitative comparison was made.

[a] *Aeration was limited to 0.1 vvm and the media contained no initial protocatechuic acid.*

[b] *Evolved strain after prolonged cultivation in CGXII media with D-glucose as sole carbon and energy source.*

CO_2 formation are the only considered carbon sinks (any other by-product formation could be excluded for all strains under investigation). The quantity ω_C has been reported several times in the literature: Marx et al. (1996) reported 0.408 g_C g_{CDW}^{-1} for *C. glutamicum* MH20-22B, a L-lysine producer strain, determined in freeze-dried biomass with a CHNS elemental analyzer. More recently, Buchholz et al. (2014) reported a value of 0.514 g_C g_{CDW}^{-1} for *C. glutamicum* ATCC 13032, which was determined by separately quantifying the total carbon in liquid bioreactor samples (supernatant and biomass) and the total inorganic carbon (total dissolved carbon) in the supernatant. In this work, we experimentally quantified ω_C for wild-type *C. glutamicum* to be around 0.4–0.42 g_C g_{CDW}^{-1}. The uncertainty of this parameter notwithstanding, its value was assumed to be 0.45 g_C g_{CDW}^{-1} for all following calculations. In face of the apparent uncertainty, its standard error was assumed to be 0.05 g_C g_{CDW}^{-1}. The arising interval covers all available literature information on this quantity. The uncertainty in derived quantities thereof can be computed by Gaussian error propagation.

From **Figure 2B** it becomes apparent that the evolved Δ*ppc* Δ*pyc* strain grows with a higher relative CO_2-formation rate with respect to the uptake rate. At the same time, the sum of the specific rates at which carbon flows into sinks amounts to the same relative value with respect to the carbon uptake rate as in other strains. Therefore, it seems plausible that a higher decarboxylation activity explains the lower relative growth rate in the *C. glutamicum* Δ*ppc* Δ*pyc* mutant. This higher relative CO_2-formation rate further substantiates the hypothesis that an altered ratio of ICL and ICD activity involves the glyoxylate shunt as anaplerotic reaction sequence in this mutant. Exclusive anaplerotic activity through the glyoxylate shunt would release two equivalents CO_2 per C4-body of oxaloacetate formed, instead of fixing one CO_2 as in the case of alternative ME or reversible PEPCk activities.

One result holds true irrespective of the genetic background: The recovery of carbon at any given time in the reactions that act as carbon sinks amounts to 80% of the carbon equivalent of the uptake rate (**Figure 2B** and **Table 2**). The non-closed instantaneous carbon balance may hint to extensive by-product formation or indicate systematically biased extracellular rates. The former is unlikely since *C. glutamicum* WT is known to produce only minor by-products under aerobic conditions (the DO was maintained at 30%). Notwithstanding, the genetic alterations may induce a more extensive overflow metabolism in some deletion mutants. However, all organic acids, sugar phosphates and amino acids in the culture supernatant measured by targeted LC-MS/MS account for a total of 274–786 $\mu mol_C\ g_{CDW}^{-1}$, depending on the strain. Therefore, the exometabolome can be neglected as carbon sink since the gap in the balance of specific rates amounts to several $mmol_C\ g_{CDW}^{-1}\ h^{-1}$ (**Figure 2B**).

Remarkably, the value of 80% for the instantaneous carbon balance matches the determined carbon balance closure in the study of Buchholz et al. (2014). This study convincingly showed that the gap in carbon balance can be traced back to the fact that part of the CO_2-production at any given time dissolves as HCO_3^- in the culture broth. This share is not recovered as gaseous CO_2 at the detector, leading to an underestimation of the CO_2-production rate.

Proteomic and Metabolomic Responses to Gene Deletions in Anaplerotic Reactions

To gain further insight into the metabolism of each mutant, untargeted proteome and targeted metabolome analyses were performed. To ensure comparability, eight strains were cultivated in parallel and subjected to identical and isochronous sample processing in subsequent steps (see section Materials and Methods for detailed descriptions). In total, we analyzed 1199 cytosolic proteins and 48 metabolites of central metabolism.

Since the Δ*ppc* mutant showed no altered phenotype and has been thoroughly characterized before, it was omitted from the set of strains to be analyzed. The evolved strain *C. glutamicum* Δ*ppc* Δ*pyc* showed significant changes in specific proteins and metabolites, which will be discussed separately in the next section.

Further differentially expressed proteins were found in *C. glutamicum* Δ*pck* and *C. glutamicum* Δ*pyc* (**Figure 3**). In none of the other tested deletion mutants significantly changed protein abundances [$p < 0.05$, $|\text{Log2(fold change)}| \geq 0.5$] were found (data not shown).

Only one protein encoded by *cybD* (cg0282) and which might be involved in stress response was found to be up-regulated in the *C. glutamicum* Δ*pck* mutant (**Table 3**). In *C. glutamicum* Δ*pyc* the enzyme quinolinate synthase A encoded by the *nadA* gene (cg1216) was up-regulated. This enzyme catalyzes the condensation of iminoaspartate with dihydroxyacetone phosphate to form quinolinate, and represents the second step of the *de novo* synthesis of NAD^+. The latter starts from L-aspartate and up-regulation of this enzyme could be a cellular response to the limited availability of this amino acid following the inactivation of PCx and to ensure sufficient NAD^+ supply. In addition, the putative transcriptional regulator (cg0787) and the 50S ribosomal protein L36 encoded by the *rpmJ* gene (cg2791) were found to be down-regulated in *C. glutamicum* Δ*pyc*.

Figure 4 shows intracellular and extracellular concentrations of selected metabolites. The L-aspartate pool is most closely correlated with the growth rate, i.e., the lowest concentrations were observed for all mutants with reduced growth rate. Apparently, its supply appears to be limiting the growth as the restored growth rate of the Δ*pck* Δ*malE* mutant in comparison to the single deletion strain Δ*pck* goes hand in hand with increased L-aspartate supply. The concentration pattern of L-aspartate seems to reflect itself in the L-homoserine pool, which is derived from the former through three intermediate reaction steps, consuming two NAD(P)H molecules and one ATP molecule. In contradistinction to L-aspartate, however, L-homoserine is clearly higher concentrated in the Δ*pck* mutant. Since the reaction sequence between both intermediates is redox-dependent, one may be tempted to attribute this observation to redox balancing. The biosynthesis of L-glutamate from α-ketoglutarate and of L-proline from L-glutamate are also redox-dependent. Conspicuously, both pools are also higher concentrated in this strain (**Figure 4**).

Moreover, we analyzed intracellular levels of NADPH and NADH alongside their oxidized analogs. No significant difference was detected in the reduced forms of these co-factors (data not shown). However, the mean of relative standard deviation over all mutants for NADH and NADPH concentrations amounts to 46% and 48%, respectively. This high technical error, impeding a precise quantification, cannot be traced back to inaccuracies in pipetting or BV concentration measurements since these factors also apply to all other metabolite quantifications in the same sample. Since the mean relative standard deviation for other metabolite pools was below 10% these factors appear to have been controlled quite well. The most likely reason for the observed coefficients of variation is metabolite instability. The redox equivalents are known to be quite sensitive to oxidation and degradation (Siegel et al., 2014). Slightly different temperature time courses, residual enzymatic activity in metabolite extracts and oxidation most likely account for the observed differences. Therefore, no accurate conclusion about the redox state in each mutant could be drawn. Nonetheless, the fact that the removal of a redox-dependent enzyme like ME restores the growth rate of the *C. glutamicum* Δ*pck* mutant suggests an involvement of the redox balance mediating some of the observed changes in metabolite pools.

Glyoxylate Shunt Enables Growth of *C. glutamicum* Δ*ppc* Δ*pyc* on D-Glucose as Sole Carbon and Energy Source

Whole-genome sequencing of evolved *C. glutamicum* Δ*ppc* Δ*pyc* confirmed the absence of genes *ppc* and *pyc* across the cell population (**Table 4**), excluding any growth contamination effect. Two insertions and some SNPs (see **Supplementary Table 6**) were detected in the coding region for ICD. Moreover, ICL (cg2560), MS (cg2559), and *cis*-aconitase (ACN, cg1737) are highly up-regulated in *C. glutamicum* Δ*ppc* Δ*pyc* (**Figure 3** and

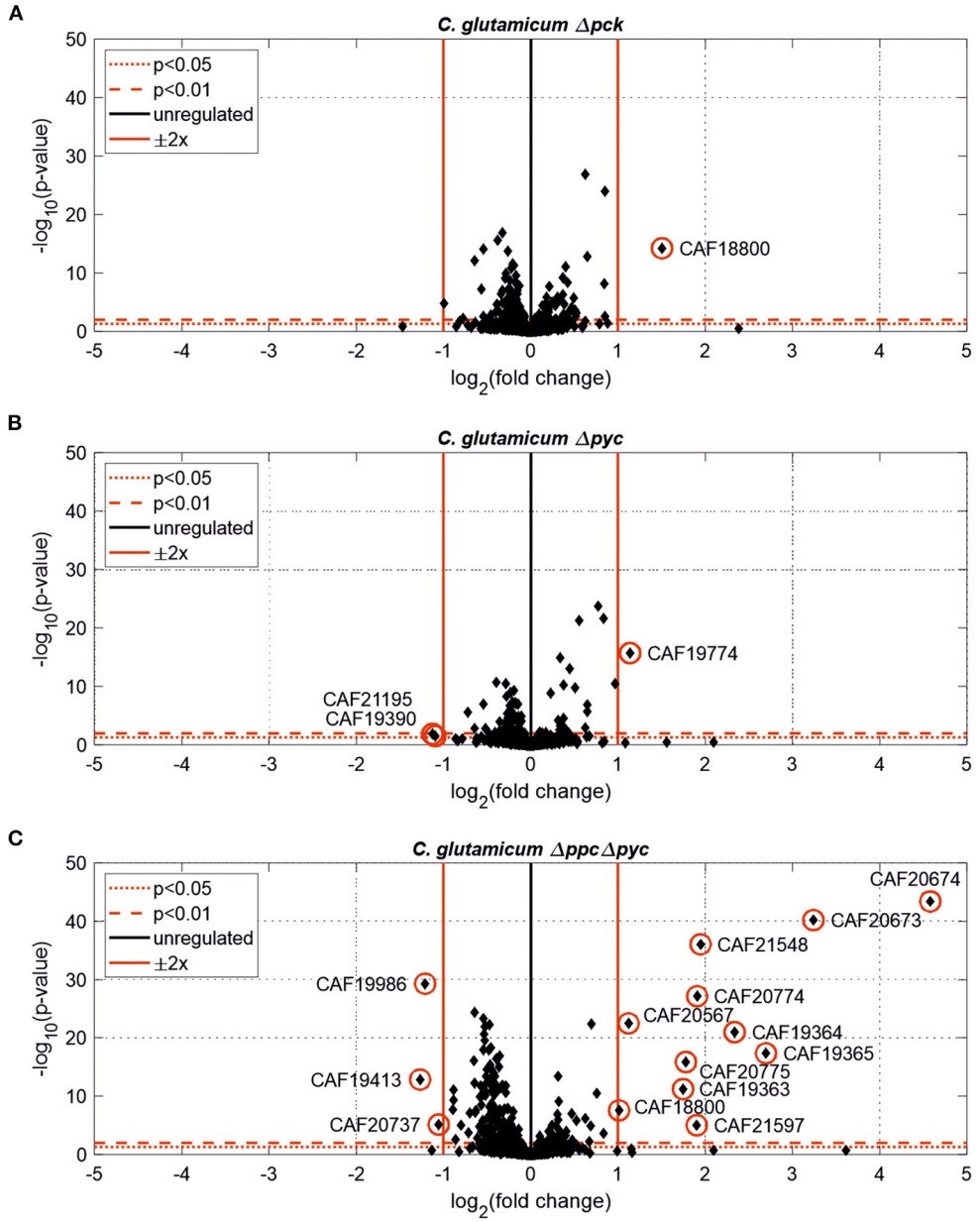

FIGURE 3 | Estimated protein fold-changes for selected *C. glutamicum* deletion mutants in comparison to the wild type. **(A)** *C. glutamicum* Δ*pck*. **(B)** *C. glutamicum* Δ*pyc*. **(C)** *C. glutamicum* Δ*ppc* Δ*pyc*. Volcano plots with significantly changed proteins [$p < 0.05$, |Log2(fold change)| ≥ 0.5] highlighted in red.

Table 3) and only in this mutant intracellular and extracellular accumulation of glyoxylate was detected (**Figure 4**).

These findings are in agreement with the study of Schwentner et al. and point to a redirection of carbon flux in our evolved strain from the oxidative decarboxylation branch of the TCA cycle into the glyoxylate shunt (Schwentner et al., 2018). In the absence of C3-carboxylation activity at the anaplerotic node, accumulation of the substrate pools phosphoenolpyruvate and pyruvate can be expected. Indeed, phosphoenolpyruvate was significantly higher concentrated in the evolved Δ*ppc* Δ*pyc* strain, while the intracellular pyruvate pool remained unaffected (**Figure 4**). However, metabolite levels of L-alanine and L-valine, which are directly derived from pyruvate, were strongly increased and this finding is also consistent with previous data (Schwentner et al., 2018). The lack of statistical significance of strain differences in the pyruvate pool is most likely due to higher technical errors during metabolite quantification. It is well-established that the accurate quantification of organic acids in cell extracts represents a veritable challenge (Zimmermann et al., 2014).

TABLE 3 | Differentially expressed proteins of *C. glutamicum* anaplerotic deletion mutants in comparison to the wild-type strain.

Strain	Protein ID	Cg no.	Gene	Annotated function	Fold change	*p*-value
C. glutamicum Δ*pck*	CAF18800	cg0282	*cybD*	Putative protein, CsbD-family, probably involved in stress response	2.84	5.90e-15
C. glutamicum Δ*pyc*	CAF19774	cg1216	*nadA*	Quinolinate synthase A	2.20	2.03e-16
	CAF19390	cg0787	–	Transcriptional regulator	0.47	3.11e-02
	CAF21195	cg2791	*rpmJ*	50S ribosomal protein L36	0.46	1.40e-02
C. glutamicum Δ*ppc* Δ*pyc*	CAF20674	cg2560	*aceA*	Isocitrate lyase	23.94	3.79e-44
	CAF20673	cg2559	*aceB*	Malate synthase	9.45	6.63e-41
	CAF19365	cg0762	*prpC2*	2-methylcitrate synthase	6.49	4.73e-18
	CAF19364	cg0760	*prpB2*	2-methylcitrate lyase	5.05	1.07e-21
	CAF21548	cg1737	*acn*	Aconitase	3.86	8.53e-37
	CAF20774	cg3047	*ackA*	Acetate kinase	3.75	7.39e-28
	CAF21597	cg1792	*whiA*	Putative transcriptional regulator-WhiA homolog	3.75	9.38e-06
	CAF20775	cg3048	*pta*	Phosphate acetyltransferase	3.43	1.42e-16
	CAF19363	cg0759	*prpD2*	2-methylcitrate dehydratase	3.36	5.83e-12
	CAF20567	–	–	Hypothetical protein	2.18	3.42e-23
	CAF18800	cg0282	–	Conserved hypothetical protein	2.02	2.79e-08
	CAF20737	cg3008	*porA*	Porin	0.48	7.16e-06
	CAF19986	cg1451	*serA*	Phosphoglycerate dehydrogenase	0.43	5.03e-30
	CAF19413	cg0812	*dtsR1*	Acetyl/ propionyl-CoA carboxylase beta chain	0.42	1.34e-13

All proteins with significant changes [$p < 0.05$, Log2(fold change) > 0.5 for upregulated proteins and Log2(fold change) < -0.5 for down-regulated proteins] are listed.

Moreover, the metabolite pool of L-glycine shows one of the most significant concentration changes, clearly distinguishing the evolved Δ*ppc* Δ*pyc* strain. L-glycine, in turn, is derived from L-serine, which also showed an increased concentration (**Figure 4**). It appears that the missing carboxylation rate cannot be matched by the pyruvate dehydrogenase activity in the Δ*ppc* Δ*pyc* mutant for substrate pools like phosphoenolpyruvate as well as amino acids derived from the lower glycolytic intermediates appear to accumulate intracellularly. This would also explain why the phosphoglycerate dehydrogenase encoded by *serA* (cg1451) was found to be significantly down-regulated in this mutant (**Table 3**). The enzyme catalyzes the first step in the biosynthesis of L-glycine, L-serine and L-cysteine and its down-regulation could be the cellular response to the higher availability of 3-phosphoglycerate.

In terms of glyoxylate shunt regulation, Wendisch et al. suggested that the carbon-source dependent regulation of this pathway is mediated by intracellular acetyl-CoA concentrations (Wendisch et al., 1997). However, intracellular acetyl-CoA concentrations did not vary significantly with respect to strain background (**Figure 4**), and therefore this hypothesis could not be validated with the made intracellular measurements. Unfortunately, acetyl-CoA measurements are notoriously error-prone due to the high instability of thioesthers. Though taking strenuous efforts to keep the sample below−20°C and immediate analysis after extraction, we still obtained a highly variable signal within each treatment group.

The corresponding genes *aceA* and *aceB* of ICL and MS, respectively, are thought to be repressed by the regulator protein RamB (cg0444) under glycolytic conditions (Auchter et al., 2011). Moreover, it has been established that RamA (cg2831) acts as transcriptional activator of both genes when acetate is the carbon source. However, no significant change in the abundances of RamA and RamB were found in Δ*ppc* Δ*pyc* mutant compared to the wild type. The fact that a Δ*ramA* mutant is not able to grow on acetate suggests that RamA is strictly required as transcriptional activator for increased expression of at least one of the essential enzymes of acetate assimilation, which are acetate kinase (AK) encoded by *ackA* (cg3047), phosphotransacetylase (PTA) encoded by *pta* (cg3048), ICL and MS (Cramer and Eikmanns, 2007). Indeed, AK and PTA are also significantly up-regulated in the Δ*ppc* Δ*pyc* mutant (**Table 3**).

Most interestingly, this strain also shows an up-regulation of the three enzymes of the methylcitrate cycle in *C. glutamicum* (Claes et al., 2002), namely 2-methylcitrate synthase (PrpC2) encoded by *prpC2* (cg0762), 2-methylcitrate dehydratase (PrpD2) encoded by *prpD2* (cg0759) and 2-methylcitrate lyase (PrpB2) encoded by *prpB2* (cg0760) (**Table 3**). Together with the activities of AK and PTA this cycle is known to be the predominant route for the degradation of propionate into pyruvate and succinate (**Figure 1**). In the presence of propionate all three genes are transcriptionally activated by the regulator PrpR (Plassmeier et al., 2012). Under the applied D-glucose conditions, however, no change in the PrpR abundance was detected. Moreover, it was found that the *prpDBC2* operon is transcriptionally activated by RamA, but not affected by RamB (Auchter et al., 2011). This makes the conclusion compelling that the concentration of at least one, still unknown, metabolite effector binding to RamA was altered, leading to the activation of the aforementioned genes. Following the strong up-regulation of the *prpDBC2* cluster in combination with the glyoxylate shunt it might be speculated that the surplus of pyruvate (from PEPCx and PCx inactivation) and succinate (from ICL activity) is channeled into the methylcitrate cycle,

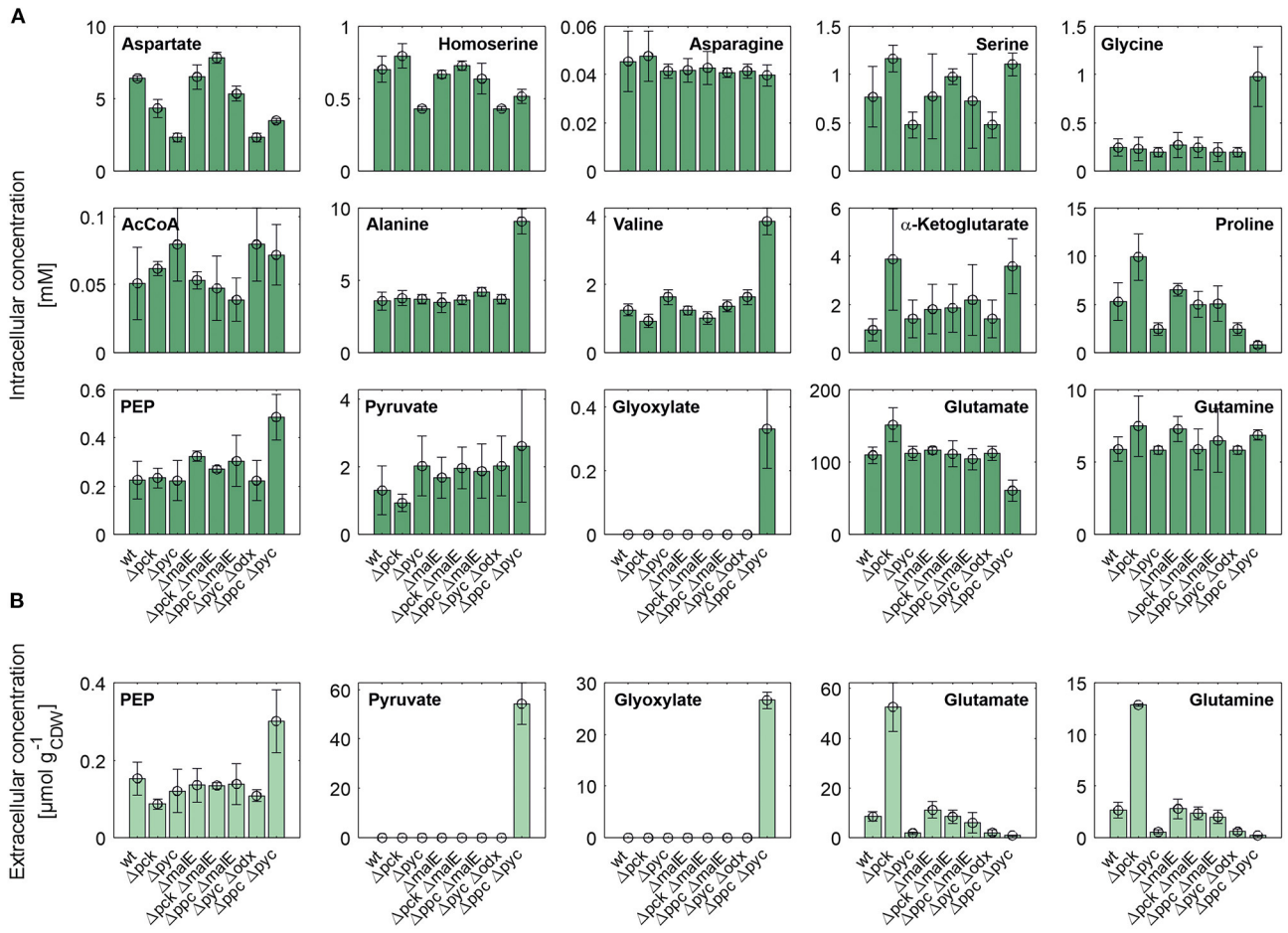

FIGURE 4 | Intracellular **(A)** and specific extracellular **(B)** concentrations of selected metabolites in *C. glutamicum* wild type and anaplerotic deletion mutants cultivated under controlled bioreactor conditions in CGXII medium with D-glucose as sole carbon and energy source. For gene to protein references see **Figure 2**.

operating in the reverse direction. This route would represent a by-pass of the TCA cycle reactions succinate: quinone oxidoreductase (SQO), fumarase (FUM) and malate: quinone oxidoreductase (MQO) to provide oxaloacetate as biomass precursor (**Figure 1**). From a thermodynamic point of view, the PrpB2 reaction in direction of 2-methylisocitrate is favored ($\Delta_r G'^0 = -9.3\ kJ/mol$) in comparison to the SQO reaction leading to fumarate ($\Delta_r G'^0 = 14.5\ kJ/mol$). However, the potentially last step of the methylcitrate cycle catalyzed by PrpC2 is thermodynamically very unfavorable ($\Delta_r G'^0 = 39.2\ kJ/mol$), but might still work under *in vivo* conditions due to very low concentrations of oxaloacetate (<100 nM of lower detection limit of applied LC-QqQ MS). Indeed, Plassmeier et al. showed that the *prpDBC2* operon is also expressed under normal cell growth conditions in wild-type *C. glutamicum*, independent of the application of propionate as carbon source (Plassmeier et al., 2007). Moreover, a high up-regulation of the *prpDBC2* operon was found in a *C. glutamicum* strain engineered for overproduction of L-isoleucine (Ma et al., 2018). Here it was speculated that this up-regulation was due to a high intracellular formation of propionyl-CoA, which was derived from the intermediate 2-ketobutyrate of the L-isoleucine biosynthesis. The resulting propionyl-CoA was then further converted into a polyhydroxyalkanoate by heterologous expression of the *phaCAB* gene cluster. In our case, however, we can exclude propionyl-CoA formation from 2-ketobutyrate because L-aspartate is limiting. Additionally, it remains open what happens with propionyl-CoA as the second product of the PrpC2 reaction when running in reverse direction (**Figure 1**). Therefore, further investigations on the interplay between the different pathways are required to substantiate our hypothesis.

Moreover, we found a SNP in the intergenic region between cg3314 and cg3315, four nucleotides upstream from the translation start of MalR (*malR*, cg3315). This protein has been originally identified as repressor of the *malE* gene in the study of Krause et al. (2012) and was recently reported to bind to several other loci (Hünnefeld et al., 2019). Since the mutation occurred outside the coding sequence of this regulator, only expression changes of the gene are able to affect metabolism. Unfortunately, the specific protein data for MalR was not very accurate ($p > 0.5$) to enable any conclusion, but ME appeared to be down-regulated in the evolved Δ*ppc* Δ*pyc* strain when grown on D-glucose

TABLE 4 | Structural variants identified in the *C. glutamicum* Δ*ppc* Δ*pyc* mutant adapted to D-glucose as sole carbon source in comparison to *C. glutamicum* WT as reference.

Affected region	Character	nt Region	Length	Reads of position	Rel. frequency
In cg2353, putative protein	Deletion	2,236,684..2,238,317	1,634	47	1
In cg2854, *tnp2c*, transposase	Deletion	2,716,280..2,717,915	1,636	59	1
In cg0691, *groEL'*, 60 kDa chaperonin, N-terminal fragment	Deletion	610,994..612,446	1,453	85	0.99
In cg0791, *pyc*, pyruvate carboxylase	Deletion	707,185..709,613	2,429	76	0.99
In cg1787, *ppc*, phosphoenolpyruvate carboxylase	Deletion	1,679,298..1,681,219	1,922	60	0.98
Intergenic region of cg1860 (putative membrane protein) and cg1861 (*rel*, ppGpp synthetase / ppGpp pyro-phosphorylase)	Replacement	1,754,002..1,754,038	37	73	0.98
Upstream of cg0756, *cstA*, carbon starvation protein A	Deletion	669,585..669,597	13	46	0.9
In cg2262, *ftsY*, signal recognition particle GTPase	Deletion	2,144,947..2,144,964	18	13	0.4
In cg0766, *icd*, isocitrate dehydrogenase	Insertion	681,078..681,079	57	27	0.38
In cg0766, *icd*, isocitrate dehydrogenase	Insertion	681,136..681,137	57	26	0.32
In cg0953, *mctC*, monocarboxylic acid transporter	Deletion	884,479..884,487	9	13	0.31

The column "Reads of position" refers to the number of sequencing reads supporting the alteration. The relative frequency refers to the number of reads supporting the alteration relative to the total number of reads of this position or region.

as sole carbon and energy source (0.54-fold, $p < 4.73e\text{-}10$). Since purified ME of *C. glutamicum* was shown to carboxylate pyruvate in *in vitro* assays with an apparent K_m constant of 13.8 mM (Gourdon et al., 2000) it was speculated that ME serves as anaplerotic enzyme under circumstances when PEPCx and PCx activities are absent and pyruvate availability is still ensured through running glycolysis. In our case, however, the amount of ME was significantly reduced with respect to the wild type and its intracellular substrate pool of pyruvate is not significantly altered and well below the K_m value (**Figure 4A**). Therefore, it can be excluded that ME catalyzes a flux compensating for the missing PCx and PEPCx activity in the evolved Δ*ppc* Δ*pyc* strain.

Finally, a deletion was detected in the *mctC* gene (cg0953), which has been shown to be essential in *C. glutamicum* for the uptake of pyruvate (Jolkver et al., 2009). Based on this, it can be hypothesized that the genetic alteration in this transporter may lead to a decreased uptake of pyruvate from the medium, which would explain the extracellular accumulation of pyruvate exclusively found in the Δ*ppc* Δ*pyc* mutant (**Figure 4B**).

CONCLUSIONS

We characterized eight different mutant strains of *C. glutamicum* carrying single or double deletions in five anaplerotic enzymes. The metabolism and adaptation of each mutant during growth under defined D-glucose conditions in lab-scale bioreactors was investigated by quantification of its extracellular rates, central metabolic intermediates by LC-QqQ MS and proteome by SWATH acquisition using a LC-QqTOF MS platform.

In comparison to the wild type the four deletion mutants *C. glutamiucm* Δ*pyc*, *C. glutamiucm* Δ*pyc* Δ*odx*, *C. glutamiucm* Δ*ppc* Δ*pyc*, and *C. glutamiucm* Δ*pck* showed lowered specific growth rates and D-glucose uptake rates, underlining the importance of PCx and PEPCk activity for a balanced carbon and energy flux at the anaplerotic node.

Detailed analyses of the *C. glutamicum* Δ*ppc* Δ*pyc* mutant evolved to grow on D-glucose revealed the strong up-regulation of a few genes that are under control of the transcriptional regulator RamA. Higher protein abundances were found for the enzymes of the glyxoylate shunt as well as the methylcitrate cycle under solely glycolytic conditions, under which condition the corresponding genes were thought to be repressed. It is inferred that this adaptation must be due to a changed concentration of a metabolite affecting the activity of regulator protein RamA, brought about by a concentration change of the former. This metabolite pool, however, could not be identified from the set of metabolites from glycolysis, TCA cycle and amino acids that was targeted in this study. Since the encoding genes of the altered proteins represent just a small subset of the RamA regulon, it can be concluded that the binding affinities

of RamA to all target genes may be regulated by various effector metabolites and not a single one. Further research, especially based on untargeted metabolomics, will be needed to identify the metabolite regulator(s) active on RamA under D-glucose conditions.

In conjunction with the intracellular metabolomics data we generally conclude that *C. glutamicum* is able to compensate missing carboxylation activities of PEPCx and PCx by activation of the glyoxylate shunt, potentially in combination with the methylcitrate cycle to channel the higher levels of PEP/ pyruvate as well as succinate and thereby also contributing to replenish oxaloacetate. To further substantiate the hypothesis on the reverse operation of the methylcitrate cycle isotope-based metabolic flux analyses with the evolved *C. glutamicum* Δ*ppc* Δ*pyc* strain could be conducted in further studies.

Finally, the reproducible effect of bicarbonate formation under excess D-glucose conditions and its consequences for carbon balancing also requires further investigations. For example, a combination of batch experiments under variation of pH and gassing rate as well as thorough modeling of the resulting CO_2-dynamics in the gas and liquid phase could be an approach for a more accurate determination of CO_2-formation rates.

DATA AVAILABILITY STATEMENT

The mass spectrometry proteomics data have been deposited to the ProteomeXchange Consortium via the PRIDE (Perez-Riverol et al., 2019) partner repository with the dataset identifier PXD022622. The reads data of the Δ*ppc* Δ*pyc* strain are available in NCBI's SRA via BioProject ID PRJNA678589. The other datasets generated for this study are available on request to the corresponding author.

AUTHOR CONTRIBUTIONS

JK and SN designed the research. JK performed data analysis and wrote the manuscript. JK and MP performed the bioreactor cultivations of *C. glutamicum*. BK lysed and digested all samples and performed the LC-MS/MS measurements. JL constructed the *C. glutamicum* double deletion mutants used in this manuscript. TP performed the whole-genome sequencing. SN, TP, and WW revised the manuscript. SN, RT, and BB supervised the research. All authors have given approval to the final version of the manuscript.

FUNDING

This work was partly funded by the Deutsche Forschungsgemeinschaft (priority program SPP2170, Grant No. 427904493).

ACKNOWLEDGMENTS

We thank Lothar Eggeling for critical comments on the manuscript.

SUPPLEMENTARY MATERIAL

The Supplementary Material for this article can be found online at: https://www.frontiersin.org/articles/10.3389/fbioe.2020.602936/full#supplementary-material

REFERENCES

Auchter, M., Cramer, A., Hüser, A., Rückert, C., Emer, D., Schwarz, P., et al. (2011). RamA and RamB are global transcriptional regulators in *Corynebacterium glutamicum* and control genes for enzymes of the central metabolism. *J. Biotechnol.* 154, 126–139. doi: 10.1016/j.jbiotec.2010.07.001

Baumgart, M., Unthan, S., Kloß, R., Radek, A., Polen, T., Tenhaef, N., et al. (2018). *Corynebacterium glutamicum* chassis C1*: building and testing a novel platform host for synthetic biology and industrial biotechnology. *ACS Synth. Biol.* 7, 132–144. doi: 10.1021/acssynbio.7b00261

Baumgart, M., Unthan, S., Rückert, C., Sivalingam, J., Grünberger, A., Kalinowski, J., et al. (2013). Construction of a prophage-free variant of *Corynebacterium glutamicum* ATCC 13032 for use as a platform strain for basic research and industrial biotechnology. *Appl. Environ. Microbiol.* 79, 6006–6015. doi: 10.1128/AEM.01634-13

Becker, J., Rohles, C. M., and Wittmann, C. (2018). Metabolically engineered *Corynebacterium glutamicum* for bio-based production of chemicals, fuels, materials, and healthcare products. *Metab. Eng.* 50, 122–141. doi: 10.1016/j.ymben.2018.07.008

Blombach, B., Buchholz, J., Busche, T., Kalinowski, J., and Takors, R. (2013). Impact of different CO_2/HCO_3^- levels on metabolism and regulation in *Corynebacterium glutamicum*. *J. Biotechnol.* 168, 331–340. doi: 10.1016/j.jbiotec.2013.10.005

Blombach, B., Riester, T., Wieschalka, S., Ziert, C., Youn, J. W., Wendisch, V. F., et al. (2011). *Corynebacterium glutamicum* tailored for efficient isobutanol production. *Appl. Environ. Microbiol.* 77, 3300–3310. doi: 10.1128/AEM.02972-10

Buchholz, J., Graf, M., Blombach, B., and Takors, R. (2014). Improving the carbon balance of fermentations by total carbon analyses. *Biochem. Eng. J.* 90, 162–169. doi: 10.1016/j.bej.2014.06.007

Claes, W. A., Pühler, A., and Kalinowski, J. (2002). Identification of two *prpDBC* gene clusters in *Corynebacterium glutamicum* and their involvement in propionate degradation via the 2-methylcitrate cycle. *J. Bacteriol.* 184, 2728–2739. doi: 10.1128/JB.184.10.2728-2739.2002

Cocaign-Bousquet, M., Guyonvarch, A., and Lindley, N. D. (1996). Growth rate-dependent modulation of carbon flux through central metabolism and the kinetic consequences for glucose-limited chemostat cultures of *Corynebacterium glutamicum*. *Appl. Environ. Microbiol.* 62, 429–436. doi: 10.1128/AEM.62.2.429-436.1996

Cramer, A., and Eikmanns, B. J. (2007). RamA, the transcriptional regulator of acetate metabolism in *Corynebacterium glutamicum*, is subject to negative autoregulation. *J. Mol. Microbiol. Biotechnol.* 12, 51–59. doi: 10.1159/000096459

Dalman, T., Dornemann, T., Juhnke, E., Weitzel, M., Wiechert, W., Nöh, K., et al. (2013). Cloud MapReduce for monte carlo bootstrap applied to metabolic flux analysis. *Future Gener. Comp. Sy.* 29, 582–590. doi: 10.1016/j.future.2011.10.007

Eikmanns, B. J., Thum-Schmitz, N., Eggeling, L., Lüdtke, K.-U., and Sahm, H. (1994). Nucleotide sequence, expression and transcriptional analysis of the *Corynebacterium glutamicum gltA* gene encoding citrate synthase. *Microbiology* 140, 1817–1828. doi: 10.1099/13500872-140-8-1817

Flamholz, A., Noor, E., Bar-Even, A., and Milo, R. (2012). eQuilibrator–the biochemical thermodynamics calculator. *Nucleic Acids Res.* 40, D770–775. doi: 10.1093/nar/gkr874

Fränzel, B., Fischer, F., Trötschel, C., Poetsch, A., and Wolters, D. (2009). The two-phase partitioning system–a powerful technique to purify integral membrane proteins of *Corynebacterium glutamicum* for quantitative shotgun analysis. *Proteomics* 9, 2263–2272. doi: 10.1002/pmic.200800766

Gourdon, P., Baucher, M. F., Lindley, N. D., and Guyonvarch, A. (2000). Cloning of the malic enzyme gene from *Corynebacterium glutamicum* and role of the enzyme in lactate metabolism. *Appl. Environ. Microbiol.* 66, 2981–2987. doi: 10.1128/AEM.66.7.2981-2987.2000

Hünnefeld, M., Persicke, M., Kalinowski, J., and Frunzke, J. (2019). The MarR-type regulator MalR is involved in stress-responsive cell envelope remodeling in *Corynebacterium glutamicum*. *Front. Microbiol.* 10:1039. doi: 10.3389/fmicb.2019.01039

Jolkver, E., Emer, D., Ballan, S., Kramer, R., Eikmanns, B. J., and Marin, K. (2009). Identification and characterization of a bacterial transport system for the uptake of pyruvate, propionate, and acetate in *Corynebacterium glutamicum*. *J. Bacteriol.* 191, 940–948. doi: 10.1128/JB.01155-08

Kappelmann, J., Wiechert, W., and Noack, S. (2016). Cutting the gordian knot: identifiability of anaplerotic reactions in *Corynebacterium glutamicum* by means of ^{13}C-metabolic flux analysis. *Biotechnol. Bioeng.* 113, 661–674. doi: 10.1002/bit.25833

Klaffl, S., and Eikmanns, B. J. (2010). Genetic and functional analysis of the soluble oxaloacetate decarboxylase from *Corynebacterium glutamicum*. *J. Bacteriol.* 192, 2604–2612. doi: 10.1128/JB.01678-09

Kogure, T., and Inui, M. (2018). Recent advances in metabolic engineering of *Corynebacterium glutamicum* for bioproduction of value-added aromatic chemicals and natural products. *Appl. Microbiol. Biotechnol.* 102, 8685–8705. doi: 10.1007/s00253-018-9289-6

Kranz, A., Vogel, A., Degner, U., Kiefler, I., Bott, M., Usadel, B., et al. (2017). High precision genome sequencing of engineered *Gluconobacter oxydans* 621H by combining long nanopore and short accurate illumina reads. *J. Biotechnol.* 258, 197–205. doi: 10.1016/j.jbiotec.2017.04.016

Krause, J. P., Polen, T., Youn, J. W., Emer, D., Eikmanns, B. J., and Wendisch, V. F. (2012). Regulation of the malic enzyme gene *malE* by the transcriptional regulator MalR in *Corynebacterium glutamicum*. *J. Biotechnol.* 159, 204–215. doi: 10.1016/j.jbiotec.2012.01.003

Küberl, A., Franzel, B., Eggeling, L., Polen, T., Wolters, D. A., and Bott, M. (2014). Pupylated proteins in *Corynebacterium glutamicum* revealed by MudPIT analysis. *Proteomics* 14, 1531–1542. doi: 10.1002/pmic.201300531

Lee, J. H., and Wendisch, V. F. (2017). Production of amino acids - genetic and metabolic engineering approaches. *Bioresour. Technol.* 245, 1575–1587. doi: 10.1016/j.biortech.2017.05.065

Ma, W. J., Wang, J. L., Li, Y., Yin, L. H., and Wang, X. Y. (2018). Poly(3-hydroxybutyrate-co-3-hydroxyvalerate) co-produced with L-isoleucine in *Corynebacterium glutamicum* WM001. *Microb. Cell Fact* 17:93. doi: 10.1186/s12934-018-0942-7

Marx, A., De Graaf, A. A., Wiechert, W., Eggeling, L., and Sahm, H. (1996). Determination of the fluxes in the central metabolism of *Corynebacterium glutamicum* by nuclear magnetic resonance spectroscopy combined with metabolite balancing. *Biotechnol. Bioeng.* 49, 111–129. doi: 10.1002/(SICI)1097-0290(19960120)49:2<111::AID-BIT1>3.0.CO;2-T

Noack, S., Voges, R., Gätgens, J., and Wiechert, W. (2017). The linkage between nutrient supply, intracellular enzyme abundances and bacterial growth: New evidences from the central carbon metabolism of *Corynebacterium glutamicum*. *J. Biotechnol.* 258, 13–24. doi: 10.1016/j.jbiotec.2017.06.407

Paczia, N., Nilgen, A., Lehmann, T., Gätgens, J., Wiechert, W., and Noack, S. (2012). Extensive exometabolome analysis reveals extended overflow metabolism in various microorganisms. *Microb. Cell Fact* 11:122. doi: 10.1186/1475-2859-11-122

Perez-Riverol, Y., Csordas, A., Bai, J., Bernal-Llinares, M., Hewapathirana, S., Kundu, D. J., et al. (2019). The PRIDE database and related tools and resources in 2019: improving support for quantification data. *Nucleic Acids Res.* 47, D442–D450. doi: 10.1093/nar/gky1106

Petersen, S., Mack, C., De Graaf, A. A., Riedel, C., Eikmanns, B. J., and Sahm, H. (2001). Metabolic consequences of altered phosphoenolpyruvate carboxykinase activity in *Corynebacterium glutamicum* reveal anaplerotic regulation mechanisms *in vivo*. *Metab. Eng.* 3, 344–361. doi: 10.1006/mben.2001.0198

Peters-Wendisch, P. G., Eikmanns, B. J., Thierbach, G., Bachmann, B., and Sahm, H. (1993). Phosphoenolpyruvate carboxylase in *Corynebacterium glutamicum* is dispensable for growth and lysine production. *FEMS Microbiol. Lett.* 114, 243–243.

Peters-Wendisch, P. G., Kreutzer, C., Kalinowski, J., Pátek, M., Sahm, H., and Eikmanns, B. J. (1998). Pyruvate carboxylase from *Corynebacterium glutamicum*: characterization, expression and inactivation of the *pyc* gene. *Microbiology* 144, 915–927. doi: 10.1099/00221287-144-4-915

Peters-Wendisch, P. G., Wendisch, V. F., Degraaf, A. A., Eikmanns, B. J., and Sahm, H. (1996). C-3-carboxylation as an anaplerotic reaction in phosphoenolpyruvate carboxylase-deficient *Corynebacterium glutamicum*. *Arch. Microbiol.* 165, 387–396. doi: 10.1007/s002030050342

Plassmeier, J., Barsch, A., Persicke, M., Niehaus, K., and Kalinowski, J. (2007). Investigation of central carbon metabolism and the 2-methylcitrate cycle in *Corynebacterium glutamicum* by metabolic profiling using gas chromatography-mass spectrometry. *J. Biotechnol.* 130, 354–363. doi: 10.1016/j.jbiotec.2007.04.026

Plassmeier, J., Persicke, M., Puhler, A., Sterthoff, C., Ruckert, C., and Kalinowski, J. (2012). Molecular characterization of PrpR, the transcriptional activator of propionate catabolism in *Corynebacterium glutamicum*. *J. Biotechnol.* 159, 1–11. doi: 10.1016/j.jbiotec.2011.09.009

Riedel, C., Rittmann, D., Dangel, P., Mockel, B., Petersen, S., Sahm, H., et al. (2001). Characterization of the phosphoenolpyruvate carboxykinase gene from *Corynebacterium glutamicum* and significance of the enzyme for growth and amino acid production. *J. Mol. Microbiol. Biotechnol.* 3, 573–583.

Schwentner, A., Feith, A., Münch, E., Busche, T., Rückert, C., Kalinowski, J., et al. (2018). Metabolic engineering to guide evolution – Creating a novel mode for L-valine production with *Corynebacterium glutamicum*. *Metab. Eng.* 47, 31–41. doi: 10.1016/j.ymben.2018.02.015

Siegel, D., Permentier, H., Reijngoud, D. J., and Bischoff, R. (2014). Chemical and technical challenges in the analysis of central carbon metabolites by liquid-chromatography mass spectrometry. *J. Chromatogr. B Analyt Technol. Biomed. Life Sci.* 966, 21–33. doi: 10.1016/j.jchromb.2013.11.022

Stella, R. G., Wiechert, J., Noack, S., and Frunzke, J. (2019). Evolutionary engineering of *Corynebacterium glutamicum*. *Biotechnol. J.* 14:e1800444. doi: 10.1002/biot.201800444

Tillack, J., Paczia, N., Noh, K., Wiechert, W., and Noack, S. (2012). Error propagation analysis for quantitative intracellular metabolomics. *Metabolites* 2, 1012–1030. doi: 10.3390/metabo2041012

Trötschel, C., Albaum, S. P., and Poetsch, A. (2013). Proteome turnover in bacteria: current status for *Corynebacterium glutamicum* and related bacteria. *Microb. Biotechnol.* 6, 708–719. doi: 10.1111/1751-7915.12035

Unthan, S., Baumgart, M., Radek, A., Herbst, M., Siebert, D., Brühl, N., et al. (2015). Chassis organism from *Corynebacterium glutamicum* – a top-down approach to identify and delete irrelevant gene clusters. *Biotechnol. J.* 10, 290–301. doi: 10.1002/biot.201400041

Unthan, S., Grünberger, A., Van Ooyen, J., Gätgens, J., Heinrich, J., Paczia, N., et al. (2014). Beyond growth rate 0.6: What drives *Corynebacterium glutamicum* to higher growth rates in defined medium. *Biotechnol. Bioeng.* 111, 359–371. doi: 10.1002/bit.25103

Uy, D., Delaunay, S., Engasser, J. M., and Goergen, J. L. (1999). A method for the determination of pyruvate carboxylase activity during the glutamic acid fermentation with *Corynebacterium glutamicum*. *J. Microbiol. Methods* 39, 91–96. doi: 10.1016/S0167-7012(99)00104-9

Van Der Rest, M. E., Lange, C., and Molenaar, D. (1999). A heat shock following electroporation induces highly efficient transformation of *Corynebacterium glutamicum* with xenogeneic plasmid DNA. *Appl. Microb. Biotechnol.* 52, 541–545. doi: 10.1007/s002530051557

Voges, R., Corsten, S., Wiechert, W., and Noack, S. (2015). Absolute quantification of *Corynebacterium glutamicum* glycolytic and anaplerotic enzymes by QconCAT. *J. Proteomics* 113, 366–377. doi: 10.1016/j.jprot.2014.10.008

Voges, R., and Noack, S. (2012). Quantification of proteome dynamics in *Corynebacterium glutamicum* by ^{15}N-labeling and selected reaction monitoring. *J. Proteomics* 75, 2660–2669. doi: 10.1016/j.jprot.2012.03.020

Wendisch, V. F., Spies, M., Reinscheid, D. J., Schnicke, S., Sahm, H., and Eikmanns, B. J. (1997). Regulation of acetate metabolism in *Corynebacterium*

glutamicum: transcriptional control of the isocitrate lyase and malate synthase genes. *Arch. Microbiol.* 168, 262–269. doi: 10.1007/s002030050497

Zelle, R. M., Harrison, J. C., Pronk, J. T., and Van Maris, A. J. (2011). Anaplerotic role for cytosolic malic enzyme in engineered *Saccharomyces cerevisiae* strains. *Appl. Environ. Microbiol.* 77, 732–738. doi: 10.1128/AEM.02132-10

Zimmermann, M., Sauer, U., and Zamboni, N. (2014). Quantification and mass isotopomer profiling of alpha-keto acids in central carbon metabolism. *Anal. Chem.* 86, 3232–3237. doi: 10.1021/ac500472c

Conflict of Interest: The authors declare that the research was conducted in the absence of any commercial or financial relationships that could be construed as a potential conflict of interest.

frontiers in Bioengineering and Biotechnology

ORIGINAL RESEARCH
published: 30 March 2021
doi: 10.3389/fbioe.2021.650961

Coenzyme Q_{10} Biosynthesis Established in the Non-Ubiquinone Containing *Corynebacterium glutamicum* by Metabolic Engineering

*Arthur Burgardt[1], Ayham Moustafa[1], Marcus Persicke[2], Jens Sproß[3], Thomas Patschkowski[2], Joe Max Risse[4], Petra Peters-Wendisch[1], Jin-Ho Lee[5] and Volker F. Wendisch[1]**

[1] Genetics of Prokaryotes, Faculty of Biology and Center for Biotechnology (CeBiTec), Bielefeld University, Bielefeld, Germany, [2] Technology Platform Genomics, Center for Biotechnology (CeBiTec), Bielefeld University, Bielefeld, Germany, [3] Industrial Organic Chemistry and Biotechnology, Department of Chemistry, Bielefeld University, Bielefeld, Germany, [4] Fermentation Technology, Technical Faculty and Center for Biotechnology (CeBiTec), Bielefeld University, Bielefeld, Germany, [5] Major in Food Science & Biotechnology, School of Food Biotechnology & Nutrition, Kyungsung University, Busan, South Korea

OPEN ACCESS

Edited by:
Jens O. Krömer,
Helmholtz Centre for Environmental Research (UFZ), Germany

Reviewed by:
Michael Bott,
Institute for Bio and Earth Sciences Biotechnology (IBG-1), Germany
Nils Jonathan Helmuth Averesch,
Stanford University, United States

***Correspondence:**
Volker F. Wendisch
volker.wendisch@uni-bielefeld.de

Specialty section:
This article was submitted to Synthetic Biology, a section of the journal Frontiers in Bioengineering and Biotechnology

Received: 08 January 2021
Accepted: 22 February 2021
Published: 30 March 2021

Citation:
Burgardt A, Moustafa A, Persicke M, Sproß J, Patschkowski T, Risse JM, Peters-Wendisch P, Lee J-H and Wendisch VF (2021) Coenzyme Q_{10} Biosynthesis Established in the Non-Ubiquinone Containing Corynebacterium glutamicum by Metabolic Engineering. Front. Bioeng. Biotechnol. 9:650961. doi: 10.3389/fbioe.2021.650961

Coenzyme Q_{10} (CoQ10) serves as an electron carrier in aerobic respiration and has become an interesting target for biotechnological production due to its antioxidative effect and benefits in supplementation to patients with various diseases. For the microbial production, so far only bacteria have been used that naturally synthesize CoQ10 or a related CoQ species. Since the whole pathway involves many enzymatic steps and has not been fully elucidated yet, the set of genes required for transfer of CoQ10 synthesis to a bacterium not naturally synthesizing CoQ species remained unknown. Here, we established CoQ10 biosynthesis in the non-ubiquinone-containing Gram-positive *Corynebacterium glutamicum* by metabolic engineering. CoQ10 biosynthesis involves prenylation and, thus, requires farnesyl diphosphate as precursor. A carotenoid-deficient strain was engineered to synthesize an increased supply of the precursor molecule farnesyl diphosphate. Increased farnesyl diphosphate supply was demonstrated indirectly by increased conversion to amorpha-4,11-diene. To provide the first CoQ10 precursor decaprenyl diphosphate (DPP) from farnesyl diphosphate, DPP synthase gene *ddsA* from *Paracoccus denitrificans* was expressed. Improved supply of the second CoQ10 precursor, *para*-hydroxybenzoate (pHBA), resulted from metabolic engineering of the shikimate pathway. Prenylation of pHBA with DPP and subsequent decarboxylation, hydroxylation, and methylation reactions to yield CoQ10 was achieved by expression of *ubi* genes from *Escherichia coli*. CoQ10 biosynthesis was demonstrated in shake-flask cultivation and verified by liquid chromatography mass spectrometry analysis. To the best of our knowledge, this is the first report of CoQ10 production in a non-ubiquinone-containing bacterium.

Keywords: coenzyme Q_{10} (CoQ 10), *Corynebacterium glutamicum*, metabolic engineering, isoprenoids, aromatic compounds, fermentation

INTRODUCTION

Coenzyme Q_{10} (CoQ10), also referred to as ubiquinone-10, is a lipid-soluble quinone (CoQ) that serves as an electron carrier in the electron transport chain of aerobic respiration and is widely distributed among organisms (Kawamukai, 2002). Besides its function in cell respiration, it is known to act as an antioxidant by protection of lipids against peroxidation and prevention of oxidative damage to mitochondrial proteins and DNA (Ernster and Dallner, 1995), a property that makes it interesting as an agent against skin aging in the cosmetic industry (Vinson and Anamandla, 2006). Medical studies showed that the supplementation of CoQ10 may be beneficial for patients with diabetes and heart failures (Hodgson et al., 2002; Weant and Smith, 2005) as well as for patients with neurologic diseases like Alzheimer's and Parkinson's disease (Yang et al., 2010; Mischley et al., 2012).

Coenzyme Q_{10} consists of the aromatic 2,3-dimethoxy-5-methyl-benzoquinone and a side chain of ten isoprenoid units. It is naturally synthesized from the two precursors decaprenyl diphosphate (DPP) and *para*-hydroxybenzoate (pHBA). The length of the polyprenyl diphosphate determines the CoQ species in *E. coli* (Asai et al., 1994). The condensation of octaprenyl diphosphate at the C3 position of pHBA is mediated by octaprenyltransferase UbiA and several subsequent modifications at the aromatic ring yield coenzyme Q_8 (CoQ8) (Young et al., 1972). In fact, UbiA promiscuously recognizes isoprenoid diphosphates of different lengths (Suzuki et al., 1994; Cheng and Li, 2014), which enabled production of CoQ10 in *E. coli* by merely expressing *ddsA* from *P. denitrificans*, coding for decaprenyl diphosphate synthase, to provide the precursor DPP (Takahashi et al., 2003).

The precursors for CoQ10, DPP, and pHBA are derived from the isoprenoid and shikimate pathways, respectively (**Figure 1**). The isoprenoid diphosphate DPP is synthesized in the 2-C-methyl-D-erythritol 4-phosphate (MEP) pathway that yields the two isomers dimethylallyl diphosphate (DMAPP) and isopentenyl diphosphate (IPP). In archaea, bacteria, and eukarya, they serve as the basis for a variety of isoprenoids like sterols, carotenoids, and ubiquinone, menaquinone, or secondary metabolites like mono-, sesqui-, and diterpenes (Rohmer and Rohmer, 1999). The *E. coli* farnesyl diphosphate (FPP) synthase IspA catalyzes the condensation of two IPP units with DMAPP or one IPP unit with geranyl diphosphate (GPP) to FPP (Fujisaki et al., 1990). Polyprenyltransferases add IPP units to FPP to generate polyprenyl diphosphates of various lengths. In CoQ10-containing bacteria such as *P. denitrificans*, *Agrobacterium tumefaciens*, and *Rhodobacter sphaeroides*, DPP is synthesized from FPP, e.g., by decaprenyl diphosphate synthase DdsA (Collins and Jones, 1981). The aromatic pHBA is synthesized from the shikimate pathway metabolite chorismate by chorismate-pyruvate lyase UbiC. The UbiC enzyme from *E. coli* shows product inhibition; however, this could be overcome in the feedback-resistant mutant $UbiC^{L31A}$. Use of $UbiC^{L31A}$ increased production of pHBA by engineered *C. glutamicum* by about 55% as compared to wild-type UbiC (Purwanto et al., 2018).

As a key step in CoQ10 synthesis, pHBA is prenylated with DPP by a 4-hydroxybenzoate polyprenyltransferase, yielding 3-decaprenyl-4-hydroxybenzoate (Takahashi et al., 2003). This intermediate is then modified in a series of reactions involving a decarboxylation, three hydroxylation, and three methylation steps (**Figure 1** and **Supplementary Figure 1**). In *E. coli*, enzymes UbiD, UbiI, UbiG, UbiH, UbiE, and UbiF are known to catalyze these reactions; however, the functions of other proteins such as UbiB, UbiJ, and UbiK in CoQ8 biosynthesis have not yet been fully elucidated (Aussel et al., 2014b). Because *ubiX* and *ubiD* mutants both accumulated 3-octaprenyl-4-hydroxybenzoate and produced low levels of CoQ8, both gene products were thought to act as decarboxylases (Gulmezian et al., 2007), More recently, it was discovered that UbiX actually prenylates flavin mononucleotide with DMAP to generate a cofactor required for UbiD activity (White et al., 2015). The first hydroxylation step is catalyzed by UbiI (not by UbiB as formerly believed) (Hajj Chehade et al., 2013). UbiB lacks conserved motifs characteristic for hydroxylases but might act as a putative kinase that is involved in CoQ synthesis; however, studies on UbiB activity are lacking (Hajj Chehade et al., 2013). To date, the catalytic mechanism of UbiJ and UbiK is not fully understood, but mutants of *ubiJ* and *ubiK* showed decreased amounts of CoQ8 and accumulation of the precursor octaprenylphenol. Additionally, UbiJ and UbiK form a complex that interacts with the major lipid palmitoleic acid in *E. coli* (Loiseau et al., 2017). While the catalytic functions of many of these enzymes are known, the roles of UbiB, UbiJ, and UbiK remain elusive. Thus, since the set of enzymes required and sufficient for CoQ synthesis is not known, approaches to biotechnological CoQ10 production were hitherto based on microorganisms that natively contain ubiquinones and, thus, possess all necessary genes for CoQ biosynthesis.

Biotechnological CoQ10 production was achieved after classical mutagenesis and screening of native CoQ10-producing bacteria like *A. tumefaciens* and *R. sphaeroides*, (Ha et al., 2008; Kien et al., 2010; Yuan et al., 2012). These bacteria were also subjected to metabolic engineering (Koo et al., 2010; Lu et al., 2015; Zhang et al., 2018; Chen et al., 2019) as well as the model bacterium *E. coli* (Takahashi et al., 2003; Park et al., 2005; Zahiri et al., 2006). Metabolically engineered *A. tumefaciens* and *R. sphaeroides* strains outperformed engineered *E. coli* strains with regard to CoQ10 production. For instance, cellular CoQ10 contents of 4.59 mg g^{-1} DCW (Zhang et al., 2018) and 12.94 mg g^{-1} DCW (Lu et al., 2015) were achieved with metabolically engineered *R. spharoides* strains as compared to 0.29 mg g^{-1} DCW (Park et al., 2005) and 2.43 mg g^{-1} DCW (Zahiri et al., 2006) with recombinant *E. coli* strains.

Electron carriers in the electron transport chain of aerobic bacteria that lack CoQ are, for example, menaquinones (MK) and dihydromenaquinones [MK(H2)] (Collins et al., 1977; Collins and Jones, 1981). The Gram-positive, rod-shaped bacterium *C. glutamicum* belongs to this type of bacteria, and it possesses MK9(H2) and MK8(H2) as electron carriers. Similar to ubiquinones, dihydromenaquinones contain an aromatic and a prenyl moiety. The aromatic moiety in MK is a bicyclic menaquinone, not a monocyclic ubiquinone. Moreover, as

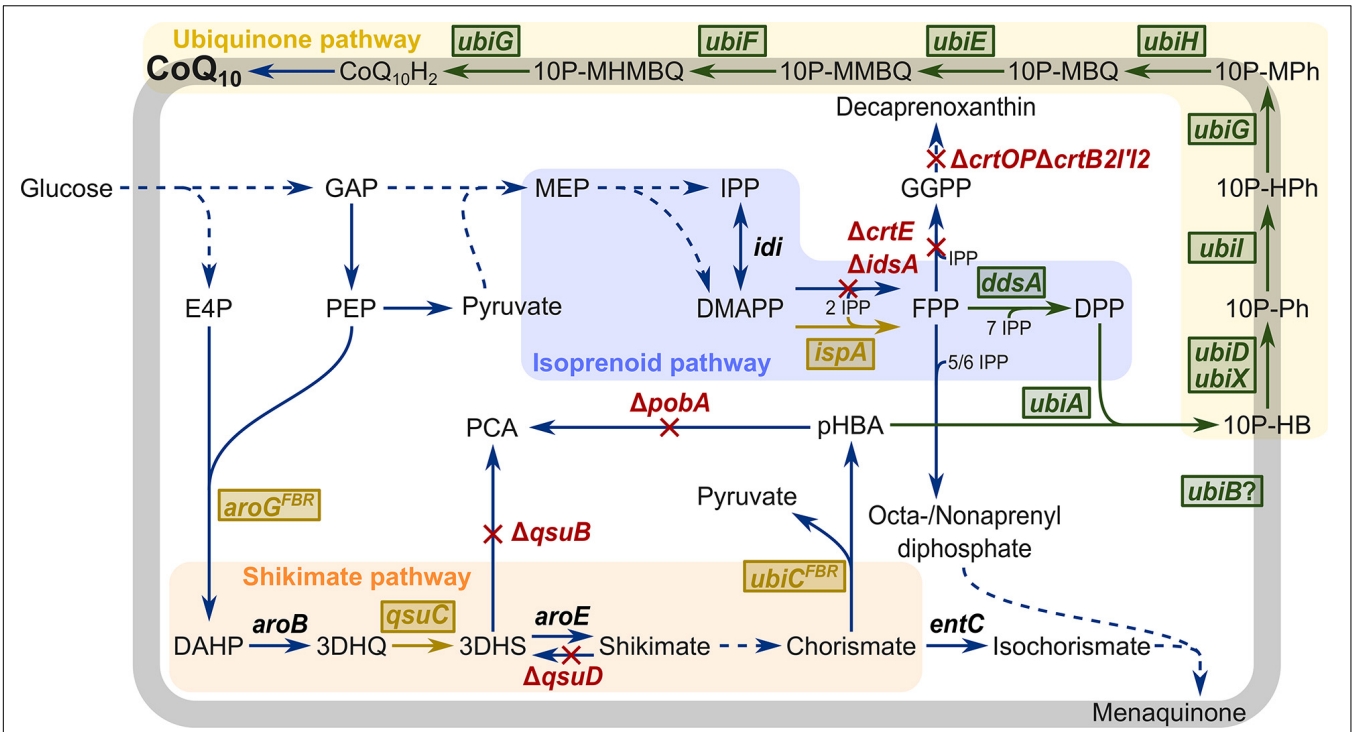

FIGURE 1 | Schematic overview of metabolic engineering of *C. glutamicum* for CoQ10 production. Heterologous plasmid-driven expression of genes is visualized in green boxes. Chromosomal overexpression of native and heterologous genes is visualized in yellow boxes. Deletion of genes is visualized in red. E4P, erythrose 4-phosphate; DAHP, 3-deoxy-D-arabinoheptulosonate 7-phosphate; 3DHQ, 3-dehydroquinate; 3DHS, 3-dehydroshikimic acid; PCA, protocatechuic acid; pHBA, *para*-hydroxybenzoate; GAP, glyceraldehyde 3-phosphate; PEP, phosphoenolpyruvate; MEP, 2-C-methylerythritol 4-phosphate; IPP, isopentenyl diphosphate; DMAPP, dimethylallyl diphosphate; GPP, geranyl diphosphate; FPP, farnesyl diphosphate; GGPP, geranylgeranyl diphosphate; DPP, decaprenyl diphosphate, 10P-HB, 3-decaprenyl-4-hydroxybenzoate; 10P-Ph, 2-decaprenylphenol; 10P-HPh, 2-decaprenyl-6-hydroxyphenol; 10P-MPh, 2-decaprenyl-6-methoxyphenol; 10P-MBQ, 2-decaprenyl-6-methoxy-1,4-benzoquinol; 10P-MMBQ, 2-decaprenyl-3-methyl-6-methoxy-1,4-benzoquinol; 10P-MHMBQ, 2-decaprenyl-3-methyl-5-hydroxy-6-methoxy-1,4-benzoquinol; $CoQ_{10}H_2$, ubiquinol-10; CoQ_{10}, ubiquinone-10; *aroG*^{FBR}, feedback-resistant DAHP synthase from *E. coli*; *aroB*, 3-dehydroquinate synthase; *qsuC*, 3-dehydroquinate dehydratase; *qsuB*, 3-dehydroshikimate dehydratase; *qsuD*, shikimate dehydrogenase; *aroE*, shikimate dehydrogenase; *ubiC*^{FBR}, feedback-resistant chorismate-pyruvate lyase from *E. coli*; *entC*, isochorismate synthase; *pobA*, *para*-hydroxybenzoate hydroxylase; *idi*, isopentenyl diphosphate isomerase; *crtE*, geranylgeranyl diphosphate synthase; *idsA*, geranylgeranyl diphosphate synthase; *ispA*, farnesyl diphosphate synthase; *crtOP*, cg0717-cg0723; *crtB2I'I2*, cg2668-cg2672; *ddsA*, decaprenyl diphosphate synthase from *P. denitrificans*; *ubiA*, 4-hydroxybenzoate octaprenyltransferase; *ubiD*, 3-octaprenyl-4-hydroxybenzoate decarboxylase; *ubiX*, flavin prenyltransferase; *ubiI*, 2-octaprenylphenol hydroxylase; *ubiG*, 2-octaprenyl-6-hydroxyphenol/2-octaprenyl-3-methyl-5-hydroxy-6-methoxy-1,4-benzoquinol methyltransferase; *ubiH*, 2-octaprenyl-6-methoxyphenol hydroxylase; *ubiE*, ubiquinone/menaquinone biosynthesis methyltransferase; *ubiF*, 2-octaprenyl-3-methyl-6-methoxy-1,4-benzoquinol hydroxylase; *ubiB*, probably protein kinase, function unknown.

opposed to CoQ biosynthesis, the aromatic precursor is almost fully modified before being prenylated in the second to last step of MK biosynthesis (Meganathan and Kwon, 2009). *C. glutamicum* is used in the food and feed industry for the million-ton-scale amino acid production (Eggeling and Bott, 2015; Wendisch, 2020). *C. glutamicum* shows stable growth to high cell densities (Riesenberg and Guthke, 1999; Pfeifer et al., 2017) and has been engineered for production of, e.g., *N*-functionalized amino acids (Mindt et al., 2020), diamines (Wendisch et al., 2018; Chae et al., 2020), alcohols (Jojima et al., 2015; Siebert and Wendisch, 2015), and organic acids (Wieschalka et al., 2013; Purwanto et al., 2018). With respect to production of molecules originating from the shikimate or isoprenoid pathways, metabolic engineering enabled production of terpenoids such as pinene (Kang et al., 2014), patchoulol (Henke et al., 2018), valencene (Frohwitter et al., 2014), or various carotenoids (Heider et al., 2014b,c; Henke et al., 2016) and of aromatic or aromatic-derived compounds such as muconic acid (Becker et al., 2018; Shin et al., 2018), phenylpropanoids (Kallscheuer et al., 2016, 2017), 4-aminobenzoate (Kubota et al., 2016), shikimate (Sato et al., 2020), protocatechuate (Kogure et al., 2020), 4-hydroxybenzyl alcohol (Kim et al., 2020), and pHBA (Kitade et al., 2018; Purwanto et al., 2018).

Therefore, in this work, in a step-by-step approach CoQ10 biosynthesis was enabled in *C. glutamicum*. Based on our previous work (Henke et al., 2018; Purwanto et al., 2018), a modular approach was followed: (1) supply of isoprenoid precursor FPP and its conversion to DPP, (2) supply of aromatic precursor pHBA, and (3) prenylation of pHBA followed by sequential modification of the aromatic moiety leading to CoQ10. Establishing CoQ10 production in a microorganism naturally lacking ubiquinone was achieved.

MATERIALS AND METHODS

Bacterial Strains and Growth Conditions

Bacterial strains used in this study are listed in **Table 1**. *E. coli* DH5α (Hanahan, 1983) was used for plasmid construction. *C. glutamicum* ATCC 13032 was used as platform strain for metabolic engineering. *E. coli ubi* mutants were used for experimental verification of plasmid expression. Pre-cultures of *E. coli* and *C. glutamicum* were performed in lysogeny broth (LB) and brain heart infusion (BHI) medium at 37°C and 30°C in baffled shake flasks on a rotary shaker at 160 rpm and 120 rpm, respectively. Cultures were inoculated from fresh LB agar plates. For growth and production experiments, *C. glutamicum* cells from pre-cultures were washed once with TN buffer pH 6.3 (10 mM Tris–HCl, 150 mM NaCl), inoculated to an optical density at 600 nm (OD_{600}) of 1 in CGXII minimal medium (Eggeling and Bott, 2005) with 40 g L^{-1} glucose as sole carbon source and incubated at 30°C and 120 rpm (shaking diameter 16.5 cm). OD_{600} was measured using a V-1200 spectrophotometer (VWR, Radnor, PA, United States). For amorpha-4,11-diene (amorphadiene) production, 10% (v/v) of dodecane and 1 mM of isopropyl-β-D-1-thiogalactopyranoside (IPTG) were added to the minimal medium after 6 hours of cultivation to capture the volatile product. The *E. coli ubi* mutant complementation experiment was performed in an M9 minimal medium (Sambrook et al., 1989) with 20 mM of succinate as sole carbon source. LB pre-cultures were washed once in TN buffer, inoculated to an OD_{600} of 0.1 or 0.01 in 3 mL of M9 minimal medium in Duetz plates (Duetz et al., 2000) and incubated at 37°C and 220 rpm. When necessary, kanamycin (25 μg mL^{-1}), spectinomycin (100 μg mL^{-1}), and tetracycline (5 μg mL^{-1}) were added to the medium. To induce gene expression from the vectors pVWEx1 (Peters-Wendisch et al., 2001), pEKEx3 (Stansen et al., 2005), and pEC-XT99A (Kirchner and Tauch, 2003), 1 mM of IPTG was added. For expression of *ddsA* and *ubiA* from pRG_Duet2 (Gauttam et al., 2019), 1 mM of IPTG and 0.25 μg mL^{-1} of anhydrotetracycline (ATc) were added, respectively.

Recombinant DNA Work and Strain Construction

Standard molecular genetic techniques were performed as described (Green and Sambrook, 2012). Competent *E. coli* DH5α cells were prepared according to the RbCl method and transformation was performed by heat shock (Green and Sambrook, 2012). *C. glutamicum* was transformed via electroporation (Eggeling and Bott, 2005) at 2.5 kV, 200 Ω, and 25 μF. PCR amplification was performed with Phusion High-Fidelity DNA polymerase and ALLin™ HiFi DNA Polymerase according to the manufacturer (New England Biolabs, United Kingdom, or highQu GmbH, Germany) using the primers specified in **Table 3**. As template for all *ubi* genes, genomic DNA from *E. coli* K-12 MG1655 was used, *ddsA* was amplified from *P. denitrificans* genomic DNA, and the construct P_{tuf}-*ispA* was amplified from pSH1-*ispA*. For the restriction of plasmids pVWEx1, pEKEx3, pEC-XT99A, and pK19*mobsacB* (Schäfer et al., 1994), *Bam*HI was used. Restriction of the dual-inducible plasmid pRG_Duet2 was carried out with *Bam*HI for insertion of *ddsA* and with *Nhe*I for insertion of *ubiA*. Plasmid construction was performed via Gibson Assembly (Gibson et al., 2009), and plasmids are listed in **Table 2**. Correctness of constructs was verified by insert sequencing. Deletion and replacement of chromosomal regions were carried out by using the suicide vector pK19*mobsacB* and two-step homologous recombination as described (Heider et al., 2014b). Transfer of the suicide vectors was done by trans-conjugation using *E. coli* S17-1 as donor strain (Eggeling and Bott, 2005), and selection of recombinants was made by kanamycin resistance after the first recombination and sucrose sensitivity after the second recombination. Mutants were verified by PCR and sequencing using the primers specified in **Table 3**.

Quantification of Amorphadiene

For analysis of amorphadiene production, dodecane supernatants from shake-flask cultivation were analyzed via gas chromatography-mass spectroscopy (GC-MS) as described (Henke et al., 2018) using a TraceGC gas chromatograph (Thermo Scientific, Waltham, MA, United States) and ISQ ion trap mass spectrometer (Thermo Scientific, Waltham, MA, United States) equipped with an AS 3000 autosampler (Thermo Scientific, Schwerte, Germany). A 30 m × 0.25 mm VF-5 column coated with 0.25 μm of 5% diphenyl and 95% of dimethylsiloxane (Varian GmbH, Darmstadt, Germany) was used. Temperatures for injector, interface, and ion source were set to 250°C, 250°C, and 220°C, respectively. 1 μl of sample was injected in splitless mode. Helium was used as carrier gas at 1 mL min^{-1}. The oven temperature was set to 80°C for one minute, raised to 120°C at 10°C min^{-1}, raised to 160°C at 3°C min^{-1} and further to 270°C at 10 °C min^{-1}, held for 2 min. Mass spectra were recorded after the dodecane peak eluted at 12 min with a scanning range of *m/z* 50–750 at 20 scans s^{-1}. Chromatograms were evaluated with Xcalibur software version 2.0.7 (Thermo Scientific, Germany). The NIST 05 library (National Institute of Standards and Technology, Gaithersburg, MD, United States; Thermo Finnigan) was used to identify valencene and amorphadiene. Due to the lack of a commercial amorphadiene standard, valencene was used as a standard equivalent and internal standard.

Crude Extract Preparation and SDS–PAGE

Cultures for crude extract preparation were inoculated in the BHI medium with 1 mM IPTG and antibiotics as described above and grown overnight. Cells were harvested, washed in TN buffer, and stored at −20°C until further use. All following steps were performed on ice. Cells were resuspended in 2 mL TN buffer and sonicated (UP200S, Hielscher Ultrasonics GmbH, Teltow, Germany) for 9 min at an amplitude of 60% and a cycle of 0.5. The lysed cells were centrifuged at 20,200 *g* and 4°C for 60 min. The protein concentration of the supernatant was determined by the Bradford method (Bradford, 1976) with bovine serum albumin as reference. Sodium dodecyl sulfate

TABLE 1 | Strains used in this work.

Strains	Description	Source
C. glutamicum		
WT	Wild type, ATCC 13032	ATCC
WT (pVWEx1)	WT carrying pVWEx1	This work
WT (pVWEx1-*ddsA*)	WT carrying pVWEx1-*ddsA*	This work
WT (pVWEx1-ADS)	WT carrying pVWEx1-ADS	This work
Δ*crtOP*Δ*idsA*Δ*crtB2I'I2*	WT carrying deletion of *crtOP* (cg0717-cg0723), *idsA* (cg2384), and *crtB2I'I2* (cg2668-cg2672)	Henke et al., 2018
UBI000	LP4::P_{tuf}-*ispA* mutant of *C. glutamicum* Δ*crtOP*Δ*idsA*Δ*crtB2I'I2*	This work
UBI000 (pVWEx1-ADS)	UBI000 carrying pVWEx1-ADS	This work
UBI000 (pEC-XT99A)	UBI000 carrying pEC-XT99A	This work
UBI000 (pEC-XT99A-*ubiDIBX*)	UBI000 carrying pEC-XT99A-*ubiDIBX*	This work
UBI000 (pEKEx3)	UBI000 carrying pEKEx3	This work
UBI000 (pEKEx3-*ubiGHEF*)	UBI000 carrying pEKEx3-*ubiGHEF*	This work
UBI100	Δ*pobA* mutant of UBI000	This work
UBI200	Δ*pcaHG*::P_{sod}-*ubiC*^{FBR} mutant of UBI100	This work
UBI300	Δ*vdh*::P_{llvC}-*aroG*^{FBR} mutant of UBI200	This work
UBI400	Δ*qsuABCD*::P_{tuf}-*qsuC* mutant of UBI300	This work
UBI401	UBI400 carrying pVWEx4	This work
UBI405	UBI400 carrying pRG_Duet2-*ddsA*-*ubiA*	This work
UBI412	UBI400 carrying pRG_Duet2-*ddsA*-*ubiA* and pEC-XT99A-*ubiDIBX*	This work
UBI413	UBI400 carrying pRG_Duet2-*ddsA*-*ubiA*, pEC-XT99A-*ubiDIBX* and pEKEx3-*ubiGHEF*	This work
E. coli		
K-12	K-12 MG1655 wild type, ATCC 47076	ATCC
DH5α	*F-thi-1 endA1 hsdr17(r-, m-) supE44 1lacU169 (Φ80lacZ1M15) recA1 gyrA96*	Hanahan, 1983
S17-1	*recA pro hsdR* RP4-2-Tc::Mu-Km::Tn7	Simon et al., 1983
Δ*ubiG*	F-, Δ*(araD-araB)567*, Δ*lacZ4787*(::rrnB-3), λ$^-$, Δ*ubiG785::kan*, *rph-1*, Δ*(rhaD-rhaB)568*, *hsdR514*	Baba et al., 2006
Δ*ubiG* (pEKEx3)	Δ*ubiG* carrying pEKEx3	This work
Δ*ubiG* (pEKEx3-*ubiG*)	Δ*ubiG* carrying pEKEx3-*ubiG*	This work
Δ*ubiH*	F-, Δ*(araD-araB)567*, Δ*lacZ4787*(::rrnB-3), λ$^-$, Δ*ubiH758::kan*, *rph-1*, Δ*(rhaD-rhaB)568*, *hsdR514*	Baba et al., 2006
Δ*ubiH* (pEKEx3)	Δ*ubiH* carrying pEKEx3	This work
Δ*ubiH* (pEKEx3-*ubiG*)	Δ*ubiH* carrying pEKEx3-*ubiG*	This work
Δ*ubiH* (pEKEx3-*ubiGH*)	Δ*ubiH* carrying pEKEx3-*ubiGH*	This work
Δ*ubiE*	F-, Δ*(araD-araB)567*, Δ*lacZ4787*(::rrnB-3), λ$^-$, Δ*ubiE778::kan*, *rph-1*, Δ*(rhaD-rhaB)568*, *hsdR514*	Baba et al., 2006
Δ*ubiE* (pEKEx3)	Δ*ubiE* carrying pEKEx3	This work
Δ*ubiE* (pEKEx3-*ubiGH*)	Δ*ubiE* carrying pEKEx3-*ubiGH*	This work
Δ*ubiE* (pEKEx3-*ubiGHEF*)	Δ*ubiE* carrying pEKEx3-*ubiGHEF*	This work
Δ*ubiF*	F-, Δ*(araD-araB)567*, Δ*lacZ4787*(::rrnB-3), λ$^-$, Δ*ubiF722::kan*, *rph-1*, Δ*(rhaD-rhaB)568*, *hsdR514*	Baba et al., 2006
Δ*ubiF* (pEKEx3)	Δ*ubiF* carrying pEKEx3	This work
Δ*ubiF* (pEKEx3-*ubiGH*)	Δ*ubiF* carrying pEKEx3-*ubiGH*	This work
Δ*ubiF* (pEKEx3-*ubiGHEF*)	Δ*ubiF* carrying pEKEx3-*ubiGHEF*	This work

polyacrylamide electrophoresis (SDS–PAGE) was performed as described (Green and Sambrook, 2012), loading 10 μg of protein samples.

LC-MS/MS Analysis of Ubi Proteins

To verify the expression of *ubi* genes, proteins were, on the one hand, isolated from induced cells and, on the other hand, excised from SDS–PAGE at their expected positions for LC-MS/MS analysis. Proteins from SDS–PAGE were transferred to tubes which had previously been washed with trifluoroacetic acid:acetonitrile:H_2O (0.1:60:40 *v*/v) and were digested with trypsin (Trypsin Gold, Promega) overnight as previously described (Shevchenko et al., 2006). For protein isolates, a simple "single-tube" preparation protocol was used (Wang et al., 2005). Bacterial cell pellets were resuspended in 200 μl 100 mM ammonium bicarbonate and subsequently transferred into 2-ml screw caps with 0.5 g of zirconia/silica micro beads of the size 0.01 mm (Bio Spec Products Inc., Bartlesville, OK, United States). Cells were disrupted five times in a Precellys homogenizer (VWR, Darmstadt, Germany) at 6.5 m/s for 30 s. 100 μl of lysed cell extract was mixed with 100 μl of the organic solvent 2,2,2-trifluoroethanol and 5 μl 200 mM of the reducing agent dithiothreitol (DTT) and incubated for 60 min at 60°C. Alkylation of cysteines was performed by adding 20 μl of 200 mM 2-iodoacetamide and incubation for 90 min in the dark at room temperature. Alkylation was stopped by adding 5 ml of 200 mM DTT and incubation for 60 min at room

TABLE 2 | Plasmids used in this work.

Plasmids	Description	Source
pVWEx1	Kan^R, P_{tac}, $lacI^q$, pHM1519 $oriV_{Cg}$, *C. glutamicum/E. coli* expression shuttle vector	Peters-Wendisch et al., 2001
pVWEx1-*ddsA*	Kan^R, pVWEx1 overexpressing *ddsA* from *P. denitrificans*	This work
pVWEx1-ADS	Kan^R, pVWEx1 overexpressing ADS from *A. annua*	This work
pSH1-*ispA*	Kan^R, P_{tuf}. pHM1519 $oriV_{Cg}$, *C. glutamicum/E. coli* expression shuttle vector overexpressing *ispA* from *E. coli*	This work
pRG_Duet2	Kan^R, P_{tac}, $lacI^q$, $P_{tetR/tetA}$, *tetR*, pBL1 $oriV_{Cg}$, dual-inducible *C. glutamicum/E. coli* expression shuttle vector	Gauttam et al., 2019
pRG_Duet2-*ddsA*-*ubiA*	Kan^R, pRG_Duet2 overexpressing *ddsA* from *P. denitrificans* (induced by IPTG) and *ubiA* from *E. coli* (induced by ATc)	This work
pEKEx3	$Spec^R$, P_{tac}, $lacI^q$, pBL1 $oriV_{Cg}$, *C. glutamicum/E. coli* expression shuttle vector	Stansen et al., 2005
pEKEx3-*ubiG*	$Spec^R$, pEKEx3 overexpressing *ubiG* from *E. coli*	This work
pEKEx3-*ubiGH*	$Spec^R$, pEKEx3 overexpressing *ubiG* and *ubiH* from *E. coli*	This work
pEKEx3-*ubiGHEF*	$Spec^R$, pEKEx3 overexpressing *ubiG*, *ubiH*, *ubiE* and *ubiF* from *E. coli*	This work
pEC-XT99A	Tet^R, P_{trc}, $lacI^q$, pGA1 $oriV_{Cg}$, *C. glutamicum/E. coli* expression shuttle vector	Kirchner and Tauch, 2003
pEC-XT99A-*ubiDIBX*	Tet^R, pEC-XT99A overexpressing *ubiD*, *ubiI*, *ubiB* and *ubiX* from *E. coli*	This work
pK19*mobsacB*	Km^R, pK19 $oriV_{Ec}$, *sacB*, *lacZα*, *E. coli/C. glutamicum* shuttle vector for construction of insertion and deletion mutants in *C. glutamicum*	Schäfer et al., 1994
pK19*mobsacB*-LP4::P_{tuf}-*ispA*	pK19*mobsacB* with a construct for insertion of *ispA* from *E. coli* K-12 under control of *C. glutamicum* promoter P_{tuf} into CgLP4	This work
pK19*mobsacB*-Δ*pobA*	pK19*mobsacB* with a construct for deletion of *pobA* (cg1226), which has been amplified from APS529 (Purwanto et al., 2018) with the primers pobA-fw and pobA-rv	This work
pK19*mobsacB*-Δ*pcaHG*::P_{sod}-*ubiC*^{FBR}	pK19*mobsacB* with a construct for deletion of *pcaHG* (cg2631-cg2630) and insertion of *ubiC*^{L31A} from *E. coli* K-12 under control of *C. glutamicum* promoter P_{sod}	Purwanto et al., 2018
pK19*mobsacB*-Δ*vdh*::P_{ilvC}-*aroG*^{FBR}	pK19*mobsacB* with a construct for deletion of *vdh* (cg2953) and insertion of *aroG*^{D146N} from *E. coli* K-12 under control of *C. glutamicum* promoter P_{ilvC}, which has been amplified from APS529 (Purwanto et al., 2018) with the primers vdh-fw and vdh-rv	This work
pK19*mobsacB*-Δ*qsuABCD*::P_{tuf}-*qsuC*	pK19*mobsacB* with a construct for deletion of *qsuABCD* (cg0501-cg0504) and insertion of *qsuC* (cg0503) under control of *C. glutamicum* promoter P_{tuf}	Walter et al., 2020

temperature. For tryptic digestion, samples were diluted 1:10 with 50 mM ammonium bicarbonate. Tryptic digestion was performed at 37°C overnight. Digested peptides were purified using Sep-Pak® Vac 1cc C18 columns (Waters, Milford, CT, United States). Peptide quantification was done using NanoDrop™ 2000 (Peqlab).

Peptides were analyzed by a nanoLC (Ultimate 3000, Thermo Fisher Scientific, Germany) coupled to an ESI-Orbitrap MS/MS (QExactive Plus, Thermo Fisher Scientific, Germany). The effective gradient length of the 25-cm Acclaim™ PepMap™ 100 C18 analytical column was adjusted to 60 min from 4 to 30% of 80% acetonitrile and 0.1% formic acid followed by 7 min from 30 to 50% of 80% acetonitrile and 0.1% formic acid at a flow rate of 300 nl min^{-1}. All samples were measured in full MS mode using a resolution of 70.000 (AGC target of 3e6 and 64 ms maximum IT). For the dd-MS2, a resolution of 17.500 (AGC target of 2e5 and 200 ms maximum IT) was used.

Data analysis was done using the Proteome Discoverer™ Software version 2.4 (Thermo Fisher Scientific, Germany). A *C. glutamicum* protein database, supplemented with the FASTA sequences of the overexpressed *E. coli* proteins, was used. For protein identification, a digestion enzyme was set to trypsin and the maximum number of missed cleavages was set to two. Carbamidomethylation of cysteine was set as a fixed modification. Variable modifications were set as follows: oxidation of methionine, N-terminal acetylation, and N-terminal loss of methionine. A false discovery rate (FDR) of 0.01 was selected for protein and peptide identification.

Quantification of Metabolites via HPLC

High-performance liquid chromatography (HPLC) was applied for analysis of total carotenoids, pHBA, and protocatechuate (PCA) and quinones, following different sample preparation and HPLC protocols. For all analytes, the Agilent 1200 series system (Agilent Technologies Deutschland GmbH, Böblingen, Germany) with a precolumn (LiChrospher 100 RP18 EC-5 μ (40 × 4 mm), CS Chromatographie Service GmbH, Langerwehe, Germany), and a main column (LiChrospher 100 RP18 EC-5 μ (125 × 4 mm), CS Chromatographie Service GmbH) was used.

For carotenoid analysis from *C. glutamicum*, 1 mL of the culture was harvested by centrifugation (20,200 *g*, 10 min) and the pellet was treated with 800 μl methanol:acetone (7:3) containing 0.05% butylhydroxytoluol at 60°C for 15 min under continuous shaking. Cell debris was spun down (20,000 g, 10 min), and the supernatant was used for HPLC analysis. The detection was carried out with a diode array detector (DAD) at 470 nm. Methanol/water (9:1) (A) and methanol (B) were used as mobile phase with the following gradient at a flow rate of 1.5 mL min^{-1}: 0 min B 100%, 10 min B 0%, 32.5 min B 0%. Total carotenoids were quantified by integration of all detected peaks and calculation of their sum.

TABLE 3 | Primers used in this work.

Primers	Sequence (5′ to 3′)
pVW-ddsA-fw / pRG-ddsA-fw	CCTGCAGGTCGACTCTAGAG**GAAAGGAGGCCCTTCAG**ATGGGCATGAACGAAAACGT
pVW-ddsA-rv / pRG-ddsA-rv	GAGCTCGGTACCCGGGGATCTCAGGACAGGCGCGAGACGA
pRG-ubiA-fw	AGAGGAGGAAAGGGTATACG**GAAAGGAGGCCCTTCAG**ATGGAGTGGAGTCTGACGCA
pRG-ubiA-rv	CAATTTAAATCCTAGGGCTATCAGAAATGCCAGTAACTCA
pG-ubiG-fw	CCTGCAGGTCGACTCTAGAGGTATAC**GAAAGGAGGCCCTTCAG**ATGAATGCCGAAAAATCGC
pG-ubiG-rv	GAGCTCGGTACCCGGGGATCTCACTTATTCTGCGTGTGC
pGH-ubiG-rv	GTAAGTCACTTATTCTGCGTGTGC
pGH-ubiH-fw	GCACACGCAGAATAAGTGACTTACCCGCGG**GAAAGGAGGCCCTTCAG**ATGAGCGTAATCATCGTCGGTGG
pGH-ubiH-rv	GAGCTCGGTACCCGGGGATCTCAACGCGCCACCCAACC
pGHEF-ubiH-rv	AAGAGTCAACGCGCCACCCAACC
pGHEF-ubiE-fw	GGTTGGGTGGCGCGTTGACTCTTCCATGG**GAAAGGAGGCCCTTCAG**ATGGTGGATAAGTCACAAG
pGHEF-ubiE-rv	GTGACTCAGAACTTATAACCACGATGC
pGHEF-ubiF-fw	GCATCGTGGTTATAAGTTCTGAGTCACGCTAGC**GAAAGGAGGCCCTTCAG**ATGACAAATCAACCAACGGAAATTGC
pGHEF-ubiF-rv	GAGCTCGGTACCCGGGGATCCTACAACCCTAACGCATATTTCAG
pDIBX-ubiD-fw	ACACAGGAAACAGACCATGGGCGGCCGC**GAAAGGAGGCCCTTCAG**ATGGACGCCATGAAATATAAC
pDIBX-ubiD-rv	GTAAGTCAGGCGCTTTTACCGTTG
pDIBX-ubiI-fw	CAACGGTAAAAGCGCCTGACTTACACTAGT**GAAAGGAGGCCCTTCAG**ATGCAAAGTGTTGATGTAGC
pDIBX-ubiI-rv	AAGAGTTAACGCAGCCATTCAGG
pDIBX-ubiB-fw	CCTGAATGGCTGCGTTAACTCTTGTTTAAAC**GAAAGGAGGCCCTTCAG**ATGACGCCAGGTGAAGTACG
pDIBX-ubiB-rv	GTGACTCAGCGTGTTTTGCGCCAAC
pDIBX-ubiX-fw	GTTGGCGCAAAACACGCTGAGTCACGCGATCGC**GAAAGGAGGCCCTTCAG**ATGAAACGACTCATTGTAGGCATCAG
pDIBX-ubiX-rv	CCGGGTACCGAGCTCGAATTTTATGCGCCCTGCCAGC
LP4-US-fw	CCTGCAGGTCGACTCTAGAGCCGTTCGGCTGACTCCTTC
LP4-US-rv	CATTCGCAGGGTAACGGCCACATCAAAAAATCCGCCGTTCCTTG
Ptuf-ispA-fw	CAAGGAACGGCGGATTTTTTGATGTGGCCGTTACCCTGCGAATG
ispA-Term-rv	CTTCCGCATCCAAACTCACTTAGTCAAAAGAGTTTGTAGAAACGCAAAAAGG
LP4-DS-fw	CCTTTTTGCGTTTCTACAAACTCTTTTGACTAAGTGAGTTTGGATGCGGAAG
LP4-DS-rv	GAGCTCGGTACCCGGGGATCCTCACTAGTACGCGGATAAATG
LP4-conf-fw	TCCGCTGATTGCAGATGGTC
LP4-conf-rv	GCTCCGACACAGAGTCAATG
pobA-fw	CCTGCAGGTCGACTCTAGAGAAATGCGGTGGTCCAGGCGTAGC
pobA-rv	GAGCTCGGTACCCGGGGATCCCAACCAAAGCCGTCGATAAGGAA
pobA-conf-fw	AAGGCCTGGTGTGAGTGCGTGAAA
pobA-conf-rv	GTACGGCACCTGCGATGAAC
pca-conf-fw	GGCGTACGTACATCAGTGGA
pca-conf-rv	CCCACTGCGGATCAAAAAGG
vdh-fw	CCTGCAGGTCGACTCTAGAGTCGAGGAACACCACGTTGTGG
vdh-rv	GAGCTCGGTACCCGGGGATCATTATTTGGCTGCTCTTCCTCAG
vdh-conf-fw	GCACTTCCCGGAGGCTACCA
vdh-conf-rv	TGCATCTGCTGCAACGGTGG
qsu-conf-fw	GTTCGTGGACAAGTGTGGTGG
qsu-conf-rv	CTACCGCGCGGATTAAACC

Ribosomal binding sites are in bold, and binding regions of Gibson primers are underlined.

For analysis of pHBA and PCA, the supernatant from *C. glutamicum* cultures was collected by centrifugation (20,200 *g*, 10 min) and used for HPLC analysis. The detection was done with a DAD at 254 nm. The mobile phase consisted of 0.1 M sodium acetate pH 3.3 (with 0.03% sodium azide) (A) and methanol (B) with the following gradient: 0 min B 8% at 0.7 mL min^{-1}, 10 min B 25% at 1.2 mL min^{-1}, 15 min B 25% at 1.2 mL min^{-1}.

Extraction of quinones was carried out as described (Tian et al., 2010a). Cells from 2 mL of culture were harvested by centrifugation (20,200 *g*, 10 min), and the pellet was treated with 3 M hydrochloric acid [10.8 mL g^{-1} dry cell weight (DCW)] at 84 °C for 35 min. After centrifugation (10,000 *g*, 1 min) the acid was removed and cell debris was resuspended in 400 µl of water. For extraction, the same amount of petroleum ether was added and mixed vigorously. After centrifugation, the organic phase was collected, followed by a second round of extraction. The solvent was evaporated in a Concentrator plus (Eppendorf AG, Hamburg, Germany), and the residue was dissolved in ethanol

for HPLC analysis. Detection was done with a DAD at 275 nm, the UV/visible (Vis) spectrum was recorded in the range from 230 to 450 nm. The mobile phase consisted of ethanol (A) and methanol (B) with the following gradient at a flow rate of 1 mL min^{-1}: 0 min B 100%, 10 min B 0%, 20 min B 0%.

Identification of CoQ10 by HPLC-ESI-MS and NanoESI-Q-TOF-MS

For identification of CoQ10, produced in shake flasks, quinone extracts were prepared as described above and analyzed via LC-ESI-MS. A Thermo Scientific UltiMate 3000 (Thermo Scientific, Germering, Germany) UHPLC system coupled to a microTOF-Q hybrid quadrupole/time-of-flight mass spectrometer (Bruker Daltonics, Bremen, Germany) equipped with an electrospray ionization (ESI) source was used. For separation, 5 µl of the samples and of the CoQ10 standard was injected and separated by an Accucore Polar Premium column (100 × 4.6 mm, 2.6 µm particle size) at 40°C. The mobile phase consisted of ethanol (A) and methanol (B), both with 10 mM of ammonium acetate for the formation of adducts $[M + NH4]^+$, with the following gradient at a flow rate of 0.3 mL min^{-1}: 0 min B 100%, 10 min B 0%, 30 min B 0%, 35 min B 100%, 50 min B 100%. UV detection was at 280 nm, and the ESI source was operated in positive ionization mode. The temperature of the dry gas and the capillary was set to 180°C. The scan range of the MS was set to *m/z* 300–1500. The software DataAnalysis Version 4.0 SP 5 (Bruker Daltonics, Bremen, Germany) was used.

In addition, extracts were analyzed via static nanoESI-Q-TOF-MS. Prior to that, they were separated by HPLC as described above; fractions were collected and evaporated, then incubated for 30 min with ethanol with 10 mM of ammonium acetate for the formation of adducts and again evaporated. Nano-ESI measurements were performed using a Synapt G2Si Q-IMS-TOF mass spectrometer (Waters GmbH, Manchester, United Kingdom) in resolution mode, interfaced to a nano-ESI ion source. Nitrogen served as both the nebulizer gas and the dry gas for nano-ESI. Nitrogen was generated by a nitrogen generator NGM 11. Samples were dissolved in acetonitrile and introduced by static nano-ESI using *in-house* pulled glass emitters. The mass axis was externally calibrated with fragment ions of GluFib as calibration standard. Scan accumulation and data processing were performed with MassLynx 4.1 (Waters GmbH, Manchester, United Kingdom) on a PC Workstation. Determination of exact masses was performed using centroided data.

Bioreactor Fermentation of UBI413

Batch fermentation of *C. glutamicum* UBI413 was performed in a volume of 2 L in a bioreactor (3.7 L KLF, Bioengineering AG, 8636 Wald, Switzerland) at 30°C and an aeration rate of 2 NL min^{-1}. The relative dissolved oxygen saturation (rDOS) was maintained at 30% by control of stirrer frequency. The pH was maintained at pH 7.0 with 4 M KOH and 10% phosphoric acid (w/w). Antifoam 204 (1.2 mL) was added to the medium initially; during growth, it was added manually when necessary. Samples were taken every 8 h and cooled down to 4°C until further use. For inoculation, the first pre-culture of *C. glutamicum* UBI413 was grown in the LB medium; cells were transferred to a second pre-culture in CGXII pH 7.0 with 40 g L^{-1} glucose with the required antibiotics and without IPTG and ATc. The culture was spun down and resuspended in a small volume of fresh CGXII medium to inoculate the bioreactor medium to an OD_{600} of 1.0. The bioreactor medium consisted of CGXII medium without 3-(*N*-morpholino) propanesulfonic acid (MOPS), supplemented with 0.5 g L^{-1} of L-methionine, with antibiotics and 1 mM of IPTG and 0.25 µg mL^{-1} of ATc.

RESULTS

Functional Expression of DPP Synthase Gene *ddsA* From *P. denitrificans* in *C. glutamicum*

Ubiquinones with different isoprenoid side-chain lengths exist. The chain length of the isoprenoid side chain is determined by biosynthesis of the precursor isoprenoid diphosphate prior to prenylation of pHBA. Therefore, in order to produce CoQ10 with its decaprenyl side chain, DPP synthase DdsA from *P. denitrificans* that converts FPP to DPP was chosen. *C. glutamicum* possesses two isoprenoid synthases, IdsA and CrtE, that convert IPP and DMAPP to GGPP via GPP and FPP (Heider et al., 2014a), and GGPP serves as precursor for the biosynthesis of the carotenoid pigment decaprenoxanthin in *C. glutamicum*. Expression of *ddsA* from *P. denitrificans* was expected to reduce decaprenoxanthin biosynthesis since DdsA competes with carotenogenesis for the isoprenoid diphosphates FPP, DMAPP, and IPP. *C. glutamicum* WT (pVWEx1) and WT (pVWEx1-*ddsA*) were cultivated in CGXII medium for 24 h, followed by carotenoid extraction and HPLC analysis (**Figure 2**). The expression of *ddsA*, which was verified by SDS-PAGE (data not shown), decreased carotenoid synthesis around 12-fold. Although DPP production could not be directly verified by analytical methods, a decrease of carotenoid synthesis may indirectly confirm functional expression of *ddsA* from *P. denitrificans*.

Metabolic Engineering for Improved Supply of Isoprenoid Precursor FPP

To avoid competition for isoprenoid diphosphates by carotenogenesis, the strain *C. glutamicum* Δ*crtOP*Δ*idsA*Δ*crtB2I'I2* (Henke et al., 2018) that produces no carotenoids but synthesizes IPP and DMAPP in the MEP pathway was chosen for heterologous expression of FPP synthase gene *ispA* from *E. coli*. The gene *ispA* was expressed from the chromosome from promoter P_{tuf} by insertion into landing pad 4 of the *C. glutamicum* chromosome (Lange et al., 2018), yielding strain UBI000. Since a direct quantification of FPP was not possible, we chose an indirect method, i.e., by conversion to amorphadiene. This precursor molecule of the antimalarial drug artemisinin is generated from FPP by amorphadiene synthase (ADS) from *Artemisia annua*. Plasmid-borne expression of the ADS gene yielded *C. glutamicum* strains WT (pVWEx1-ADS) and UBI000 (pVWEx1-ADS), respectively.

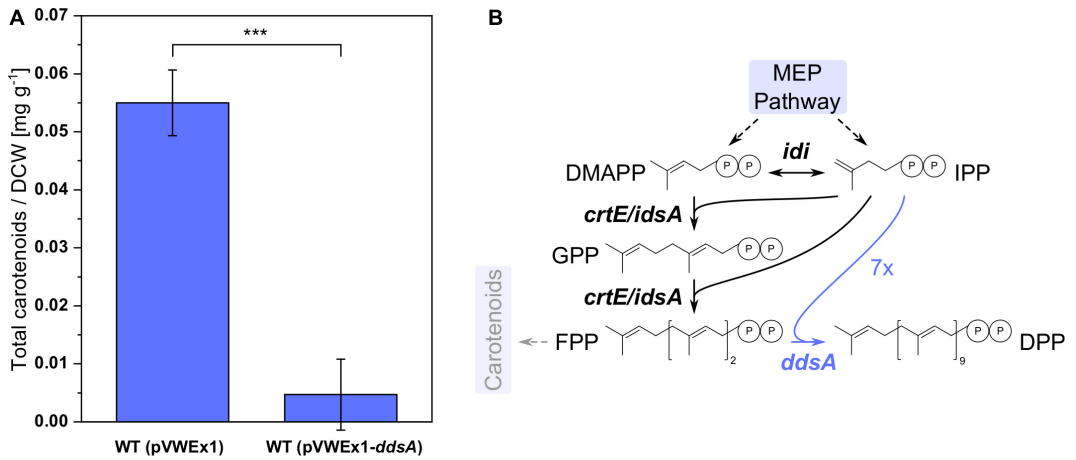

FIGURE 2 | Carotenoid synthesis in *C. glutamicum* WT with and without expression of *ddsA*. **(A)** Total carotenoid amount per dry cell weight from WT (pVWEx1) and WT (pVWEx1-*ddsA*). **(B)** Pathway of isoprenoids with diverging reactions from FPP to DPP and carotenoids. The heterologous expression of *ddsA* is highlighted in blue. MEP, 2-C-methylerythritol 4-phosphate; IPP, isopentenyl diphosphate; DMAPP, dimethylallyl diphosphate; GPP, geranyl diphosphate; FPP, farnesyl diphosphate; DPP, decaprenyl diphosphate; *idi*, isopentenyl diphosphate isomerase; *crtE*, geranylgeranyl diphosphate synthase; *idsA*, geranylgeranyl diphosphate synthase; *ddsA*, decaprenyl diphosphate synthase from *P. denitrificans*. Values and error bars represent means and standard deviations ($n = 3$). Statistical significance is based on a two-sided unpaired Student's *t*-test (***: $p < 0.001$).

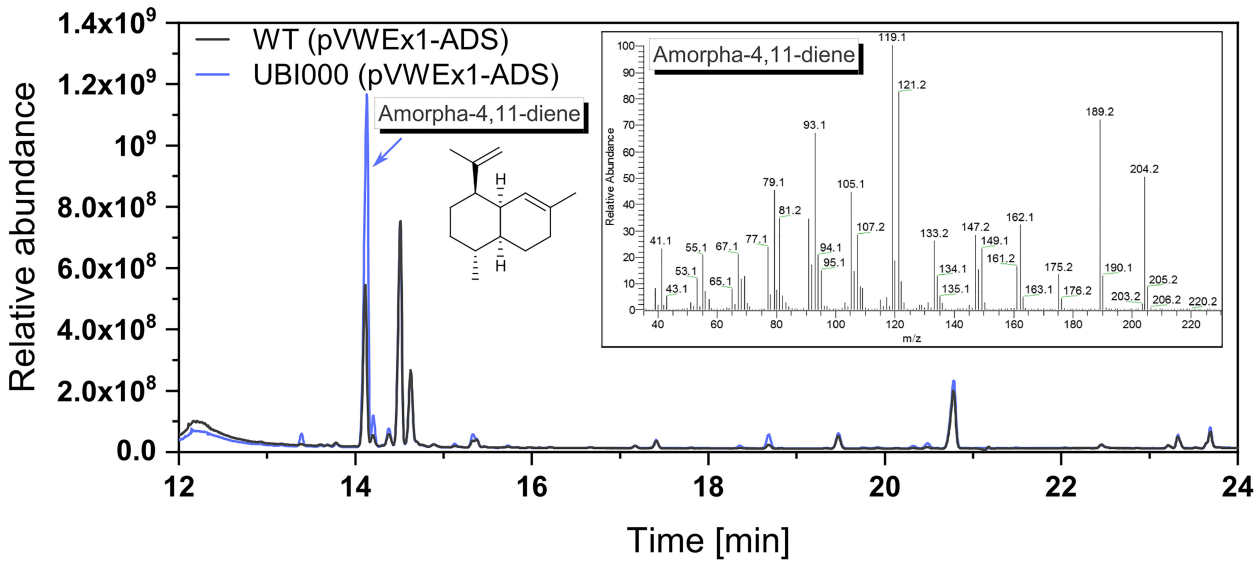

FIGURE 3 | Production of amorphadiene as a means to quantify FPP supply. The extracts of dodecane overlay cultivation with WT (pVWEx1-ADS), shown in black, and UBI000 (pVWEx1-ADS), shown in blue, were analyzed via GC-MS. For quantification, valencene was used as a standard equivalent. Shown are the chromatogram and in the insert the mass spectrum of produced amorphadiene.

These strains were cultivated in the CGXII medium with an overlay of 10% dodecane (v/v) to capture the volatile product amorphadiene. After 75 h of shake-flask cultivation, the dodecane phase was separated from the medium and samples were analyzed by GC-MS analysis (**Figure 3**). GC-MS confirmed production of amorphadiene. For its quantification, valencene was used as a chemically similar standard equivalent as amorphadiene could not be purchased. It could be shown that UBI000 (pVWEx1-ADS) produced 10.9 ± 0.1 mg L^{-1} valencene equivalents of amorphadiene, thus 2.5 times more than WT (pVWEx1-ADS). This indicated an increased FPP supply in the strain UBI000 (pVWEx1-ADS).

Metabolic Engineering for Improved Supply of Aromatic Precursor pHBA

The aromatic ring of CoQ10 originates from pHBA, a product of the shikimate pathway synthesized naturally by *E. coli*, but not by *C. glutamicum*. Following our previously developed metabolic engineering strategy to enable pHBA production

by *C. glutamicum* (Purwanto et al., 2018), the CoQ10 base strain UBI000 was engineered for increased supply of pHBA. First, *pobA*, encoding pHBA hydroxylase, was deleted to avoid degradation of pHBA to PCA, resulting in the strain UBI100. Second, UBI200 was constructed by integration of feedback-resistant (L31A) chorismate-pyruvate lyase gene $ubiC^{FBR}$ from *E. coli* under control of the promoter P_{sod} by simultaneous deletion of *pcaHG*, encoding PCA dioxygenase. It was reported that deletion of *pcaHG* together with deletion of *qsuB* led to a significantly reduced PCA production compared to *qsuB* deletion alone (Kallscheuer et al., 2016). To generate increased flux into the shikimate pathway and reduced by-product formation, UBI300 was engineered by integration of $aroG^{FBR}$, which codes for feedback-resistant (D146N) 3-deoxy-D-arabinoheptulosonate 7-phosphate (DAHP) synthase from *E. coli*, with the simultaneous deletion of *vdh*, coding for vanillin dehydrogenase. Fourth, the operon *qsuABCD*, encoding putative shikimate importer, 3-dehydroshikimate dehydratase, 3-dehydroquinate dehydratase, and shikimate dehydrogenase, was deleted and *qsuC* was overexpressed from the P_{tuf} promoter to reduce formation of PCA as by-product, yielding strain UBI400.

To compare the production of pHBA and formation of the by-product PCA, the strains UBI000, UBI100, UBI200, UBI300, and UBI400 were cultivated in CGXII medium and supernatants were analyzed after 24 h by HPLC (**Figure 4**). As expected, strains UBI000 and UBI100 did not produce pHBA because they lack *ubiC*. As a result of the integration of *ubiC*, UBI200 accumulated 0.9 ± 0.1 mM of pHBA and 0.1 ± 0.0 mM of PCA. Production of pHBA by UBI300 doubled due to an increased flux into the shikimate pathway, but accumulation of PCA as by-product exceeded pHBA production. PCA accumulation was almost abolished using strain UBI400 that carried a *qsuB* deletion and *qsuC* overexpression, and pHBA production by this strain was increased to 2.5 ± 0.1 mM (**Figure 4**). These results suggested that supply of the precursor pHBA in strain UBI400 was sufficient to synthesize CoQ10 to a similar concentration.

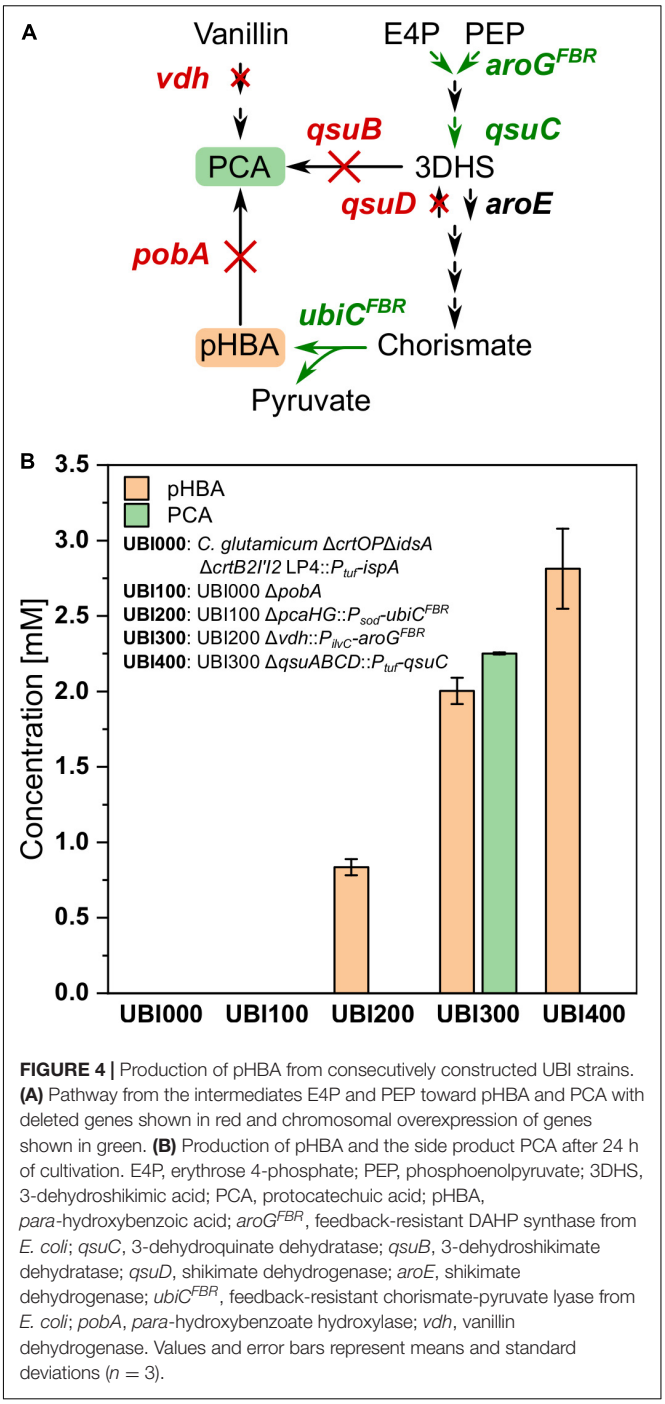

FIGURE 4 | Production of pHBA from consecutively constructed UBI strains. **(A)** Pathway from the intermediates E4P and PEP toward pHBA and PCA with deleted genes shown in red and chromosomal overexpression of genes shown in green. **(B)** Production of pHBA and the side product PCA after 24 h of cultivation. E4P, erythrose 4-phosphate; PEP, phosphoenolpyruvate; 3DHS, 3-dehydroshikimic acid; PCA, protocatechuic acid; pHBA, *para*-hydroxybenzoic acid; $aroG^{FBR}$, feedback-resistant DAHP synthase from *E. coli*; *qsuC*, 3-dehydroquinate dehydratase; *qsuB*, 3-dehydroshikimate dehydratase; *qsuD*, shikimate dehydrogenase; *aroE*, shikimate dehydrogenase; $ubiC^{FBR}$, feedback-resistant chorismate-pyruvate lyase from *E. coli*; *pobA*, *para*-hydroxybenzoate hydroxylase; *vdh*, vanillin dehydrogenase. Values and error bars represent means and standard deviations ($n = 3$).

Functional Expression of Polyprenyl Transferase Gene *ubiA* From *E. coli*

For expression of polyprenyl transferase *ubiA* from *E. coli*, this gene and *ddsA* were cloned into the dual-inducible expression vector pRG_Duet2 (Gauttam et al., 2019). This vector allowed for independent expression of both genes: IPTG inducible expression of *ddsA* and ATc inducible expression of *ubiA*.

Since UbiA condenses pHBA with decaprenyl diphosphate to 3-decaprenyl-4-hydroxybenzoate (10P-HB), pHBA accumulation was examined to estimate if UbiA from *E. coli* was active in recombinant *C. glutamicum*. UBI400 (pRG_Duet2-*ddsA*-*ubiA*) was cultivated in the CGXII minimal medium in the presence or absence of the inducers IPTG and/or ATc (**Figure 5**). Without any inducer and with IPTG only, around 4.7 mM pHBA accumulated after 48 h. In the presence of ATc (alone or with IPTG), only 3.5 mM pHBA accumulated in the supernatant. It was expected that pHBA would be prenylated by the activity of UbiA, decreasing the intracellular pHBA concentration and, as consequence, secretion of pHBA to the culture medium. The finding that pHBA accumulation in the culture medium decreased upon *ubiA* expression was considered as indirect evidence for functional expression of polyprenyl transferase gene *ubiA* from *E. coli* in the recombinant *C. glutamicum* strain. IPTG induction of *ddsA* expression did not reduce pHBA further, which may indicate that supply of pHBA is not limiting its prenylation.

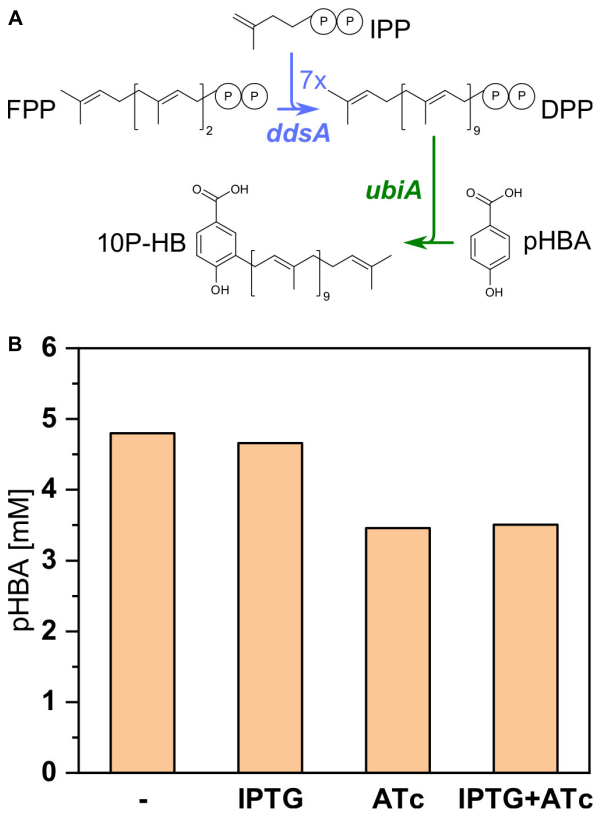

FIGURE 5 | Influence of *ubiA* expression on pHBA production by the strain UBI400 (pRG_Duet2-*ddsA*-*ubiA*). **(A)** Pathway from the precursor FPP toward the intermediate 10P-HB with heterologously expressed *ddsA* and *ubiA* marked in blue and green, respectively. **(B)** The expression of *ubiA* was induced or not induced via addition of ATc either with or without the additional induction of *ddsA* expression via addition of IPTG. The concentration of pHBA was measured in the respective supernatants. IPP, isopentenyl diphosphate; FPP, farnesyl diphosphate; DPP, decaprenyl diphosphate; DPP, decaprenyl diphosphate; 10P-HB, 3-decaprenyl-4-hydroxybenzoate; *ddsA*, decaprenyl diphosphate synthase from *P. denitrificans*; *ubiA*, 4-hydroxybenzoate octaprenyltransferase from *E. coli*.

Functional Expression of Genes for the Ubiquinone Modification Pathway

After condensation of pHBA with decaprenyl diphosphate to 10P-HB, CoQ10 biosynthesis proceeds via a number of reactions modifying the aromatic ring. The respective *ubi* genes from *E. coli* were cloned into the *C. glutamicum*/*E. coli* shuttle vectors pEC-XT99A and pEKEx3. The resulting vectors pEC-XT99A-*ubiDIBX* and pEKEx3-*ubiGHEF* are compatible and allow for IPTG inducible gene expression in *C. glutamicum* as well as *E. coli*. The vectors were tested in genetic complementation experiments since samples of CoQ10 pathway intermediates are scarce, if available at all, and only few enzyme assays have been developed (Poon et al., 1999; Cheng and Li, 2014). Genetically defined ubiquinone biosynthesis mutants of *E. coli* are available, and these mutants are unable to catabolize succinate as sole carbon and energy source (Wallace and Young, 1977). The constructed vectors pEC-XT99A-*ubiDIBX* and pEKEx3-*ubiGHEF* and their derivatives were used to test for genetic complementation of the *ubi* mutants *E. coli* $ubiD^{G452R}$, *ubiI*::*kan*, *ubiX*::*kan*, *ubiG*::*kan*, *ubiH*::*kan*, *ubiE*::*kan*, and *ubiF*::*kan*. These strains and *E. coli* MG1655 as a control strain were grown in M9 medium with succinate as sole carbon source. The mutants *ubiG*::*kan*, *ubiH*::*kan*, *ubiE*::*kan*, and *ubiF*::*kan* only grew with succinate as sole carbon source if they carried the respective vector for complementation (**Figure 6A**). The *E. coli* mutants *ubiI*::*kan* and *ubiX*::*kan* were able to grow without complementation; thus, they were not informative to judge functional expression of *ubiI* and *ubiX* from plasmid pEC-XT99A-*ubiDIBX*. *E. coli* $ubiD^{G452R}$ did not grow within 48 h, even when complemented with pEC-XT99A-*ubiD*. We speculate that expression of *ubiD* was too low or that the mutation $ubiD^{G452R}$ is dominant negative (**Figure 6A**). Therefore, the identity of Ubi proteins was analyzed by peptide mass fingerprints after excision of protein bands from SDS-PAGE gels, digestion with trypsin, and LC-MS/MS analysis (**Supplementary Table 2**). While UbiD, UbiI, UbiB, UbiX, UbiG, UbiH, and UbiF could be detected, detection of UbiE was unsuccessful. In addition, proteins were isolated from bacterial cells and whole-proteome LC-MS/MS analysis confirmed presence of all Ubi proteins including UbiE in the respective strains as well as absence of Ubi proteins from the empty vector control strains. In summary, evidence for expression of all cloned *ubi* genes was gained.

CoQ10 Biosynthesis by Metabolically Engineered *C. glutamicum*

After having established provision of FPP and pHBA as precursors, as well as functional expression of genes for prenylation of pHBA and for modification of the condensation product 10-HB to CoQ10, all engineered pathways were assembled stepwise in a series of recombinant *C. glutamicum* strains: UBI401, UBI405, UBI412, and UBI413 (**Table 1**). UBI401 is an empty vector control, UBI405 carried only pRG_Duet2-*ddsA*-*ubiA*, UBI412 possessed pRG_Duet2-*ddsA*-*ubiA*, and pECXT-*ubiDIBX*, and UBI413 carried three vectors, pRG_Duet2-*ddsA*-*ubiA*, pECXT-*ubiDIBX*, and pEKEx3-*ubiGHEF*. Strains UBI405 and UBI412 were expected to synthesize 3-decaprenyl-4-hydroxybenzoate and/or 2-decaprenyl-6-hydroxyphenol, whereas strain UBI413 was expected to synthesize CoQ10.

C. glutamicum strains UBI401, UBI405, UBI412, and UBI413 were cultivated in CGXII medium for 72 h, followed by extraction of quinones from whole cells and HPLC analysis (**Figure 7A**). While all strains grew to similar biomass concentrations with ODs of 40 to 45, the specific growth rates of strains UBI413 and UBI412 with 0.08 and 0.10 h^{-1} were considerably lower than of UBI401 and UBI405 with 0.30 h^{-1} (**Figure 7C**). The slowed growth of strains UBI412 and UBI413 may indicate interference of CoQ10 or its precursors with the native respiratory chain. As expected, extracts of the control strain UBI401 carrying an empty vector showed two major peaks in the chromatogram that likely are the native dihydromenaquinones MK9(H2) and MK8(H2). These reduced menaquinones have previously been described to occur in corynebacteria (Collins and Jones, 1981), and they do

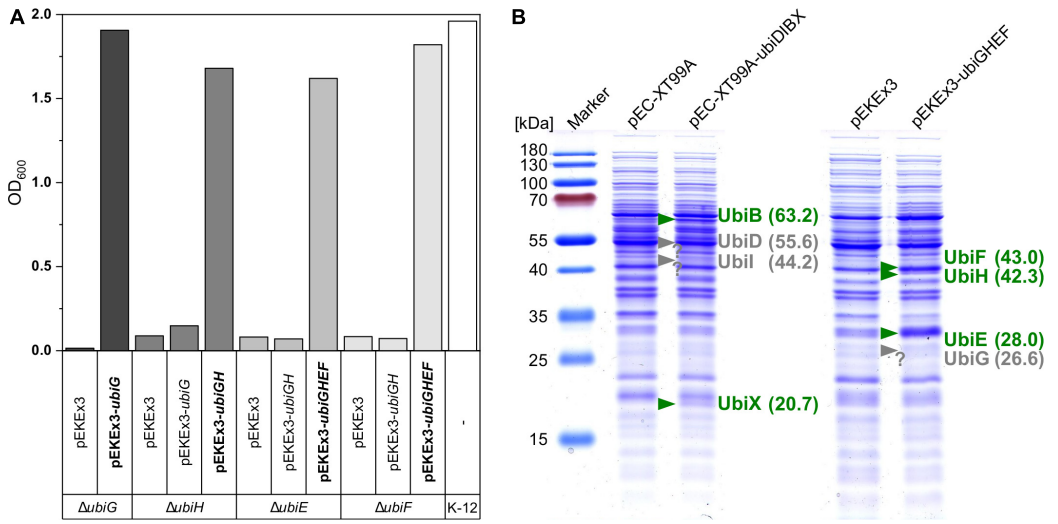

FIGURE 6 | Verification of *ubi* gene function and expression. **(A)** *E. coli* deletion mutants were transformed with control vectors and complementation vectors (bold) and inoculated into M9 minimal medium with 20 mM succinate as sole carbon source. Complementation enabled growth after 45/48 h as can be compared with the positive control strain K-12. **(B)** SDS–PAGE of UBI000 crude extracts carrying different vectors for expression analysis. Confirmed expression based on theoretical protein weights is depicted in green, missing bands are shown in gray at the expected position.

occur in all tested strains, but at reduced levels in strains UBI405, UBI412, and UBI413. Extracts of strain UBI405 contained two additional compounds, likely MK10(H2) as result of the expression of *ddsA*, and the CoQ10 biosynthesis intermediate 3-decaprenyl-4-hydroxybenzoate, the condensation product of decaprenyl diphosphate, and pHBA generated by UbiA. Extracts of strain UBI412, which further expressed the genes *ubiDIBX*, showed several additional peaks, likely early intermediates of CoQ10 biosynthesis. Alternatively, their prenyl side-chain lengths may be shorter (8 or 9 instead of 10) since pHBA prenyltransferase UbiA is promiscuous for prenyl diphosphates of different lengths and *C. glutamicum* possesses a putative octaprenyl diphosphate synthase encoded by *ispB* (Heider et al., 2014a).

Surprisingly, chromatograms of extracts of strain UBI413 did not contain an extra peak although having been engineered for the complete CoQ10 biosynthesis. One of the peaks present in extracts of strains UBI412 and UBI413 co-eluted with the CoQ10 standard. Their absorption spectra, however, differed from that of CoQ10 (**Supplementary Figure 2**). The non-identity of the UV spectra of the standard and the CoQ10 formed by strain UBI413 is striking. We hypothesize that at least one other compound co-elutes with CoQ10. Addition of reducing or oxidizing agents to the extracts had no effect on the chromatograms or UV spectra, which supports the notion that the standard and the CoQ10 formed by strain UBI413 do not differ by the oxidation states. Therefore, the samples and the standard were subjected to LC-MS analysis (**Figures 7B,D**). Extracts of strain UBI413, but not those of the tested other strains, revealed a mass of 880.72 for the peak co-eluting with the CoQ10 standard, which corresponded to CoQ10 $[M+NH_4]^+$. The results were confirmed in another independent shake-flask experiment with subsequent Q-TOF-MS analysis of the quinone extracts. The LC-MS analysis did not provide a clue on the nature of the compound co-eluting with CoQ10, which, thus, remains elusive.

Moreover, to prevent that *S*-adenosyl-L-methionine (SAM)-dependent methylation reactions may limit CoQ10 biosynthesis, 0.5 g L^{-1} of L-methionine was added. Addition of L-methionine has been shown to improve vanillin production in *E. coli* by increased SAM availability (Kunjapur et al., 2016). Indeed, addition of L-methionine altered the ratios of compounds present in quinone extracts including a substance eluting with/near CoQ10, which indicated that flux in the ubiquinone pathway was altered by increased SAM availability (**Supplementary Figure 3**).

In order to test if CoQ10 production is stable in a bioreactor, a 2-L batch fermentation with strain UBI413 was performed (**Figure 8**). Moreover, bioreactor fermentation may provide better cultivation conditions than flask cultivation with respect to molecular oxygen, which is required for CoQ10 biosynthesis since UbiI, UbiH, and UbiF are oxygenases. The strain UBI413 was cultivated for 96 h, rDOS was set to 30%, and the agitator frequency was controlled to keep the rDOS constant. The cells reached an OD_{600} of 42; glucose was consumed after around 56 h. A pHBA titer of 0.6 g L^{-1} (4.4 mM) was reached after 72 h, which was comparable with observed titers in shake flasks. Although CoQ10 was not quantifiable due to background peaks, we made an upper estimate: under the assumption that the corresponding peak at the CoQ10 retention time consists only of CoQ10 a titer $\leq$ 0.43 mg L^{-1} and a cellular content $\leq$ 36 µg g^{-1} DCW after 96 h were observed.

Taken together, by metabolically engineering non-ubiquinone-containing *C. glutamicum* to produce the precursors DPP and pHBA from extended isoprenoid and shikimate pathways, respectively, and introducing ubiquinone modification genes from *E. coli*, the biosynthesis of CoQ10 was unequivocally documented by the *C. glutamicum* strain UBI413.

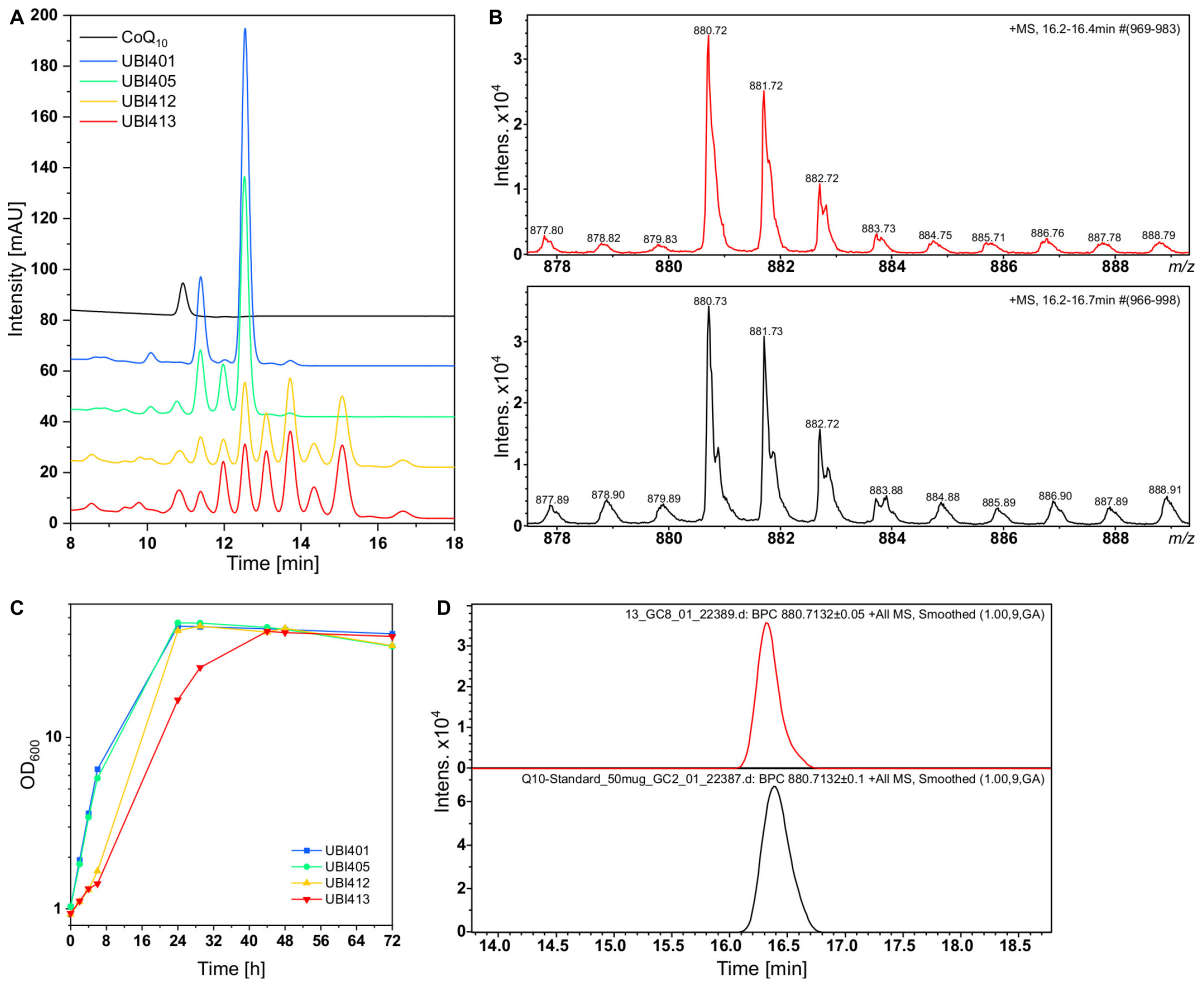

FIGURE 7 | High performance liquid chromatography (HPLC) and LC-MS analyses of quinone extracts from different UBI strains for CoQ10 detection. **(A)** Overlaid chromatograms of the CoQ10 standard and UBI strains with UBI413 (red) carrying the vectors pRG_Duet2-*ddsA-ubiA*, pEC-XT99A-*ubiDIBX*, and pEKEx3-*ubiGHEF* to facilitate CoQ10 production. **(B)** Isotope pattern of CoQ10 from quinone extract of UBI413 (red) and from the CoQ10 standard (black). **(C)** Growth curves of strains that were used for quinone extraction. **(D)** Base peak chromatogram of *m/z* 880.71, the ammonium adduct mass of CoQ10 in the quinone extract of UBI413 (red) and in the CoQ10 standard (black).

DISCUSSION

Biosynthesis of CoQ10 was established in the non-ubiquinone-containing bacterium *C. glutamicum*. Supply of the aromatic precursor pHBA was enabled following a previously developed strategy (Purwanto et al., 2018). Supply of FPP as isoprenoid precursor upon introduction of the FPP synthase from *E. coli* was demonstrated by production of amorphadiene (10.9 ± 0.1 mg L^{-1} valencene equivalents) when the gene for amorphadiene synthase from *A. annua* was expressed in addition and endogenous carotenogenesis was abolished. Upon expression of heterologous genes for decaprenyl diphosphate synthase from *P. denitrificans* and 4-hydroxybenzoate polyprenyltransferase and ubiquinone modification enzymes from *E. coli*, pHBA was prenylated and CoQ10 was produced as evidenced by MS analysis.

The intracellular concentration of the aromatic precursor pHBA was not measured; however, its supply for CoQ10 biosynthesis appears not to be limiting, since the metabolic engineering strategy followed here to provide pHBA was used previously to establish pHBA overproduction and 19 g L^{-1} (138 mM) pHBA was secreted to the culture medium in a fed-batch fermentation (Purwanto et al., 2018). The finding that strains constructed here secreted up to 5 mM pHBA (**Figure 5B**) suggested that Co10 biosynthesis was not limited by pHBA supply.

Competition for isoprenoid diphosphates in naturally CoQ10-synthesizing bacteria such as *P. denitrificans* (Yoshida et al., 1998), *Rhodospirillum rubrum* (Tian et al., 2010b), and *R. sphaeroides* was reduced by abolishment/reduction of carotenogenesis, which increased CoQ10 content. However, *R. sphaeroides* suffered from the deletion of the carotenoid gene cluster as the biomass decreased to half of that of the wild type (Zhu et al., 2017). To overcome this detrimental problem (the titer of cell-bound products depends on content per cell as well as on the biomass concentration achieved), it was

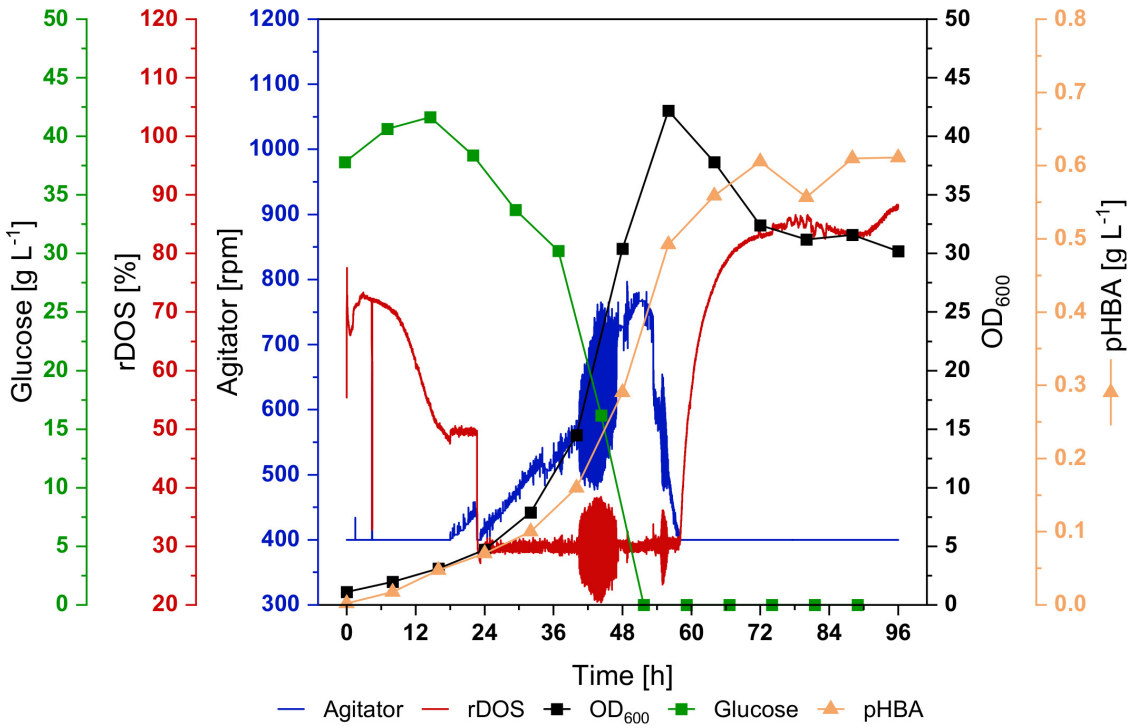

FIGURE 8 | Batch fermentation of *C. glutamicum* UBI413 in 2-L scale. The cultivation was performed in CGXII medium with 40 g L^{-1} glucose, supplemented with 0.5 g L^{-1} of L-methionine, antibiotics, 1 mM of IPTG and 0.25 μg mL^{-1} of ATc for induction of gene expression at 30°C, pH 7.0 and an aeration rate of 2 NL min^{-1}. The rDOS was maintained at 30% by control of agitator frequency. Glucose concentration (green) and OD_{600} (black) are shown in squares, rDOS (red) and agitator frequency (blue) are indicated by lines, production of pHBA is shown in triangles. An upper estimate of CoQ10 production is given in the results.

required to downregulate the carotenoid genes of *R. sphaeroides* by overexpression of the transcriptional repressor gene *ppsR* and of the GGPP synthase gene *crtE* to maintain biomass formation at a higher CoQ10 content (Zhu et al., 2017). By contrast, *C. glutamicum* does not suffer from carotenoid deficiency (data not shown) and therefore constitutes an adequate host for the production of isoprenoid-derived compounds as shown for patchoulol production. The carotenoid-deficient strain *C. glutamicum* Δ*crtOP*Δ*idsA*Δ*crtB2I'I2* (pECXT_*ispA-PcPS*)(pVWEx1) produced 60 mg L^{-1} patchoulol and reached a biomass concentration of 4.2 ± 0.6 g L^{-1} (Henke et al., 2018), which is only slightly lower than that of the wild type (5.4 g L^{-1}) under the same conditions (Frohwitter et al., 2014), presumably due to the plasmids it carried. Thus, further improving isoprenoid diphosphate precursor supply may be beneficial for CoQ10 production by the strains constructed in this study without compromising biomass formation. In *R. sphaeroides*, this was achieved by self-regulated overexpression of the genes *dxs*, *dxr*, *idi*, and *ispD* from the MEP pathway (Lu et al., 2014).

To provide DPP for prenylation of pHBA, we chose to express the heterologous decaprenyl diphosphate synthase gene *ddsA* from *P. denitrificans*. The enzyme has K_m values of 5.0, 0.06, and 2.9 μM for GPP, FPP, and GGPP, respectively, and yields DPP and undecaprenyl diphosphate (UPP), but not shorter diphosphates. The ratio of DPP to UPP synthesized by DdsA depended on the Mg^{2+} concentrations and ranged from 23:1 at 1 mM Mg^{2+} to 5:1 at 5 mM Mg^{2+} (Ishii et al., 1985). In *E. coli*, plasmid-borne expression of *ddsA* alone was sufficient to enable CoQ10 biosynthesis in addition to and independent of native CoQ8 biosynthesis via IspB (Takahashi et al., 2003). In the MK-containing, but CoQ-lacking *C. glutamicum*, we observed a 12-fold reduction of carotenoid content upon expression of *ddsA* (**Figure 2**), indicating competition for the substrate FPP between DdsA and GGPP synthases IdsA and CrtE on the one hand and competition between DdsA and phytoene synthase CrtB for the substrate GGPP on the other hand. IdsA and CrtE have K_m values of 8 and 0.1 μM for GPP and 20 and 6 for FPP, respectively (Heider et al., 2014a); thus, the fact that DdsA shows higher affinity for both substrates may explain the reduced carotenoid accumulation as consequence of *ddsA* expression. To abolish any competition, the carotenoid-deficient mutant *C. glutamicum* Δ*crtOP*Δ*idsA*Δ*crtB2I'I2* was chosen and the FPP synthase gene *ispA* from *E. coli* was integrated into the chromosome.

For condensation of DPP and pHBA, we chose prenyltransferase UbiA from *E. coli*. When *ubiA* was induced, the amount of pHBA accumulated outside the cells was reduced (**Figure 5**), which may serve as indirect evidence for functional expression of this prenyltransferase gene. UbiA is highly specific for pHBA, accepting only very similar compounds like 3-chloro-4-hydroxybenzoic acid and 2,4-dihydroxybenzoic acid to some extent (Bräuer et al., 2004); however, these are not known to occur in *C. glutamicum*. By contrast, UbiA is promiscuous for isoprenoid diphosphates of different chain

lengths (Suzuki et al., 1994; Cheng and Li, 2014); thus, the product of prenylation depends on the availability of isoprenoid diphosphate species. Biosynthesis of menaquinones MK8 and MK9 in *C. glutamicum* involves prenylation by MenA using either octa- or nonaprenyl diphosphate that are synthesized by the native octa- or nonaprenyl diphosphate synthases such as IspB (Heider et al., 2014a). Hence, it is conceivable that heterologous UbiA accepts octa- or nonaprenyl diphosphate for prenylation of pHBA, yielding CoQ8 and CoQ9 as byproducts of CoQ10 biosynthesis. HPLC analysis revealed that upon expression of *ddsA* and *ubiA* (strain UBI405), new quinone compounds arise, which are absent from the precursor strain and from *C. glutamicum* wild type (data not shown). These compounds could either be pHBA prenylation products CoQ8 and/or CoQ9 or, alternatively, be MK10 synthesized by MenA using DPP instead of octa- or nonaprenyl diphosphate. Thus, selection and/or engineering of prenyltransferases that show as strict substrate specificity for isoprenoid diphosphate substrate as for the aromatic substrate may improve CoQ10 production by decoupling native MK8 and MK9 biosynthesis from engineered CoQ10 biosynthesis.

The product of prenylation of pHBA with DPP, 10P-HB, is modified further by a sequence of enzymes. This process may be limiting. Several studies have shown that UbiG is a bottleneck in ubiquinone biosynthesis and its overexpression increased CoQ10 titers in *E. coli* (Zhu et al., 1995; Zhang et al., 2007) and *R. spharoides* (Lu et al., 2013). In the strain constructed here, UbiG levels may be low since genetic complementation of an *E. coli* Δ*ubiG* mutant by plasmid-borne expression of *ubiG* was successful, whereas SDS–PAGE did not reveal a protein band of UbiG (**Figure 6**). One option to improve *ubiG* expression is in the form of a membrane-anchored fusion protein of UbiG and UbiE, which improved CoQ10 productivity by recombinant *R. sphaeroides* (Lu et al., 2015). Moreover, certain steps of 10P-HB modification have not been assigned to a protein unambiguously. For instance, an *E. coli* Δ*ubiB* deletion strain accumulates 3-octaprenylphenol and does not produce CoQ8, but the function of UbiB remains unknown (Hajj Chehade et al., 2013). UbiB was believed to catalyze the first monooxygenase step (Poon et al., 2000), which is actually performed by UbiI, and UbiB may function in regulation of ubiquinone synthesis through its putative kinase activity. In our design we included *ubiB* and CoQ10 biosynthesis was successful, but we did not test if *ubiB* is essential for CoQ10 biosynthesis. The CoQ10-synthesizing strain developed here lacked heterologous expression of *ubiJ* and *ubiK*. In *E. coli*, the membrane-bound UbiJ-UbiK complex is believed to facilitate locating the Ubi enzymes at the membrane, where ubiquinone synthesis takes place (Loiseau et al., 2017). Deletion of *ubiK* decreased the CoQ8 content to 18% compared to the wild type, while *ubiJ* was shown to be essential for ubiquinone synthesis in *E. coli* under aerobic conditions (Aussel et al., 2014a). Heterologous expression of *ubiJ* and *ubiK* may improve CoQ10 biosynthesis by recombinant *C. glutamicum*.

While we have achieved a proof-of-concept for biosynthesis of CoQ10 in the first non-ubiquinone-containing bacterium, the demanding pathway may be optimized with regard to (a) efficient provision of DPP, (b) prenylation of pHBA with DPP as sole prenyl diphosphate, and efficient modification of 10P-HB for overproduction of CoQ10 by recombinant *C. glutamicum*.

DATA AVAILABILITY STATEMENT

The original contributions presented in the study are included in the article/**Supplementary Material**, further inquiries can be directed to the corresponding author/s.

AUTHOR CONTRIBUTIONS

AB, AM, MP, JS, JR, and TP carried out experimental procedures of the present study. AB, AM, MP, JS, TP, PP-W, J-HL, and VW analyzed data. AB prepared a draft of the manuscript. AB and VW finalized the manuscript. J-HL and VW coordinated the study. All authors read and approved the final version of the manuscript.

FUNDING

VW and J-HL acknowledge support by the German-Korean MOBKOR program jointly funded by the National Research Foundation of Korea (NRF-2016K1A3A1A04940618) and the German Federal Ministry of Education and Research. J-HL acknowledges support by Basic Science Research Program through the National Research Foundation of Korea (NRF-2018R1D1A1B07047207) and the BB21+ Project in 2020. VW acknowledges support for the article processing charge from the Deutsche Forschungsgemeinschaft and the Open Access Publication Fund of Bielefeld University. This work was funded in part by the state of North Rhine Westphalia (NRW) and the "European Regional Development Fund (EFRE)," Project "Cluster Industrial Biotechnology (CLIB) Kompetenzzentrum Biotechnologie (CKB)" 34.EFRE0300095/1703FI04. The funders had no role in study design and data analysis and interpretation.

ACKNOWLEDGMENTS

The authors thank Thomas Schäffer from the Department of Fermentation Technology at Bielefeld University and Florian Meyer for their support during the batch fermentations. The authors also thank Bernhard J. Eikmanns from the Institute of Microbiology and Biotechnology at University of Ulm for providing the vector pRG_Duet2, Jonas Frohwitter for constructing the vector pVWEx1-ADS, and Sabine A. E. Heider for constructing the vector pSH1-*ispA*.

SUPPLEMENTARY MATERIAL

The Supplementary Material for this article can be found online at: https://www.frontiersin.org/articles/10.3389/fbioe.2021.650961/full#supplementary-material

REFERENCES

Asai, K., Fujisaki, S., Nishimura, Y., Nishino, T., Okada, K., Nakagawa, T., et al. (1994). The identification of *Escherichia coli ispB* (cel) gene encoding the octaprenyl diphosphate synthase. *Biochem. Biophys. Res. Commun.* 202, 340–345. doi: 10.1006/bbrc.1994.1933

Aussel, L., Loiseau, L., Chehade, M. H., Pocachard, B., Fontecave, M., Pierrel, F., et al. (2014a). *UbiJ*, a new gene required for aerobic growth and proliferation in macrophage, is involved in coenzyme Q biosynthesis in *Escherichia coli* and *Salmonella enterica* serovar typhimurium. *J. Bacteriol.* 196, 70–79. doi: 10.1128/JB.01065-13

Aussel, L., Pierrel, F., Loiseau, L., Lombard, M., Fontecave, M., and Barras, F. (2014b). Biosynthesis and physiology of coenzyme Q in bacteria. *Biochim. Biophys. Acta Bioenerg.* 1837, 1004–1011. doi: 10.1016/j.bbabio.2014.01.015

Baba, T., Ara, T., Hasegawa, M., Takai, Y., Okumura, Y., Baba, M., et al. (2006). Construction of *Escherichia coli* K-12 in-frame, single-gene knockout mutants: the Keio collection. *Mol. Syst. Biol.* 2, 2006.0008. doi: 10.1038/msb4100050

Becker, J., Kuhl, M., Kohlstedt, M., Starck, S., and Wittmann, C. (2018). Metabolic engineering of *Corynebacterium glutamicum* for the production of *cis,cis*-muconic acid from lignin. *Microb. Cell Fact.* 17:115. doi: 10.1186/s12934-018-0963-2

Bradford, M. M. (1976). A rapid and sensitive method for the quantitation of microgram quantities of protein utilizing the principle of protein-dye binding. *Anal. Biochem.* 72, 248–254. doi: 10.1016/0003-2697(76)90527-3

Bräuer, L., Brandt, W., and Wessjohann, L. A. (2004). Modeling the *E. coli* 4-hydroxybenzoic acid oligoprenyltransferase (ubiA transferase) and characterization of potential active sites. *J. Mol. Model.* 10, 317–327. doi: 10.1007/s00894-004-0197-6

Chae, T. U., Ahn, J. H., Ko, Y.-S., Kim, J. W., Lee, J. A., Lee, E. H., et al. (2020). Metabolic engineering for the production of dicarboxylic acids and diamines. *Metab. Eng.* 58, 2–16. doi: 10.1016/j.ymben.2019.03.005

Chen, X., Jiang, X., Xu, M., Zhang, M., Huang, R., Huang, J., et al. (2019). Co-production of farnesol and coenzyme Q10 from metabolically engineered *Rhodobacter sphaeroides*. *Microb. Cell Fact.* 18:98. doi: 10.1186/s12934-019-1145-6

Cheng, W., and Li, W. (2014). Structural insights into ubiquinone biosynthesis in membranes. *Science* 343, 878–881. doi: 10.1126/science.1246774

Collins, M. D., and Jones, D. (1981). Distribution of isoprenoid quinone structural types in bacteria and their taxonomic implication. *Microbiol. Rev.* 45, 316–354.

Collins, M. D., Pirouz, T., Goodfellow, M., and Minnikin, D. E. (1977). Distribution of menaquinones in actinomycetes and corynebacteria. *J. Gen. Microbiol.* 100, 221–230. doi: 10.1099/00221287-100-2-221

Duetz, W. A., Rüedi, L., Hermann, R., O'Connor, K., Büchs, J., and Witholt, B. (2000). Methods for intense aeration, growth, storage, and replication of bacterial strains in microtiter plates. *Appl. Environ. Microbiol.* 66, 2641–2646. doi: 10.1128/AEM.66.6.2641-2646.2000

Eggeling, L., and Bott, M. (2005). *Handbook of Corynebacterium Glutamicum*. Boca Raton, FL: CRC press.

Eggeling, L., and Bott, M. (2015). A giant market and a powerful metabolism: L-lysine provided by *Corynebacterium glutamicum*. *Appl. Microbiol. Biotechnol.* 99, 3387–3394. doi: 10.1007/s00253-015-6508-2

Ernster, L., and Dallner, G. (1995). Biochemical, physiological and medical aspects of ubiquinone function. *Biochim. Biophys. Acta* 1271, 195–204.

Frohwitter, J., Heider, S. A. E., Peters-Wendisch, P., Beekwilder, J., and Wendisch, V. F. (2014). Production of the sesquiterpene (+)-valencene by metabolically engineered *Corynebacterium glutamicum*. *J. Biotechnol.* 191, 205–213. doi: 10.1016/j.jbiotec.2014.05.032

Fujisaki, S., Hara, H., Nishimura, Y., Horiuchi, K., and Nishino, T. (1990). Cloning and nucleotide sequence of the *ispA* gene responsible for farnesyl diphosphate synthase activity in *Escherichia coli*. *J. Biochem.* 108, 995–1000.

Gauttam, R., Desiderato, C., Jung, L., Shah, A., and Eikmanns, B. J. (2019). A step forward: compatible and dual-inducible expression vectors for gene co-expression in *Corynebacterium glutamicum*. *Plasmid* 101, 20–27. doi: 10.1016/j.plasmid.2018.12.004

Gibson, D. G., Young, L., Chuang, R. Y., Venter, J. C., Hutchison, C. A., and Smith, H. O. (2009). Enzymatic assembly of DNA molecules up to several hundred kilobases. *Nat. Methods* 6, 343–345. doi: 10.1038/nmeth.1318

Green, M. R., and Sambrook, J. (2012). *Molecular Cloning: A Laboratory Manual*, 4th Edn. Cold Spring Harbor, NY: Cold Spring Harbor Laboratory Press.

Gulmezian, M., Hyman, K. R., Marbois, B. N., Clarke, C. F., and Javor, G. T. (2007). The role of UbiX in *Escherichia coli* coenzyme Q biosynthesis. *Arch. Biochem. Biophys.* 467, 144–153. doi: 10.1016/j.abb.2007.08.009

Ha, S.-J., Kim, S.-Y., Seo, J.-H., Sim, W.-I., Moon, H.-J., and Lee, J.-K. (2008). Lactate increases coenzyme Q10 production by *Agrobacterium tumefaciens*. *World J. Microbiol. Biotechnol.* 24, 887–890. doi: 10.1007/s11274-007-9547-8

Hajj Chehade, M., Loiseau, L., Lombard, M., Pecqueur, L., Ismail, A., Smadja, M., et al. (2013). *ubiI*, a new gene in *Escherichia coli* coenzyme Q biosynthesis, is involved in aerobic C5-hydroxylation. *J. Biol. Chem.* 288, 20085–20092. doi: 10.1074/jbc.M113.480368

Hanahan, D. (1983). Studies on transformation of *Escherichia coli* with plasmids. *J. Mol. Biol.* 166, 557–580.

Heider, S. A. E., Peters-Wendisch, P., Beekwilder, J., and Wendisch, V. F. (2014a). IdsA is the major geranylgeranyl pyrophosphate synthase involved in carotenogenesis in *Corynebacterium glutamicum*. *FEBS J.* 281, 4906–4920. doi: 10.1111/febs.13033

Heider, S. A. E., Peters-Wendisch, P., Netzer, R., Stafnes, M., Brautaset, T., and Wendisch, V. F. (2014b). Production and glucosylation of C50 and C40 carotenoids by metabolically engineered *Corynebacterium glutamicum*. *Appl. Microbiol. Biotechnol.* 98, 1223–1235. doi: 10.1007/s00253-013-5359-y

Heider, S. A. E., Wolf, N., Hofemeier, A., Peters-Wendisch, P., and Wendisch, V. F. (2014c). Optimization of the IPP precursor supply for the production of lycopene, decaprenoxanthin and astaxanthin by *Corynebacterium glutamicum*. *Front. Bioeng. Biotechnol.* 2:28. doi: 10.3389/fbioe.2014.00028

Henke, N. A., Heider, S. A. E., Peters-Wendisch, P., and Wendisch, V. F. (2016). Production of the marine carotenoid astaxanthin by metabolically engineered *Corynebacterium glutamicum*. *Mar. Drugs* 14:124. doi: 10.3390/md14070124

Henke, N. A., Wichmann, J., Baier, T., Frohwitter, J., Lauersen, K. J., Risse, J. M., et al. (2018). Patchoulol production with metabolically engineered *Corynebacterium glutamicum*. *Genes* 9:219. doi: 10.3390/genes9040219

Hodgson, J., Watts, G., Playford, D., Burke, V., and Croft, K. (2002). Coenzyme Q10 improves blood pressure and glycaemic control: a controlled trial in subjects with type 2 diabetes. *Eur. J. Clin. Nutr.* 56, 1137–1142. doi: 10.1038/sj.ejcn.1601464

Ishii, K., Sagami, H., and Ogura, K. (1985). Decaprenyl pyrophosphate synthetase from *Paracoccus denitrificans*. *Biochim. Biophys. Acta (BBA) Lipids Lipid Metab.* 835, 291–297. doi: 10.1016/0005-2760(85)90284-X

Jojima, T., Noburyu, R., Sasaki, M., Tajima, T., Suda, M., Yukawa, H., et al. (2015). Metabolic engineering for improved production of ethanol by *Corynebacterium glutamicum*. *Appl. Microbiol. Biotechnol.* 99, 1165–1172. doi: 10.1007/s00253-014-6223-4

Kallscheuer, N., Vogt, M., Bott, M., and Marienhagen, J. (2017). Functional expression of plant-derived O -methyltransferase, flavanone 3-hydroxylase, and flavonol synthase in *Corynebacterium glutamicum* for production of pterostilbene, kaempferol, and quercetin. *J. Biotechnol.* 258, 190–196. doi: 10.1016/j.jbiotec.2017.01.006

Kallscheuer, N., Vogt, M., Stenzel, A., Gätgens, J., Bott, M., and Marienhagen, J. (2016). Construction of a *Corynebacterium glutamicum* platform strain for the production of stilbenes and (2S)-flavanones. *Metab. Eng.* 38, 47–55. doi: 10.1016/j.ymben.2016.06.003

Kang, M.-K., Eom, J.-H., Kim, Y., Um, Y., and Woo, H. M. (2014). Biosynthesis of pinene from glucose using metabolically-engineered *Corynebacterium glutamicum*. *Biotechnol. Lett.* 36, 2069–2077. doi: 10.1007/s10529-014-1578-2

Kawamukai, M. (2002). Biosynthesis, bioproduction and novel roles of ubiquinone. *J. Biosci. Bioeng.* 94, 511–517. doi: 10.1016/S1389-1723(02)80188-8

Kien, N. B., Kong, I.-S., Lee, M.-G., and Kim, J. K. (2010). Coenzyme Q10 production in a 150-l reactor by a mutant strain of *Rhodobacter sphaeroides*. *J. Ind. Microbiol. Biotechnol.* 37, 521–529. doi: 10.1007/s10295-010-0699-4

Kim, B., Jung, H., Lee, J.-Y., Ferrer, L., Purwanto, H. S., and Lee, J. (2020). Production of 4-hydroxybenzyl alcohol by metabolically engineered *Corynebacterium glutamicum*. *Microbiol. Biotechnol. Lett.* 48, 506–514. doi: 10.48022/mbl.2010.10008

Kirchner, O., and Tauch, A. (2003). Tools for genetic engineering in the amino acid-producing bacterium *Corynebacterium glutamicum*. *J. Biotechnol.* 104, 287–299. doi: 10.1016/S0168-1656(03)00148-2

Kitade, Y., Hashimoto, R., Suda, M., Hiraga, K., and Inui, M. (2018). Production of 4-hydroxybenzoic acid by an aerobic growth-arrested bioprocess using metabolically engineered *Corynebacterium glutamicum*. *Appl. Environ. Microbiol.* 84:e02587-17. doi: 10.1128/AEM.02587-17

Kogure, T., Suda, M., Hiraga, K., and Inui, M. (2020). Protocatechuate overproduction by *Corynebacterium glutamicum* via simultaneous engineering of native and heterologous biosynthetic pathways. *Metab. Eng.* (in press). doi: 10.1016/j.ymben.2020.11.007

Koo, B.-S., Gong, Y.-J., Kim, S.-Y., Kim, C.-W., and Lee, H.-C. (2010). Improvement of coenzyme Q 10 production by increasing the NADH/NAD + Ratio in *Agrobacterium tumefaciens*. *Biosci. Biotechnol. Biochem.* 74, 895–898. doi: 10.1271/bbb.100034

Kubota, T., Watanabe, A., Suda, M., Kogure, T., Hiraga, K., and Inui, M. (2016). Production of para-aminobenzoate by genetically engineered *Corynebacterium glutamicum* and non-biological formation of an *N*-glucosyl byproduct. *Metab. Eng.* 38, 322–330. doi: 10.1016/j.ymben.2016.07.010

Kunjapur, A. M., Hyun, J. C., and Prather, K. L. J. (2016). Deregulation of S-adenosylmethionine biosynthesis and regeneration improves methylation in the *E. coli de novo* vanillin biosynthesis pathway. *Microb. Cell Fact.* 15:61. doi: 10.1186/s12934-016-0459-x

Lange, J., Müller, F., Takors, R., and Blombach, B. (2018). Harnessing novel chromosomal integration loci to utilize an organosolv-derived hemicellulose fraction for isobutanol production with engineered *Corynebacterium glutamicum*. *Microb. Biotechnol.* 11, 257–263. doi: 10.1111/1751-7915.12879

Loiseau, L., Fyfe, C., Aussel, L., Hajj Chehade, M., Hernández, S. B., Faivre, B., et al. (2017). The UbiK protein is an accessory factor necessary for bacterial ubiquinone (UQ) biosynthesis and forms a complex with the UQ biogenesis factor UbiJ. *J. Biol. Chem.* 292, 11937–11950. doi: 10.1074/jbc.M117.789164

Lu, W., Shi, Y., He, S., Fei, Y., Yu, K., and Yu, H. (2013). Enhanced production of CoQ10 by constitutive overexpression of 3-demethyl ubiquinone-9 3-methyltransferase under *tac* promoter in *Rhodobacter sphaeroides*. *Biochem. Eng. J.* 72, 42–47. doi: 10.1016/j.bej.2012.12.019

Lu, W., Ye, L., Lv, X., Xie, W., Gu, J., Chen, Z., et al. (2015). Identification and elimination of metabolic bottlenecks in the quinone modification pathway for enhanced coenzyme Q10 production in *Rhodobacter sphaeroides*. *Metab. Eng.* 29, 208–216. doi: 10.1016/j.ymben.2015.03.012

Lu, W., Ye, L., Xu, H., Xie, W., Gu, J., and Yu, H. (2014). Enhanced production of coenzyme Q10 by self-regulating the engineered MEP pathway in *Rhodobacter sphaeroides*. *Biotechnol. Bioeng.* 111, 761–769. doi: 10.1002/bit.25130

Meganathan, R., and Kwon, O. (2009). Biosynthesis of menaquinone (Vitamin K2) and ubiquinone (Coenzyme Q). *EcoSal Plus* 3, 149–159. doi: 10.1128/ecosalplus.3.6.3.3

Mindt, M., Walter, T., Kugler, P., and Wendisch, V. F. (2020). Microbial engineering for production of *N*-functionalized amino acids and amines. *Biotechnol. J.* 15:1900451. doi: 10.1002/biot.201900451

Mischley, L. K., Allen, J., and Bradley, R. (2012). Coenzyme Q10 deficiency in patients with Parkinson's disease. *J. Neurol. Sci.* 318, 72–75. doi: 10.1016/j.jns.2012.03.023

Park, Y.-C., Kim, S.-J., Choi, J.-H., Lee, W.-H., Park, K.-M., Kawamukai, M., et al. (2005). Batch and fed-batch production of coenzyme Q10 in recombinant *Escherichia coli* containing the decaprenyl diphosphate synthase gene from *Gluconobacter suboxydans*. *Appl. Microbiol. Biotechnol.* 67, 192–196. doi: 10.1007/s00253-004-1743-y

Peters-Wendisch, P. G., Schiel, B., Wendisch, V. F., Katsoulidis, E., Möckel, B., Sahm, H., et al. (2001). Pyruvate carboxylase is a major bottleneck for glutamate and lysine production by *Corynebacterium glutamicum*. *J. Mol. Microbiol. Biotechnol.* 3, 295–300.

Pfeifer, E., Gätgens, C., Polen, T., and Frunzke, J. (2017). Adaptive laboratory evolution of *Corynebacterium glutamicum* towards higher growth rates on glucose minimal medium. *Sci. Rep.* 7:16780. doi: 10.1038/s41598-017-17014-9

Poon, W. W., Barkovich, R. J., Hsu, A. Y., Frankel, A., Lee, P. T., Shepherd, J. N., et al. (1999). Yeast and rat Coq3 and *Escherichia coli* UbiG polypeptides catalyze both O-methyltransferase steps in coenzyme Q biosynthesis. *J. Biol. Chem.* 274, 21665–21672. doi: 10.1074/jbc.274.31.21665

Poon, W. W., Davis, D. E., Ha, H. T., Jonassen, T., Rather, P. N., and Clarke, C. F. (2000). Identification of *Escherichia coli ubiB*, a gene required for the first monooxygenase step in ubiquinone biosynthesis. *J. Bacteriol.* 182, 5139–5146. doi: 10.1128/JB.182.18.5139-5146.2000

Purwanto, H. S., Kang, M., Ferrer, L., Han, S., Lee, J.-Y., Kim, H., et al. (2018). Rational engineering of the shikimate and related pathways in *Corynebacterium glutamicum* for 4-hydroxybenzoate production. *J. Biotechnol.* 282, 92–100. doi: 10.1016/j.jbiotec.2018.07.016

Riesenberg, D., and Guthke, R. (1999). High-cell-density cultivation of microorganisms. *Appl. Microbiol. Biotechnol.* 51, 422–430. doi: 10.1007/s002530051412

Rohmer, M., and Rohmer, M. (1999). The discovery of a mevalonate-independent pathway for isoprenoid biosynthesis in bacteria, algae and higher plants. *Nat. Prod. Rep.* 16, 565–574. doi: 10.1039/a709175c

Sambrook, J., Fritsch, E. F., and Maniatis, T. (1989). *Molecular Cloning: A Laboratory Manual*, 2nd Edn. Cold Spring Harbor, NY: Cold Spring Harbor Laboratory Press.

Sato, N., Kishida, M., Nakano, M., Hirata, Y., and Tanaka, T. (2020). Metabolic engineering of shikimic acid-producing *Corynebacterium glutamicum* from glucose and cellobiose retaining its phosphotransferase system function and pyruvate kinase activities. *Front. Bioeng. Biotechnol.* 8:569406. doi: 10.3389/fbioe.2020.569406

Schäfer, A., Tauch, A., Jäger, W., Kalinowski, J., Thierbach, G., and Pühler, A. (1994). Small mobilizable multi-purpose cloning vectors derived from the *Escherichia coli* plasmids pK18 and pK19: selection of defined deletions in the chromosome of *Corynebacterium glutamicum*. *Gene* 145, 69–73. doi: 10.1016/0378-1119(94)90324-7

Shevchenko, A., Tomas, H., Havli, J., Olsen, J. V., and Mann, M. (2006). In-gel digestion for mass spectrometric characterization of proteins and proteomes. *Nat. Protoc.* 1, 2856–2860. doi: 10.1038/nprot.2006.468

Shin, W. S., Lee, D., Lee, S. J., Chun, G. T., Choi, S. S., Kim, E. S., et al. (2018). Characterization of a non-phosphotransferase system for *cis,cis*-muconic acid production in *Corynebacterium glutamicum*. *Biochem. Biophys. Res. Commun.* 499, 279–284. doi: 10.1016/j.bbrc.2018.03.146

Siebert, D., and Wendisch, V. F. (2015). Metabolic pathway engineering for production of 1,2-propanediol and 1-propanol by *Corynebacterium glutamicum*. *Biotechnol. Biofuels* 8:91. doi: 10.1186/s13068-015-0269-0

Simon, R., Priefer, U., and Pühler, A. (1983). A broad host range mobilization system for *In Vivo* genetic engineering: transposon mutagenesis in gram negative bacteria. *Bio Technology* 1, 784–791. doi: 10.1038/nbt1183-784

Stansen, C., Uy, D., Delaunay, S., Eggeling, L., Goergen, J.-L., and Wendisch, V. F. (2005). Characterization of a *Corynebacterium glutamicum* lactate utilization operon induced during temperature-triggered glutamate production. *Appl. Environ. Microbiol.* 71, 5920–5928. doi: 10.1128/AEM.71.10.5920-5928.2005

Suzuki, K., Ueda, M., Yuasa, M., Nakagawa, T., Kawamukai, M., and Matsuda, H. (1994). Evidence that *Escherichia coli ubiA* product is a functional homolog of yeast COQ2, and the regulation of *ubiA* gene expression. *Biosci. Biotechnol. Biochem.* 58, 1814–1819. doi: 10.1271/bbb.58.1814

Takahashi, S., Nishino, T., and Koyama, T. (2003). Isolation and expression of *Paracoccus denitrificans* decaprenyl diphosphate synthase gene for production of ubiquinone-10 in *Escherichia coli*. *Biochem. Eng. J.* 16, 183–190. doi: 10.1016/S1369-703X(03)00035-4

Tian, Y., Yue, T., Pei, J., Yuan, Y., Li, J., and Lo, Y. M. (2010a). Effects of cell lysis treatments on the yield of coenzyme Q10 following *Agrobacterium tumefaciens* fermentation. *Food Sci. Technol. Int.* 16, 195–203. doi: 10.1177/1082013210366788

Tian, Y., Yue, T., Yuan, Y., Soma, P. K., and Lo, Y. M. (2010b). Improvement of cultivation medium for enhanced production of coenzyme Q10 by photosynthetic *Rhodospirillum rubrum*. *Biochem. Eng. J.* 51, 160–166. doi: 10.1016/j.bej.2010.06.011

Vinson, J., and Anamandla, S. (2006). Comparative topical absorption and antioxidant effectiveness of two forms of coenzyme Q10 after a single dose and after long-term supplementation in the skin of young and middle-aged subjects. *Int. J. Cosmet. Sci.* 28, 148–148. doi: 10.1111/j.1467-2494.2006.00307_3.x

Wallace, B. J., and Young, I. G. (1977). Role of quinones in electron transport to oxygen and nitrate in *Escherichia coli*. Studies with a *ubiA- menA-* double quinone mutant. *BBA Bioenerg.* 461, 84–100. doi: 10.1016/0005-2728(77)90071-8

Walter, T., Al Medani, N., Burgardt, A., Cankar, K., Ferrer, L., Kerbs, A., et al. (2020). Fermentative *N*-methylanthranilate production by engineered *Corynebacterium glutamicum*. *Microorganisms* 8:866. doi: 10.3390/microorganisms8060866

Wang, H., Qian, W.-J., Mottaz, H. M., Clauss, T. R. W., Anderson, D. J., Moore, R. J., et al. (2005). Development and evaluation of a micro- and nanoscale proteomic sample preparation method. *J. Proteome Res.* 4, 2397–2403. doi: 10.1021/pr050160f

Weant, K. A., and Smith, K. M. (2005). The role of coenzyme Q 10 in heart failure. *Ann. Pharmacother.* 39, 1522–1526. doi: 10.1345/aph.1E554

Wendisch, V. F. (2020). Metabolic engineering advances and prospects for amino acid production. *Metab. Eng.* 58, 17–34. doi: 10.1016/j.ymben.2019.03.008

Wendisch, V. F., Mindt, M., and Pérez-García, F. (2018). Biotechnological production of mono- and diamines using bacteria: recent progress, applications, and perspectives. *Appl. Microbiol. Biotechnol.* 102, 3583–3594. doi: 10.1007/s00253-018-8890-z

White, M. D., Payne, K. A. P., Fisher, K., Marshall, S. A., Parker, D., Rattray, N. J. W., et al. (2015). UbiX is a flavin prenyltransferase required for bacterial ubiquinone biosynthesis. *Nature* 522, 502–506. doi: 10.1038/nature14559

Wieschalka, S., Blombach, B., Bott, M., and Eikmanns, B. J. (2013). Bio-based production of organic acids with *Corynebacterium glutamicum*. *Microb. Biotechnol.* 6, 87–102. doi: 10.1111/1751-7915.12013

Yang, X., Dai, G., Li, G., and Yang, E. S. (2010). Coenzyme Q10 reduces β-amyloid plaque in an APP/PS1 transgenic mouse model of Alzheimer's disease. *J. Mol. Neurosci.* 41, 110–113. doi: 10.1007/s12031-009-9297-1

Yoshida, H., Kotani, Y., Ochiai, K., and Araki, K. (1998). Production of ubiquinone-10 using bacteria. *J. Gen. Appl. Microbiol.* 44, 19–26. doi: 10.2323/jgam.44.19

Young, I. G., Leppik, R. A., Hamilton, J. A., and Gibson, F. (1972). Biochemical and genetic studies on ubiquinone biosynthesis in *Escherichia coli* K-12:4-hydroxybenzoate octaprenyltransferase. *J. Bacteriol.* 110, 18–25.

Yuan, Y., Tian, Y., and Yue, T. (2012). Improvement of coenzyme Q10 production: mutagenesis induced by high hydrostatic pressure treatment and optimization of fermentation conditions. *J. Biomed. Biotechnol.* 2012:607329. doi: 10.1155/2012/607329

Zahiri, H. S., Yoon, S. H., Keasling, J. D., Lee, S. H., Won Kim, S., Yoon, S. C., et al. (2006). Coenzyme Q10 production in recombinant *Escherichia coli* strains engineered with a heterologous decaprenyl diphosphate synthase gene and foreign mevalonate pathway. *Metab. Eng.* 8, 406–416. doi: 10.1016/j.ymben.2006.05.002

Zhang, D., Shrestha, B., Li, Z., and Tan, T. (2007). Ubiquinone-10 production using *Agrobacterium tumefaciens dps* gene in *Escherichia coli* by coexpression system. *Mol. Biotechnol.* 35, 1–14.

Zhang, J., Gao, D., Cai, J., Liu, H., and Qi, Z. (2018). Improving coenzyme Q10 yield of *Rhodobacter sphaeroides* via modifying redox respiration chain. *Biochem. Eng. J.* 135, 98–104. doi: 10.1016/j.bej.2018.04.006

Zhu, X., Yuasa, M., Okada, K., Suzuki, K., Nakagawa, T., Kawamukai, M., et al. (1995). Production of ubiquinone in *Escherichia coli* by expression of various genes responsible for ubiquinone biosynthesis. *J. Ferment. Bioeng.* 79, 493–495. doi: 10.1016/0922-338X(95)91268-A

Zhu, Y., Lu, W., Ye, L., Chen, Z., Hu, W., Wang, C., et al. (2017). Enhanced synthesis of Coenzyme Q10 by reducing the competitive production of carotenoids in *Rhodobacter sphaeroides*. *Biochem. Eng. J.* 125, 50–55. doi: 10.1016/j.bej.2017.03.019

Conflict of Interest: The authors declare that the research was conducted in the absence of any commercial or financial relationships that could be construed as a potential conflict of interest.

frontiers in Microbiology

MINI REVIEW
published: 07 April 2021
doi: 10.3389/fmicb.2021.654058

Advances and Perspectives for Genome Editing Tools of *Corynebacterium glutamicum*

Qingzhuo Wang[1], Jiao Zhang[2,3], Naief H. Al Makishah[4], Xiaoman Sun[1], Zhiqiang Wen[1,5]*, Yu Jiang[6] and Sheng Yang[2,6]*

[1] School of Food Science and Pharmaceutical Engineering, Nanjing Normal University, Nanjing, China, [2] Key Laboratory of Synthetic Biology, CAS Center for Excellence in Molecular Plant Sciences, Shanghai Institute of Plant Physiology and Ecology, Chinese Academy of Sciences, Shanghai, China, [3] University of Chinese Academy of Sciences, Beijing, China, [4] Environmental Sciences Department, Faculty of Meteorology, Environment and Arid Land Agriculture, King Abdulaziz University, Jeddah, Saudi Arabia, [5] School of Environmental and Biological Engineering, Nanjing University of Science & Technology, Nanjing, China, [6] Huzhou Center of Industrial Biotechnology, Shanghai Institutes of Biological Sciences, Chinese Academy of Sciences, Shanghai, China

OPEN ACCESS

Edited by:
Yu Wang,
Chinese Academy of Sciences, China

Reviewed by:
Suiping Zheng,
South China University of Technology, China
Xixian Xie,
Tianjin University of Science and Technology, China
Lothar Eggeling,
Julich-Forschungszentrum, Helmholtz-Verband Deutscher Forschungszentren (HZ), Germany

***Correspondence:**
Zhiqiang Wen
zqwen@njnu.edu.cn;
zqwen@njust.edu.cn
Xiaoman Sun
xiaomansun@njnu.edu.cn

Specialty section:
This article was submitted to Microbiotechnology, a section of the journal Frontiers in Microbiology

Received: *15 January 2021*
Accepted: *01 March 2021*
Published: *07 April 2021*

Citation:
Wang Q, Zhang J, Al Makishah NH, Sun X, Wen Z, Jiang Y and Yang S (2021) Advances and Perspectives for Genome Editing Tools of Corynebacterium glutamicum. Front. Microbiol. 12:654058. doi: 10.3389/fmicb.2021.654058

Corynebacterium glutamicum has been considered a promising synthetic biological platform for biomanufacturing and bioremediation. However, there are still some challenges in genetic manipulation of *C. glutamicum*. Recently, more and more genetic parts or elements (replicons, promoters, reporter genes, and selectable markers) have been mined, characterized, and applied. In addition, continuous improvement of classic molecular genetic manipulation techniques, such as allelic exchange via single/double-crossover, nuclease-mediated site-specific recombination, RecT-mediated single-chain recombination, actinophages integrase-mediated integration, and transposition mutation, has accelerated the molecular study of *C. glutamicum.* More importantly, emerging gene editing tools based on the CRISPR/Cas system is revolutionarily rewriting the pattern of genetic manipulation technology development for *C. glutamicum*, which made gene reprogramming, such as insertion, deletion, replacement, and point mutation, much more efficient and simpler. This review summarized the recent progress in molecular genetic manipulation technology development of *C. glutamicum* and discussed the bottlenecks and perspectives for future research of *C. glutamicum* as a distinctive microbial chassis.

Keywords: *Corynebacterium*, molecular genetic modification, CRISPR/Cas system, genome editing, toolbox

INTRODUCTION

Corynebacterium glutamicum has been widely used in the food industry for amino acid production (Wendisch et al., 2016). It is also being considered as a promising general-purpose chassis strain for other high-value chemicals (Woo and Park, 2014; Heider and Wendisch, 2015; Becker et al., 2018), as well as an emerging heterologous protein expression host (Liu et al., 2016). However, there are some challenges in developing *C. glutamicum* as a synthetic biology platform (Woo and Park, 2014), especially in the aspect of genome editing tools, lagging far behind *Escherichia coli*.

The genetic modification of *C. glutamicum* can be traced back to 1984 (Ozaki et al., 1984), but the development and application of genetic manipulation technology are progressing slowly (Nesvera and Patek, 2011; Suzuki and Inui, 2013; Yang et al., 2020), which may be attributed to the fact that *C. glutamicum* is a type of Gram-positive actinomyces with high GC content in the genome (Ikeda and Nakagawa, 2003). Unusual cell wall together with deficient homologous

recombination (HR) (for DNA repair) of *C. glutamicum* results in extremely low efficiency in shuttle plasmid transformation and subsequent gene editing (Nesvera and Patek, 2011; Ruan et al., 2015; Yang et al., 2020). In the post-genomic era of *C. glutamicum* (Kalinowski et al., 2003; Lv et al., 2011, 2012), genomics and transcriptomics have promoted the mining and characterization of synthetic biological elements (such as promoters, replicons, and selectable markers) to a certain extent (Tauch et al., 2003; Nesvera et al., 2012; Patek et al., 2013; Rytter et al., 2014; Shang et al., 2018). More and more genetic manipulation tools have been applied in *C. glutamicum* (Nesvera and Patek, 2011; Suzuki and Inui, 2013), including type strain ATCC 13032 and no-model industrial strains such as *Brevibacterium flavum* and *Corynebacterium crenatum* (Xu et al., 2010; Shu et al., 2018). Most importantly, the gene editing technology mediated by CRISPR/Cas system has been successfully developed in *C. glutamicum*, revolutionizing the study of genetic manipulation technology (Jiang et al., 2017).

Here, we reviewed recent advances in genome editing technology of *C. glutamicum*, as summarized in **Table 1**, with a special focus on the CRISPR/Cas system. Technical bottlenecks and future development trends are also discussed.

CLASSIC ALLELIC-EXCHANGE-BASED GENOME EDITING TOOLS

Since *C. glutamicum* can hardly repair DNA through Non-Homologous End Joining (NHEJ), allelic exchange based on HR is the most commonly used genetic manipulation tool (Suzuki and Inui, 2013; Yang et al., 2020). In *C. glutamicum*, both suicide plasmid and replicable plasmid can be used for allelic exchange (Wang et al., 2019a; Wu et al., 2020). Allelic exchange could be achieved by single crossover and double crossover, the results of which vary dependent on the characteristic of homology arms (**Figures 1A,B**).

In *C. glutamicum*, genetic tools based on allelic exchange can basically implement genetic manipulation such as insertion, substitution, deletion, and point mutation (Nesvera and Patek, 2011; Suzuki and Inui, 2013; Yang et al., 2020) and have been widely used in metabolic engineering and chassis development (Woo and Park, 2014). However, there are some drawbacks for allelic exchange. For example, it usually takes a long period (about 8 days) to complete one round of gene editing. Besides, the low efficiency of the second single crossover prevents the desired mutant to be obtained, even after a large number of colony PCR screening (Wen et al., 2020). To ensure the availability of desired mutant strains, counter-selectable markers and nuclease systems are introduced.

SacB gene encoding a levansucrase, which can convert sucrose into a toxic metabolite, is the most commonly used counter-selectable marker in *C. glutamicum*. Schäfer et al. (1994) successfully deleted the hom-*thrB* gene of *C. glutamicum* by SacB-assisted allelic exchange. In later studies, the streptomycin-sensitive gene *rspl* and 5-fluorouracil-lethal gene *upp* were also introduced as negative markers in *C. glutamicum* (Kim et al., 2011; Ma et al., 2015). Screening marker-mediated conditional lethality can help filter out strains that have not undergone the secondary crossover, because only strains that have lost the lethal gene through the second crossover can survive. Therefore, the screening workload is drastically reduced. However, it does not improve the efficiency of HR.

In *C. glutamicum*, nuclease systems such as Cre-loxP and I-SceI system (Yang et al., 2020) have been introduced to force the host to activate a second crossover (by specifically cutting DNA) to survive (Zhang et al., 2015). It not only filters out the transformants that have not undergone the second crossover but also stimulates recombination. However, low-efficiency DNA repair still hinders the acquisition of desired transformants. Therefore, the RecT recombinase system was employed. RecT is a single-stranded DNA annealing protein (SSAPs) (Zhang et al., 1998), which can mediate binding of template DNA strand and homologous DNA by annealing, to realize subsequent exchange and invasion. Accordingly, artificially synthesized ssDNA substrates can effectively achieve site-directed mutagenesis, insertion, and deletion, through recombination (**Figure 1C**).

RecT-mediated ssDNA single-stranded recombination does not rely on the RecA recombination system of the bacteria, but relies on the RecT recombination system encoded by the *recT* gene from the prophage Rac (Zhang et al., 1998). Compared with the natural recombination system in hosts, it is easier to operate and is not affected by DNA sequence and length, which can achieve high-efficiency recombination using even very short homologous DNA sequences as substrates (Murphy et al., 2000; Sawitzke et al., 2011). Binder et al. (2013) introduced RecT recombinase into *C. glutamicum* for the first time. In later studies, Krylov et al. (2014) and Wu et al. (2020) optimized the ssDNA chain length, concentration, base modification, and DNA strand tendency (leading or lagging strand), which further improved the recombination efficiency of ssDNA in *C. glutamicum*. The exonuclease–recombinase pair RecE + RecT (RecET) has also be adapted to promote dsDNA recombination. Recently, Huang et al. (2017) reported an effective and sequential deletion method based on RecET and Cre/loxP system, which has been successfully applied for L-leucine production in *C. glutamicum* (Luo et al., 2020).

Although RecT/ssDNA- or RecET/dsDNA-mediated recombineering simplifies the operation of genome editing, only one gene can be edited at one round in *C. glutamicum*. By contrast, in *E. coli*, oligonucleotide-mediated multiple-site editing of the genome has been successfully applied for over 10 years (Wang et al., 2009; Isaacs et al., 2011). It implied that ssDNA/dsDNA electroporation efficiency and the expression level of the RecT/RecET in *C. glutamicum* need to be further optimized.

REVOLUTIONARY CRISPR/CAS-BASED GENOME EDITING TOOLS

The CRISPR/Cas system has achieved great success in various prokaryotic and eukaryotic microorganisms and is regarded as a revolutionary gene manipulation technology

TABLE 1 | Comparison of different genetic tools applicable in *C. glutamicum*.

Genome editing tools	Principles or outcome(s)	Advantages	Putative drawbacks	References
Allelic exchange	HR (homologous recombination)-mediated in-frame deletion or insertion	Versatile and broadly applicable	Limited to low HR efficiency	Niebisch and Bott, 2001; Unthan et al., 2015; Baumgart et al., 2016; Baumgart et al., 2018
Counter-marker-assisted allelic exchange	Marker-mediated conditional lethality to retain mutants with second crossover	Filtering out false positives to reduce workload	Failing to stimulate HR	Niebisch and Bott, 2001; Kim et al., 2011; Ma et al., 2015
Cre-loxP or I-SceI system-assisted allelic exchange	DNA cleavage by Cre or I-SceI to accelerate second crossover	Filtering out false positives to reduce workload; stimulating HR	Remaining recognition site may interference next round of operation	Suzuki et al., 2005b; Suzuki et al., 2005d; Ma et al., 2015; Huang et al., 2017; Zhan et al., 2019; Luo et al., 2020; Marques et al., 2020; Wu et al., 2020
RecET/ssDNA(dsDNA)-mediated recombination	RecT recombination system-mediated HR	Independent of host recombination system; straightforward procedure	Limited to RecET expression and ssDNA/ds DNA transformation efficiency	Binder et al., 2013; Krylov et al., 2014; Huang et al., 2017; Su et al., 2018; Luo et al., 2020
CRISPR/Cas9	Cas9-mediated DSB to stimulate DNA repair	Broadly applicable and function diversity	Toxicity of DSB; limited to host DNA repair capability	Liu et al., 2017; Peng et al., 2017; Coates et al., 2019
CRISPR/Cas9 + RecT/ssDNA	Cas9-mediated DSB and RecT recombination system mediated HR	Enhanced recombination efficiency	Limited to RecT expression and ssDNA transformation efficiency	Cho et al., 2017; Liu et al., 2018; Wang B. et al., 2018
CRISPR/dCas9	Steric hindrance effect of dCas9 to repress transcription	Fine transcription level regulation of any given gene	Dependent on sgRNA and target gene	Cleto et al., 2016; Lee et al., 2018; Yoon and Woo, 2018; Gauttam et al., 2019
CRISPR/Cpf1	Cas9-mediated DSB to stimulate DNA repair	Decreased toxicity; multiple sites editing; broadly applicable	Toxicity of DSB; limited to host DNA repair capability	Jiang et al., 2017; Krumbach et al., 2019; Zhang et al., 2019; Dong et al., 2020; Li M. et al., 2020
CRISPR/Cpf1 + RecT/ssDNA	Cas9-mediated DSB and RecT recombination system mediated HR	Enhanced recombination efficiency and multiple sites editing	Limited to RecT expression and ssDNA transformation efficiency	Jiang et al., 2017; Wang et al., 2019b; Zhang J. et al., 2020; Zhao et al., 2020
CRISPR/dCpf1	Steric hindrance effect of dCpf1 to repress transcription	Fine transcription level regulation of any given gene	Dependent on sgRNA and target gene	Li M. et al., 2020
Cytosine base editor (CBE)	Activation-induced cytidine deaminase (AID) and CRISPR/dCas9 convert C to T in editing window	High efficiency and multiple sites editing	Limited base transition capability	Wang Y. et al., 2018; Deng et al., 2020; Li J. et al., 2020
Adenine base editor (ABE)	tRNA adenosine deaminase and CRISPR/dCas9 convert A to G in editing window	High efficiency and multiple sites editing	Limited base transition capability	Wang et al., 2019c; Deng et al., 2020
TadA-dCas9-AID	Combination of CBE and ABE	Bi-directional base conversion to achieve C–T, C–G and A–G conversion	Limited base transition capability	Deng et al., 2020
Base editor (BE3)	Cytidine deaminase and uracil DNA glycosylase inhibitor; converting specific C·G nucleotide base pairs to T·A	High efficiency and multiple sites editing	Limited base transition capability	Huang et al., 2020
MACBETH	Robotic system-assisted multiplex automated base editing	Automated, ultra-high-throughput multiple sites editing	Limited base transition capability	Wang Y. et al., 2018
Actinophages integrase mediated integration	TP901-1, ϕC31 or ϕBT1 integrase mediated integration	Site-directed integration of long DNA fragment	Attachment sites need to be installed in advance	Shen et al., 2017; Marques et al., 2020
Transposon	Random transposon disruption or inactivation	Easy to construct single-gene disruptant mutant library	Inaccurate genome editing	Vertes et al., 1994; Inui et al., 2005; Suzuki et al., 2006; Gorshkova et al., 2018
Transposon + Cre-loxP system	Random long or short DNA fragments deletion	Easy to construct reduced genome mutant library	Inaccurate genome reducing	Tsuge et al., 2007

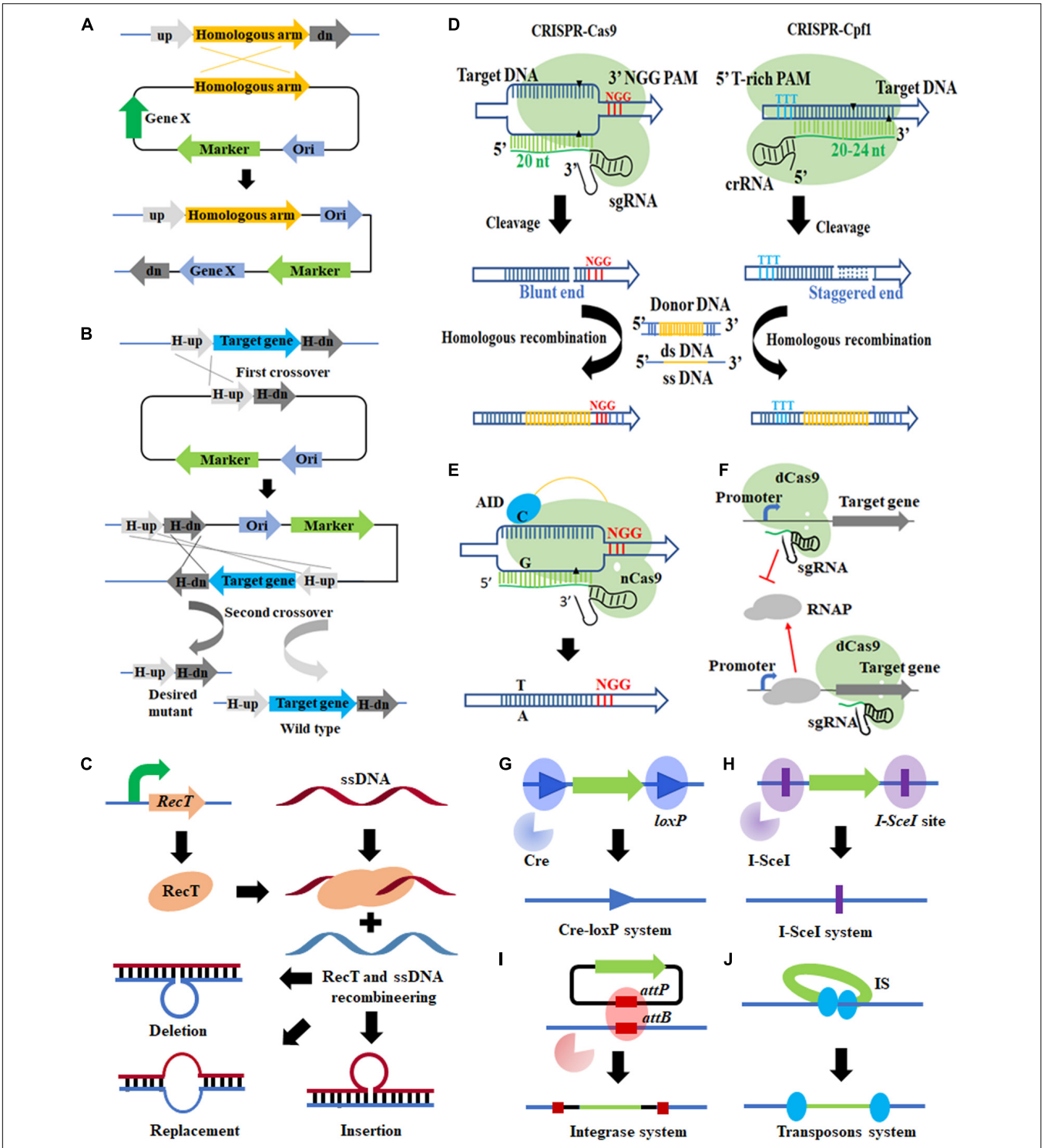

FIGURE 1 | Genome editing tools applicable in *Corynebacterium glutamicum*. **(A,B)** Allelic exchange-based tools (single and double crossover); **(C)** RecT-ssDNA-mediated recombination; **(D)** CRISPR/Cas system; **(E)** CRISPR/Cas system-assisted base editing system; **(F)** CRISPR/Cas system-assisted transcription regulation; **(G)** Cre-loxP system; **(H)** I-SceI system; **(I)** integrase-mediated site-specific integration; **(J)** transposon.

(Jinek et al., 2012; Cong et al., 2013). A lot of effort has been paid to introduce the CRISPR/Cas system into *C. glutamicum*, but progress was not smooth initially, because *C. glutamicum* cannot tolerate the toxicity of Cas9 expression (Cho et al., 2017; Jiang et al., 2017). This explains why CRISPR interference (CRISPRi) mediated by CRISPR/dCas9 [dead

Cas9, harboring D10A and H840A mutations in Cas9, no nuclease activity (Bikard et al., 2013)], but not CRISPR/Cas9-based genome editing, was first applied to *C. glutamicum* (Cleto et al., 2016).

CRISPRi can be used to regulate the transcriptional level of any given gene by steric hindrance effect (**Figure 1F**) and is especially suitable to down-regulate essential genes because they cannot be inactivated directly (Wen et al., 2017). In *C. glutamicum*, CRISPR/dCas9-mediated single-gene transcriptional repression (Cleto et al., 2016; Lee et al., 2018; Yoon and Woo, 2018; Gauttam et al., 2019) and CRISPR-dCpf1-mediated down-regulation of multiple genes have been achieved (Liu et al., 2019; Li M. et al., 2020), but hardly no study about transcriptional activation has been reported.

As for genome editing, after observing lethality of Cas9 expression to *C. glutamicum*, Jiang et al. (2017) developed a gene editing tool based on *Francisella novicida* (Fn) CRISPR/Cpf1 (**Figure 1D**), in which DSB created by Cpf1 (a staggered end) can be repaired by DNA templates. When ssDNA and RecT recombination systems were introduced, more types of gene editing including gene deletion/insertion/point mutation were realized (Jiang et al., 2017). It represented a milestone in gene editing tools development of *C. glutamicum* and was successfully applied in six other industrial *Corynebacterium* strains.

Immediately after this work, breakthroughs in CRISPR/Cas9 system development were achieved. Cho et al. (2017) found that the codon optimization of the Cas9 gene reduced the toxicity of Cas9 expression; in addition, when RecT and ssDNA recombineering were employed to further facilitate recombination at the target loci, genome editing based on the CRISPR/Cas9 system in *C. glutamicum* was realized for the first time. In parallel studies, controlling the expression of Cas9 under an inducible promoter also achieved the goal of reducing toxicity (Liu et al., 2017; Peng et al., 2017).

The CRISPR/Cas system was subsequently optimized in the aspects of Cas9 expression stability (Wang B. et al., 2018), the convenience of curing Cas9 plasmids (Cho et al., 2017), transformation efficiency of Cas9 plasmids (Coates et al., 2019), crRNA delivery vector design (Krumbach et al., 2019), protospacer adjacent motif (PAM) sequence, the length of the spacer sequence, and the type of repair template (Wang et al., 2019c; Zhang et al., 2019), among others. Moreover, counter-selectable markers (Zhang J. et al., 2020) and ssDNA-RecT recombination engineering (Liu et al., 2018; Wang B. et al., 2018; Zhao et al., 2020) have also been introduced to further optimize the gene editing system. The application of the CRISPR/Cas system has been expanded from single gene editing to multiplex gene editing and large DNA fragment deletion (Liu et al., 2017; Wang B. et al., 2018; Zhao et al., 2020). However, it is still conditioned to the inefficient HR of *C. glutamicum*.

Base editing can create a missense mutation or null mutation in a gene via base substitution without introducing a DSB (Komor et al., 2016; Nishida et al., 2016), which is especially suitable for strains with inefficient HR (like *C. glutamicum*), and has attracted increasing attention (Wen et al., 2020). Wang Y. et al. (2018) developed a cytosine base editor (CBE) applicable in *C. glutamicum* based on activation-induced cytidine deaminase (AID) and the CRISPR/Cas9 system (**Figure 1E**), which can efficiently achieve C–T conversion with efficiencies up to 100%, 87.2%, and 23.3% for single-, double-, and triple-locus editing, respectively. In subsequent work, they fused tRNA adenosine deaminase from *E. coli* (TadA) with different Cas9 variants to construct different adenine base editors (ABEs), which can convert specific A·T nucleotide base pairs in the CRISPR-Cas9 targeting window sequence to G·C (Wang et al., 2019c). By combining the above CBE and ABE tools in one system, Deng et al. (2020) developed a bi-directional base conversion tool TadA-dCas9-AID, which achieved the base conversion of C–T, C–G, and A–G in the editing window. Most recently, Huang et al. developed a BE3 Cytidine Base Editor by fusing the cytidine deaminase (rat Apobec1), nCas9, and uracil DNA glycosylase inhibitor (UGI). It can convert C to T with a conversion efficiency up to 90% (Huang et al., 2020), which provided more tools for base editing.

Parallel to base editing tools development to explore different base transition capability, the system optimization has also made progress. Wang et al. found that some Cas9 variants can accept different PAM sequences, which increased their genome-targeting scope for base editing. Besides, base editing window was expanded from 5 to 7 bp when truncated or extended guide RNAs were adapted (Wang et al., 2019c). They also provided an online tool (gBIG[1]) for designing guide RNAs for base editing-mediated inactivation (Wang et al., 2019c). It is particularly exciting that an integrated robotic system-assisted automation base editing platform based on MACBETH was constructed (Wang Y. et al., 2018), which represented a new trend in future studies.

CRISPR/Cas system-based genome and base editing tools have brought the development of genetic manipulation technology into a new era due to its multiple functions, higher efficiency, shorter cycle, and more sophisticated modification over the traditional allelic exchange (Cho et al., 2017; Jiang et al., 2017; Wang Y. et al., 2018). Currently, the CRISPR/Cas system is generally preferred and increasingly applied in strain breeding (Bott and Eggeling, 2017), including rapid identification of unknown genes (Lee et al., 2018), complicated metabolic engineering (Zhang J. et al., 2020), and rational genome evolution (Zhao et al., 2020).

INDISPENSABLE HR-INDEPENDENT GENOME EDITING TOOLS

There are some HR-independent genome editing tools applicable in *C. glutamicum*, such as the aforementioned Cre-loxP and I-SceI systems. Nuclease Cre mediates intramolecular recombination of two loxP sites (**Figure 1G**), so that the DNA sequence between the loxP sites is deleted or rearranged, leaving a loxP site in chromosome (Suzuki et al., 2005a,d). Suzuki et al. (2005c; 2005d) realized large fragment deletion and genome rearrangement in *C. glutamicum* using the Cre-loxP system. A total of 11 distinct genomic regions (up to 250 kb, 7.5% of the genome) were successfully deleted. A putative problem is

[1]http://www.ibiodesign.net/gBIG

that the loxP sites remaining in chromosome may interfere with subsequent rounds of Cre/loxP recombination (Suzuki et al., 2005a). To avoid that, a pair of mutant lox sites (lox66 and lox71) was introduced to replace the loxP site. The lox72 site, generated from Cre, caused site-specific recombination of lox66 and lox71 and cannot be recognized by Cre, which facilitated continuous Cre-lox recombination (Suzuki et al., 2005a; Hu et al., 2014).

As for the I-SceI system (**Figure 1H**), it consists of a homing endonuclease I-SceI and an 18-bp specific sequence (5′-TAGGGATAACAGGGTAAT-3′) (Zhang et al., 2015). The system has been adapted in *C. glutamicum* for genes knock-out and knock-in (Suzuki et al., 2005b; Ma et al., 2015; Wu et al., 2020). In addition, it is often used in conjunction with counter-selectable markers such as *SacB*, *Upp*, and the Cre-loxP system (Suzuki et al., 2005d; Ma et al., 2015; Wu et al., 2020).

It should be noted that the specific recognition sequence of the nuclease is difficult to customize, and the recognition site of the recombinase must be introduced into the chromosome in advance (Nesvera and Patek, 2011; Suzuki and Inui, 2013; Yang et al., 2020). It explained why site-specific recombination tools are usually used in combination with allelic exchange-based tools.

Different from Cre-loxP and I-SceI systems, transposon is a simple tool that can perform genome editing independently (**Figure 1J**). It can cause interruption or inactivation of some genes by random transposon insertion (Alain et al., 1994). Many transposable elements have been identified and used in *C. glutamicum*, such as IS31831 (Vertes et al., 1994), miniTn31831 (Alain et al., 1994), Tn14751 (Inui et al., 2005), IS1249 (Tauch et al., 1995), Tn5 (Suzuki et al., 2006), and mini-Mu (Gorshkova et al., 2018). These transposons have different transposition efficiency, sequence preference (AT-rich regions or GC-rich regions preference), and cargo delivery capacity. The combined application of different transposable elements can make up for each other's deficiencies, thereby identifying more genes with unknown functions. For example, a combination of the miniTn31831 and Tn5 transposome systems successfully constructed a pool of 13,000 transposon mutants, equal to a library of 2300 different single-gene disruptant mutants, covering 75% of genes in *C. glutamicum* (Suzuki et al., 2006).

Transposon can be used not only for random knockout of single gene but also for random deletion of chromosome fragments when it is combined with nuclease systems (Goryshin et al., 2003; Tsuge et al., 2007). Random segment deletion based on IS31831 and Cre/loxP excision system has been applied for genome reduction of *C. glutamicum* by random deletion of DNA fragments (Tsuge et al., 2007). Compared with conventional strategies (genomic analysis combined with precise deletion) (Baumgart et al., 2013, 2016, 2018; Unthan et al., 2015), this strategy has been considered as a faster way to create a minimum bacterial genome (Suzuki and Inui, 2013).

Unfortunately, transposons are rarely used for random integration of heterogenous genes, because the length of cargo fragments is usually limited (Gorshkova et al., 2018). By contrast, integrase-mediated site-directed integration of heterologous genes can integrate fragments up to tens of kb (**Figure 1I**) (Huang et al., 2019). Shen et al. (2017) employed a phage integrase TP901-1-mediated chromosomal integration method in *C. glutamicum*, which realized the integration of two reporter genes, implying good application potential. In another study, Marques et al. (2020) developed two markerless integrative systems, respectively, based on actinophage ϕC31 and ϕBT1 for stable inheritance of the introduced genetic traits. Similar to the Cre-loxP and I-SceI system, the prerequisite for integrase-mediated site-directed integration is that the attB site has been integrated into the chromosome by allelic exchange in advance (Shen et al., 2017; Marques et al., 2020). To realize one-step site-directed integration, Strecker et al. (2019) and Klompe et al. (2019), respectively, developed CRISPR-associated transposon-mediated RNA-guided programmable DNA integration methods in *E. coli*. These methods do not rely on HR and have achieved multi-site and multi-copy integration of heterologous genes in *E. coli* and *Tatumella citrea* (Vo et al., 2020; Zhang Y. et al., 2020). It is expected to be introduced into *C. glutamicum* for high-efficiency, multiplexed chromosome integration.

Table 1 summarizes and compares the principles, effects, advantages, and putative drawbacks of various genetic manipulation tools in *C. glutamicum*. According to the table, the CRISPR/Cas system has obvious advantages over other methods but is far from perfect. Classic tools such as counter-selectable markers, ssDNA-RecT recombineering, transposons, and nuclease could be employed in the CRISPR/Cas system to further improve efficiency and expand functions. The combination of different genetic manipulation tools to achieve new editing purposes has become a trend (Suzuki and Inui, 2013; Yang et al., 2020). Besides, many efforts have been paid to overcome barriers to introduce these tools to non-model *Corynebacterium* strains (Jiang et al., 2017; Coates et al., 2019).

Synthetic biology is profoundly rewriting the development pattern of genetic modification of *C. glutamicum*. Artificial intelligence-assisted massive omics data mining may greatly enrich the genetic element library of *C. glutamicum*; advanced models or algorithms could rationally guide chassis cells design; coupled with a new generation of high-throughput, automated biological casting platform, they should enable the future development of more effective *C. glutamicum*.

AUTHOR CONTRIBUTIONS

QW, XS, and ZW conceived the project and wrote the manuscript. All authors participated in the discussion, revised the manuscript, and approved the final manuscript.

FUNDING

This study was supported by grants from the National Natural Science Foundation of China (21706133, 21825804, 31670094, and 31971343), the Funds for Creative Research Groups of China (31921006), and the Key Laboratory of Biomass Chemical Engineering of Ministry of Education, Zhejiang University (2018BCE003).

REFERENCES

Alain, A. V., Asai, Y., Inui, M., Kobayashi, M., Kurusu, Y., and Yukawa, H. (1994). Transposon mutagenesis of coryneform bacteria. *Mol. Gen. Genet.* 245, 397–405.

Baumgart, M., Unthan, S., Kloss, R., Radek, A., Polen, T., Tenhaef, N., et al. (2018). *Corynebacterium glutamicum* chassis C1*: building and testing a novel platform host for synthetic biology and industrial biotechnology. *Acs Synth. Biol.* 7, 132–144. doi: 10.1021/acssynbio.7b00261

Baumgart, M., Unthan, S., Radek, A., Herbst, M., Siebert, D., Bruehl, N., et al. (2016). Chassis organism from *Corynebacterium glutamicum*–Genome reduction as a tool toward improved strains for synthetic biology and industrial biotechnology. *N. Biotechnol.* 33, S25–S25. doi: 10.1016/j.nbt.2016.06.814

Baumgart, M., Unthan, S., Rueckert, C., Sivalingam, J., Gruenberger, A., Kalinowski, J., et al. (2013). Construction of a prophage-free variant of *Corynebacterium glutamicum* ATCC 13032 for use as a platform strain for basic research and industrial biotechnology. *Appl. Environ. Microbiol.* 79, 6006–6015. doi: 10.1128/aem.01634-13

Becker, J., Rohles, C. M., and Wittmann, C. (2018). Metabolically engineered *Corynebacterium glutamicum* for bio-based production of chemicals, fuels, materials, and healthcare products. *Metab. Eng.* 50, 122–141. doi: 10.1016/j.ymben.2018.07.008

Bikard, D., Jiang, W. Y., Samai, P., Hochschild, A., Zhang, F., and Marraffini, L. A. (2013). Programmable repression and activation of bacterial gene expression using an engineered CRISPR-Cas system. *Nucleic Acids Res.* 41, 7429–7437.

Binder, S., Siedler, S., Marienhagen, J., Bott, M., and Eggeling, L. (2013). Recombineering in *Corynebacterium glutamicum* combined with optical nanosensors: a general strategy for fast producer strain generation. *Nucleic Acids Res.* 41, 6360–6369. doi: 10.1093/nar/gkt312

Bott, M., and Eggeling, L. (2017). "Novel technologies for optimal strain breeding," in *Advances in Biochemical Engineering/Biotechnology: Amino Acid Fermentation*, eds A. Yokota and M. Ikeda (Tokyo: Springer Japan), 227–254. doi: 10.1007/10_2016_33

Cho, J. S., Choi, K. R., Prabowo, C. P. S., Shin, J. H., Yang, D., Jang, J., et al. (2017). CRISPR/Cas9-coupled recombineering for metabolic engineering of *Corynebacterium glutamicum*. *Metab. Eng.* 42, 157–167. doi: 10.1016/j.ymben.2017.06.010

Cleto, S., Jensen, J. V. K., Wendisch, V. F., and Lu, T. K. (2016). *Corynebacterium glutamicum* metabolic engineering with CRISPR interference (CRISPRi). *ACS Synth. Biol.* 5, 375–385. doi: 10.1021/acssynbio.5b00216

Coates, R. C., Blaskowski, S., Szyjka, S., van Rossum, H. M., Vallandingham, J., Patel, K., et al. (2019). Systematic investigation of CRISPR-Cas9 configurations for flexible and efficient genome editing in *Corynebacterium glutamicum* NRRL-B11474. *J. Ind. Microbiol. Biotechnol.* 46, 187–201. doi: 10.1007/s10295-018-2112-7

Cong, L., Ran, F. A., Cox, D., Lin, S., Barretto, R., Habib, N., et al. (2013). Multiplex genome engineering using CRISPR/cas systems. *Science* 339, 819–823. doi: 10.1126/science.1231143

Deng, C., Lv, X., Li, J., Liu, Y., Du, G., and Liu, L. (2020). Development of a DNA double-strand break-free base editing tool in *Corynebacterium glutamicum* for genome editing and metabolic engineering. *Metab. Eng. Commun.* 11:e00135. doi: 10.1016/j.mec.2020.e00135

Dong, J., Kan, B., Liu, H., Zhan, M., Wang, S., Xu, G., et al. (2020). CRISPR-Cpf1-assisted engineering of *Corynebacterium glutamicum* SNK118 for enhanced l-ornithine production by NADP-Dependent Glyceraldehyde-3-Phosphate Dehydrogenase and NADH-Dependent Glutamate Dehydrogenase. *Appl. Biochem. Biotechnol.* 191, 955–967. doi: 10.1007/s12010-020-03231-y

Gauttam, R., Seibold, G. M., Mueller, P., Weil, T., Weiss, T., Handrick, R., et al. (2019). A simple dual-inducible CRISPR interference system for multiple gene targeting in *Corynebacterium glutamicum*. *Plasmid* 103, 25–35. doi: 10.1016/j.plasmid.2019.04.001

Gorshkova, N. V., Lobanova, J. S., Tokmakova, I. L., Smirnov, S. V., Akhverdyan, V. Z., Krylov, A. A., et al. (2018). Mu-driven transposition of recombinant mini-Mu unit DNA in the *Corynebacterium glutamicum* chromosome. *Appl. Microbiol. Biotechnol.* 102, 2867–2884. doi: 10.1007/s00253-018-8767-1

Goryshin, I. Y., Naumann, T. A., Apodaca, J., and Reznikoff, W. S. (2003). Chromosomal deletion formation system based on Tn5 double transposition: use for making minimal genomes and essential gene analysis. *Genome Res.* 13, 644–653.

Heider, S. A. E., and Wendisch, V. F. (2015). Engineering microbial cell factories: metabolic engineering of *Corynebacterium glutamicum* with a focus on non-natural products. *Biotechnol. J.* 10, 1170–1184. doi: 10.1002/biot.201400590

Hu, J., Li, Y., Zhang, H., Tan, Y., and Wang, X. (2014). Construction of a novel expression system for use in *Corynebacterium glutamicum*. *Plasmid* 75, 18–26. doi: 10.1016/j.plasmid.2014.07.005

Huang, H., Bai, L., Liu, Y., Li, J., Wang, M., and Hua, E. (2020). Development and application of BE3 cytidine base editor in *Corynebacterium glutamicum*. *Biotechnol. Bull.* 36, 95–101.

Huang, H., Chai, C., Yang, S., Jiang, W., and Gu, Y. (2019). Phage serine integrase-mediated genome engineering for efficient expression of chemical biosynthetic pathway in gas-fermenting *Clostridium ljungdahlii*. *Metab. Eng.* 52, 293–302. doi: 10.1016/j.ymben.2019.01.005

Huang, Y., Li, L., Xie, S., Zhao, N., Han, S., Lin, Y., et al. (2017). Recombineering using RecET in *Corynebacterium glutamicum* ATCC14067 via a self-excisable cassette. *Sci. Rep.* 7:7916. doi: 10.1038/s41598-017-08352-9

Ikeda, M., and Nakagawa, S. (2003). The *Corynebacterium glutamicum* genome: features and impacts on biotechnological processes. *Appl. Microbiol. Biotechnol.* 62, 99–109. doi: 10.1007/s00253-003-1328-1

Inui, M., Tsuge, Y., Suzuki, N., Vertes, A. A., and Yukawa, H. (2005). Isolation and characterization of a native composite transposon, Tn14751, carrying 17.4 kilobases of *Corynebacterium glutamicum* chromosomal DNA. *Appl. Environ. Microbiol.* 71, 407–416. doi: 10.1128/aem.71.1.407-416.2005

Isaacs, F. J., Carr, P. A., Wang, H. H., Lajoie, M. J., Sterling, B., Kraal, L., et al. (2011). Precise manipulation of chromosomes in vivo enables genome-wide codon replacement. *Science* 333, 348–353.

Jiang, Y., Qian, F., Yang, J., Liu, Y., Dong, F., Xu, C., et al. (2017). CRISPR-Cpf1 assisted genome editing of *Corynebacterium glutamicum*. *Nat. Commun.* 8:15179. doi: 10.1038/ncomms15179

Jinek, M., Chylinski, K., Fonfara, I., Hauer, M., Doudna, J. A., and Charpentier, E. (2012). A programmable dual-RNA-guided DNA endonuclease in adaptive bacterial immunity. *Science* 337, 816–821. doi: 10.1126/science.1225829

Kalinowski, J., Bathe, B., Bartels, D., Bischoff, N., Bott, M., Burkovski, A., et al. (2003). The complete *Corynebacterium glutamicum* ATCC 13032 genome sequence and its impact on the production of L-aspartate-derived amino acids and vitamins. *J. Biotechnol.* 104, 5–25. doi: 10.1016/s0168-1656(03)00154-8

Kim, I. K., Jeong, W. K., Lim, S. H., Hwang, I. K., and Kim, Y. H. (2011). The small ribosomal protein S12P gene rpsL as an efficient positive selection marker in allelic exchange mutation systems for *Corynebacterium glutamicum*. *J. Microbiol. Methods* 84, 128–130. doi: 10.1016/j.mimet.2010.10.007

Klompe, S. E., Vo, P. L. H., Halpin-Healy, T. S., and Sternberg, S. H. (2019). Transposon-encoded CRISPR-Cas systems direct RNA-guided DNA integration. *Nature* 571, 219–225. doi: 10.1038/s41586-019-1323-z

Komor, A. C., Kim, Y. B., Packer, M. S., Zuris, J. A., and Liu, D. R. (2016). Programmable editing of a target base in genomic DNA without double-stranded DNA cleavage. *Nature* 533, 420–424.

Krumbach, K., Sonntag, C. K., Eggeling, L., and Marienhagen, J. (2019). CRISPR/Cas12a mediated genome editing to introduce amino acid substitutions into the mechanosensitive channel MscCG of *Corynebacterium glutamicum*. *ACS Synth. Biol.* 8, 2726–2734. doi: 10.1021/acssynbio.9b00361

Krylov, A. A., Kolontaevsky, E. E., and Mashko, S. V. (2014). Oligonucleotide recombination in corynebacteria without the expression of exogenous recombinases. *J. Microbiol. Methods* 105, 109–115. doi: 10.1016/j.mimet.2014.07.028

Lee, S. S., Shin, H., Jo, S., Lee, S.-M., Um, Y., and Woo, H. M. (2018). Rapid identification of unknown carboxyl esterase activity in *Corynebacterium glutamicum* using RNA-guided CRISPR interference. *Enzyme Microb. Technol.* 114, 63–68. doi: 10.1016/j.enzmictec.2018.04.004

Li, J., Liu, Y., Wang, Y., Yu, P., Zheng, P., and Wang, M. (2020). Optimization of base editing in *Corynebacterium glutamicum*. *Chin. J. Biotechnol.* 36, 143–151. doi: 10.13345/j.cjb.190192

Li, M., Chen, J., Wang, Y., Liu, J., Huang, J., Chen, N., et al. (2020). Efficient multiplex gene repression by CRISPR-dCpf1 in *Corynebacterium glutamicum*. *Front. Bioeng. Biotechnol.* 8:357. doi: 10.3389/fbioe.2020.00357

Liu, J., Wang, Y., Lu, Y., Zheng, P., Sun, J., and Ma, Y. (2017). Development of a CRISPR/Cas9 genome editing toolbox for *Corynebacterium glutamicum*. *Microb. Cell Fact.* 16:205. doi: 10.1186/s12934-017-0815-5

Liu, J., Wang, Y., Zheng, P., and Sun, J. (2018). CRISPR/Cas9-mediated ssDNA Recombineering in *Corynebacterium glutamicum*. *Bio Protoc.* 8:e3038. doi: 10.21769/BioProtoc.3038

Liu, W., Tang, D., Wang, H., Lian, J., Huang, L., and Xu, Z. (2019). Combined genome editing and transcriptional repression for metabolic pathway engineering in *Corynebacterium glutamicum* using a catalytically active Cas12a. *Appl. Microbiol. Biotechnol.* 103, 8911–8922. doi: 10.1007/s00253-019-10118-4

Liu, X., Yang, Y., Zhang, W., Sun, Y., Peng, F., Jeffrey, L., et al. (2016). Expression of recombinant protein using *Corynebacterium Glutamicum*: progress, challenges and applications. *Crit. Rev. Biotechnol.* 36, 652–664. doi: 10.3109/07388551.2015.1004519

Luo, G., Zhao, N., Jiang, S., and Zheng, S. (2020). Application of RecET-Cre/loxPsystem in *Corynebacterium glutamicum* ATCC14067 forl-leucine production. *Biotechnol. Lett* 43, 297–306. doi: 10.1007/s10529-020-03000-1

Lv, Y., Liao, J., Wu, Z., Han, S., Lin, Y., and Zheng, S. (2012). Genome Sequence of *Corynebacterium glutamicum* ATCC 14067, which provides insight into amino acid biosynthesis in coryneform bacteria. *J. Bacteriol.* 194, 742–743. doi: 10.1128/jb.06514-11

Lv, Y., Wu, Z., Han, S., Lin, Y., and Zheng, S. (2011). Genome sequence of *Corynebacterium glutamicum* S9114, a strain for industrial production of glutamate. *J. Bacteriol.* 193, 6096–6097. doi: 10.1128/jb.06074-11

Ma, W., Wang, X., Mao, Y., Wang, Z., Chen, T., and Zhao, X. (2015). Development of a markerless gene replacement system in *Corynebacterium glutamicum* using upp as a counter-selection marker. *Biotechnol. Lett.* 37, 609–617. doi: 10.1007/s10529-014-1718-8

Marques, F., Luzhetskyy, A., and Mendes, M. V. (2020). Engineering *Corynebacterium glutamicum* with a comprehensive genomic library and phage-based vectors. *Metab. Eng.* 62, 221–234. doi: 10.1016/j.ymben.2020.08.007

Murphy, K. C., Campellone, K. G., and Poteete, A. R. (2000). PCR-mediated gene replacement in *Escherichia coli*. *Gene* 246, 321–330.

Nesvera, J., Holatko, J., and Patek, M. (2012). Analysis of *Corynebacterium glutamicum* promoters and their applications. *Subcell. Biochem.* 64, 203–221. doi: 10.1007/978-94-007-5055-5_10

Nesvera, J., and Patek, M. (2011). Tools for genetic manipulations in *Corynebacterium glutamicum* and their applications. *Appl. Microbiol. Biotechnol.* 90, 1641–1654. doi: 10.1007/s00253-011-3272-9

Niebisch, A., and Bott, M. (2001). Molecular analysis of the cytochrome bc1-aa3 branch of the *Corynebacterium glutamicum* respiratory chain containing an unusual diheme cytochrome c1. *Arch. Microbiol.* 175, 282–294. doi: 10.1007/s002030100262

Nishida, K., Arazoe, T., Yachie, N., Banno, S., Kakimoto, M., Tabata, M., et al. (2016). Targeted nucleotide editing using hybrid prokaryotic and vertebrate adaptive immune systems. *Science* 353:aaf8729.

Ozaki, A., Katsumata, R., Oka, T., and Furuya, A. (1984). Functional expression of the genes of *Escherichia coli* in gram-positive *Corynebacterium glutamicum*. *Mol. Gen. Genet.* 196, 175–178. doi: 10.1007/bf00334113

Patek, M., Holatko, J., Busche, T., Kalinowski, J., and Nesvera, J. (2013). *Corynebacterium glutamicum* promoters: a practical approach. *Microb. Biotechnol.* 6, 103–117. doi: 10.1111/1751-7915.12019

Peng, F., Wang, X., Sun, Y., Dong, G., Yang, Y., Liu, X., et al. (2017). Efficient gene editing in *Corynebacterium glutamicum* using the CRISPR/Cas9 system. *Microb. Cell Fact.* 16:201. doi: 10.1186/s12934-017-0814-6

Ruan, Y., Zhu, L., and Li, Q. (2015). Improving the electro-transformation efficiency of *Corynebacterium glutamicum* by weakening its cell wall and increasing the cytoplasmic membrane fluidity. *Biotechnol. Lett.* 37, 2445–2452. doi: 10.1007/s10529-015-1934-x

Rytter, J. V., Helmark, S., Chen, J., Lezyk, M. J., Solem, C., and Jensen, P. R. (2014). Synthetic promoter libraries for Corynebacterium glutamicum. *Appl. Microbiol. Biotechnol.* 98, 2617–2623. doi: 10.1007/s00253-013-5481-x

Sawitzke, J. A., Costantino, N., Li, X. T., Thomason, L. C., Bubunenko, M., Court, C., et al. (2011). Probing cellular processes with oligo-mediated recombination and using the knowledge gained to optimize recombineering. *J. Mol. Biol.* 407, 45–59.

Schafer, A., Tauch, A., Jager, W., Kalinowski, J., Thierbach, G., and Puhler, A. (1994). Small mobilizable multi-purpose cloning vectors derived from the *Escherichia coli* plasmids pK18 and pK19: selection of defined deletions in the chromosome of *Corynebacterium glutamicum*. *Gene* 145, 69–73. doi: 10.1016/0378-1119(94)90324-7

Shang, X., Chai, X., Lu, X., Li, Y., Zhang, Y., Wang, G., et al. (2018). Native promoters of *Corynebacterium glutamicum* and its application in l-lysine production. *Biotechnol. Lett.* 40, 383–391. doi: 10.1007/s10529-017-2479-y

Shen, J., Chen, J., Jensen, P. R., and Solem, C. (2017). A novel genetic tool for metabolic optimization of *Corynebacterium glutamicum*: efficient and repetitive chromosomal integration of synthetic promoter-driven expression libraries. *Appl. Microbiol. Biotechnol.* 101, 4737–4746. doi: 10.1007/s00253-017-8222-8

Shu, Q., Xu, M., Li, J., Yang, T., Zhang, X., Xu, Z., et al. (2018). Improved l-ornithine production in *Corynebacterium crenatum* by introducing an artificial linear transacetylation pathway. *J. Indust. Microbiol. Biotechnol.* 45, 393–404. doi: 10.1007/s10295-018-2037-1

Strecker, J., Ladha, A., Gardner, Z., Schmid-Burgk, J. L., Makarova, K. S., Koonin, E. V., et al. (2019). RNA-guided DNA insertion with CRISPR-associated transposases. *Science* 365, 48–53. doi: 10.1126/science.aax9181

Su, T., Jin, H., Zheng, Y., Zhao, Q., Chang, Y., Wang, Q., et al. (2018). Improved ssDNA recombineering for rapid and efficient pathway engineering in *Corynebacterium glutamicum*. *J. Chem. Technol. Biotechnol.* 93, 3535–3542. doi: 10.1002/jctb.5726

Suzuki, N., and Inui, M. (2013). *Genome Engineering of Corynebacterium glutamicum*. Berlin: Springer.

Suzuki, N., Nonaka, H., Tsuge, Y., Inui, M., and Yukawa, H. (2005a). New multiple-deletion method for the *Corynebacterium glutamicum* genome, using a mutant lox sequence. *Appl. Environ. Microbiol.* 71, 8472–8480. doi: 10.1128/aem.71.12.8472-8480.2005

Suzuki, N., Nonaka, H., Tsuge, Y., Okayama, S., Inui, M., and Yukawa, H. (2005b). Multiple large segment deletion method for *Corynebacterium glutamicum*. *Appl. Microbiol. Biotechnol.* 69, 151–161. doi: 10.1007/s00253-005-1976-4

Suzuki, N., Okai, N., Nonaka, H., Tsuge, Y., Inui, M., and Yukawa, H. (2006). High-throughput transposon mutagenesis of *Corynebacterium glutamicum* and construction of a single-gene disruptant mutant library. *Appl. Environ. Microbiol.* 72, 3750–3755. doi: 10.1128/aem.72.5.3750-3755.2006

Suzuki, N., Okayama, S., Nonaka, H., Tsuge, Y., Inui, M., and Yukawa, H. (2005c). Large-scale engineering of the *Corynebacterium glutamicum* genome. *Appl. Environ. Microbiol.* 71, 3369–3372. doi: 10.1128/aem.71.6.3369-3372.2005

Suzuki, N., Tsuge, Y., Inui, M., and Yukawa, H. (2005d). Cre/loxP-mediated deletion system for large genome rearrangements in *Corynebacterium glutamicum*. *Appl. Microbiol. Biotechnol.* 67, 225–233. doi: 10.1007/s00253-004-1772-6

Tauch, A., Kassing, F., Kalinowski, J. R., and Alfred, P. (1995). The erythromycin resistance gene of the *Corynebacterium xerosis* R-plasmid pTP10 also carrying chloramphenicol, kanamycin, and tetracycline resistances is capable of transposition in *Corynebacterium glutamicum*. *Plasmid* 33, 168–179.

Tauch, A., Puhler, A., Kalinowski, J., and Thierbach, G. (2003). Plasmids in *Corynebacterium glutamicum* and their molecular classification by comparative genomics. *J. Biotechnol.* 104, 27–40. doi: 10.1016/s0168-1656(03)00157-3

Tsuge, Y., Suzuki, N., Inui, M., and Yukawa, H. (2007). Random segment deletion excision system in based on IS31831 and Cre/loxP *Corynebacterium glutamicum*. *Appl. Microbiol. Biotechnol.* 74, 1333–1341. doi: 10.1007/s00253-006-0788-5

Unthan, S., Baumgart, M., Radek, A., Herbst, M., Siebert, D., Bruehl, N., et al. (2015). Chassis organism from *Corynebacterium glutamicum*–a top-down approach to identify and delete irrelevant gene clusters. *Biotechnol. J.* 10, 290–301. doi: 10.1002/biot.201400041

Vertes, A. A., Inui, M., Kobayashi, M., Kurusu, Y., and Yukawa, H. (1994). Isolation and characterization of IS31831, a transposable element from *Corynebacterium glutamicum*. *Mol. Microbiol.* 11, 739–746. doi: 10.1111/j.1365-2958.1994.tb00351.x

Vo, P. L. H., Ronda, C., Klompe, S. E., Chen, E. E., Acree, C., Wang, H. H., et al. (2020). CRISPR RNA-guided integrases for high-efficiency, multiplexed bacterial genome engineering. *Nat. Biotechnol.* doi: 10.1038/s41587-020-00745-y

Wang, B., Hu, Q., Zhang, Y., Shi, R., Chai, X., Liu, Z., et al. (2018). A RecET-assisted CRISPR-Cas9 genome editing in *Corynebacterium glutamicum*. *Microb. Cell Fact.* 17:63. doi: 10.1186/s12934-018-0910-2

Wang, H. H., Isaacs, F. J., Carr, P. A., Sun, Z. Z., Xu, G., Forest, C. R., et al. (2009). Programming cells by multiplex genome engineering and accelerated evolution. *Nature* 460, 894–898.

Wang, T., Li, Y., Li, J., Zhang, D., Cai, N., Zhao, G., et al. (2019a). An update of the suicide plasmid-mediated genome editing system in *Corynebacterium glutamicum*. *Microb. Biotechnol.* 12, 907–919. doi: 10.1111/1751-7915.13444

Wang, T., Ma, H., Zhao, G., Cai, N., Zhang, D., and Chen, N. (2019b). Optimization of a CRISPR-Cpf1 /ssDNA genome editing system for *Corynebacterium glutamicum*. *Food Ferment. Ind.* 45, 1–7.

Wang, Y., Liu, Y., Li, J., Yang, Y., Ni, X., Cheng, H., et al. (2019c). Expanding targeting scope, editing window, and base transition capability of base editing in *Corynebacterium glutamicum*. *Biotechnol. Bioeng.* 116, 3016–3029. doi: 10.1002/bit.27121

Wang, Y., Liu, Y., Liu, J., Guo, Y., Fan, L., Ni, X., et al. (2018). MACBETH: multiplex automated *Corynebacterium glutamicum* base editing method. *Metab. Eng.* 47, 200–210. doi: 10.1016/j.ymben.2018.02.016

Wen, Z., Lu, M., Ledesma-Amaro, R., Li, Q., Jin, M., and Yang, S. (2020). TargeTron technology applicable in *Solventogenic Clostridia*: revisiting 12 years'. *Adv. Biotechnol. J.* 15:e1900284. doi: 10.1002/biot.201900284

Wen, Z., Minton, N. P., Zhang, Y., Li, Q., Liu, J., Jiang, Y., et al. (2017). Enhanced solvent production by metabolic engineering of a twin-clostridial consortium. *Metab. Eng.* 39, 38–48. doi: 10.1016/j.ymben.2016.10.013

Wendisch, V. F., Jorge, J. M. P., Perez-Garcia, F., and Sgobba, E. (2016). Updates on industrial production of amino acids using *Corynebacterium glutamicum*. *World J. Microbiol. Biotechnol.* 32:105. doi: 10.1007/s11274-016-2060-1

Woo, H. M., and Park, J. B. (2014). Recent progress in development of synthetic biology platforms and metabolic engineering of *Corynebacterium glutamicum*. *J. Biotechnol.* 180, 43–51. doi: 10.1016/j.jbiotec.2014.03.003

Wu, M., Xu, Y., Yang, J., and Shang, G. (2020). Homing endonuclease I-SceI-mediated *Corynebacterium glutamicum* ATCC 13032 genome engineering. *Appl. Microbiol. Biotechnol.* 104, 3597–3609. doi: 10.1007/s00253-020-10517-y

Xu, D., Tan, Y., Huan, X., Hu, X., and Wang, X. (2010). Construction of a novel shuttle vector for use in *Brevibacterium flavum*, an industrial amino acid producer. *J. Microbiol. Methods* 80, 86–92. doi: 10.1016/j.mimet.2009.11.003

Yang, J., Ma, X., Wang, X., Zhang, Z., Wang, S., Qin, H., et al. (2020). Advances in gene editing of *Corynebacterium glutamate*. *Chin. J. Biotechnol.* 36, 820–828. doi: 10.13345/j.cjb.190403

Yoon, J., and Woo, H. M. (2018). CRISPR interference-mediated metabolic engineering of *Corynebacterium glutamicum* for homo-butyrate production. *Biotechnol. Bioeng.* 115, 2067–2074. doi: 10.1002/bit.26720

Zhan, M., Kan, B., Zhang, H., Dong, J., Xu, G., Han, R., et al. (2019). Comparison of CRISPR-Cpf1 with Cre/loxP for gene knockout in *Corynebacterium glutamicum*. *Microbiol. China* 46, 278–291. doi: 10.13344/j.microbiol.china.180225

Zhang, J., Qian, F., Dong, F., Wang, Q., Yang, J., Jiang, Y., et al. (2020). De novo engineering of *Corynebacterium glutamicum* for L-proline production. *ACS Synth. Biol.* 9, 1897–1906. doi: 10.1021/acssynbio.0c00249

Zhang, J., Yang, F., Yang, Y., Jiang, Y., and Huo, Y.-X. (2019). Optimizing a CRISPR-Cpf1-based genome engineering system for *Corynebacterium glutamicum*. *Microb. Cell Fact.* 18:60. doi: 10.1186/s12934-019-1109-x

Zhang, N., Shao, L., Jiang, Y., Gu, Y., Li, Q., Liu, J., et al. (2015). I-SceI-mediated scarless gene modification via allelic exchange in *Clostridium*. *J. Microbiol. Methods* 108, 49–60. doi: 10.1016/j.mimet.2014.11.004

Zhang, Y., Buchholz, F., Muyrers, J. P., and Stewart, F. A. (1998). A new logic for DNA engineering using recombination in *Escherichia coli*. *Nat. Genet.* 20, 123–128. doi: 10.1038/2417

Zhang, Y., Sun, X., Wang, Q., Xu, J., Dong, F., Yang, S., et al. (2020). Multicopy chromosomal integration using CRISPR-associated transposases. *ACS Synth. Biol.* 9, 1998–2008. doi: 10.1021/acssynbio.0c00073

Zhao, N., Li, L., Luo, G., Xie, S., Lin, Y., Han, S., et al. (2020). Multiplex gene editing and large DNA fragment deletion by the CRISPR/Cpf1-RecE/T system in *Corynebacterium glutamicum*. *J. Ind. Microbiol. Biotechnol.* 47, 599–608. doi: 10.1007/s10295-020-02304-5

Conflict of Interest: The authors declare that the research was conducted in the absence of any commercial or financial relationships that could be construed as a potential conflict of interest.

frontiers in Bioengineering and Biotechnology

ORIGINAL RESEARCH
published: 07 May 2021
doi: 10.3389/fbioe.2021.668513

Droplet-Based Microfluidic High Throughput Screening of *Corynebacterium glutamicum* for Efficient Heterologous Protein Production and Secretion

Suvasini Balasubramanian[1], Jun Chen[2], Vinoth Wigneswaran[1], Claus Heiner Bang-Berthelsen[1] and Peter Ruhdal Jensen[1]**

[1] Research Group for Microbial Biotechnology and Biorefining, National Food Institute, Technical University of Denmark, Kongens Lyngby, Denmark, [2] Samplix ApS, Herlev, Denmark

OPEN ACCESS

Edited by:
Yu Wang,
Tianjin Institute of Industrial Biotechnology, Chinese Academy of Sciences, China

Reviewed by:
Chong Zhang,
Tsinghua University, China
Alexander Grünberger,
Bielefeld University, Germany

***Correspondence:**
Jun Chen
jcn@samplix.com
Peter Ruhdal Jensen
perj@food.dtu.dk

Specialty section:
This article was submitted to Synthetic Biology, a section of the journal Frontiers in Bioengineering and Biotechnology

Received: *16 February 2021*
Accepted: *12 April 2021*
Published: *07 May 2021*

Citation:
Balasubramanian S, Chen J, Wigneswaran V, Bang-Berthelsen CH and Jensen PR (2021) Droplet-Based Microfluidic High Throughput Screening of Corynebacterium glutamicum for Efficient Heterologous Protein Production and Secretion. Front. Bioeng. Biotechnol. 9:668513. doi: 10.3389/fbioe.2021.668513

With emerging interests in heterologous production of proteins such as antibodies, growth factors, nanobodies, high-quality protein food ingredients, etc. the demand for efficient production hosts increases. *Corynebacterium glutamicum* is an attractive industrial host with great secretion capacity to produce therapeutics. It lacks extracellular protease and endotoxin activities and easily achieves high cell density. Therefore, this study focuses on improving protein production and secretion in *C. glutamicum* with the use of droplet-based microfluidic (DBM) high throughput screening. A library of *C. glutamicum* secreting β-glucosidase was generated using chemical mutagenesis coupled with DBM screening of 200,000 mutants in just 20 min. Among 100 recovered mutants, 16 mutants exhibited enhanced enzyme secretion capacity, 13 of which had unique mutation profiles. Whole-genome analysis showed that approximately 50–150 SNVs had occurred on the chromosome per mutant. Functional enrichment analysis of genes with non-synonymous mutations showed overrepresentation of genes involved in protein synthesis and secretion relevant biological processes, such as DNA and ribosome RNA synthesis, protein secretion and energy turnover. Two mutants JCMT1 and JCMT8 exhibited the highest secretion with a six and a fivefold increase in the β-glucosidase activity in the supernatant, respectively, relative to the reference strain JC0190. After plasmid curing, a new plasmid with the gene encoding α-amylase was cloned into these two mutants. The new strains SB024 and SB025 also exhibited a five and a sixfold increase in α-amylase activity in the supernatant, respectively, relative to the reference strain SB023. The results demonstrate how DBM screening can serve as a powerful development tool to improve cell factories for the production and secretion of heterologous proteins.

Keywords: droplet-based microfluidics, high throughput screening, heterologous protein production, β-glucosidase, α-amylase, *Corynebacterium glutamicum*

INTRODUCTION

Genetic engineering of microbes has diverse applications in biotechnology, enabling improved and valuable products for human consumption, industrial applications and therapeutic solutions. Significant advances have been made from rational gene over-expression and the introduction of heterologous genes with fine control of gene expression and modulating the regulatory networks of the host cell (Jensen and Hammer, 1998; Solem and Jensen, 2002). Over the years, the integration of systems biology and synthetic biology has allowed for the development of high performing cell factories. The production of proteins and chemicals have proven to be economical and environmentally sustainable by endowing desirable properties on microorganisms by rerouting existing metabolic pathways or introducing entirely new ones (Lee et al., 2012). In order to exploit cell factories for efficient heterologous expression, optimization of the properties of the strains and enabling secretion of proteins into the culture media at high efficiency are important. It is also critical to understand the complex molecular mechanisms of the cells in order to fully harness the technology in delivering the desired phenotypes and products.

Challenges remain in rational engineering of hosts for improved protein production and secretion, as protein synthesis is a complex machinery, and multi-level cellular processes must be well coordinated to achieve high-yield production and secretion. Incorporating traditional techniques like random mutagenesis and screening is again becoming an alternative to rational engineering. This technique involves introducing random mutations into the genome of the cell to construct a cell library with diverse phenotypic variations followed by screening for a desired phenotype. Due to the random nature of mutagenesis, a high throughput screening technology capable of screening about 10^6–10^8 mutants is required for screening a large cell library efficiently (Derkx et al., 2014).

Droplet-based microfluidics (DBM) is an emerging high-throughput technology with a lot of potential for screening large sets of mutant libraries individually (Chen et al., 2017). The platform generates compartments of volumes as low as femtolitres and perform reactions individually at the single cell level enabling rapid screening (Seemann et al., 2012). Monodisperse water-in-oil droplets (media containing cells enclosed by oil) are generated with tunable size at a high frequency in a microfluidic chip. These compartments of single-cell in a droplet increase the cell density in post-incubation and enable accumulation of the secretion in droplets, which are then screened individually at the frequency of 0.1–1 kHz (Theberge et al., 2010). All the reagents and equipment used for droplets screening are biocompatible and therefore target cells with improved performance can be recovered for further use.

C. glutamicum is an attractive candidate for the expression and secretion of heterologous proteins into the culture media enabling simpler downstream processing. This gram-positive soil bacterium is already prevalent as an industrial workhorse for generating essential biomolecules with applications in food, feed and pharmaceutical products such as vitamins and amino acids (Izumi et al., 1978; Krömer et al., 2005). *C. glutamicum* has several advantages such as GRAS (generally recognized as safe) and low nutrient requirements. It also lacks extracellular proteases, providing an oxidative environment for proper folding, and disulfide bond formation over the widely used production host *E. coli* (Berlec and Štrukelj, 2013) and has both twin arginine transporter (TAT) and secretion (SEC) pathways to transport the proteins across the cytoplasmic membrane (Liu et al., 2017).

Previous work has facilitated improved traits in the organism including over-expression tools and higher biomass to improve its potential as an industrial host for recombinant protein production (Kikuchi et al., 2009; Unthan et al., 2014). In this study, we used random mutagenesis and DBM high throughput screening to successfully improve heterologous protein production and secretion in *C. glutamicum*. The study demonstrated that DBM screening served as a high-throughput and cost-effective toolbox for improving protein production and secretion in Gram-positive bacteria. The results of the study will also facilitate reverse engineering strategies for further developing cell factories based on the valuable mutations identified.

RESULTS AND DISCUSSION

Random Mutagenesis and Microfluidic Screening

The parent strain JC0190 secreting β-glucosidase was mutagenized with ethyl methanesulfonate (EMS) and by the end of a 3-h treatment, 0.32% of the cells survived (**Figure 1**). We chose the library after 3-h EMS mutagenesis for the further experiment, as an approximately 99% killing rate would be eligible for droplet screening (Chen et al., 2017). Encapsulation of mutants in droplets was carried out along with the fluorogenic substrate Fluorescein Di-β-DGlucopyranoside (FDGlu) (**Figure 2**). The calculation of cell density for encapsulation

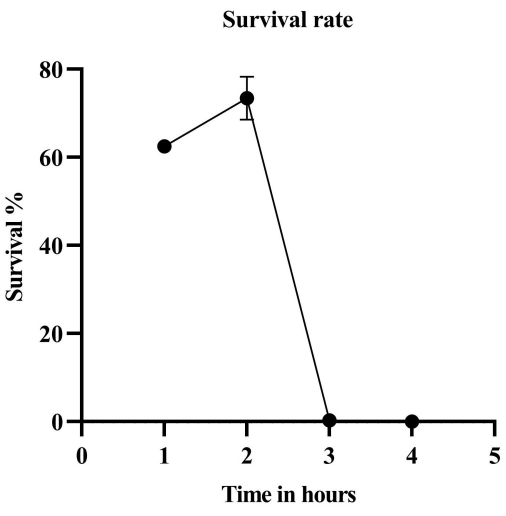

FIGURE 1 | Survival rate after EMS treatment. The survival percentage of the cells by the end of the third hour was 0.315.

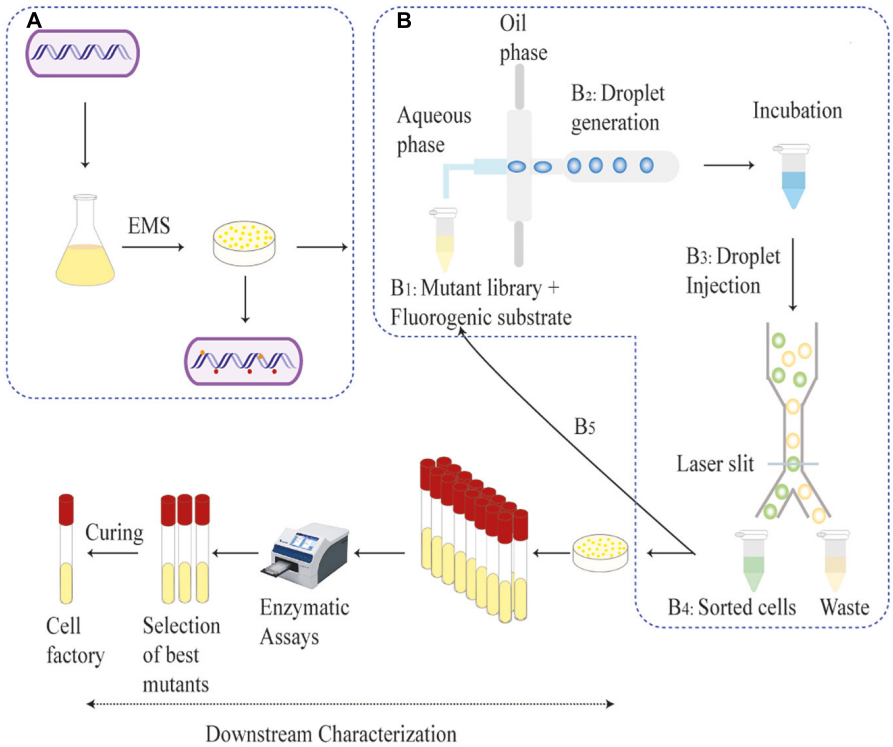

FIGURE 2 | Schematic overview of development and screening of the mutant library: A whole genome mutated library was generated with EMS chemical mutagenesis on shake flask culture and were recovered on an agar as shown in **(A)**. Steps **B_1–B_5** represents the microfluidic process—The recovered mutants were diluted to 10^7 mutant libraries mixed with fluorogenic substrate **(B_1)**. The droplets generated incubates for the cells to accumulate secretion **(B_2)**. Post incubation, droplets are injected into the sorting chip and sorted based on the fluorescence intensity and collected in an Eppendorf tube. The sorted cells are then released and injected into the device for a second round of droplet generation and screening **(B_5)**. The sorted cells are then released and cultivated on agar plates. The outgrown single colonies are picked for downstream characterization, e.g., shake flask fermentation and protein secretion tests.

utilizes the Poisson distribution, where the ratio of having single cells to multiple cells can be optimized and controlled by varying the cell density (Beneyton et al., 2017). In this study, a λ of 0.5 was used to generate an average of 0.5 cells per droplet. More than 200 K droplets were generated because of high single cell to multi-cell ratio will lead to a large fraction of empty droplets (Chen et al., 2018). The droplets were then incubated for 3–4 h, where the cells could proliferate and secrete β-glucosidase into droplets to hydrolyze the substrate, after which fluorescein was released to generate the green fluorescence for detection. Sorting of the mutants occurs based on the threshold set for the intensity of the fluorescent signals. 3.2% of the droplets with the highest signals were sorted from a screening of 140 K positive droplets in total in 20 min. The sorted droplets were collected in a 1.5-mL Eppendorf tube. The cells were then released and were re-injected into the device for the second round of encapsulation and sorting to further improve the purity. The second round of sorting yielded 3,900 sorted droplets (1.95%) resulting from screening a library of 200 K positive droplets.

After being released from the sorted droplets, the cells were recovered on agar plates. Among the formed single colonies, 100 colonies were randomly picked and printed on a BHI agar plate containing IPTG, esculin and $FeCl_3$ for indication of β-glucosidase activity. β-glucosidase cleaves esculin to produce esculetin and glucose molecule. The hydrolytic product esculetin reduces the ferric ions in the medium to produce iron, which causes browning on the agar. Therefore, the colonies producing brown color on the agar are esculin positive and possess β-glucosidase activity, and the shade of brown color could indicate the capacity of protein secretion, which served as an effective secondary screening (Veena et al., 2011). Sixteen colonies exhibiting the strongest dark red color were picked for further characterization. The growth of the strains was analyzed in microplates on Biolector (**Figure 3**).

Characterization of the Selected Mutants

The β-glucosidase secretion capacity of the selected mutants was validated by testing the activity in the supernatant of the cultures. Thirteen of sixteen mutants had higher β-glucosidase activity in the supernatants compared to the reference strain JC0190. The supernatants were concentrated and analyzed on an SDS-PAGE gel, which showed improved protein secretion in the mutants. Although a native protein band overlaps with the β-glucosidase band on the SDS-PAGE gel in **Figure 4** the protein concentration of the band from the strain JC0190 supernatant is higher relative to the negative control proving the presence of β-glucosidase. Based on the growth profiles generated by Biolector shown in **Figure 3**, 13 mutants were fast-growing strains with higher

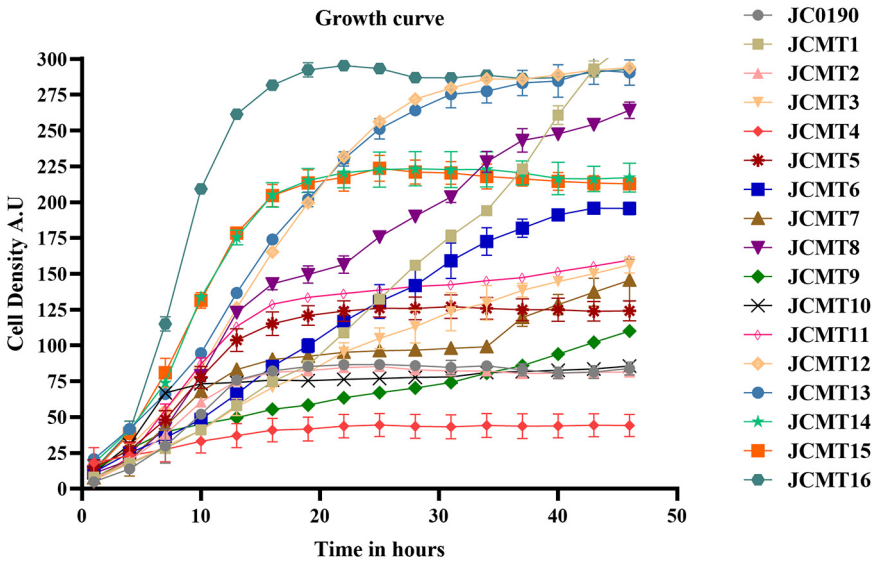

FIGURE 3 | Growth curves of the parent and mutant strains carried out in BioLector. The growth of the strains were monitored in a 48-well flower plate (culture volume: 1,000 μL, temperature: 30°C, agitation: 800 rpm) by measuring scattered light (ex: 620 nm, Gain: 20).

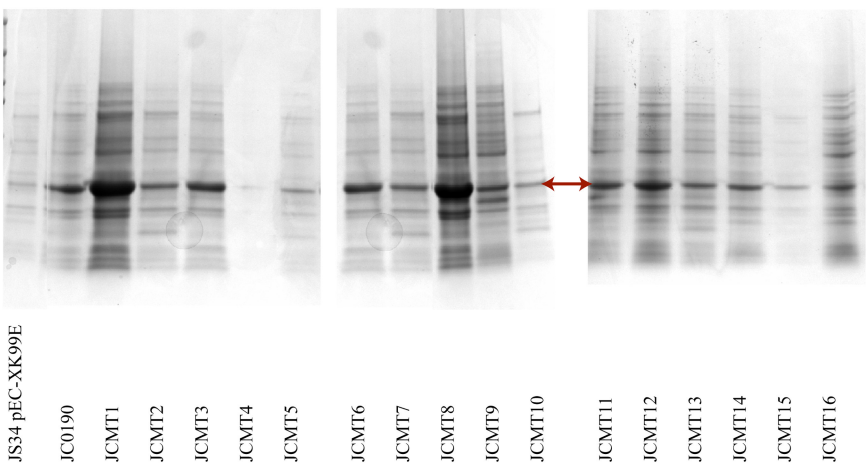

FIGURE 4 | SDS PAGE analysis of the supernatant of the selected mutants. The arrow points the band β-glucosidase. The lanes from left to right are the wild-type strain with empty plasmid, and the reference strain followed by the mutants. 15 μL of acetone precipitated protein samples were loaded on the wells.

biomass and the strains JCMT02, JCMT09, JCMT10 had a similar profile compared to the reference strain JC0190. Amongst the mutant strains, JCMT08 had the highest biomass production. By analyzing the supernatant, the mutant JCMT1 and JCMT8 had the highest activity of β-glucosidase and total protein content in the supernatant (**Figures 5A,B**), where approximately six and fivefold higher enzyme activity, respectively, than the reference strain JC0190 were observed. However, JCMT8 had higher total protein content in the supernatant than JCMT1 (**Figure 5B**).

As JCMT1 and JCMT8 showed a better performance than the parent strain and the other mutants, they could potentially serve as platform strains for producing other proteins in *C. glutamicum*. To test this, the plasmid in JCMT1 and JCMT8 were cured using bactericidal antibiotic penicillin. The successful plasmid curing was confirmed by a growth inhibition in the presence of kanamycin and lack of β-glucosidase in the supernatant. The plasmid-cured mutants were transformed with a new plasmid with α-amylase gene (pECXCαAmy), which resulted in the strains SB024 and SB025 derived from JCMT1 and JCMT8, respectively. The new strains SB024 and SB025 harboring the gene coding for α-amylase exhibited similar growth rate as that of the uncured counterparts (**Supplementary Figure 1**) and had a 5.6 and 7-fold higher secretion of α-amylase compared to the reference strain SB023 (JS034 harboring pECXCαAmy), respectively (**Figure 5C**). These results demonstrates both the mutant's stability and its potential for use as a host for producing other essential proteins. With mutagenesis and DBM screening experiment, we have thus established *C. glutamicum* strains

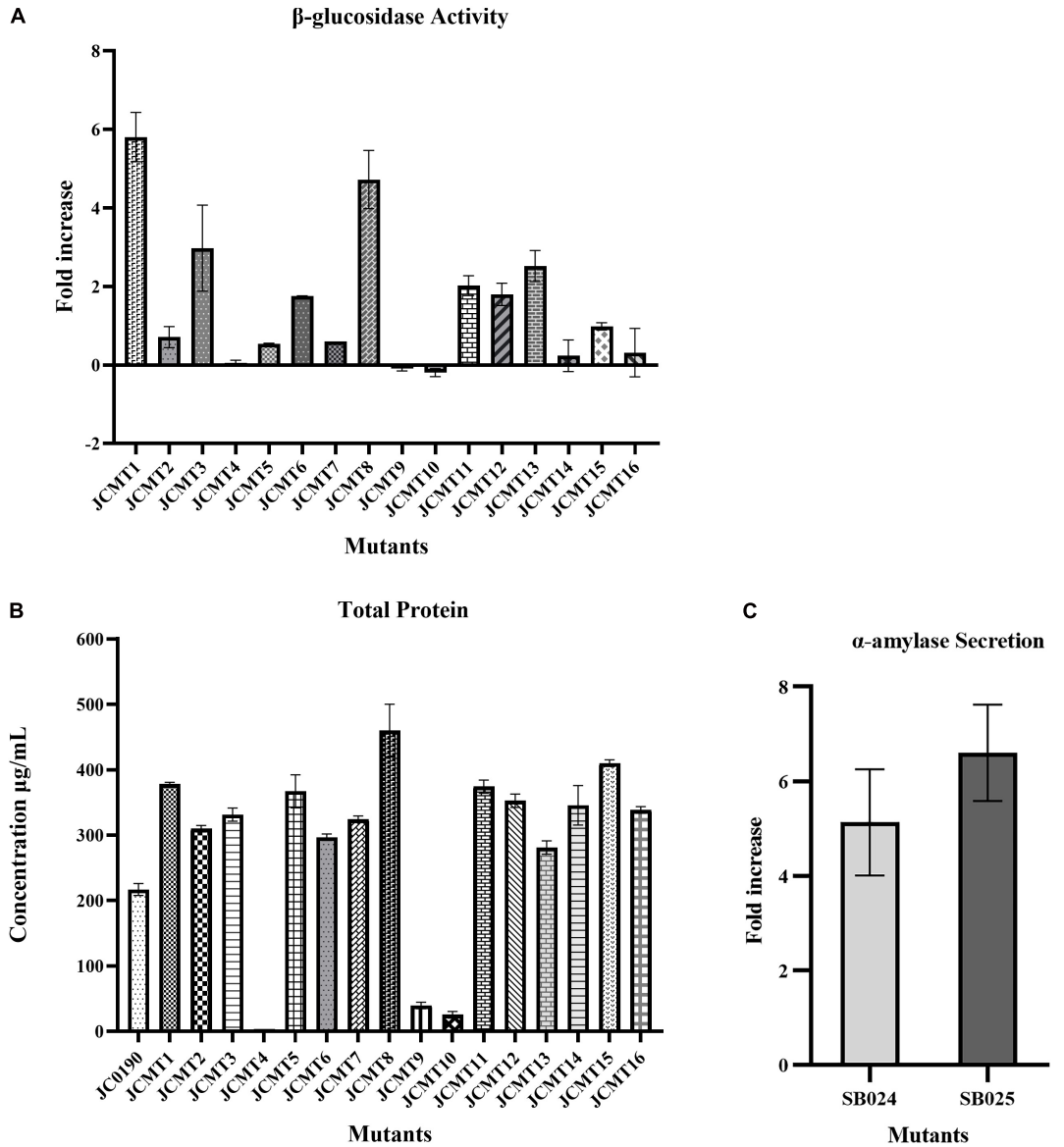

FIGURE 5 | Protein secretion capacity of selected mutant strains: **(A)** β-glucosidase activity: fold increase in the relative fluorescence activity of the mutant strains secreting β-glucosidase in comparison to the reference strain JC0190. **(B)** Total protein: total protein content of the reference and mutant strains in the supernatants. The protein content of mutant 4 is around 4 µg and hence negligible in the graph. **(C)** α-Amylase secretion: fold increase in the α-amylase enzyme units of the strains SB024 and SB025 derived from mutants JCMT1 and JCMT8, respectively, compared to the reference strain SB023.

with up to sixfold higher activity in the supernatant, which is comparable to the previous work with other organisms such as yeasts, where the enzyme activity was improved between two and fourfold by mutagenesis and DBM screening (Huang et al., 2015; Beneyton et al., 2017).

Genome Resequencing and SNV Identification

The genomes of all the 16 mutants and the parent strain JC0190 were sequenced in an attempt to disclose the link between genetic and phenotypic changes. Single nucleotide variants (SNVs) of the 16 mutants were called and filtered against the SNVs identified in JC0190 to eliminate background noises. It was found that the mutants JCMT03, JCMT06, JCMT12, and JCMT13 had the identical SNV profiles, which indicates that they originated from the same mutant, and were repetitively picked during the secondary selection on agar plates. Therefore, JCMT03 was used to represent the four strains in the subsequent analysis.

In the 13 mutants with unique SNV profiles, we found approximately 50–150 SNVs per genome, and 0–1 SNV on the expression plasmid in each strain. The occurrence of SNVs on the genome and the plasmids were thus 0.002–0.005% and 0–0.012%, which were not significantly biased. In total, 1,002

mutations were identified across 13 mutants of which 313 were silent mutations, 566 were missense and 123 were in the non-coding region. To explore the patterns of these mutations, we first pooled all the genes that had non-synonymous SNVs in the coding regions in the 13 mutants and submitted this pool, which had 713 unique gene entries, to DAVID (Huang et al., 2009) for functional enrichment and clustering. The GO and KEGG terms were chosen for the analysis, which resulted in 13 functional clusters (**Figure 6**).

In the cluster 1, 3 terms in relation to membrane transport activity were enriched. They mostly consisted of different ABC transporter permeases and cation transporters. In the plasma membranes, the subunits b, c and γ of the ATP synthase F_0F_1 were enriched. The F_0F_1 synthase protein complex consisting of the subunits α_3, β_3, γ_1, δ_1, ε_1, a_1, b_2, and c_n (n—varies from species to species) present on the bacterial membranes are responsible for the synthesis of ATP from ADP, being a key parameter of energy production of aerobic cells (Soga et al., 2017). The α_3, β_3, γ_1, δ_1, ε_1 subunits catalyzes ATP hydrolysis, while the a_1, b_2, and c_n mediates proton transport across the membrane (Ueno et al., 2005). In *E. coli,* the deletion of the ATP operon encoding ATPase has resulted in decreased ATP synthesis despite the increased respiration rate (Jensen and Michelsen, 1992), which resulted in decreased growth rate (74–78%) and yield (55–58%) than the wild type strains. The mutants JCMT1, JCMT10, JCMT14 had missense mutations on the subunits γ, b,

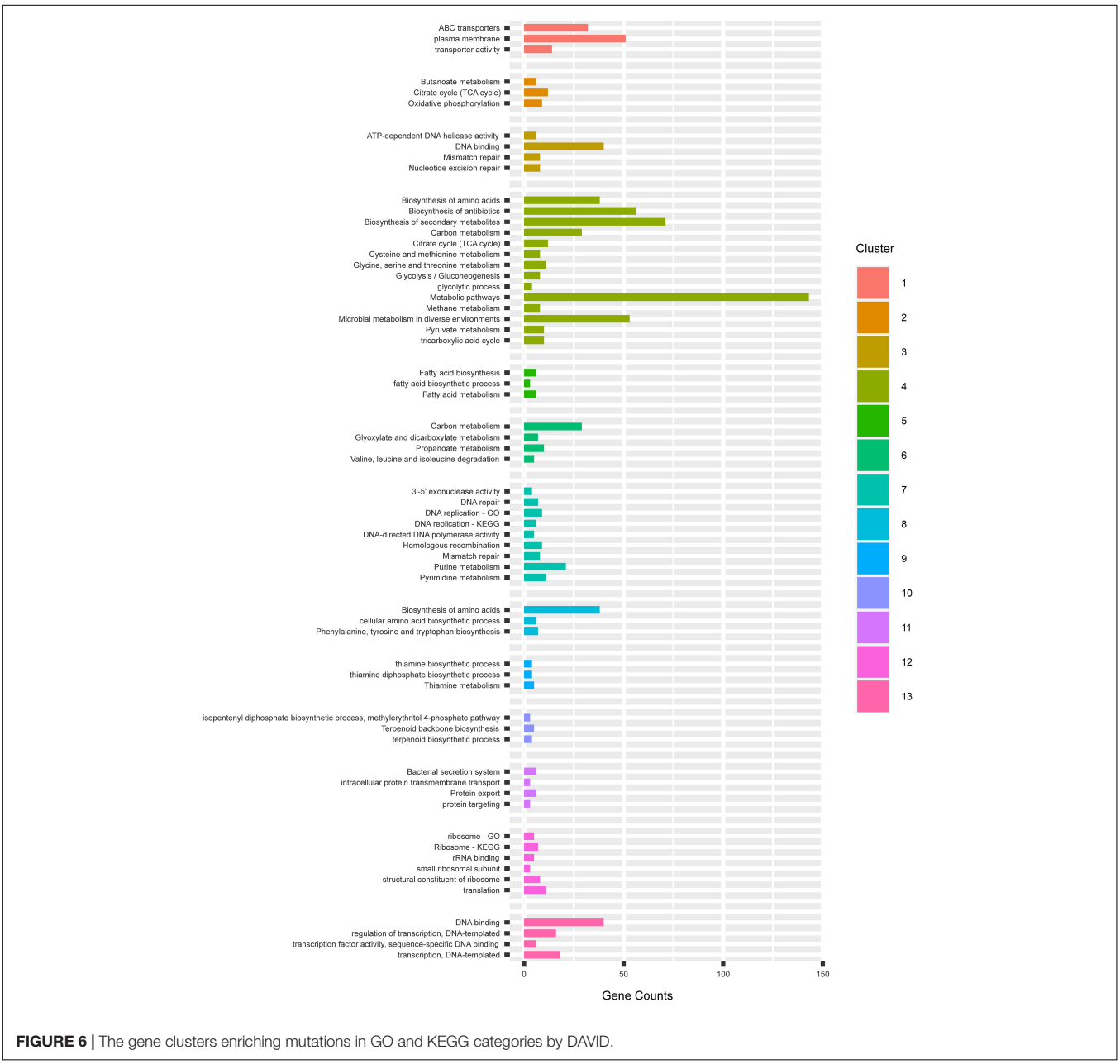

FIGURE 6 | The gene clusters enriching mutations in GO and KEGG categories by DAVID.

and c of ATP synthase, respectively, while the mutant JCMT16 had a silent mutation on the γ subunit, which indicates the capacity of ATP synthesis could be altered in the mutants in favor of protein synthesis.

In the cluster oxidative phosphorylation, the three subunits of the ATP synthase F_0F_1 in the cluster 1 reoccurred. In the term plasma membrane, we also found non-synonymous SNVs also existed in the genes *secA2*, *secD* and *secF* in the sec pathway. *SecA* is responsible for transferring of secretory proteins to the membrane-embedded translocon, and *SecD* and *F* are responsible for releasing the mature peptides into periplasm (Chatzi et al., 2014). The mutations on *SecA* were enriched in mutants 11 and 16 while the mutation on *SecD* is only in 11. However, in this study, a tat signal peptide was used for mediating protein secretion, and hence the effect of this mutation on secretion is unclear.

In the cluster 2, we found two interesting terms, namely, TCA cycle and oxidative phosphorylation. Non-synonymous SNVs were found in 12 genes in the TCA cycle e.g., pyruvate carboxylase (*pyc*), acetate (*ace*), fumarase (*fum*) and succinic dehydrogenase (*sdh*) (**Figure 7**). The TCA cycle provides several metabolic precursors and cofactors for cell growth and amino acid production. The pyruvate OAA node is one of the factors regulating the carbon flux in the TCA cycle by interconnecting different metabolic pathways responsible for carbon metabolism. The pyruvate carboxylase (*pyc*) which is part of the anaplerotic pathway enhances the cell growth and amino acid production on glucose by renewing OAA, and the expression levels of *pyc*, *ace*, *fum* and *sdh* are enhanced with biotin supplementation (Xu et al., 2018). The mutants JCMT7, JCMT10, and JCMT14 possessed a mutation in the *pyc* gene, where the mutants JCMT7 and JCMT10 had a non-synonymous mutation with R/C and P/L substitutions while JCMT14 had a synonymous mutation. Similarly, three mutants—JCMT1, JCMT8 and JCMT11 had SNV mutations in the *sdh* gene, of which JCMT1 had a non-synonymous mutation with S/L substitution and the rest had silent mutations. The high number of mutations in the genes involved in the primary metabolic pathways such as TCA cycle indicated an enhanced metabolic activity could be critical for protein synthesis and secretion.

Moreover, three genes encoding cytochrome b subunit of the bc complex, cytochrome bd-type quinol oxidase, subunit 1 and 2, respectively, which are involved in the respiratory chain were found in cluster 2. The efficiency of the respiratory chain depends on the expression levels of the bc1 complex and the cytochrome bd oxidase. The bc1-aa3 branch is important for aerobic growth in minimal media such as CGXII while the cytochrome bd oxidase inhibits the growth, biomass and the protein production levels when overexpressed (Bott and Niebisch, 2003). The S/L mutation in the cytochrome bd-type quinol oxidase, subunit 1 could have positively influenced the capacity of respiration in the strain JCMT1.

In the cluster 3, it mostly consists of terms that have relations to DNA replication and repair. Forty genes were allocated in term

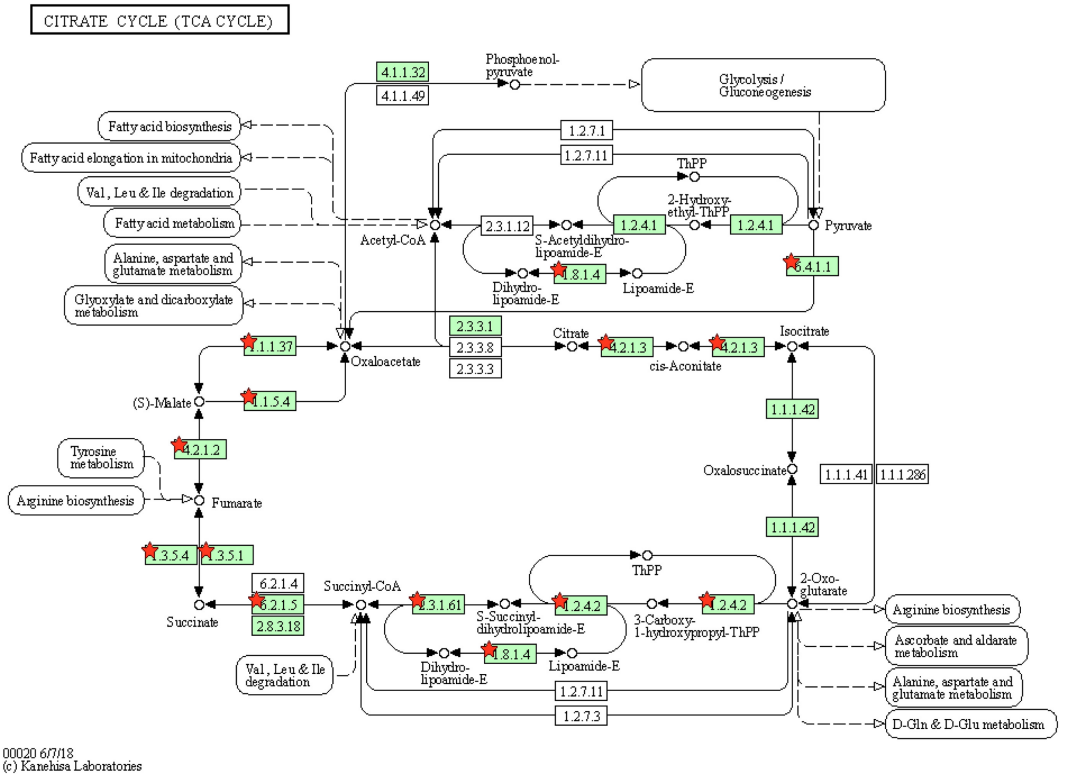

FIGURE 7 | Tricarboxylic acid cycle with genes enriching mutations. The red stars represent the genes with presence of mutations.

DNA binding. Among others, we found several genes that encode DNA gyrases, DNA polymerases, helicases and regulators.

The cluster 4 is the biggest group containing 14 terms. These terms mostly consist of primary and secondary metabolisms, in which the TCA cycle occurred in cluster 2. Furthermore, we found 8 genes involved in the glycolysis pathway. In cluster 5, we found that 6 genes in the fatty acid synthesis had non-synonymous SNVs. Considering the fatty acid synthesis pathway is composed of 9 genes in total. The frequency of mutations was high in the fatty acid biosynthesis pathway. The cluster 6, 8, 9, and 10 consist of genes involved in primary and secondary metabolism, which also occurred in cluster 4.

The cluster 7 resembles the cluster 3 involved in DNA replication and repair, but the cluster 7 had more detailed classification. In addition, we also found that 21 genes were involved in purine metabolism, and 11 genes were involved in pyrimidine metabolism. In the cluster 11, it is interesting to see that 6 genes involved in protein secretion were mutated. These genes encode accessory Sec system translocase SecA2, inner membrane protein translocase YidC, preprotein translocase subunit SecD, preprotein translocase subunit SecF, preprotein translocase subunit YajC, signal recognition particle GTPase.

The cluster 12 contains terms involved in translation and ribosome process. We saw mutations in several genes that encode ribosome 30s and 50s subunits, which play a critical role in translation. Terms in the cluster 13 were mostly involved in the regulation of transcription, in which transcriptional regulators were clustered.

For the mutations on the plasmid, in the 13 unique mutants, we found a single SNV on the expression plasmid in the strain JCMT01, 03, 05, and 08. In JCMT16, there were two SNVs on the plasmid. In JCMT01 and JCMT03, the SNV is non-synonymous and changed the coding sequence of the kanamycin resistance gene. In JCMT05, the SNV was also located in the kanamycin resistance gene, but it was synonymous. The rest were in the intergenic regions. The mutation on the resistance gene or on the plasmid is not critical. As by plasmid curing and introducing the newly constructed plasmid expressing α-amylase, the high protein production and secretion traits remained in the mutants, indicating that the improvement was a result of the mutations on the chromosome rather than those on the plasmid (**Figure 5C**).

CONCLUSION

DBM has previously been explored to screen mutants generated using random mutagenesis for optimization of strains producing native and non-native metabolites (Huang et al., 2015; Chen et al., 2018). Results from the current study has shown how one can improve phenotypic traits of *C. glutamicum* for increasing protein secretion using high-throughput droplet screening. Furthermore, the diversity of mutations profiles within a single mutant disclosed in this study gives multiple possibilities for future metabolic engineering aimed at improving protein secretion.

MATERIALS AND METHODS

Strains and Plasmids

In this study, *C. glutamicum* JS34, a derivative of ATCC 13032, Shen et al. (2017) was used as the host for strain construction. The vectors used for the construction of expression/secretion plasmid were pEC-XK99E and pEC-XC99E harboring kanamycin and chloramphenicol resistance, respectively. For construction, the β-glucosidase expression/secretion plasmid (pECXKBGL), the SD sequence of the *tpiA* gene (30 bp before the start codon) from *C. glutamicum* followed by Cgr0949 signal peptide and the β-glucosidase gene from *S. degradans* were cloned onto the *Xba*I site on pEC-XK99E, and the plasmid was transformed into JS34, which resulted in JC0190. JCMT1 to JCMT16 are the mutants derived from JC0190 after mutagenesis and DBM screening. For the construction of the amylase expression/secretion strains, the mutant strains JCMT1 and JCMT8 were cured and transformed with the plasmid pECXCαAmy containing α-amylase gene from *G. stearothermophilus*, named SB024 and SB025, respectively. **Table 1** summarizes the strains and plasmids used in this study.

TABLE 1 | Summary of strains and plasmids used.

Strains and plasmids	Description	References
JS34	A derivative of the wild-type strain ATCC 13032 carrying an *attB* site in its chromosome	Shen et al., 2017
JC0190	JS34 strain expressing and secreting β-glucosidase	This work
JCMT1–JCMT16	Mutant derivatives of JC0190	This work
SB023	JS34 strain expressing and secreting α-amylase	This work
SB024	Cured JCMT1 expressing and secreting α-amylase	This work
SB025	Cured JCMT8 expressing and secreting α-amylase	This work
pEC-XK99E	Cloning vector Km^r, *Ptrc* promoter, *lacIq* regulatory gene	Kirchner and Tauch, 2003
pEC-XC99E	Cloning vector Cm^r, *Ptrc* promoter, *lacIq* regulatory gene	Kirchner and Tauch, 2003
pECXKBGL	pEC-XK99E vector containing the SD sequence of the *tpiA* gene, signal peptide Cg0949, and gene coding β-glucosidase	This work
pECXCαAmy	pEC-XC99E vector containing the SD sequence of the *tpiA* gene, signal peptide Cg0949, and gene coding α-amylase gene	This work

Media and Culture Conditions

For all fermentations, CGXII media supplemented with 0.1% brain heart infusion broth (BHI, Sigma, St. Louis, MO, United States) was used (Unthan et al., 2014). The media composition per liter is 1 g BHI, 20g $(NH_4)_2SO_4$, 1gK_2HPO_4, 1g KH_2PO_4, 5g urea, 13.25mg $CaCl_2{\cdot}2H_2O$, 0.25g $MgSO_4{\cdot}7H_2O$, 10mg $FeSO_4{\cdot}7H_2O$, 10mg $MnSO_4{\cdot}H_2O$, 0.02mg $NiCl_2{\cdot}6H_2O$, 0.313mg $CuSO_4{\cdot}5H_2O$, 1mg $ZnSO_4{\cdot}7H_2O$, 42 g MOPS, 0.2mg biotin, 30 mg protocatechuic acid and 40g D-glucose. For the preparation of electro-competent cells, the standard procedure in the Handbook of *C. glutamicum* was followed (Eggeling and Bott, 2005). For β-glucosidase hydrolysis in the droplet, 50 μM FDGlu substrate from Invitrogen, CA, United States was used (Hardiman et al., 2010). The antibiotic concentrations were 25 μg/mL and 8 μg/mL for kanamycin and chloramphenicol, respectively. The Isopropyl ß-D-1-thiogalactopyranoside (IPTG, Sigma-Aldrich, St. Louis, MO, United States) concentration for induction was 1 mM. Ethyl methanesulfonate (EMS) from Sigma-Aldrich, St. Louis, MO, United States was used for chemical mutagenesis at a concentration of 2%. For indication of amylase activity on agar plates, 5 g/L starch, 15/L g agar, 1.5 g/L iodine and 1.5 g/L potassium iodide were added to the CGXII/BHI medium. All strains were grown at 30°C aerobically for 24 h.

C. glutamicum Mutant Library Construction

A single colony of the *C. glutamicum* construct JC0190 was inoculated into 10-ml BHI broth and cultivated 30 ml test tube with 220 RPM shaking at 30°C overnight. The outgrown culture was first washed in PBS buffer (pH = 7.4) (Sigma-Aldrich, St. Louis, MO, United States) twice and resuspended in PBS, in which the cell density was adjusted to 10^9 cells per mL. EMS was spiked into the culture at a concentration of 2%. It was incubated for 4 h at room temperature and sampled at a 1-h interval. Meanwhile, a tube with 10^9/mL JC0190 cells without EMS was also incubated and sampled for calculation of the killing rate. During post mutagenesis, the samples were washed twice with CGXII—0.1% BHI to remove residual EMS. Both treated and untreated samples were plated on BHI agar plates with appropriate dilutions for counting CFUs and calculating the killing rate.

Microfluidic Chip Fabrication

The two chips used for encapsulation and sorting of the droplets (**Figure 8**) are both made of structured polydimethylsiloxane (PDMS) slab bonded to a glass slide, which was fabricated by Droplet Genomics (Vilnius, 10223 Lithuania). The procedure is briefly described as follows: the 10:1 w/w mixture of PDMS (Sylgard 184, Dow Corning) is cast over a mold, created using regular UV-photolithography to pattern a layer of SU-8 2075 (MicroChem) on a 4-inch silicon wafer. The PDMS was cured overnight at 60°C, cut into separate devices and carefully removed from the mold. The molded chips are transparent with a dimension of 6.2 × 2 × 0.5 cm. Holes for in- and outlets were made using Ø:0.75 mm biopsy punches. Both glass slides and PDMS parts were exposed to a 50 W 13.56 MHz air plasma for 60 s (Atto Plasma cleaner, Diener), then immediately bonded and placed under the weight (400 g/slide) at 90°C for 10 min. After cooling down, the channels were flushed with filtered Aquapel and subsequently quickly purged by applying vacuum to the outlets. The sorting chips were heated on an 85°C hotplate, allowing a low-temperature solder wire (Indalloy #19, Indium Corp) to be inserted and fill the electrode cavities. Before cooling the device, small pieces of wire were inserted as connectors to the electrodes. The design of droplet generation and sorting chip from Mazutis et al. (2013) were used in this study.

Experimental Setup of Microfluidic Devices

The setup of microfluidic devices published in our previous studies was used (Chen et al., 2017). The system described here again in brief. A custom-built fluorescence microscope, with a 488-nm laser (06-01; Cobolt, Solna, Sweden) guiding through a 1,000-mm cylindrical lens (LJ1516RM-A; Thorlabs, Newton, NJ, United States) and a 10× microscope objective (N10X-PF; Thorlabs) was used to form a narrow line for fluorescence detection. The chips are placed on a 3D printed microscope stage. The fluorescent light emitted was transmitted through a dichroic mirror (MD499; Thorlabs) and a bandpass filter (MF530-43; Thorlabs) before being measured by a photomultiplier tube (PMT) (PMTSS; Thorlabs). A field-programmable gate array (FPGA) (PCIe-7842R; National Instruments, Austin, United States) was programmed to sample the PMT signal every 7 μs (>143 kHz) and continuously evaluate both the signal width and intensity. When a signal fell within the preset gating, the on-chip electrodes are activated with a square voltage wave (15 kHz) amplified to ±400 V (Trek 623B; Trek, Inc., Lockport, NY, United States). For droplet generation, the fluidic inlets/outlet were connected to a vertically oriented syringe pump (PHD 2000; Harvard Apparatus, Inc., Holliston, MA, United States) using PTFE tubing (TW30; Adtech, Stroud, United Kingdom) with an internal diameter of 320 μm. For sorting, fluorinated ethylene propylene (FEP) tubing (JR-T-6794-M10; VICI-Jour, Schekon, Switzerland) with an inner diameter of 100 μm was used instead for the fluidic outlets to ensure that the sorted drops were immediately pushed out of the tubing and collected into Eppendorf tubes. The controlling software package consists of two main parts: a LabVIEW FPGA code that is downloaded to the external processor (for fast and reliable operation) and a regular LabVIEW code (**Supplementary File**) supplying the user interface, which runs on the laboratory PC.

Encapsulation of Mutants in Droplets

The library was diluted in CGXII media containing kanamycin, IPTG and FDGlu to get a final concentration of 10^7 cells/ml. The culture, which forms the aqueous phase, and the oil-containing surfactant (Dolomite Pico-Surf 2.5%; Royston, United Kingdom) was set to 10 μL/min inflow rates to result in a droplet diameter of 50 μm (Chen et al., 2017). A 1-ml syringe (BD Medical, Sandy, UT, United States) was connected to the outlet to collect the emulsions and incubated for 3–4 h at 25°C. Post incubation, the droplet emulsion containing the cells

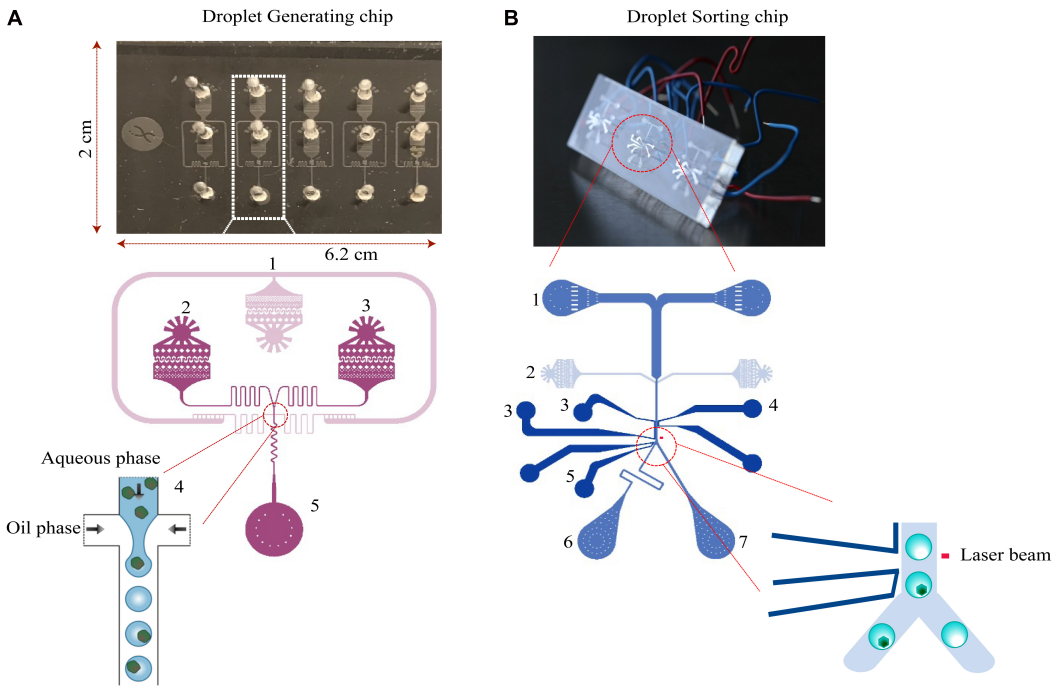

FIGURE 8 | Design of microfluidic chips. **(A)** The droplet generation chip for cell encapsulation consists of an oil phase inlet (1), and two aqueous phase inlets (2 and 3). The fluid resistors (4) dampen fluctuations arising from the mechanical instability of syringe pumps and PDMS device. Due to the surface tension of the water–oil interface, the aqueous phase breaks up into droplets at the flow-focusing junction. Droplets are collected into a syringe or an Eppendorf tube from the outlet (5). **(B)** The droplet-sorting chip consists of two inlets for droplets (1) and spacing oil (2). The flow rate ratio of the oil and injected emulsions are varied to control the distance between adjacent droplets. The droplets at the sorting junction are sorted based on the fluorescence intensity. Downstream to the detection, electrodes—ground (3, 4), high voltage (5) are located. Next to the electrodes, the channel is split into two outlets for collecting sorted droplets (6) and unsorted/waste cells (7).

were examined on a microscope (**Supplementary Figure 2**). For the second round of screening, the sorted cells from the first round were reinjected for encapsulation followed by collection and incubation.

Sorting the Cells Encapsulated in Microdroplets

The syringe containing the droplet emulsion were reinjected into the sorting chip at a rate of 1 μl/min, and the oil phase at 10 μl/min. The cells were sorted based on the fluorescence intensity of the preset threshold level; when the cells with fluorescence exceeding the threshold pass, an electric field is activated by supplying a voltage to the on-chip electrodes. The threshold is set to sort roughly 2–3% of droplets with the highest fluorescent readouts. For each sorting operation, the electrical field was triggered for 1,750 μs after a 250-μs delay to allow droplets to pass the gap between the laser spot and the electrodes.

Extraction of Cells After Sorting

The collected emulsions were centrifuged at 100 g for 30 s. The oil layer was carefully removed and 300 μl of PFOH (1*H*,1*H*,2*H*,2*H* perfluorooctan-1-ol) (Sigma-Aldrich, St. Louis, MO, United States) was added to disrupt the droplets and release the cells into the aqueous layer. The cells were then plated onto BHI agar plates to form colonies.

BioLector Cultivations

Strains were cultured in a 48 well flower plate (m2p-labs GmbH, Baesweiler, Germany) with 1 mM IPTG concentration and 25 μg/mL kanamycin at 30°C with continuous shaking at 800 rpm and the increase of biomass was monitored through BioLector (m2p-labs GmbH, Baesweiler, Germany). The humidity and gain were set to 95% and 20, respectively.

Fermentation in Shake Flasks

For further large-scale analysis, fermentations were carried in 250 mL baffled shake flasks with a culture volume of 25 mL with 220-RPM shaking at 30°C for 24 h. Upon completion, the cultures were centrifuged at 6,000 g for 30 min at 4°C and the supernatants were collected for further analysis.

Plasmid Curing

Plasmid curing is the process of eliminating the production plasmid from the hosts. From the overnight cultures of JCMT1 and JCMT8, a subculture was cultivated under selective pressure. During the log phase, penicillin (Sigma-Aldrich, St. Louis, MO, United States) at a concentration of 100 μg/mL was added (Tomás and Kay, 1984). During their decline phase, the cells were plated on a non-selective BHI agar and incubated for 24 h at 30°C. Post incubation, the colonies were replicated on a new BHI agar

plate with kanamycin and incubated for 24 h at 30°C to identify the colonies without the production plasmid.

Qualitative and Quantitative Assays

Enzyme Activity Measurement

The activity of β-glucosidase was measured by the hydrolysis of FDGlu at 525 nm. Cellulose from *T. reesei* (Sigma-Aldrich, St. Louis, MO, United States) was used as a standard. For α-amylase activity, ceralpha kit (Megazyme, Bray, Ireland) was used with α-amylase from *Aspergillus oryzae* (Sigma-Aldrich, St. Louis, MO, United States) as a standard.

Bradford Assay

Total protein concentration was measured using the Bradford assay. The Bradford reagent (Sigma-Aldrich, St. Louis, MO, United States) and samples were mixed to a ratio of 30:1. The samples were vortexed, incubated for 15 min and measured using a UV spectrophotometer at 595 nm. A standard calibration curve was plot using five concentrations of Bovine Serum Albumin (BSA, Sigma-Aldrich, St. Louis, MO, United States) 0.125, 0.25, 0.5, 1, and 1.5 mg/mL. The supernatant of JS34 bearing pEC-XK99E was used as a blank.

SDS PAGE

The supernatants from the fermentations were treated with acetone (Sigma-Aldrich, St. Louis, MO, United States) at −20°C to precipitate the proteins. The protein pellets after centrifugation at 5,000 g for 10 min, were boiled with 4× laemmli buffer (Bio-Rad Laboratories, Hercules, California, United States) at 95°C for 5 min. The samples were then loaded on a gradient (4–20%) mini-PROTEAN stain-free TGX precast polyacrylamide gels (Bio-Rad Laboratories, Hercules, California, United States) and analyzed on a Bio-Rad imager after electrophoresis.

Genome Sequencing Analysis

Genomic DNA was purified from the mutant using DNeasy blood and tissue kit (Qiagen, Hilden, Germany), and the quality was assessed using DNA electrophoresis and a NanoDrop 1,000 spectrophotometer (Thermo Fisher Scientific, Waltham, MA, United States). Library preparation and sequencing were provided by BGI China (Shenzhen, China). The sequencing was performed on a BGIseq 500 next-generation sequencer, from which data sets (paired) per sample were obtained. Afterwards, adaptor sequences, contaminants, and low-quality reads were removed from the raw reads. CLC Genomics Workbench (Qiagen, Hilden, Germany) was used to map the reads, detect single-nucleotide variations (SNVs) and insertion/deletion events (INDELs), and identify genomic rearrangements using the published genomic sequence of *C. glutamicum* ATCC13032 (Kalinowski et al., 2003). To explore the patterns of mutations, all the genes that had non-synonymous SNVs in the coding regions in the 13 mutants were pooled and submitted to DAVID (Huang et al., 2009) for functional enrichment and clustering. The GO and KEGG terms were chosen for the analysis. All the sequencing data are deposited in the NCBI SRA database under the accession number PRJNA682818.

DATA AVAILABILITY STATEMENT

The datasets presented in this study can be found in online repositories. The names of the repository/repositories and accession number(s) can be found below: https://www.ncbi.nlm.nih.gov/, PRJNA682818.

AUTHOR CONTRIBUTIONS

JC designed and performed the experiments. SB performed the experiments and wrote the manuscript. All authors discussed the results and contributed to the final manuscript.

SUPPLEMENTARY MATERIAL

The Supplementary Material for this article can be found online at: https://www.frontiersin.org/articles/10.3389/fbioe.2021.668513/full#supplementary-material

Supplementary Figure 1 | Growth curves of cured and uncured mutants. The growth of the strains were monitored in a 48-well flower plate (culture volume: 1000 μL, temperature: 30°C, agitation: 800 rpm) by measuring scattered light (ex: 620 nm, Gain: 20) on biolector.

Supplementary Figure 2 | Microscopic view of droplet emulsion containing cells.

REFERENCES

Beneyton, T., Thomas, S., Griffiths, A. D., Nicaud, J. M., Drevelle, A., and Rossignol, T. (2017). Droplet-based microfluidic high-throughput screening of heterologous enzymes secreted by the yeast *Yarrowia lipolytica*. *Microbial Cell Fact.* 16:18. doi: 10.1186/s12934-017-0629-5

Berlec, A., and Štrukelj, B. (2013). Current state and recent advances in biopharmaceutical production in *Escherichia coli*, yeasts and mammalian cells. *J. Ind. Microbiol. Biotechnol.* 40, 257–274. doi: 10.1007/s10295-013-1235-0

Bott, M., and Niebisch, A. (2003). The respiratory chain of *Corynebacterium glutamicum*. *J. Biotechnol.* 104, 129–153. doi: 10.1016/s0168-1656(03)00144-5

Chatzi, K. E., Sardis, M. F., Economou, A., and Karamanou, S. (2014). SecA-mediated targeting and translocation of secretory proteins. *Biochim. Biophys. Acta* 1843, 1466–1474. doi: 10.1016/j.bbamcr.2014.02.014

Chen, J., Vestergaard, M., Jensen, T. G., Shen, J., Dufva, M., Solem, C., et al. (2017). Finding the needle in the haystack-the use of microfluidic droplet technology to identify vitamin-secreting lactic acid bacteria. *mBio* 8:e00526-17. doi: 10.1128/mBio.00526-17

Chen, J., Vestergaard, M., Shen, J., Solem, C., Dufva, M., and Jensen, P. R. (2018). Droplet-based microfluidics as a future tool for strain improvement in lactic acid bacteria. *FEMS Microbiol. Lett.* 365, 1–7. doi: 10.1093/femsle/fny258

Derkx, P. M. F., Janzen, T., Sørensen, K. I., Christensen, J. E., Stuer-Lauridsen, B., and Johansen, E. (2014). The art of strain improvement of industrial lactic acid bacteria without the use of recombinant DNA technology. *Microbial Cell Fact.* 13 (Suppl. 1):S5. doi: 10.1186/1475-2859-13-S1-S5

Eggeling, L., and Bott, M. (eds) (2005). *Handbook of Corynebacterium glutamicum*. Boca Raton, FL: CRCpress.

Hardiman, E., Gibbs, M., Reeves, R., and Bergquist, P. (2010). Directed evolution of a thermophilic beta-glucosidase for cellulosic bioethanol production. *Appl. Biochem. Biotechnol.* 161, 301–312. doi: 10.1007/s12010-009-8794-6

Huang, D. W., Sherman, B. T., and Lempicki, R. A. (2009). Systematic and integrative analysis of large gene lists using DAVID bioinformatics resources. *Nat. Protocols* 4, 44–57. doi: 10.1038/nprot.2008.211

Huang, M., Bai, Y., Sjostrom, S. L., Hallström, B. M., Liu, Z., Petranovic, D., et al. (2015). Microfluidic screening and whole-genome sequencing identifies mutations associated with improved protein secretion by yeast. *Proc. Natl. Acad. Sci. U S A.* 112, E4689–E4696. doi: 10.1073/pnas.1506460112

Izumi, Y., Chibata, I., and Itoh, T. (1978). Production and utilization of amino acids. *Angewandte Chemie Int. Ed. English* 17, 176–183. doi: 10.1002/anie.197801761

Jensen, P. R., and Hammer, K. (1998). Artificial promoters for metabolic optimization. *Biotechnol. Bioeng.* 58, 191–195.

Jensen, P. R., and Michelsen, O. (1992). Carbon and energy metabolism of atp mutants of *Escherichia coli*. *J. Bacteriol.* 174, 7635–7641. doi: 10.1128/jb.174.23.7635-7641.1992

Kalinowski, J., Bathe, B., Bartels, D., Bischoff, N., Bott, M., Burkovski, A., et al. (2003). The complete *Corynebacterium glutamicum* ATCC 13032 genome sequence and its impact on the production of L-aspartate-derived amino acids and vitamins. *J. Biotechnol.* 104, 5–25. doi: 10.1016/s0168-1656(03)00154-8

Kikuchi, Y., Itaya, H., Date, M., Matsui, K., and Wu, L. F. (2009). TatABC overexpression improves *Corynebacterium glutamicum* Tat-dependent protein secretion. *Appl. Environ. Microbiol.* 75, 603–607. doi: 10.1128/AEM.01874-08

Kirchner, O., and Tauch, A. (2003). Tools for genetic engineering in the amino acid-producing bacterium *Corynebacterium glutamicum*. *J. Biotechnol.* 104, 287–299. doi: 10.1016/s0168-1656(03)00148-2

Krömer, J. O., Fritz, M., Heinzle, E., and Wittmann, C. (2005). In vivo quantification of intracellular amino acids and intermediates of the methionine pathway in *Corynebacterium glutamicum*. *Anal. Biochem.* 340, 171–173. doi: 10.1016/j.ab.2005.01.027

Lee, J. W., Na, D., Park, J. M., Lee, J., Choi, S., and Lee, S. Y. (2012). Systems metabolic engineering of microorganisms for natural and non-natural chemicals. *Nat. Chem. Biol.* 8, 536–546. doi: 10.1038/nchembio.970

Liu, X., Zhang, W., Zhao, Z., Dai, X., Yang, Y., and Bai, Z. (2017). Protein secretion in *Corynebacterium glutamicum*. *Crit. Rev. Biotechnol.* 37, 541–551. doi: 10.1080/07388551.2016.1206059

Mazutis, L., Gilbert, J., Ung, W. L., Weitz, D. A., Griffiths, A. D., and Heyman, J. A. (2013). Single-cell analysis and sorting using droplet-based microfluidics. *Nat. Protocols* 8, 870–891. doi: 10.1038/nprot.2013.046

Seemann, R., Brinkmann, M., Pfohl, T., and Herminghaus, S. (2012). Droplet based microfluidics. *Rep. Prog. Phys.* 75:016601. doi: 10.1088/0034-4885/75/1/016601

Shen, J., Chen, J., Jensen, P. R., and Solem, C. (2017). A novel genetic tool for metabolic optimization of *Corynebacterium glutamicum*: efficient and repetitive chromosomal integration of synthetic promoter-driven expression libraries. *Appl. Microbiol. Biotechnol.* 101, 4737–4746. doi: 10.1007/s00253-017-8222-8

Soga, N., Kimura, K., Kinosita, K. Jr., Yoshida, M., and Suzuki, T. (2017). Perfect chemomechanical coupling of FoF1-ATP synthase. *Proc. Natl. Acad. Sci. U S A.* 114, 4960–4965. doi: 10.1073/pnas.1700801114

Solem, C., and Jensen, P. R. (2002). Modulation of gene expression made easy. *Appl. Environ. Microbiol.* 68, 2397–2403. doi: 10.1128/AEM.68.5.2397-2403.2002

Theberge, A. B., Courtois, F., Schaerli, Y., Fischlechner, M., Abell, C., Hollfelder, F., et al. (2010). Microdroplets in microfluidics: an evolving platform for discoveries in chemistry and biology. *Angewandte Chemie - Int. Ed.* 49, 5846–5868. doi: 10.1002/anie.200906653

Tomás, J. M., and Kay, W. W. (1984). A simple and rapid method for the elimination of r plasmids from enteric bacteria. *Curr. Microbiol.* 11, 155–157. doi: 10.1007/bf01567341

Ueno, H., Suzuki, T., Kinosita, K. Jr., and Yoshida, M. (2005). ATP-driven stepwise rotation of FoF1-ATP synthase. *Proc. Natl. Acad. Sci. U S A.* 102, 1333–1338. doi: 10.1073/pnas.0407857102

Unthan, S., Grünberger, A., van Ooyen, J., Gätgens, J., Heinrich, J., Paczia, N., et al. (2014). Beyond growth rate 0.6: what drives *Corynebacterium glutamicum* to higher growth rates in defined medium. *Biotechnol. Bioeng.* 111, 359–371. doi: 10.1002/bit.25103

Veena, V., Poornima, P., Parvatham, R., Sivapriyadharshini, and Kalaiselvi, K. (2011). Isolation, and characterization of β-Glucosidase producing bacteria from different sources. *African J. Biotechnol.* 10, 14907–14912. doi: 10.5897/ajb09.314

Xu, J. Z., Wu, Z. H., Gao, S. J., and Zhang, W. (2018). Rational modification of tricarboxylic acid cycle for improving L-lysine production in *Corynebacterium glutamicum*. *Microbial Cell Fact.* 17:105. doi: 10.1186/s12934-018-0958-z

Conflict of Interest: The authors declare that the research was conducted in the absence of any commercial or financial relationships that could be construed as a potential conflict of interest.

frontiers in Bioengineering and Biotechnology

ORIGINAL RESEARCH
published: 28 May 2021
doi: 10.3389/fbioe.2021.669093

Evolving a New Efficient Mode of Fructose Utilization for Improved Bioproduction in *Corynebacterium glutamicum*

*Irene Krahn[1], Daniel Bonder[2], Lucía Torregrosa-Barragán[2], Dominik Stoppel[1], Jens P. Krause[1], Natalie Rosenfeldt[3], Tobias M. Meiswinkel[1], Gerd M. Seibold[3,4], Volker F. Wendisch[1] and Steffen N. Lindner[1,2]**

[1] Chair of Genetics of Prokaryotes, Faculty of Biology and CeBiTec, Bielefeld University, Bielefeld, Germany, [2] Systems and Synthetic Metabolism, Max Planck Institute of Molecular Plant Physiology, Potsdam-Golm, Germany, [3] Institute of Biochemistry, University of Cologne, Cologne, Germany, [4] Department of Biotechnology and Biomedicine, Technical University of Denmark, Lyngby, Denmark

Fructose utilization in *Corynebacterium glutamicum* starts with its uptake and concomitant phosphorylation *via* the phosphotransferase system (PTS) to yield intracellular fructose 1-phosphate, which enters glycolysis upon ATP-dependent phosphorylation to fructose 1,6-bisphosphate by 1-phosphofructokinase. This is known to result in a significantly reduced oxidative pentose phosphate pathway (oxPPP) flux on fructose (∼10%) compared to glucose (∼60%). Consequently, the biosynthesis of NADPH demanding products, e.g., L-lysine, by *C. glutamicum* is largely decreased when fructose is the only carbon source. Previous works reported that fructose is partially utilized *via* the glucose-specific PTS presumably generating fructose 6-phosphate. This closer proximity to the entry point of the oxPPP might increase oxPPP flux and, consequently, NADPH availability. Here, we generated deletion strains lacking either the fructose-specific PTS or 1-phosphofructokinase activity. We used these strains in short-term evolution experiments on fructose minimal medium and isolated mutant strains, which regained the ability of fast growth on fructose as a sole carbon source. In these fructose mutants, the deletion of the glucose-specific PTS as well as the 6-phosphofructokinase gene, abolished growth, unequivocally showing fructose phosphorylation *via* glucose-specific PTS to fructose 6-phosphate. Gene sequencing revealed three independent amino acid substitutions in PtsG (M260V, M260T, and P318S). These three PtsG variants mediated faster fructose uptake and utilization compared to native PtsG. In-depth analysis of the effects of fructose utilization *via* these PtsG variants revealed significantly increased ODs, reduced side-product accumulation, and increased L-lysine production by 50%.

Keywords: metabolic engineering, synthetic biology, PTS, NADPH, lysine, fructose, adaptive laboratory evolution

OPEN ACCESS

Edited by:
Pablo Ivan Nikel, Novo Nordisk Foundation Center for Biosustainability (DTU Biosustain), Denmark

Reviewed by:
Stephan Noack, Julich-Forschungszentrum, Helmholtz-Verband Deutscher Forschungszentren (HZ), Germany
Fabien Létisse, UMR 5504 Laboratoire d'Ingénierie des Systèmes Biologiques et des Procédés (LISBP), France

***Correspondence:**
Steffen N. Lindner
Lindner@mpimp-golm.mpg.de

Specialty section:
This article was submitted to Synthetic Biology, a section of the journal Frontiers in Bioengineering and Biotechnology

Received: *17 February 2021*
Accepted: *14 April 2021*
Published: *28 May 2021*

Citation:
Krahn I, Bonder D, Torregrosa-Barragán L, Stoppel D, Krause JP, Rosenfeldt N, Meiswinkel TM, Seibold GM, Wendisch VF and Lindner SN (2021) Evolving a New Efficient Mode of Fructose Utilization for Improved Bioproduction in Corynebacterium glutamicum. Front. Bioeng. Biotechnol. 9:669093. doi: 10.3389/fbioe.2021.669093

INTRODUCTION

Canonical metabolic routes evolved for superior performance in the natural habitat but often they do not represent the ideal choice from a biotechnological perspective (Erb et al., 2017). If more suitable alternative pathways are known, rational approaches of metabolic engineering can redirect metabolic pathways into more advantageous directions. In the absence of a known and better-suited natural alternative, adapted laboratory evolution (ALE) may select for efficient pathway variants. *Corynebacterium glutamicum* is employed in the million-ton scale bioproduction of amino acids, with the lion's share split between L-glutamate and L-lysine (Wendisch, 2020). Beyond amino acids, amines, organic acids, and alcohols are produced with this bacterium (Becker et al., 2018; Mindt et al., 2020).

NADPH is an important cofactor for anabolic reactions and hence a limiting factor in the production of metabolites with a particularly high demand for NADPH, e.g., L-lysine, which requires four molecules of NADPH per molecule of L-lysine produced (Marx et al., 1996). To provide NADPH, *C. glutamicum* possesses several dehydrogenases, which use $NADP^+$ as cofactor. These are the glucose 6-phosphate dehydrogenase (Zwf), and the 6-phosphogluconate dehydrogenase (Gnd) of the oxidative part of the pentose phosphate pathway (oxPPP), the isocitrate dehydrogenase (Icd) in the TCA cycle, and the malic enzyme (MalE), and their overexpression improved production of L-lysine (Georgi et al., 2005; Becker et al., 2007). NADPH provision was optimized by heterologous expression of genes encoding the membrane-bound transhydrogenase from *Escherichia coli* (Kabus et al., 2007). Although *C. glutamicum* lacks transhydrogenase, it is known to run an ATP-consuming transhydrogenase-like cycle between the anaplerotic reactions, malate dehydrogenase, and MalE, transferring electrons from NADH to $NADP^+$ (Blombach et al., 2011). However, the predominant way of NADPH generation is *via* the oxPPP.

Metabolic engineering was used to broaden the substrate spectrum of *C. glutamicum* toward second generation feedstocks such as non-food wastes from biodiesel (glycerol) (Rittmann et al., 2008) or hemicellulose biomasses (xylose and arabinose) (Zhao et al., 2018). Yet, the sugars glucose, derived from starch hydrolysates as well as sucrose and fructose derived from molasses, are still the preferred carbon sources for amino acid production (Anaya-Reza and Lopez-Arenas, 2017). The decrease in L-lysine titers when fructose is used instead of glucose is drastic, resulting in a 40–75% lower L-lysine yield (Georgi et al., 2005). Although the entry points of glucose and fructose are only two reactions apart, the fluxes through the oxPPP, and hence the prevalent NADPH generating reactions, are significantly different. On fructose, a very low flux is described (10%), whereas glucose leads to a high flux (60%) (Kiefer et al., 2004). As a result, a low L-lysine product yield is reached on fructose compared to glucose (Georgi et al., 2005). Moreover, the reported high oxPPP fluxes on glucose may still be limiting for overproduction of high NADPH-consuming products, such as amino acids (Murai et al., 2020).

While for glucose an ATP-dependent pathway, which can replace the phosphoenolpyruvate-dependent phosphotransferase system (PTS), is present in *C. glutamicum* (Moon et al., 2007; Lindner et al., 2011), fructose and sucrose are exclusively phosphorylated by the PTS (Ikeda, 2012). Glucose is phosphorylated to glucose 6-P by a glucose-specific PTS compound (PtsG). Sucrose is phosphorylated to sucrose 6-P *via* its PTS (PtsS) and subsequently cleaved to glucose 6-P and fructose; the latter is exported outside *via* a so far unidentified exporter. Fructose, regardless if added to the medium as a carbon source or originating from sucrose catabolism, is taken up and phosphorylated to fructose 1-P by a fructose specific PTS (PtsF) (Dominguez and Lindley, 1996; Parche et al., 2001). After a second ATP-dependent phosphorylation of fructose 1-P catalyzed by 1-phosphofructokinase (FruK), it enters glycolysis at the level of fructose 1,6-BP. Additionally, a minor fraction of fructose (<10%) is taken up and phosphorylated by PtsG to generate fructose 6-phosphate (Kiefer et al., 2004; **Figure 1**). Most strikingly, overexpression of fructose 1,6-bisphosphatase increased L-lysine production when fructose was used as the carbon source (Georgi et al., 2005), pointing to an advantage of fructose 6-P over fructose 1,6-BP for increasing oxPPP-flux as fructose 6-P is rapidly converted to glucose 6-phosphate by phosphoglucoisomerase and, consequently, increasing NADPH regeneration and productivity. Thus, shifting the carbon flux slightly closer to the entry point of the oxPPP allows a higher flux through the oxPPP and a higher NADPH regeneration rate. Similarly, L-lysine production from molasses was optimized by overexpression of fructose 1,6-bisphosphatase and fructokinase (Xu et al., 2013).

Here, we aimed at increasing the efficiency of the PtsG-catalyzed conversion of fructose to fructose 6-P. We generated strains unable to utilize fructose *via* its usual route and selected fast-growing strains after short-term evolution in fructose minimal medium. Isolated PtsG variants were identified

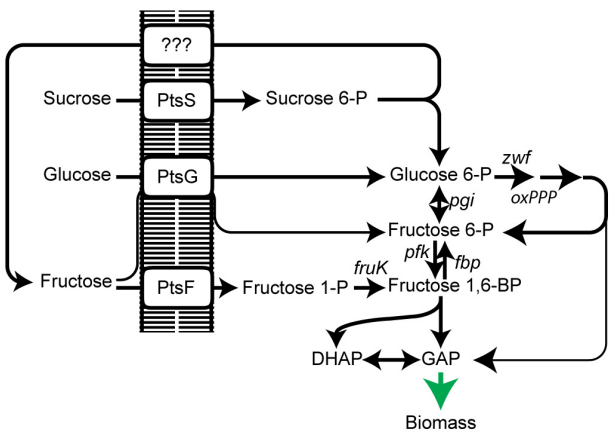

FIGURE 1 | Scheme of PTS-dependent uptake and utilization of sugars sucrose, glucose, and fructose in *C. glutamicum*. PtsS, sucrose PTS; PtsG, glucose PTS; PtsF, fructose PTS; oxPPP, oxidative pentose phosphate pathway; pgi, phosphoglucose isomerase; pfk, 6-phosphofructokinase; fbp, fructose 1,6-bisphosphatase; fruK, 1-phosphofruktokinase; DHAP, dihydroxyacetone phosphate; GAP, glyceraldehyde 3-phosphate. Data represent one of two individual cultivations, which differed <5%.

and reverse engineering complemented fructose utilization in the deletion strains. Deletion of 6-phosphofructokinase in the mutants and overexpression of the PtsG variants in a fructose 1,6-bisphosphatase deletion strain confirmed fructose phosphorylation to fructose 6-P by the PtsG variants. ^{13}C-labeling experiments revealed that a higher oxPPP flux is present in the reverse-engineered strains. Finally, the alternative way of fructose utilization was tested on L-lysine production, showing an increase in L-lysine yield from fructose.

MATERIALS AND METHODS

Strains and Plasmids Used

Corynebacterium glutamicum strains and plasmids used are listed in **Tables 1**, **2**, respectively. For plasmid construction, the primers listed in **Supplementary Table 1** were used. For cloning, genes were amplified from genomic DNA and cloned by the indicated restriction sides (**Supplementary Table 1**) into similarly restricted pVWEx1. Deletion plasmids were constructed by cloning PCR-fused products of primer pairs A + B and C + D and cloned blunt-ended into *Sma*I-digested pK19mobsacB.

Culture Conditions and Growth Experiments

Corynebacterium glutamicum strains were cultivated in LB (1% NaCl, 1% tryptone, and 0.5% yeast extract) or CgXII minimal medium [20 g/L $(NH_4)_2$ SO_4, 5 g/L urea, 1 g/L KH_2PO_4, 1 g/L K_2HPO_4, 42 g/L MOPS, 10 mg/L $CaCl_2$, 250 mg/L $MgSO_4 \times 7$ H_2O, 0.01 mg/L $FeSO_4 \times 7$ H_2O, 0.01 mg/L $MnSO_4 \times 7$ H_2O, 0.001 mg/L $ZnSO_4 \times 7$ H_2O, 0.0002 mg/L $CuSO_4$, and 0.00002 mg/L $NiCl_2 \times 6$ H_20, pH 7) (Eggeling and Bott, 2005). For growth experiments, the strains grew in 50-ml LB cultures overnight, harvested by centrifugation (3220 × *g*), washed twice in CgXII without carbon source, and inoculated to an optical density (OD) of 1 in 50 ml of CgXII containing the indicated carbon sources. For plasmid construction, *E. coli* DH5α was used and cultured in LB medium. Precultures for growth experiments with *C. glutamicum* and all *E. coli* cultures were carried out in LB. For selection on pVWEx1 and derivatives, 50 and 25 mg/ml kanamycin was added to *E. coli* and *C. glutamicum* cultures, respectively. CgXII minimal medium (Eggeling and Bott, 2005) was used for growth, sugar uptake, and L-lysine production experiments. Cells were

TABLE 1 | *Corynebacterium glutamicum* strains used in this study.

Strain	Deletion of gene, function	Derived from	Source
C. glutamicum	Wild-type (WT), ATCC13032	–	ATCC
Δ*ptsF*	*ptsF*, fructose specific PTS compound	WT	Radek et al., 2016
Δ*ptsF* Δ*ptsG*	*ptsG*, glucose-specific PTS compound	Δ*ptsF*	This study
Δ*fruK1*	*fruK1*, 1-phosphofructokinase 1	WT	This study
Δ*fruK2*	*fruK2*, 1-phosphofructokinase 2	WT	This study
Δ*fruK1* Δ*fruK2*	*fruK1*, *fruK2*, 1-phosphofructokinase 1 + 2	Δ*fruK1*	This study
Δ*fbp*	*fbp*, fructose 1,6-bisphosphatase	WT	Rittmann et al., 2003
Δ*fruK1* Δ*fruk2* Δ*pfk*	*pfk*, 6-phosphofructokinase	Δ*fruK1* Δ*fruK2*	This study
Δ*fruK1* Δ*fruk2* Δ*ptsG*	*ptsG*, glucose-specific PTS compound	Δ*fruK1* Δ*fruK2*	This study
Δ*fruK1* Δ*fruk2* Δ*hpr*	*hpr*, general PTS compound Hpr	Δ*fruK1* Δ*fruK2*	This study
CgLYS4	DM1729 Δ*pta-ackA* Δ*cat* Δace*AB* Δ*ldhA* Δ*nanR*	DM1729	Sgobba et al., 2018
CgLYS4 Δ*ptsF*	CgLYS4 deleted in Δ*ptsF*	CgLYS4	Sgobba et al., 2018

TABLE 2 | Plasmids used in this study.

Name	Properties/use	Source
pVWEx1	Km^R, pHM1519, P_{tac}, $lacI^q$, for IPTG inducible expression	Peters-Wendisch et al., 2001
pVWEx1-*ptsG*	pVWEx1, carrying WT *ptsG*	This study
pVWEx1-$ptsG^{M260V}$	pVWEx1, carrying *ptsG* mutated in M260V	This study
pVWEx1-$ptsG^{M260T}$	pVWEx1, carrying *ptsG* mutated in M260T	This study
pVWEx1-$ptsG^{P318S}$	pVWEx1, carrying *ptsG* mutated in P318S	This study
pVWEx1-*ptsF*	pVWEx1, carrying WT *ptsF*	This study
pVWEx1-$lysC^{fbr}$	pVWEx1, carrying feedback resistant version of *lysC* (T311I)	This study
pK19*mobsacB*	Km^R, RP4; *mob*; $oriV_{Ec}$; *sacB; lacZα;* for allelic exchange	Schafer et al., 1994
pK19*mobsacB* Δ*fruK1*	pK19*mobsacB* based for *fruK1* deletion	This study
pK19*mobsacB* Δ*fruK2*	pK19*mobsacB* based for *fruK2* deletion	This study
pK19*mobsacB* Δ*pfk*	pK19*mobsacB* based for *pfk* deletion	This study
pK19*mobsacB* Δ*ptsG*	pK19*mobsacB* based for *ptsG* deletion	This study
pK19*mobsacB* Δ*ptsF*	pK19*mobsacB* based for *ptsF* deletion	Radek et al., 2016
pK19*mobsacB* Δ*hpr*	pK19*mobsacB* based for *hpr* deletion	Lindner et al., 2011

harvested in the exponential growth phase by centrifugation (RT, 3220 × *g* for 10 min) and washed twice in CgXII medium without carbon source. Gene expression was induced by addition of up to 1 mM isopropyl β-D-1-thiogalactopyranoside (IPTG). Ideal concentration of IPTG for *ptsF*/*G* expression was determined to be at 30 μM IPTG. Cultivations were carried out in 50-ml solutions in 500-ml baffled shaking flasks at 120 rpm and 30°C.

Analysis of Sugars and Organic Acid Concentration, and Amino Acid Production

Lysine production: to verify L-lysine production, strains were inoculated to OD_{600} of 1 in CgXII media supplXemented with 4% fructose (w/v), 30 μM IPTG, and, if carrying a pVWEx1 variant, 25 μg/ml kanamycin in 500-ml baffled shake flasks. Supernatants were collected at 4, 8, 12, 24, 48, and 72 h after inoculation. L-lysine concentrations were determined in up to 1:5000 serial dilution of supernatants using an ICS-6000 HPIC Ion Chromatography equipped with an AminoPac PA10 IC column, ICS-6000 CD Conductivity Detector, and ADRS 600 Anion Dynamically Regenerated Suppressor (Dionex, CA, United States). The column was set with a 10–250 mM NaOH gradient at a 0.25 ml/min flow rate. Sugars and organic acid concentrations were quantified *via* HPLC as described previously (Rittmann et al., 2008).

^{13}C Isotopic Labeling of Proteinogenic Amino Acids

^{13}C-isotope tracing was performed to indirectly analyze carbon flux. Cells were cultured in 4 ml of CgXII medium containing ^{13}C-1-glucose or ^{13}C-1-fructose (Sigma-Aldrich, Taufkirchen, Germany) as sole carbon sources. Cultures were inoculated from CgXII + 20 mM pyruvate overnight cultures to an OD_{600} 0.01 and grown at 30°C until early stationary phase. Before inoculation, cells were washed twice (RT, 6000 × *g*, 3 min) in carbon source free CgXII medium. 10^9 cells (∼1 ml of OD_{600} = 1) were pelleted, washed with ddH_2O, and hydrolyzed in 1 ml of 6N hydrochloric acid at 95°C for 24 h. Subsequently to hydrolysis, HCl was evaporated by heating at 95°C under an air stream. Hydrolyzed biomass was resuspended in 1 ml of ddH_2O. Amino acid masses were analyzed after separation by ultra-performance liquid chromatography (Acquity, Waters, Milford, MA, United States) using a C18-reversed-phase column (Waters, Eschborn, Germany) as previously described (Giavalisco et al., 2011). Mass spectra were acquired by an Exactive mass spectrometer (Thermo Scientific, Dreieich, Germany). Data were analyzed using Xcalibur (Thermo Scientific, Dreieich, Germany). Amino acid standards (Merck, Darmstadt, Germany) were used to determine specific retention times.

Sugar Uptake Measurements

For ^{14}C-labeled fructose uptake studies, strains were grown to early exponential growth phase with 50 mM fructose as sole carbon source and 30 μM IPTG, if appropriate. Cells were harvested by centrifugation, washed two times in ice-cold CgXII medium (without carbon source), resuspended to an optical density OD_{600} of 2 in CgXII medium, and stored on ice until measurement. Prior to the transport assay, cells were incubated for 3 min at 30°C. The assay was started by addition of 1 μM to 1 mM ^{14}C-labeled fructose (specific activity of 45 mCi mmol^{-1}; Hartmann Analytik, Braunschweig, Germany). At given time intervals (15, 30, 45, 60, and 120 s), 200-μl samples were filtered through glass fiber filters (type F; Millipore, Eschborn, Germany) and washed twice with 2.5 ml of 100 mM LiCl. The radioactivity of the filter samples was determined using scintillation fluid (Rotiszinth; Roth, Germany) and a scintillation counter (LS 6500; Beckmann, Krefeld, Germany).

RESULTS

Construction and Characterization of Strains Lacking Fructose-Specific PTS and 1-Phosphofructokinase Genes

Previous studies suggested a PtsG-mediated fructose utilization to fructose 6-P in *C. glutamicum* (Kiefer et al., 2004). We expected that the direct generation of fructose 6-P instead of fructose 1,6-BP from fructose increases oxidative PPP flux leading to higher NADPH availability, which is advantageous for high NADPH-demanding bioproductions, such as L-lysine. In fact, overexpression of fructose 1,6-bisphosphatase increased L-lysine production from fructose (Georgi et al., 2005). The aim of this study was to explore the promiscuous reaction of PtsG and evolve it for increased activity. To be able to select for this route of fructose utilization and to evolve it, we generated two strains, which are deficient in the canonical route of fructose utilization. The first lacks the fructose-specific PTS compound (Δ*ptsF*), and the second lacks 1-phosphofructokinase activity (Δ*fruK1* Δ*fruK2*) (**Figure 1**). As expected, growth of these strains on fructose was strongly affected. The Δ*ptsF* strain grew with a very low growth rate and the Δ*fruK1* Δ*fruK2* strain did not grow at all within 24 h. Growth analysis of the individual 1-phosphofructokinase deletion strains on fructose revealed no effect by the deletion of *fruK2*, but slower growth when *fruK1* was deleted (**Figure 2**). Similarly to effects observed for Δ*ptsF* and Δ*fruK1* Δ*fruK2*, an *E. coli* 1-phosphofruktokinase deletion strain was reported to be unable to grow on fructose, and moreover growth on other carbon sources of this strain was inhibited when fructose or fructose 1-P were added to the medium, indicating a growth perturbing effect of fructose 1-P caused by regulatory or inhibitory function of this metabolite (Ferenci and Kornberg, 1973). In *C. glutamicum*, fructose 1-P acts as a negative effector of sugar regulator SugR and hence accumulation in the absence of 1-phosphofructokinase activity might affect sugar uptake and utilization (Dietrich et al., 2009), thus causing the growth difference of Δ*ptsF* and Δ*fruK1* Δ*fruK2* observed here. Both, Δ*ptsF* and Δ*fruK1* Δ*fruK2* were considered suitable for performing shake-flask short-term evolution experiments. In particular, the slow growth of Δ*ptsF* indicates the presence of an alternative way for fructose utilization in our background strain, suggesting a good starting point for optimization of the reaction

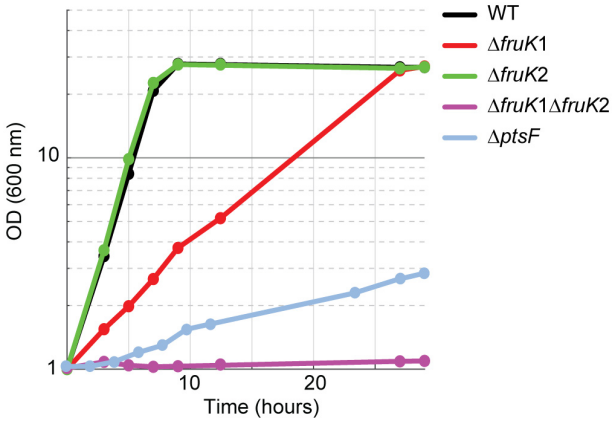

FIGURE 2 | Growth on 2% fructose of strains lacking parts of the canonical fructose utilization pathway, fructose-specific PTS (*ptsF*), or 1-phosphofructokinases (*fruK1*, *fruK2*). Data represent one of two individual cultivations that differed <5%.

through evolution. In contrast to the results obtained with Δ*ptsF*, a deletion strain lacking the general PTS compound HPR is unable to grow on fructose, also after prolonged incubation, pointing to the contribution of PtsG as reported earlier (Kiefer et al., 2004; Moon et al., 2007) (data not shown).

Adaptive Evolution for Growth on Fructose

To evolve the specificity of the glucose-specific PTS compound toward fructose, *C. glutamicum* strains Δ*ptsF* and Δ*fruK1*Δ*fruK2* were incubated in CgXII minimal media containing 2% fructose (w/v) as a sole carbon source. After incubation for 3–4 days, all strains had grown to stationary phase. Samples from each culture were transferred to LB plates for single colony isolation. When subsequently transferred to fructose minimal medium, the isolated strains immediately showed fast growth, indicating that a mutation compensating for the growth deficiency had occurred. To increase the variance, 20 cultures of each genetic background (Δ*ptsF* and Δ*fruK1*Δ*fruK2*) were incubated for 4 days in fructose minimal medium. All strains reached stationary phase within this time. To identify if mutations in PtsG are responsible for the growth recovery, the *ptsG* locus of the isolated mutants was amplified by PCR and sequenced by Sanger sequencing. Sequencing results revealed that all strains analyzed (n = 40) had non-synonymous substitution in the coding sequence of *ptsG*. Among these mutants, only three different point mutations were found. These mutations altered the amino acids M260V, M260T, or P318S. The most abundant mutation among the three was M260V (**Supplementary Figure 1**).

Mutants from both the Δ*ptsF* and the Δ*fruK1* Δ*fruK2* background representing all three PtsG variants were analyzed for growth in fructose, sucrose, as well as in fructose + glucose minimal medium (**Figure 3**). The six analyzed mutants showed restored, fast growth with fructose as a sole source of carbon; moreover, they grew to slightly higher ODs than the WT strain. In sucrose minimal medium as well as in glucose + fructose medium, the strains grew similarly to the WT control and reached ODs twofold higher than their parental strains (Δ*ptsF* or Δ*fruK1*Δ*fruK2*), since the latter can only efficiently utilize the glucose part of the provided carbon sources. While the mutant strains reached comparable maximal ODs in medium containing sucrose only, they grew to slightly higher maximal ODs with glucose + fructose and to significantly higher maximal ODs when fructose was used as the sole carbon source.

After having shown that the mutants derived from the parental Δ*fruK1* Δ*fruK2* strain grew with fructose and contained non-synonymous mutations in the *ptsG* locus, either the gene encoding the general PTS subunit *hpr* or the glucose-specific subunit PtsG was deleted in these mutants. Both deletions *ptsG* and *hpr* in the Δ*fruK1* Δ*fruK2* mutants abolished growth with fructose in these strains (**Supplementary Figure 2**). Thus, the activity of the glucose-specific PTS is responsible for fructose utilization in these mutants.

Evidence for Generation of Fructose 6-Phosphate From Fructose *via* Glucose-Specific PTS

To test the hypothesis that PtsG phosphorylates fructose to yield fructose 6-P, genetic experiments were performed. First, it was determined if 6-phosphofructokinase is required for fructose catabolism *via* glucose-specific PTS. Therefore, the 6-phosphofructokinase gene (*pfkA*) was deleted in strain Δ*fruK1* Δ*fruK2*, which lacked both 1-phosphofructokinase genes, as well as in the evolved Δ*fruK1* Δ*fruK2* ALE mutant PtsG^{M260T}. Both of these *pfkA* deletion mutants were not able to grow in fructose minimal medium (**Figure 4A**), indicating that PtsG phosphorylates fructose exclusively to fructose 6-phosphate.

The deletion of *pfkA* in the WT background did not alter growth of the strain with fructose, as fructose utilized *via* PtsF and FruK enters glycolysis at fructose 1,6-bisphosphate. In the absence of 6-phosphofructokinase in the strain Δ*fruK1* Δ*fruK2* and the Δ*fruK1* Δ*fruK2* ALE mutant PtsG^{M260T} (see **Figure 4A**), the only way fructose 6-P can be catabolized is *via* the oxPPP. From three molecules of fructose 6-P entering the oxPPP, one molecule of glyceraldehyde 3-phosphate (GAP) and three molecules of carbon dioxide are produced, while two molecules of fructose 6-P are regenerated. This low feed to the "lower" metabolism seemingly is not sufficient to allow for growth. One reason might be due to sugar phosphate stress. It might also be the case that metabolism probably does not utilize the GAP produced efficiently enough as it must be used to provide PEP for fructose phosphorylation, in order to keep the stoichiometric influx of fructose 6-P.

Based on previous findings that fructose 1,6-bisphosphatase is important for fructose catabolism *via* PtsF and 1-phosphofructokinases/FruK1 and/or FruK2 (Becker et al., 2005; Georgi et al., 2005), we hypothesized that strains growing on fructose *via* PtsG, synthesizing fructose 6-P directly from fructose, do not require fructose 1,6-bisphosphatase for growth. To test this, we overexpressed the PtsG variants in a Δ*fbp* strain and analyzed its growth on fructose (**Figure 4B**). This

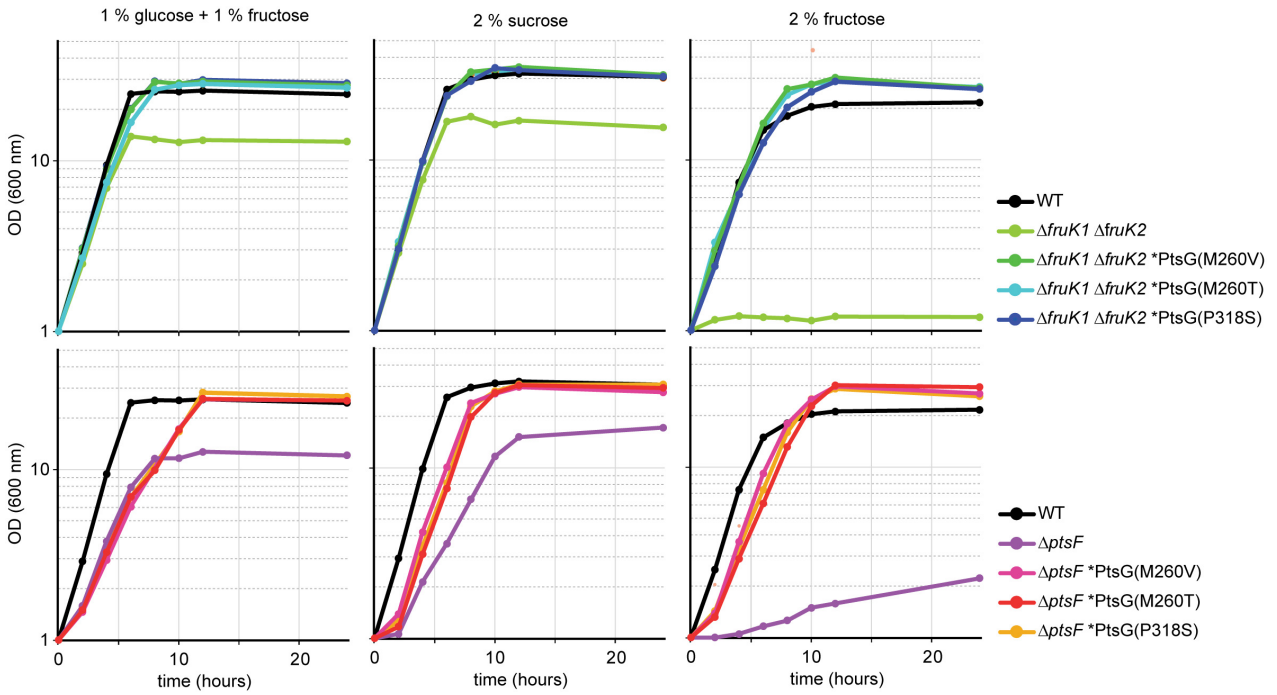

FIGURE 3 | Growth of isolated fructose mutants on glucose + fructose, sucrose, and fructose. Data represent one of two individual cultivations that differed <5%.

experiment tests only for the small flux to fructose 6-P, which is necessary to generate essential PPP intermediates (erythrose 4-P, ribose 5-P, and glucose 6-P). Notably, some residual growth on fructose was observed for Δ*fbp*. This might be, similar to Δ*ptsF*, due to the presence of the genomic *ptsG* in this strain, which is commensurate with some flux of fructose phosphorylation in the WT as observed previously (Kiefer et al., 2004). However, all PtsG variants allowed the Δ*fbp* strain to regain growth with fructose as fast as the WT strain (**Figure 4B**). Thus, fructose 1,6-bisphosphatase is dispensable for growth if fructose catabolism is mediated *via* PtsG with fructose being directly converted to fructose 6-P.

Complementation of Δ*ptsG*Δ*ptsF* by *ptsG* Overexpression

After having shown that PtsG-mediated fructose catabolism complemented the growth impairment due to the absence of fructose 1,6-bisphosphatase, a more rigorous test was attempted. A strain lacking the genes for both fructose- and glucose-specific PTS subunits was constructed (Δ*ptsG*Δ*ptsF*), and it was tested if PtsG and/or the selected PtsG variants support growth with fructose as the sole carbon source. Strain Δ*ptsF* Δ*ptsG* revealed a clean phenotype as growth with fructose as the sole carbon source was completely abolished (**Figure 5**). With glucose, however, Δ*ptsG*Δ*ptsF* showed some residual growth, which likely depended on PTS-independent glucose catabolism (Ikeda et al., 2011; Lindner et al., 2011). The observed reduction of OD to 50% with sucrose as the sole carbon source reflects the fact that only the glucose moiety can be utilized after its activation by PtsS and cleavage to glucose 6-P and fructose, but not the fructose moiety of the disaccharide, which can be catabolized by strain Δ*ptsF* Δ*ptsG*. Under the chosen conditions, PTS-independent fructose catabolism is irrelevant as indicated by this finding and the inability of strain Δ*ptsF* Δ*ptsG* to grow with fructose alone.

To test for *ptsG*-mediated fructose utilization, strain Δ*ptsG* Δ*ptsF* was transformed with expression plasmids overexpressing either native *ptsG*, one of the three newly identified *ptsG* variants, or, as positive control, native *ptsF*. Growth of the resulting strains in minimal media containing either fructose, glucose, or sucrose is shown in **Figure 5**. Growth of Δ*ptsF* Δ*ptsG* with glucose was complemented to a similar extent with all PtsG variants, including native PtsG, whereas overexpression of the fructose-specific PTS gene *ptsF* did not. On fructose, all constructs complemented the growth phenotype of Δ*ptsF* Δ*ptsG*, but to varying extent. Native *ptsG* supported a significantly lower growth rate (0.19 h^{-1}) as compared to the growth achieved with the three mutated *ptsG*-versions (0.36–0.39 h^{-1}) and with *ptsF* (0.44 h^{-1}). Lag phases were observed only with native PtsG and with variant $PtsG^{P318S}$ (**Figure 5**). Similar to the observed higher ODs reached by the ALE mutants as compared to their parent strains (**Figure 3**), the reverse-engineered strains analyzed also grew to about 20% higher OD in fructose minimal medium than strain Δ*ptsG*Δ*ptsF* (**Table 3**). With sucrose as the sole carbon source, all strains grew similar to WT except for Δ*ptsF* Δ*ptsG* carrying the empty vector as negative control, which showed a lag phase, grew slower, and reached about half of the OD compared to the other strains. Analysis of supernatants from sucrose grown Δ*ptsF* Δ*ptsG* revealed stoichiometric production of fructose from sucrose (data not shown).

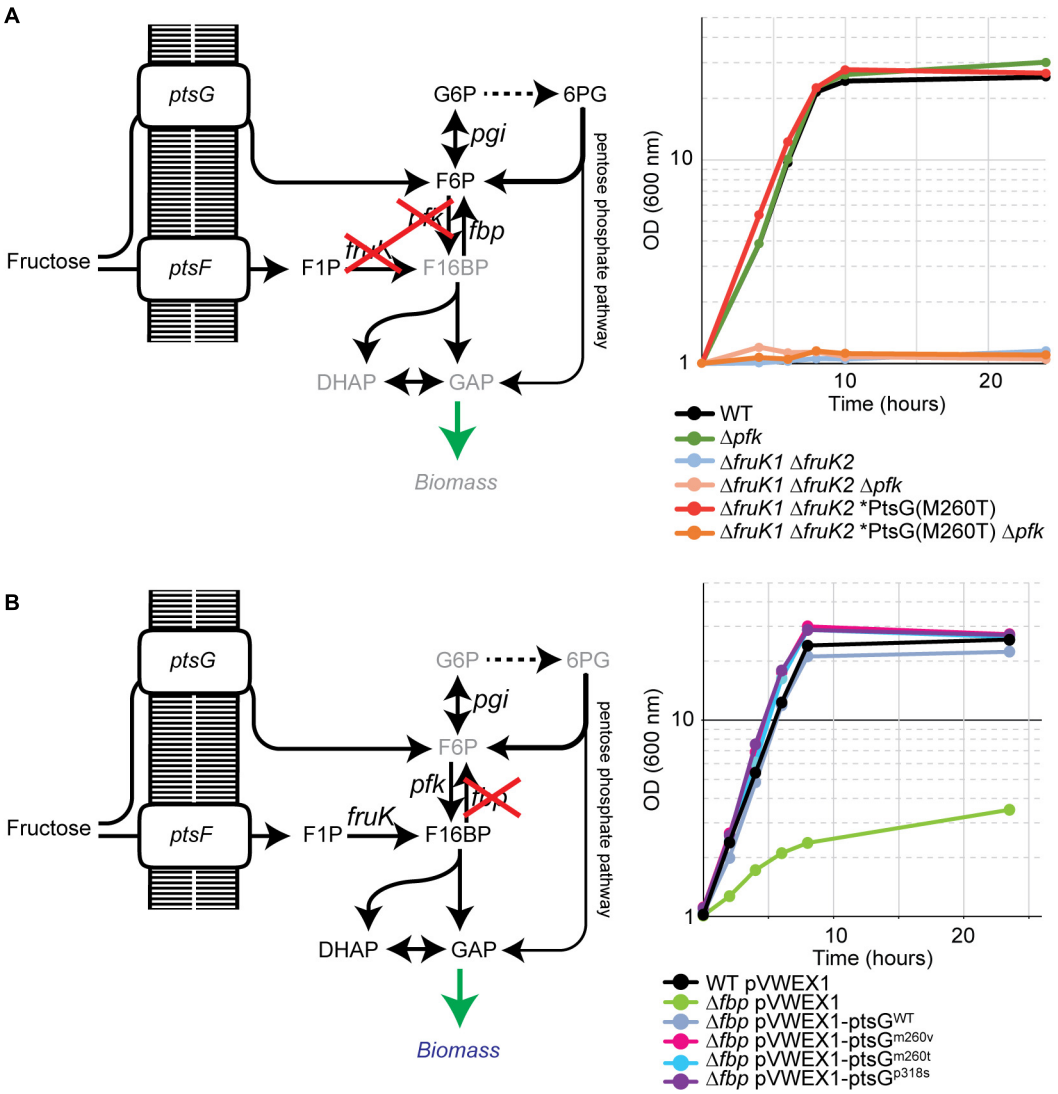

FIGURE 4 | Genetic elucidation of fructose phosphorylation to fructose 6-P by PtsG. **(A)** Deletion of 6-phosphofruktokinase (Δ*pfk*) in Δ*fruK1* Δ*fruK2* fructose mutant abolishes growth. **(B)** Overexpression of PtsG variants improve growth of a fructose 1,6-bisphosphatase deletion strain (Δ*fbp*). Data represent one of two individual cultivations that differed <5%.

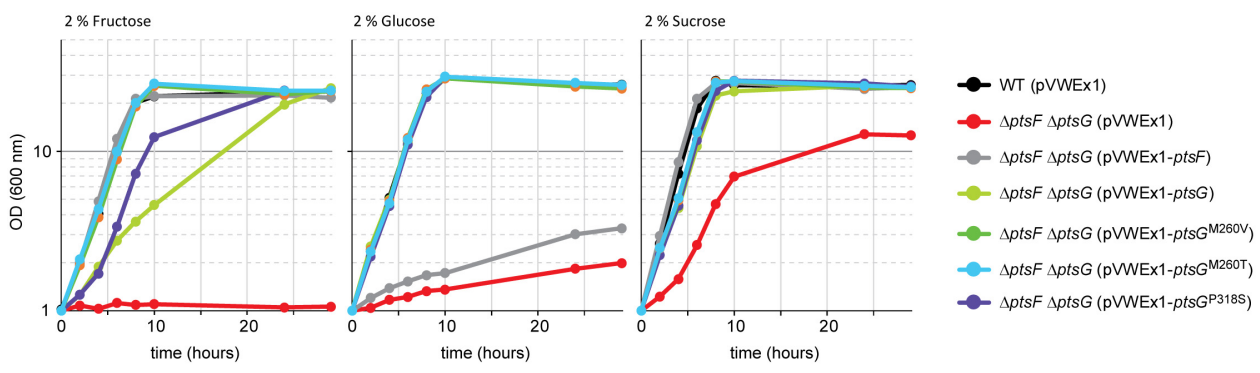

FIGURE 5 | Growth complementation of the Δ*ptsF* Δ*ptsG* strain by overexpressing PtsG variants. Data represent one of two individual cultivations that differed <5%.

TABLE 3 | Growth rates and changes in OD (600 nm) during growth of recombinant strains on 2% glucose, 2% fructose, or 2% sucrose.

	2% glucose	2% fructose	2% sucrose
Growth rates (h^{-1})			
WT (pVWEx1)	0.40 ± 0.00	0.41 ± 0.01	0.49 ± 0.00
Δ*ptsF* Δ*ptsG* (pVWEx1)	0.03 ± 0.00	0.00 ± 0.00	0.26 ± 0.01
Δ*ptsF* Δ*ptsG* (pVWEx1-*ptsF*)	0.03 ± 0.00	0.45 ± 0.01	0.50 ± 0.01
Δ*ptsF* Δ*ptsG* (pVWEx1-*ptsG*)	0.37 ± 0.01	0.19 ± 0.01	0.33 ± 0.00
Δ*ptsF* Δ*ptsG* (pVWEx1-*ptsG*^{P318S})	0.40 ± 0.01	0.36 ± 0.00	0.41 ± 0.00
Δ*ptsF* Δ*ptsG* (pVWEx1-*ptsG*^{M260V})	0.40 ± 0.00	0.39 ± 0.01	0.42 ± 0.01
Δ*ptsF* Δ*ptsG* (pVWEx1-*ptsG*^{M260T})	0.40 ± 0.00	0.38 ± 0.00	0.42 ± 0.00
ΔOD(600 nm)			
WT (pVWEx1)	27.8 ± 0.2	21.1 ± 0.2	25.6 ± 0.2
Δ*ptsF* Δ*ptsG* (pVWEx1)	0.8 ± 0.2	0.0 ± 0.0	11.8 ± 0.0
Δ*ptsF* Δ*ptsG* (pVWEx1-*ptsF*)	25.6 ± 0.1	21.7 ± 0.5	25.8 ± 1.6
Δ*ptsF* Δ*ptsG* (pVWEx1-*ptsG*)	27.7 ± 0.5	25.1 ± 0.1	24.8 ± 0.6
Δ*ptsF* Δ*ptsG* (pVWEx1-*ptsG*^{P318S})	28.1 ± 0.3	24.6 ± 0.3	26.7 ± 0.3
Δ*ptsF* Δ*ptsG* (pVWEx1-*ptsG*^{M260V})	27.7 ± 0.7	24.8 ± 0.9	27.2 ± 0.4
Δ*ptsF* Δ*ptsG* (pVWEx1-*ptsG*^{M260T})	28.4 ± 0.0	25.6 ± 0.6	26.8 ± 0.4

Faster Fructose Uptake Mediated by the Selected PtsG Variants

The three observed mutations M260T, M260V, and P318S are located within the EIIC permease subunit of the PTS-transporter domain, which mediates substrate translocation and transiently binds the substrate, until it becomes phosphorylated. In the well-characterized EIIC ChbC of *Bacillus cereus*, residues E334 and H250 interact with the substrate *N,N′*-diacetylchitobiose *via* hydrogen bonds (McCoy et al., 2015) and are located at the beginning of the transmembrane domain (TM) 7 and between TM8 and TM9, respectively. The topology of this region in ChbC is quite different from the (predicted) topology of BglF (beta-glucoside-specific) and MtlA (mannitol specific) EIIC proteins from *E. coli*. Based on the localization of predicted TM domains in *C. glutamicum* PtsG, the residues M260 and P318 are located as the first amino acid of TM5 and within TM6, respectively. P318 is very close to H322, which together with E389 are the two amino acids likely involved in substrate binding in *C. glutamicum* PtsG. Thus, the location of the mutations can be related to a change in substrate binding ability.

To analyze the kinetics of the PtsG-mediated fructose transport, we used ^{14}C-labeled fructose as a tracer. The kinetic data obtained from these experiments are shown in **Table 4**. Strains that possess PtsF showed sigmoidal dependence of the uptake rate on the fructose concentration with Hill coefficients between 2 and 3, while Δ*ptsF* mutants did not (**Table 4** and **Supplementary Figure 3**). No fructose uptake was detected by mutant Δ*ptsF* Δ*ptsG*. Fructose uptake was detected in the absence of PtsF; however, the K_M value was about 20-fold higher than the $K_{1/2}$ value observed for strains that possess PtsF (**Table 4**). Moreover, fructose uptake was 5- to 10-fold faster in the presence of PtsF as compared to its absence. Thus, PtsF allowed for fast fructose uptake with high affinity, whereas PtsG supported slower uptake with lower affinity (**Table 4**).

The PtsG variants showed higher affinity for fructose than WT PtsG. Graphs of fructose uptake are shown in **Supplementary Figure 3**. The lowest apparent K_M was determined for PtsG^{P318S} (325 μM), which is lower than half of WT PtsG (739 μM), but still 10-fold higher than the $K_{1/2}$ value of PtsF. Two of the three PtsG variants (M260V and P318S) supported about 1.5- to 2-fold faster fructose uptake than WT PtsG {change of 6.7–10 and 12.4 nmol/[min × mg(CDW)], respectively}. Thus, the PtsG mutations showed improved kinetic parameters for fructose uptake as compared to WT PtsG. Notably, since the maximal uptake rates observed for the PtsG mutants did not reach that supported by PtsF, their improved kinetic parameters may not explain the fast growth observed for the respective strains *in vivo*. All growth experiments performed here exceed the K_M concentrations by more than 100-fold; thus, all PtsG variants should work under saturation conditions and affinity should not be a limiting factor.

^{13}C-Labeling Experiments Reveal Substantially Higher oxPPP Flux

In order to analyze altered flux distributions in the strains utilizing fructose *via* PtsG, we performed ^{13}C-labeling experiments. As the flux *via* the oxPPP and the associated NADPH provision is low during growth of *C. glutamicum* WT on fructose and depends at least in part on fructose 1,6-bisphosphatase, we hypothesized that PtsG-mediated fructose catabolism directly leading to fructose 6-P instead of fructose 1,6-BP might result in a higher flux *via* the oxPPP. To test this hypothesis, we performed ^{13}C-labeling experiments with ^{13}C-1-fructose as the sole carbon source for growth. For comparison, cells were grown with ^{13}C-1-glucose. During fructose and glucose catabolism *via* the oxPPP, the labeled C1 is lost as $^{13}CO_2$ in the oxidative decarboxylation of gluconate 6-P to ribulose 5-P. Thus, only unlabeled ribose 5-P is present and, hence, histidine, which is derived from ribose 5-P, is expected not to carry ^{13}C label from the carbons derived from ribose 5-P. If the non-oxPPP is used to provide C_5 building blocks, ^{13}C-labeling of xylulose 5-P (generated by transketolase reactions) and other pentose phosphate molecules is expected. Specifically, the non-oxPPP converts two molecules of fructose 6-P (fully labeled at C1) and one molecule of GAP (50% labeling at C3) to two molecules of xylulose 5-P (fully labeled at C1 and 50% labeled at C3), and one molecule of unlabeled ribose 5-P as shown in detail in **Supplementary Figure 4**.

To obtain a clean negative control devoid of labeling patterns from the oxPPP, we included strain Δ*zwf*, which lacks glucose 6-P dehydrogenase, the entry point of the oxPPP. **Figure 6** shows the labeling patterns of histidine and alanine in the ^{13}C-labeling experiments performed with *C. glutamicum* WT and the indicated mutants. Our results confirmed previous findings that the relative flux *via* the oxPPP is lower during growth with fructose than during growth with glucose (Kiefer et al., 2004) since labeling in L-alanine and L-histidine was higher with ^{13}C-1-fructose than with ^{13}C-1-glucose. In the WT, the oxPPP is barely active during growth on fructose, indicated by the high ^{13}C-labeling in L-alanine and L-histidine during growth with ^{13}C-1-fructose, which was almost as high as in the Δ*zwf* strain, which lacks the oxPPP. The Δ*ptsF* Δ*ptsG* strain expressing *ptsF* showed a labeling pattern similar to WT, which indicated a low

TABLE 4 | Kinetics parameters of fructose uptake by PtsF and PtsG.

Strain	Hill coefficient	Sigmoid	$K_{1/2}$ (μM)	K_M (μM)	V_{max} {nmol/[min × mg (CDW)]}
WT	3.00	Yes	45.7	–	73.5
Δ*ptsF*	/	X	–	841	8.4
Δ*ptsG*	2.38	Yes	44.8	–	41.6
Δ*ptsF* Δ*ptsG*	/	X	–	n.u.	–
Δ*ptsF* Δ*ptsG* (pVWEx1)	/	X	–	n.u.	–
Δ*ptsF* Δ*ptsG* (pVWEx1-*ptsF*)	2.57	Yes	30.0	–	40.8
Δ*ptsF* Δ*ptsG* (pVWEx1-*ptsG*)	/	X	–	739	6.7
Δ*ptsF* Δ*ptsG* (pVWEx1-$ptsG^{M260V}$)	/	X	–	520	10.0
Δ*ptsF* Δ*ptsG* (pVWEx1-$ptsG^{M260T}$)	/	X	–	459	7.1
Δ*ptsF* Δ*ptsG* (pVWEx1-$ptsG^{P318S}$)	/	X	–	325	12.4

n.u., no uptake.

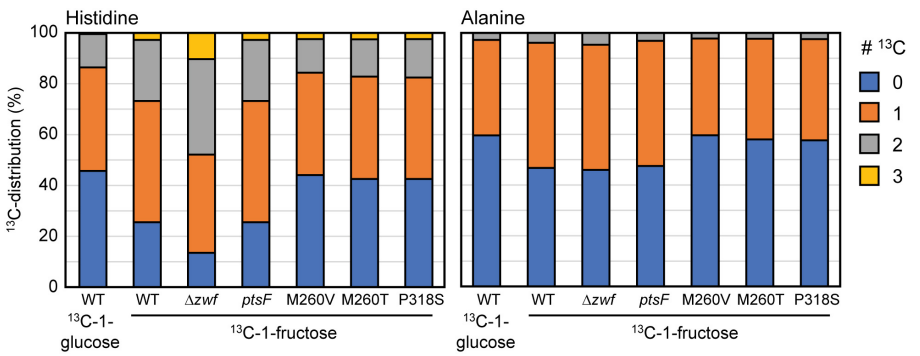

FIGURE 6 | ^{13}C-labeling in L-histidine and L-alanine in WT, Δ*zwf*, and the Δ*ptsF* Δ*ptsG* strain overexpressing *ptsF* or the *ptsG* variants upon feeding ^{13}C-1-fructose or ^{13}C-1-glucose. Data represent means of three independent experiment errors <5%.

relative oxPPP flux when fructose was catabolized *via* PtsF. On the other hand, Δ*ptsF* Δ*ptsG* strains overexpressing the PtsG variants showed reduced absolute labeling of L-alanine and L-histidine. This provided evidence for a higher relative oxPPP flux when fructose is utilized *via* PtsG with direct conversion to fructose 6-P. Notably, the observed labeling is similar to the labeling observed when WT and the other strains grew on ^{13}C-1-glucose (**Figure 6** and data not shown). The absolute labeling in L-alanine and L-histidine (^{13}C-abundance reduced by about 20% in Δ*ptsF* Δ*ptsG* strains overexpressing the PtsG variants compared to the Δ*zwf* strain used as reference lacking the oxPPP) allowed us to calculate that about 20% of the fructose molecules were catabolized *via* the oxPPP, which was comparable to the glucose utilized *via* the oxPPP in the WT.

Evolved and Reverse-Engineered Strains Showed Reduced Overflow Metabolism

Fast growth with glucose is known to be associated with intermittent lactate accumulation in the culture medium. During the exponential growth phase, NAD-dependent L-lactate dehydrogenase reduced pyruvate to L-lactate, which is secreted (Dominguez et al., 1998). L-lactate generation is significantly higher (fourfold) when fructose is the carbon source compared to glucose (Kiefer et al., 2004). L-lactate is re-utilized after induction of LldR by L-lactate and derepression of the *lld* operon for L-lactate catabolism (Georgi et al., 2008). The observed higher relative oxPPP flux when fructose is catabolized *via* the PtsG variants as compared to PtsF prompted us to investigate metabolic consequences. As already described above, the isolated mutants as well as the reverse-engineered strains grew to higher ODs than the *C. glutamicum* WT. Here, we investigated whether metabolic consequences can be observed with regard to by-product formation. Besides growing to higher ODs, the mutant and the reverse-engineered strain accumulated less L-lactate during growth (**Figure 7**).

PtsG Catalyzed Fructose Utilization Improved L-Lysine Production

L-lysine production benefits from improved NADPH provision and reduced by-product formation. Since we have shown that PtsG-mediated fructose catabolism is characterized by increased oxPPP flux relevant for NADPH provision as well as reduced intermittent formation of L-lactate as by-product, the metabolic consequence on L-lysine production was determined. First, low-level L-lysine production by the ALE mutants was enabled *via* transformation using a plasmid for overexpression of a feedback-resistant aspartokinase gene (pVWEx1-$lysC^{fbr}$). Compared to the control, i.e., *C. glutamicum* WT(pVWEx1-$lysC^{fbr}$) L-lysine production in minimal medium containing 40 g/L fructose was increased about fivefold. The ALE mutants overexpressing $lysC^{fbr}$ produced about 26 mM, while the WT overexpressing $lysC^{fbr}$ produced 4.5 mM.

After these initial and very promising results, we constructed the PtsG pathway as the sole route for fructose utilization in the

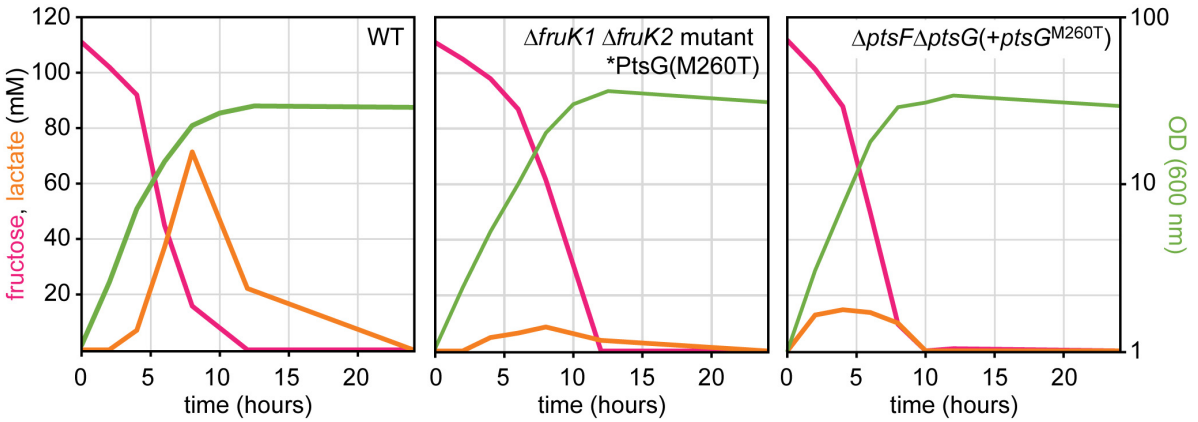

FIGURE 7 | Transient lactate accumulation in cultures of WT, mutant, and reconstructed strain during growth on fructose. Data represent one of two individual cultivations that differed <5%.

L-lysine producer CgLYS4 Δ*ptsF* (Sgobba et al., 2018). This strain is a *ptsF* deletion strain derived from CgLYS4 and, thus, lacks native fructose utilization *via* PtsF. CgLYS4 produces L-lysine due to feedback-resistant aspartokinase, attenuated homoserine dehydrogenase, and improved pyruvate carboxylase ($lysC^{T311I}$, hom^{V59A}, pyc^{P458S}), and the strain shows reduced by-product formation as it carries deletions in the lactate dehydrogenase gene (*ldhA*) and acetate production genes (*pta-ackA*). Production of L-lysine was analyzed after growth with 40 g/L fructose as the sole carbon source and compared to the production achieved with the parental strain CgLYS4 (Sgobba et al., 2018). All tested strains utilizing fructose *via* PtsG accumulated about 50% more L-lysine than the PtsF-positive CgLYS4 (about 45 mM as compared to about 30 mM; **Table 5**). Notably, the strain overexpressing native PtsG reached a similar final L-lysine concentration to the strains overexpressing the new PtsG variants, but much later since this strain grew significantly slower (data not shown). Interestingly, overexpression of *ptsF* reduced L-lysine production compared to CgLYS4. Taken together, fructose catabolism *via* the isolated PtsG variants is a promising strategy to improve L-lysine production. These results might be of relevance for an increased bioproduction efficiency when using molasses as the feedstock, as molasses contain significant shares of fructose of their sugar compounds.

TABLE 5 | L-lysine production of strains utilizing fructose *via* PtsG.

Strain	l-lysine (mM)
CgLYS4	29.7
CgLYS4 Δ*ptsF*[a]	0.8
CgLYS4 Δ*ptsF* pVWEx1-*ptsG*	43.1
CgLYS4 Δ*ptsF* pVWEx1-$ptsG^{P318S}$	44.2
CgLYS4 Δ*ptsF* pVWEx1-$ptsG^{M260V}$	46.9
CgLYS4 Δ*ptsF* pVWEx1-$ptsG^{M260T}$	46.2
CgLYS4 Δ*ptsF* pVWEx1-*ptsF*	24.0

Data represent means of three independent experiment with errors <5%.
[a]*L-lysine produced by CgLYS4 ΔptsF after 96 h of cultivation.*

DISCUSSION

In this study, ALE was used to isolate mutants able to catabolize fructose *via* PtsG. The PtsG variants enabled fast growth with fructose with increased relative oxPPP flux. Production of L-lysine was chosen as an application example and improved L-lysine titers associated with fast growth on fructose. However, it should be made clear at this point that fructose is not purely used in bioproduction of commodities and only makes a fraction of the sugar content of molasses (besides sucrose and glucose).

As shown here, only a few days of cultivation under selective conditions were sufficient to achieve the desired growth phenotype, indicating that mutation of a single gene was sufficient and that several mutations in this gene resulted in the desired growth phenotype. This is not unprecedented as earlier studies revealed the ability of *C. glutamicum* to evolve relatively quickly into a niche or to overcome a genetic impairment (Youn et al., 2009; Lindner et al., 2011; Uhde et al., 2013). The present study and the studies mentioned above share that they selected for utilization of a carbon and energy source. In addition, ALE has been used to select *C. glutamicum* mutants withstanding adverse conditions, e.g., due to methanol or indole (Lessmeier and Wendisch, 2015; Hennig et al., 2020; Kuepper et al., 2020; Walter et al., 2020) or mutants that have overcome the requirement for an additive such as iron chelator PCA (Graf et al., 2019) or production of, e.g., putrescine (Jorge et al., 2017; Li and Liu, 2017). Thus, ALE has proven valuable for *C. glutamicum* metabolic engineering (Stella et al., 2019).

Apart from *C. glutamicum*'s PtsG, the mannose PTS system of *E. coli* also generates fructose 6-P from fructose (Kornberg, 2001); this tendency of promiscuity of the PTS system compounds also applies to some sugar kinases, e.g., *E. coli*'s enzymes xylulokinase is active with xylulose and ribulose (Di Luccio et al., 2007) and fuculokinase is active with fuculose and ribulose (LeBlanc and Mortlock, 1971). One explanation for their promiscuity is that carbohydrate kinases are ancient enzymes, which needed to evolve into niches of present carbon sources (Roy et al., 2019). A good example for enzyme promiscuity

is the fast evolution for utilization of new substrates shown for *E. coli* (Guzman et al., 2019). Regarding PTS specificity, a prominent and promiscuous example is probably *E. coli*'s mannose PTS compound, which, besides mannose, also takes glucose, fructose, N-acetylglucosamine, and glucosamine (Curtis and Epstein, 1975; Chou et al., 1994). Similar to the approach described here, Wang et al. (2016) used a *C. glutamicum* Δ*ptsF* strain, evolved it on sucrose, and found suppressor mutants with inactivated 1-phosphofructokinase gene, indicating the role of sugar phosphates in transcriptional repression, likely of *ptsG*, which might explain the enhanced NADPH and L-lysine production from sucrose and fructose. The responsible regulator of sugar utilization, SugR, represses expression of *ptsG* (Engels and Wendisch, 2007), and deletion of *sugR* derepressed *ptsG* transcription and consequently facilitates glucose utilization and improved L-lysine productivity (Perez-Garcia et al., 2016).

The results deduced from the ^{13}C-labeling obtained in our study show some differences to the data described by Kiefer et al. (2004), which might be explained by the use of an L-lysine producer strain in the study by Kiefer et al. (2004) since L-lysine overproduction provides a strong NADPH sink. *C. glutamicum* can respond to different metabolic burdens differing in their NADPH requirements, as was shown in a metabolic flux comparison of *C. glutamicum* WT grown either under standard conditions or upon triggering L-glutamate production and of an L-lysine-producing strain (Marx et al., 1997). Flux in the oxPPP and, thus, NADPH generation was highest in the L-lysine producer, intermediate in WT and lowest under L-glutamate production (Icd provides NADPH and 2-oxoglutarate to balance the NADPH requirement of glutamate dehydrogenase for reductive amination of 2-oxoglutarate to yield glutamate) (Bormann et al., 1992).

We used L-lysine production as a readout to prove the increased NADPH availability in the engineered strains. It is important to state that all experiments were carried out in shake flasks and a transfer to a robust bioreactor culture is needed as the first step of up-scaling experiments to describe oxygen transfer, pressure, and foaming as highly relevant parameters that do not scale well when transferring from shake flasks to technical scale bioreactors (Takors, 2012). In addition to its NADPH demand, L-lysine production highly depends on strong fluxes toward anaplerosis, providing oxaloacetate as the precursor for aspartate biosynthesis, the starting point of L-lysine biosynthesis. The supply of anaplerotic precursors might be negatively affected by the PEP-dependent sugar phosphorylation carried out by the PTS system, as PTS-independent sugar utilizations improved L-lysine production (Lindner et al., 2011). However, using ATP-dependent sugar phosphorylation, e.g., fructokinase was shown to have a negative effect on ATP availability and hence sugar uptake (Xu et al., 2020). Recently, for L-lysine and L-threonine production (both high-NADPH demanding products), optimal flux ratio between oxPPP and glycolysis was determined (Murai et al., 2020), indicating a high demand of oxPPP for these products. Similar to the effects seen for L-lysine, our discovery might be of value for biotechnological use for high-NADPH-dependent products, e.g., threonine or 1,5-diaminopentane. This approach may be paired with others: Further approaches tackling NADPH recovery for increased bioproductions are overexpression of membrane-bound transhydrogenase (Kabus et al., 2007), deletion of phosphoglucose isomerase (Marx et al., 2003), overexpression of NAD kinase (Lindner et al., 2010), and overexpression of oxPPP enzymes (Becker et al., 2007). However, these studies exclusively focused on glucose as a carbon source. Indirect effects similarly to the approach described above were undertaken by overexpressing gluconeogenetic fructose 1,6-bisphosphatase, which increased L-lysine production from fructose (Georgi et al., 2005).

A new and fast way of fructose utilization *via* the optimized PtsG variants was shown in the biotechnologically important microbe *C. glutamicum*. The pathway supports higher relative oxPPP flux and consequently an improved NADPH regeneration rate, which was exploited here for the high NADPH demanding L-lysine production. The here described results and especially the PtsG mutations might also be advantageous for the production of other NADPH demanding products, e.g., other amino acids or derivatives like diamines, and fatty acids.

DATA AVAILABILITY STATEMENT

The raw data supporting the conclusions of this article will be made available by the authors, without undue reservation.

AUTHOR CONTRIBUTIONS

SNL and VFW conceived the study, designed the experiments, and analyzed the results. IK, DB, LT-B, JPK, TMM, and SNL performed metabolic engineering experiments. NR and GMS performed sugar uptake experiments. SNL, VFW, and GMS wrote the manuscript with contributions from all authors. All authors agreed with the final version of the manuscript.

FUNDING

Work of GMS was partially funded by the Novo Nordisk Fonden within the framework of the Fermentation-based Biomanufacturing Initiative (FBM) (FBM-grant: NNF17SA0031362).

ACKNOWLEDGMENTS

We thank Änne Michaelis for assistance with LC-MS analysis of ^{13}C-labeling in amino acids.

SUPPLEMENTARY MATERIAL

The Supplementary Material for this article can be found online at: https://www.frontiersin.org/articles/10.3389/fbioe.2021.669093/full#supplementary-material

REFERENCES

Anaya-Reza, O., and Lopez-Arenas, T. (2017). Comprehensive assessment of the L-lysine production process from fermentation of sugarcane molasses. *Bioprocess Biosyst. Eng.* 40, 1033–1048. doi: 10.1007/s00449-017-1766-2

Becker, J., Klopprogge, C., Herold, A., Zelder, O., Bolten, C. J., and Wittmann, C. (2007). Metabolic flux engineering of L-lysine production in *Corynebacterium glutamicum*–over expression and modification of G6P dehydrogenase. *J. Biotechnol.* 132, 99–109. doi: 10.1016/j.jbiotec.2007.05.026

Becker, J., Klopprogge, C., Zelder, O., Heinzle, E., and Wittmann, C. (2005). Amplified expression of fructose 1,6-bisphosphatase in *Corynebacterium glutamicum* increases in vivo flux through the pentose phosphate pathway and lysine production on different carbon sources. *Appl. Environ. Microbiol.* 71, 8587–8596. doi: 10.1128/aem.71.12.8587-8596.2005

Becker, J., Rohles, C. M., and Wittmann, C. (2018). Metabolically engineered *Corynebacterium glutamicum* for bio-based production of chemicals, fuels, materials, and healthcare products. *Metab. Eng.* 50, 122–141. doi: 10.1016/j.ymben.2018.07.008

Blombach, B., Riester, T., Wieschalka, S., Ziert, C., Youn, J. W., Wendisch, V. F., et al. (2011). *Corynebacterium glutamicum* tailored for efficient isobutanol production. *Appl. Environ. Microbiol.* 77, 3300–3310. doi: 10.1128/aem.02972-10

Bormann, E. R., Eikmanns, B. J., and Sahm, H. (1992). Molecular analysis of the *Corynebacterium glutamicum gdh* gene encoding glutamate dehydrogenase. *Mol. Microbiol.* 6, 317–326. doi: 10.1111/j.1365-2958.1992.tb01474.x

Chou, C. H., Bennett, G. N., and San, K. Y. (1994). Effect of modulated glucose uptake on high-level recombinant protein production in a dense *Escherichia coli* culture. *Biotechnol. Prog.* 10, 644–647. doi: 10.1021/bp00030a009

Curtis, S. J., and Epstein, W. (1975). Phosphorylation of D-glucose in *Escherichia coli* mutants defective in glucosephosphotransferase, mannosephosphotransferase, and glucokinase. *J. Bacteriol.* 122, 1189–1199. doi: 10.1128/jb.122.3.1189-1199.1975

Di Luccio, E., Petschacher, B., Voegtli, J., Chou, H. T., Stahlberg, H., Nidetzky, B., et al. (2007). Structural and kinetic studies of induced fit in xylulose kinase from *Escherichia coli*. *J. Mol. Biol.* 365, 783–798. doi: 10.1016/j.jmb.2006.10.068

Dietrich, C., Nato, A., Bost, B., Le Marechal, P., and Guyonvarch, A. (2009). Regulation of *ldh* expression during biotin-limited growth of *Corynebacterium glutamicum*. *Microbiology* 155, 1360–1375. doi: 10.1099/mic.0.022004-0

Dominguez, H., and Lindley, N. D. (1996). Complete Sucrose Metabolism Requires Fructose Phosphotransferase Activity in *Corynebacterium glutamicum* To Ensure Phosphorylation of Liberated Fructose. *Appl. Environ. Microbiol.* 62, 3878–3880. doi: 10.1128/aem.62.10.3878-3880.1996

Dominguez, H., Rollin, C., Guyonvarch, A., Guerquin-Kern, J. L., Cocaign-Bousquet, M., and Lindley, N. D. (1998). Carbon-flux distribution in the central metabolic pathways of *Corynebacterium glutamicum* during growth on fructose. *Eur. J. Biochem.* 254, 96–102. doi: 10.1046/j.1432-1327.1998.2540096.x

Eggeling, L., and Bott, M. (2005). *Handbook of Corynebacterium Glutamicum*. Florida: CRC press.

Engels, V., and Wendisch, V. F. (2007). The DeoR-type regulator SugR represses expression of *ptsG* in *Corynebacterium glutamicum*. *J. Bacteriol.* 189, 2955–2966. doi: 10.1128/jb.01596-06

Erb, T. J., Jones, P. R., and Bar-Even, A. (2017). Synthetic metabolism: metabolic engineering meets enzyme design. *Curr. Opin. Chem. Biol.* 37, 56–62. doi: 10.1016/j.cbpa.2016.12.023

Ferenci, T., and Kornberg, H. L. (1973). The utilization of fructose by *Escherichia coli*. Properties of a mutant defective in fructose 1-phosphate kinase activity. *Biochem. J.* 132, 341–347. doi: 10.1042/bj1320341

Georgi, T., Engels, V., and Wendisch, V. F. (2008). Regulation of L-lactate utilization by the FadR-type regulator LldR of *Corynebacterium glutamicum*. *J. Bacteriol.* 190, 963–971. doi: 10.1128/jb.01147-07

Georgi, T., Rittmann, D., and Wendisch, V. F. (2005). Lysine and glutamate production by *Corynebacterium glutamicum* on glucose, fructose and sucrose: roles of malic enzyme and fructose-1,6-bisphosphatase. *Metab. Eng.* 7, 291–301. doi: 10.1016/j.ymben.2005.05.001

Giavalisco, P., Li, Y., Matthes, A., Eckhardt, A., Hubberten, H. M., Hesse, H., et al. (2011). Elemental formula annotation of polar and lipophilic metabolites using 13C, 15N and 34S isotope labelling, in combination with high−resolution mass spectrometry. *Plant J.* 68, 364–376. doi: 10.1111/j.1365-313x.2011.04682.x

Graf, M., Haas, T., Muller, F., Buchmann, A., Harm-Bekbenbetova, J., Freund, A., et al. (2019). Continuous Adaptive Evolution of a Fast-Growing *Corynebacterium glutamicum* Strain Independent of Protocatechuate. *Front. Microbiol.* 10:1648. doi: 10.3389/fmicb.2019.01648

Guzman, G. I., Sandberg, T. E., Lacroix, R. A., Nyerges, A., Papp, H., De Raad, M., et al. (2019). Enzyme promiscuity shapes adaptation to novel growth substrates. *Mol. Syst. Biol.* 15:e8462.

Hennig, G., Haupka, C., Brito, L. F., Ruckert, C., Cahoreau, E., Heux, S., et al. (2020). Methanol-Essential Growth of *Corynebacterium glutamicum*: adaptive Laboratory Evolution Overcomes Limitation due to Methanethiol Assimilation Pathway. *Int. J. Mol. Sci.* 21:3617. doi: 10.3390/ijms21103617

Ikeda, M. (2012). Sugar transport systems in *Corynebacterium glutamicum*: features and applications to strain development. *Appl. Microbiol. Biotechnol.* 96, 1191–1200. doi: 10.1007/s00253-012-4488-z

Ikeda, M., Mizuno, Y., Awane, S., Hayashi, M., Mitsuhashi, S., and Takeno, S. (2011). Identification and application of a different glucose uptake system that functions as an alternative to the phosphotransferase system in *Corynebacterium glutamicum*. *Appl. Microbiol. Biotechnol.* 90, 1443–1451. doi: 10.1007/s00253-011-3210-x

Jorge, J. M., Nguyen, A. Q., Perez-Garcia, F., Kind, S., and Wendisch, V. F. (2017). Improved fermentative production of gamma-aminobutyric acid via the putrescine route: systems metabolic engineering for production from glucose, amino sugars, and xylose. *Biotechnol. Bioeng.* 114, 862–873. doi: 10.1002/bit.26211

Kabus, A., Georgi, T., Wendisch, V. F., and Bott, M. (2007). Expression of the *Escherichia coli pntAB* genes encoding a membrane-bound transhydrogenase in *Corynebacterium glutamicum* improves L-lysine formation. *Appl. Microbiol. Biotechnol.* 75, 47–53. doi: 10.1007/s00253-006-0804-9

Kiefer, P., Heinzle, E., Zelder, O., and Wittmann, C. (2004). Comparative metabolic flux analysis of lysine-producing *Corynebacterium glutamicum* cultured on glucose or fructose. *Appl. Environ. Microbiol.* 70, 229–239. doi: 10.1128/aem.70.1.229-239.2004

Kornberg, H. L. (2001). Routes for fructose utilization by *Escherichia coli*. *J. Mol. Microbiol. Biotechnol.* 3, 355–359.

Kuepper, J., Otto, M., Dickler, J., Behnken, S., Magnus, J., Jager, G., et al. (2020). Adaptive laboratory evolution of *Pseudomonas putida* and *Corynebacterium glutamicum* to enhance anthranilate tolerance. *Microbiology* 166, 1025–1037. doi: 10.1099/mic.0.000982

LeBlanc, D. J., and Mortlock, R. P. (1971). Metabolism of D-arabinose: origin of a D-ribulokinase activity in *Escherichia coli*. *J. Bacteriol.* 106, 82–89. doi: 10.1128/jb.106.1.82-89.1971

Lessmeier, L., and Wendisch, V. F. (2015). Identification of two mutations increasing the methanol tolerance of *Corynebacterium glutamicum*. *BMC Microbiol.* 15:216. doi: 10.1186/s12866-015-0558-6

Li, Z., and Liu, J. Z. (2017). Transcriptomic Changes in Response to Putrescine Production in Metabolically Engineered *Corynebacterium glutamicum*. *Front. Microbiol.* 8:1987. doi: 10.3389/fmicb.2017.01987

Lindner, S. N., Niederholtmeyer, H., Schmitz, K., Schoberth, S. M., and Wendisch, V. F. (2010). Polyphosphate/ATP-dependent NAD kinase of *Corynebacterium glutamicum*: biochemical properties and impact of *ppnK* overexpression on lysine production. *Appl. Microbiol. Biotechnol.* 87, 583–593. doi: 10.1007/s00253-010-2481-y

Lindner, S. N., Seibold, G. M., Henrich, A., Kramer, R., and Wendisch, V. F. (2011). Phosphotransferase system-independent glucose utilization in *corynebacterium glutamicum* by inositol permeases and glucokinases. *Appl. Environ. Microbiol.* 77, 3571–3581. doi: 10.1128/aem.02713-10

Marx, A., De Graaf, A. A., Wiechert, W., Eggeling, L., and Sahm, H. (1996). Determination of the fluxes in the central metabolism of *Corynebacterium glutamicum* by nuclear magnetic resonance spectroscopy combined with metabolite balancing. *Biotechnol. Bioeng.* 49, 111–129. doi: 10.1002/(sici)1097-0290(19960120)49:2<111::aid-bit1>3.0.co;2-t

Marx, A., Hans, S., Mockel, B., Bathe, B., De Graaf, A. A., Mccormack, A. C., et al. (2003). Metabolic phenotype of phosphoglucose isomerase mutants of *Corynebacterium glutamicum*. *J. Biotechnol.* 104, 185–197. doi: 10.1016/s0168-1656(03)00153-6

Marx, A., Striegel, K., De Graaf, A. A., Sahm, H., and Eggeling, L. (1997). Response of the central metabolism of *Corynebacterium glutamicum* to

different flux burdens. *Biotechnol. Bioeng.* 56, 168–180. doi: 10.1002/(SICI)1097-0290(19971020)56:2<168::AID-BIT6>3.0.CO;2-N

McCoy, J. G., Levin, E. J., and Zhou, M. (2015). Structural insight into the PTS sugar transporter EIIC. *Biochim. Biophys. Acta* 1850, 577–585. doi: 10.1016/j.bbagen.2014.03.013

Mindt, M., Walter, T., Kugler, P., and Wendisch, V. F. (2020). Microbial Engineering for Production of *N*-Functionalized Amino Acids and Amines. *Biotechnol. J.* 15:1900451. doi: 10.1002/biot.201900451

Moon, M. W., Park, S. Y., Choi, S. K., and Lee, J. K. (2007). The phosphotransferase system of *Corynebacterium glutamicum*: features of sugar transport and carbon regulation. *J. Mol. Microbiol. Biotechnol.* 12, 43–50. doi: 10.1159/000096458

Murai, K., Sasaki, D., Kobayashi, S., Yamaguchi, A., Uchikura, H., Shirai, T., et al. (2020). Optimal Ratio of Carbon Flux between Glycolysis and the Pentose Phosphate Pathway for Amino Acid Accumulation in *Corynebacterium glutamicum*. *ACS Synth. Biol.* 9, 1615–1622. doi: 10.1021/acssynbio.0c00181

Parche, S., Burkovski, A., Sprenger, G. A., Weil, B., Kramer, R., and Titgemeyer, F. (2001). *Corynebacterium glutamicum*: a dissection of the PTS. *J. Mol. Microbiol. Biotechnol.* 3, 423–428.

Perez-Garcia, F., Peters-Wendisch, P., and Wendisch, V. F. (2016). Engineering *Corynebacterium glutamicum* for fast production of L-lysine and L-pipecolic acid. *Appl. Microbiol. Biotechnol.* 100, 8075–8090. doi: 10.1007/s00253-016-7682-6

Peters-Wendisch, P. G., Schiel, B., Wendisch, V. F., Katsoulidis, E., Mockel, B., Sahm, H., et al. (2001). Pyruvate carboxylase is a major bottleneck for glutamate and lysine production by *Corynebacterium glutamicum*. *J. Mol. Microbiol. Biotechnol.* 3, 295–300.

Radek, A., Muller, M. F., Gatgens, J., Eggeling, L., Krumbach, K., Marienhagen, J., et al. (2016). Formation of xylitol and xylitol-5-phosphate and its impact on growth of D-xylose-utilizing *Corynebacterium glutamicum* strains. *J. Biotechnol.* 231, 160–166. doi: 10.1016/j.jbiotec.2016.06.009

Rittmann, D., Lindner, S. N., and Wendisch, V. F. (2008). Engineering of a glycerol utilization pathway for amino acid production by *Corynebacterium glutamicum*. *Appl. Environ. Microbiol.* 74, 6216–6222. doi: 10.1128/aem.00963-08

Rittmann, D., Schaffer, S., Wendisch, V. F., and Sahm, H. (2003). Fructose-1,6-bisphosphatase from *Corynebacterium glutamicum*: expression and deletion of the *fbp* gene and biochemical characterization of the enzyme. *Arch. Microbiol.* 180, 285–292. doi: 10.1007/s00203-003-0588-6

Roy, S., Vivoli Vega, M., and Harmer, N. J. (2019). Carbohydrate Kinases: a Conserved Mechanism Across Differing Folds. *Catalysts* 9:29. doi: 10.3390/catal9010029

Schafer, A., Tauch, A., Jager, W., Kalinowski, J., Thierbach, G., and Puhler, A. (1994). Small mobilizable multi-purpose cloning vectors derived from the *Escherichia coli* plasmids pK18 and pK19: selection of defined deletions in the chromosome of *Corynebacterium glutamicum*. *Gene* 145, 69–73. doi: 10.1016/0378-1119(94)90324-7

Sgobba, E., Stumpf, A. K., Vortmann, M., Jagmann, N., Krehenbrink, M., Dirks-Hofmeister, M. E., et al. (2018). Synthetic *Escherichia coli-Corynebacterium glutamicum* consortia for L-lysine production from starch and sucrose. *Bioresour. Technol.* 260, 302–310. doi: 10.1016/j.biortech.2018.03.113

Stella, R. G., Wiechert, J., Noack, S., and Frunzke, J. (2019). Evolutionary engineering of *Corynebacterium glutamicum*. *Biotechnol. J.* 14:e1800444.

Takors, R. (2012). Scale-up of microbial processes: impacts, tools and open questions. *J. Biotechnol.* 160, 3–9. doi: 10.1016/j.jbiotec.2011.12.010

Uhde, A., Youn, J. W., Maeda, T., Clermont, L., Matano, C., Kramer, R., et al. (2013). Glucosamine as carbon source for amino acid-producing *Corynebacterium glutamicum*. *Appl. Microbiol. Biotechnol.* 97, 1679–1687. doi: 10.1007/s00253-012-4313-8

Walter, T., Al Medani, N., Burgardt, A., Cankar, K., Ferrer, L., Kerbs, A., et al. (2020). Fermentative *N*-Methylanthranilate Production by Engineered *Corynebacterium glutamicum*. *Microorganisms* 8:866. doi: 10.3390/microorganisms8060866

Wang, Z., Chan, S. H. J., Sudarsan, S., Blank, L. M., Jensen, P. R., and Solem, C. (2016). Elucidation of the regulatory role of the fructose operon reveals a novel target for enhancing the NADPH supply in *Corynebacterium glutamicum*. *Metab. Eng.* 38, 344–357. doi: 10.1016/j.ymben.2016.08.004

Wendisch, V. F. (2020). Metabolic engineering advances and prospects for amino acid production. *Metab. Eng.* 58, 17–34. doi: 10.1016/j.ymben.2019.03.008

Xu, J., Zhang, J., Guo, Y., Zai, Y., and Zhang, W. (2013). Improvement of cell growth and L-lysine production by genetically modified *Corynebacterium glutamicum* during growth on molasses. *J. Ind. Microbiol. Biotechnol.* 40, 1423–1432. doi: 10.1007/s10295-013-1329-8

Xu, J. Z., Ruan, H. Z., Yu, H. B., Liu, L. M., and Zhang, W. (2020). Metabolic engineering of carbohydrate metabolism systems in *Corynebacterium glutamicum* for improving the efficiency of L-lysine production from mixed sugar. *Microb. Cell Fact.* 19:39. doi: 10.21775/9781910190050.04

Youn, J. W., Jolkver, E., Kramer, R., Marin, K., and Wendisch, V. F. (2009). Characterization of the dicarboxylate transporter DctA in *Corynebacterium glutamicum*. *J. Bacteriol.* 191, 5480–5488. doi: 10.1128/jb.00640-09

Zhao, N., Qian, L., Luo, G., and Zheng, S. (2018). Synthetic biology approaches to access renewable carbon source utilization in *Corynebacterium glutamicum*. *Appl. Microbiol. Biotechnol.* 102, 9517–9529. doi: 10.1007/s00253-018-9358-x

Conflict of Interest: The authors declare that the research was conducted in the absence of any commercial or financial relationships that could be construed as a potential conflict of interest.

frontiers in Microbiology

ORIGINAL RESEARCH
published: 21 July 2021
doi: 10.3389/fmicb.2021.718511

Development of a Hyperosmotic Stress Inducible Gene Expression System by Engineering the MtrA/MtrB-Dependent *NCgl1418* Promoter in *Corynebacterium glutamicum*

Jingwen Huang[1,2†], Jiuzhou Chen[2†], Yu Wang[2], Tuo Shi[2], Xiaomeng Ni[2], Wei Pu[2], Jiao Liu[2], Yingyu Zhou[2,3], Ningyun Cai[2], Shuangyan Han[1], Ping Zheng[2] and Jibin Sun[1,2*]*

[1]School of Biology and Biological Engineering, South China University of Technology, Guangzhou, China, [2]Key Laboratory of Systems Microbial Biotechnology, Tianjin Institute of Industrial Biotechnology, Chinese Academy of Sciences, Tianjin, China, [3]College of Biotechnology, Tianjin University of Science and Technology, Tianjin, China

OPEN ACCESS

Edited by:
Xiao-Jun Ji,
Nanjing Tech University, China

Reviewed by:
Guoqiang Xu,
Jiangnan University, China
Dong Liu,
Nanjing Tech University, China

***Correspondence:**
Ping Zheng
zheng_p@tib.cas.cn
Jibin Sun
sun_jb@tib.cas.cn

[†]These authors have contributed equally to this work

Specialty section:
This article was submitted to Microbiotechnology, a section of the journal Frontiers in Microbiology

Received: 01 June 2021
Accepted: 28 June 2021
Published: 21 July 2021

Citation:
Huang J, Chen J, Wang Y, Shi T, Ni X, Pu W, Liu J, Zhou Y, Cai N, Han S, Zheng P and Sun J (2021) Development of a Hyperosmotic Stress Inducible Gene Expression System by Engineering the MtrA/MtrB-Dependent NCgl1418 Promoter in Corynebacterium glutamicum. Front. Microbiol. 12:718511. doi: 10.3389/fmicb.2021.718511

Corynebacterium glutamicum is an important workhorse for industrial production of diversiform bioproducts. Precise regulation of gene expression is crucial for metabolic balance and enhancing production of target molecules. Auto-inducible promoters, which can be activated without expensive inducers, are ideal regulatory tools for industrial-scale application. However, few auto-inducible promoters have been identified and applied in *C. glutamicum*. Here, a hyperosmotic stress inducible gene expression system was developed and used for metabolic engineering of *C. glutamicum*. The promoter of *NCgl1418* ($P_{NCgl1418}$) that was activated by the two-component signal transduction system MtrA/MtrB was found to exhibit a high inducibility under hyperosmotic stress conditions. A synthetic promoter library was then constructed by randomizing the flanking and space regions of $P_{NCgl1418}$, and mutant promoters exhibiting high strength were isolated *via* fluorescence activated cell sorting (FACS)-based high-throughput screening. The hyperosmotic stress inducible gene expression system was applied to regulate the expression of *lysE* encoding a lysine exporter and repress four genes involved in lysine biosynthesis (*gltA*, *pck*, *pgi*, and *hom*) by CRISPR interference, which increased the lysine titer by 64.7% (from 17.0 to 28.0 g/L) in bioreactors. The hyperosmotic stress inducible gene expression system developed here is a simple and effective tool for gene auto-regulation in *C. glutamicum* and holds promise for metabolic engineering of *C. glutamicum* to produce valuable chemicals and fuels.

Keywords: *Corynebacterium glutamicum*, hyperosmotic stress, inducible promoter, MtrA, fluorescence activated cell sorting, lysine

INTRODUCTION

The nonpathogenic Gram-positive *Corynebacterium glutamicum* is a biosafe strain recognized by FDA and widely used in biomanufacturing of amino acids, organic acids, proteins, and other chemicals (Woo and Park, 2014; Lee et al., 2016; Tsuge and Matsuzawa, 2021). Regulation and optimization of target gene expression is crucial for balance of metabolic pathway and

improvement of product biosynthesis. Promoters with different properties are one of the most effective tools to control gene expression. At present, a series of promoters have been identified or developed to regulate gene expression in *C. glutamicum* (Becker et al., 2005; Kind et al., 2010; Patek and Nesvera, 2011; Dostalova et al., 2017; Zhang et al., 2018; Sun et al., 2020; Wang et al., 2020; Wiechert et al., 2020a,b; Henke et al., 2021). In general, there are two types of promoters: constitutive promoters and inducible promoters. The strong constitutive promoters, such as the *tuf* and *sod* promoters, are widely used to enhance the expression of target genes (Becker et al., 2005; Kind et al., 2010). However, in some cases, gene expression controlled by strong constitutive promoters may cause cellular burden and metabolic unbalance, which hinders bioproduction (Giacalone et al., 2006; Terpe, 2006). Compared to constitutive promoters, inducible promoters can initiate the gene expression at any time when required, so they are preferred for the regulation and redistribution of metabolic flux and the expression of proteins with cytotoxicity (Lipscomb et al., 2004). At the moment, *tac*, *trc*, and other inducible promoters are extensive applied in the metabolic regulation of *C. glutamicum* (Ben Samoun et al., 1999; Okibe et al., 2010; Lausberg et al., 2012; Sun et al., 2020; Wiechert et al., 2020b; Henke et al., 2021), but there are also limitations. The requirement of inducers that are toxic [such as isopropyl-β-D-thiogalactopyranoside (IPTG)] or exhaustible (such as gluconate) limits the use in a large scale. Besides, inducers are usually added during the cultivation, so monitoring the cell growth state and optimizing the timing of inducer addition are required (Nocadello and Swennen, 2012). Therefore, there is a demand in development of auto-inducible systems without the use of external inducers.

Recently, auto-inducible promoters that can automatically turn on gene expression in response to environmental factors, metabolites, and cell growth state have been identified and applied in several bacteria. For example, a dynamic turn-off switch (dTFS) and a dynamic turn-on switch (dTNS) in *Escherichia coli* were constructed using the growth phase-dependent promoter and degron (Lemke et al., 2011). This bifunctional molecular switch was used to uncouple cell growth from the biosynthesis of shikimic acid and glucaric acid (Hou et al., 2020). Pyruvate-responsive genetic circuits were constructed in *Bacillus subtilis* by the hybrid promoter that contained the PdhR-binding site and the pyruvate-responsive transcription factor PdhR from *E. coli*, which were used to balance and optimize the metabolic flux toward the production of glucaric acid (Ogasawara et al., 2007; Xu et al., 2020a). An endogenous quorum-sensing (QS) based CRISPRi circuit in *Streptomyces* was constructed, in which the *dcas9* gene was regulated by a native QS signal-responsive promoter. The system was used for downregulating three key nodes in essential pathways to divert metabolic flux toward rapamycin biosynthesis (Tian et al., 2020). In *C. glutamicum*, some auto-inducible promoters have also been reported and applied. For example, based on the LysR-type transcriptional regulator (LTTR) LysG and the *lysE* promoter with the LysG-binding site, a sensor suitable for intracellular lysine detection was developed (Binder et al., 2012). Two growth-regulated promoters (P_{cg3141} and $P_{CP\ 2836}$) had been identified (Kim et al., 2016; Ma et al., 2018). The P_{cg3141} promoter was verified with the production of glutathione S-transferase as a model protein, and the P_{CP_2836} promoter was used for improving the production of valine and 5-aminolevulinic acid (Kim et al., 2016; Ma et al., 2018; Zhang et al., 2020).

With strict control of fermentation conditions such as pH and dissolved oxygen, the titer of target metabolites in the bioreactors can reach 100 g/L or even 200 g/L, Lys production by *C. glutamicum*, for example (Xu et al., 2020b). Therefore, in the mid- and late-stage of fermentation, the accumulation of high concentrations of products or the feeding of substrates will inevitably lead to a high-salt or hyperosmotic stress, which can be used as a natural inducer that exits in almost all fermentation processes (Varela et al., 2003; Chung et al., 2017). However, hyperosmotic stress inducible promoters have not been identified so far. MtrA/MtrB, one of the two-component systems that are highly conserved in corynebacteria and mycobacteria, regulates the expression of genes involved in osmoprotection (Moker et al., 2004; Bott and Brocker, 2012). Some target genes and the consensus binding sites of MtrA have also been identified in *C. glutamicum* (Brocker et al., 2011). However, the MtrA/MtrB-dependent promoters responding to the hyperosmotic stress have not been identified and applied in gene regulation.

In this study, a hyperosmotic stress inducible gene expression system based on the hyperosmotic stress inducible promoter was developed in *C. glutamicum*. Among eight promoters regulated by the two-component system MtrA/MtrB, the promoter of *NCgl1418* ($P_{NCgl1418}$) showed high expression intensity and induction activity under a hyperosmotic stress. The core sequence of $P_{NCgl1418}$ was identified and the activity and inducibility was further enhanced by mutagenesis and fluorescence activated cell sorting (FACS)-based high-throughput screening. To demonstrate an application of this inducible system in metabolic engineering of *C. glutamicum*, it was used for overexpression of lysine exporter and CRISPR-dCpf1-mediated multiplex gene repression of four endogenous genes (Li et al., 2020) to maximize lysine production. This MtrA/MtrB-dependent hyperosmotic stress inducible system may also be useful for gene regulation in microorganisms beyond *C. glutamicum*.

MATERIALS AND METHODS

Bacterial Strains and Cultivation Conditions

The bacterial strains used in this study are listed in **Supplementary Table S1**. *E. coli* Trans1-T1 and Trans DB 3.1 were used as the host for cloning and plasmid maintenance. Wild-type *C. glutamicum* ATCC 13032 was used as the host for gene expression and promoter screening. *C. glutamicum* SCgL30, the derivative of *C. glutamicum* ATCC 13032 with a feedback deregulated aspartokinase (T311I; Becker and Wittmann, 2012), was used for lysine production. *E. coli* was cultivated at 37°C in Luria-Bertani (LB) medium (5 g/L yeast extract, 10 g/L tryptone, and 10 g/L NaCl). Kanamycin (50 μg/ml) or chloramphenicol (20 μg/ml) was added to LB

medium as required. *C. glutamicum* was cultivated at 30°C in BHI medium containing 37 g/L bovine brain heart extract, 10 g/L $(NH_4)_2SO_4$, 0.2 g/L K_2HPO_4, 0.3 g/L NaH_2PO_4, and 0.5 g/L $MgSO_4{\cdot}7H_2O$. For fluorescence intensity determination, *C. glutamicum* was cultivated in a defined medium (CGXIIY medium) containing 50 g/L glucose, 2 g/L yeast extract, 16.5 g/L NH_4Cl, 5 g/L urea, 1 g/L KH_2PO_4, 1 g/L K_2HPO_4, 42 g/L MOPS, 0.25 g/L $MgSO_4$, 0.01 g/L $FeSO_4{\cdot}2H_2O$, 0.01 g/L $MnSO_4{\cdot}H_2O$, 0.001 g/L $ZnSO_4{\cdot}7H_2O$, 0.2 mg/L $CuSO_4$, 0.02 mg/L $NiCl{\cdot}6H_2O$, 0.01 g/L $CaCl_2$, 0.03 g/L protocatechuic acid, 0.2 mg/L biotin, and 0.1 mg/L vitamin B1. Kanamycin (25 μg/ml), chloramphenicol (5 μg/ml) or IPTG (1 mM) was added when necessary.

Plasmid Manipulation

The plasmids and primers used in this study are listed in **Supplementary Tables S1** and **S2**, respectively. The promoter regions [about 300 bp upstream of the coding sequence (CDS)] of *abgT*, *csbD*, *betP*, *NCgl1418*, *NCgl1756*, *NCgl1838*, *NCgl2841*, and *proP* were amplified from the genomic DNA of *C. glutamicum* ATCC 13032 by PCR with eight primer pairs abgT-F/R, csbD-F/R, betP-F/R, 1418-F/R, 1756-F/R, 1838-F/R, 2841-F/R, and proP-F/R, respectively. *E. coli-C. glutamicum* shuttle expression vector pXM-*gfp* (Sun et al., 2019) was used to characterize the promoter strength. The backbone of pXM-*gfp* was amplified by PCR with the primer pair pGFP-F/R and self-cyclized to construct the control plasmid pXM-con-*gfp* harboring no promoter for *gfp*. The promoters P_{abgT}, P_{csbD}, P_{betP}, $P_{NCgl1418}$, $P_{NCgl1756}$, $P_{NCgl1838}$, $P_{NCgl2841}$, and P_{proP} were individually inserted to pXM-con-*gfp* for *gfp* expression. The *tuf* promoter (the 349 bp upstream of the *tuf* gene) was amplified from the genomic DNA of *C. glutamicum* ATCC 13032 by PCR with the primer pair tuf-F/R. The backbone of pXM-$P_{NCgl1418}$-*gfp* was amplified by PCR with the primer pair pGFP-tuf-F/pGFP-R. Then these two PCR fragments were purified and ligated using the CloneExpress® MultiS One Step Cloning Kit (Vazyme Biotech, Nanjing, China) to generate the plasmid pXM-P_{tuf}-*gfp*. The backbone of pXM-*gfp* was amplified by PCR with the primer pair tac-F/R and then self-cyclized to generate the plasmid pXM-P_{tac}-*gfp*. To test truncated $P_{NCgl1418}$ promoters, the $P_{NCgl1418}$ in pXM-$P_{NCgl1418}$-*gfp* was replaced with truncated promoters, $P_{NCgl1418\text{-}203}$, $P_{NCgl1418\text{-}145}$, and $P_{NCgl1418\text{-}94}$, by PCR using the forward primer 1418-203-F, 1418-145-F, and 1418-94-F, respectively, with the reverse primer pGFP-R.

E. coli-C. glutamicum shuttle expression vector pEC-XK99E was used to express *lysE*. The $P_{NCgl1418}$ promoter and the *lysE* gene were amplified by PCR using the primer pairs 1418-E-F/R and lysE-F/R from the genomic DNA of *C. glutamicum* ATCC 13032, respectively. Then the backbone of pEC-XK99E was amplified with the primer pair pEC-F/R. These three PCR fragments were purified and ligated to generate the plasmid pEC-$P_{NCgl1418}$-*lysE*. The $P_{NCgl1418}$ on pEC-$P_{NCgl1418}$-*lysE* was replaced with the $P_{NCgl1418}$ variant ($P_{NCgl1418\text{-}A10}$) by PCR using the primer pair A10-E-F/R, generating the plasmid pEC-$P_{NCgl1418\text{-}A10}$-*lysE*.

A previously developed CRISPR-dCpf1 system (Li et al., 2020) was modified to repress the expression of target genes in response to the hyperosmotic stress. To construct an all-in-one CRISPRi tool plasmid, the backbone of pXM-07 expressing dCpf1 was divided into three parts, which were amplified with the primer pairs pXM-07-F1/R1, pXM-07-F2/R2, and pXM-07-F3/R3, respectively. A gRNA cassette consisting of a constitutive promoter (P_{11F}), two direct repeats (DRs), a *ccdB* flanked by two *Bbs*I sites, and a terminator was amplified from pEC-02 (Li et al., 2020) with the primer pair ccdB-F/R. These four PCR fragments were purified and ligated to generate the plasmid pXM-*dCpf1*. Two oligonucleotides (RFP-F/R) were annealed and assembled into *Bbs*I-digested pXM-*dCpf1* backbone using a Golden Gate assembly method, resulting in the plasmid pXM-*dCpf1*-RFP. Similarly, array-F1/R1, array-F2/R2, array-F3/R3, and array-F4/R4 were annealed, respectively, and assembled into *Bbs*I-digested pXM-*dCpf1* backbone, resulting in the plasmid pXM-*dCpf1*-4crRNA (the crRNA array targeting *gltA*, *pgi*, *hom*, and *pck*). All crRNAs used in this study are listed in **Supplementary Table S3**. To construct a hyperosmotic stress inducible CRISPRi system, the $P_{NCgl1418}$ promoter was amplified from the genomic DNA of *C. glutamicum* ATCC 13032 by PCR using the primer pair 1418-D-F/R. The backbone of pXM-*dCpf1* or pXM-*dCpf1*-4crRNA was amplified with the primer pairs pXM-D-F1/R1 and pXM-D-F2/R2, respectively. Then these three PCR fragments were purified and ligated to generate the plasmids pXM-$P_{NCgl1418}$-con and pXM-$P_{NCgl1418}$-*dCpf1*-4crRNA, respectively. The $P_{NCgl1418}$ on pXM-$P_{NCgl1418}$-con and pXM-$P_{NCgl1418}$-*dCpf1*-4crRNA was replaced with the $P_{NCgl1418\text{-}A10}$ variant by PCR using the primer pairs A10-D-F1/R1 and A10-D-F2/R2, generating the plasmid pXM-$P_{NCgl1418\text{-}A10}$-con and pXM-$P_{NCgl1418\text{-}A10}$-*dCpf1*-4crRNA, respectively.

Construction of the MtrA-Deleted Strain

Deletion of the *mtrA* gene in *C. glutamicum* ATCC 13032 chromosome was performed by the CRISPR-Cas9 system (Liu et al., 2017). Plasmid pgRNA-ΔmtrA was construct by inserting the flanking regions of *mtrA* into pgRNA2 and replacing the base-pairing region of gRNA targeting *ldhA* with a base-pairing region targeting *mtrA* (N20, 5'-GTGGTGCTCGGTTTGGA ATC-3'). A part of pgRNA2 backbone was amplified by PCR using primer pair gRNA-mtrA/pgRNA-1. N20 for *mtrA* was added to the backbone by primer gRNA-mtrA. A second part of pgRNA2 backbone was amplified by PCR using primer pair pgRNA-2/pgRNA-3. The 979 and 1,008 bp flanking regions of *mtrA* were amplified from the genomic DNA of *C. glutamicum* ATCC 13032 using the primer pairs mtrA-del-up-F/R and mtrA-del-down-F/R, respectively. The four fragments were ligated using the CloneExpress® MultiS One Step Cloning Kit (Vazyme Biotech, Nanjing, China) to yield pgRNA-ΔmtrA. The two plasmids (pgRNA-ΔmtrA and pCas9) were transformed into *C. glutamicum* ATCC 13032 by electroporation, and the screening of *ΔmtrA* mutants was performed in BHI plate with 0.05 mM IPTG. Gene deletion was verified by checking the sizes of the colony PCR fragments. Tool plasmids were

cured from the edited mutant before it was used for subsequent experiments.

Construction of Synthetic Promoter Libraries

The synthetic promoter libraries of $P_{NCgl1418}$ were constructed using the primer pairs P-Library-F1/R1 and P-Library-F2/R2 containing degenerated oligonucleotides (Ns) by PCR using pXM-$P_{NCgl1418}$-*gfp* as a template. The PCR product was self-ligated with T4 ligase. The ligation products were transformed into strain *E. coli* Trans1-T1. The quality of randomization was checked by sequencing 24 randomly picked transformants. The synthetic promoter libraries were extracted and then transformed into *C. glutamicum* ATCC 13032 by electroporation.

FACS Screening

The *C. glutamicum* library was inoculated into BHI medium and cultivated overnight at 30°C and 220 rpm. The overnight cultures were transferred into 24-well plates with 1 ml CGXIIY medium containing 0.6 M Na_2SO_4 to an optical density at 600 nm (OD_{600}) of 0.5. Then, cells were cultivated for 6 h at 30°C and with shaking at 800 rpm in INFORS Microtron (INFORS HT Multitron Pro, Switzerland). The cell suspension was diluted by proper times with distilled water and sorted on FACS (MoFlo XDP, Beckman Coulter, Inc., Miami, FL, United States) using green fluorescent protein (GFP) as the reporter protein. The cells were excited by 488-nm laser and detected through a 520 band-pass filter. In the first-round screening, cells showing high fluorescence intensity (the top 0.01%) were sorted (positive sorting). The sorted cells were poured directly into 5 ml BHI medium and cultivated overnight, and then the cells were transferred into 24-well plates with 1 ml CGXIIY medium for the next round of screening. In the second-round screening, cells showing low fluorescence intensity (the bottom 1%) were sorted (negative sorting). Similarly, the third-round screening (positive sorting) was performed. After the three-round sorting, the sorted cells were spread on BHI agar plate and incubated at 30°C.

Fluorescence Intensity Determination

The *C. glutamicum* was inoculated into BHI medium and cultivated overnight at 30°C and 220 rpm. The overnight cultures were transferred into 24-well plates with 1 ml CGXIIY medium with or without 0.6 M Na_2SO_4 to an OD_{600} of 0.5. After cultivated at 30°C and with shaking at 800 rpm for 18 h, cells were harvested and diluted by proper times with distilled water. GFP fluorescence intensities were determined using a microplate reader (SpectraMax M5, Molecular Devices, λ excitation = 488 nm, λ emission = 520 nm). The fluorescence intensities were normalized with OD_{600}.

Lysine Production in 24-Well Plates

C. glutamicum SCgL30 with a feedback deregulated aspartokinase (T311I; Becker and Wittmann, 2012) was used for lysine production. Strain SCgL30 and its derivatives were cultivated in BHI medium at 30°C and with shaking at 220 rpm. The overnight cultures were transferred into 24-well plates containing 1 ml fermentation medium each well to an initial OD_{600} of 0.5. The fermentation medium contains 80 g/L glucose, 8 g/L yeast extract, 9 g/L urea, 1.5 g/L $K_2HPO_4{\cdot}3H_2O$, 0.01 g/L $MnSO_4$, 0.6 g/L $MgSO_4{\cdot}7H_2O$, 0.01 g/L $FeSO_4{\cdot}7H_2O$, and 42 g/L MOPS (Li et al., 2020). Then, cells were cultivated for 24 or 36 h at 30°C and with shaking at 800 rpm in INFORS Microtron (INFORS HT Multitron Pro, Switzerland).

Lysine Production in 1-L Bioreactors

Colonies grown on a BHI plate at 30°C for 24 h were picked and used to inoculate 50 ml LSS1 medium (Ohnishi et al., 2002) in 500 ml shake flasks. The cultures were then cultivated overnight at 30°C and with shaking at 220 rpm. The cultures were transferred into a 1-L jar bioreactor [T&J-MiniBox, T&J Bio-engineering (Shanghai) Co., Ltd., China] containing 500 ml LPG1 medium (Ohnishi et al., 2002) with an inoculation volume of 10%. After the sugar initially added to the bioreactor was exhausted, glucose solution (50%, w/v) containing 0.5 mg/L biotin was continuously fed to maintain the glucose concentration at about 1.5% $(NH_4)_2SO_4$ solution (5.56%, w/v) was also fed to supply nitrogen source for lysine biosynthesis and cell growth. The fermentation was performed at 34°C with an agitation speed of 900 rpm and an aeration at 2.5 L/min. The pH was maintained at 7.3 with NH_4OH. LSS1 medium (Ohnishi et al., 2002) contains 50 g/L sucrose, 40 g/L corn steep liquor, 8.3 g/L $(NH_4)_2SO_4$, 1 g/L urea, 2 g/L KH_2PO_4, 0.83 g/L $MgSO_4{\cdot}7H_2O$, 10 mg/L $FeSO_4{\cdot}7H_2O$, 1 mg/L $CuSO_4{\cdot}5H_2O$, 10 mg/L $ZnSO_4{\cdot}7H_2O$, 10 mg/L β-alanine, 5 mg/L vitamin B3, 1.5 mg/L vitamin B1, 0.5 mg/L biotin, and 30 g/L $CaCO_3$. LPG1 medium (Ohnishi et al., 2002) contains 50 g/L glucose, 20 g/L corn steep liquor, 15 g/L $(NH_4)_2SO_4$, 1 g/L urea, 2.5 g/L KH_2PO_4, 0.75 g/L $MgSO_4{\cdot}7H_2O$, 50 mg/L $FeSO_4{\cdot}7H_2O$, 13 mg/L $MnSO_4{\cdot}5H_2O$, 50 mg/L $CaCl_2{\cdot}2H_2O$, 6.3 mg/L $CuSO_4{\cdot}5H_2O$, 1.3 mg of $ZnSO_4{\cdot}7H_2O$, 5 mg/L $NiCl_2{\cdot}6H_2O$, 1.3 mg/L $CoCl_2{\cdot}6H_2O$, 1.3 mg/L $(NH_4)_6Mo_7O_{24}{\cdot}4H_2O$, 23 mg/L β-alanine, 14 mg/L vitamin B3, 7 mg/L vitamin B1, and 0.5 mg/L biotin. Samples were taken periodically and glucose and lysine concentrations were quantified using an SBA-40D biosensor analyzer (Institute of Biology of Shandong Province Academy of Sciences, Shandong, China). Cell biomass was determined as OD_{600} with a UV-1800 spectrophotometer (Shimadzu, Kyoto, Japan) after proper dilution with distilled water.

RESULTS

Identification of Hyperosmotic Stress Inducible Promoters

To identify the hyperosmotic stress inducible promoters, we tested the promoters of the genes showing MtrA-dependent behaviors. Eight promoters (P_{abgT}, P_{csbD}, P_{betP}, $P_{NCgl1418}$, $P_{NCgl1756}$, $P_{NCgl1838}$, $P_{NCgl2841}$, and P_{proP}), which control the expression of *abgT* (secondary transporter of the AbgT family), *csbD*, *betP*

(glycine betaine transporter), *NCgl1418*, *NCgl1756*, *NCgl1838*, *NCgl2841*, and *proP* (proline/ectoine carrier), respectively, were selected based on a previous study (Brocker et al., 2011). These genes showed significantly decreased transcription levels (<10% of the control) upon the deletion of *mtrA* in *C. glutamicum*. Besides, the MtrA binding sites of these promoters have also been identified (Brocker et al., 2011). Since most of the exact promoters and regulatory regions of those genes have not been fully defined yet, the ~300 bp upstream of each CDS was investigated. In order to assess these MtrA-dependent promoters, GFP was used as a reporter to study the transcriptional strength of these promoters with or without 0.6 M NaCl. P_{abgT}, $P_{NCgl1418}$, $P_{NCgl1838}$, and P_{proP} showed more than 2.0-fold NaCl-induced expression activity. Among them, $P_{NCgl1418}$ showed the highest induced expression intensity (**Figure 1**). Therefore, we chose $P_{NCgl1418}$ for further analysis.

Characterization of the *NCgl1418* Promoter

Next, the effects of different types or concentrations of inducers on induction of $P_{NCgl1418}$ were investigated. Using GFP as a reporter, it was found that sulfate was the best inducer, which induced the expression activity of $P_{NCgl1418}$ up to 4.0-fold (**Figure 2A**). $P_{NCgl1418}$ showed obvious gradient induction activity in the range of 0~0.6 M Na_2SO_4 (**Figure 2B**). Compared with the endogenous strong constitutive promoter P_{tuf} and the widely used IPTG-inducible promoter P_{tac} (Becker et al., 2005; Kind et al., 2010; Rytter et al., 2014), $P_{NCgl1418}$ showed about 62% expression strength upon hyperosmotic stress induction (**Figure 2C**). These results demonstrate that $P_{NCgl1418}$ is a relative strong hyperosmotic stress inducible promoter, which has application potential for initiating the expression of target genes during the fermentation process.

To determine the key functional region of $P_{NCgl1418}$, three truncated variants (94, 145, and 203 bp) were constructed and used for GFP expression (**Figure 3A**). Although the 94 bp $P_{NCgl1418}$ promoter contained the core −35 and −10 regions (Pfeifer Sancar et al., 2013), the function of the promoter completely lost. The 145 bp promoter contained the MtrA binding site but showed a decreased expression activity (74%) under hyperosmotic stress. In contrast, the 203 bp promoter maintained almost the same activity (94%) to the whole-length promoter (243 bp) under hyperosmotic stress (**Figure 3B**). To confirm the necessity of MtrA for $P_{NCgl1418}$ functioning, a *mtrA*-deleted *C. glutamicum* strain was constructed and the plasmid harboring the $P_{NCgl1418}$-controlled *gfp* cassette was transformed into the mutant. As expect, no GFP expression could be detected with *mtrA* deletion (**Supplementary Figure S1**). These results suggest that MtrA and its specific binding site are essential to the inducible activity of $P_{NCgl1418}$. However, considering the partial activity loss of the 145 bp truncation, unknown mechanisms may also have an impact on the promoter.

Construction of $P_{NCgl1418}$ Libraries and Isolation of Variants With Enhanced Inducible Activity

Although $P_{NCgl1418}$ exhibited a relatively high inducible activity, its expression intensity was still lower than that of P_{tuf} and P_{tac}, which may hinder the application in high-level gene expression. Therefore, further engineering of this promoter is needed to increase its strength. To engineer the $P_{NCgl1418}$, random promoter libraries were constructed based on the

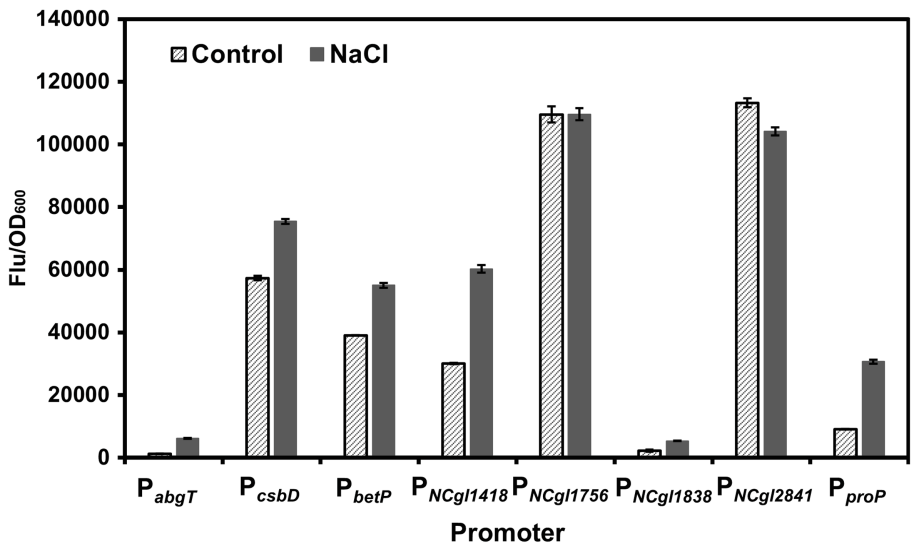

FIGURE 1 | Screening of hyperosmotic stress inducible promoters. Expression of *gfp* was controlled by different MtrA/MtrB-dependent promoters (P_{abgT}, P_{csbD}, P_{betP}, $P_{NCgl1418}$, $P_{NCgl1756}$, $P_{NCgl1838}$, $P_{NCgl2841}$, and P_{proP}) in *C. glutamicum* with or without high salt stress induction. Cell fluorescence intensity was normalized to cell density and the background value of the strain containing the control vector pXM-con-*gfp* without a promoter was deducted. All data represent mean values from three biological replicates including standard deviations (SDs).

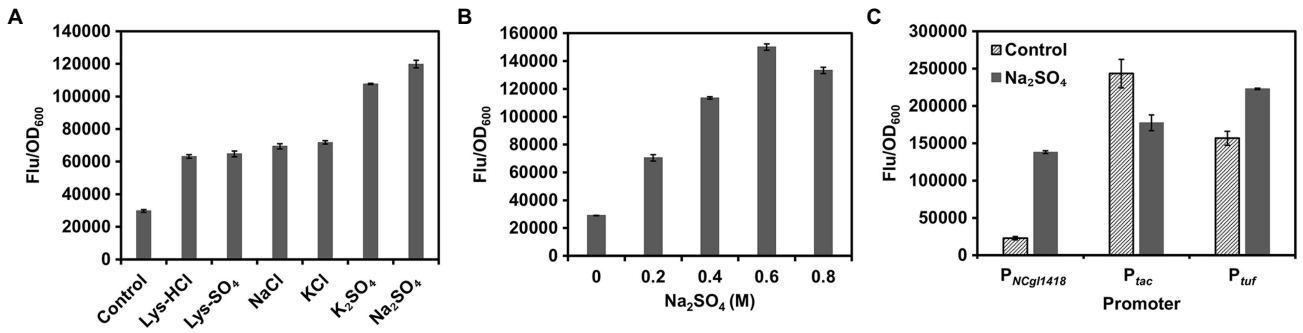

FIGURE 2 | Characterization of $P_{NCgl1418}$ promoter. **(A)** Expression of *gfp* under the control of $P_{NCgl1418}$ in *C. glutamicum* induced by different salts. **(B)** Expression of *gfp* under the control of $P_{NCgl1418}$ in *C. glutamicum* induced by different concentrations of sodium sulfate. **(C)** Comparison of $P_{NCgl1418}$ with P_{tuf} and P_{tac} promoters. Expression of *gfp* was assayed with or without 0.6 M sodium sulfate. Cell fluorescence intensity was normalized to cell density and the background value of the strain containing the control vector pXM-con-*gfp* without a promoter was deducted. All data represent mean values from three biological replicates including SDs.

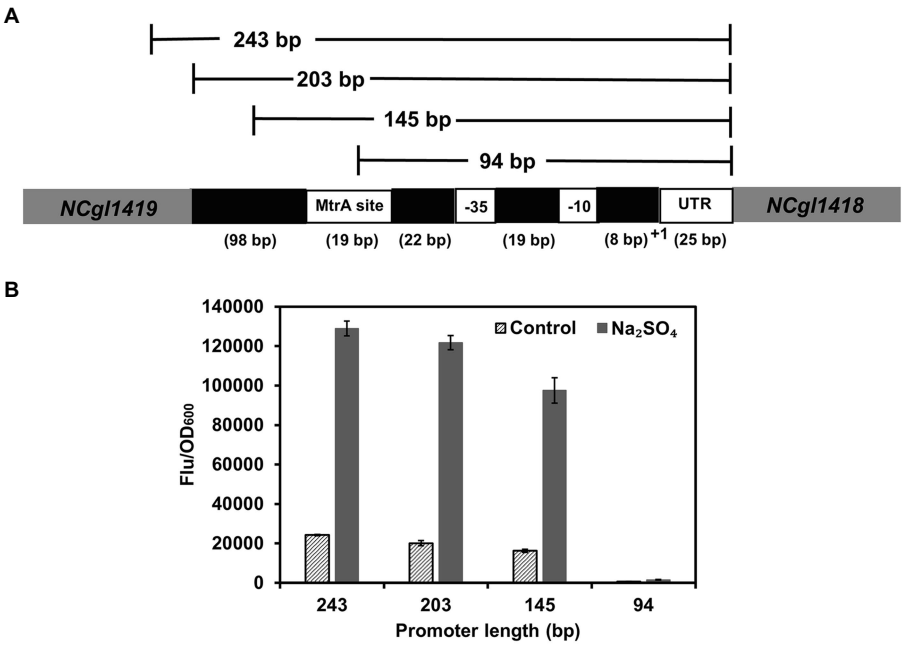

FIGURE 3 | Identification of the core functional region of $P_{NCgl1418}$ promoter. **(A)** Schematic diagram of the $P_{NCgl1418}$ promoter truncation strategy. **(B)** Expression of *gfp* under the control of $P_{NCgl1418}$ promoter variants with different length (243, 203, 145, and 94 bp) with or without 0.6 M sodium sulfate. Cell fluorescence intensity was normalized to cell density and the background value of the strain containing the control vector pXM-con-*gfp* without a promoter was deducted. All data represent mean values from three biological replicates including SDs.

243 bp wild-type promoter. The deduced −10 and −35 regions of $P_{NCgl1418}$ were fixed to allow sigma factor binding, and the 29 bp spacer and left flanking regions were designed to have fully randomized nucleotides (**Figure 4A**). The randomized promoters were cloned to the upstream of the GFP reporter gene and subjected to a three-step positive-negative-positive screening to identify promoter variants with improved induction activity and expression strength. During this screening process, positive screening in the presence of 0.6 M Na_2SO_4 was conducted to identify high-fluorescence variants (isolation of the top 0.01% fluorescing cells) and the negative screening in the absence of 0.6 M Na_2SO_4 was conducted to exclude the variants with too high fluorescence intensity without induction (isolation of the bottom 1% non-fluorescing cells; **Figure 4B**). After three rounds of screening, the sorted cells were cultivated on agar plates, and 90 clones were randomly picked and characterized. After a secondary screening in microtiter plates, a total of 10 promoter variants with different sequences (**Supplementary Figure S2**) and inducible activities were obtained (**Figure 4C**). One promoter variant A10

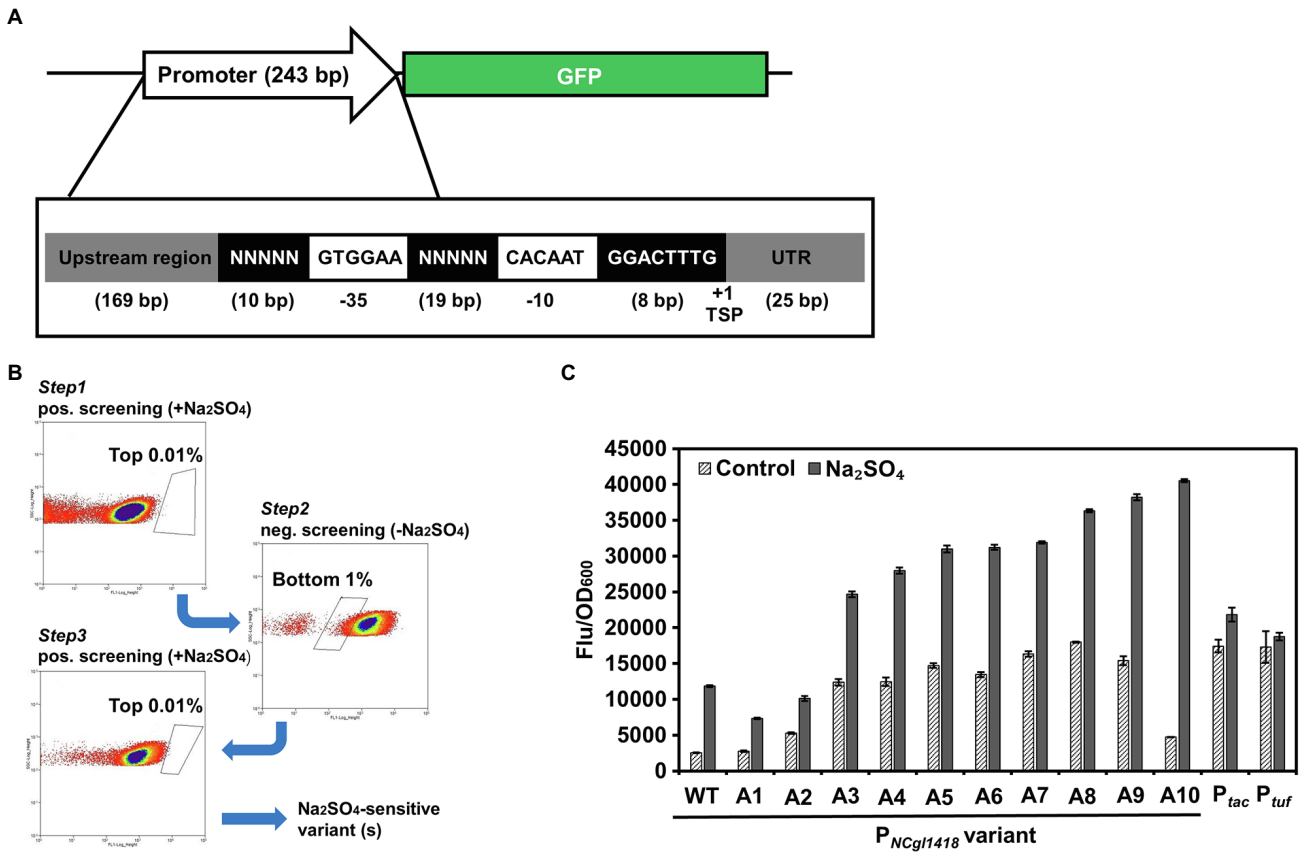

FIGURE 4 | FACS-based positive/negative screening of the random promoter library to identify $P_{NCgl1418}$ promoter variants with enhanced inducible activity. **(A)** Design of the random promoter library. **(B)** FACS plots of the three rounds of positive/negative screening. **(C)** Characterization of the isolated promoter variants. Cell fluorescence intensity was normalized to cell density and the background value of the strain containing the control vector pXM-con-*gfp* without a promoter was deducted. All data represent mean values from three biological replicates including SDs.

($P_{NCgl1418\text{-}A10}$) showed the highest inducible activity and was chosen for further analysis. $P_{NCgl1418\text{-}A10}$ was then compared with the strong constitutive promoter P_{tuf} and IPTG-inducible promoter P_{tac} with or without 0.6 M Na_2SO_4. The expression of GFP under the control of $P_{NCgl1418\text{-}A10}$ showed an 8.5-fold induction by 0.6 M Na_2SO_4. The induced GFP expression level was approximately 1.8-fold higher than those of P_{tuf} and P_{tac} (**Figure 4C**).

Application of the Hyperosmotic Stress Inducible Promoter to Optimize Lysine Biosynthesis

To demonstrate the usability of the hyperosmotic stress inducible promoters in metabolic engineering, the wild-type $P_{NCgl1418}$ and $P_{NCgl1418\text{-}A10}$ variant were used to regulate five genes related to lysine biosynthesis and excretion in *C. glutamicum* (**Figure 5A**). One target gene *lysE* encodes a lysine efflux protein and overexpression of *lysE* can increase lysine production by enhancing excretion of lysine (Zhou and Zeng, 2015). The other four genes, *gltA*, *pck*, *pgi*, and *hom*, are involved in the metabolic flux competition with lysine biosynthesis and their repression by CRISPRi has been proven to enhance the lysine production (Li et al., 2020).

Firstly, we constructed an all-in-one CRIPSRi tool plasmid pXM-*dCpf1* based on the previously developed two plasmids system expressing dCpf1 under the control of IPTG-inducible P_{tac} and crRNA array under the control of constitutive P_{11F} (Li et al., 2020). To determine the gene repression efficiency of the all-in-one CRIPSRi system, a crRNA targeting the template strand of red fluorescent protein (RFP) encoding gene was designed and assembled to the plasmid pXM-*dCpf1*. A repression efficiency of 77% was achieved (**Supplementary Figure S3**), which was similar with the previous system using two plasmids. For combinational repression of the four target genes (*gltA*, *pck*, *pgi*, and *hom*), a crRNA array harboring four spacers was assembled to pXM-*dCpf1*. To achieve hyperosmotic stress inducible gene repression, the IPTG-inducible P_{tac} was replaced with $P_{NCgl1418}$ and $P_{NCgl1418\text{-}A10}$, respectively, for controlling dCpf1 expression. The two CRISPRi plasmids and a control plasmid without targeting crRNA array were individually transformed into the lysine-producing strain SCgL30 with a feedback deregulated aspartokinase (T311I; Becker and Wittmann, 2012). Fermentation in 24-well plates was performed to evaluate lysine

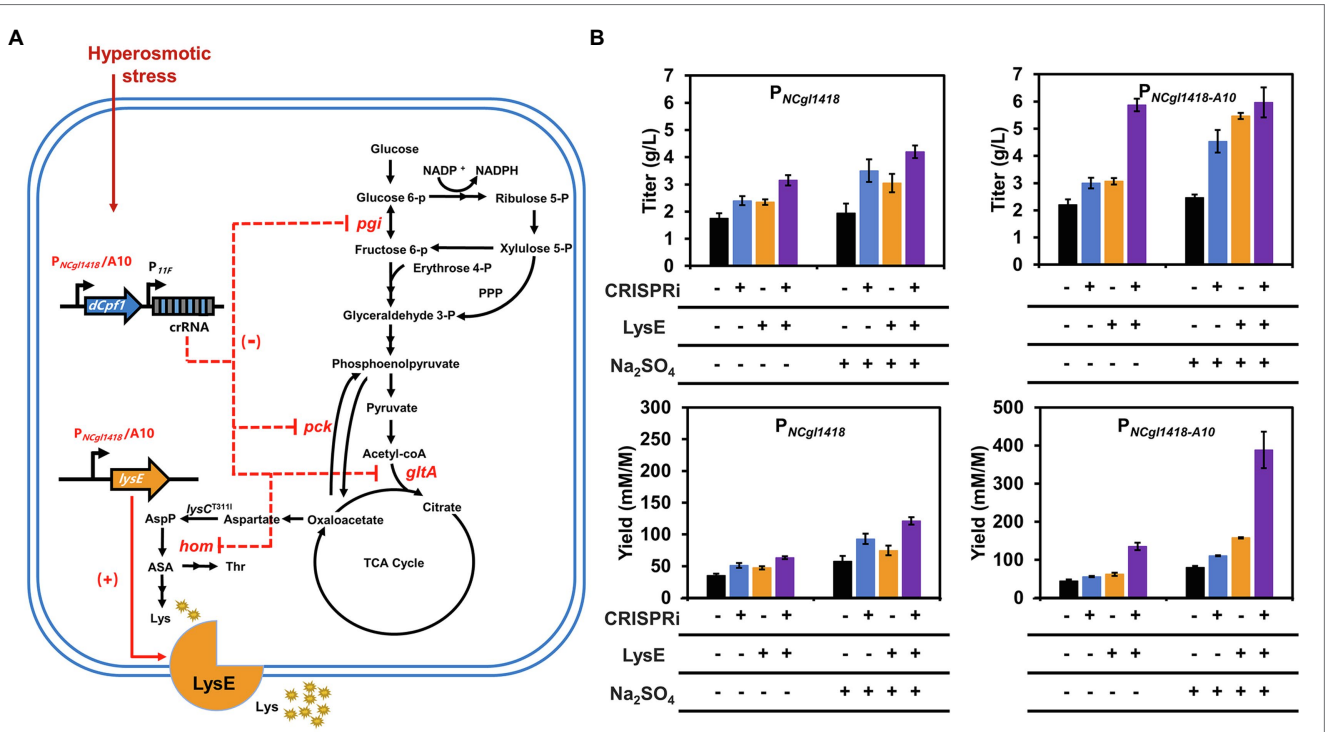

FIGURE 5 | Enhancing lysine production by regulating the expression of target genes using the hyperosmotic stress inducible promoters. **(A)** Lysine biosynthesis pathway of *C. glutamicum*. (+) Represents gene overexpression and (–) represents gene repression. AspP, aspartyl phosphate; ASA, aspartate semialdehyde; Thr, threonine; Lys, lysine. **(B)** Effects of $P_{NCgl1418}$ and $P_{NCgl1418\text{-}A10}$ promoter-regulated *lysE* overexpression and/or multiple genes (*gltA*, *pgi*, *hom*, and *pck*) repression on lysine production. SCgL30 strains expressing LysE and/or dCpf1 with a crRNA array were cultivated in fermentation medium for 24 h (for $P_{NCgl1418}$ promoter) or 36 h (for $P_{NCgl1418\text{-}A10}$ promoter). SCgL30 strains containing the empty vector pEC-XK99E and/or the plasmid pXM-$P_{NCgl1418}$-con without the crRNA array were used as controls. All data represent mean values from three biological replicates including SDs.

production. Without addition of 0.6 M Na_2SO_4 to provide a hyperosmotic stress, repression of four target genes using $P_{NCgl1418}$ enhanced lysine titer and yield by 37 and 45%, respectively (**Figure 5B**). When the hyperosmotic stress was exerted to cells by adding 0.6 M Na_2SO_4, repression of four target genes enhanced lysine titer and yield by 79 and 62%, respectively (**Figure 5B**). The lysine titer was improved by 92% (reached 4.5 g/L) when the stronger promoter variant $P_{NCgl1418\text{-}A10}$ was used in the presence of hyperosmotic stress. The results suggest that the hyperosmotic stress inducible promoters can be used for efficiently regulating gene expression under high salt conditions for metabolic engineering purposes.

For further testing the application of the hyperosmotic stress inducible promoters in gene upregulation, *lysE* was selected and overexpressed in SCgL30. Without the addition of 0.6 M Na_2SO_4, overexpression of *lysE* slightly increased the lysine titer and yield. However, under the hyperosmotic stress, *lysE* overexpression controlled by $P_{NCgl1418\text{-}A10}$ exhibited much higher lysine titer (2.3-fold) and yield (about 2.0-fold) compared with the control strain (**Figure 5B**). Finally, overexpression of *lysE* and repression of *gltA*, *pck*, *pgi*, and *hom* by CRISPRi were simultaneously performed for lysine production using the strain SLDEA10. Under the hyperosmotic stress, this combinational strategy improved lysine titer and the yield by 2.5- and 4.8-fold compared to the control, respectively (**Figure 5B**). It was noticed that the lysine titers of strain SLDEA10 cultivated with or without 0.6 M Na_2SO_4 were almost the same. This is may be due to the slower growth rate of strain SLDEA10 under hyperosmotic stress (**Supplementary Figure S4**). The growth retardation might be caused by the higher expression of dCpf1 and LysE or the stronger repression of the endogenous genes under hyperosmotic stress. However, the lysine yield reached 388.7 mM/M, which improved by 4.8-fold when 0.6 M Na_2SO_4 was added (**Figure 5B**). The results indicate that the promoter variant $P_{NCgl1418\text{-}A10}$ has strong inductivity and the rebalance between growth and production is necessary to increase the performance of engineered strains.

Feed Batch Fermentation of the Lysine Producer With the Auto-Inducible System

Because of the limited substrate supplement and the lack of fermentation condition control, fermentation in 24-well plates cannot result in high-titer lysine production. Therefore, 0.6 M Na_2SO_4 was added to provide a hyperosmotic stress to induce gene expression controlled by $P_{NCgl1418}$ and $P_{NCgl1418\text{-}A10}$. Fed-batch fermentations are usually used to obtain high concentrations of products, which can serve as inducers for hyperosmotic stress inducible promoters such as $P_{NCgl1418\text{-}A10}$. To demonstrate the auto-inducible system based on $P_{NCgl1418\text{-}A10}$, fed-batch

fermentations without exogenous Na_2SO_4 addition were conducted in 1-L bioreactors using the best lysine producer strain SLDEA10 and a control strain SLDEcon2 without the auto-inducible CRISPRi and *lysE* overexpression system. Overall, SLDEA10 had a better balance between growth and production than the control strain (**Figure 6**). Strain SLDEcon2 entered the stationary phage at 15 h with a relatively high OD_{600nm} peak value, while the highest OD_{600nm} was significantly reduced by 32.3% for strain SLDEA10 (**Figure 6**). On the contrary, the lysine biosynthesis rate of SLDEA10 was significantly higher than that of strain SLDEcon2 in the mid- and late-stage. After 33 h fermentation, 28.0 g/L of lysine was produced by strain SLDEA10, representing a 64.7% improvement compared to strain SLDEcon2 (17.0 g/L; **Figure 6**). These results suggest that the metabolic flux is directed from biomass synthesis to product synthesis by using the auto-inducible system based on the hyperosmotic stress inducible promoter.

DISCUSSION

In the last few decades, *C. glutamicum* has been engineered for the production of a variety of value-added products, including amino acids, organic acids, polymer precursors, and proteins (Baritugo et al., 2018; Lee and Kim, 2018). Gene expression regulation technologies based on CRISPR and synthetic small RNAs for *C. glutamicum* have been developed (Liu et al., 2017; Wang et al., 2018; Gauttam et al., 2019; Sun et al., 2019; Li et al., 2020). By combining these technologies with metabolic- or QS-responding elements, dynamic regulation strategies have been developed for precise regulation of gene expression to maximize the biosynthesis of target products (Gupta et al., 2017; Chen et al., 2018; Shen et al., 2019; Liang et al., 2020; Tian et al., 2020; Hartline et al., 2021). However, the metabolic-responding elements are specific for certain metabolites and thus they are not universal for various fermentation processes. Although QS systems have good universality, their application in large-scale fermentation usually suffers from the low threshold. As an alternative, the environmental parameter-responding elements have the advantages of high universality and good controllability, which can be used to develop universal dynamic regulation systems. At present, dynamic regulation strategies based on external environmental conditions such as temperature, dissolved oxygen, pH, and illumination have been successfully developed and applied in metabolic engineering (Jong Uk et al., 2008; Binder et al., 2016; Hwang et al., 2017; Harder et al., 2018; Zhao et al., 2018; Banares et al., 2020). However, in large-scale fermentation, these environmental factors including temperature, dissolved oxygen, and pH mostly need to be controlled at a steady level to maintain cellular activity, and optogenetics tools are limited by the nonhomogeneity in large fermenters. Hyperosmotic stress, which commonly presents in the mid- and late-phase of almost all the fermentation processes, can serve as a naturally occurring inducer. Compared with the promoters based on metabolic- or QS-responding elements and those responding to external environmental conditions such as temperature, dissolved oxygen, pH, and illumination, the hyperosmotic stress inducible promoters have good universality and economy in the large-scale industrialization applications. In this study, a hyperosmotic stress inducible gene expression system was developed in *C. glutamicum*. The promoter of *NCgl1418* identified here exhibits high expression intensity and induction activity under hyperosmotic stress caused by different salt inducers. More importantly, the induction activity was closely related to product concentration, which can be conveniently used to regulate the expression of key genes according to the product concentration. Considering the different expression intensities and induction activities by different types or concentrations of salts, optimization tests for different media may be required in practical applications.

Promoters are the core elements of the dynamic regulation systems and synthetic biology researches. Identification and modification of novel promoters with special functions can provide necessary tools for the development of new gene circuits and hyperproducing strains. At present, omics analysis

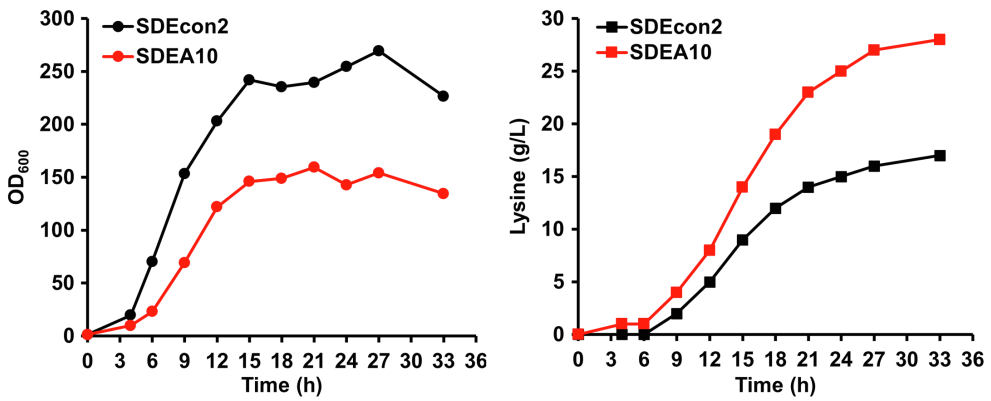

FIGURE 6 | Fed-batch fermentation for lysine production using strains SDEcon2 (black lines) and SDEA10 (red lines). Strain SDEcon2 is strain SCgL30 harboring the empty vector pEC-XK99E and the plasmid pXM-$P_{NCgl1418}$-con without the crRNA array. Strain SDEA10 is strain SCgL30 with overexpression of *lysE* and repression of *gltA*, *pgi*, *hom*, and *pck* controlled by $P_{NCgl1418\text{-}A10}$ promoter. Cultivation was performed in 1-L bioreactors with fermentation medium.

under different culture conditions and bioinformatics analysis of specific recognition sequences of transcriptional regulators are the main strategies for the identification of new promoters (Dahl et al., 2013; Liu et al., 2015; Kim et al., 2016; Ma et al., 2018). However, the strength and induction activity of natural promoters are often not sufficient for practical applications. To engineer more suitable promoters, random mutation followed by high-throughput screening and redesign of the natural promoters with components from other different promoters are usually performed (Kim et al., 2016; Zhang et al., 2018; Henke et al., 2021). In this study, for isolation of engineered promoters with enhanced inducibility by hyperosmotic stress, we used a FACS screening strategy that combined three rounds of positive and negative screening. The isolated promoters showed up to a 3.4-fold increased GFP expression level compared to the original *NCgl1418* promoter with much higher inducibility (up to 8.5-fold). As a proof-of-concept, lysine production was improved by regulating key genes expression with the hyperosmotic stress inducible promoters, demonstrating the great potential in metabolic engineering of *C. glutamicum*. Also, we observed leaky expression of the *NCgl1418* promoter, like all the other kinds of inducible promoters. For a stricter control of the *NCgl1418* promoter, conditional overexpression of its regulator MtrA/MtrB may be a useful strategy. In addition, promoter variants with low-level leaky expression could also be further screened by FACS. In conclusion, we identified the MtrA/MtrB-dependent *NCgl1418* promoter as a hyperosmotic stress inducible promoter and developed a hyperosmotic stress inducible gene expression system in *C. glutamicum*. To the best of our knowledge, this is the first report on the development of a hyperosmotic stress inducible promoter in *C. glutamicum*. We believe this hyperosmotic stress inducible gene expression system will contribute to extend the usefulness of *C. glutamicum* in the industrial-scale production of various value-added biochemicals.

DATA AVAILABILITY STATEMENT

The original contributions presented in the study are included in the article/**Supplementary Material**, further inquiries can be directed to the corresponding authors.

AUTHOR CONTRIBUTIONS

JH, JC, YW, PZ, and JS conceptualized the project, designed the study, and composed the manuscript. JH, JC, TS, YZ, and NC conducted the experiments and collected data. JH, JC, YW, XN, WP, and JL performed the data analysis. PZ, JS, and SH provided the critical feedback on the manuscript and resources. All authors contributed to the article and approved the submitted version.

FUNDING

This work was supported by the National Key R&D Program of China (2018YFA0901400 and 2019YFA0904900), Tianjin Synthetic Biotechnology Innovation Capacity Improvement Project (TSBICIP-KJGG-005), and the National Natural Science Foundation of China (32000023).

SUPPLEMENTARY MATERIAL

The Supplementary Material for this article can be found online at: https://www.frontiersin.org/articles/10.3389/fmicb.2021.718511/full#supplementary-material

REFERENCES

Banares, A. B., Valdehuesa, K. N. G., Ramos, K. R. M., Nisola, G. M., Lee, W. K., and Chung, W. J. (2020). A pH-responsive genetic sensor for the dynamic regulation of D-xylonic acid accumulation in *Escherichia coli*. *Appl. Microbiol. Biotechnol.* 104, 2097–2108. doi: 10.1007/s00253-019-10297-0

Baritugo, K. A. G., Kim, H. T., David, Y. C., Choi, J. H., Choi, J.i., Kim, T. W., et al. (2018). Recent advances in metabolic engineering of *Corynebacterium glutamicum* as a potential platform microorganism for biorefinery. *Biofuels Bioprod. Biorefin.* 12, 899–925. doi: 10.1002/bbb.1895

Becker, J., Klopprogge, C., Zelder, O., Heinzle, E., and Wittmann, C. (2005). Amplified expression of fructose 1,6-bisphosphatase in *Corynebacterium glutamicum* increases in vivo flux through the pentose phosphate pathway and lysine production on different carbon sources. *Appl. Environ. Microbiol.* 71, 8587–8596. doi: 10.1128/AEM.71.12.8587-8596.2005

Becker, J., and Wittmann, C. (2012). Bio-based production of chemicals, materials and fuels *Corynebacterium glutamicum* as versatile cell factory. *Curr. Opin. Biotechnol.* 23, 631–640. doi: 10.1016/j.copbio.2011.11.012

Ben Samoun, K., Leblon, G., and Reyes, O. (1999). Positively regulated expression of the *Escherichia coli araBAD* promoter in *Corynebacterium glutamicum*. *FEMS Microbiol. Lett.* 174, 125–130. doi: 10.1111/j.1574-6968.1999.tb13558.x

Binder, D., Frohwitter, J., Mahr, R., Bier, C., Grünberger, A., Loeschcke, A., et al. (2016). Light-controlled cell factories: employing photocaged isopropyl-β-D-thiogalactopyranoside for light-mediated optimization of *lac* promoter-based gene expression and (+)-valencene biosynthesis in *Corynebacterium glutamicum*. *Appl. Environ. Microbiol.* 82, 6141–6149. doi: 10.1128/AEM.01457-16

Binder, S., Schendzielorz, G., Staebler, N., Krumbach, K., Hoffmann, K., Bott, M., et al. (2012). A high-throughput approach to identify genomic variants of bacterial metabolite producers at the single-cell level. *Genome Biol.* 13:R40. doi: 10.1186/gb-2012-13-5-r40

Bott, M., and Brocker, M. (2012). Two-component signal transduction in *Corynebacterium glutamicum* and other corynebacteria: on the way towards stimuli and targets. *Appl. Microbiol. Biotechnol.* 94, 1131–1150. doi: 10.1007/s00253-012-4060-x

Brocker, M., Mack, C., and Bott, M. (2011). Target genes, consensus binding site, and role of phosphorylation for the response regulator MtrA of *Corynebacterium glutamicum*. *J. Bacteriol.* 193, 1237–1249. doi: 10.1128/JB.01032-10

Chen, Y., Ho, J. M. L., Shis, D. L., Gupta, C., Long, J., Wagner, D. S., et al. (2018). Tuning the dynamic range of bacterial promoters regulated by ligand-inducible transcription factors. *Nat. Commun.* 9:64. doi: 10.1038/s41467-017-02473-5

Chung, S. C., Park, J. S., Yun, J., and Park, J. H. (2017). Improvement of succinate production by release of end-product inhibition in *Corynebacterium glutamicum*. *Metab. Eng.* 40, 157–164. doi: 10.1016/j.ymben.2017.02.004

Dahl, R. H., Zhang, F., Alonso Gutierrez, J., Baidoo, E., Batth, T. S., Redding Johanson, A. M., et al. (2013). Engineering dynamic pathway regulation

using stress-response promoters. *Nat. Biotechnol.* 31, 1039–1046. doi: 10.1038/nbt.2689

Dostalova, H., Holatko, J., Busche, T., Rucka, L., Rapoport, A., Halada, P., et al. (2017). Assignment of sigma factors of RNA polymerase to promoters in *Corynebacterium glutamicum*. *AMB Express* 7:133. doi: 10.1186/s13568-017-0436-8

Gauttam, R., Seibold, G. M., Mueller, P., Weil, T., Weiss, T., Handrick, R., et al. (2019). A simple dual-inducible CRISPR interference system for multiple gene targeting in *Corynebacterium glutamicum*. *Plasmid* 103, 25–35. doi: 10.1016/j.plasmid.2019.04.001

Giacalone, M. J., Gentile, A. M., Lovitt, B. T., Berkley, N. L., Gunderson, C. W., and Surber, M. W. (2006). Toxic protein expression in *Escherichia coli* using a rhamnose-based tightly regulated and tunable promoter system. *BioTechniques* 40, 355–364. doi: 10.2144/000112112

Gupta, A., Reizman, I. M. B., Reisch, C. R., and Prather, K. L. J. (2017). Dynamic regulation of metabolic flux in engineered bacteria using a pathway-independent quorum-sensing circuit. *Nat. Biotechnol.* 35:273. doi: 10.1038/nbt.3796

Harder, B. J., Bettenbrock, K., and Klamt, S. (2018). Temperature-dependent dynamic control of the TCA cycle increases volumetric productivity of itaconic acid production by *Escherichia coli*. *Biotechnol. Bioeng.* 115, 156–164. doi: 10.1002/bit.26446

Hartline, C. J., Schmitz, A. C., Han, Y., and Zhang, F. (2021). Dynamic control in metabolic engineering: theories, tools, and applications. *Metab. Eng.* 63, 126–140. doi: 10.1016/j.ymben.2020.08.015

Henke, N. A., Krahn, I., and Wendisch, V. F. (2021). Improved plasmid-based inducible and constitutive gene expression in *Corynebacterium glutamicum*. *Microorganisms* 9:204. doi: 10.3390/microorganisms9010204

Hou, J., Gao, C., Guo, L., Nielsen, J., Ding, Q., Tang, W., et al. (2020). Rewiring carbon flux in *Escherichia coli* using a bifunctional molecular switch. *Metab. Eng.* 61, 47–57. doi: 10.1016/j.ymben.2020.05.004

Hwang, H. J., Kim, J. W., Ju, S. Y., Park, J. H., and Lee, P. C. (2017). Application of an oxygen-inducible nar promoter system in metabolic engineering for production of biochemicals in *Escherichia coli*. *Biotechnol. Bioeng.* 114, 468–473. doi: 10.1002/bit.26082

Jong Uk, P., Jo, J. H., Kim, Y. J., Chung, S. S., Lee, J. H., and Lee, H. H. (2008). Construction of heat-inducible expression vector of *Corynebacterium-glutamicum* and C-ammoniagenes: fusion of iambda operator with promoters isolated from C-ammoniagenes. *J. Microbiol. Biotechnol.* 18, 639–647. doi: 10.1016/S1369-8001(00)00115-3

Kim, M. J., Yim, S. S., Choi, J. W., and Jeong, K. J. (2016). Development of a potential stationary-phase specific gene expression system by engineering of SigB-dependent *cg3141* promoter in *Corynebacterium glutamicum*. *Appl. Microbiol. Biotechnol.* 100, 4473–4483. doi: 10.1007/s00253-016-7297-y

Kind, S., Jeong, W. K., Schroeder, H., and Wittmann, C. (2010). Systems-wide metabolic pathway engineering in *Corynebacterium glutamicum* for bio-based production of diaminopentane. *Metab. Eng.* 12, 341–351. doi: 10.1016/j.ymben.2010.03.005

Lausberg, F., Chattopadhyay, A. R., Heyer, A., Eggeling, L., and Freudl, R. (2012). A tetracycline inducible expression vector for *Corynebacterium glutamicum* allowing tightly regulable gene expression. *Plasmid* 68, 142–147. doi: 10.1016/j.plasmid.2012.05.001

Lee, M. J., and Kim, P. (2018). Recombinant protein expression system in *Corynebacterium glutamicum* and its application. *Front. Microbiol.* 9:2523. doi: 10.3389/fmicb.2018.02523

Lee, J. Y., Na, Y. A., Kim, E., Lee, H. S., and Kim, P. (2016). The *Actinobacterium Corynebacterium glutamicum*, an industrial workhorse. *J. Microbiol. Biotechnol.* 26, 807–822. doi: 10.4014/jmb.1601.01053

Lemke, J. J., Sanchez Vazquez, P., Burgos, H. L., Hedberg, G., Ross, W., and Gourse, R. L. (2011). Direct regulation of *Escherichia coli* ribosomal protein promoters by the transcription factors ppGpp and DksA. *Proc. Natl. Acad. Sci. U. S. A.* 108, 5712–5717. doi: 10.1073/pnas.1019383108

Li, M., Chen, J., Wang, Y., Liu, J., Huang, J., Chen, N., et al. (2020). Efficient multiplex gene repression by CRISPR-dCpf1 in *Corynebacterium glutamicum*. *Front. Bioeng. Biotechnol.* 8:357. doi: 10.3389/fbioe.2020.00357

Liang, C., Zhang, X., Wu, J., Mu, S., Wu, Z., Jin, J. M., et al. (2020). Dynamic control of toxic natural product biosynthesis by an artificial regulatory circuit. *Metab. Eng.* 57, 239–246. doi: 10.1016/j.ymben.2019.12.002

Lipscomb, M. L., Mowry, M. C., and Kompala, D. S. (2004). Production of a secreted glycoprotein from an inducible promoter system in a perfusion bioreactor. *Biotechnol. Prog.* 20, 1402–1407. doi: 10.1021/bp049973j

Liu, Y., Li, Q., Zheng, P., Zhang, Z., Liu, Y., Sun, C., et al. (2015). Developing a high-throughput screening method for threonine overproduction based on an artificial promoter. *Microb. Cell Factories* 14:121. doi: 10.1186/s12934-015-0311-8

Liu, J., Wang, Y., Lu, Y., Zheng, P., Sun, J., and Ma, Y. (2017). Development of a CRISPR/Cas9 genome editing toolbox for *Corynebacterium glutamicum*. *Microb. Cell Factories* 16:205. doi: 10.1186/s12934-017-0815-5

Ma, Y., Cui, Y., Du, L., Liu, X., Xie, X., and Chen, N. (2018). Identification and application of a growth-regulated promoter for improving L-valine production in *Corynebacterium glutamicum*. *Microb. Cell Factories* 17:185. doi: 10.1186/s12934-018-1031-7

Moker, N., Brocker, M., Schaffer, S., Kramer, R., Morbach, S., and Bott, M. (2004). Deletion of the genes encoding the MtrA-MtrB two-component system of *Corynebacterium glutamicum* has a strong influence on cell morphology, antibiotics susceptibility and expression of genes involved in osmoprotection. *Mol. Microbiol.* 54, 420–438. doi: 10.1111/j.1365-2958.2004.04249.x

Nocadello, S., and Swennen, E. F. (2012). The new pLAI (lux regulon based auto-inducible) expression system for recombinant protein production in *Escherichia coli*. *Microb. Cell Factories* 11:3. doi: 10.1186/1475-2859-11-3

Ogasawara, H., Ishida, Y., Yamada, K., Yamamoto, K., and Ishihama, A. (2007). PdhR (pyruvate dehydrogenase complex regulator) controls the respiratory electron transport system in *Escherichia coli*. *J. Bacteriol.* 189, 5534–5541. doi: 10.1128/JB.00229-07

Ohnishi, J., Mitsuhashi, S., Hayashi, M., Ando, S., Yokoi, H., Ochiai, K., et al. (2002). A novel methodology employing *Corynebacterium glutamicum* genome information to generate a new L-lysine-producing mutant. *Appl. Microbiol. Biotechnol.* 58, 217–223. doi: 10.1007/s00253-001-0883-6

Okibe, N., Suzuki, N., Inui, M., and Yukawa, H. (2010). Isolation, evaluation and use of two strong, carbon source-inducible promoters from *Corynebacterium glutamicum*. *Lett. Appl. Microbiol.* 50, 173–180. doi: 10.1111/j.1472-765X.2009.02776.x

Patek, M., and Nesvera, J. (2011). Sigma factors and promoters in *Corynebacterium glutamicum*. *J. Biotechnol.* 154, 101–113. doi: 10.1016/j.jbiotec.2011.01.017

Pfeifer Sancar, K., Mentz, A., Rueckert, C., and Kalinowski, J. (2013). Comprehensive analysis of the *Corynebacterium glutamicum* transcriptome using an improved RNA-seq technique. *BMC Genomics* 14:888. doi: 10.1186/1471-2164-14-888

Rytter, J. V., Helmark, S., Chen, J., Lezyk, M. J., Solem, C., and Jensen, P. R. (2014). Synthetic promoter libraries for *Corynebacterium glutamicum*. *Appl. Microbiol. Biotechnol.* 98, 2617–2623. doi: 10.1007/s00253-013-5481-x

Shen, X., Wang, J., Li, C., Yuan, Q., and Yan, Y. (2019). Dynamic gene expression engineering as a tool in pathway engineering. *Curr. Opin. Biotechnol.* 59, 122–129. doi: 10.1016/j.copbio.2019.03.019

Sun, D., Chen, J., Wang, Y., Li, M., Rao, D., Guo, Y., et al. (2019). Metabolic engineering of *Corynebacterium glutamicum* by synthetic small regulatory RNAs. *J. Ind. Microbiol. Biotechnol.* 46, 203–208. doi: 10.1007/s10295-018-02128-4

Sun, M., Gao, X., Zhao, Z., Li, A., Wang, Y., Yang, Y., et al. (2020). Enhanced production of recombinant proteins in *Corynebacterium glutamicum* by constructing a bicistronic gene expression system. *Microb. Cell Factories* 19:113. doi: 10.1186/s12934-020-01370-9

Terpe, K. (2006). Overview of bacterial expression systems for heterologous protein production: from molecular and biochemical fundamentals to commercial systems. *Appl. Microbiol. Biotechnol.* 72, 211–222. doi: 10.1007/s00253-006-0465-8

Tian, J., Yang, G., Gu, Y., Sun, X., Lu, Y., and Jiang, W. (2020). Developing an endogenous quorum-sensing based CRISPRi circuit for autonomous and tunable dynamic regulation of multiple targets in *Streptomyces*. *Nucleic Acids Res.* 48, 8188–8202. doi: 10.1093/nar/gkaa602

Tsuge, Y., and Matsuzawa, H. (2021). Recent progress in production of amino acid-derived chemicals using *Corynebacterium glutamicum*. *World J. Microbiol. Biotechnol.* 37:49. doi: 10.1007/s11274-021-03007-4

Varela, C., Agosin, E., Baez, M., Klapa, M., and Stephanopoulos, G. (2003). Metabolic flux redistribution in *Corynebacterium glutamicum* in response to osmotic stress. *Appl. Microbiol. Biotechnol.* 60, 547–555. doi: 10.1007/s00253-002-1120-7

Wang, Y., Gao, X., Liu, X., Li, Y., Sun, M., Yang, Y., et al. (2020). Construction of a 3A system from BioBrick parts for expression of recombinant hirudin variants III in *Corynebacterium glutamicum*. *Appl. Microbiol. Biotechnol.* 104, 8257–8266. doi: 10.1007/s00253-020-10835-1

Wang, Y., Liu, Y., Liu, J., Guo, Y., Fan, L., Ni, X., et al. (2018). MACBETH: Multiplex automated *Corynebacterium glutamicum* base editing method. *Metab. Eng.* 47, 200–210. doi: 10.1016/j.ymben.2018.02.016

Wiechert, J., Filipchyk, A., Huennefeld, M., Gaetgens, C., Brehm, J., Heermann, R., et al. (2020a). Deciphering the rules underlying xenogeneic silencing and counter-silencing of Lsr2-like proteins using CgpS of *Corynebacterium glutamicum* as a model. *mBio* 11, e02273–e02219. doi: 10.1128/mBio.02273-19

Wiechert, J., Gaetgens, C., Wirtz, A., and Frunzke, J. (2020b). Inducible expression systems based on xenogeneic silencing and counter-silencing and design of a metabolic toggle switch. *ACS Synth. Biol.* 9, 2023–2038. doi: 10.1021/acssynbio.0c00111

Woo, H. M., and Park, J. B. (2014). Recent progress in development of synthetic biology platforms and metabolic engineering of *Corynebacterium glutamicum*. *J. Biotechnol.* 180, 43–51. doi: 10.1016/j.jbiotec.2014.03.003

Xu, X., Li, X., Liu, Y., Zhu, Y., Li, J., Du, G., et al. (2020a). Pyruvate-responsive genetic circuits for dynamic control of central metabolism. *Nat. Chem. Biol.* 16, 1261–1268. doi: 10.1038/s41589-020-0637-3

Xu, J. Z., Ruan, H. Z., Yu, H. B., Liu, L. M., and Zhang, W. (2020b). Metabolic engineering of carbohydrate metabolism systems in *Corynebacterium glutamicum* for improving the efficiency of L-lysine production from mixed sugar. *Microb. Cell Factories* 19:39. doi: 10.1186/s12934-020-1294-7

Zhang, C., Li, Y., Zhu, F., Li, Z., Lu, N., Li, Y., et al. (2020). Metabolic engineering of an auto-regulated *Corynebacterium glutamicum* chassis for biosynthesis of 5-aminolevulinic acid. *Bioresour. Technol.* 318:124064. doi: 10.1016/j.biortech.2020.124064

Zhang, S., Liu, D., Mao, Z., Mao, Y., Ma, H., Chen, T., et al. (2018). Model-based reconstruction of synthetic promoter library in *Corynebacterium glutamicum*. *Biotechnol. Lett.* 40, 819–827. doi: 10.1007/s10529-018-2539-y

Zhao, E. M., Zhang, Y., Mehl, J., Park, H., Lalwani, M. A., Toettcher, J. E., et al. (2018). Optogenetic regulation of engineered cellular metabolism for microbial chemical production. *Nature* 555, 683–687. doi: 10.1038/nature26141

Zhou, L., and Zeng, A. (2015). Engineering a lysine-ON riboswitch for metabolic control of lysine production in *Corynebacterium glutamicum*. *ACS Synth. Biol.* 4, 1335–1340. doi: 10.1021/acssynbio.5b00075

Conflict of Interest: The authors declare that the research was conducted in the absence of any commercial or financial relationships that could be construed as a potential conflict of interest.

frontiers in Bioengineering and Biotechnology

ORIGINAL RESEARCH
published: 29 July 2021
doi: 10.3389/fbioe.2021.704681

A Timed Off-Switch for Dynamic Control of Gene Expression in *Corynebacterium Glutamicum*

Daniel Siebert[1,2], *Josef Altenbuchner*[3] *and Bastian Blombach*[1,2]*

[1] Microbial Biotechnology, Campus Straubing for Biotechnology and Sustainability, Technical University of Munich, Straubing, Germany, [2] SynBiofoundry@TUM, Technical University of Munich, Straubing, Germany, [3] Institute of Industrial Genetics, University of Stuttgart, Stuttgart, Germany

OPEN ACCESS

Edited by:
Ping Zheng,
Tianjin Institute of Industrial Biotechnology, Chinese Academy of Sciences (CAS), China

Reviewed by:
Guoqiang Xu,
Jiangnan University, China
Xinqing Zhao,
Shanghai Jiao Tong University, China

***Correspondence:**
Bastian Blombach
bastian.blombach@tum.de

Specialty section:
This article was submitted to Synthetic Biology, a section of the journal Frontiers in Bioengineering and Biotechnology

Received: 03 May 2021
Accepted: 30 June 2021
Published: 29 July 2021

Citation:
Siebert D, Altenbuchner J and Blombach B (2021) A Timed Off-Switch for Dynamic Control of Gene Expression in Corynebacterium Glutamicum. Front. Bioeng. Biotechnol. 9:704681. doi: 10.3389/fbioe.2021.704681

Dynamic control of gene expression mainly relies on inducible systems, which require supplementation of (costly) inducer molecules. In contrast, synthetic regulatory circuits, which allow the timed shutdown of gene expression, are rarely available and therefore represent highly attractive tools for metabolic engineering. To achieve this, we utilized the VanR/P_{vanABK}* regulatory system of *Corynebacterium glutamicum*, which consists of the transcriptional repressor VanR and a modified promoter of the *vanABK* operon (P_{vanABK}*). VanR activity is modulated by one of the phenolic compounds ferulic acid, vanillin or vanillic acid, which are co-metabolized with D-glucose. Thus, gene expression in the presence of D-glucose is turned off if one of the effector molecules is depleted from the medium. To dynamically control the expression of the *aceE* gene, encoding the E1 subunit of the pyruvate dehydrogenase complex that is essential for growth on D-glucose, we replaced the native promoter by *vanR*/P_{vanABK}* yielding *C. glutamicum* ΔP_{aceE}::*vanR*-P_{vanABK}*. The biomass yield of this strain increased linearly with the supplemented amount of effector. After consumption of the phenolic compounds growth ceased, however, *C. glutamicum* ΔP_{aceE}::*vanR*-P_{vanABK}* continued to utilize the residual D-glucose to produce significant amounts of pyruvate, L-alanine, and L-valine. Interestingly, equimolar concentrations of the three phenolic compounds resulted in different biomass yields; and with increasing effector concentration, the product spectrum shifted from pyruvate over L-alanine to L-valine. To further test the suitability of the VanR/P_{vanABK}* system, we overexpressed the L-valine biosynthesis genes *ilvBNCE* in *C. glutamicum* ΔP_{aceE}::*vanR*-P_{vanABK}*, which resulted in efficient L-valine production with a yield of about 0.36 mol L-valine per mol D-glucose. These results demonstrate that the VanR/P_{vanABK}* system is a valuable tool to control gene expression in *C. glutamicum* in a timed manner by the cheap and abundant phenolic compounds ferulic acid, vanillin, and vanillic acid.

Keywords: ***Corynebacterium glutamicum*, dynamic expression control, lignin, L-valine production, ferulic acid, vanillin, vanillic acid, pyruvate dehydrogenase complex**

INTRODUCTION

Controlling gene expression is one of the key tasks to manipulate the metabolism of a host cell for application in a biotechnological process. Regarding the targeted induction of gene expression in prokaryotes, several systems are well-established and widely applied, such as LacI/P_{tac}, AraC/P_{araBAD}, PrpR/P_{prp}, RhaR-RhaS/P_{rhaBAD}, and T7 RNA polymerase-based versions (Lee and Keasling, 2005; Terpe, 2006; Brautaset et al., 2009). While these systems are usually easy to handle and well-suited for lab scale studies, their application in the industrial environment is often hampered by, e.g., the price or availability of the effector molecule (Ferreira et al., 2018; Cardoso et al., 2020). Moreover, since most effector molecules show a high stability and cannot easily be removed from the culture broth, dynamic control of gene expression is still challenging and therefore subject of recent studies in different organisms (Jayaraman et al., 2018; Baumschlager et al., 2020; Wiechert et al., 2020; Glasscock et al., 2021).

Corynebacterium glutamicum is a Gram-positive facultative anaerobic organism that grows on a variety of sugars, organic acids, and phenolic compounds as single or combined carbon and energy sources (Eggeling and Bott, 2005; Merkens et al., 2005; Nishimura et al., 2007; Takeno et al., 2007; Becker and Wittmann, 2019). The organism is regarded as powerhouse for large-scale production of amino acids (if mentioned here, always the L-form is meant), such as glutamate and lysine at a level of 6 million tons per year (Becker et al., 2018). Moreover, many studies exploited *C. glutamicum* for the production of commodity chemicals, such as the biofuels isobutanol, ethanol, and *n*-propanol (Inui et al., 2004; Blombach and Eikmanns, 2011; Blombach et al., 2011; Yamamoto et al., 2013; Siebert and Wendisch, 2015; Lange et al., 2018; Hasegawa et al., 2020), the diamines cadaverine and putrescine (Kind and Wittmann, 2011; Wendisch, 2017), and other amino acids such as histidine (Schwentner et al., 2019) and valine (Oldiges et al., 2014; Schwentner et al., 2018). This impressive progress in metabolic engineering of *C. glutamicum* is based on wealth of knowledge about the central metabolism, physiology, and regulation of relevant pathways, and the development of systems biology approaches and genetic engineering tools (Eggeling and Bott, 2005; Burkovski, 2008; Yukawa and Inui, 2013; Inui and Toyoda, 2020; Wang et al., 2021). Although numerous tools to manipulate the metabolism of *C. glutamicum* have been developed and standard heterologous inducible promotor systems are established and optimized (Goldbeck and Seibold, 2018; Gauttam et al., 2019), the set of available native promoters to drive synthetic and dynamic expression control is still small (Wiechert et al., 2020). Recently, Wiechert et al. (2020) constructed a GntR-dependent metabolic toggle switch that is regulated by the effector gluconate and can be applied to dynamically control gene expression in *C. glutamicum* (Wiechert et al., 2020).

Corynebacterium glutamicum is able to grow on the lignin-derived phenolic compounds ferulic acid (FA), vanillin (Van), and vanillic acid (VA) and, compared with other microbial systems, is less susceptible to growth inhibition by these molecules (Shen et al., 2012; Ding et al., 2015; Becker and Wittmann, 2019). The degradation of Van and VA proceeds *via* the vanillate pathway yielding protocatechuic acid (PCA), which is subsequently converted by the β-ketoadipate pathway to acetyl-CoA and succinyl-CoA entering eventually the tricarboxylic acid (TCA) cycle [**Figure 1** (Merkens et al., 2005; Brinkrolf et al., 2006; Shen et al., 2012; Kallscheuer et al., 2016; Okai et al., 2017)]. Within the vanillate pathway, FA might be converted in a cascade *via* Van and VA to PCA (Merkens et al., 2005; Brinkrolf et al., 2006; Shen et al., 2012). However, FA utilization essentially requires the action of the β-oxidative deacetylation pathway yielding VA [**Figure 1** (Kallscheuer et al., 2016)]. The vanillate utilization genes are transcribed as *vanABK* operon from the promotor P_{vanABK}, which is under control of the PadR-like repressor VanR. This transcriptional regulator is *in vitro* inhibited only by VA but not by FA, Van, or PCA; whereas *in vivo* the presence of FA, Van, and VA leads to a de-repression of the *vanABK* operon [**Figure 1** (Morabbi Heravi et al., 2015)]. The crystal structure of VanR of *C. glutamicum* was recently elucidated (Yao et al., 2020) and the VanR operator sequence, which is located downstream of the $P_{vanABK}-10$ region, has been identified (Morabbi Heravi et al., 2015).

In this study, we utilized the VanR/P_{vanABK} regulatory system to dynamically control gene expression in *C. glutamicum*. As a proof of concept, we show that the expression of the *aceE* gene, encoding the E1 subunit of the pyruvate dehydrogenase complex (PDHC), can be switched off in a timed manner, which was achieved by replacing the native *aceE* promoter with a modified VanR/P_{vanABK} system (subsequently indicated as VanR/P_{vanABK}*). This dynamically controlled off-switch essentially relies on the utilization of one of the compounds, FA, Van, or VA (**Figure 1**), and was applied to control biomass formation and to induce the production of pyruvate and its derived products alanine and valine.

MATERIALS AND METHODS

Microorganisms, Media, and Cultivation Conditions

All *C. glutamicum* strains and plasmids used in this study are given in **Table 1**. The *Escherichia coli* strain DH5α (Hanahan, 1983) was used as shuttle organism for all cloning purposes. For cultivation of *E. coli* as well as for the precultures of *C. glutamicum*, 2x TY complex medium (Green and Sambrook, 2012) was applied. The growth experiments with *C. glutamicum* were all conducted aerobically with a modified version of CGXII minimal medium (Buchholz et al., 2014) either with 5 g ammonium sulfate L^{-1}, if nothing else is mentioned, or 20 g L^{-1}, set to a pH of 7.4 and 20 g glucose L^{-1} as standard carbon source. Because of the phenotype of *aceE*-deficient strains (Schreiner et al., 2005), 5 g acetate L^{-1} (as potassium salt) was supplemented in precultivation steps for all *C. glutamicum* strains in this study. The standard conditions for liquid cultures were 37°C (*E. coli*) and 30°C (*C. glutamicum*) in an orbital shaker (Ø 25 mm, Multitron®2, INFORS GmbH, Einsbach, Germany) at 180 rpm applying glass tubes with 5-mL medium or 500-mL cultivation flasks with four baffles containing 50 mL medium. Solid medium

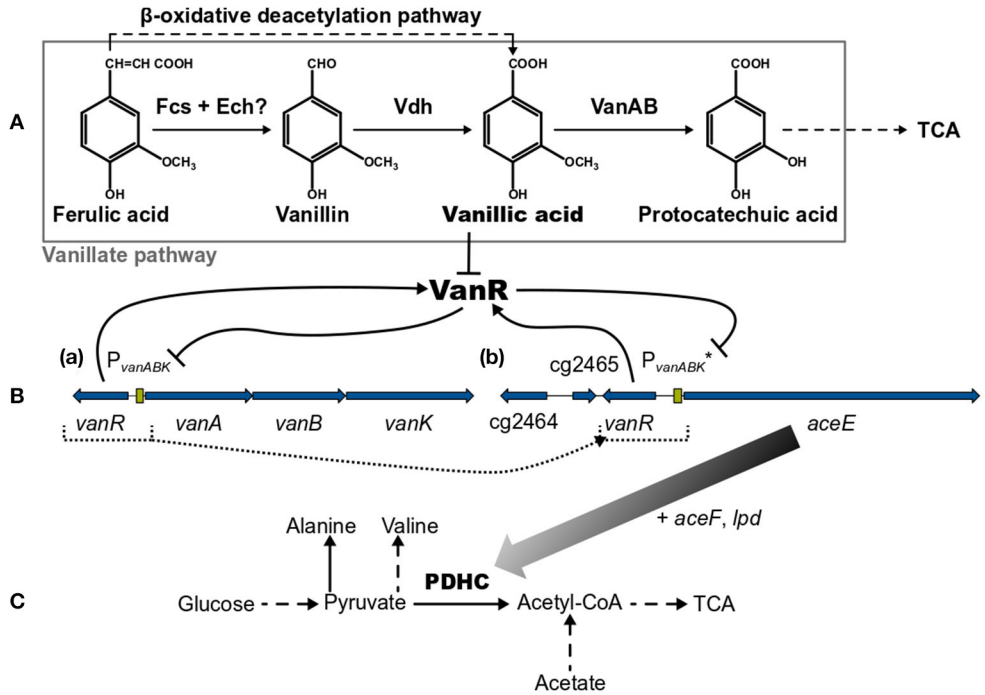

FIGURE 1 | (A) Overview of the vanillate and β-oxidative deacetylation pathways, (**B**, a) the native *vanR-vanABK* gene cluster, (**B**, b) the *aceE* gene under synthetic control of VanR/P_{vanABK}* (in *C. glutamicum* ΔP_{aceE}::*vanR*-P_{vanABK}*) and **(C)** relevant pathways around the pyruvate dehydrogenase complex (PDHC). Black arrows represent pathways or gene products and are dashed if indicating more than one reaction. Flat-headed lines point to inhibition. Blue arrows are genes and green boxes promotor regions. Color gradient of black arrow implies decreasing expression of *aceE* due to the utilization of phenolic compounds. Dotted lines represent the promotor exchange from P_{aceE} to VanR/P_{vanABK}*. (?) marks that this pathway is only predicted yet. Fcs, feruloyl-CoA synthetase; Ech, enoyl-CoA hydratase/aldolase; Vdh, vanillin dehydrogenase; VanAB, A and B subunits of vanillate demethylase encoded by *vanA* and *vanB*; TCA, tricarboxylic acid cycle; VanR, PadR-type repressor encoded by *vanR*; *vanK*, gene coding for vanillate transport protein VanK; cg2464 + cg2465, genes coding for hypothetical proteins; *aceE*, *aceF*, and *lpd*, genes coding for E1-, E2- and E3-subunits of pyruvate dehydrogenase complex (PDHC), respectively; P_{vanABK}, promotor region of *vanABK* and its −10-region-optimized derivative indicated by (*). This figure was adapted and compiled with information from diverse references (Kalinowski et al., 2003; Merkens et al., 2005; Brinkrolf et al., 2006; Chaudhry et al., 2007; Shen et al., 2012; Pfeifer-Sancar et al., 2013; Eikmanns and Blombach, 2014; Ding et al., 2015; Morabbi Heravi et al., 2015; Kallscheuer et al., 2016; Okai et al., 2017).

TABLE 1 | Strains and plasmids used in this study.

Strain or plasmid	Relevant characteristics	Reference or source
***C. glutamicum* strains**		
WT	Wild type (ATCC13032)	Abe et al., 1967; Ikeda and Nakagawa, 2003
ΔP_{aceE}::*vanR*-P_{vanABK}*	Wild type with insertion of the native *vanR* gene and the optimized *vanABK* promotor sequence (indicated by asterisk, derived from pJOE7747.1) in exchange for the *aceE* promotor sequence	This study
Plasmids		
pK19*mobsacB*	Mobilizable *E. coli* vector for the construction of deletion and insertion mutants, Km^R, *sacB*, *lacZα* with multiple cloning site, *oriV*, *oriT*	Schäfer et al., 1994
pK19*mobsacB*-ΔP_{aceE}::*vanR*-P_{vanABK}*	pK19*mobsacB*to replace the native *aceE* promotor sequence with the native *vanR* gene and the optimized *vanABK* promotor sequence (indicated by asterisk, derived from pJOE7747.1)	This study
pJOE7747.1	*ori*pBR322, *ori*pCG1, *rop,* Km^R, *vanR*192-P*vanR*-P*vanABK-eGFP-terrrnB* (optimized−10 region of P*vanABK*)	Morabbi Heravi et al., 2015
pJC4	*E. coli-C. glutamicum* shuttle vector, derivative of pACYC177-pHM1519 hybrid pZ1, ori_{p15A}, ori_{pCG1}, Km^R	Menkel et al., 1989; Cordes et al., 1992
pJC4-*ilvBNCE*	pJC4 with coding sequence for native *ilvBNCE* genes from *C. glutamicum* WT	Radmacher et al., 2002

was prepared by adding 18 g agar–agar L^{-1} to liquid medium in 9-cm Petri dishes, which were incubated at the above-mentioned temperature after inoculation. When appropriate, the medium was supplemented with 50 μg kanamycin mL^{-1}. For the dynamic control of gene expression, FA (product no: 128708; Sigma-Aldrich Chemie GmbH, Schnelldorf, Germany), Van (product no: 7887.1; Carl Roth GmbH + Co. KG, Karlsruhe, Germany), VA (product no: H36001; Sigma-Aldrich Chemie GmbH, Schnelldorf, Germany), or protocatechuic acid (product no: B24016; Alfa Aesar by Thermo Fisher Scientific, Kandel, Germany) was dissolved in DMSO to prepare 1 M stock solutions, which were applied in appropriate dilutions to reach the final concentrations given in the results. The seed train for all cultivation experiments with *C. glutamicum* was the following: cells out of glycerol cultures (30% glycerol and stored at −80°C) were streaked out on 2x TY-agar plates, which were incubated for 3 days. A single colony was used to inoculate 2x TY medium in a glass tube, which was incubated for 6–8 h. Then, the whole suspension was transferred into 2x TY medium in cultivation flasks and incubated overnight. The culture was centrifuged (4,000 × g, 10 min, room temperature), the cells were resuspended in CGXII medium and used to inoculate the main culture (flask or FlowerPlate, see below) to a start OD_{600} (optical density at a wavelength of 600 nm) of 1. To follow the growth *via* determination of $OD_{600,}$ a spectrophotometer (ULTROSPEC® 10, Biochrom, Holliston, MA, United States) was used, diluting the samples into a range of 0.1–0.3 OD_{600} units. The cell dry weight (CDW) in gL^{-1} was calculated by the conversion factor 0.23 × OD_{600}. The growth rate (h^{-1}) was determined *via* linear regression in a semi-logarithmic blot by maximizing the coefficient of determination (R^2) in the exponential phase. Additionally, a microbioreactor system (BioLector® I, m2p-labs GmbH, Baesweiler, Germany) for microliter scale cultivation was employed. The seed train was the same as described above but using a cultivation volume of 1 ml in a 48-well FlowerPlate (product no: MTP-48-B; m2p-labs GmbH, Baesweiler, Germany) covered with a gas permeable sealing foil (product no: F-GP-10; m2p-labs GmbH, Baesweiler, Germany). The process parameters were set to 30°C, 85% humidity, and 1,000 rpm shaking frequency. The growth was followed by measurement of the backscatter light at 620 nm with a gain of 20. In all cultivation experiments 1-mL samples were taken at the time points given in the results and centrifuged (10 min; 21300 × g) and the resulting supernatants were stored at −20°C until further analysis.

Recombinant DNA Work and Construction of *C. glutamicum* Insertion Mutant

All oligonucleotides used in this study were purchased from Sigma-Aldrich Chemie GmbH (Steinheim, Germany) and are listed in **Table 2**. For purification of PCR products and isolation of plasmid and genomic DNA, the kit systems "NucleoSpin® Gel and PCR Clean-up," "NucleoSpin® Plasmid," and "NucleoSpin® Microbial DNA" were employed, respectively, as recommended by the manufacturer MACHEREY-NAGEL GmbH & Co. KG (Düren, Germany). All enzymes were purchased from New England Biolabs GmbH [(NEB), Frankfurt am Main, Germany] and the appropriate reactions were carried out as recommended by NEB. For the construction of pK19*mobsacB*-ΔP_{aceE}::*vanR*-P_{vanABK}* the flanking regions were PCR-amplified from the genomic DNA of *C. glutamicum* with the primer pairs #1 + #2 and #3 + #4 and the fragment containing the native gene *vanR* with its native promotor and the optimized *vanABK* promotor sequence from pJOE7747.1 with the primer pair #5 + #6 *via* Phusion® High-Fidelity DNA Polymerase. These fragments were cloned into SmaI-linearized pK19*mobsacB* via Gibson assembly (Gibson, 2011), preparing the assembly master mix in-house with purchased enzymes and applying the assembled plasmid for transformation of *E. coli* DH5α with the calcium chloride method (Green and Sambrook, 2012). Positive clones were identified by colony PCR using the QuickLoad® Taq 2X Master Mix adding primers #7 + #8, and the purified plasmids were further validated by restriction enzyme digestion with KpnI and sequencing of the inserted fragments *via* "TubeSeq Service" at Eurofins Genomics (Ebersberg, Germany). The plasmid pK19*mobsacB*-ΔP_{aceE}::*vanR*-P_{vanABK}* was then used for transformation of electrocompetent *C. glutamicum* wild-type cells (Tauch et al., 2002) *via* electroporation (van der Rest et al., 1999). The integration of the plasmid was tested phenotypically *via* kanamycin resistance and sucrose sensitivity on 2x TY agar plates, and the whole recombination procedure *via* double cross-over events was carried out as described previously (Schäfer et al., 1994). The successful exchange of the *aceE* promotor sequence against the native *vanR* with its native promotor and the optimized *vanABK* promotor sequence in the *C. glutamicum* wild-type background was proven *via* colony PCR applying primer pair #12 + #13 and further confirmed by "TubeSeq Service" as described above, providing the purified product from the colony PCR for sequencing. The resulting strain *C. glutamicum*ΔP_{aceE}::*vanR*-P_{vanABK}* was further modified by transformation with pJC4 (Cordes et al., 1992) or pJC4-*ilvBNCE* (Radmacher et al., 2002), confirming the presence of the appropriate plasmid *via* colony PCR with primer pair #17 + #18 or #16 + #17, respectively.

HPLC Measurement

In this study, the concentration of all compounds besides that of biomass were determined *via* high-performance liquid chromatography (HPLC) employing a 1260 Infinity II system (Agilent Technologies, Waldbronn, Germany). All columns were purchased from Agilent Technologies and only HPLC-grade solvents were used. In the case of glucose and pyruvate measurements, the system was equipped with a Hi-Plex H column (7.7 × 300 mm, 8 μm) protected by a Hi-Plex H guard cartridge (3 × 5 mm, 8 μm) hold at 50°C. The isocratic, mobile phase was 5 mM sulfuric acid (H_2SO_4) in water with a flow rate of 0.4 mL min^{-1}. The signals were acquired *via* refractive index detector (RID) hold at 50°C. This method (Ball et al., 2011) was adapted from the manufacturer Agilent Technologies as well as the procedure for the analysis of the primary amino acids alanine and valine (Agilent Technologies, 2020). Therefore, an AdvanceBio Amino Acid Analysis (AAA)

TABLE 2 | Oligonucleotides used in this study.

#	Name	Sequence (5′→ 3′)
1	Pace_ex_upstrm_fw_pK19	*GTCGACTCTAGAGGATCCCCG*CCTCGAAAGCAACGAGTGAAATA
2	Pace_ex_upstrm_rv	*CAAAGCTGTAGACGCATGCA*GCTCACTGGGATTTCAGGTATCC
3	Pace_ex_dwnstrm_fw	*TAGTTCTTTAGGAGTTCCAT*ATGGCCGATCAAGCAAAACTTG
4	Pace_ex_dwnstrm_rv_pK19	*TGAATTCGAGCTCGGTACCC*GTGCACCATCCTGGTCCTTC
5	vanRP_fw_Pace_ex	*TACCTGAAATCCCAGTGAGC*TGCATGCGTCTACAGCTTTGATAC
6	vanRP_rv_Pace_ex	*AGTTTTGCTTGATCGGCCAT*ATGGAACTCCTAAAGAACTATATAACCAAATACCT
7	pK19lacZ_fw	ATGACCATGATTACGCCAAGCTTG
8	pK19lacZ_rv	TTAGCAGCCCTTGCGCC
9	pK19lacI_fw	TCAGTGAGCGAGGAAGCG
10	aceP_ex_fw_2	CGGAGCGTCGGCCAC
11	aceP_ex_rv	GGTGATGCGTGGCCCTG
12	vanRP_fw_Pace_ex_2	TTTTCTCATGCATACCCAATGCGTAC
13	vanRP_rv_Pace_ex_2	AGCTCGCTTGTAGGCTGC
14	vanR_fw	GTGGGCTTTGTGTGGAGTGG
15	vanR_rv	CTAAAGGGTATCGAGTAGTTTCAAGCC
16	fw_ilvC-2_seq	GAGTTCGGTGGCTACCTC
17	fw_pJC4_seq	CGATTGAAGACCGTCAAC
18	rev_pJC4_seq	GTCATCAGACCAAGGAG

Italic letters: Overlapping sequence for Gibson assembly.

column (4.6 × 100 mm, 2.7 μm) protected by an AdvanceBio AAA guard column (4.6 × 5 mm, 2.7 μm) was installed and heated to 40°C. The separation was carried out *via* a gradient with an aqueous, polar phase (10 mM Na_2HPO_4, 10 mM Na_2B_4O7, pH 8.2) and a non-polar phase (45 vol% acetonitrile, 45 vol% methanol, 10 vol% water). For detection of the primary amino acids, an automated online derivatization with *ortho*-phthaldialdehyde (OPA) was conducted, and signals were acquired *via* fluorescence detector (FLD) at an excitation wavelength of 340 nm, an emission wavelength of 450 nm, and a PMT gain of 10. As internal standard, 100 μM norvaline was added to each sample. The measurement of the phenolic compounds FA, Van, and VA was adapted from Mollerup Andersen and Batsberg Pedersen (1983) and Merkens et al. (2005) using the same column described in the amino acids analysis. For the separation, a gradient from 95% 30 mM formic acid in water decreasing to 65% within 15 min was adjusted, applying as second phase pure methanol with an overall constant flow rate of 1 mL min^{-1}. FA and Van were detected at 280 nm and VA at 264 nm in a diode-array detector (DAD). For all HPLC analysis peak detection, integration and calculation of the final concentrations were carried out with the software "OpenLab CDS ChemStation Edition Rev. C.01.10 [236]" (Agilent Technologies, Waldbronn, Germany), which was also employed for the instrument controls. For the calibration curves, external reference standards were prepared for each compound ranging from 1 to 200 mM with seven points (glucose and pyruvate), 10 to 400 μM with seven points (alanine and valine), or 0.01 to 25 mM with 11 points (phenolics). Sample preparation was carried out by thawing of the supernatants, additional centrifugation (10 min; 21300 × g) and transfer of the resulting supernatants into HPLC glass vials. The samples were diluted if appropriate.

RESULTS

Influence of the Phenolic Compounds Ferulic Acid, Vanillin, and Vanillic Acid on Growth of *C. glutamicum*

While the general ability to utilize ferulic acid, vanillin, and vanillic acid as sole carbon source for growth was already shown (Merkens et al., 2005; Brinkrolf et al., 2006), we aimed at first to investigate which concentrations of these potential antimicrobial compounds may hamper the growth of the *C. glutamicum* wild type. We cultivated the wild type strain in a microliter scale (Biolector® I, M2PLabs, Baesweiler, Germany) with the CGXII minimal medium and 20 g glucose L^{-1} supplemented with different concentrations of FA, Van, and VA. Interestingly, FA and Van at concentrations up to 10 mM did not inhibit growth (**Figure 2**). In contrast, low concentrations (0–5 mM) of both phenolic compounds even increased the growth rate by maximal 24 and 27%, respectively. Only at 10 and 20 mM of FA and Van growth was negatively affected. VA showed the strongest inhibitory effect with 2 mM already leading to a decrease of 30% in the growth rate. While the finally reached backscatter values were almost the same, the lag phase was prolonged with higher concentrations of the supplemented substances (**Supplementary Figure 1**). Based on these results, we conducted the characterization of the strain *C. glutamicum* ΔP_{aceE}::*vanR*-P_{vanABK}* with concentration up to 10 mM for all the three compounds.

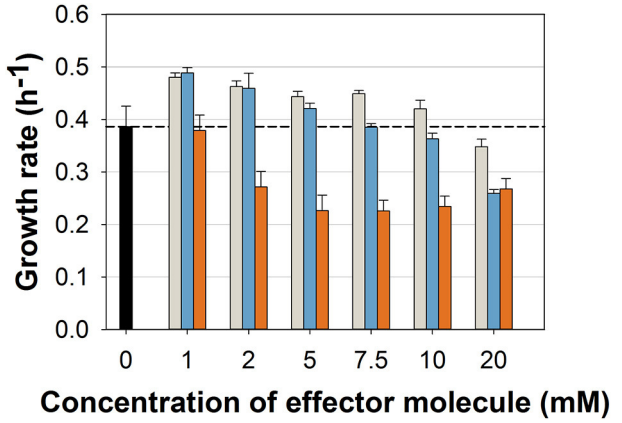

FIGURE 2 | Growth rates of *C. glutamicum* wild type in microliter scale cultivations with CGXII minimal medium and 20 g glucose L^{-1} without (black) and with different concentrations of ferulic acid (gray), vanillin (blue), and vanillic acid (orange). Black dashed line indicates mean growth rate of the wild type without any effector molecule. Growth rate was determined for all cultivations between 20 and 400 backscatter units *via* linear regression in a semi-logarithmic plot (**Supplementary Figure 1**). Error bars represent standard deviation of at least three cultivations.

Adjusting Growth of *C. glutamicum* ΔP_{aceE}::*vanR*-P_{vanABK}* With the Effectors Ferulic Acid, Vanillin, and Vanillic Acid

To test the suitability of the VanR/P_{vanABK}* regulatory system to dynamically control the gene expression in *C. glutamicum*, we constructed *C. glutamicum* ΔP_{aceE}::*vanR*-P_{vanABK}* *via* exchange of the native *aceE* promotor by P_{vanABK}*(Morabbi Heravi et al., 2015) and an additional copy of *vanR* (**Figure 1**). P_{vanABK}* carries a single point mutation in the −10 region (CAATAT → TAATAT) leading to a 73-fold induction compared with its native version (Morabbi Heravi et al., 2015) and we anticipated that the regulatory circuit drives *aceE* expression as long as the effector molecule is present in the medium. After utilization, growth should arrest due to the abolished *aceE* expression and, consequently, the loss of PDHC activity. *C. glutamicum* ΔP_{aceE}::*vanR*-P_{vanABK}* was cultivated in a microliter scale (Biolector® I, M2PLabs, Baesweiler, Germany) with the CGXII minimal medium and 20 g glucose L^{-1} supplemented with 0–10 mM of the potential effector molecules FA, Van, and VA. Without an effector in the medium, *C. glutamicum* ΔP_{aceE}::*vanR*-P_{vanABK}* showed negligible growth (**Supplementary Figure 2**). In the presence of the phenolic compounds, we observed a linear correlation between the introduced effector concentration and the finally reached biomass, but equimolar amounts led to different reads in the backscatter (**Figures 3A–C**;

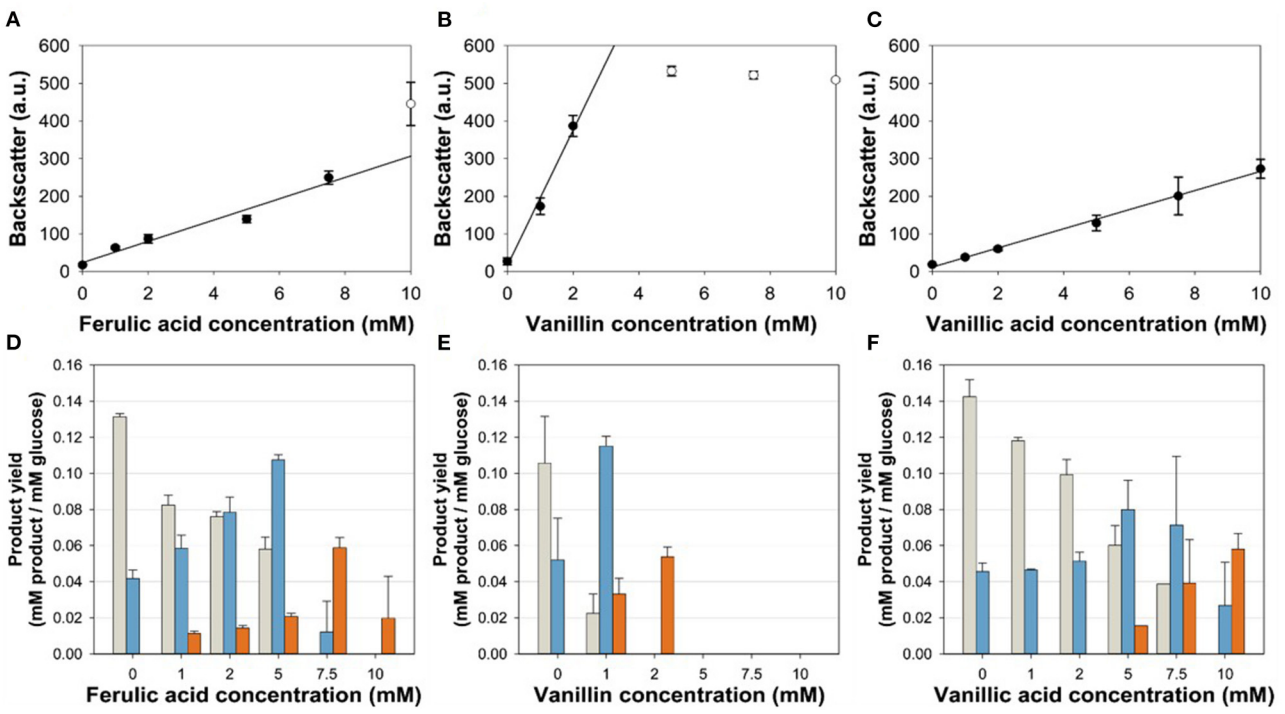

FIGURE 3 | (A,C) Correlation of the final backscatter against the effector molecule concentration of *C. glutamicum* ΔP_{aceE}::*vanR*-P_{vanABK}* in microliter scale cultivations with CGXII minimal medium and 20 g glucose L^{-1} with different concentrations of **(A)** ferulic acid ($m = 28$ backscatter units/mM; $R^2 = 0.966$), **(B)** vanillin ($m = 180$ backscatter units/mM; $R^2 = 0.989$), and **(C)** vanillic acid ($m = 25$ backscatter units/mM; $R^2 = 0.996$). Black line represents linear regression of black dots, while empty dots are excluded from this regression. **(D–F)** Product yields of the aforementioned cultivations for pyruvate (gray), alanine (blue), and valine (orange). Error bars represent standard deviation of at least three cultivations.

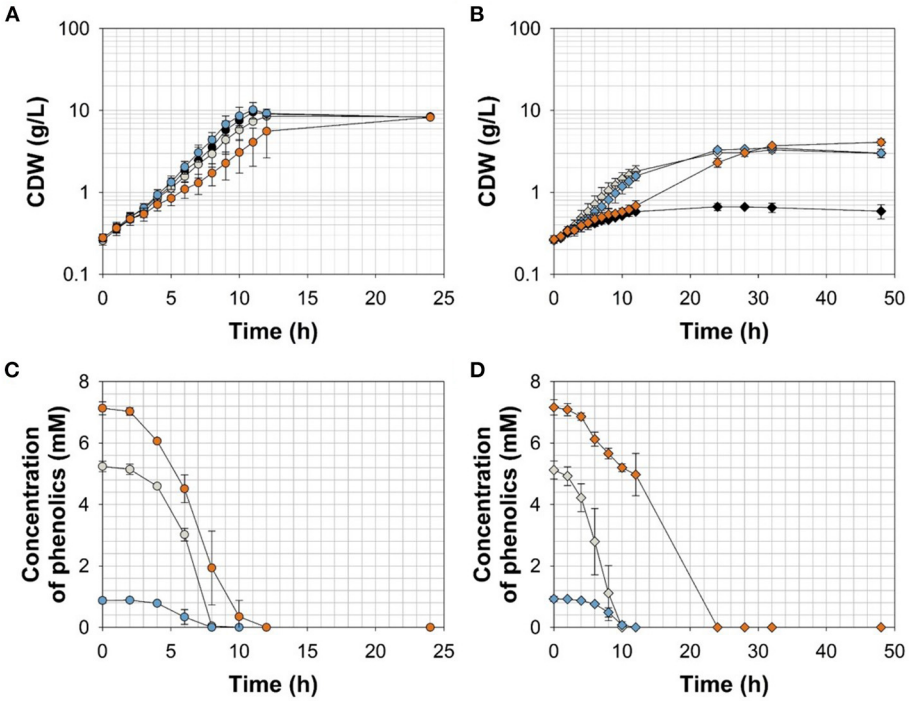

FIGURE 4 | (A,B) Growth and **(C,D)** effector molecule consumption of *C. glutamicum* wild type (circles) and *C. glutamicum* ΔP_{aceE}::*vanR*-P_{vanABK}* (diamonds) in shaking flasks with CGXII minimal medium and 20 g glucose L^{-1} without (black) and with ferulic acid (gray), vanillin (blue), or vanillic acid (orange). Error bars represent standard deviation of cultivations of at least three biological replicates.

Supplementary Figure 2). While Van concentration >2 mM was already sufficient to reach final biomass comparable to the wild type (**Supplementary Figures 1**, **2**), >7.5 mM FA was required and even 10 mM VA was not enough. No growth occurred for this mutant strain if PCA was added as effector molecule in the same concentration range (data not shown). The cell cultures were harvested at the end of the cultivation and the supernatants were analyzed by HPLC to determine the amounts of glucose and the three metabolites pyruvate, alanine, and valine. The product yields for all three metabolites showed a strong dependence on the applied effector molecule concentration. With increasing effector concentrations, the product spectrum shifted from pyruvate over alanine to valine, and at about half-maximal biomass concentration, highest cumulated product yields were observed (**Figures 3D–F**).

Kinetic Analysis of *C. glutamicum* ΔP_{aceE}::*vanR*-P_{vanABK}* and the Wild Type

To further resolve the kinetics of growth and product formation in dependence of the effector molecules, we cultivated *C. glutamicum* ΔP_{aceE}::*vanR*-P_{vanABK}* and the wild type in CGXII minimal medium with 20 g glucose L^{-1} at effector concentrations, which yielded around half of the maximal biomass concentration in comparison with the outgrown wild type. Thus, 5 mM FA, 1 mM Van, and 7.5 mM VA were applied (**Figure 4**; **Table 3**). The *C. glutamicum* wild type showed a growth rate of 0.35, 0.31, 0.39, and 0.23 h^{-1} in the medium without and with FA, Van, and VA (**Figure 4A**; **Table 3**), which is in accordance with the microscale cultivations (**Figure 2**). Furthermore, in the exponential growth phase, all the three phenolic compounds were consumed completely and in parallel to glucose (**Figure 4C**; **Supplementary Figure 3A**), which led to increased glucose-specific biomass yields correlating to the amount of additional carbon source provided by the phenolic compounds (**Table 3**). *C. glutamicum* did not secrete pyruvate, alanine, or valine into the culture broth. Interestingly, we observed the temporary accumulation of traces of VA in cultivations with FA (up to 0.1 mM VA) and Van (up to 0.03 mM VA; data not shown). *C. glutamicum* ΔP_{aceE}::*vanR*-P_{vanABK}* showed 40–60% decreased growth rates compared with the wild type in the presence of the respective phenolic compounds and negligible growth without an effector (**Figure 4B**; **Table 3**). Furthermore, applying the correlation from the microscale cultivation (**Figures 3A–C**) allowed to adjust the final biomass concentration and the cells grew only until the effector molecule was fully depleted (**Figures 4B,D**). Although growth ceased, the cells remained metabolically active and started to secrete pyruvate, alanine, and valine (**Supplementary Figures 3B–D**; **Table 3**) and the reached product yields (**Table 3**) are in good accordance with the microliter scale experiments (**Figures 3D–F**). Also, the temporary accumulation of traces of VA, as described for the wild type, could be observed if the strain *C. glutamicum* ΔP_{aceE}::*vanR*-P_{vanABK}* was cultivated with

TABLE 3 | Growth rates, biomass yields, and product yields of *C. glutamicum* wild type, *C. glutamicum* ΔP_{aceE}::*vanR*-P_{vanABK}*, and *C. glutamicum* ΔP_{aceE}::*vanR*-P_{vanABK}* (pJC4-*ilvBNCE*) in shaking flasks with CGXII minimal medium and 20 g glucose L^{-1} without and with ferulic acid, vanillin, or vanillic acid. Standard deviation was determined *via* cultivations of at least three biological replicates.

Concentration of effector molecule (mM)	Growth rate μ (h^{-1})	Biomass yield ($g_{CDW}/g_{glucose}$)	Pyruvate yield ($mol/mol_{glucose}$)	Alanine yield ($mol/mol_{glucose}$)	Valine yield ($mol/mol_{glucose}$)
***C. glutamicum* wild type**					
–	0.35 ± 0.01	0.47 ± 0.01	b.d.	b.d.	b.d.
FA (5.2 ± 0.2)	0.31 ± 0.03	0.52 ± 0.02	b.d.	b.d.	b.d.
Van (0.9 ± 0.1)	0.39 ± 0.01	0.50 ± 0.04	b.d.	b.d.	b.d.
VA (7.1 ± 0.2)	0.23 ± 0.04	0.58 ± 0.03	b.d.	b.d.	b.d.
C. glutamicum* ΔP_{aceE}::*vanR*-P_{vanABK}					
–	n.d.	n.d.	0.18 ± 0.02	0.07 ± 0.01	b.d.
FA (5.1 ± 0.3)	0.19 ± 0.03	0.58 ± 0.09	0.08 ± 0.05	0.11 ± 0.02	0.01 ± 0.01
Van (0.9 ± 0.1)	0.16 ± 0.01	0.40 ± 0.01	0.06 ± 0.02	0.10 ± 0.01	0.02 ± 0.01
VA (7.2 ± 0.2)	0.10 ± 0.02	0.34 ± 0.03	0.07 ± 0.06	0.09 ± 0.01	0.02 ± 0.01
***C. glutamicum* ΔP_{aceE}::*vanR*-P_{vanABK}* (pJC4-*ilvBNCE*)**					
–	n.d.	n.d.	0.10 ± 0.05	0.04 ± 0.01	0.27 ± 0.03
FA (4.9 ± 0.1)	0.17 ± 0.01	0.52 ± 0.01	b.d.	0.02 ± 0.01	0.36 ± 0.02
Van (1.0 ± 0.1)	0.14 ± 0.02	0.34 ± 0.03	0.02 ± 0.03	0.03 ± 0.01	0.38 ± 0.01
VA (7.3 ± 0.1)	0.08 ± 0.01	0.38 ± 0.06	0.03 ± 0.05	0.03 ± 0.01	0.35 ± 0.04

b.d., below detection limit; n.d., not determined.

FA (up to 0.5 mM VA) and Van (up to 0.02 mM VA; data not shown).

Dynamically Induced Valine Production With *C. glutamicum* ΔP_{aceE}::*vanR*-P_{vanABK}* Overexpressing *ilvBNCE*

To channel the carbon flux more efficiently from pyruvate toward valine, we transformed *C. glutamicum* ΔP_{aceE}::*vanR*-P_{vanABK}* with the plasmid pJC4-*ilvBNCE* (Radmacher et al., 2002) to overexpress the valine biosynthesis genes *ilvBNCE* encoding acetohydroxyacid synthase (*ilvBN*), isomeroreductase (*ilvC*), and transaminase B (*ilvE*). *C. glutamicum* ΔP_{aceE}::*vanR*-P_{vanABK}* (pJC4-*ilvBNCE*) and the control strain *C. glutamicum* ΔP_{aceE}::*vanR*-P_{vanABK}* (pJC4) were cultivated in shaking flasks with CGXII minimal medium and 20 g glucose L^{-1} supplemented with 5 mM FA, 1 mM Van, and 7.5 mM VA (**Figure 5**; **Table 3**). Under the conditions tested, *C. glutamicum* ΔP_{aceE}::*vanR*-P_{vanABK}* and its plasmid carrying derivatives showed very similar growth and consumption of glucose and the phenolic compounds, and all the strains induced production after consumption of the respective effector molecule (**Figures 5A**, **4B**; **Supplementary Figures 5**, **6**; **Table 3**). *C. glutamicum* ΔP_{aceE}::*vanR*-P_{vanABK}* and the derivative with the empty vector secreted similar amounts of pyruvate, alanine, and valine into the medium (**Supplementary Figures 3B–D, 6C,E**). However, overexpression of the *ilvBNCE* genes in *C. glutamicum* ΔP_{aceE}::*vanR*-P_{vanABK}* shifted the product spectrum toward valine. In the medium containing FA, Van, or VA *C. glutamicum* ΔP_{aceE}::*vanR*-P_{vanABK}* (pJC4-*ilvBNCE*) produced 40 ± 3.6, 40.6 ± 1.7, and 29.3 ± 7.1 mM valine after 48 h with a product yield of 0.36 ± 0.02, 0.38 ± 0.01, and 0.35 ± 0.04 mol valine per mol glucose (**Figure 5B**; **Table 3**). The concentration of pyruvate and alanine was, under all conditions, below 5 mM over the whole cultivation time (**Supplementary Figures 4B,C**).

DISCUSSION

In this study, the VanR/P_{vanABK}* regulatory system was utilized to dynamically control gene expression in *C. glutamicum*. We applied this circuit to switch off the *aceE* expression in a timed manner when the lignin-derived effectors FA, Van, and VA were depleted from the medium. Finally, we showed the feasibility of this approach to adjust biomass formation and to induce the production of valine.

The ability of *C. glutamicum* to tolerate higher concentrations of aromatics than other bacteria was already described (Shen et al., 2012; Morabbi Heravi et al., 2015; Becker and Wittmann, 2019) as well as to utilize the phenolic compounds FA, Van, and VA as sole carbon sources (Merkens et al., 2005; Brinkrolf et al., 2006; Shen et al., 2012; Kallscheuer et al., 2016). Here, we show that these molecules are also co-utilized with glucose (**Figure 4C**; **Supplementary Figure 3A**; **Table 3**), which is a promising feature of *C. glutamicum* with regard to the application of lignocellulosic hydrolysates as feedstock for industrial biotechnology. While minimum inhibitory concentrations (MIC) for the phenolic compounds tested in this study range for *E. coli* between 0.5 and 15 mM (Fitzgerald et al., 2004; Mourtzinos et al., 2009; Borges et al., 2013), *C. glutamicum* still shows, in the presence of up to 20 mM of each molecule, about 67–90% growth rate compared with reference conditions (**Figure 2**). Remarkably, low concentrations (up to 2 mM) of FA and Van significantly (p-value $\leq$ 0.01) increased the growth rate of *C. glutamicum* (**Figure 2**). It is known that diphenolic compounds, such as catechol or PCA,

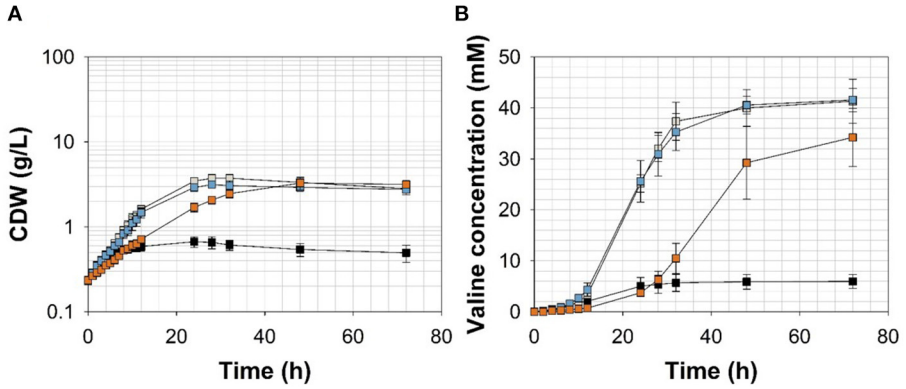

FIGURE 5 | (A) Growth and **(B)** valine accumulation in the supernatant of *C. glutamicum* ΔP_{aceE}::*vanR*-P_{vanABK}*(pJC4-*ilvBNCE*) in shaking flasks with CGXII minimal medium (with 20 g ammonium sulfate L^{-1}) and 20 g glucose L^{-1} without (black) and with ferulic acid (gray), vanillin (blue), or vanillic acid (orange) (for detailed concentration of effector molecules see **Supplementary Figure 5**; **Table 3**). Error bars represent standard deviation of cultivations of at least three biological replicates.

facilitate the growth of *C. glutamicum* (Liebl et al., 1989). Recently, it has been shown that this effect is based on the potential of diphenols, with two adjacent hydroxyl groups or a mix of amino and hydroxyl groups, to chelate iron and/or reduce Fe_3^+, thus improving the overall iron availability (Müller et al., 2020). If the positive effect of FA and Van is directly mediated by these molecules or if it is the effect of the degradation intermediate PCA (Brinkrolf et al., 2006; Shen et al., 2012; Kallscheuer et al., 2016) remains to be investigated. For VA, no positive effect on growth was observed at the applied concentrations (**Figure 2**). In general, VA has a much higher antimicrobial potential, especially in comparison with Van (Mourtzinos et al., 2009). Thus, it has to be tested if lower concentrations (<1 mM) of VA have a growth-promoting effect.

All the three phenolic compounds proved suitability to induce the VanR/P_{vanABK}* regulatory circuit, providing flexibility with regard to the intended application. However, since 2 mM VA already reduced the growth rate of the *C. glutamicum* wild type significantly (**Figure 2**; *p*-value $\leq$0.01), Van and FA are the preferred inducer molecules. VA, FA, and Van, compared with common inducers such as IPTG or rhamnose, are cheaper and abundant, since these molecules can be derived from lignocellulosic material. Therefore, VA, FA, and Van are, in principle, well-suited for industrial application if the main substrate of the process is not a lignocellulosic hydrolysate containing significant amounts of effector molecules. Future studies have to evaluate if the VanR/P_{vanABK}* regulatory circuit can be applied in large scale as well as in other hosts. As a prerequisite, the microbial system of choice should show considerable tolerance against the aromatic inducer molecules such as *Pseudomonads* (Becker and Wittmann, 2019). Moreover, if applied as synthetic off-switch, the organism should be able to metabolize the inducer molecules and its metabolism should not be under control of catabolite repression, which might result in inducer exclusion.

The final biomass of *C. glutamicum* ΔP_{aceE}::*vanR*-P_{vanABK}* correlated directly with the applied amount of effector molecule. FA and VA showed almost identical slopes of the linear regression, while Van yielded an about 7-fold higher slope, i.e., seven times less Van has to be added to the culture in order to achieve the same biomass as with VA or FA (**Figures 3A–C**). The reason for this effect remains unclear, especially since in cultivations with FA and Van small amounts of the VanR effector VA were secreted into the medium, indicating a limitation in the conversion of VA to PCA catalyzed by vanillate demethylase VanAB. While biochemical data for VanAB are not available yet specifically for *C. glutamicum*, it is known that this enzyme complex shares significant similarity to VanABs of other microorganisms such as *Pseudomonas* species (Merkens et al., 2005; Brinkrolf et al., 2006), where it is described to convert VA to PCA, demanding NAD(P)H_2 plus molecular oxygen and releasing NAD(P), water, and formaldehyde, which has to be further detoxified (Priefert et al., 1997; Hibi et al., 2005). This energy- and oxygen-demanding reaction, along with the release of formaldehyde, is a good indicator for the strict regulation of VanABK in *C. glutamicum* (Merkens et al., 2005; Brinkrolf et al., 2006; Morabbi Heravi et al., 2015).

The PDHC of *C. glutamicum* is a promising target for metabolic engineering (Eikmanns and Blombach, 2014), and it has been shown that the PDHC-deficient strain *C. glutamicum* Δ*aceE* is unable to grow on glucose unless supplemented with acetate (Schreiner et al., 2005). This feature has been utilized to adjust biomass formation over the provided amount of acetate. After its depletion, the growth of *C. glutamicum*Δ*aceE* stopped, but the cells remained metabolically active and started to produce pyruvate, alanine, and valine from glucose (Blombach et al., 2007). More recently, Wiechert et al. (2020) designed an inducible metabolic toggle switch, which efficiently controls the *aceE* expression by the effector molecule gluconate. However, compared with acetate as well as gluconate as inducers, at least 50 times lower molar amounts of Van have to be introduced into the process to achieve similar biomass concentrations (Blombach et al., 2007; Wiechert et al., 2020).

Compared with *C. glutamicum* P_{gntK}-*aceE* (Wiechert et al., 2020), *C. glutamicum* ΔP_{aceE}::*vanR*-P_{vanABK}* showed an around 50% slower growth rate with Van and FA, indicating further potential to optimize the VanR/P_{vanABK}* system. Data relating the promotor strength of P_{aceE}, P_{vanABK}*, and P_{gntK} under comparable conditions are not available. However, while the ribosomal binding site "AGGAG" was utilized in the promoter regions of P_{gntK} and P_{vanABK}* (Wiechert et al., 2020), the spacer regions are quite different, potentially impacting gene expression (Schneider et al., 2012).

In microliter cultivations, the product pattern of *C. glutamicum* ΔP_{aceE}::*vanR*-P_{vanABK}* (**Figures 3D–F**) shifted from pyruvate over alanine to valine with increasing effector and final biomass concentrations. This effect was observed for all three phenolic compounds, indicating biomass-dependent metabolic changes, which promote valine synthesis. However, to channel the carbon flux toward valine, plasmid-based overexpression of the valine biosynthesis genes *ilvBNCE* was more efficient. *C. glutamicum* ΔP_{aceE}::*vanR*-P_{vanABK}* (pJC4-*ilvBNCE*) showed product yields of about 0.36 mol valine per mol glucose, which are about 6-fold higher compared with the yields of *C. glutamicum* ΔP_{aceE}::*vanR*-P_{vanABK}* at optimal effector concentrations (**Figures 3D–F**; **Table 3**). Although the glucose-based product yield of *C. glutamicum* ΔP_{aceE}::*vanR*-P_{vanABK}* (pJC4-*ilvBNCE*) is considerably lower in comparison with 0.47 mol valine per mol glucose of *C. glutamicum*Δ*aceE* (pJC4-*ilvBNCE*) and 0.52 mol valine per mol glucose of *C. glutamicum* P_{gntK}-*aceE* (pJC4-P_{ilvB}-*ilvBNC*-P_{ilvE}-*ilvE*), the overall yield (including the amount of effector) of 0.36 C-mol per C-mol of *C. glutamicum* ΔP_{aceE}::*vanR*-P_{vanABK}* (pJC4-*ilvBNCE*) with Van is at least identical to the latter two strains with values of 0.32 and 0.36 C-mol per C-mol, respectively (Blombach et al., 2007; Wiechert et al., 2020).

Concluding, this study shows the suitability of the VanR/P_{vanABK}* system as a tool to control gene expression in *C. glutamicum*. The regulatory circuit can be toggled by the cheap and abundant lignin-derived phenolic compounds FA, Van, and VA. Since these three molecules are consumed in parallel to the main substrate glucose, the regulatory circuit represents a valuable genetic control element to adjust gene expression on demand.

DATA AVAILABILITY STATEMENT

The original contributions presented in the study are included in the article/**Supplementary Material**. Further inquiries can be directed to the corresponding author/s.

AUTHOR CONTRIBUTIONS

DS and BB conceived and supervised the study and designed the experiments. DS performed the experiments and analyzed the data. DS, JA, and BB wrote the manuscript. All authors contributed to the article and approved the submitted version.

ACKNOWLEDGMENTS

We thank Marie-Theres Wirth for supporting the cloning work, Sebastian Roth for his assistance in the HPLC analysis, and Dr. Felix Thoma for his expertise in the fields of phenolic compounds and *C. glutamicum*.

SUPPLEMENTARY MATERIAL

The Supplementary Material for this article can be found online at: https://www.frontiersin.org/articles/10.3389/fbioe.2021.704681/full#supplementary-material

REFERENCES

Abe, S., Takayama, K.-I., and Kinoshita, S. (1967). Taxonomical studies on glutamic acid-producing bacteria. *J. Gen. Appl. Microbiol.* 13, 279–301. doi: 10.2323/jgam.13.279

Agilent Technologies (2020). *Agilent Biocolumns: Amino Acid Analysis. "How-To" Guide*. Available online at: https://www.agilent.com/cs/library/brochures/5991-7694EN_AdvanceBio%20AAA_How-To%20Guide_LR.pdf (accessed March 29, 2021).

Ball, S., Bullock, S., Lloyd, L., and Mapp, K. (2011). *Agilent Hi-Plex Columns Applications Compendium*. Available online at: https://www.agilent.com/cs/library/applications/5990-8801EN%20Hi-Plex%20Compendium.pdf (accessed March 29, 2021).

Baumschlager, A., Rullan, M., and Khammash, M. (2020). Exploiting natural chemical photosensitivity of anhydrotetracycline and tetracycline for dynamic and setpoint chemo-optogenetic control. *Nat. Comm.* 11:3834. doi: 10.1038/s41467-020-17677-5

Becker, J., Rohles, C. M., and Wittmann, C. (2018). Metabolically engineered *Corynebacterium glutamicum* for bio-based production of chemicals, fuels, materials, and healthcare products. *Metab. Eng.* 50, 122–141. doi: 10.1016/j.ymben.2018.07.008

Becker, J., and Wittmann, C. (2019). A field of dreams: Lignin valorization into chemicals, materials, fuels, and health-care products. *Biotechnol. Adv.* 37:107360. doi: 10.1016/j.biotechadv.2019.02.016

Blombach, B., and Eikmanns, B. J. (2011). Current knowledge on isobutanol production with *Escherichia coli*, *Bacillus subtilis* and *Corynebacterium glutamicum*. *Bioeng. Bugs.* 2, 346–350. doi: 10.4161/bbug.2.6.17845

Blombach, B., Riester, T., Wieschalka, S., Ziert, C., Youn, J.-W., Wendisch, V. F., et al. (2011). *Corynebacterium glutamicum* tailored for efficient isobutanol production. *Appl. Environ. Microb.* 77, 3300–3310. doi: 10.1128/AEM.02972-10

Blombach, B., Schreiner, M. E., Holátko, J., Bartek, T., Oldiges, M., and Eikmanns, B. J. (2007). L-valine production with pyruvate dehydrogenase complex-deficient *Corynebacterium glutamicum*. *Appl. Environ. Microb.* 73, 2079–2084. doi: 10.1128/AEM.02826-06

Borges, A., Ferreira, C., Saavedra, M. J., and Simões, M. (2013). Antibacterial activity and mode of action of ferulic and gallic acids against pathogenic bacteria. *Microb. Drug. Resist.* 19, 256–265. doi: 10.1089/mdr.2012.0244

Brautaset, T., Lale, R., and Valla, S. (2009). Positively regulated bacterial expression systems. *Microb. Biotechnol.* 2, 15–30. doi: 10.1111/j.1751-7915.2008.00048.x

Brinkrolf, K., Brune, I., and Tauch, A. (2006). Transcriptional regulation of catabolic pathways for aromatic compounds in *Corynebacterium glutamicum*. *Genet. Mol. Res* 5, 773–789.

Buchholz, J., Graf, M., Blombach, B., and Takors, R. (2014). Improving the carbon balance of fermentations by total carbon analyses. *Biochem. Eng. J.* 90, 162–169. doi: 10.1016/j.bej.2014.06.007

Burkovski, A. (ed.). (2008). *Corynebacteria: Genomics and Molecular Biology*. Wymondham: Caister Academic.

Cardoso, V. M., Campani, G., Santos, M. P., Silva, G. G., Pires, M. C., Gonçalves, V. M., et al. (2020). Cost analysis based on bioreactor cultivation conditions: Production of a soluble recombinant protein using *Escherichia coli* BL21(DE3). *Biotechnol. Rep.* 26:e00441. doi: 10.1016/j.btre.2020.e00441

Chaudhry, M. T., Huang, Y., Shen, X.-H., Poetsch, A., Jiang, C.-Y., and Liu, S.-J. (2007). Genome-wide investigation of aromatic acid transporters in *Corynebacterium glutamicum*. *Microbiology* 153, 857–865. doi: 10.1099/mic.0.2006/002501-0

Cordes, C., Möckel, B., Eggeling, L., and Sahm, H. (1992). Cloning, organization and functional analysis of *ilvA*, *ilvB* and *ilvC* genes from *Corynebacterium glutamicum*. *Gene* 112, 113–116. doi: 10.1016/0378-1119(92)90311-C

Ding, W., Si, M., Zhang, W., Zhang, Y., Chen, C., Zhang, L., et al. (2015). Functional characterization of a vanillin dehydrogenase in *Corynebacterium glutamicum*. *Sci. Rep.* 5:8044. doi: 10.1038/srep08044

Eggeling, L., and Bott, M. (eds.). (2005). *Handbook of Corynebacterium glutamicum*. Boca Raton, FL: CRC Press.

Eikmanns, B. J., and Blombach, B. (2014). The pyruvate dehydrogenase complex of *Corynebacterium glutamicum*: an attractive target for metabolic engineering. *J. Biotechnol.* 192 (Pt B0, 339–345. doi: 10.1016/j.jbiotec.2013.12.019

Ferreira, R., d,. G., Azzoni, A. R., and Freitas, S. (2018). Techno-economic analysis of the industrial production of a low-cost enzyme using *E. coli*: the case of recombinant β-glucosidase. *Biotechnol. Biofuels*. 11:81. doi: 10.1186/s13068-018-1077-0

Fitzgerald, D. J., Stratford, M., Gasson, M. J., Ueckert, J., Bos, A., and Narbad, A. (2004). Mode of antimicrobial action of vanillin against *Escherichia coli*, *Lactobacillus plantarum* and *Listeria innocua*. *J. Appl. Microbiol.* 97, 104–113. doi: 10.1111/j.1365-2672.2004.02275.x

Gauttam, R., Desiderato, C., Jung, L., Shah, A., and Eikmanns, B. J. (2019). A step forward: compatible and dual-inducible expression vectors for gene co-expression in *Corynebacterium glutamicum*. *Plasmid* 101, 20–27. doi: 10.1016/j.plasmid.2018.12.004

Gibson, D. G. (2011). Enzymatic assembly of overlapping DNA fragments. *Method. Enzymol.* 498, 349–361. doi: 10.1016/B978-0-12-385120-8.00015-2

Glasscock, C. J., Biggs, B. W., Lazar, J. T., Arnold, J. H., Burdette, L. A., Valdes, A., et al. (2021). Dynamic control of gene expression with riboregulated switchable feedback promoters. *ACS. Synth. Biol.* 10, 1199–1213. doi: 10.1021/acssynbio.1c00015

Goldbeck, O., and Seibold, G. M. (2018). Construction of pOGOduet - An inducible, bicistronic vector for synthesis of recombinant proteins in *Corynebacterium glutamicum*. *Plasmid* 95, 11–15. doi: 10.1016/j.plasmid.2018.01.001

Green, M. R., and Sambrook, J. (2012). *MOLECULAR cloning: A Laboratory Manual*. Cold Spring Harbor, N.Y: Cold Spring Harbor Laboratory Press.

Hanahan, D. (1983). Studies on transformation of *Escherichia coli* with plasmids. *J. Mol. Biol.* 166, 557–580. doi: 10.1016/S0022-2836(83)80284-8

Hasegawa, S., Jojima, T., Suda, M., and Inui, M. (2020). Isobutanol production in *Corynebacterium glutamicum*: suppressed succinate by-production by *pckA* inactivation and enhanced productivity via the Entner-Doudoroff pathway. *Metab. Eng.* 59, 24–35. doi: 10.1016/j.ymben.2020.01.004

Hibi, M., Sonoki, T., and Mori, H. (2005). Functional coupling between vanillate-O-demethylase and formaldehyde detoxification pathway. *FEMS Microbiol. Lett.* 253, 237–242. doi: 10.1016/j.femsle.2005.09.036

Ikeda, M., and Nakagawa, S. (2003). The *Corynebacterium glutamicum* genome: features and impacts on biotechnological processes. *Appl. Microbiol. Biot.* 62, 99–109. doi: 10.1007/s00253-003-1328-1

Inui, M., Kawaguchi, H., Murakami, S., Vertès, A. A., and Yukawa, H. (2004). Metabolic engineering of *Corynebacterium glutamicum* for fuel ethanol production under oxygen-deprivation conditions. *J. Mol. Microb. Biotech.* 8, 243–254. doi: 10.1159/000086705

Inui, M., and Toyoda, K. (2020). *Corynebacterium glutamicum: Biology and Biotechnology*. Cham: Springer International Publishing.

Jayaraman, P., Yeoh, J. W., Zhang, J., and Poh, C. L. (2018). Programming the dynamic control of bacterial gene expression with a chimeric ligand- and light-lased promoter system. *ACS Synth. Biol.* 7, 2627–2639. doi: 10.1021/acssynbio.8b00280

Kalinowski, J., Bathe, B., Bartels, D., Bischoff, N., Bott, M., Burkovski, A., et al. (2003). The complete *Corynebacterium glutamicum* ATCC 13032 genome sequence and its impact on the production of L-aspartate-derived amino acids and vitamins. *J. Biotechnol.* 104, 5–25. doi: 10.1016/S0168-1656(03)00154-8

Kallscheuer, N., Vogt, M., Kappelmann, J., Krumbach, K., Noack, S., Bott, M., et al. (2016). Identification of the *phd* gene cluster responsible for phenylpropanoid utilization in *Corynebacterium glutamicum*. *Appl. Microbiol. Biot.* 100, 1871–1881. doi: 10.1007/s00253-015-7165-1

Kind, S., and Wittmann, C. (2011). Bio-based production of the platform chemical 1,5-diaminopentane. *Appl. Microbiol. Biot.* 91, 1287–1296. doi: 10.1007/s00253-011-3457-2

Lange, J., Müller, F., Takors, R., and Blombach, B. (2018). Harnessing novel chromosomal integration loci to utilize an organosolv-derived hemicellulose fraction for isobutanol production with engineered *Corynebacterium glutamicum*. *Microb. Biotechnol.* 11, 257–263. doi: 10.1111/1751-7915.12879

Lee, S. K., and Keasling, J. D. (2005). A propionate-inducible expression system for enteric bacteria. *Appl. Environ. Microb.* 71, 6856–6862. doi: 10.1128/AEM.71.11.6856-6862.2005

Liebl, W., Klamer, R., and Schleifer, K.-H. (1989). Requirement of chelating compounds for the growth of *Corynebacterium glutamicum* in synthetic media. *Appl. Microbiol. Biot.* 32, 205–210. doi: 10.1007/BF00165889

Menkel, E., Thierbach, G., Eggeling, L., and Sahm, H. (1989). Influence of increased aspartate availability on lysine formation by a recombinant strain of *Corynebacterium glutamicum* and utilization of fumarate. *Appl. Environ. Microb.* 55, 684–688. doi: 10.1128/aem.55.3.684-688.1989

Merkens, H., Beckers, G., Wirtz, A., and Burkovski, A. (2005). Vanillate metabolism in *Corynebacterium glutamicum*. *Curr. Microbiol.* 51, 59–65. doi: 10.1007/s00284-005-4531-8

Mollerup Andersen, J., and Batsberg Pedersen, W. (1983). Analysis of plant phenolics by high-performance liquid chromatography. *J. Chromatogr. A* 259, 131–139. doi: 10.1016/S0021-9673(01)87986-3

Morabbi Heravi, K., Lange, J., Watzlawick, H., Kalinowski, J., and Altenbuchner, J. (2015). Transcriptional regulation of the vanillate utilization genes (*vanABK* Operon) of *Corynebacterium glutamicum* by VanR, a PadR-like repressor. *J. Bacteriol.* 197, 959–972. doi: 10.1128/JB.02431-14

Mourtzinos, I., Konteles, S., Kalogeropoulos, N., and Karathanos, V. T. (2009). Thermal oxidation of vanillin affects its antioxidant and antimicrobial properties. *Food Chem.* 114, 791–797. doi: 10.1016/j.foodchem.2008.10.014

Müller, F., Rapp, J., Hacker, A.-L., Feith, A., Takors, R., and Blombach, B. (2020). CO_2/HCO_3^- accelerates iron reduction through phenolic compounds. *mBio.* 11. doi: 10.1128/mBio.00085-20

Nishimura, T., Vertès, A. A., Shinoda, Y., Inui, M., and Yukawa, H. (2007). Anaerobic growth of *Corynebacterium glutamicum* using nitrate as a terminal electron acceptor. *Appl. Microbiol. Biot.* 75, 889–897. doi: 10.1007/s00253-007-0879-y

Okai, N., Masuda, T., Takeshima, Y., Tanaka, K., Yoshida, K.-I., Miyamoto, M., et al. (2017). Biotransformation of ferulic acid to protocatechuic acid by *Corynebacterium glutamicum* ATCC 21420 engineered to express vanillate O-demethylase. *AMB Exp.* 7:130. doi: 10.1186/s13568-017-0427-9

Oldiges, M., Eikmanns, B. J., and Blombach, B. (2014). Application of metabolic engineering for the biotechnological production of L-valine. *Appl. Microbiol. Biot.* 98, 5859–5870. doi: 10.1007/s00253-014-5782-8

Pfeifer-Sancar, K., Mentz, A., Rückert, C., and Kalinowski, J. (2013). Comprehensive analysis of the *Corynebacterium glutamicum* transcriptome using an improved RNAseq technique. *BMC Genom.* 14:888. doi: 10.1186/1471-2164-14-888

Priefert, H., Rabenhorst, J., and Steinbüchel, A. (1997). Molecular characterization of genes of *Pseudomonas sp.* strain HR199 involved in bioconversion of vanillin to protocatechuate. *J. Bacteriol.* 179, 2595–2607. doi: 10.1128/jb.179.8.2595-2607.1997

Radmacher, E., Vaitsikova, A., Burger, U., Krumbach, K., Sahm, H., and Eggeling, L. (2002). Linking central metabolism with increased pathway flux: L-valine accumulation by *Corynebacterium glutamicum*. *Appl. Environ. Microb.* 68, 2246–2250. doi: 10.1128/AEM.68.5.2246-2250.2002

Schäfer, A., Tauch, A., Jäger, W., Kalinowski, J., Thierbach, G., and Pühler, A. (1994). Small mobilizable multi-purpose cloning vectors derived from

the *Escherichia coli* plasmids pK18 and pK19: selection of defined deletions in the chromosome of *Corynebacterium glutamicum*. *Gene* 145, 69–73. doi: 10.1016/0378-1119(94)90324-7

Schneider, J., Eberhardt, D., and Wendisch, V. F. (2012). Improving putrescine production by *Corynebacterium glutamicum* by fine-tuning ornithine transcarbamoylase activity using a plasmid addiction system. *Appl. Microbiol. Biot.* 95, 169–178. doi: 10.1007/s00253-012-3956-9

Schreiner, M. E., Fiur, D., Holátko, J., Pátek, M., and Eikmanns, B. J. (2005). E1 enzyme of the pyruvate dehydrogenase complex in *Corynebacterium glutamicum*: molecular analysis of the gene and phylogenetic aspects. *J. Bacteriol.* 187, 6005–6018. doi: 10.1128/JB.187.17.6005-6018.2005

Schwentner, A., Feith, A., Münch, E., Busche, T., Rückert, C., Kalinowski, J., et al. (2018). Metabolic engineering to guide evolution - Creating a novel mode for L-valine production with *Corynebacterium glutamicum*. *Metab. Eng.* 47, 31–41. doi: 10.1016/j.ymben.2018.02.015

Schwentner, A., Feith, A., Münch, E., Stiefelmaier, J., Lauer, I., Favilli, L., et al. (2019). Modular systems metabolic engineering enables balancing of relevant pathways for L-histidine production with *Corynebacterium glutamicum*. *Biotechnol. Biofuels* 12:65. doi: 10.1186/s13068-019-1410-2

Shen, X.-H., Zhou, N.-Y., and Liu, S.-J. (2012). Degradation and assimilation of aromatic compounds by *Corynebacterium glutamicum*: another potential for applications for this bacterium? *Appl. Microbiol. Biot.* 95, 77–89. doi: 10.1007/s00253-012-4139-4

Siebert, D., and Wendisch, V. F. (2015). Metabolic pathway engineering for production of 1,2-propanediol and 1-propanol by *Corynebacterium glutamicum*. *Biotechnol. Biofuels.* 8:91. doi: 10.1186/s13068-015-0269-0

Takeno, S., Ohnishi, J., Komatsu, T., Masaki, T., Sen, K., and Ikeda, M. (2007). Anaerobic growth and potential for amino acid production by nitrate respiration in *Corynebacterium glutamicum*. *Appl. Microbiol. Biot.* 75, 1173–1182. doi: 10.1007/s00253-007-0926-8

Tauch, A., Kirchner, O., Löffler, B., Götker, S., Pühler, A., and Kalinowski, J. (2002). Efficient electrotransformation of *Corynebacterium diphtheriae* with a mini-replicon derived from the *Corynebacterium glutamicum* plasmid pGA1. *Curr. Microbiol.* 45, 362–367. doi: 10.1007/s00284-002-3728-3

Terpe, K. (2006). Overview of bacterial expression systems for heterologous protein production: from molecular and biochemical fundamentals to commercial systems. *Appl. Microbiol. Biot.* 72, 211–222. doi: 10.1007/s00253-006-0465-8

van der Rest, M. E., Lange, C., and Molenaar, D. (1999). A heat shock following electroporation induces highly efficient transformation of *Corynebacterium glutamicum* with xenogeneic plasmid DNA. *Appl. Microbiol. Biot.* 52, 541–545. doi: 10.1007/s002530051557

Wang, Q., Zhang, J., Al Makishah, N. H., Sun, X., Wen, Z., Jiang, Y., et al. (2021). Advances and perspectives for genome editing tools of *Corynebacterium glutamicum*. *Front. Microbiol.* 12:654058. doi: 10.3389/fmicb.2021.654058

Wendisch, V. F. (2017). "Microbial production of amino acid-related compounds," in *Amino Acid Fermentation*, eds A. Yokota, and M. Ikeda (Tokyo: Springer Japan), 255–269.

Wiechert, J., Gätgens, C., Wirtz, A., and Frunzke, J. (2020). Inducible expression systems based on xenogeneic silencing and counter-silencing and design of a metabolic toggle switch. *ACS Synth. Biol.* 9, 2023–2038. doi: 10.1021/acssynbio.0c00111

Yamamoto, S., Suda, M., Niimi, S., Inui, M., and Yukawa, H. (2013). Strain optimization for efficient isobutanol production using *Corynebacterium glutamicum* under oxygen deprivation. *Biotechnol. Bioeng.* 110, 2938–2948. doi: 10.1002/bit.24961

Yao, J., He, Y., Su, N., Bharath, S. R., Tao, Y., Jin, J.-M., et al. (2020). Developing a highly efficient hydroxytyrosol whole-cell catalyst by de-bottlenecking rate-limiting steps. *Nat. Comm.* 11:1515. doi: 10.1038/s41467-020-14918-5

Yukawa, H., and Inui, M. (eds.). (2013). *Corynebacterium glutamicum*. Berlin, Heidelberg: Springer Berlin Heidelberg.

Conflict of Interest: The authors declare that the research was conducted in the absence of any commercial or financial relationships that could be construed as a potential conflict of interest.

Publisher's Note: All claims expressed in this article are solely those of the authors and do not necessarily represent those of their affiliated organizations, or those of the publisher, the editors and the reviewers. Any product that may be evaluated in this article, or claim that may be made by its manufacturer, is not guaranteed or endorsed by the publisher.

frontiers in Bioengineering and Biotechnology

ORIGINAL RESEARCH
published: 21 September 2021
doi: 10.3389/fbioe.2021.748155

Exploring the Potential of *Corynebacterium glutamicum* to Produce the Compatible Solute Mannosylglycerate

Andreas Schwentner[1], *Heiko Neugebauer*[1], *Serin Weinmann*[1], *Helena Santos*[2] *and Bernhard J. Eikmanns*[1]*

[1]*Institute of Microbiology and Biotechnology, Ulm University, Ulm, Germany,* [2]*Instituto de Tecnologia Química e Biológica António Xavier, Universidade Nova de Lisboa, Oeiras, Portugal*

OPEN ACCESS

Edited by:
Volker F. Wendisch, Bielefeld University, Germany

Reviewed by:
Fernando Pérez-García, Norwegian University of Science and Technology, Norway
K. Madhavan Nampoothiri, National Institute for Interdisciplinary Science and Technology (CSIR), India

***Correspondence:**
Bernhard J. Eikmanns
bernhard.eikmanns@uni-ulm.de

Specialty section:
This article was submitted to Synthetic Biology, a section of the journal Frontiers in Bioengineering and Biotechnology

Received: *27 July 2021*
Accepted: *26 August 2021*
Published: *21 September 2021*

Citation:
Schwentner A, Neugebauer H, Weinmann S, Santos H and Eikmanns BJ (2021) Exploring the Potential of Corynebacterium glutamicum *to Produce the Compatible Solute Mannosylglycerate. Front. Bioeng. Biotechnol. 9:748155. doi: 10.3389/fbioe.2021.748155*

The compatible solute mannosylglycerate (MG) has exceptional properties in terms of protein stabilization and protection under salt, heat, and freeze-drying stresses as well as against protein aggregation. Due to these characteristics, MG possesses large potential for clinical and biotechnological applications. To achieve efficient MG production, *Corynebacterium glutamicum* was equipped with a bifunctional MG synthase (encoded by *mgsD* and catalyzing the condensation of 3-phosphoglycerate and GDP-mannose to MG) from *Dehalococcoides mccartyi*. The resulting strain *C. glutamicum* (pEKEx3 *mgsD*) intracellularly accumulated about 111 mM MG (60 ± 9 mg g_{CDW}^{-1}) with 2% glucose as a carbon source. To enable efficient mannose metabolization, the native *manA* gene, encoding mannose 6-phosphate isomerase, was overexpressed. Combined overexpression of *manA* and *mgsD* from two plasmids in *C. glutamicum* resulted in intracellular MG accumulation of up to ca. 329 mM [corresponding to 177 mg $g_{\text{cell dry weight (CDW)}}^{-1}$] with glucose, 314 mM (168 mg g_{CDW}^{-1}) with glucose plus mannose, and 328 mM (176 mg g_{CDW}^{-1}) with mannose as carbon source(s), respectively. The product was successfully extracted from cells by using a cold water shock, resulting in up to 5.5 mM MG (1.48 g L^{-1}) in supernatants. The two-plasmid system was improved by integrating the *mgsD* gene into the *manA*-bearing plasmid and the resulting strain showed comparable production but faster growth. Repeated cycles of growth/production and extraction of MG in a bacterial milking-like experiment showed that cells could be recycled, which led to a cumulative MG production of 19.9 mM (5.34 g L^{-1}). The results show that the newly constructed *C. glutamicum* strain produces MG from glucose and mannose and that a cold water shock enables extraction of MG from the cytosol into the medium.

Keywords: mannosylglycerate, compatible solute, metabolic engineering, Corynebacterium glutamicum, bacterial milking, mannose metabolization, bifunctional mannosylglycerate synthase

INTRODUCTION

Compatible solutes are compounds of low molecular weight that are readily accumulated in the cytoplasm of microorganisms up to molar concentrations as a reaction to increasing extracellular osmolality (Santos and da Costa, 2001; Santos et al., 2006). Particularly, microorganisms adapted to extreme environments, such as hyperthermophiles and halophiles, accumulate compatible solutes not only as a response to salt stress but also in response to supraoptimal growth temperatures (Silva et al., 1999; Esteves et al., 2014). In contrast to compatible solutes from mesophilic organisms, which commonly accumulate neutral and nitrogen-containing compounds, such as L-proline, betaine, or ectoine, compatible solutes from (hyper)thermophilic organisms commonly are negatively charged and carbohydrate-based (Borges et al., 2014). One of the most widespread compatible solutes in (hyper)thermophilic microorganisms is α-D-mannopyranosyl-(1--°2)-D-glycerate, also known as mannosylglycerate (MG), digeneaside, or firoin (Empadinhas and da Costa, 2008; Borges et al., 2014).

Most known native producers synthesize MG *via* a two-step pathway in which the enzymes mannosyl 3-phosphoglycerate synthase (MPGS) and mannosyl 3-phosphoglycerate phosphatase (MPGP) subsequently convert guanosine diphosphate mannose (GDP-Man) and 3-phosphoglycerate (3-PG) to MG (Borges et al., 2004; Borges et al., 2014). However, there are also organisms, e.g., the mesophilic bacterium *Dehalococcoides mccartyi (*formerly *D. ethenogenes),* which uses a single-step pathway *via* a bifunctional synthase/phosphatase called mannosylglycerate synthase (MgsD), encoded by *mgsD* and converting 3-PG and GDP-Man to MG (Empadinhas et al., 2004). Heterologous expression of the *mgsD* gene resulted in intracellular accumulation of MG in *Saccharomyces cerevisiae*, confirming the functionality of MgsD of *D. mccartyi* as bifunctional MG synthase/phosphatase (Empadinhas et al., 2004).

MG is a molecule with outstanding characteristics in protein stabilization *in vitro* and *in vivo*, which opens up a vast field of applications (Lentzen and Schwarz, 2006; Jorge et al., 2016). MG was shown to protect model proteins (e.g., lactate dehydrogenase and glucose oxidase; Borges et al., 2002), against heat inactivation and freeze-drying and prevented heat-induced aggregation; it led to enhanced stability of cutinase (Melo et al., 2001), recombinant nuclease (Faria et al., 2004), and retroviral vaccines (Cruz et al., 2006). Strikingly, MG was also effective in suppressing aggregation of soluble β-amyloid peptides into fibrils, one of the key pathological features of Alzheimer's disease (Ryu et al., 2008). In a yeast model of Parkinson's disease, MG prevented aggregation of α-synuclein, the major component of the intraneuronal inclusions in the brain of patients suffering from this disease (Faria et al., 2013). These characteristics render MG an attractive target for microbial production.

Corynebacterium glutamicum is a Gram-positive, facultatively anaerobic bacterium that natively grows on a variety of sugars, alcohols, organic acids, and other substrates (Becker and Wittmann, 2015). Furthermore, the organism has been engineered to metabolize nonnative carbon sources such as xylose (Kawaguchi et al., 2006; Meiswinkel et al., 2013; Lange et al., 2017), N-acetylmuramic acid (Sgobba et al., 2018), mannitol (Laslo et al., 2012), starch (Seibold et al., 2006), or cellobiose (Adachi et al., 2013). Generally, *C. glutamicum* is well known for the large-scale industrial production of amino acids, mainly L-glutamate and L-lysine (Eggeling and Bott, 2015; Wendisch et al., 2016). During the past decade, however, the range of products has been expanded drastically and comprises nowadays not only other proteinogenic amino acids, such as L-valine (Blombach et al., 2007a; Schwentner et al., 2018), L-arginine (Park et al., 2014), L-tryptophan (Zhang et al., 2015), or L-histidine (Schwentner et al., 2019), but also organic acids (Wieschalka et al., 2013), alcohols (Blombach et al., 2011), carotenoids (Henke and Wendisch, 2019), and proteins (Bakkes et al., 2020; Hemmerich et al., 2020). Moreover, *C. glutamicum* has been engineered to overproduce native compatible solutes such as trehalose (Carpinelli et al., 2006) and L-proline (Jensen and Wendisch, 2013), as well as the nonnative α-D-glucosylglycerol (Roenneke et al., 2018), L-pipecolic acid (Pérez-García et al., 2019), and ectoine/hydroxyectoine (Gießelmann et al., 2019), principally demonstrating the capability of *C. glutamicum* to serve as a host for production of compatible solutes. Very recently, *C. glutamicum* has been also engineered to produce MG from glucose plus glycerate and from mannose plus glycerate in an artificially designed starch-mannose-fermentation biotransformation process, respectively (Tian et al., 2020).

Mannose is a C-2 epimer of glucose, which is widespread in lignocellulosic biomass and makes up 20% of the sugars from biomass hydrolysates of wood (Sasaki et al., 2011). Sasaki and coworkers showed that uptake of mannose in *C. glutamicum* strain R is mainly mediated *via* the glucose-specific phosphoenolpyruvate- (PEP-) dependent phosphotransferase system PtsG, which can be substituted for by the fructose-dependent PtsF in absence of PtsG. The WT strain as well as a *manA* (encoding MPI) overexpressing strain consumed glucose preferentially over mannose when both substrates were present; however, mannose consumption was drastically increased when *manA* was overexpressed. *C. glutamicum* only consumed glucose and mannose simultaneously when *ptsF* was overexpressed. Furthermore, MPI was shown to be essential not only for mannose catabolism but also for the synthesis of GDP-mannose from fructose 6-phosphate (Sasaki et al., 2011).

In this study, we aimed to produce the compatible solute MG from glucose with the heterologous host organism *C. glutamicum,* which natively possesses the pathways for the synthesis of the MG precursors GDP-mannose and 3-phosphoglycerate (see **Figure 1**) by implementing an MG synthase from the native MG producer *D. mccartyi*. The MG-producing *C. glutamicum* was engineered to grow with mannose as a carbon source by overexpressing the native *manA* gene and eventually we produced MG from glucose and/or mannose.

MATERIALS AND METHODS

Bacterial Strains and Plasmids

All bacterial strains, plasmids, and oligonucleotides used in this work and their corresponding characteristics, sequences, and sources are given in **Table 1**.

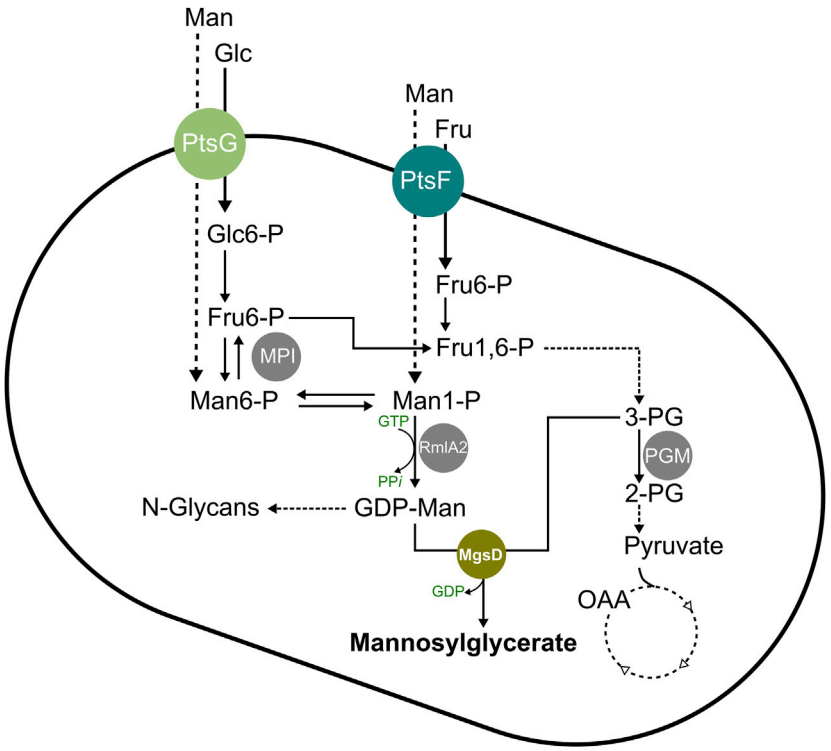

FIGURE 1 | Schematic overview of the mannosylglycerate synthesis pathway in *C. glutamicum*. Abbreviations: 2-PG, 2-phosphoglycerate; 3-PG, 3-phosphoglycerate; Fru, fructose; Fru1,6-P, fructose-1,6-bisphosphate; Fru6-P, fructose 6-phosphate; Glc, glucose; Glc6-P, glucose 6-phosphate; GDP, guanosine diphosphate; GTP, guanosine triphosphate; Man, mannose; Man1-P, mannose 1-phosphate; Man6-P, mannose 6-phosphate; MgsD, mannosylglycerate synthase (encoded by *mgsD* from *Dehalococcoides mccartyi*); MPI, mannose 6-phosphate isomerase (encoded by *manA*); OAA, oxaloacetate; PGM, phosphoglycerate mutase (encoded by *pgm*); PP_i, inorganic pyrophosphate; PtsF, fructose-specific phosphoenolpyruvate-dependent phosphotransferase system (encoded by *ptsF*); PtsG, glucose-specific phosphoenolpyruvate-dependent phosphotransferase system (encoded by *ptsG*); RmlA2, GDP-mannose pyrophosphorylase (encoded by *rmlA2*).

Media and Cultivation Conditions

E. coli DH5α cells were cultivated aerobically in 5 ml 2xYT complex medium (Green and Sambrook, 2012) at 37 ºC in glass test tubes on a rotary shaker at 130 rpm. Cultivation of *C. glutamicum* cells was performed in glass test tubes or baffled shaking flasks at 30°C on a rotary shaker at 130 rpm. Precultivations of *C. glutamicum* cells were done by streaking cell material from a glycerol stock (30% glycerol [v v^{-1}]) on 2xYT agar medium, which then was incubated for 2–3 days at 30°C. Inoculation of the first liquid culture was done by transferring a single colony in 5 ml 2xYT medium in 20 ml glass test tubes, which was incubated for about 7 h. Then, the culture was transferred completely into 50 ml 2xYT medium in a 500 ml baffled shaking flask and incubated overnight (about 14 h). The overnight culture was harvested by centrifugation (4.500 × g, 10 min, 4°C) and the resulting cell pellet was washed in 0.9% (w v^{-1}) sodium chloride solution, centrifuged again, resuspended in sodium chloride solution, and then used to inoculate 50 ml modified CGXII minimal medium (Eikmanns et al., 1991) in 500 ml baffled shaking flasks to a starting optical density at 600 nm (OD_{600}) of 1. The modified CGXII minimal medium contained 5 g $(NH_4)_2SO_4$ L^{-1}, 5 g urea L^{-1}, 21 g 3-morpholinopropanesulfonic acid (MOPS) L^{-1}, 1 g K_2HPO_4 L^{-1}, 1 g KH_2PO_4 L^{-1}, 0.25 g $MgSO_4$ L^{-1}, and 0.01 g $CaCl_2$ L^{-1}. Before the medium was autoclaved, the pH was set to 7.4 by adding 5 M KOH and after autoclaving, 16.4 mg $FeSO_4 \times 7\ H_2O$ L^{-1}, 10 mg $MnSO_4 \times H_2O$ L^{-1}, 0.2 mg $CuSO_4$ L^{-1}, 1 mg $ZnSO_4 \times 7\ H_2O$ L^{-1}, 0.02 mg $NiCl_2 \times 6\ H_2O$ L^{-1}, 0.2 mg biotin L^{-1}, and either 10 or 20 g glucose L^{-1} and/or 10 or 20 g mannose L^{-1} (as indicated in the Results section) were added under sterile conditions. The expression of genes under control of the P_{tac} promoter was induced by adding 0.5 mM isopropyl β-d-1-thiogalactopyranoside (IPTG) directly before inoculation into the main culture. For strains carrying plasmids, 50 µg kanamycin mL^{-1} or 100 µg spectinomycin mL^{-1} was added to the media where required. For strains carrying two plasmids, the antibiotic concentrations were reduced to 25 µg kanamycin ml^{-1} and 50 µg spectinomycin mL^{-1}. Formation of biomass was followed by measuring OD_{600} with a photometer (Ultrospec® 3000 pro, Amersham Pharmacia Biotech Europe GmbH, Freiburg, Germany). Cell dry weight (in g_{CDW} L^{-1}) of the biomass was calculated by applying the correlation CDW = $OD_{600} \times 0.30$ g L^{-1} (Blombach et al., 2007b).

Growth rates µ [h^{-1}] were calculated by applying linear regressions of ln(OD_{600}) plotted over time in h during the exponential growth phase (between 4 and 10 h of incubation after inoculation).

TABLE 1 | Strains, plasmids, and oligonucleotides used in this study.

Strain, plasmid, or oligonucleotide	Relevant characteristic(s) or sequence	Source, reference, or purpose
Strains		
E. coli DH5α	F-ϕ80*lacZ*ΔM15 Δ(*lacZYA-argF*)U169 *endA1 recA1 hsdR17* (r_K^- m_K^+) *supE44 thi-1 gyrA96 relA1 phoA*	Hanahan (1983)
C. glutamicum WT	Wild-type (WT) strain ATCC 13032	American Type Culture Collection
C. glutamicum (pEKEx3 *mgsD*)	*C. glutamicum* WT carrying the heterologous *mgsD* gene from *Dehalococcoides mccartyi* in plasmid pEKEx3	This work
C. glutamicum (pVWEx1 *manA*)	*C. glutamicum* WT carrying the native gene *manA* in plasmid pVWEx1	This work
C. glutamicum (*pEKEx3 mgsD*) (*pVWEx1 manA*)	*C. glutamicum* WT carrying the heterologous *mgsD* gene and the native *manA* gene in plasmids pEKEx3 and pVWEx1, respectively	This work
C. glutamicum (*pVWEx1 manA mgsD*)	*C. glutamicum* WT carrying *manA* and *mgsD* genes in plasmid pVWEx1	This work
Plasmids		
pEX-K4 *mgsD*	pEX-K4 containing a codon-optimized *mgsD* gene from *D. mccartyi*	Eurofins Genomics GmbH, Ebersberg, Germany
pEKEx2	*E. coli-C. glutamicum* shuttle vector, P_{tac}, *lacI*^{q}, Km^R, and pBL1 ori	Eikmanns et al. (1994)
pEKEx3	*E. coli-C. glutamicum* shuttle vector, P_{tac},*lacI*^{q}, $Spec^R$, and pBL1 ori	Stansen et al. (2005)
pVWEx1	*E. coli-C. glutamicum* shuttle vector, P_{tac}, *lacI*^{q}, Km^R, and pCG1 ori	Peters-Wendisch et al. (2001)
pEKEx2 *mgsD*	pEKEx2 containing a codon-optimized *mgsD* gene from *D. mccartyi* under control of P_{tac}	This work
pEKEx3 *mgsD*	pEKEx3 containing a codon-optimized *mgsD* gene from *D. mccartyi* under control of P_{tac}	This work
pVWEx1 *manA*	pVWEx1 containing the *manA* gene from *C. glutamicum* under control of P_{tac}	This work
pVWEx1 *manA mgsD*	pVWEx1 *manA* containing a codon-optimized *mgsD* gene from *D. mccartyi* under control of P_{tac}	This work
Oligonucleotides		
mgsD-2.1	5′-CCTCCCGGAGCGAATCAGTC-3′	Sequencing of *mgsD* insert in pEKEx2 *mgsD*
mgsD-2.2	5′-CGGTGGAGTAGGAGTATGTC-3′	Sequencing of *mgsD* insert in pEKEx2 *mgsD*
mgsD-2.3	5′-CAGACCGCTTCTGCGTTCTG-3′	Sequencing of *mgsD* insert in pEKEx2 *mgsD*
mgsD1	5′- CACTCCCGTTCTGGATAATG-3′	Sequencing of *mgsD* insert in pEKEx3 *mgsD*
mgsD2	5′-ATACTCCATGGTCCGTGTTC-3′	Sequencing of *mgsD* insert in pEKEx3 *mgsD*
mgsD3	5′-ATGGACCTCGCGAAGTTCTC-3′	Sequencing of *mgsD* insert in pEKEx3 *mgsD*
mgsD4	5′- GCTACGGCGTTTCACTTCTG-3′	Sequencing of *mgsD* insert in pEKEx3 *mgsD*
manA_fwd	5′-GACGGTCTAGATAAAGGAGTTTTATGGAGCTATTGGAAGG-3′	Amplification of *manA* (*Xba*I site underlined)
manA_rev	5′-CAGCTGGTACCCTAAACCCTAGCGAGGAATA-3′	Amplification of *manA* (*Kpn*I site underlined)
mgsD-for	5′-TAGGGTACCAGGAGGACATACAATGCGCATCGAGAGCCTGCG-3′	Amplification of *mgsD* (*Kpn*I site underlined)
mgsD-rev	5′-GCTGGTACCCTTACTCCATAGGCAGGATAATG-3′	Amplification of *mgsD* (*Kpn*I site underlined)
mgsD5	5′-GACAACTACATCCCTGG-3′	Sequencing of *mgsD* insert in pVWEx1 *manA mgsD*
mgsD6	5′-CTGCCGTGATTGAGAAG-3′	Sequencing of *mgsD* insert in pVWEx1 *manA mgsD*
mgsD7	5′-CGCTCCACTAATATCGTG-3′	Sequencing of *mgsD* insert in pVWEx1 *manA mgsD*

Recombinant DNA Work

Standardized methods of molecular cloning such as PCR, DNA restriction, and ligation were carried out according to Green and Sambrook (2012). Plasmids were isolated and PCR fragments purified with the E.Z.N.A.® Plasmid Mini Kit I (Omega Bio-Tek, Inc., Norcross, United States) and the NucleoSpin® Gel and PCR Clean-Up Kit (Macherey Nagel GmbH & Co. KG, Düren, Germany), respectively, according to the manufacturer's instructions. Genomic DNA from *C. glutamicum* was isolated and purified with NucleoSpin Microbial DNA Mini kit (Macherey Nagel GmbH & Co. KG, Düren, Germany) according to the manufacturer's instructions.

Electrocompetent cells of *E. coli* DH5α and of *C. glutamicum* were prepared as has been described before (Dower et al., 1988;

Tauch et al., 2002). Transformation of *E. coli* and *C. glutamicum* with plasmids was performed as described before (Dower et al., 1988; van der Rest et al., 1999). Transformation of *C. glutamicum* included a heat shock for 6 min at 46°C. *E. coli* DH5α and all *C. glutamicum* strains were electroporated with a MicroPulser Electroporator (Bio-Rad Laboratories GmbH, München, Germany) at 2.5 kV with 600 Ω resistance. Enzymes for recombinant DNA work were obtained from Thermo Fisher Scientific Inc. (Darmstadt, Germany) or New England Biolabs GmbH (Frankfurt am Main, Germany). Oligonucleotides used in this work were ordered from biomers.net GmbH (Ulm, Germany) and are listed in **Table 1**.

A codon-optimized variant of the *mgsD* gene, encoding mannosylglycerate synthase (MgsD) from *D. mccartyi* strain ATCC BAA-2266/KCTC 15142/195 (formerly *D. ethenogenes* strain 195), was deduced from UniProt protein Q3Z6S5 and synthesized commercially and equipped with restriction sites for *Sal*I and *Kpn*I and ligated into pEX-K4 (Eurofins Genomics GmbH, Ebersberg, Germany). *E. coli* DH5α was transformed with the resulting vector pEX-K4 *mgsD* and the plasmid from transformants was isolated and restricted with *Sal*I and *Kpn*I. The *mgsD* fragment was purified and ligated into pEKEx2 as an intermediate step. The sequence identity of the resulting plasmid pEKEx2 *mgsD* was checked by PCR using primers mgsD-2.1, mgsD-2.2, and mgsD-2.3 (Eurofins Genomics GmbH, Ebersberg, Germany). Plasmid pEKEx2 *mgsD* was then restricted with *Sal*I and *Eco*RI and the *mgsD* fragment was ligated into pEKEx3 under control of the IPTG-inducible *tac* promoter, resulting in pEKEx3 *mgsD*, whose sequence identity was verified *via* restriction control and sequencing (Eurofins Genomics GmbH, Ebersberg, Germany) with primers mgsD1, mgsD2, mgsD3, and mgsD4.

The *manA* gene (cg0856), encoding mannose 6-phosphate isomerase (MPI), was amplified *via* PCR with primers manA_fwd and manA_rev from genomic DNA of *C. glutamicum* wild type (WT). The purified product was restricted with *Xba*I and *Kpn*I and cloned into the shuttle expression vector pVWEx1 under the control of the IPTG-inducible *tac* promoter. Sequence identity was verified *via* control digestions and sequencing using the primers mentioned above.

Gene *mgsD* was cloned into pVWEx1 *manA* by amplifying *mgsD* with primers mgsD-for (containing the ribosomal binding site of the *tuf* gene [cg0587] of *C. glutamicum*) and mgsD-rev from plasmid pEKEx3 *mgsD*. Plasmid pVWEx1 and the resulting PCR product were cut with *Kpn*I and purified *mgsD* was cloned into the cut plasmid *via* ligation. The resulting plasmid was sequenced with primers mgsD5, mgsD6, and mgsD7 to check sequence identity and correct orientation of *mgsD*.

Determination of Specific Mannose 6-Phosphate Isomerase Activities

Determination of specific MPI activities was performed as described before (Sasaki et al., 2011). In brief, cells were grown in CGXII minimal medium with the respective carbon source(s) and harvested by centrifugation (4,200 × g, 10 min, 4°C). Cells were washed twice in 8 ml extraction buffer [2 mM dithiothreitol, 0.1 mM ethylenediaminetetraacetic acid, 20 mM KCl, 20 mM $MgCl_2$, 5 mM $MnSO_4$, and 100 mM tris(hydroxyethyl)aminomethane (TRIS), pH was adjusted to 7.5 with 2 M HCl] and resuspended in 1 ml extraction buffer. Before performing the assay, cells were disrupted in a Precellys 24 tissue homogenizer (Bertin Technologies SAS, Montigny-le-Bretonneux, France) for three rounds (45 s each, 6,500 × g, 4°C) with intermitted cooling on ice. The cell lysate was centrifuged (12,100 × g, 20 min, 4°C) and the supernatant was used for the assay in a final volume of 1 ml at 37°C. The assay contained 1 U glucose 6-phosphate dehydrogenase from yeast (Roche Diagnostics GmbH, Mannheim, Germany), 0.7 U phosphoglucose isomerase from yeast (Roche Diagnostics GmbH), 5 mM $MgSO_4$, 25 mM TRIS-HCl (pH 7.5), 1 mM $NADP^+$, 1 mM mannose 6-phosphate, and 100 µl of the respective (diluted) supernatant.

Quantification of Substrates and Products

To quantify the substrates glucose and mannose and the product MG, 1 ml of cell suspension was harvested from the respective cultures by centrifugation (12,100 × g, 5 min, RT). Supernatants were either frozen and stored at −20°C or directly used for further analysis. Quantification of glucose, mannose, and mannosylglycerate was performed with an Agilent 1200 series apparatus (Agilent Technologies, Santa Clara, CA, United States) equipped with an organic acid/sugar column and precolumn (organic-acid resin; 300 × 8 mm; from CS Chromatographie, Langerwehe, Germany). Isocratic chromatography was realized with a mobile phase of 5 mM H_2SO_4 and a constant flow rate of 0.8 ml min^{-1} at 60°C. Detection occurred with a variable wavelength detector and a refractive index detector. Quantification of the analytes was conducted by using an eight-point calibration curve for each of the components (glucose, mannose, MG) as an external reference standard. MG was purchased as firoin from *Rhodothermus marinus* (Sigma Aldrich Chemie GmbH, Taufkirchen, Germany). The detection limit of the applied analytical system for MG in cell extracts was determined to be around 0.5 mM.

Intracellular MG concentrations were determined by harvesting 5 ml cell suspension from the cultures, centrifugation (4,200 × g, 20 min, RT), and resuspending the cell pellet in 1 ml 0.9% (w v^{-1}) NaCl. Cells were disrupted in a Precellys 24 tissue homogenizer (Bertin Technologies SAS, Montigny-le-Bretonneux, France) for three rounds (45 s each, 6,500 × g, 4°C) with intermitted cooling at 4°C. The lysate was centrifuged (12,100 × g, 20 min, 4°C) and the supernatant was used for HPLC analysis, as described above.

Extracellular MG was determined by taking 1 ml samples from the culture medium, centrifugation at 12,100 × g, 5 min, RT, and directly using the supernatant for HPLC analysis as described above. The intracellular MG content was estimated using the following correlations:

(i) OD_{600} = 0.30 g_{CDW} L^{-1} (Blombach et al., 2007b).
(ii) 1 mg CDW = 2 µl cytoplasmic volume (Gutmann et al., 1992).

Extraction of Mannosylglycerate and Bacterial-Milking-Like Experiment

MG was extracted from the cells by applying a cold water shock with ultrapure water (HiPerSolv CHROMANORM®, VWR

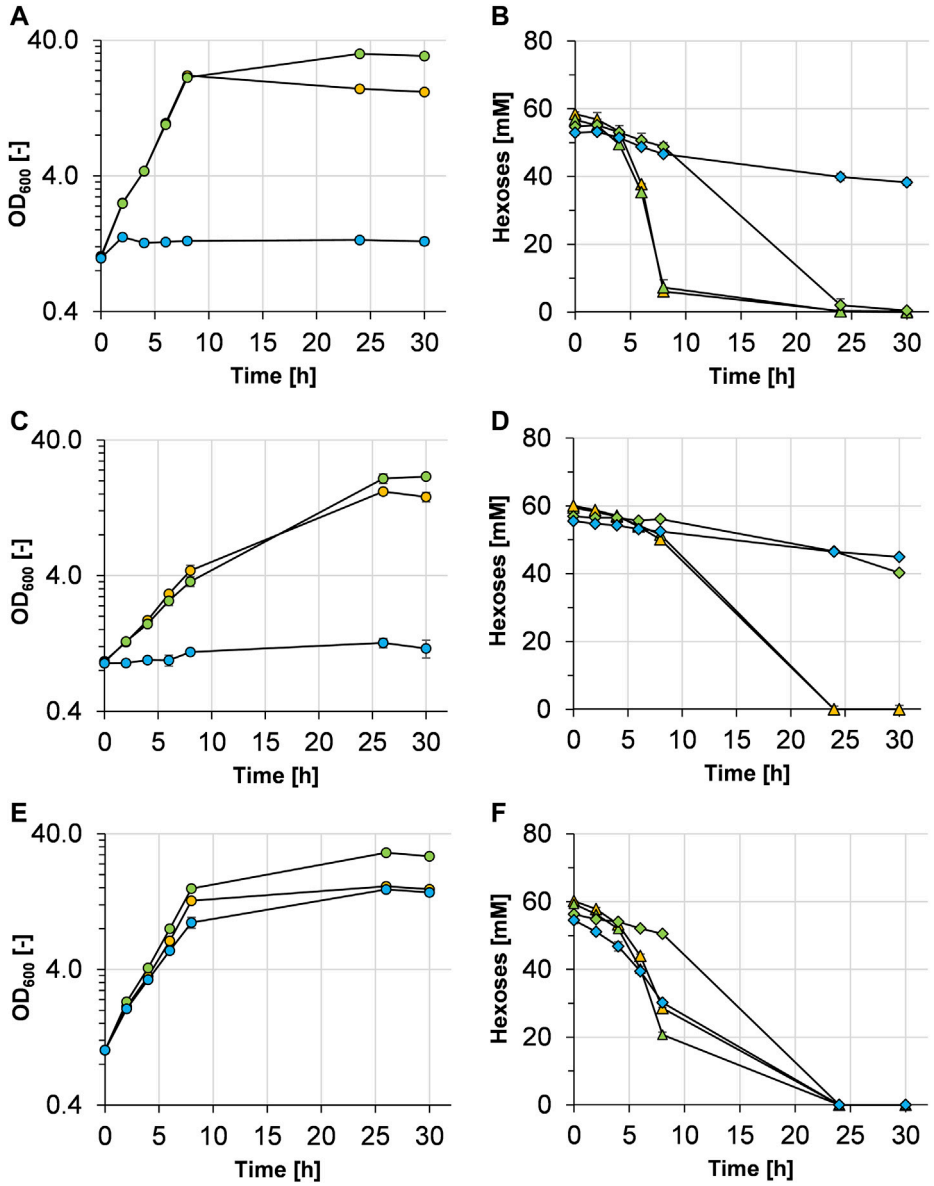

FIGURE 2 | Growth and hexose (glucose and/or mannose) consumption of *C. glutamicum* WT **(A,B)**, *C. glutamicum* (pEKEx3 *mgsD*) **(C,D)**, and *C. glutamicum* (pVWEx1 *manA*) **(E,F)** grown in CGXII minimal medium containing either 1% glucose (orange symbols), 1% glucose plus 1% mannose (green symbols), or 1% mannose (blue symbols). The growth of the three strains is represented by colored circles in **(A,C,E)**. Glucose and mannose consumption in **(B,D,F)** is represented by triangles and diamonds and corresponds to the colors given in the growth diagrams, respectively. Experiments have been performed in triplicate and the standard deviation is given as error bars.

International GmbH, Darmstadt, Germany) chilled to 4°C. This was done by harvesting 5 ml of the cell suspension at the respective time point, centrifugation (4,200 × g, 20 min, RT), resuspending the cell pellet in 5 ml ice-cold water, and incubating for 30 min on ice. After incubation, the cell suspension was centrifuged and samples were taken from the supernatant for extracellular MG analysis *via* HPLC as described above. To determine the amount of MG that remained intracellularly after the cold water shock, the cell pellet was treated as described above. It is noteworthy to mention that the viability of the cells was not affected by the cold water shock as the number of colony-forming units on 2xYT agar medium was the same before and after the cold shock treatment.

For a bacterial-milking-like experiment, cells were cultivated as described above with glucose and mannose as carbon sources. After 24 h, the complete content of a shaking flask was centrifuged and cells were resuspended in 20 ml of ice-cold ultrapure H_2O and incubated for 60 min on ice. Afterward, the suspension was centrifuged again, and the supernatant was collected and stored at 4°C. The cell pellet was resuspended in

2 ml 0.9% (w v^{-1}) NaCl solution and used to inoculate fresh medium. Cells were grown for 24 h at 30°C with 130 rpm shaking followed by another round of extraction with the supernatant from the first round of extraction. This procedure was repeated several times and the ice-cold supernatant (extract) was used repeated times to release MG from the cells, which led to the accumulation of MG.

RESULTS

C. glutamicum WT Does Not Produce Mannosylglycerate, Does Not Metabolize It, and Is Not Inhibited by Mannosylglycerate

In the first experiments, *C. glutamicum* WT was cultivated in minimal medium with either glucose (10 g L^{-1}), glucose plus mannose (10 g L^{-1} each), or mannose (10 g L^{-1}) as carbon and energy source(s) (**Figure 2A**). With glucose and with a mixture of glucose and mannose, *C. glutamicum* WT grew with similar growth rates of 0.41 ± 0.01 and 0.40 ± 0.01 h^{-1}, respectively. Due to the higher amount of carbon, the final OD_{600} of the cultures with glucose plus mannose was higher compared with that of the cultures with glucose alone. The WT strain was not able to grow at all with mannose as a sole carbon source (**Figure 2A**), although the mannose concentration in the medium slightly but steadily decreased over time (**Figure 2B**) with a rate of about 0.65 ± 0.02 mmol mannose g_{CDW}^{-1} h^{-1}). When both substrates were supplied, both carbon sources were metabolized; however, glucose was preferentially taken up and mannose was mainly metabolized after glucose was depleted (**Figure 2B**), indicating at least partially sequential metabolization of the two sugars.

Cells and supernatants of *C. glutamicum* WT cultures characterized above were then analyzed for the presence of MG. HPLC analysis of the intracellular and extracellular samples revealed that there was no MG detectable, suggesting that *C. glutamicum* natively is not able to synthesize MG.

To test whether MG exhibits negative effects on the growth of and whether MG is metabolized by *C. glutamicum*, the WT strain was inoculated and incubated in minimal medium with glucose (10 g L^{-1}) and different concentrations of MG (6–24 mM) and the growth and MG concentration were followed. Growth of *C. glutamicum* WT in medium with glucose and MG was the same as that with glucose alone (data not shown) and the MG concentrations in the medium remained constant during cultivations, indicating that *C. glutamicum* is not able to take up MG and use it as a carbon source. In accordance, there was no growth observable in cultivations in medium with MG and without glucose (data not shown).

Overexpression of a Heterologous *mgsD* Gene Leads to Mannosylglycerate Production

With the aim of enabling MG production in *C. glutamicum*, the heterologous *mgsD* gene from *D. mccartyi* was ligated into plasmid pEKEx3 and *C. glutamicum* WT was transformed with the resulting plasmid pEKEx3 *mgsD*. The resulting strain *C. glutamicum* (pEKEx3 *mgsD*) was cultivated in minimal medium with glucose, glucose plus mannose, or mannose as carbon source(s) (**Figure 2C**). The growth rates of *C. glutamicum* (pEKEx3 *mgsD*) in medium with glucose and with glucose plus mannose were 0.21 ± 0.02 and 0.18 ± 0.02 h^{-1}, respectively. These growth rates are considerably lower than those of the plasmid-free host strain (see above, **Figure 2A**). As expected from the results obtained with *C. glutamicum* WT (**Figure 2A**), *C. glutamicum* (pEKEx3 *mgsD*) as well did not grow with mannose as a sole carbon source, although the mannose concentration in the medium again slowly decreased (**Figure 2D**) with a rate of 0.40 ± 0.09 mmol mannose g_{CDW}^{-1} h^{-1}.

Cells and supernatants of the *C. glutamicum* (pEKEx3 *mgsD*) cultures containing glucose as a carbon source were analyzed for the presence of MG. Using HPLC analysis, 111 ± 16 mM MG (60 ± 9 mg g_{CDW}^{-1}) were detected intracellularly after 24 h of cultivation when cells were grown with 20 g glucose L^{-1}. No MG was detectable in supernatants of these cultivations, indicating that MG manifested as an intracellular metabolite in *C. glutamicum* and was not exported into the medium under these conditions, at least not in detectable amounts.

Overexpression of *manA* Leads to Growth of *C. glutamicum* on Mannose

In *D. mccartyi* and some other organisms, MG is synthesized in a single-step reaction by the bifunctional enzyme MgsD from the glycolysis intermediate 3-PG and the activated sugar GDP-Man (Empadinhas et al., 2004; Löffler et al., 2013). Since GDP-Man can be formed from mannose in only one or two steps (see **Figure 1**), mannose represented an interesting substrate for a potential MG-producing *C. glutamicum* cell factory. Since *C. glutamicum* WT was not able to grow with mannose as a sole carbon source (**Figure 2A**), we aimed to exploit growth with metabolization of mannose by overexpressing the native *manA* gene. Overexpression of *manA* has been shown before to improve the growth of *C. glutamicum* strain R with mannose as a sole carbon source (Sasaki et al., 2011). Thus, plasmid pVWEx1 *manA* was constructed and used to transform *C. glutamicum,* resulting in strain *C. glutamicum* (pVWEx1 *manA*).

To evaluate the growth characteristics of *C. glutamicum* (pVWEx1 *manA*), it was cultivated in minimal medium containing glucose, glucose plus mannose, or mannose, and growth and substrate consumption were monitored (**Figures 2E,F**). With glucose and glucose plus mannose, *C. glutamicum* (pVWEx1 *manA*) showed slightly lower growth rates (0.32 ± 0.01 and 0.34 ± 0.01 h^{-1}, respectively), when compared with that of *C. glutamicum* WT (0.40 ± 0.01 h^{-1}). As observed with *C. glutamicum* WT, *C. glutamicum* (pVWEx1 *manA*) showed sequential metabolization of glucose and mannose (**Figure 2F**). However, in contrast to the WT strain, *C. glutamicum* (pVWEx1 *manA*) was able to grow with mannose as a sole carbon source (**Figure 2E**), showing a growth rate of 0.24 ± 0.01 h^{-1} and a mannose consumption rate of 2.49 ±

TABLE 2 | Specific enzyme activities of mannose 6-phosphate isomerase (MPI) in cell extracts of *C. glutamicum* WT and *C. glutamicum* (pVWEx1 *manA*) cells, harvested during mid-exponential phase with either glucose, glucose plus mannose, or mannose as carbon source(s).

Strain	Specific MPI activity U (mg protein)$^{-1}$		
	1% glucose	1% glucose plus 1% mannose	1% mannose
C. glutamicum WT	0.07 ± 0.02	0.10 ± 0.08	n.g.
C. glutamicum (pVWEx1 *manA*)	0.39 ± 0.10	0.40 ± 0.10	0.38 ± 0.01

n.g., no growth on this substrate. Experiments have been performed in triplicate and the standard deviation is given.

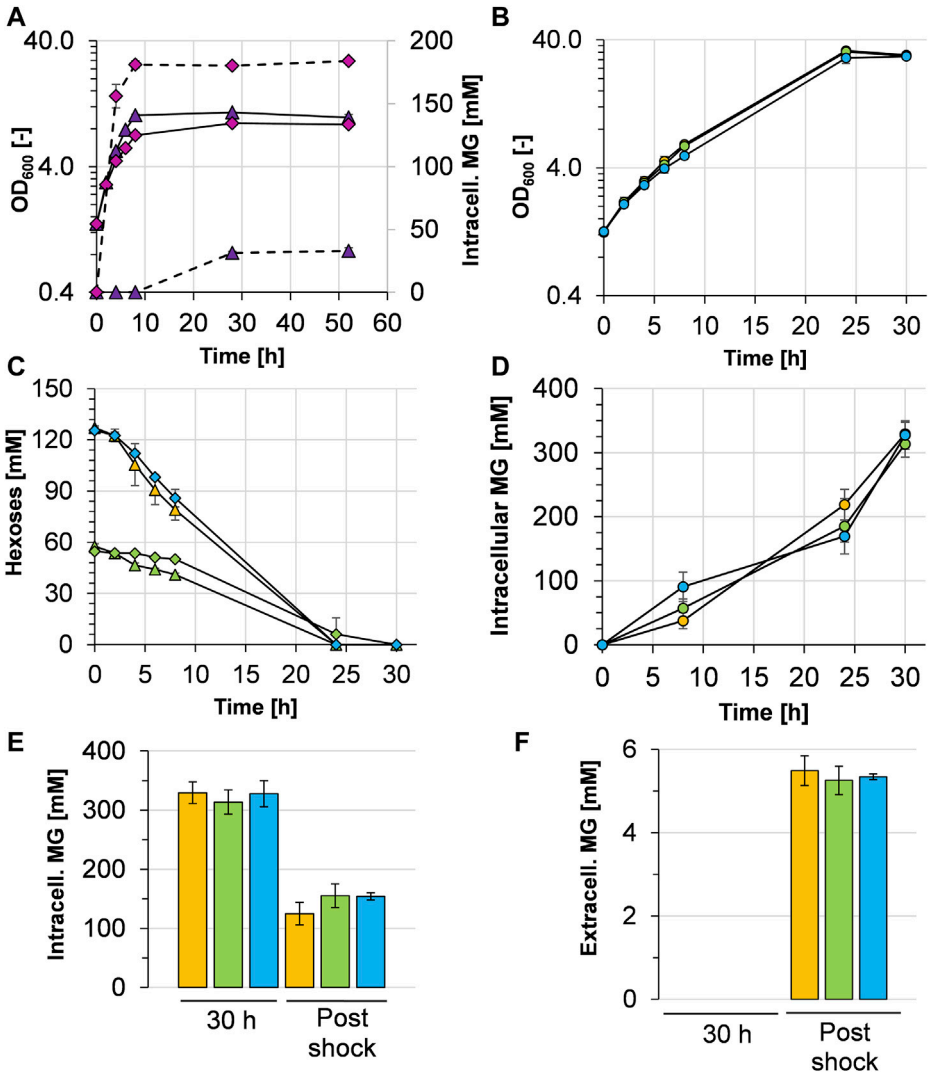

FIGURE 3 | Growth characteristics and mannosylglycerate (MG) production behavior of *C. glutamicum* (pEKEx3 *mgsD*) (pVWEx1 *manA*) grown in different media. **(A)** Growth (solid lines) and intracellular MG concentration (dashed lines) in 2xYT complex medium with IPTG-induction (pink diamonds) and without IPTG-induction (purple triangles). **(B)** Growth and **(C)** hexose (glucose and mannose) consumption of *C. glutamicum* (pEKEx3 *mgsD*) (pVWEx1 *manA*) in CGXII minimal medium containing either 2% glucose (orange symbols), 1% glucose plus 1% mannose (green symbols), or 2% mannose (blue symbols) with the corresponding intracellular **(D)** and extracellular **(E)** MG concentrations, the latter upon cold shock with ultrapure H_2O. Before the cold shock, extracellular MG concentrations were below the detection limit. Growth in **(B)** is represented by closed circles; glucose and mannose concentrations in **(C)** are represented by triangles and diamonds, respectively. Experiments were conducted in biological triplicates and the standard deviation is given as error bars.

0.07 mmol mannose g_{CDW}^{-1} h^{-1} within the first 7.5 h of incubation.

Overexpression of *manA* was evaluated by determination of the specific MPI activities in *C. glutamicum* WT and *C. glutamicum* (pVWEx1 *manA*) cells from the cultures characterized above (**Figures 2A,E**). As shown in **Table 2**, the specific MPI activities in extracts of *C. glutamicum* (pVWEX1 *manA*) were four- to sixfold higher in cells grown with glucose, with glucose plus mannose, and with mannose, when compared to the activities in extracts of *C. glutamicum* WT cells grown with glucose or with glucose plus mannose.

Taken together, our results show that the plasmid-borne, native *manA* gene in *C. glutamicum* (pVWEx1 *manA*) is overexpressed and that *manA* overexpression and thus, higher MPI activities enable *C. glutamicum* WT to grow on mannose as a sole carbon source.

Combined Overexpression of *manA* and *mgsD* Enhances Mannosylglycerate Production and a Cold Shock Releases Mannosylglycerate From the Cytosol

With the aim of facilitating MG production from mannose as a carbon source, *C. glutamicum* (pEKEx3 *mgsD*) was transformed with plasmid pVWEx1 *manA*. The capacity of the resulting strain *C. glutamicum* (pEKEx3 *mgsD*)(pVWEx1 *manA*) to produce MG was investigated first by cultivations in a 2xYT complex medium (**Figure 3A**). When P_{tac}-based expression of *mgsD* and *manA* was not induced with IPTG, *C. glutamicum* (pEKEx3 *mgsD*) (pVWEx1 *manA*) grew to a maximal OD_{600} of about 11 and accumulated a maximum of 33 ± 3 mM (18 ± 1 mg g_{CDW}^{-1}) of intracellular MG, which was probably due to leaky *mgsD* and *manA* expressions based on P_{tac}. With the induction of IPTG, the strain grew to a slightly lower maximal OD_{600} of about 9 and accumulated up to 184 ± 2 mM (99 ± 1 mg g_{CDW}^{-1}) of intracellular MG. Importantly, the intracellular MG concentration remained stable in the stationary phase for ca. forty-two hours (**Figure 3A**), corroborating our previous conclusion that MG is not metabolized by *C. glutamicum* (see above).

To evaluate MG production in defined minimal medium, *C. glutamicum* (pEKEx3 *mgsD*) (pVWEx1 *manA*) was cultivated with 1% (w/v) glucose, 1% (wt/vol) glucose plus 1% (wt/vol) mannose, and 1% (wt/vol) mannose (**Figure 3B**). The growth rates between t = 0 and t = 8 h were 0.17 ± 0.01 h^{-1} with glucose, 0.17 ± 0.01 h^{-1} with glucose plus mannose, and 0.15 ± 0.01 h^{-1} with mannose. The respective consumption rates were 4.12 ± 0.43 mmol glucose g_{CDW}^{-1} h^{-1} within the first 8 h of incubation, 1.49 ± 0.09 mmol glucose g_{CDW}^{-1} h^{-1}, and 0.41 ± 0.10 mmol mannose g_{CDW}^{-1} h^{-1} and 4.49 ± 0.54 mmol mannose g_{CDW}^{-1} h^{-1}, respectively. The substrates (about 120 mM in every culture) were consumed within 24 h (**Figure 3C**), and the intracellular MG concentrations raised steadily (**Figure 3D**). After 30 h, the glucose-grown cells intracellularly accumulated 329 ± 18 mM, the glucose plus mannose-grown cells 314 ± 21 mM and the mannose-grown cells 328 ± 21 mM (**Figure 3E**), corresponding to 177 ± 10, 168 ± 11, and 176 ± 12 mg MG g_{CDW}^{-1}, respectively. However, analysis of MG in the culture supernatants revealed that the *C. glutamicum* (pEKEx3 *mgsD*) (pVWEx1 *manA*) cells under these conditions did not release MG in detectable amounts into the medium (data not shown). In summary, the results obtained with *C. glutamicum* (pEKEx3 *mgsD*) (pVWEx1 *manA*) reflect that mannose can substitute for glucose as a carbon source for intracellular MG production.

For biotechnological production processes, it is always of interest when the desired product can be harvested from culture broth. To enable the release of MG from the *C. glutamicum* cells into the medium, an osmotic temperature shock (cold water shock) with 4°C cold ultrapure water followed by 30 min incubation on ice was applied. As shown in **Figure 3E**, this treatment lowered the intracellular MG concentration by about 51–62%, leaving 125 ± 19, 155 ± 20, and 154 ± 6 mM in the cytosol of *C. glutamicum* (pVWEx1 *manA*) (pEKEx3 *mgsD*), respectively. Moreover, the cold water shock resulted in a release of MG from the cytosol into the medium, which led to extracellular MG concentrations of 5.5 ± 0.4 mM (1.48 g L^{-1}) for glucose-grown cells, 5.3 ± 0.3 mM (1.42 g L^{-1}) for glucose plus mannose-grown cells, and 5.3 ± 0.1 mM (1.42 g L^{-1}) for mannose-grown cells (**Figure 3F**). The yields thus were in the range of about 1.45 g MG per 20 g of sugar, corresponding to 0.073 g MG g_{sugar}^{-1} or 7.3%.

Constructing a One-Plasmid System for Mannose Utilization and Mannosylglycerate Production and Applying It for Cumulative Mannosylglycerate Production

To construct a one-plasmid system for combining efficient mannose utilization and MG production, the *mgsD* gene was cloned into the pVWEx1 *manA* plasmid and the resulting plasmid pVWEx1 *manA mgsD* was used to transform *C. glutamicum*. The resulting strain *C. glutamicum* (pVWEx1 *manA mgsD*) was cultivated in minimal medium with glucose plus mannose (**Figure 4A**). The growth rate of *C. glutamicum* (pVWEx1 *manA mgsD*) was significantly higher when compared to that of the strain carrying two plasmids, *C. glutamicum* (pVWEx1 *manA*) (pEKEx3 *mgsD*) (0.32 ± 0.01 vs. 0.17 ± 0.01 h^{-1}, see also **Figure 3B**). Both strains showed very similar MG production capacities (**Figure 4B**); the intracellular MG concentration in *C. glutamicum* (pVWEx1 *manA mgsD*) was determined to be 327 ± 31 mM (= 175 ± 17 mg MG g_{CDW}^{-1}), compared to 314 ± 21 mM in the two-plasmid-strain. After cold water shock, the released MG reached 5.6 ± 0.6 mM, leaving 143 ± 6 mM of intracellular MG in the cytosol, compared to 5.3 ± 0.34 mM extracellularly and 155 ± 20 mM intracellularly with *C. glutamicum* (pVWEx1 *manA*) (pEKEx3 *mgsD*). These values correspond to recoveries after cold water shock of about 56% for the one-plasmid system and 51% for the two-plasmid system.

To test whether cells can be recycled and applied for repeated cycles of cultivation and production, we set up an experiment similar to what has previously been termed *bacterial milking* (Sauer and Galinski, 1998). For that purpose, *C. glutamicum* (pVWEx1 *manA mgsD*) was cultivated for 24 h in minimal medium with mannose and glucose (**Figure 5A**) and cells were harvested and exposed to a cold

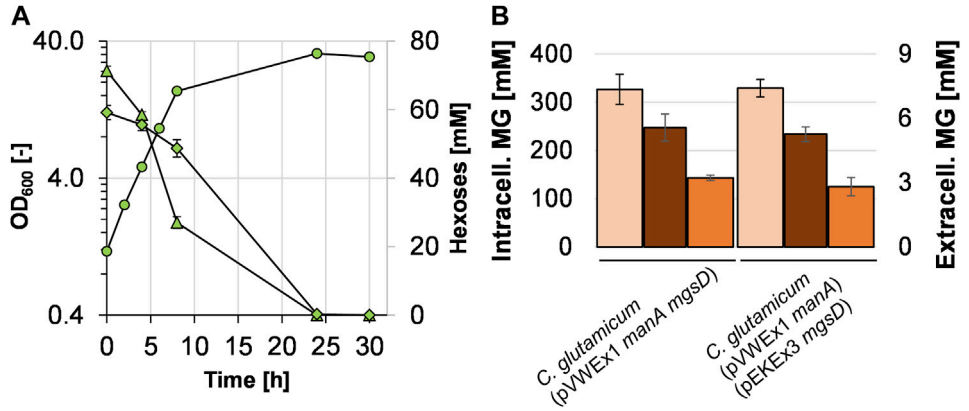

FIGURE 4 | Growth of *C. glutamicum* (pVWEx1 *manA mgsD*) with 1% glucose (triangles) and 1% mannose (diamonds) in CGXII minimal medium **(A)** and comparison of intracellularly accumulated MG (light red bars), released MG (dark bars), and remaining intracellular MG (orange bars) obtained with *C. glutamicum* (pVWEx1 *manA*) (pEKEx3 *mgsD*) under the same conditions **(B)**.

water shock, which released MG from the cytosol. Afterward, these cells were used to inoculate fresh medium, the culture was incubated again for 24 h, and the cells were again subjected to cold water shock treatment. The initial OD_{600} dropped from ca. 32–12, which is due to the previous sampling for determination of OD_{600}, of the substrates, and of intra- and extracellular MG. The growth-and-extraction cycle was repeated three times, leading to repeated increase and decrease in the intracellular MG concentration (**Figure 5B**) and stepwise increase in the MG concentration of the "milking extract" (**Figure 5C**). Four extractions (E1–E4 in **Figure 5C**) led to the release of 3.8 ± 0.3, 5.0 ± 1.2, 4.9 ± 0.1, and 6.2 ± 1.3 mM MG, respectively, which eventually summed up to 19.9 ± 2.9 mM MG (5.34 g L^{-1}) in the extract solution. The final yield of this experiment was 5.34 g MG per 80 g of sugar, corresponding to 0.067 g MG g_{sugar}^{-1} or 6.7%.

DISCUSSION

MG is a compatible solute that occurs mainly in (hyper) thermophilic organisms (Santos and da Costa, 2002; Borges et al., 2014) and red algae of the order Ceramiales (Kremer, 1980) and represents an interesting product for microbial production due to its superior protective properties on protein structures *in vivo* and *in vitro*. Therefore, it might have great potential to promote the development of new drugs for protein-misfolding diseases, such as Parkinson's and Alzheimer's disease (Faria et al., 2013; Jorge et al., 2016). However, in contrast to other compatible solutes like ectoine (Fallet et al., 2010; He et al., 2015; Zhao et al., 2019) or trehalose (Schiraldi et al., 2002; Song et al., 2016), whose production has been exploited intensely, the knowledge on the production of MG is more restricted.

C. glutamicum not only is a suitable host for MG production due to the vast set of established engineering tools and its genetic accessibility (Becker and Wittmann, 2015; Pérez-García and Wendisch, 2018) but also does not take up and metabolize MG (as shown here) like other industrially relevant organisms, such as *E. coli* and *Bacillus subtilis* (Sampaio et al., 2004). *C. glutamicum* has been engineered to produce the native compatibles solutes trehalose (Carpinelli et al., 2006) and L-proline (Jensen and Wendisch, 2013) and the nonnative compatible solutes α-D-glucosylglycerol (Roenneke et al., 2018), L-pipecolic acid (Pérez-García et al., 2019), ectoine/hydroxyectoine (Gießelmann et al., 2019), and very recently also MG (Tian et al., 2020). In the latter work, MG production has been reported from glucose and mannose plus glycerate and authors applied MG synthase from *Rhodothermus marinus* DSM 4252 and additionally overexpressed the genes *nahK* from *Bifidobacterium longum*, encoding N-acetylhexosamine 1-kinase, *manB*, encoding phosphomannomutase from *E. coli*, and *manC*, encoding mannose 1-phosphate guanylyl transferase from *E. coli* to convert glucose/mannose to MG (Tian et al., 2020). This strain produced 2.1 g MG L^{-1} from 20 g glucose and 5 g glycerate L^{-1}, 5.5 g MG L^{-1} from 20 g mannose and 5 g glycerate L^{-1}, and 7.2 g MG L^{-1} from mixed sugar substrates containing 30.6 g mannose L^{-1}, 5.1 g fructose L^{-1}, 5.0 g glucose L^{-1}, and 10 g glycerate L^{-1} in a high cell density fermentation processes with an inoculation OD_{600} of 25. Interestingly, production from mannose and glycerate was 2.6-fold higher than from glucose and glycerate. In the data presented in this work, production from glucose, from glucose plus mannose, and from mannose alone yielded similar results, not highlighting one over the other carbon source. This might have to do with the fact that 0.5% glycerate was supplemented by Tian et al. and served as an additional carbon source.

Besides *C. glutamicum*, also *S. cerevisiae* has been genetically modified to produce MG (Faria et al., 2018). The MG-producing *S. cerevisiae* strain (over)expressed the heterologous *mgsD* gene of *D. mccartyi* and the homologous PMI40 (encoding mannose-6-phosphate isomerase) and PSA1 (encoding GDP-mannose pyrophosphorylase) genes, resulting in an accumulation of up to 16 mg MG g_{CDW}^{-1}. Compared to this intracellular MG content, the herein presented 177 mg g_{CDW}^{-1} in *C. glutamicum* is more than tenfold higher. The respective value of the *C. glutamicum* strain constructed by Tian et al. (2020) accumulated even more than 400 mg MG g_{CDW}^{-1}; however, this was produced from a mixture of several sugars and the direct precursor glycerate at quite high concentrations. Up to about 86 mg MG g_{CDW}^{-1} and a final titer of

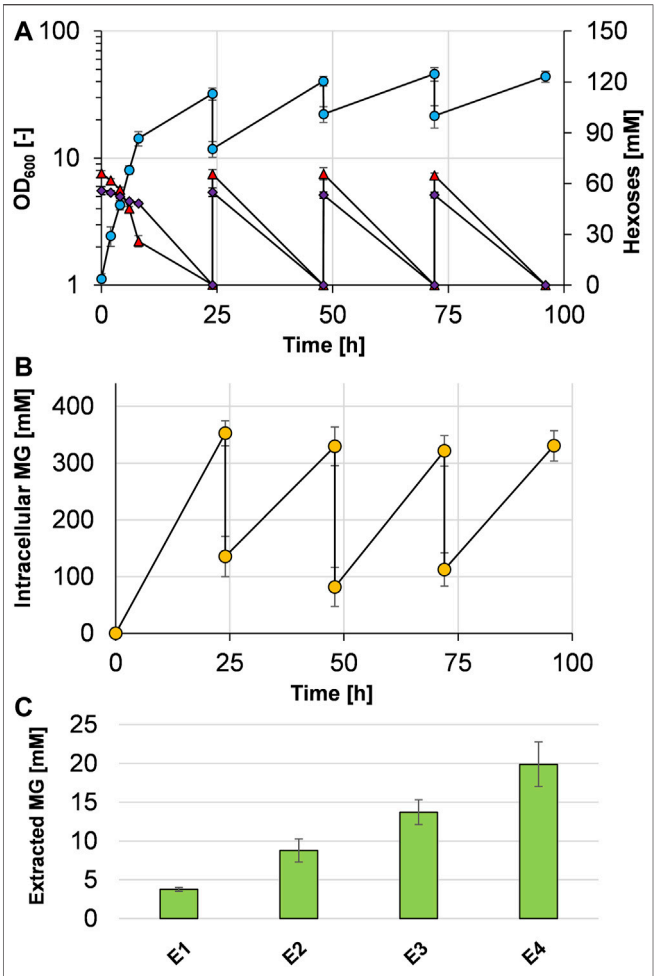

FIGURE 5 | Bacterial milking experiment with *C. glutamicum* (pVWEx1 *manA mgsD*) in CGXII minimal medium with 1% glucose and 1% mannose. Cells were cultivated 24 h in repeated cycles and growth (blue circles), mannose (purple diamonds), and glucose (red triangles) concentrations are given **(A)**. After 24 h of cultivation, the cells were harvested by centrifugation and shocked with ultrapure ice-cold water, leading to the release of MG from the cytosol, determined by analysis of intracellular MG concentrations **(B)**. The extract solution was collected by centrifugation and stored at 4°C; the cell pellet was used to inoculate the fresh medium. The procedure was repeated three times; the stored extract was used for another round of extraction 24 h later. This procedure led to stepwise accumulation of MG in the extract **(C)**. Concentrations of the released and cumulated MG that were measured in the supernatant after the single extraction steps (E1–E4) are shown as bars. Experiments were conducted in biological triplicates and the standard deviation is given as error bars.

1.7 g MG L^{-1} have been produced in a fed-batch fermentation in a complex medium using a trehalose-deficient mutant of *Thermus thermophilus* RQ-1 (Egorova et al., 2007), a thermophilic bacterium that natively forms MG in response to osmotic stress (Nunes et al., 1995). Commercially, MG has been reported to be produced by bitop AG (Witten, Germany) *via* fermentation of a natural producer, *Rhodothermus marinus*, but this resulted in low titers and high production costs (Faria et al., 2018).

Since MG by the deployed MG synthase from *D. mccartyi* is synthesized from 3-phosphoglycerate and the activated sugar GDP-mannose, it was logical to test mannose as a sole and additional carbon source for MG production. However, the basis strain *C. glutamicum* ATCC 13032 naturally does not grow on mannose (**Figure 2A**). In contrast, *C. glutamicum* R at least showed minimal growth with mannose as a sole carbon source (Sasaki et al., 2011). As in *C. glutamicum* R (Sasaki et al., 2011), overexpression of the native *manA* gene led to efficient mannose metabolization in *C. glutamicum* ATCC 13032, thereby enabling exploitation of this carbon source for MG production. Determination of specific mannose 6-phosphate isomerase activities in *C. glutamicum* (pVWEx1 *manA*) demonstrated successful overexpression of *manA* and resulted in about 8-fold increased specific activities on all tested carbon sources/mixtures during the exponential growth phase, when compared to *C. glutamicum* WT. It has been shown that the EII subunit of the phosphoenolpyruvate- (PEP-) dependent phosphotransferase system (PTS) for glucose (encoded by *ptsG*) has very limited transport capacities for mannose besides its main substrate glucose (Moon et al., 2007). Further research indicated that both the fructose and glucose PTS are involved in mannose uptake (Sasaki et al., 2011). These authors also observed increased mannose uptake of a *manA*-overexpressing strain when a mixture of mannose and glucose was present compared with mannose as a sole carbon source. Glucose in all cases was strongly preferred over mannose (Sasaki et al., 2011), which could be observed in this work as well. Nevertheless, the exact mechanism of mannose uptake in *C. glutamicum* remains unclear and requires further research. So far, mannose is a neglected carbon source for cultivations of *C. glutamicum* and its use is limited to those products whose precursor is GDP-mannose and to which mannose lies in close spaciotemporal vicinity, such as GDP-L-fucose (Lee et al., 2009; Chin et al., 2013), mannosyl-oligosaccharides, and MG (Tian et al., 2020). Interestingly, the overexpression of *manA* in a GDP-L-fucose-producing *C. glutamicum* strain showed negative effects on the formation of the product (Chin et al., 2013). In contrast to Tian and coworkers, we aimed to produce MG from glucose and mannose as sole carbon source(s), without supplementations like glycerate. For that purpose, *manA*, enabling mannose utilization, and *mgsD*, enabling MG synthesis, were combined in a two-plasmid system, showing solid production of MG, which accumulated intracellularly. When *manA* and *mgsD* genes were combined in one plasmid, MG production behavior remained similar; however, the resulting strain showed faster growth, which most likely is connected to the omitted spectinomycin for maintenance of the second plasmid.

When comparing the MG-producing strains *C. glutamicum* (pEKEx3 mgsD) and *C. glutamicum* (pEKEx3-mgsD) (pVWEx1 manA), the growth rates on glucose medium were almost the same (**Figures 2C**, **3B**; 0.21 ± 0.02 vs. 0.17 ± 0.01 h^{-1}). The former strain accumulated intracellularly 111 mM MG with glucose as a substrate, and the latter accumulated 329 mM MG, indicating that additional overexpression of manA in fact is very favorable for MG synthesis. This is probably due to the fact that the ManA protein (MPI) is very favorable in converting fructose-6-phosphate to mannose-6-phosphate (see **Figure 1**) and thus provides this precursor of MG synthesis very efficiently.

Extraction of MG from the cytosol into the medium was accomplished with a cold water shock. This method principally was shown before to extract isotopically labeled MG from the *E. coli* cytosol (Sampaio et al., 2003). Preliminary experiments

indicated that mainly the temperature is responsible for the release, since a physiological ice-cold sodium chloride solution extracted MG to a small percentage, whereas ultrapure water at room temperature did not lead to a release of detectable amounts of MG (data not shown). In contrast to the work of Sampaio and colleagues, where almost 100% of radioactively labeled MG could be released from the *E. coli* cytosol into the medium (Sampaio et al., 2003), we here report on the release of up to 62% of MG release from the *C. glutamicum* cytosol. This difference might have to do with the transport capacities for MG, which most likely differs in both organisms. Interestingly, the release of MG from the *C. glutamicum* cytosol into the medium has been reported before to occur without application of a shock leading to the release of about 48% of the MG into the medium (Tian et al., 2020). Since the intracellular concentrations in these strains were higher than in the herein reported ones, it might be speculated that intracellular concentrations of MG in *C. glutamicum* have a certain threshold and upon reaching it, MG leaks out of the cell. In contrast to the export of MG, which has not been studied in detail, the import of MG has been elucidated for *E. coli*, which in contrast to *C. glutamicum* is able to grow with MG as a sole carbon source. In *E. coli*, uptake is mediated by the PEP-dependent PTS with protein MngA as an MG-inducible specific EIIABC complex (Sampaio et al., 2004).

Since the production of compatible solutes with native producers has been achieved successfully before by the so-called *bacterial milking* (Sauer and Galinski, 1998; Egorova et al., 2007), *C. glutamicum* (pVWEx1 *manA mgsD*) was employed for a similar process. Alternating rounds of growth/production and osmotic shocks were used to extract the produced MG from the cells, eventually leading to 5.34 g MG L^{-1} after repeating the extraction three times. In principle, these cycles could be repeated several times more on a larger scale to increase the amount of extracted MG. Similar techniques have been applied before for the production of compatible solutes in their native hosts, e.g., ectoine/hydroxyectoine with *Halomonas elongata* (Sauer and Galinski, 1998; up to 4.1 g L^{-1}) and MG with *Thermus thermophilus* RQ-1 (Egorova et al., 2007; 4.6 g L^{-1}). Recombinant *C. glutamicum* cells grown under elevated osmotic pressure released L-pipecolic acid (about 2.8 g L^{-1}) after an osmotic down-shock (Perez-Garcia et al., 2019), in principle also enabling bacterial milking with repeated cycles. However, the former two processes in contrast to the one that is described here required increased concentrations of sodium chloride of up to 30 g L^{-1}, which is well known to act corrosively on steel reactors and thus might hamper industrial feasibility (Speidel, 1981; Chisti, 1992).

Sustainable production of biochemicals and pharmaceuticals is an intensively discussed and increasingly important topic (Meyer, 2011; Koenig et al., 2019; Matthews et al., 2019). Utilizing green substrates with as little impact on the environment as possible and leading production away from fossil-based resources nowadays has top priorities. Optimally, such sustainable bioprocesses use renewable and not food-carbohydrates-based substrates, to circumvent the *food vs. fuel* debate (Inderwildi and King, 2009). One source for such microbial substrates is hexose and pentose sugars derived from lignocellulose-based materials, which are not intended for food or feed production and often arise from processing plant materials in biorefineries (Valdivia et al., 2016). Conversion of the input lignocellulosic biomass, which is heterogenous in plant origin and composition, results in side streams as byproducts, such as spent sulfite liquor (SSL), a waste stream in pulp and paper manufacturing processes. SSL contains mannose (up to more than 40% of the total sugars), glucose (up to more than 20%), and xylose (up to 20%) as the main carbohydrates, depending on the wood type used in fluctuating proportions (Nigam, 2001; He and Chen, 2020; Hoheneder et al., 2021). However, although SSL in general contains potential inhibitors for bacterial growth (Al-Rudainy et al., 2017), *C. glutamicum* carrying our plasmid pVWEx1-manA has recently been shown to grow in minimal medium containing 20% of ultrafiltrated SSL from softwood pulping, consuming completely both glucose and mannose (Sinner et al., 2021). Moreover, Perez-Gracia et al. (2021) used synthetic SSL, containing glucose, mannose, and xylose, as a substrate for a riboflavin-producing *C. glutamicum* strain with the plasmid-bound expression of *manA* and *xylAB* genes, the latter enabling xylose utilization. Thus, it might be attractive to use *C. glutamicum* (pVWEx1 *manA mgsD*) constructed here for MG production from SSL, a green substrate, that is available in large quantities from lignocellulosic biomass.

CONCLUSION

Taken together, we showed that *C. glutamicum* can be engineered to produce the compatible solute MG by expressing *mgsD* from *D. mccartyi* from glucose and from glucose plus mannose and when the native *manA* is overexpressed from mannose alone as well. The intracellular MG accumulated up to 177 mg MG g_{CDW}^{-1} and up to 62% thereof could be released with a cold water shock, resulting in up to 1.48 g MG L^{-1}. A *bacterial milking*-like experiment with repeated cycles of production and extraction led to 5.34 g MG L^{-1}. Our results provide valuable information to develop *C. glutamicum* as a promising host for industrial production of MG from waste streams containing glucose and/or mannose, such as SSL derived from processed lignocellulosic biomass.

DATA AVAILABILITY STATEMENT

The original contributions presented in the study are included in the article/supplementary material; further inquiries can be directed to the corresponding author.

AUTHOR CONTRIBUTIONS

AS, HS, and BE designed and planned the experiments. AS, HN, and SW performed the experiments. AS, HS, and BE wrote and revised the manuscript.

ACKNOWLEDGMENTS

The authors thankfully acknowledge the help of Andrea Roth with HPLC analyses and Marco Mannes for help with the construction of plasmid pEKEx2 *mgsD* and they thank Gerd Seibold for valuable discussions.

REFERENCES

Adachi, N., Takahashi, C., Ono-Murota, N., Yamaguchi, R., Tanaka, T., and Kondo, A. (2013). Direct L-Lysine Production from Cellobiose by *Corynebacterium glutamicum* Displaying Beta-Glucosidase on its Cell Surface. *Appl. Microbiol. Biotechnol.* 97, 7165–7172. doi:10.1007/s00253-013-5009-4

Al-Rudainy, B., Galbe, M., and Wallberg, O. (2017). Influence of Prefiltration on Membrane Performance During Isolation of Lignin-Carbohydrate Complexes from Spent Sulfite Liquor. *Sep. Purif. Tech.* 187, 380–388. doi:10.1016/j.seppur.2017.06.031

Bakkes, P. J., Ramp, P., Bida, A., Dohmen-Olma, D., Bott, M., and Freudl, R. (2020). Improved pEKEx2-Derived Expression Vectors for Tightly Controlled Production of Recombinant Proteins in *Corynebacterium glutamicum*. *Plasmid* 112, 102540. doi:10.1016/j.plasmid.2020.102540

Becker, J., and Wittmann, C. (2015). Advanced Biotechnology: Metabolically Engineered Cells for the Bio-Based Production of Chemicals and Fuels, Materials, and Health-Care Products. *Angew. Chem. Int. Ed.* 54, 3328–3350. doi:10.1002/anie.201409033

Blombach, B., Riester, T., Wieschalka, S., Ziert, C., Youn, J.-W., Wendisch, V. F., et al. (2011). *Corynebacterium glutamicum* Tailored for Efficient Isobutanol Production. *Appl. Environ. Microbiol.* 77, 3300–3310. doi:10.1128/AEM.02972-10

Blombach, B., Schreiner, M. E., Hola´tko, J., Bartek, T., Oldiges, M., and Eikmanns, B. J. (2007a). l -Valine Production with Pyruvate Dehydrogenase Complex-Deficient *Corynebacterium glutamicum*. *Appl. Environ. Microbiol.* 73, 2079–2084. doi:10.1128/AEM.02826-06

Blombach, B., Schreiner, M. E., Moch, M., Oldiges, M., and Eikmanns, B. J. (2007b). Effect of Pyruvate Dehydrogenase Complex Deficiency on L-Lysine Production with *Corynebacterium glutamicum*. *Appl. Microbiol. Biotechnol.* 76, 615–623. doi:10.1007/s00253-007-0904-1

Borges, N., Jorge, C. D., Gonçalves, L. G., Gonçalves, S., Matias, P. M., and Santos, H. (2014). Mannosylglycerate: Structural Analysis of Biosynthesis and Evolutionary History. *Extremophiles* 18, 835–852. doi:10.1007/s00792-014-0661-x

Borges, N., Marugg, J. D., Empadinhas, N., Costa, M. S. d., and Santos, H. (2004). Specialized Roles of the Two Pathways for the Synthesis of Mannosylglycerate in Osmoadaptation and Thermoadaptation of *Rhodothermus marinus*. *J. Biol. Chem.* 279, 9892–9898. doi:10.1074/jbc.M312186200

Borges, N., Ramos, A., Raven, N., Sharp, R., and Santos, H. (2002). Comparative Study of the Thermostabilizing Properties of Mannosylglycerate and Other Compatible Solutes on Model Enzymes. *Extremophiles* 6, 209–216. doi:10.1007/s007920100236

Carpinelli, J., Krämer, R., and Agosin, E. (2006). Metabolic Engineering of *Corynebacterium glutamicum* for Trehalose Overproduction: Role of the TreYZ Trehalose Biosynthetic Pathway. *Appl. Environ. Microbiol.* 72, 1949–1955. doi:10.1128/AEM.72.3.1949-1955.2006

Chin, Y.-W., Park, J.-B., Park, Y.-C., Kim, K. H., and Seo, J.-H. (2013). Metabolic Engineering of *Corynebacterium glutamicum* to Produce GDP-L-Fucose from Glucose and Mannose. *Bioproc. Biosyst. Eng.* 36, 749–756. doi:10.1007/s00449-013-0900-z

Chisti, Y. (1992). Build Better Industrial Bioreactors. *Chem. Eng. Prog.* 88, 55–58.

Cruz, P. E., Silva, A. C., Roldão, A., Carmo, M., Carrondo, M. J. T., and Alves, P. M. (2006). Screening of Novel Excipients for Improving the Stability of Retroviral and Adenoviral Vectors. *Biotechnol. Prog.* 22, 568–576. doi:10.1021/bp050294y

Dower, W. J., Miller, J. F., and Ragsdale, C. W. (1988). High Efficiency Transformation of *E. coli* by High Voltage Electroporation. *Nucleic Acids Res.* 16, 6127–6145. doi:10.1093/nar/16.13.6127

Eggeling, L., and Bott, M. (2015). A Giant Market and a Powerful Metabolism: L-Lysine Provided by *Corynebacterium glutamicum*. *Appl. Microbiol. Biotechnol.* 99, 3387–3394. doi:10.1007/s00253-015-6508-2

Egorova, K., Grudieva, T., Morinez, C., Kube, J., Santos, H., da Costa, M. S., et al. (2007). High Yield of Mannosylglycerate Production by Upshock Fermentation and Bacterial Milking of Trehalose-Deficient Mutant *Thermus thermophilus* RQ-1. *Appl. Microbiol. Biotechnol.* 75, 1039–1045. doi:10.1007/s00253-007-0915-y

Eikmanns, B. J., Metzger, M., Reinscheid, D., Kircher, M., and Sahm, H. (1991). Amplification of Three Threonine Biosynthesis Genes inCorynebacterium Glutamicum and its Influence on Carbon Flux in Different Strains. *Appl. Microbiol. Biotechnol.* 34, 617–622. doi:10.1007/BF00167910

Eikmanns, B. J., Thum-Schmitz, N., Eggeling, L., Lüdtke, K.-U., and Sahm, H. (1994). Nucleotide Sequence, Expression and Transcriptional Analysis of the *Corynebacterium glutamicum gltA* Gene Encoding Citrate Synthase. *Microbiology* 140, 1817–1828. doi:10.1099/13500872-140-8-1817

Empadinhas, N., Albuquerque, L., Costa, J., Zinder, S. H., Santos, M. A. S., Santos, H., et al. (2004). A Gene from the Mesophilic Bacterium *Dehalococcoides Ethenogenes* Encodes a Novel Mannosylglycerate Synthase. *J. Bacteriol.* 186, 4075–4084. doi:10.1128/JB.186.13.4075-4084.2004

Empadinhas, N., and da Costa, M. S. (2008). To be or Not to be a Compatible Solute: Bioversatility of Mannosylglycerate and Glucosylglycerate. *Syst. Appl. Microbiol.* 31, 159–168. doi:10.1016/j.syapm.2008.05.002

Esteves, A. M., Chandrayan, S. K., McTernan, P. M., Borges, N., Adams, M. W. W., and Santos, H. (2014). Mannosylglycerate and Di- myo -Inositol Phosphate Have Interchangeable Roles during Adaptation of Pyrococcus Furiosus to Heat Stress. *Appl. Environ. Microbiol.* 80, 4226–4233. doi:10.1128/AEM.00559-14

Fallet, C., Rohe, P., and Franco-Lara, E. (2010). Process Optimization of the Integrated Synthesis and Secretion of Ectoine and Hydroxyectoine under Hyper/Hypo-Osmotic Stress. *Biotechnol. Bioeng.* 107, 124–133. doi:10.1002/bit.22750

Faria, C., Borges, N., Rocha, I., and Santos, H. (2018). Production of Mannosylglycerate in *Saccharomyces cerevisiae* by Metabolic Engineering and Bioprocess Optimization. *Microb. Cell Fact* 17, 178. doi:10.1186/s12934-018-1023-7

Faria, C., Jorge, C. D., Borges, N., Tenreiro, S., Outeiro, T. F., and Santos, H. (2013). Inhibition of Formation of α-synuclein Inclusions by Mannosylglycerate in a Yeast Model of Parkinson's Disease. *Biochim. Biophys. Acta* 1830, 4065–4072. doi:10.1016/j.bbagen.2013.04.015

Faria, T. Q., Lima, J. C., Bastos, M., Maçanita, A. L., and Santos, H. (2004). Protein Stabilization by Osmolytes from Hyperthermophiles. *J. Biol. Chem.* 279, 48680–48691. doi:10.1074/jbc.M408806200

Gießelmann, G., Dietrich, D., Jungmann, L., Kohlstedt, M., Jeon, E. J., Yim, S. S., et al. (2019). Metabolic Engineering of Corynebacterium Glutamicum for High-Level Ectoine Production: Design, Combinatorial Assembly, and Implementation of a Transcriptionally Balanced Heterologous Ectoine Pathway. *Biotechnol. J.* 14, 1800417. doi:10.1002/biot.201800417

Green, M. R., and Sambrook, J. (2012). *Molecular Cloning: A Laboratory Manual*. New York: Cold Spring Harbor Laboratory Press.

Gutmann, M., Hoischen, C., and Krämer, R. (1992). Carrier-mediated Glutamate Secretion by *Corynebacterium glutamicum* under Biotin Limitation. *Biochim. Biophys. Acta (Bba) - Biomembranes* 1112, 115–123. doi:10.1016/0005-2736(92)90261-J

Hanahan, D. (1983). Studies on Transformation of *Escherichia coli* with Plasmids. *J. Mol. Biol.* 166, 557–580. doi:10.1016/S0022-2836(83)80284-8

He, Q., and Chen, H. (2020). Increased Efficiency of Butanol Production from Spent Sulfite Liquor by Removal of Fermentation Inhibitors. *J. Clean. Prod.* 263, 121356. doi:10.1016/j.jclepro.2020.121356

He, Y.-Z., Gong, J., Yu, H.-Y., Tao, Y., Zhang, S., and Dong, Z.-Y. (2015). High Production of Ectoine from Aspartate and Glycerol by Use of Whole-Cell Biocatalysis in Recombinant *Escherichia coli*. *Microb. Cell Fact* 14, 55. doi:10.1186/s12934-015-0238-0

Hemmerich, J., Labib, M., Steffens, C., Reich, S. J., Weiske, M., Baumgart, M., et al. (2020). Screening of a Genome-reduced Corynebacterium Glutamicum Strain Library for Improved Heterologous Cutinase Secretion. *Microb. Biotechnol.* 13, 2020–2031. doi:10.1111/1751-7915.13660

Henke, N. A., and Wendisch, V. F. (2019). Improved Astaxanthin Production with *Corynebacterium Glutamicum* by Application of a Membrane Fusion Protein. *Mar. Drugs* 17, 621. doi:10.3390/md17110621

Hoheneder, R., Fitz, E., Bischof, R. H., Russmayer, H., Ferrero, P., Peacock, S., et al. (2021). Efficient Conversion of Hemicellulose Sugars from Spent Sulfite Liquor into Optically Pure L-Lactic Acid by *Enterococcus mundtii*. *Bioresour. Tech.* 333, 125215. doi:10.1016/j.biortech.2021.125215

Inderwildi, O. R., and King, D. A. (2009). Quo Vadis biofuels? *Energy Environ. Sci.* 2, 343–346. doi:10.1039/B822951C

Jensen, J. V., and Wendisch, V. F. (2013). Ornithine Cyclodeaminase-Based Proline Production by *Corynebacterium glutamicum*. *Microb. Cell Fact* 12, 63. doi:10.1186/1475-2859-12-63

Jorge, C. D., Borges, N., Bagyan, I., Bilstein, A., and Santos, H. (2016). Potential Applications of Stress Solutes from Extremophiles in Protein Folding Diseases and Healthcare. *Extremophiles* 20, 251–259. doi:10.1007/s00792-016-0828-8

Kawaguchi, H., Vertès, A. A., Okino, S., Inui, M., and Yukawa, H. (2006). Engineering of a Xylose Metabolic Pathway in *Corynebacterium glutamicum*. *Appl. Environ. Microbiol.* 72, 3418–3428. doi:10.1128/aem.72.5.3418-3428.2006

Koenig, S. G., Bee, C., Borovika, A., Briddell, C., Colberg, J., Humphrey, G. R., et al. (2019). A green Chemistry Continuum for a Robust and Sustainable Active Pharmaceutical Ingredient Supply Chain. *ACS Sust. Chem. Eng.* 7, 16937–16951. doi:10.1021/acssuschemeng.9b02842

Kremer, B. P. (1980). Taxonomic Implications of Algal Photoassimilate Patterns. *Br. Phycological J.* 15, 399–409. doi:10.1080/00071618000650401

Lange, J., Müller, F., Takors, R., and Blombach, B. (2017). Harnessing Novel Chromosomal Integration Loci to Utilize an Organosolv-Derived Hemicellulose Fraction for Isobutanol Production with engineeredCorynebacterium Glutamicum. *Microb. Biotechnol.* 11, 257–263. doi:10.1111/1751-7915.12879

Laslo, T., von Zaluskowski, P., Gabris, C., Lodd, E., Rückert, C., Dangel, P., et al. (2012). Arabitol Metabolism of *Corynebacterium glutamicum* and its Regulation by AtlR. *J. Bacteriol.* 194, 941–955. doi:10.1128/JB.06064-11

Lee, W.-H., Han, N.-S., Park, Y.-C., and Seo, J.-H. (2009). Modulation of Guanosine 5′-Diphosphate-D-Mannose Metabolism in Recombinant *Escherichia coli* for Production of Guanosine 5′-Diphosphate-L-Fucose. *Bioresour. Tech.* 100, 6143–6148. doi:10.1016/j.biortech.2009.07.035

Lentzen, G., and Schwarz, T. (2006). Extremolytes: Natural Compounds from Extremophiles for Versatile Applications. *Appl. Microbiol. Biotechnol.* 72, 623–634. doi:10.1007/s00253-006-0553-9

Löffler, F. E., Yan, J., Ritalahti, K. M., Adrian, L., Edwards, E. A., Konstantinidis, K. T., et al. (2013). *Dehalococcoides Mccartyi* gen. nov., sp. nov., Obligately Organohalide-Respiring Anaerobic Bacteria Relevant to Halogen Cycling and Bioremediation, Belong to a Novel Bacterial Class, *Dehalococcoidia* Classis nov., Order *Dehalococcoidales* ord. Nov. And Family *Dehalococcoidaceae* fam. nov., within the Phylum Chloroflexi. *Int. J. Syst. Evol. Microbiol.* 63, 625–635. doi:10.1099/ijs.0.034926-0

Matthews, N. E., Cizauskas, C. A., Layton, D. S., Stamford, L., and Shapira, P. (2019). Collaborating Constructively for Sustainable Biotechnology. *Sci. Rep.* 9, 19033. doi:10.1038/s41598-019-54331-7

Meiswinkel, T. M., Gopinath, V., Lindner, S. N., Nampoothiri, K. M., and Wendisch, V. F. (2013). Accelerated Pentose Utilization byCorynebacterium Glutamicumfor Accelerated Production of Lysine, Glutamate, Ornithine and Putrescine. *Microb. Biotechnol.* 6, 131–140. doi:10.1111/1751-7915.12001

Melo, E. P., Faria, T. Q., Martins, L. O., Gonçalves, A. M., and Cabral, J. M. S. (2001). Cutinase Unfolding and Stabilization by Trehalose and Mannosylglycerate. *Proteins* 42, 542–552. doi:10.1002/1097-0134(20010301)42:4<542::AID-PROT120>3.0.CO;2-4

Meyer, H.-P. (2011). Sustainability and Biotechnology. *Org. Process. Res. Dev.* 15, 180–188. doi:10.1021/op100206p

Moon, M.-W., Park, S.-Y., Choi, S.-K., and Lee, J.-K. (2007). The Phosphotransferase System of *Corynebacterium glutamicum*: Features of Sugar Transport and Carbon Regulation. *J. Mol. Microbiol. Biotechnol.* 12, 43–50. doi:10.1159/000096458

Nigam, J. N. (2001). Ethanol Production from Hardwood Spent Sulfite Liquor Using an Adapted Strain of *Pichia Stipitis*. *J. Ind. Microbiol. Biotechnol.* 26, 145–150. doi:10.1038/sj.jim.7000098

Nunes, O. C., Manaia, C. M., Da Costa, M. S., and Santos, H. (1995). Compatible Solutes in the Thermophilic Bacteria *Rhodothermus marinus* and "*Thermus thermophilus*". *Appl. Environ. Microbiol.* 61, 2351–2357. doi:10.1128/aem.61.6.2351-2357.1995

Park, S. H., Kim, H. U., Kim, T. Y., Park, J. S., Kim, S.-S., and Lee, S. Y. (2014). Metabolic Engineering of *Corynebacterium glutamicum* for L-Arginine Production. *Nat. Commun.* 5. doi:10.1038/ncomms5618

Pérez-García, F., Brito, L. F., and Wendisch, V. F. (2019). Function of L-Pipecolic Acid as Compatible Solute in *Corynebacterium glutamicum* as Basis for its Production under Hyperosmolar Conditions. *Front. Microbiol.* 10. doi:10.3389/fmicb.2019.00340

Pérez-García, F., Burgardt, A., Kallman, D. R., Wendisch, V. F., and Bar, N. (2021). Dynamic Co-Cultivation Process of Corynebacterium Glutamicum Strains for the Fermentative Production of Riboflavin. *Fermentation* 7, 11. doi:10.3390/fermentation7010011

Pérez-García, F., and Wendisch, V. F. (2018). Transport and Metabolic Engineering of the Cell Factory *Corynebacterium Glutamicum*. *FEMS Microbiol. Lett.* 365, fny166. doi:10.1093/femsle/fny166

Peters-Wendisch, P. G., Schiel, B., Wendisch, V. F., Katsoulidis, E., Möckel, B., Sahm, H., et al. (2001). Pyruvate Carboxylase Is a Major Bottleneck for Glutamate and Lysine Production by *Corynebacterium glutamicum*. *J. Mol. Microbiol. Biotechnol.* 3, 295–300.

Roenneke, B., Rosenfeldt, N., Derya, S. M., Novak, J. F., Marin, K., Krämer, R., et al. (2018). Production of the Compatible Solute α-d-glucosylglycerol by Metabolically Engineered Corynebacterium Glutamicum. *Microb. Cell Fact* 17, 1. doi:10.1186/s12934-018-0939-2

Ryu, J., Kanapathipillai, M., Lentzen, G., and Park, C. B. (2008). Inhibition of β-amyloid Peptide Aggregation and Neurotoxicity by α-d-mannosylglycerate, a Natural Extremolyte. *Peptides* 29, 578–584. doi:10.1016/j.peptides.2007.12.014

Sampaio, M.-M., Chevance, F., Dippel, R., Eppler, T., Schlegel, A., Boos, W., et al. (2004). Phosphotransferase-mediated Transport of the Osmolyte 2-O-α-Mannosyl-D-Glycerate in *Escherichia coli* Occurs by the Product of the mngA (hrsA) Gene and Is Regulated by the mngR (farR) Gene Product Acting as Repressor. *J. Biol. Chem.* 279, 5537–5548. doi:10.1074/jbc.M310980200

Sampaio, M.-M., Santos, H., and Boos, W. (2003). Synthesis of GDP-Mannose and Mannosylglycerate from Labeled Mannose by Genetically Engineered *Escherichia coli* without Loss of Specific Isotopic Enrichment. *Appl. Environ. Microbiol.* 69, 233–240. doi:10.1128/AEM.69.1.233-240.2003

Santos, H., and da Costa, M. S. (2001). "[26] Organic Solutes from Thermophiles and Hyperthermophiles," in *Methods in Enzymology Hyperthermophilic Enzymes, Part C*. Editors M. W. Adams and R. M. Kelly (Cambridge, MA: Academic Press), 302–315. doi:10.1016/S0076-6879(01)34478-6

Santos, H., and da Costa, M. S. (2002). Compatible Solutes of Organisms that Live in Hot saline Environments. *Environ. Microbiol.* 4, 501–509. doi:10.1046/j.1462-2920.2002.00335.x

Santos, H., Lamosa, P., and Borges, N. (2006). "8 Characterization and Quantification of Compatible Solutes in (Hyper) thermophilic Microorganisms," in *Methods in Microbiology*. Editor F. A. Rainey (Cambridge, MA: Academic Press), 173–199. doi:10.1016/S0580-9517(08)70011-4

Sasaki, M., Teramoto, H., Inui, M., and Yukawa, H. (2011). Identification of Mannose Uptake and Catabolism Genes in *Corynebacterium glutamicum* and Genetic Engineering for Simultaneous Utilization of Mannose and Glucose. *Appl. Microbiol. Biotechnol.* 89, 1905–1916. doi:10.1007/s00253-010-3002-8

Sauer, T., and Galinski, E. A. (1998). Bacterial Milking: A Novel Bioprocess for Production of Compatible Solutes. *Biotechnol. Bioeng.* 57, 306–313. doi:10.1002/(SICI)1097-0290(19980205)57:3<306::AID-BIT7>3.0.CO;2-L

Schiraldi, C., Di Lernia, I., and De Rosa, M. (2002). Trehalose Production: Exploiting Novel Approaches. *Trends Biotechnol.* 20, 420–425. doi:10.1016/S0167-7799(02)02041-3

Schwentner, A., Feith, A., Münch, E., Busche, T., Rückert, C., Kalinowski, J., et al. (2018). Metabolic Engineering to Guide Evolution - Creating a Novel Mode for L-Valine Production with Corynebacterium Glutamicum. *Metab. Eng.* 47, 31–41. doi:10.1016/j.ymben.2018.02.015

Schwentner, A., Feith, A., Münch, E., Stiefelmaier, J., Lauer, I., Favilli, L., et al. (2019). Modular Systems Metabolic Engineering Enables Balancing of Relevant Pathways for L-Histidine Production with *Corynebacterium glutamicum*. *Biotechnol. Biofuels* 12, 65. doi:10.1186/s13068-019-1410-2

Seibold, G., Auchter, M., Berens, S., Kalinowski, J., and Eikmanns, B. J. (2006). Utilization of Soluble Starch by a Recombinant *Corynebacterium glutamicum* Strain: Growth and Lysine Production. *J. Biotechnol.* 124, 381–391. doi:10.1016/j.jbiotec.2005.12.027

Sgobba, E., Blöbaum, L., and Wendisch, V. F. (2018). Production of Food and Feed Additives from Non-food-competing Feedstocks: Valorizing N-Acetylmuramic Acid for Amino Acid and Carotenoid Fermentation with *Corynebacterium glutamicum*. *Front. Microbiol.* 9, 1. doi:10.3389/fmicb.2018.02046

Silva, Z. x. l., Borges, N., Martins, L. x. g. O., Wait, R., da Costa, M. S., and Santos, H. (1999). Combined Effect of the Growth Temperature and Salinity of the Medium on the Accumulation of Compatible Solutes by *Rhodothermus Marinus* and *Rhodothermus obamensis*. *Extremophiles* 3, 163–172. doi:10.1007/s007920050112

Sinner, P., Stiegler, M., Herwig, C., and Kager, J. (2021). Noninvasive Online Monitoring of Corynebacterium Glutamicum Fed-Batch Bioprocesses Subject to Spent Sulfite Liquor Raw Material Uncertainty. *Bioresource Technol.* 321, 124395. doi:10.1016/j.biortech.2020.124395

Song, X., Tang, S., Jiang, L., Zhu, L., and Huang, H. (2016). Integrated Biocatalytic Process for Trehalose Production and Separation from Maltose. *Ind. Eng. Chem. Res.* 55, 10566–10575. doi:10.1021/acs.iecr.6b02276

Speidel, M. O. (1981). Stress Corrosion Cracking of Stainless Steels in NaCl Solutions. *Mta* 12, 779–789. doi:10.1007/BF02648342

Stansen, C., Uy, D., Delaunay, S., Eggeling, L., Goergen, J.-L., and Wendisch, V. F. (2005). Characterization of a *Corynebacterium glutamicum* Lactate Utilization Operon Induced during Temperature-Triggered Glutamate Production. *Appl. Environ. Microbiol.* 71, 5920–5928. doi:10.1128/AEM.71.10.5920-5928.2005

Tauch, A., Kirchner, O., Löffler, B., Götker, S., Pühler, A., and Kalinowski, J. (2002). Efficient Electrotransformation of *Corynebacterium diphtheriae* with a Mini-Replicon Derived from the *Corynebacterium glutamicum* Plasmid pGA1. *Curr. Microbiol.* 45, 362–367. doi:10.1007/s00284-002-3728-3

Tian, C., Yang, J., Li, Y., Zhang, T., Li, J., Ren, C., et al. (2020). Artificially Designed Routes for the Conversion of Starch to Value-Added Mannosyl Compounds through Coupling *In Vitro* and *In Vivo* Metabolic Engineering Strategies. *Metab. Eng.* 61, 215–224. doi:10.1016/j.ymben.2020.06.008

Valdivia, M., Galan, J. L., Laffarga, J., and Ramos, J. L. (2016). Biofuels 2020: Biorefineries Based on Lignocellulosic Materials. *Microb. Biotechnol.* 9, 585–594. doi:10.1111/1751-7915.12387

van der Rest, M. E., Lange, C., and Molenaar, D. (1999). A Heat Shock Following Electroporation Induces Highly Efficient Transformation of *Corynebacterium glutamicum* with Xenogeneic Plasmid DNA. *Appl. Microbiol. Biotechnol.* 52, 541–545. doi:10.1007/s002530051557

Wendisch, V. F., Jorge, J. M. P., Pérez-García, F., and Sgobba, E. (2016). Updates on Industrial Production of Amino Acids Using *Corynebacterium glutamicum*. *World J. Microbiol. Biotechnol.* 32. doi:10.1007/s11274-016-2060-1

Wieschalka, S., Blombach, B., Bott, M., and Eikmanns, B. J. (2013). Bio-based Production of Organic Acids with *Corynebacterium glutamicum*. *Microb. Biotechnol.* 6, 87–102. doi:10.1111/1751-7915.12013

Zhang, C., Zhang, J., Kang, Z., Du, G., and Chen, J. (2015). Rational Engineering of Multiple Module Pathways for the Production of L-Phenylalanine in *Corynebacterium glutamicum*. *J. Ind. Microbiol. Biotechnol.* 42, 787–797. doi:10.1007/s10295-015-1593-x

Zhao, Q., Li, S., Lv, P., Sun, S., Ma, C., Xu, P., et al. (2019). High Ectoine Production by an Engineered *Halomonas hydrothermalis* Y2 in a Reduced Salinity Medium. *Microb. Cell Fact* 18, 184. doi:10.1186/s12934-019-1230-x

Conflict of Interest: The authors declare that the research was conducted in the absence of any commercial or financial relationships that could be construed as a potential conflict of interest.

Publisher's Note: All claims expressed in this article are solely those of the authors and do not necessarily represent those of their affiliated organizations or those of the publisher, the editors, and the reviewers. Any product that may be evaluated in this article or claim that may be made by its manufacturer is not guaranteed or endorsed by the publisher.

frontiers in Bioengineering and Biotechnology

ORIGINAL RESEARCH
published: 23 September 2021
doi: 10.3389/fbioe.2021.748510

Metabolic Engineering of *Corynebacterium glutamicum* for Production of UDP-N-Acetylglucosamine

Rahul Gauttam[1†], *Christian K. Desiderato*[1], *Dušica Radoš*[2], *Hannes Link*[2†], *Gerd M. Seibold*[1†] *and Bernhard J. Eikmanns*[1*]

[1]*Institute of Microbiology and Biotechnology, University of Ulm, Ulm, Germany,* [2]*Max Planck Institute for Terrestrial Microbiology, Marburg, Germany*

OPEN ACCESS

Edited by:
Yu Wang,
Tianjin Institute of Industrial Biotechnology, (CAS), China

Reviewed by:
Yanfeng Liu,
Jiangnan University, China
Dave Siak-Wei Ow,
*Bioprocessing Technology Institute (A*STAR), Singapore*

***Correspondence:**
Bernhard J. Eikmanns
bernhard.eikmanns@uni-ulm.de

[†]**Present address:**
Rahul Gauttam,
Biological Systems and Engineering Division, Lawrence Berkeley National Laboratory, Berkeley, CA, United States
Hannes Link,
University of Tübingen Cluster of Excellence CMFI – Bacterial Metabolomics, Tübingen, Germany
Gerd M. Seibold,
Section for Synthetic Biology, Department of Biotechnology and Biomedicine, Technical University of Denmark, Denmark

Specialty section:
This article was submitted to Synthetic Biology, a section of the journal Frontiers in Bioengineering and Biotechnology

Received: *28 July 2021*
Accepted: *13 September 2021*
Published: *23 September 2021*

Citation:
Gauttam R, Desiderato CK, Radoš D, Link H, Seibold GM and Eikmanns BJ (2021) Metabolic Engineering of Corynebacterium glutamicum *for Production of UDP-N-Acetylglucosamine. Front. Bioeng. Biotechnol. 9:748510. doi: 10.3389/fbioe.2021.748510*

Uridine diphosphate-N-acetylglucosamine (UDP-GlcNAc) is an acetylated amino sugar nucleotide that naturally serves as precursor in bacterial cell wall synthesis and is involved in prokaryotic and eukaryotic glycosylation reactions. UDP-GlcNAc finds application in various fields including the production of oligosaccharides and glycoproteins with therapeutic benefits. At present, nucleotide sugars are produced either chemically or *in vitro* by enzyme cascades. However, chemical synthesis is complex and non-economical, and *in vitro* synthesis requires costly substrates and often purified enzymes. A promising alternative is the microbial production of nucleotide sugars from cheap substrates. In this study, we aimed to engineer the non-pathogenic, Gram-positive soil bacterium *Corynebacterium glutamicum* as a host for UDP-GlcNAc production. The native *glmS*, *glmU*, and *glmM* genes and *glmM* of *Escherichia coli*, encoding the enzymes for UDP-GlcNAc synthesis from fructose-6-phosphate, were over-expressed in different combinations and from different plasmids in *C. glutamicum* GRS43, which lacks the glucosamine-6-phosphate deaminase gene (*nagB*) for glucosamine degradation. Over-expression of *glmS*, *glmU* and *glmM,* encoding glucosamine-6-phosphate synthase, the bifunctional glucosamine-1-phosphate acetyltransferase/N-acetyl glucosamine-1-phosphate uridyltransferase and phosphoglucosamine mutase, respectively, was confirmed using activity assays or immunoblot analysis. While the reference strain *C. glutamicum* GlcNCg1 with an empty plasmid in the exponential growth phase contained intracellularly only about 0.25 mM UDP-GlcNAc, the best engineered strain GlcNCg4 accumulated about 14 mM UDP-GlcNAc. The extracellular UDP-GlcNAc concentrations in the exponential growth phase did not exceed 2 mg/L. In the stationary phase, about 60 mg UDP-GlcNAc/L was observed extracellularly with strain GlcNCg4, indicating the potential of *C. glutamicum* to produce and to release the activated sugar into the culture medium. To our knowledge, the observed UDP-GlcNAc levels are the highest obtained with microbial

Abbreviations: AmpR, ampicillin resistance; AMP, adenosine monophosphate; ATc, anhydrotetracycline; CMP, cytosine monophosphate; CmR, chloramphenicol resistance; IPTG, Isopropyl-β-D-thiogalactopyranoside; KanR, kanamycin resistance; UDP, uridine diphosphate; UDP-GlcNAc, UDP-N-acetylglucosamine

hosts, emphasizing the potential of *C. glutamicum* as a suitable platform for activated sugar production.

Keywords: Corynebacterium glutamicum, metabolic engineering, activated amino sugars, sugar nucleotide, UDP-N-acetylglucosamine

INTRODUCTION

Sugar nucleotides are activated forms of sugars and are composed of two moieties, a sugar and a nucleoside mono- or di-phosphate (Kleczkowski and Decker, 2015). Depending on the nucleoside phosphate attached, these sugar nucleotides are classified as nucleoside monophosphate sugars (such as cytidine monophospho-N-acetylneuraminic acid) or nucleoside diphosphate sugars, such as adenine- or uridine-diphosphate glucose, guanosine-diphosphate mannose or the activated amino sugar uridine-diphosphate-N-acetylglucosamine (UDP-GlcNAc) (Wagner et al., 2009). UDP-linked amino sugars have attracted a great deal of attention because of their indispensable role in cell wall biosynthesis and in the synthesis of natural glycoproteins, glycolipids, oligosaccharides, and glycosides by providing the sugar moieties (Barreteau et al., 2008; Thibodeaux et al., 2008; De Bruyn et al., 2015; Mikkola, 2020). UDP-GlcNAc plays a pivotal role in several metabolic processes in both prokaryotes as well as eukaryotes. In bacteria, UDP-GlcNAc serves as a precursor of cell wall components (Mengin-Lecreulx and van Heijenoort, 1993; Brown et al., 1994). In eukaryotes, it plays an important role in the synthesis of physiologically relevant glycoconjugates such as precursors for cell wall chitin, extracellular matrix polymers and bioactive glycoproteins (Moussian, 2008; Bond and Hanover, 2015; Corfield and Berry, 2015). In biotechnology, UDP-GlcNAc and other UDP-linked amino sugars serve as sugar donors for the chemical, enzymatic and/or microbial synthesis of a variety of native and non-native oligo- and polysaccharides for clinical (Thibodeaux et al., 2008) and medical (Wagner et al., 2009) purposes and for pharmaceutically relevant glycoproteins (Mueller et al., 2018; Natarajan et al., 2020).

The UDP-GlcNAc biosynthetic pathway has been extensively elucidated in prokaryotes (Mikušová et al., 2000; Wang and Quinn, 2010; Li et al., 2012). UDP-GlcNAc is synthesized from fructose-6-phosphate (Fru-6-P) by three enzymes in four sequential enzymatic reactions (**Figure 1**). Firstly, Fru-6-P is converted to glucosamine-6-phosphate (GlcN-6-P) by glucosamine-6-phosphate synthase (GlmS). This reaction involves hydrolysis of L-glutamine to L-glutamate and ammonia, catalyzed by the N-terminal domain of GlmS, whereas the C-terminal domain is responsible for GlcN-6-P formation by utilizing the released ammonia (Durand et al., 2008). Secondly, GlcN-6-P is converted to glucosamine-1-phosphate (GlcN-1-P). This step is catalyzed by phosphoglucosamine mutase (GlmM) in a phosphorylated state in a ping-pong bi-mechanism involving glucosamine-1,6-bisphosphate as an intermediate (Jolly et al., 1999). The last two reactions, i.e., acetylation of GlcN-1-P to form GlcNAc-1-P and conversion of GlcNAc-1-P (plus UTP) to UDP-GlcNAc (plus pyrophosphate) are catalyzed by the bifunctional glucosamine-1-phosphate acetyltransferase/N-acetyl glucosamine-1-phosphate uridyltransferase GlmU (Mengin-Lecreulx and van Heijenoort, 1993; Mengin-Lecreulx and van Heijenoort, 1996; Milewski et al., 2006). The C-terminal GlmU domain is responsible for the acetylation, whereas the N-terminal domain catalyzes the uridylation reaction (Mengin-Lecreulx and van Heijenoort, 1994).

C. glutamicum is a non-pathogenic, aerobic, Gram-positive, biotin-auxotrophic soil bacterium that was initially described to be a natural producer of L-glutamate (Kinoshita et al., 1957). Since its discovery, the most appreciated application for this organism is L-glutamate and L-lysine production (Eggeling and Bott, 2015), however, the organism has also been employed for the production of other industrially relevant amino acids such as L-methionine, L-threonine, L-valine, L-tryptophan, phenylalanine, and isoleucine (Becker and Whittmann, 2015; Eggeling and Bott, 2015; Wendisch et al., 2016). The ease of cultivation of *C. glutamicum* combined with the generally regarded as safe (GRAS) status and robustness towards environmental stress contributed to the success of this bacterium in biotechnology. Furthermore, the utility of *C. glutamicum* in the production of a diverse range of bioproducts can be attributed to the sophisticated understanding of metabolic pathways regulation and the availability of advanced metabolic engineering strategies (Becker et al., 2016; Baritugo et al., 2018). Another advantageous feature of this organism is its ability to use a variety of sugars and to co-utilize different substrates (Blombach and Seibold, 2010; Wendisch et al., 2016). Owing to these advantageous traits, *C. glutamicum* has been engineered to produce numerous bioproducts other than amino acids, including isobutanol (Blombach et al., 2011), diamines (Schneider and Wendisch, 2011), polyhydroxybutyrate (Jo et al., 2006), 1,2-propanediol (Niimi et al., 2011), lactate (Okino et al., 2008), ethanol (Inui et al., 2004), cadaverine (Mimitsuka et al., 2007), xylitol (Sasaki et al., 2010) and GDP-L-fucose (Chin et al., 2013). Recently, it has been shown that metabolically engineered strains of *C. glutamicum* are also able to produce hyaluronic acid (Cheng et al., 2019a) and chondroitin (Cheng et al., 2019b), two products that include activated sugars (UDP-Glc, UDP-GlcNAc) in their synthesis.

The present study demonstrates for the first time the potential of *C. glutamicum* to intra- and extracellularly accumulate the UDP-linked activated amino sugar UDP-GlcNAc by modifying the biosynthetic pathway using metabolic engineering strategies. The employed enzymatic approach for *in vivo* UDP-GlcNAc biosynthesis in *C. glutamicum* provides a promising economical

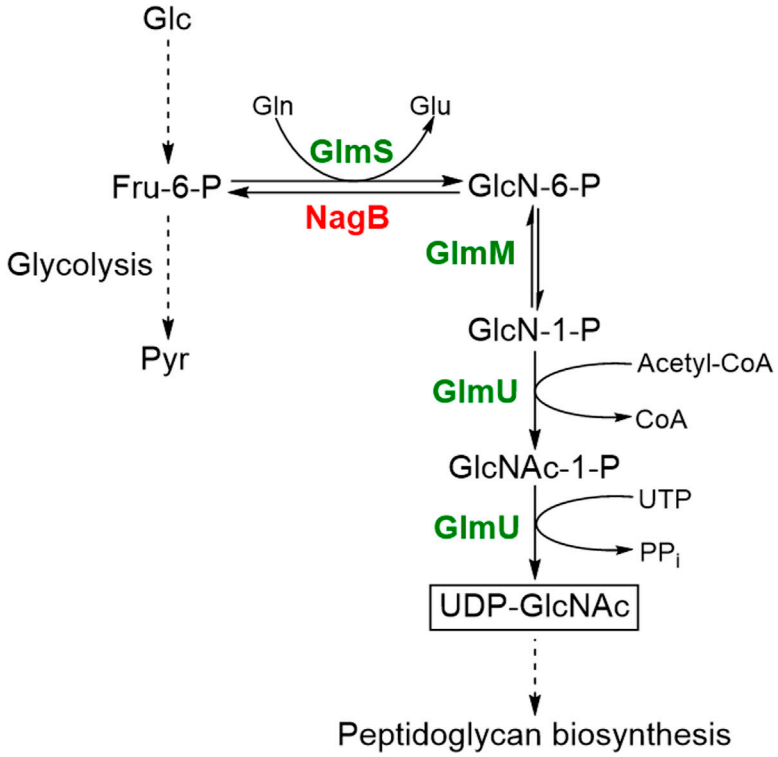

Glc	glucose
Fru-6-P	fructose-6-phosphate
Pyr	pyruvate
Gln	glutamine
Glu	glutamate
GlcN-6-P	glucosamine-6-phosphate
GlcN-1-P	glucosamine-1-phosphate
GlcNAc-1-P	N-acetylglucosamine-1-phosphate
UDP-GlcNAc	uridine-5´-diphospho-N-acetylglucosamine
CoA	coenzyme A
UTP	uridine-5´-triphosphate
PP_i	pyrophosphate
GlmS	glucosamine-6-phosphate synthase
GlmM	phosphoglucosamine mutase
GlmU	bifunctional glucosamine-1-phosphate acetyltransferase/N-acetyl glucosamine-1-phosphate uridyltransferase
NagB	glucosamine-6-phosphate deaminase

FIGURE 1 | Schematic overview of the metabolic pathway responsible for UDP-GlcNAc biosynthesis in *C. glutamicum* and metabolic engineering strategies implemented to overproduce UDP-GlcNAc. Abbreviations are given in the box. The desired product UDP-GlcNAc is boxed. Product of genes that are knocked out or over-produced are shown in red or green text, respectively.

alternative to the complex chemical route and also provides the room for scaling up the production process to larger amounts.

MATERIAL AND METHODS

Bacterial Strains, Plasmids, and Culture Conditions

Bacterial strains and plasmids used in this study are listed in **Table 1**. For recombinant plasmid construction, genomic DNA of *E. coli* and of *C. glutamicum* was isolated and used as the template for specific gene amplification. *E. coli* DH5α was used for gene cloning.

E. coli strains were cultivated aerobically in 2xTY complex medium (Green and Sambrook, 2012) at 37°C on a rotary shaker at 150 rpm. For *C. glutamicum* cultivation, a single colony picked from a freshly prepared 2xTY agar plate was inoculated in 5 ml 2xTY seed culture and grown for 8 h at 30°C on a rotary shaker at 120 rpm. This seed culture was then used to inoculate a 50 ml 2xTY pre-culture in a 500 ml baffled flask and aerobically grown on a rotary shaker under the same conditions. Cells of an overnight pre-culture were harvested by centrifugation (4,200 × g, 15 min at 4°C) and washed twice with 0.9% (w/v) NaCl before inoculating modified CgXII minimal medium (Eikmanns et al., 1991) to an optical density at 600 nm (OD_{600}) of about 1.5. In CgXII medium, the cells were grown aerobically on a rotary shaker (120 rpm at 30°C) in 500 ml baffled Erlenmeyer flasks containing 50 ml medium. The growth of bacterial cultures was monitored spectrophotometrically by measuring OD_{600} in an Ultrospec 2,100 pro spectrophotometer (GE Healthcare Life Sciences, Freiburg, Germany). Glucose (2% w/v) was added to this media as a carbon source. Whenever appropriate, cultures were supplemented with antibiotics at the following concentration: for *E. coli*, kanamycin (50 μg/ml), chloramphenicol (34 μg/ml), ampicillin (100 μg/ml), and for *C. glutamicum*: kanamycin (50 μg/ml), chloramphenicol (7.5 μg/ml). Solid media for 2xTY agar plates was prepared by adding agar (18 g/L). Gene expression was induced by adding isopropyl-β-D-thiogalactopyranoside (IPTG; 1 mM) and/or anhydrotetracycline (ATc; 0.25 μg/ml) to the cultures when the OD_{600} reached 3 to 4. Samples were removed at specific time intervals for determination of enzyme activities, for Western blot analysis and for determining product concentration.

DNA Manipulation and Transformation

Standard molecular biology procedures were used for DNA isolation, gel electrophoresis, gene cloning, *E. coli* competent cells preparation, and transformation (Green and Sambrook, 2012). Restriction enzymes, T4 DNA Ligase, CloneJet^{TM} PCR Cloning Kit, and alkaline phosphatase employed in this study were obtained from Thermo Fisher Scientific (Waltham MA, United States) and used following the instructions from the

TABLE 1 | Strains and plasmids used in this study.

Strain or plasmid	Relevant characteristics	Source/References
Strains		
E. coli DH5α	F⁻ φ80*lacZ*ΔM15 Δ(*lacZYA-argF*) U169 *endA1 recA1 hsdR17* (r_k^-, m_k^+) *supE44 thi*$^{-1}$ *gyrA996 relA1 phoA*	Hanahan (1983)
E. coli BL21	ompT *hsd*SB (r_B-m_B) *gal dcm* (DE3)	Studier (1990)
E. coli BL21 (*pET28a-His6glmU*$_{cg}$)	*E. coli* BL21 carrying the coding sequence for N-terminally His-tagged GlmU from *C. glutamicum* in vector pET28a	This study
C. glutamicum GRS43	*C. glutamicum* GRS with in-frame deletion of *cg2925-2,943*	Unthan et al. (2015)
C. glutamicum GlcNCg1	strain GRS43 carrying pCLTon1; Kan^R	This study
C. glutamicum GlcNCg2	strain GRS43 carrying pCLTon1-*glmUSM*$_{Cg}$; Kan^R	This study
C. glutamicum GlcNCg3	strain GRS43 carrying pCLTon1-*glmUSM*$_{Cg}$ and pRG_Duet1; Kan^R + Cm^R	This study
C. glutamicum GlcNCg4	strain GRS43 carrying pCLTon1-*glmUSM*$_{Cg}$ and pRG_Duet1-*glmM*$_{Eco}$; Kan^R + Cm^R	This study
C. glutamicum GlcNCg5	strain GRS43 carrying pCLTon1-*glmM*$_{Eco}$*US*$_{Cg}$; Kan^R	This study
C. glutamicum GlcNCg6	strain GRS43 carrying pCLTon1-*glmM*$_{Eco}$*US*$_{Cg}$ and pRG_Duet1; Kan^R + Cm^R	This study
C. glutamicum GlcNCg7	strain GRS43 carrying pCLTon1-*glmM*$_{Eco}$*US*$_{Cg}$ and pRG_Duet1-*glmM*$_{Eco}$; Kan^R + Cm^R	This study
C. glutamicum GlcNCg8	strain GRS43 carrying pRG_Duet1; Cm^R	Gauttam et al. (2019)
C. glutamicum GlcNCg9	strain GRS43 carrying pRG_Duet1-*glmM*$_{Eco}$; Cm^R	This study
Plasmids		
pRG_Duet1	dual-inducible *E. coli/C. glutamicum* shuttle vector (P_{tac}, *lacI*^{Q}, $OriV_{C.\ glut}$ (pCG1), $OriV_{E.coli}$ (p15A), $P_{tetR/tetA}$, *tetR*); Cm^R	Gauttam et al. (2019)
pCLTon1	*E. coli/C. glutamicum* shuttle vector (P_{tet}, *tetR*); Kan^R	Lausberg et al. (2012)
pCLTon1-*glmUSM*$_{Cg}$	pCLTon1 vector carrying *glmU, glmS* and *glmM* derived from *C. glutamicum* downstream of the ATc-inducible promoter P_{tet}; Kan^R	This study
pCLTon1-*glmUS*$_{Cg}$	pCLTOn1-*glmUSM*$_{Cg}$ with removed coding sequence for *glmM*; Kan^R	This study
pCLTon1-*glmM*$_{Eco}$*US*$_{Cg}$	pCLTon1-*glmUS*$_{Cg}$ carrying *glmM* coding sequence from *E. coli* upstream of *glmU*, controlled by P_{tet}; Kan^R	This study
pET28a	Kan^R; bacterial expression vector with T7 promoter	Novagen
pET28a-His6*glmU*$_{cg}$	pET28a vector carrying the *glmU* gene from *C. glutamicum* with N-terminal histidine tag sequence	This study
pJET1.2/blunt	Linearized cloning vector for use in *E. coli*; Amp^R	CloneJET PCR Cloning Kit (Thermo Scientific)
pJET-*glmM*$_{Eco}$	pJET1.2/blunt carrying *glmM* from *E. coli* with C-terminal histidine tag sequence; Amp^R	This study
pRG_Duet1-*glmM*$_{Eco}$	pRG_Duet1 carrying *glmM* from *E. coli* with C-terminal histidine tag sequence controlled by P_{tac}; Cm^R	This study

manufacturer. Oligonucleotides used for gene amplification were ordered from biomers.net (Ulm, Germany) and are listed in **Supplementary Table S1**.

Coding sequences were first cloned into a subcloning vector (pJET1.2/blunt) and then into the respective expression vectors. Constructs were sequence-verified at Eurofins Genomics (Ebersberg, Germany). Polymerase chain reaction (PCR) conditions were optimized for each primer pair, and DNA fragments were amplified using Q5 High-Fidelity DNA polymerase (New England Biolabs). PCR products were separated by electrophoresis in agarose gels (1%; w/v) and purified using the NucleoSpin DNA extraction kit from Macherey and Nagel (Düren, Germany). Gibson Assembly Master® Mix (New England Biolabs, Ipswich, MA, United States) was used to assemble fragments to generate expression cassettes following the instructions from the manufacturer. The primers were designed to incorporate 15–20 bp overlaps using the web-based "NEBuilderHiFi assembly tool" (New England Biolabs). The recombinant plasmids were isolated from *E. coli* transformants using the NucleoSpin plasmid purification kit from Macherey and Nagel, following the instructions of the manufacturer. Basic bioinformatic tools and software were used for designing oligonucleotides (Clone Manager v.7) and genome analysis (NCBI Blast).

For transformation, electrocompetent cells of *E. coli* DH5α and of *C. glutamicum* were prepared according to Dower et al., 1988, transformation of both organisms with plasmids was performed by electroporation using a MicroPulser Electroporator (Bio-Rad Laboratories GmbH, München, Germany) at 2.5 kV with 600 Ω resistance, as described before (Dower et al., 1988; Van der Rest et al., 1999). Recombinant strains (transformants) were selected on 2xTY agar plates containing respective antibiotics.

Plasmid Construction

The *glmS, glmM,* and *glmU* genes, encoding glucosamine-6-phosphate synthase, phosphoglucosamine mutase and the bifunctional glucosamine-1-phosphate acetyltransferase/ N-acetyl glucosamine-1-phosphate uridyltransferase, respectively, were amplified from *C. glutamicum* genomic DNA, using the primer pairs *glmS*_GIB-fwd/rev, *glmM*_GIB-fwd/rev, and *glmU*_GIB-fwd/rev, respectively. To increase the translational efficiency of *glmU*, the original TTG start codon of this gene was replaced by an ATG codon. All three fragments were joined in the order (*glmU* → *glmS* → *glmM*) by Q5® Gibson assembly. The assembled fragments were then ligated into the *Sal*I/*Sac*I double-digested expression vector pCLTon1 (Lausberg et al., 2012), resulting in plasmid pCLTon1-*glmUSM*$_{cg}$. Plasmid pCLTon1 carries the (anhydro) tetracycline- (ATc-) inducible

promoter P_{tet} to control the expression of inserted genes. As host for the newly constructed plasmid, we chose *C. glutamicum* GRS43 (Unthan et al., 2015). This strain was transformed with vector pCLTon1 (empty vector as a control) and with plasmid pCLTon1-*glmUSM*$_{cg}$ to generate the *C. glutamicum* strains GlcNCg1 (carrying pCLTon1) and GlcNCg2 (carrying pCLTon1-*glmUSM*$_{cg}$).

For expression of the *E. coli glmM* gene in *C. glutamicum*, we replaced the corynebacterial *glmM* gene in pCLTon1-*glmUSM*$_{cg}$ with the respective *glmM*$_{Eco}$. For that purpose, an intermediate construct pCLTon1-*glmUS*$_{Cg}$ was created by removing the coding region for *glmM*$_{Cg}$ using *Bgl*II/*Spe*I restriction sites. The coding region for *glmM*$_{Eco}$ was amplified from *E. coli* genomic DNA using *glmM*$_{Eco}$-His6-fwd/rev primers and cloned into pJET1.2/blunt (a subcloning vector) to construct pJET-*glmM*$_{Eco}$. After sequence verification, the *glmM*$_{Eco}$ fragment was cut out using *Sbf*I and ligated into *Sbf*I-restricted pCLTon1-*glmUS*$_{Cg}$ to construct pCLTon1-*glmM*$_{Eco}$*US*$_{Cg}$. In addition, the *Sbf*I-cut-out *glmM*$_{Eco}$ fragment was ligated into *SbfI*-restricted expression plasmid pRG_Duet1 (Gauttam et al., 2019), downstream of the IPTG-inducible promoter P_{tac}, to create pRG_Duet1-*glmM*$_{Eco}$.

Preparation of Cell Extracts

In order to detect proteins using Western blot and to determine intracellular enzyme activities, cells were harvested during the mid-exponential growth phase (OD_{600} of 10–12) by centrifugation (3,200 × g, 15 min, 4°C) and washed once with 0.9% NaCl. Cells were resuspended in 1 ml resuspension buffer (50 mM Tris-HCl, pH 7.5) and filled into 2 ml screw-cap tubes containing glass beads (250 µL). The tubes were then placed in a RiboLyser (Thermo Fisher Scientific, Heidelberg, Germany), and cells were disrupted three times using a pre-optimized program at a speed of 6.5 for 45 s with 5 min of intermittent cooling on ice to prevent protein denaturation due to frictional heat generation. Cell debris and glass beads were removed from the whole cell lysate by centrifugation (18,000 × g, 30 min, 4°C).

Western Blot Analysis

To confirm *glmM* expression in cell-free extracts, the recombinant strains were grown in CgXII minimal medium, and cells were harvested at mid-exponential growth phase (OD_{600} of 10–12). Protein concentration was determined by employing a colorimetric Bradford assay using the Roti®-Nanoquant kit (Carl Roth, Karlsruhe, Germany). Prior to loading on the gel, the samples were mixed with SDS-PAGE loading dye [5-fold concentrated: 0.313 M Tris (pH 6.8), 200 mM dithiothreitol (DTT), 1% (w/v) SDS, 2% (w/v) glycerol, bromophenol blue (0.02%)], and boiled at 100°C for 10 min. The gels were prepared using TGX Stain-Free™ FastCast™ Acrylamide Kit (Bio-Rad Laboratories, Feldkirchen, Germany; Cat. #161-0,185). Cell extracts containing about 40 µg protein were loaded in each lane. Using the Trans-Blot Turbo™ transfer system (Bio-Rad Laboratories, Cat. #170-4,272), protein bands were transferred to a PVDF membrane. This step was followed by overnight membrane blocking in 5% skimmed milk at 4°C with mild agitation. Next day, the membrane was washed (3× for 5 min) in Tris-buffered saline (pH 7.5) with Tween-20 (TBST), followed by 1 h incubation in a solution containing 6×-His Tag monoclonal antibody HIS.H8 (Thermo Scientific, Rockford, IL, Cat. #MA1-21315) at room temperature with mild agitation. After incubation with the primary antibody, the membrane was washed (3× for 5 min) again in TBST, followed by incubation with horseradish peroxidase (HRP)-labelled secondary antibody (Peroxidase AffiniPure Goat Anti-Mouse IgG, Cat. #115–035-003, Thermo Fischer Scientific, Darmstadt, Germany). Following this step, the membrane was washed again in TBST before being developed to visualize the bands using a SuperSignal™ chemiluminescent substrate (Cat. #34095, Thermo Fischer Scientific) and an iBright Imaging system (Thermo Fischer Scientific).

Enzyme Activity Assays

Glucosamine-6-phosphate synthase (GlmS) activity was determined spectrophotometrically using the glutamate dehydrogenase (GDH) based assay described by Badet et al. (1987). GDH catalyzes the reduction of 3-acetylpyridine adenine dinucleotide (APAD) into APADH that can be detected directly at 365 nm. The reaction mixture contained 50 mM potassium phosphate buffer, pH 7.5, 0.3 mM APAD, 10 mM fructose-6-phosphate, 6 mM glutamine, 50 mM KCl, GDH (3 U), cell extract (variable) in a total volume of 1 ml (Badet et al., 1987). Fructose-6-phosphate was added to initiate the reaction. To calculate the specific activity of GlmS in cell extracts, the millimolar extinction coefficient of reduced APADH at 363 nm (9.1 mM^{-1} cm^{-1}) was used. One Unit (U) of activity is defined as the conversion of 1 µmole of glutamine to glutamate per minute.

Glucosamine-1-phosphate acetyltransferase/*N*-acetylglucosamine-1-phosphate uridyltransferase (GlmU) activity was determined using an enzymatic assay described previously by Mengin-Lecreulx and Van Heijenoort (1994). The assay involves the reaction between Ellman's reagent and acetyl-CoA, resulting in an increase in absorbance at 412 nm. The reaction mixture contained 50 mM Tris-HCl, pH 7.5, 3 mM $MgCl_2$, 1 mM acetyl-CoA, 1 mM 5,5-dithio-bis-2-nitrobenzoic acid (DTNB), cell extract (variable) in a total volume of 200 µL. The reaction was started by adding glucosamine-1-phosphate (1 mM). To calculate the specific activity of GlmU, the millimolar extinction coefficient of reduced DTNB at 412 nm (13.6 mM^{-1} cm^{-1}) was used. One Unit (U) of activity is defined as the amount required to acetylate 1 µmole of glucosamine-1-phosphate per minute.

For determination of phosphoglucosamine mutase (GlmM) activity, we used a coupled enzyme assay described previously by Mengin-Lecreulx and van Heijenoort (1996), involving the GlmU reaction for determination of the glucosamine-1-phosphate production by GlmM. Purification of histidine-tagged *C. glutamicum* GlmU overproduced in *E. coli* BL21 (pET28a-His6*glmU*$_{cg}$) and proof of activity of the purified enzyme is outlined in the **Supplementary Material**. The GlmM reaction mixture contained 50 mM Tris-HCl buffer

pH 7.5, 3 mM $MgCl_2$, 1 mM acetyl-CoA, 1 mM DTNB, purified GlmU (5 mg, 8.6 U/mg), cell extract (variable) in a total volume of 200 µL. The reaction was started by adding glucosamine-6-phosphate (1 mM).

Uridine Diphosphate-N-Acetylglucosamine Quantification

To determine the total UDP-GlcNAc concentration in cells and culture broth, 100 µL of the culture was taken at a specified time point and mixed with 400 µL equimolar pre-cooled (at −20°C) acetonitrile: methanol mixture (50:50 v/v), followed by 30 min incubation at −20°C. Afterwards, cell debris was removed by centrifugation (13,000 rpm, 15 min, 4°C), and the supernatant (containing the cytosol and cell-free culture broth) was collected and stored at −80°C until further analysis.

To determine the extracellular UDP-GlcNAc concentration, 100 µL of the culture was sterile-filtered (0.2 µm), and the filtrate was quenched as described above. LC-MS/MS measurements were performed following the method previously described by Guder et al. (2017). For liquid chromatography (LC), an Agilent 1,290 Infinity II UHPLC system (Agilent Technologies) was used with iHILIC-Fusion(P) (50 × 2.1 mm, 5 µm) column at 30°C. An LC method previously described by Guder et al. (2017) with standardized runtime (2 min), flow rate (0.4 ml/min), injection volume (3 µL) and time between injections (0.5 min) was applied. LC-MS grade water with ammonium carbonate (10 mM) and ammonium hydroxide (0.2%) was used as LC solvent A. Acetonitrile (ACN) was used as LC solvent B and the gradient was 0 min 90% B; 1.3 min 40% B; 1.5 min 40% B; 1.7 min 90% B; 2 min 90% B. LC-treated samples were loaded onto an Agilent 6495 triple quadrupole mass spectrometer. The obtained LC-MS/MS data were converted into a text file using MSConvert (Chambers et al., 2012). Further data analysis was performed by an in-house software (Guder et al., 2017). Determination of absolute concentrations of UDP-GlcNAc was performed by using the ^{13}C internal standard and authentic standards (Bennett et al., 2009; Guder et al., 2017).

To calculate the intracellular UDP-GlcNAc concentration, the value of the extracellular UDP-GlcNAc concentration was subtracted from the UDP-GlcNAc concentration of the whole culture broth, the resulting UDP-GlcNAc concentration was divided by the cell dry weight (CDW), that was calculated from the OD_{600} (using a ratio of 0.33 g CDW L^{-1} $OD_{600}{}^{-1}$, determined by weighing dried biomass from cultures with specific OD_{600} values). For the calculation of the intracellular UDP-GlcNAc concentration (mM), a specific cell volume of 1.95 µL/mg CDW was assumed (Gutmann et al., 1992). The intracellular UDP-GlcNAc level is also given in mg UDP-GlcNAc/g CDW to better compare extracellular and intracellular values. For that purpose, the UDP-GlcNAc concentration was multiplied with the molecular mass of UDP-GlcNAc (= 607.36 g/mol) and divided by g CDW/L. The extracellular concentration is given in mg UDP-GlcNAc/L by multiplying the measured extracellular concentration with the molecular mass of UDP-GlcNAc.

RESULTS

Overexpression of Homologous Genes Encoding Enzymes of the Pathway for UDP-GlcNAc Synthesis in *C. glutamicum*

With the aim to engineer *C. glutamicum* for the production of the activated amino sugar UDP-GlcNAc, the native genes coding for enzymes involved in the respective pathway, namely *glmS* (Gene ID: 1020224), *glmM* (Gene ID: 1018587), and *glmU* (Gene ID: 1018935) were identified and employed for the construction of plasmid pCLTon1-$glmUSM_{cg}$ (*Material and Methods* Section). The respective gene products are annotated as glucosamine-6-phosphate synthase GlmS, phosphoglucosamine mutase GlmM and bifunctional N-acetylglucosamine-1-phosphate uridyltransferase/glucosamine-1-phosphate acetyltransferase GlmU (**Figure 1**). As host for the newly constructed plasmid, we chose *C. glutamicum* GRS43, which has been generated as part of a genome-reduction project (Unthan et al., 2015) and lacks the *nagB* gene (*cg2928*) encoding glucosamine-6-phosphate deaminase (NagB) and thus, the enzyme for the backward reaction of GlmS (Uhde et al., 2013) (**Figure 1**).

To test the newly constructed strain *C. glutamicum* GlcNCg2 and the control strains *C. glutamicum* GRS43 and GlcNCg1 (with empty plasmid pCLTon1) for (over)expression of *glmU, glmS* and *glmM*, they were cultured in CgXII minimal medium with glucose as carbon source and at an OD_{600} of about 4, plasmid-borne expression was induced by addition of ATc. The cells were harvested at the mid-exponential growth phase (OD_{600} of 10–12), and crude extracts for enzyme tests were prepared. As shown in **Figure 2A**, the specific GlmU activities were found to be about 16-fold higher in the extracts of strain GlcNCg2 (0.66 ± 0.04 U/mg) when compared to those in the extracts of control strains GRS43 and GlcNcg1 (0.04 ± 0.03 U/mg). Similar results were obtained for the GlmS activities, that were approximately 10-fold higher in the extracts of strain GlcNCg2 (0.21 ± 0.02 U/mg) in comparison to those observed in the extracts of strain GlcNcg1 (0.02 ± 0.01 U/mg). For so far unknown reasons, we were not able to detect GlmM activity in either of the cell extracts, indicating either that the assay used was not functional and/or not sensitive enough or that the plasmid-borne *glmM* gene is not expressed.

Heterologous Expression of *E. coli glmM* in *C. glutamicum*

As described above, GlmM activity (and thus, *glmM* overexpression) could not be confirmed in cell extracts of *C. glutamicum* GlcNCg2, possibly due to very low (or no) expression of the native *C. glutamicum glmM*. To investigate this hypothesis and since GlmM from *E. coli* has been well characterized (Mengin-Lecreulx and van Heijenoort, 1996), we tested the heterologous expression of *glmM* from *E. coli* ($glmM_{Eco}$) in *C. glutamicum*. For that purpose, we replaced the coding region for $glmM_{Cg}$ in plasmid pCLTon1-$glmUSM_{Cg}$ with the coding region

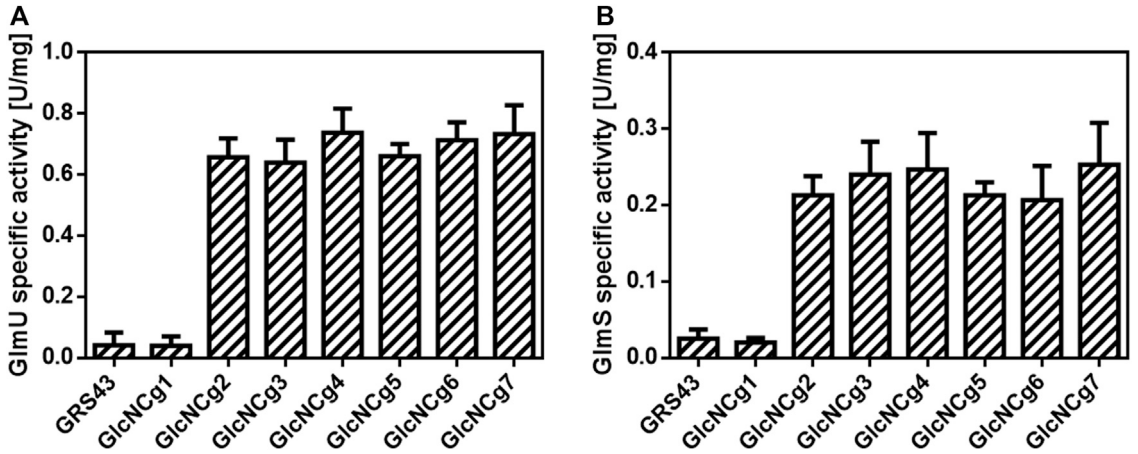

FIGURE 2 | Specific GlmU **(A)** and GlmS **(B)** activities in cell extracts of *C. glutamicum* GRS43 and the recombinant strains *C. glutamicum* GlcNCg1 to GlcNCg7. For strain description, **Table 1**. Data represent mean values of triplicate assays from at least three individual cultivations. Error bars represent standard deviations (SD).

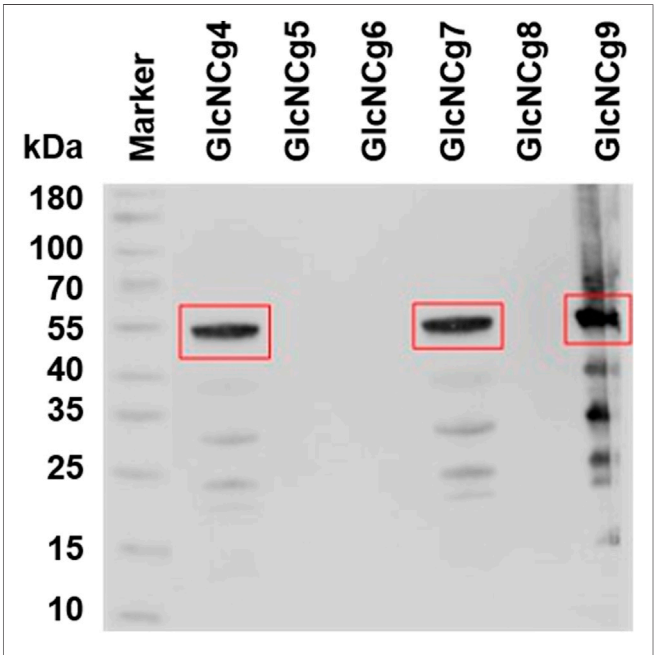

FIGURE 3 | Western blot analysis of heterologous C-terminally His-tagged GlmM in cell extracts of recombinant *C. glutamicum* strains GRS43 and GlcNCg4 to GlcNCg9 (for strain description **Table 1**). The $GlmM_{Eco}$ protein (calculated mass ~49 kDa) is highlighted with a red rectangle.

for $glmM_{Eco}$. The new construct pCLTon1-$glmM_{Eco}US_{Cg}$ is different from pCLTon1-$glmUSM_{cg}$ in the sense that $glmM_{Eco}$ was C-terminally fused with the coding sequence for a histidine-(His-) tag and placed at the first position in the expression cassette *glmM-glmU-glmS*. In addition to plasmid pCLTon1-$glmM_{Eco}US_{Cg}$, we constructed the pCLTon1-compatible plasmid pRG_Duet1-$glmM_{Eco}$, carrying $glmM_{Eco}$ under control of the IPTG-inducible *tac* promoter P_{tac}. Subsequently, *C. glutamicum* GRS43 was transformed with plasmids pCLTon1-$glmUSM_{cg}$, pCLTon1-$glmM_{Eco}US_{Cg}$, pRG_Duet1-$glmM_{Eco}$ and pRG_Duet1 in different combinations to construct *C. glutamicum* GlcNCg3, GlcNCg4, GlcNCg5, GlcNCg6, GlcNCg7, GlcNCg8, and GlcNCg9 (**Table 1**).

Enzyme assays were performed to confirm the overexpression of *glmU* and *glmS* in *C. glutamicum* GlcNCg3 to GlcNCg7. As shown in **Figure 2A**, the specific GlmU activities were found to be 15- to 18-fold higher in the extracts of strains GlcNCg3 to GlcNCg7, when compared to the specific activities in the extracts of reference strains GRS43 and GlcNCg1. In the same way, the specific GlmS activities were 11- to 15-fold higher in the extracts of strains GlcNCg3 to GlcNCg7 compared to those determined in the extracts of the control strains (**Figure 2B**).

To prove the heterologous expression of $glmM_{Eco}$ and the presence of $GlmM_{Eco}$ protein in the different *C. glutamicum* strains carrying pCLTon1-$glmM_{Eco}US_{Cg}$ and/or pRG_Duet1-$glmM_{Eco}$, Western blot analysis was performed with cell extracts of *C. glutamicum* GlcNCg4 to GlcNCg9, using the 6x-His-tag monoclonal antibody HIS.H8. As shown in **Figure 3**, a dense band well corresponding to the size of GlmM polypeptide (~49 kDa) from *E. coli* was detected in the extracts of strains GlcNCg4, GlcNCg7, and GlcNCg9. As expected, $GlmM_{Eco}$ protein was not detected in cell extracts of *C. glutamicum* GlcNCg8. However, the GlmM protein was also not detected in *C. glutamicum* GlcNCg5 and GlcNCg6 (**Figure 3**). Based on this observation, we hypothesize that ATc-inducible promoter P_{tet} is not strong enough to drive the expression of *glmM* in *C. glutamicum*, irrespective of the source of origin. A previous attempt to detect the production of His-tagged GlmM from *C. glutamicum* using the expression plasmid pCLTon1 failed too, and we could not observe a band corresponding to GlmM by immunoblot analysis of respective *C. glutamicum* extracts (data not shown).

It is noteworthy to mention that out of all recombinant strains GlcNCg4 and GlcNCg7 were the only strains which thus were

TABLE 2 | Growth rate, cell dry weight (CDW) at time of harvest and intracellular UDP-GlcNAc accumulation of recombinant *C. glutamicum* strains grown in minimal medium plus glucose and harvested in the exponential growth phase at an OD_{600} of about 10.

C. glutamicum strain	Growth rate (h^{-1})	g CDW/L	mg UDP-GlcNAc/g CDW	mM UDP-GlcNAc
GlcNCg1	0.36 ± 0.01	3.93 ± 0.05	0.29 ± 0.10	0.25 ± 0.08
GlcNCg2	0.32 ± 0.01	4.51 ± 1.73	1.68 ± 0.66	1.47 ± 0.22
GlcNCg3	0.16 ± 0.02	3.53 ± 0.20	6.92 ± 1.80	5.85 ± 1.52
GlcNCg4	0.17 ± 0.03	3.50 ± 0.10	16.75 ± 0.82	14.15 ± 0.07
GlcNCg5	0.31 ± 0.01	4.06 ± 1.60	1.68 ± 0.66	1.51 ± 0.28
GlcNCg6	0.17 ± 0.01	3.68 ± 1.45	5.49 ± 2.61	5.27 ± 1.98
GlcNCg7	0.18 ± 0.02	4.01 ± 1.52	15.69 ± 6.13	13.06 ± 1.62
GlcNCg8	0.23 ± 0.03	5.36 ± 2.15	1.49 ± 0.65	1.26 ± 0.30
GlcNCg9	0.20 ± 0.03	3.91 ± 1.48	1.84 ± 0.76	1.55 ± 0.30

Values are averages ±SD of three to six independent experiments (biological replicates).

proven to express all three genes (*glmU, glmS,* and *glmM*) involved in the prokaryotic UDP-GlcNAc biosynthesis pathway.

Intracellular and Extracellular Accumulation of UDP-GlcNAc

Overexpression of *glmS*, *glmM,* and *glmU* in different combinations or from different plasmids were shown in the previous section. LC-MS/MS was employed for the quantification of UDP-GlcNAc in cells of recombinant *C. glutamicum* strains GlcNCg1 to GlcNCg9. As shown in **Table 2**, cells of the reference strain *C. glutamicum* GlcNCg1 (GRS43 carrying empty pCLTon1) showed minimal intracellular UDP-GlcNAc levels of about 0.25 mM (corresponding to 0.29 mg UDP-GlcNAc/g CDW) and those of strain GlcNCg2 (carrying pCLTon1-$glmUSM_{cg}$) about 1.47 mM (i.e., 1.68 mg UDP-GlcNAc/g CDW). These results suggested that plasmid-based overexpression of *glmU* and *glmS* is sufficient for a significant increase of the UDP-GlcNAc content within the cells. Cells of *C. glutamicum* strain GlcNCg5 (carrying pCLTon1-$glmM_{Eco}US_{Cg}$) contained about 1.51 mM (i.e., 1.68 mg UDP-GlcNAc/g CDW) and thus, comparable concentrations as strain GlcNCg2. These are the strains which showed overexpression of *glmU* and *glmS,* but not of $glmM_{Cg}$ or $glmM_{Ec}$. Surprisingly, an up to fourfold increase in UDP-GlcNAc levels were observed in *C. glutamicum* GlcNCg3 (5.85 mM) and GlcNCg6 cells (5.27 mM), carrying the same vectors as strains GlcNCg2 and GlcNCg5, respectively, but in addition the empty plasmid pRG_Duet1 (**Table 2**). The higher UDP-GlcNAc levels in *C. glutamicum* GlcNCg3 and GlcNCg6 correlate to an about twofold lower growth rate of these strains (μ = 0.16 to 0.17 h^{-1}), when compared to their respective single-plasmid counterparts (GlcNCg2 and GlcNCg5; μ = 0.31 to 0.32 h^{-1}) (**Table 2**). Maximal intracellular UDP-GlcNAc levels were observed in *C. glutamicum* GlcNCg4, carrying pCLTon1-$glmUSM_{Cg}$ + pRG_Duet1-$glmM_{Eco}$ (14.15 mM, i.e. 16.75 mg UDP-GlcNAc/g CDW) and GlcNCg7, carrying pCLTon1-$glmM_{Eco}US_{Cg}$ + pRG_Duet1-$glmM_{Eco}$ (13.06 mM, i.e. 15.69 mg UDP-GlcNAc/g CDW) (**Table 2**). These UDP-GlcNAc levels were around 55-fold higher than that of the reference strain GlcNCg1. The increased UDP-GlcNAc levels in strains GlcNCg4 and GlcNCg7 (μ = 0.18 ± 0.02 h^{-1}) can be explained by the cumulative effect of reduced growth rate (μ = 0.17 to 0.18 h^{-1} vs 0.36 h^{-1}) and proven overexpression of $glmUS_{Cg}$ from plasmid pCLTon1 and of $glmM_{Eco}$ from plasmid pRG_Duet1 (see above). Intracellular UDP-GlcNAc levels in *C. glutamicum* GlcNCg8, carrying empty plasmid pRG_Duet1 and showing also a relatively low growth rate of 0.23 h^{-1}, were nearly as high as that of strain GlcNCg2 (1.26 vs 1.47 mM) (**Table 2**), although the former strain does not carry any plasmid-borne *glm* gene. This result indicates that a reduced growth rate is in favour of UDP-GlcNAc accumulation. *C. glutamicum* GlcNCg9 (carrying pRG_Duet1-$glmM_{Eco}$) also showed a relatively low growth rate of about 0.23 ± 0.03 h^{-1} and only slightly higher intracellular UDP-GlcNAc concentration (about 1.55 mM) than strain GlcNCg8, indicating that $glmM_{Eco}$ expression alone in combination with the reduced growth rate is not sufficient to substantially increase the intracellular UDP-GlcNAc levels.

To test also for extracellular UDP-GlcNAc accumulation, we analyzed the supernatants of *C. glutamicum* GlcNCg1 (basal intracellular UDP-GlcNAc level), *C. glutamicum* GlcNCg3 (elevated intracellular UDP-GlcNAc level), and *C. glutamicum* GlcNCg4 (highest intracellular UDP-GlcNAc level) cultures in the exponential (7 h after inoculation) and in the stationary growth phase (24 h after inoculation). In the exponential phase, the original host strain *C. glutamicum* GlcNCg1 accumulated extracellularly 0.13 ± 0.03 mg UDP-GlcNAc/L (i.e., below 0.25 µM) whereas strains GlcNCg3 and GlcNCg4 accumulated 1.8 ± 0.4 mg and 1.74 ± 0.3 mg UDP-GlcNAc/L, corresponding to roughly 3 µM in the culture supernatant (**Figure 4**), which is orders of magnitude lower than that within the cells (5.85 and 14.15 mM, respectively; **Table 2**). In the stationary phase, *C. glutamicum* GlcNCg3 showed significantly elevated extracellular UDP-GlcNAc accumulation with 10.42 ± 1.93 mg UDP-GlcNAc/L, i.e., about 17 µM, whereas the intracellular UDP-GlcNAc concentration was about 0.4 mM. An even higher extracellular accumulation of 59.80 ± 8.69 mg UDP-GlcNAc/L (about 0.1 mM) was observed for *C. glutamicum* GlcNCg4 (**Figure 4**). The intracellular concentration in stationary phase cells of *C. glutamicum* GlcNCg4 was about 0.67 mM, which is about 20-fold lower than in the exponential phase, but still 6- to 7-fold higher than the extracellular concentration (0.1 mM). This latter observation might indicate that the secretion (or the release) of UDP-GlcNAc

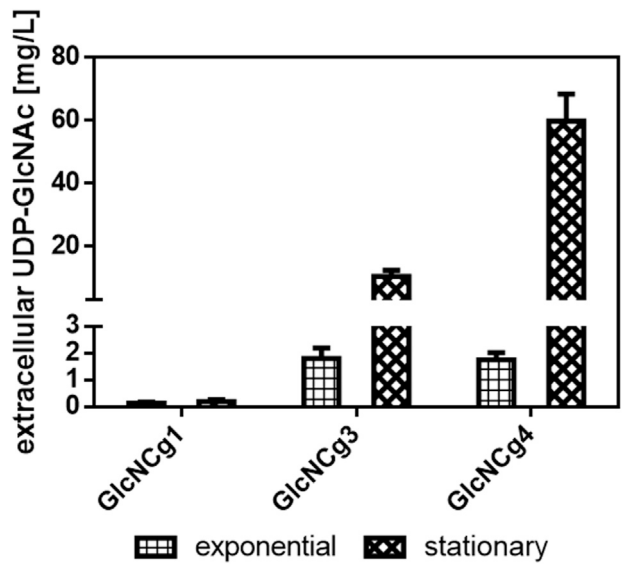

FIGURE 4 | Extracellular accumulation of UDP-GlcNAc in *C. glutamicum* GlcNCg1, GlcNCg3 and GlcNCg4. For strain description **Table 1**. The cells were cultured in CgXII minimal medium with 2% glucose supplemented with inducers (1 mM IPTG, 250 ng/ml ATc). Data represents mean values of triplicate (exponential phase) or duplicate (stationary phase) assays from individual cultivations and error bars represent deviations.

into the medium is the rate-limiting step for UDP-GlcNAc production.

DISCUSSION

UDP-linked amino sugars are difficult to synthesize, however, chemical, enzymatic and chemoenzymatic approaches have been explored (Koizumi et al., 1998; Ahmadipour and Miller 2017; Zamora et al., 2017; Ahmadipour et al., 2018; Ahmadipour et al., 2019; Mikkola, 2020). Chemical synthesis of activated carbohydrates is demanding and relies on specialized expertise in carbohydrate chemistry; however, due to the lack of alternative routes, it remains a popular choice to synthesize non-natural sugar nucleotides (e.g., fluorinated nucleotide sugars) (Wagner et al., 2009; Tedaldi et al., 2012), which may serve for the synthesis of modified oligosaccharides, as enzyme inhibitors and/or in diagnostics (Mikkola, 2020). In general, sugar nucleotides generated from chemical routes are often quite expensive due to low extraction yield, and attempts made to scale up the production proved to be non-economical or impractical (Heidlas et al., 1992; Timmons and Jakeman, 2007; Wagner et al., 2009). Moreover, chemical approaches also suffer from other major drawbacks such as lack of stereoselectivity, tedious purification processes, and a low space-time yield (Zhao et al., 2010). Chemoenzymatic syntheses use biotransformation steps together with simple chemical steps, thus improving efficiency and enabling the synthesis of chemically defined nucleotide-activated sugars (Zamora et al., 2017). Using glucosamine and ATP as substrates and hexokinase, GlmM, and GlmU, Heidlas et al. (1992) firstly showed the enzymatic synthesis of UDP-GlcNAc. Further multi-enzyme cascades coupled with regeneration systems were developed (e.g., Elling, 1997; Bülter and Elling, 1999; Wahl et al., 2016). Efficient enzymatic synthesis of UDP-GlcNAc and other nucleotide sugars has recently been described in an up to 200 ml lab scale via enzyme cascades in repetitive batch mode (Fischöder et al., 2019). Compared to the chemical synthesis, this enzymatic process seems to be quite competitive, however, all these processes often require expensive starting materials (e.g., ATP, UDP and UTP), purified enzymes and complex operations for scaling up (Mikkola, 2020; Zhao et al., 2021), and therefore, are expensive and difficult to be used for industrial production.

To address above mentioned limitations and to make amino sugars (such as UDP-GlcNAc and UDP-GalNAc) available in large scale and in a cost-effective and sustainable manner, microbial production represents an interesting alternative to traditional chemical, enzymatic and chemoenzymatic routes. However, the use of microorganisms for the production of activated amino sugars relies heavily on a sound understanding of the microbial sugar biosynthetic pathways (Thibodeaux et al., 2008). Tabata et al. (2000) were the first to set up a microbial production system for UDP-GlcNAc, using a combination of six recombinant *E. coli* strains and *Corynebacterium ammoniagenes* DN510. In a rather complicated high-density incubation process, including permeabilization of the cells, the six different *E. coli* strains synthesized GlcNAc-1-P from externally added glucosamine and acetate by overexpression of the GlmM, GlmU, glucokinase, acetate kinase, phosphotransacetylase, or pyrophosphatase genes, respectively, whereas the latter provided the UTP (required for the very last step of UDP-GlcNAc synthesis, **Figure 1**) from orotic acid. The final titer of UDP-GlcNAc was 11.4 mM; compared to the *C. glutamicum* system presented here, this is a 100-fold higher concentration. However, several recombinant strains have to be cultivated separately and permeabilized in a second step. Further, the addition of several substrates (orotic acid, fructose, glucosamine, and acetate) at high concentrations are required, whereas *C. glutamicum* is producing UDP-GlcNAc in a single cultivation step in minimal medium containing glucose as the sole carbon source. Moreover, due to the permeabilization of the *E. coli* and *C. ammoniagenes* cells, it is likely that the downstream processing of the *C. glutamicum* system is presumably much easier. However, it is obvious that improvement of the *C. glutamicum* system is still required to obtain higher UDP-GlcNAc titers. It is striking that the strains tested in this work showed satisfactory performance even under non-optimized, standard laboratory growth conditions, thus, in parallel with strain optimization, production process optimization is also envisaged to reach higher biotransformation efficiency and product titer.

Rodríguez-Díaz et al. (2012a) showed for the first time that GlmS, GlmM and GlmU are responsible for UDP-GlcNAc

biosynthesis in *Lactobacilli*, and they also found UDP-GlcNAc synthesis to be tightly regulated in *Lactobacillus casei* BL23 (Rodríguez-Díaz et al., 2012b). However, the authors constructed a recombinant *L. casei* BL23 strain overexpressing the homologous GlmS and GlmM genes and showing in complex medium with 0.5% glucose an about fourfold higher intracellular UDP-GlcNAc pool (3.18 μMol g protein^{-1}), when compared to the parental strain (0.82 μMol g protein^{-1}) (Rodríguez-Díaz et al., 2012a). Although the authors obviously did not analyze the culture broth for extracellular UDP-GlcNAc, all these observations indicated that the activities of the GlmSMU enzymes are sufficient for UDP-GlcNAc biosynthesis in prokaryotes and suggesting that it might be easily possible to use prokaryotic systems to produce UDP-GlcNAc from carbohydrates. In fact, we here were able to metabolically engineer *C. glutamicum* for production of this sugar nucleotide from glucose and could show that overexpression of *glmU*, *glmS,* and $glmM_{Eco}$ in *C. glutamicum* GRS43 led to up to 16.75 mg UDP-GlcNAc per g of CDW. This corresponds to 51.5 μmol UDP-GlcNAc per g protein and thus to an about 16-fold higher intracellular UDP-GlcNAc accumulation when compared to the recombinant *L. casei* BL23.

In the stationary phase, we detected up to 60 mg UDP-GlcNAc L^{-1} in the culture supernatant of *C. glutamicum* GlcNCg4, indicating that the organism is able to release the activated sugar into the medium. Dedicated nucleotide sugar transporters were identified in eukaryotic cells and are localized in the membrane of the Golgi apparatus, thus providing nucleotide sugars for glycosylation reactions in this organelle (Gerardy-Schahn et al., 2001; Orellana et al., 2016). However, to our knowledge, such transporters are not present in bacteria. The accumulation of nucleotide sugars in the culture supernatant most probably reduces the overall conversion of UDP-GlcNAc since the suitable glycosyltransferases and sugar acceptors are located within the cells and are absent in the culture medium. It remains unclear why and how *C. glutamicum* releases UDP-GlcNAc in the stationary phase into the medium and what mechanisms are behind it. The big difference between the intracellular and the extracellular UDP-GlcNAc concentrations, in particular in strains GlcNCg1 and GlcNCg3, argues against a simple diffusion process and is in favour of protein-mediated transport. It can be speculated that the intracellular accumulation of UDP-GlcNAc in the stationary phase leads to conditions that e.g. affect peptidoglycan synthesis and/or the membrane state and thus possibly activate a channel protein. Time-course studies on the release of UDP-GlcNAc from the exponential to the stationary growth phase and concomitantly on the intracellular UDP-GlcNAc concentrations might shed more light on the UDP-GlcNAC release mechanism. However, the extracellular UDP-GlcNAc accumulation in the stationary phase simplifies the subsequent downstream processing and contributes to cheap production of UDP-GlcNAc with *C. glutamicum* compared to conventional enzymatic or chemical synthesis.

CONCLUSION

In this study, *C. glutamicum* was engineered for the first time to produce the activated amino sugar UDP-GlcNAc. Homologous overexpression of *glmU* and *glmS* and heterologous expression of the *E. coli glmM* from two plasmids increased the intracellular concentration of UDP-GlcNAc more than 50-fold in a range that is nearly 20-fold higher than that obtained with recombinant *L. casei* BL23 cells. In addition, we demonstrate the accumulation of up to 60 mg UDP-GlcNAc/L in culture supernatants of recombinant *C. glutamicum* strains, which simplifies downstream processing and may contribute to product stability. Our results provide valuable information to develop this organism as a promising alternative to cost-intensive chemical methods for industrial production of UDP-GlcNAc. Moreover, our results indicate the potential of *C. glutamicum* to produce nucleotide sugars and their derivatives.

DATA AVAILABILITY STATEMENT

The original contributions presented in the study are included in the article/**Supplementary Material**, further inquiries can be directed to the corresponding author.

AUTHOR CONTRIBUTIONS

RG, GS, and BE conceived and designed the experiments. RG and CD performed most of the experiments, DR and HL performed the LC-MS/MS determinations. RG, CD, and BE analyzed the data and wrote the manuscript. All authors made contributions to the final manuscript.

FUNDING

This study was supported by grants from Ministry for Science, Research and Arts of the Federal State Government of Baden-Württemberg, Germany. DR acknowledges postdoctoral funding by the ERC starting grant "MapMe" (grant agreement no. 715650).

ACKNOWLEDGMENTS

We are grateful and acknowledge the financial support of the Ministry for Science, Research and Arts of the Federal State Government of Baden-Württemberg, for the Postgraduate scholarship of RG within the cooperative doctoral Research Training Group "Pharmaceutical Biotechnology".

SUPPLEMENTARY MATERIAL

The Supplementary Material for this article can be found online at: https://www.frontiersin.org/articles/10.3389/fbioe.2021.748510/full#supplementary-material

REFERENCES

Ahmadipour, S., and Miller, G. J. (2017). Recent Advances in the Chemical Synthesis of Sugar Nucleotides. *Carbohydr. Res.* 451, 95–109. doi:10.1016/j.carres.2017.08.014

Ahmadipour, S., Beswick, L., and Miller, G. J. (2018). Recent Advances in the Enzymatic Synthesis of Sugar-Nucleotides Using Nucleotidylyltransferases and Glycosyltransferases. *Carbohydr. Res.* 469, 38–47. doi:10.1016/j.carres.2018.09.002

Ahmadipour, S., Pergolizzi, G., Rejzek, M., Field, R. A., and Miller, G. J. (2019). Chemoenzymatic Synthesis of C6-Modified Sugar Nucleotides to Probe the GDP-D-Mannose Dehydrogenase from *Pseudomonas aeruginosa*. *Org. Lett.* 21, 4415–4419. doi:10.1021/acs.orglett.9b00967

Badet, B., Vermoote, P., Haumont, P. Y., Lederer, F., and Le Goffic, F. (1987). Glucosamine Synthetase from *Escherichia coli*: Purification, Properties, and Glutamine-Utilizing Site Location. *Biochemistry* 26, 1940–1948. doi:10.1021/bi00381a023

Baritugo, K.-A., Kim, H. T., David, Y., Choi, J.-i., Hong, S. H., Jeong, K. J., et al. (2018). Metabolic Engineering of *Corynebacterium Glutamicum* for Fermentative Production of Chemicals in Biorefinery. *Appl. Microbiol. Biotechnol.* 102, 3915–3937. doi:10.1007/s00253-018-8896-6

Barreteau, H., Kovač, A., Boniface, A., Sova, M., Gobec, S., and Blanot, D. (2008). Cytoplasmic Steps of Peptidoglycan Biosynthesis. *FEMS Microbiol. Rev.* 32, 168–207. doi:10.1111/j.1574-6976.2008.00104.x

Becker, J., and Wittmann, C. (2015). Advanced Biotechnology: Metabolically Engineered Cells for the Bio-Based Production of Chemicals and Fuels, Materials, and Health-Care Products. *Angew. Chem. Int. Ed.* 54, 3328–3350. doi:10.1002/anie.201409033

Becker, J., Gießelmann, G., Hoffmann, S. L., and Wittmann, C. (2016). *Corynebacterium Glutamicum* for Sustainable Bioproduction: from Metabolic Physiology to Systems Metabolic Engineering. *Adv. Biochem. Eng. Biotechnol.* 162, 217–263. doi:10.1007/10_2016_21

Bennett, B. D., Kimball, E. H., Gao, M., Osterhout, R., Van Dien, S. J., and Rabinowitz, J. D. (2009). Absolute Metabolite Concentrations and Implied Enzyme Active Site Occupancy in *Escherichia coli*. *Nat. Chem. Biol.* 5, 593–599. doi:10.1038/nchembio.186

Blombach, B., and Seibold, G. M. (2010). Carbohydrate Metabolism in *Corynebacterium Glutamicum* and Applications for the Metabolic Engineering of L-Lysine Production Strains. *Appl. Microbiol. Biotechnol.* 86, 1313–1322. doi:10.1007/s00253-010-2537-z

Blombach, B., Riester, T., Wieschalka, S., Ziert, C., Youn, J.-W., Wendisch, V. F., et al. (2011). *Corynebacterium Glutamicum* Tailored for Efficient Isobutanol Production. *Appl. Environ. Microbiol.* 77, 3300–3310. doi:10.1128/AEM.02972-10

Bond, M. R., and Hanover, J. A. (2015). A Little Sugar Goes a Long Way: the Cell Biology of O-GlcNAc. *J. Cel Biol.* 208, 869–880. doi:10.1083/jcb.201501101

Brown, E. D., Marquardt, J. L., Lee, J. P., Walsh, C. T., and Anderson, K. S. (1994). Detection and Characterization of a Phospholactoyl-Enzyme Adduct in the Reaction Catalyzed by UDP-N-Acetylglucosamine Enolpyruvoyl Transferase, MurZ. *Biochemistry* 33, 10638–10645. doi:10.1021/bi00201a010

Bülter, T., and Elling, L. (1999). Enzymatic Synthesis of Nucleotide Sugars. *Glycoconj. J.* 16, 147–159. doi:10.1023/a:1026444726698

Chambers, M. C., Maclean, B., Burke, R., Amodei, D., Ruderman, D. L., Neumann, S., et al. (2012). A Cross-Platform Toolkit for Mass Spectrometry and Proteomics. *Nat. Biotechnol.* 30, 918–920. doi:10.1038/nbt.2377

Cheng, F., Yu, H., and Stephanopoulos, G. (2019a). Engineering *Corynebacterium Glutamicum* for High-Titer Biosynthesis of Hyaluronic Acid. *Metab. Eng.* 55, 276–289. doi:10.1016/j.ymben.2019.07.003

Cheng, F., Luozhong, S., Yu, H., and Guo, Z. (2019b). Biosynthesis of Chondroitin in Engineered *Corynebacterium Glutamicum*. *J. Microbiol. Biotechnol.* 29, 392–400. doi:10.4014/jmb.1810.10062

Chin, Y.-W., Park, J.-B., Park, Y.-C., Kim, K. H., and Seo, J.-H. (2013). Metabolic Engineering of *Corynebacterium Glutamicum* to Produce GDP-L-Fucose from Glucose and Mannose. *Bioproc. Biosyst. Eng.* 36, 749–756. doi:10.1007/s00449-013-0900-z

Corfield, A. P., and Berry, M. (2015). Glycan Variation and Evolution in the Eukaryotes. *Trends Biochem. Sci.* 40, 351–359. doi:10.1016/j.tibs.2015.04.004

De Bruyn, F., Maertens, J., Beauprez, J., Soetaert, W., and De Mey, M. (2015). Biotechnological Advances in UDP-Sugar Based Glycosylation of Small Molecules. *Biotechnol. Adv.* 33, 288–302. doi:10.1016/j.biotechadv.2015.02.005

Dower, W. J., Miller, J. F., and Ragsdale, C. W. (1988). High Efficiency Transformation of E.Coli by High Voltage Electroporation. *Nucleic Acids Res.* 16, 6127–6145. doi:10.1093/nar/16.13.6127

Durand, P., Golinelli-Pimpaneau, B., Mouilleron, S., Badet, B., and Badet-Denisot, M.-A. (2008). Highlights of glucosamine-6P Synthase Catalysis. *Arch. Biochem. Biophys.* 474, 302–317. doi:10.1016/j.abb.2008.01.026

Eggeling, L., and Bott, M. (2015). A Giant Market and a Powerful Metabolism: L-Lysine provided by *Corynebacterium Glutamicum*. *Appl. Microbiol. Biotechnol.* 99, 3387–3394. doi:10.1007/s00253-015-6508-2

Eikmanns, B. J., Kleinertz, E., Liebl, W., and Sahm, H. (1991). A Family of *Corynebacterium Glutamicum/Escherichia coli* Shuttle Vectors for Cloning, Controlled Gene Expression, and Promoter Probing. *Gene* 102, 93–98. doi:10.1016/0378-1119(91)90545-m

Elling, L. (1997). Glycobiotechnology: Enzymes for the Synthesis of Nucleotide Sugars. *Adv. Biochem. Eng. Biotechnol.* 58, 89–144. doi:10.1007/bfb0103303

Fischöder, T., Wahl, C., Zerhusen, C., and Elling, L. (2019). Repetitive Batch Mode Facilitates Enzymatic Synthesis of the Nucleotide Sugars UDP-Gal, UDP-GlcNAc, and UDP-GalNAc on a Multi-Gram Scale. *Biotechnol. J.* 14, 1800386. doi:10.1002/biot.201800386

Gauttam, R., Desiderato, C., Jung, L., Shah, A., and Eikmanns, B. J. (2019). A Step Forward: Compatible and Dual-Inducible Expression Vectors for Gene Co-expression in *Corynebacterium Glutamicum*. *Plasmid* 101, 20–27. doi:10.1016/j.plasmid.2018.12.004

Gerardy-Schahn, R., Oelmann, S., and Bakker, H. (2001). Nucleotide Sugar Transporters: Biological and Functional Aspects. *Biochimie* 83, 775–782. doi:10.1016/s0300-9084(01)01322-0

Green, M. R., and Sambrook, J. (2012). *Molecular Cloning. A Laboratory Manual*. 4th edn. Cold Spring Harbor, New York: Cold Spring Harbor Laboratory Press.

Guder, J. C., Schramm, T., Sander, T., and Link, H. (2017). Time-Optimized Isotope Ratio LC-MS/MS for High-Throughput Quantification of Primary Metabolites. *Anal. Chem.* 89, 1624–1631. doi:10.1021/acs.analchem.6b03731

Gutmann, M., Hoischen, C., and Krämer, R. (1992). Carrier-mediated Glutamate Secretion by *Corynebacterium Glutamicum* under Biotin Limitation. *Biochim. Biophys. Acta Biomembr.* 1112, 115–123. doi:10.1016/0005-2736(92)90261-j

Hanahan, D. (1983). Studies on Transformation of *Escherichia coli* with Plasmids. *J. Mol. Biol.* 166, 557–580. doi:10.1016/s0022-2836(83)80284-8

Heidlas, J. E., Lees, W. J., Pale, P., and Whitesides, G. M. (1992). Gram-scale Synthesis of Uridine 5'-Diphospho-N-Acetylglucosamine: Comparison of Enzymic and Chemical Routes. *J. Org. Chem.* 57, 146–151. doi:10.1021/jo00027a028

Inui, M., Kawaguchi, H., Murakami, S., Vertès, A. A., and Yukawa, H. (2004). Metabolic Engineering of *Corynebacterium Glutamicum* for Fuel Ethanol Production under Oxygen-Deprivation Conditions. *J. Mol. Microbiol. Biotechnol.* 8, 243–254. doi:10.1159/000086705

Jo, S.-J., Maeda, M., Ooi, T., and Taguchi, S. (2006). Production System for Biodegradable Polyester Polyhydroxybutyrate by *Corynebacterium Glutamicum*. *J. Biosci. Bioeng.* 102, 233–236. doi:10.1263/jbb.102.233

Jolly, L., Ferrari, P., Blanot, D., van Heijenoort, J., Fassy, F., and Mengin-Lecreulx, D. (1999). Reaction Mechanism of Phosphoglucosamine Mutase from *Escherichia coli*. *Eur. J. Biochem.* 262, 202–210. doi:10.1046/j.1432-1327.1999.00373.x

Kinoshita, S., Udaka, S., and Shimono, M. (1957). Studies on the Amino Acid Fermentation. *J. Gen. Appl. Microbiol.* 3, 193–205. doi:10.2323/jgam.3.193

Kleczkowski, L. A., and Decker, D. (2015). Sugar Activation for Production of Nucleotide Sugars as Substrates for Glycosyltransferases in Plants. *J. Appl. Glycosci.* 62, 25–36. doi:10.5458/jag.jag.jag-2015_003

Koizumi, S., Endo, T., Tabata, K., and Ozaki, A. (1998). Large-scale Production of UDP-Galactose and Globotriose by Coupling Metabolically Engineered Bacteria. *Nat. Biotechnol.* 16, 847–850. doi:10.1038/nbt0998-847

Lausberg, F., Chattopadhyay, A. R., Heyer, A., Eggeling, L., and Freudl, R. (2012). A Tetracycline Inducible Expression Vector for *Corynebacterium Glutamicum* Allowing Tightly Regulable Gene Expression. *Plasmid* 68, 142–147. doi:10.1016/j.plasmid.2012.05.001

Li, S., Kang, J., Yu, W., Zhou, Y., Zhang, W., Xin, Y., et al. (2012). Identification of *M. tuberculosis* Rv3441c and *M. Smegmatis* MSMEG_1556 and Essentiality of

M. Smegmatis MSMEG_1556. *PLoS ONE* 7, e42769. doi:10.1371/journal.pone.0042769

Mengin-Lecreulx, D., and van Heijenoort, J. (1993). Identification of the *glmU* Gene Encoding N-Acetylglucosamine-1-Phosphate Uridyltransferase in *Escherichia coli*. *J. Bacteriol.* 175, 6150–6157. doi:10.1128/jb.175.19.6150-6157.1993

Mengin-Lecreulx, D., and van Heijenoort, J. (1994). Copurification of Glucosamine-1-Phosphate Acetyltransferase and N-Acetylglucosamine-1-Phosphate Uridyltransferase Activities of *Escherichia coli*: Characterization of the *glmU* Gene Product as a Bifunctional Enzyme Catalyzing Two Subsequent Steps in the Pathway for UDP-N-Acetylglucosamine Synthesis. *J. Bacteriol.* 176, 5788–5795. doi:10.1128/jb.176.18.5788-5795.1994

Mengin-Lecreulx, D., and van Heijenoort, J. (1996). Characterization of the Essential Gene *glmM* Encoding Phosphoglucosamine Mutase in *Escherichia coli*. *J. Biol. Chem.* 271, 32–39. doi:10.1074/jbc.271.1.32

Mikkola, S. (2020). Nucleotide Sugars in Chemistry and Biology. *Molecules* 25, 5755. doi:10.3390/molecules25235755

Mikušová, K., Yagi, T., Stern, R., McNeil, M. R., Besra, G. S., Crick, D. C., et al. (2000). Biosynthesis of the Galactan Component of the *Mycobacterial* Cell wall. *J. Biol. Chem.* 275, 33890–33897. doi:10.1074/jbc.M006875200

Mimitsuka, T., Sawai, H., Hatsu, M., and Yamada, K. (2007). Metabolic Engineering ofCorynebacterium Glutamicumfor Cadaverine Fermentation. *Biosci. Biotechnol. Biochem.* 71, 2130–2135. doi:10.1271/bbb.60699

Moussian, B. (2008). The Role of GlcNAc in Formation and Function of Extracellular Matrices. *Comp. Biochem. Physiol. B: Biochem. Mol. Biol.* 149, 215–226. doi:10.1016/j.cbpb.2007.10.009

Mueller, P., Gauttam, R., Raab, N., Handrick, R., Wahl, C., Leptihn, S., et al. (2018). High Level *In Vivo* Mucin-type Glycosylation in *Escherichia coli*. *Microb. Cel Fact.* 17, 1–15. doi:10.1186/s12934-018-1013-9

Natarajan, A., Jaroentomeechai, T., Cabrera-Sánchez, M., Mohammed, J. C., Cox, E. C., Young, O., et al. (2020). Engineering Orthogonal Human O-Linked Glycoprotein Biosynthesis in Bacteria. *Nat. Chem. Biol.* 16, 1062–1070. doi:10.1038/s41589-020-0595-9

Niimi, S., Suzuki, N., Inui, M., and Yukawa, H. (2011). Metabolic Engineering of 1,2-propanediol Pathways in *Corynebacterium Glutamicum*. *Appl. Microbiol. Biotechnol.* 90, 1721–1729. doi:10.1007/s00253-011-3190-x

Okino, S., Suda, M., Fujikura, K., Inui, M., and Yukawa, H. (2008). Production of D-Lactic Acid by *Corynebacterium Glutamicum* under Oxygen Deprivation. *Appl. Microbiol. Biotechnol.* 78, 449–454. doi:10.1007/s00253-007-1336-7

Orellana, A., Moraga, C., Araya, M., and Moreno, A. (2016). Overview of Nucleotide Sugar Transporter Gene Family Functions across Multiple Species. *J. Mol. Biol.* 428, 3150–3165. doi:10.1016/j.jmb.2016.05.021

Rodríguez-Díaz, J., Rubio-del-Campo, A., and Yebra, M. J. (2012a). Metabolic Engineering of *Lactobacillus Casei* for Production of UDP-N-Acetylglucosamine. *Biotechnol. Bioeng.* 109, 1704–1712. doi:10.1002/bit.24475

Rodríguez-Díaz, J., Rubio-del-Campo, A., and Yebra, M. J. (2012b). Regulatory Insights into the Production of UDP-N-Acetylglucosamine by *Lactobacillus Casei*. *Bioengineered* 3, 339–342. doi:10.4161/bioe.21271

Sasaki, M., Jojima, T., Inui, M., and Yukawa, H. (2010). Xylitol Production by Recombinant *Corynebacterium Glutamicum* under Oxygen Deprivation. *Appl. Microbiol. Biotechnol.* 86, 1057–1066. doi:10.1007/s00253-009-2372-2

Schneider, J., and Wendisch, V. F. (2011). Biotechnological Production of Polyamines by Bacteria: Recent Achievements and Future Perspectives. *Appl. Microbiol. Biotechnol.* 91, 17–30. doi:10.1007/s00253-011-3252-0

William Studier, F., Rosenberg, A. H., Dunn, J. J., and Dubendorff, J. W. (1990). [6] Use of T7 RNA Polymerase to Direct Expression of Cloned Genes. *Met. Enzymol.* 185, 60–89. doi:10.1016/0076-6879(90)85008-c

Tabata, K., Koizumi, S., Endo, T., and Ozaki, A. (2000). Production of UDP-N-Acetylglucosamine by Coupling Metabolically Engineered Bacteria. *Biotechnol. Let.* 22, 479–483. doi:10.1023/a:1005627820455

Tedaldi, L. M., Pierce, M., and Wagner, G. K. (2012). Optimised Chemical Synthesis of 5-substituted UDP-Sugars and Their Evaluation as Glycosyltransferase Inhibitors. *Carbohydr. Res.* 364, 22–27. doi:10.1016/j.carres.2012.10.009

Thibodeaux, C. J., Melançon, C. E., and Liu, H.-w. (2008). Natural-product Sugar Biosynthesis and Enzymatic Glycodiversification. *Angew. Chem. Int. Ed.* 47, 9814–9859. doi:10.1002/anie.200801204

Timmons, S. C., and Jakeman, D. L. (2007). Stereoselective Chemical Synthesis of Sugar Nucleotides via Direct Displacement of Acylated Glycosyl Bromides. *Org. Lett.* 9, 1227–1230. doi:10.1021/ol063068d

Uhde, A., Youn, J.-W., Maeda, T., Clermont, L., Matano, C., Krämer, R., et al. (2013). Glucosamine as Carbon Source for Amino Acid-Producing *Corynebacterium Glutamicum*. *Appl. Microbiol. Biotechnol.* 97, 1679–1687. doi:10.1007/s00253-012-4313-8

Unthan, S., Baumgart, M., Radek, A., Herbst, M., Siebert, D., Brühl, N., et al. (2015). Chassis Organism from Corynebacterium Glutamicum - a Top-down Approach to Identify and Delete Irrelevant Gene Clusters. *Biotechnol. J.* 10, 290–301. doi:10.1002/biot.201400041

Van der Rest, M. E., Lange, C., and Molenaar, D. (1999). A Heat Shock Following Electroporation Induces Highly Efficient Transformation of *Corynebacterium Glutamicum* with Xenogeneic Plasmid DNA. *Appl. Microbiol. Biotechnol.* 52, 541–545. doi:10.1007/s002530051557

Wagner, G. K., Pesnot, T., and Field, R. A. (2009). A Survey of Chemical Methods for Sugar-Nucleotide Synthesis. *Nat. Prod. Rep.* 26, 1172–1194. doi:10.1039/b909621n

Wahl, C., Hirtz, D., and Elling, L. (2016). Multiplexed Capillary Electrophoresis as Analytical Tool for Fast Optimization of Multi-Enzyme Cascade Reactions - Synthesis of Nucleotide Sugars. *Biotechnol. J.* 11, 1298–1308. doi:10.1002/biot.201600265

Wang, X., and Quinn, P. J. (2010). Lipopolysaccharide: Biosynthetic Pathway and Structure Modification. *Prog. Lipid Res.* 49, 97–107. doi:10.1016/j.plipres.2009.06.002

Wendisch, V. F., Jorge, J. M. P., Pérez-García, F., and Sgobba, E. (2016). Updates on Industrial Production of Amino Acids Using *Corynebacterium Glutamicum*. *World J. Microbiol. Biotechnol.* 32, 105. doi:10.1007/s11274-016-2060-1

Zamora, C. Y., Schocker, N. S., Chang, M. M., and Imperiali, B. (2017). Chemoenzymatic Synthesis and Applications of Prokaryote-specific UDP-Sugars. *Met. Enzymol.* 597, 145–186. doi:10.1016/bs.mie.2017.06.003

Zhao, G., Guan, W., Cai, L., and Wang, P. G. (2010). Enzymatic Route to Preparative-Scale Synthesis of UDP-GlcNAc/GalNAc, Their Analogues and GDP-Fucose. *Nat. Protoc.* 5 (4), 636–646. doi:10.1038/nprot.2010.3

Zhao, L., Ma, Z., Yin, J., Shi, G., and Ding, Z. (2021). Biological Strategies for Oligo/polysaccharide Synthesis: Biocatalyst and Microbial Cell Factory. *Carbohydr. Polym.* 258, 117695. doi:10.1016/j.carbpol.2021.117695

Conflict of Interest: The authors declare that the research was conducted in the absence of any commercial or financial relationships that could be construed as a potential conflict of interest.

frontiers in Bioengineering and Biotechnology

BRIEF RESEARCH REPORT
published: 15 October 2021
doi: 10.3389/fbioe.2021.768289

GEDpm-cg: Genome Editing Automated Design Platform for Point Mutation Construction in *Corynebacterium glutamicum*

Yi Yang[1,2†], Yufeng Mao[1,2†], Ye Liu[2], Ruoyu Wang[1,2], Hui Lu[2], Haoran Li[1,2], Jiahao Luo[1,2], Meng Wang[2], Xiaoping Liao[1,2] and Hongwu Ma[1,2*]*

[1]Biodesign Center, Key Laboratory of Systems Microbial Biotechnology, Tianjin Institute of Industrial Biotechnology, Chinese Academy of Sciences, Tianjin, China, [2]Tianjin Institute of Industrial Biotechnology, Chinese Academy of Sciences, Tianjin, China

Advances in robotic system-assisted genome editing techniques and computer-aided design tools have significantly facilitated the development of microbial cell factories. Although multiple separate software solutions are available for vector DNA assembly, genome editing, and verification, by far there is still a lack of complete tool which can provide a one-stop service for the entire genome modification process. This makes the design of numerous genetic modifications, especially the construction of mutations that require strictly precise genetic manipulation, a laborious, time-consuming and error-prone process. Here, we developed a free online tool called GEDpm-cg for the design of genomic point mutations in *C. glutamicum*. The suicide plasmid-mediated counter-selection point mutation editing method and the overlap-based DNA assembly method were selected to ensure the editability of any single nucleotide at any locus in the *C. glutamicum* chromosome. Primers required for both DNA assembly of the vector for genetic modification and sequencing verification were provided as design results to meet all the experimental needs. An *in-silico* design task of over 10,000 single point mutations can be completed in 5 min. Finally, three independent point mutations were successfully constructed in *C. glutamicum* guided by GEDpm-cg, which confirms that the *in-silico* design results could accurately and seamlessly be bridged with *in vivo* or *in vitro* experiments. We believe this platform will provide a user-friendly, powerful and flexible tool for large-scale mutation analysis in the industrial workhorse *C. glutamicum* via robotic/software-assisted systems.

Keywords: genetic modification, point mutation editing, computer-aided design automation, Corynebacterium glutamicum, GEDpm-cg

OPEN ACCESS

Edited by:
Zheng-Hong Xu,
Jiangnan University, China

Reviewed by:
Ruslan Kalendar,
University of Helsinki, Finland
Yanfeng Liu,
Jiangnan University, China

****Correspondence:***
Xiaoping Liao
liao_xp@tib.cas.cn
Hongwu Ma
ma_hw@tib.cas.cn

[†]These authors have contributed equally to this work

Specialty section:
This article was submitted to Synthetic Biology, a section of the journal Frontiers in Bioengineering and Biotechnology

Received: *31 August 2021*
Accepted: *07 October 2021*
Published: *15 October 2021*

Citation:
Yang Y, Mao Y, Liu Y, Wang R, Lu H, Li H, Luo J, Wang M, Liao X and Ma H (2021) GEDpm-cg: Genome Editing Automated Design Platform for Point Mutation Construction in Corynebacterium glutamicum. *Front. Bioeng. Biotechnol. 9:768289. doi: 10.3389/fbioe.2021.768289*

INTRODUCTION

Industrial biomanufacturing, using well-tailored microbial cell factories with economically competitive titers, synthesis rates and yields (TRY), offers a potentially green and economical alternative to current petroleum-based chemical synthesis (Clomburg et al., 2017). *Corynebacterium glutamicum*, the famous industrial workhorse for amino acid production with a current output of over 6 million tons per year (Lee et al., 2016), is increasingly being adapted as a promising chassis for the biosynthesis of other compounds (Becker et al., 2018). However, most microorganisms, including

the industrial *C. glutamicum*, strains have not evolved to naturally and/or efficiently produce the majority of petrochemical compounds (Lee et al., 2012). Despite the substantial rational engineering efforts devoted to developing efficient cell factories, it is still arduous to achieve competitive TRY values due to our current limited understanding of cellular metabolism (Nielsen and Keasling, 2016; Ding et al., 2020). Instead, most industrial workhorses are developed without in-depth genetic knowledge by random mutagenesis strategies such as adaptive laboratory evolution and chemical/physical mutagenesis (Ikeda, 2003; Zhang et al., 2014; Sandberg et al., 2019). Over the past few decades, random mutagenesis strategies combined with applicable selection methods have led to the development of various industrial *C. glutamicum* strains as well as a valuable trove of genetic diversity (Ikeda, 2003; Zhang et al., 2018; Stella et al., 2019). With the development of genome sequencing and genetic engineering tools, novel synthetic biology elements such as enzyme variants have been identified through reverse engineering (Ikeda and Takeno, 2020), which can motivate further innovation in the development of industrial *C. glutamicum* strains. Since point mutations (single nucleotide substitutions, insertions or deletions) are the predominant mutation type identified in industrial/evolved strains (Kvitek and Sherlock, 2013; Lang et al., 2013), large-scale point mutation analysis is highly desired for further understanding the genetic basis responsible for the evolved *C. glutamicum* phenotypes (Bailey et al., 2002; Nielsen and Keasling, 2016). However, one major issue in the current point mutation analysis is the genetic modification of cells to introduce the enormous numbers of point mutations needed for high-throughput screening, which appears to be an impossible task for laboratory biologists. For the case of a saturation mutation library targeting the 10 bp sequence of the core region of a bacterial promoter (−35/−10 region), the strain library size can reach 4^10, nearly one million, which is impossible to accomplish with human labor alone. Recently, a robotic system-assisted *C. glutamicum* automation genome editing platform (MACBETH) has been developed, with the capacity to generate thousands of single nucleotide mutant strains per month (Wang Y. et al., 2018), which opens the possibility for future robot-assisted large-scale point mutation editing. Unfortunately, as a CRISPR/Cas-deaminase-mediated base editing platform, MACBETH was unable to edit all the nucleotides of interest due to the limitation of genome-targeting scope, editing window, and base transition capability (Wang Y. et al., 2019).

Genome point mutation editing is a much more precise genetic modification than gene deletion or insertion. Although there are many genome editing techniques, which can be simply divided into ones based on homologous-recombination (HR) and non-homologous end-joining (NHEJ), few are suitable for strictly precise genomic point mutation editing (Wang et al., 2021). The nuclease/integrase/transposon-mediated NHEJ system, which requires a specific recognition site at the targeted chromosomal locus in advance and will inevitably generate chromosomal scars (such as the *loxP* or *attB* sites) after genome editing (Hu et al., 2014; Marques et al., 2020), is obviously inapplicable for point mutation editing. The RNA-guided CRISPR/Cas-based HR systems can provide scarless chromosomal modifications (Jiang et al., 2017; Wang et al., 2018a). However, additional mutations in protospacer and PAM regions are usually prerequisite for avoiding re-cutting by endonucleases, and editable genome regions are restricted due to the limited availability of guide RNAs (Wang T. et al., 2019), which also limits its application in point mutation editing. The RecT-mediated ssDNA/dsDNA HR system, which can support the editing of any nucleotide of interest without the need to repeatedly construct editing vectors (Binder et al., 2013), seems like an ideal technique. However, the ssDNA/dsDNA electro-transformation efficiency in Gram-positive *C. glutamicum* might be problematic (Ruan et al., 2015), especially for the industrial recombinant strains. In addition, due to the relatively short homologous arms in ssDNA/dsDNA, the off-target risk is high, especially for point mutations inside sequences with additional copies in the chromosome. In the counter-marker-assisted HR system, which is based on two rounds of single crossover HR (Schäfer et al., 1994), any nucleotide in the genome is theoretically editable without risk of introducing additional mutations/scars. The application of an editing vector carrying relatively long homologous arms can not only significantly improve the electro-transformation efficiency, but also lower the off-target risk caused by mismatching. In addition, the editing vector can be used repeatedly, which reduces the cost of vector DNA assembly. Although the efficiency of HR is relatively low, conditional lethality mediated by counter-selectable markers, such as the sucrose-lethal gene *sacB* (Schäfer et al., 1994) or streptomycin-sensitive gene *rpsL* (Kim et al., 2011), can ensure the occurrence of two rounds of single-crossover HR. Therefore, the counter-marker-assisted HR system is the most promising chromosomal point mutation technique for *C. glutamicum*.

The counter-marker HR mediated genome editing system is mostly implemented using non-replicating suicide plasmids (Wang et al., 2021), among which the suicide vector pK18*mobsacB* (GenBank: FJ437239.1) is the most widely used in *C. glutamicum* (Schäfer et al., 1994). For point mutation editing based on the pK18*mobsacB* vector, a pK18*mobsacB*-derived vector and a total of two rounds of crossover HR and mutant isolation are required (**Figure 1**). Firstly, the upstream homologous arm (UHA) and the downstream homologous arm (DHA), which contain the corresponding point mutation, are amplified from the chromosome of *C. glutamicum* by primer pairs 1/2 and 3/4 (named as primer-1/2/3/4), respectively. Then, the homologous arms as well as the linearized pK18*mobsacB* vector fragment are assembled into the pK18*mobsacB*-derived suicide vector, containing homologous arms and the desired point mutation. Subsequently, the resulting vector is electroporated into the cells and integrated into the chromosome in the 1st-round of single crossover, and the resulting transformants are selected in the 1st-round isolation based on the positive selection marker, the kanamycin resistance gene *kan*^{R}. Next, the integrated vector is eliminated in the 2nd-round of single crossover and the transformants are selected in the 2nd-round of isolation based on a negative selection marker, the sucrose-lethal gene *sacB*. Finally, the correct mutants

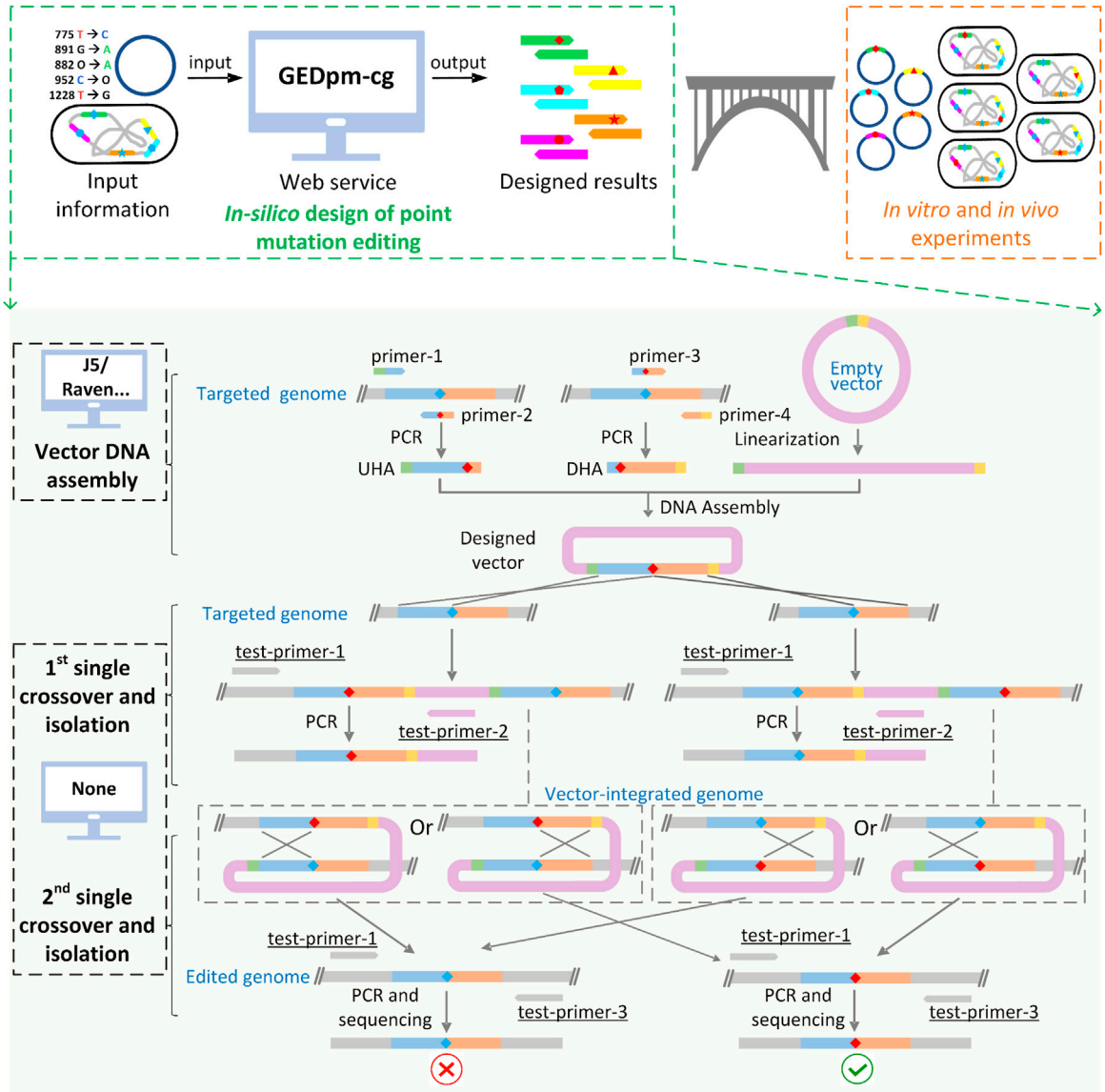

FIGURE 1 | Schematic diagram of GEDpm-cg and the point mutation editing technique based on uploaded sequences. GEDpm-cg is a web-based computer-aided design tool for the construction of genomic point mutations in *C. glutamicum*. When input files containing information of point mutations, vector and targeted genome are uploaded, GEDpm-cg is able to provide precise and high-throughput *in-silico* designed results for *in vitro* editing vector DNA assembly and *in vivo* point mutation editing in *C. glutamicum*. The design of point mutations by GEDpm-cg can be divided into the overlap-based vector DNA assembly and the suicide plasmid-mediated counter-selection point mutation genome editing. For vector DNA assembly, design tools such as j5 or Raven are able to assist the design of vector DNA assembly for biologists, while no tool is available for the design of suicide plasmid-mediated counter-selection point mutation genome editing. UHA, upstream homologous arm; DHA, downstream homologous arm; green band, homologous end between UHA and vector; yellow band, homologous end between DHA and vector, blue diamond, base before point mutation; red diamond, base after point mutation. Underlined names indicate the easily-neglected verification primers.

containing the point mutation are confirmed by sequencing. Thus, a total of two homologous arms and at least two pairs of primers (primer-1/2/3/4) are required for the whole process of point mutation editing.

Despite the development of computer-aided design (CAD) tools for the design of genetic modifications (Kalendar et al., 2011; Appleton et al., 2017a; Appleton et al., 2017b), no CAD tool is currently available for the design of counter-marker-assisted HR editing. Although some tools such as j5 (Hillson et al., 2012), Raven (Appleton et al., 2014) and FastPCR (Kalendar et al., 2017) can assist the design of optimal primers for amplifying UHA/DHA, laboratory biologists still have to manually extract and input optional templates, which is laborious, time-consuming and error-prone if it needs to be done on a large scale. In addition, the design of primers for sequence verification, one of the most important experimental steps, is often neglected by laboratory

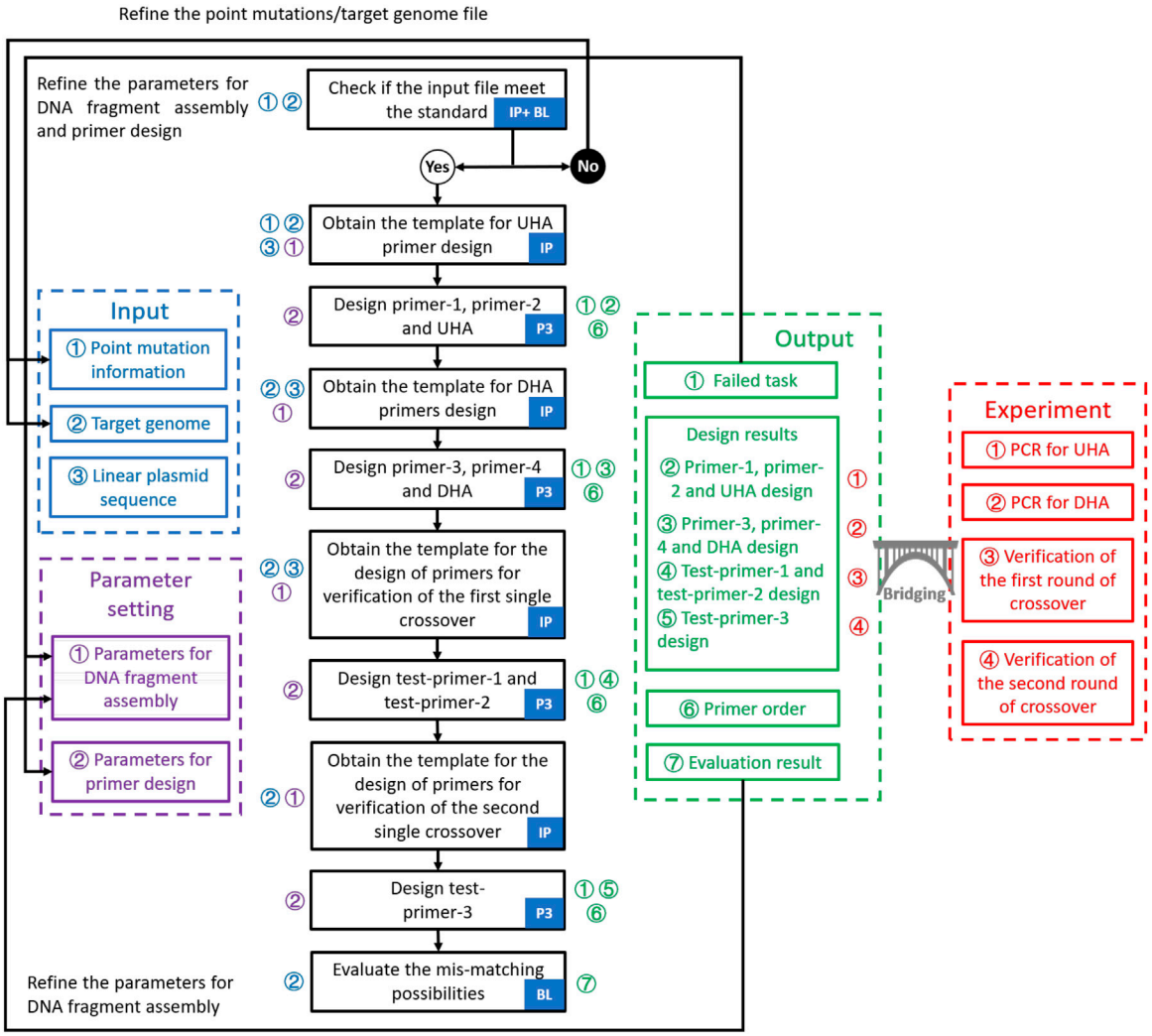

FIGURE 2 | Workflow for the design of point mutations in GEDpm-cg. The design of primers and homologous arms is performed by three programs: In-house program, Primer3 and BLAST. Logical judgment flow is divided into detailed steps which are marked with corresponding inputs (blue numbers), parameters (purple numbers) and outputs (green numbers). Moreover, output files linked to experiments are marked with red numbers. First, three input files are checked by the in-house program and BLAST. If the input file does not meet the standards, it should be refined. Otherwise, they will be submitted to the back-end program with the parameters set by the user to go through the design process. The design process consists of three main operations: determination of the templates for primer design by the in-house program, design of primers based on the templates by Primer3 and evaluation of the mis-match likelihood of UHA/DHA by BLAST. Then, the design results will be provided in four output files. "Failed task" and 'Evaluation result' can guide the user to re-optimize the parameters. "Design results" and 'Primer order' are used to guide the experiment. IP, In-house program; P3, Primer3; BL, BLAST; UHA, upstream homologous arm; DHA, downstream homologous arm; PCR, polymerase chain reaction.

beginners, which limits the ability to correct unexpected misediting/non-editing. For instance, if adding one pair of verification primers (test-primer-1/2, **Figure 1**), non-editing failures caused by false-positive transformants (Ma et al., 2015) during the 1st-round of single crossover and isolation can be avoided. In addition, unexpected mutations located around the ends (~100 bp) of UHA-DHA cannot be precisely sequenced if simply using primer-1/2 rather than test-primer-1/3 (**Figure 1**) for the final sequence verification. Thus, a one-stop, comprehensive CAD tool for the whole design process of counter-marker HR mediated genome editing is highly desirable for automated and high-throughput point mutation editing in *C. glutamicum*.

In this study, to reduce the effort and time needed for point mutation editing design and provide a comprehensive packaged result for laboratory biologists, we developed a user-friendly online tool (**Figure 1**), named the Genome Editing automated Design platform for point mutation construction in *Corynebacterium glutamicum* (GEDpm-cg, https://gedpm-cg.biodesign.ac.cn/). The counter-selection HR system (Schäfer et al., 1994; Tan et al., 2012) and the overlap-based assembly method (Casini et al., 2015) were chosen as the loading

techniques. Homologous arms and primers required for genetic modification, vector DNA assembly and sequencing verification were provided as design results. Moreover, the GEDpm-cg was built in a novel, entirely serverless architecture, with computing, as well as data storage, done in a serverless manner, which ensures flexibility in allocating computing resources. Finally, to verify the accuracy of design results generated by GEDpm-cg, three independent point mutations were experimentally implemented.

MATERIALS AND METHODS

GEDpm-cg Service Implementation and Availability

GEDpm-cg is written in the Python programming language (https://www.python.org). GEDpm-cg makes external calls to Primer3 (Untergasser et al., 2012) for primer and flanking homology sequence design, and to BLAST (Zhang et al., 2000) for checking redundant mutations inside target sequences from the input file and identifying putative mis-priming and flanking homology sequence incompatibility events. The point mutation design is conducted via the workflow integrating inhouse program, Primer3 and BLAST (**Figure 2**). A detailed user manual for GEDpm-cg is provided online (https://gedpm-cg.biodesign.ac.cn/help).

GEDpm-cg is freely available for noncommercial (e.g., academic, nonprofit, or governmental) users. The service is available through the public GEDpm-cg webserver (https://gedpm-cg.biodesign.ac.cn/).

Serverless Architecture of GEDpm-cg

The serverless architecture of GEDpm-cg allows us to devote more time to core workflows and to build scalable, reliable systems more quickly and easily. We used three-tier architecture to build our website, which is a popular pattern for user-facing applications (**Supplementary Figure S1**). All tiers that comprise this architecture are deployed on Amazon Web Service, including the front presentation tier, logic computation tier, and data storage tier. The front presentation tier represents the component that users directly interact with (such as a web page, etc.), which is hosted by AWS S3 static website functionality and accelerated by AWS CloudFront. The logic computation tier of our website manages http requests from external systems and contains the core services such as AWS Lambda, AWS API Gateway and AWS Step Functions. AWS Lambda provides core computation functionality, which runs the point mutation design processing workflows. The API Gateway handles the http requests and routes them to the correct backends. AWS Step Functions orchestrate the serverless workflow by processing messages from the API Gateway and invoking AWS Lambda asynchronously. The data storage tier manages persistent storage from our website, including AWS DynamoDB, and AWS S3.

On the GEDpm-cg home page, uploaded input files will be stored on an AWS S3 bucket. When the submit button is clicked after all parameters are set, a request is sent to the API Gateway, which passes the parameters to the AWS Step Function, and all parameters are stored on AWS DynamoDB. Then, the browser gets the response, jumps to the results page, and waits for the computing results. AWS lambda is invoked asynchronously by AWS Step Function event sources, which runs the logic code and uploads the result files to AWS S3. Each submission will trigger a computing process in parallel, regardless of how much demand there is on the website, showcasing the usefulness of serverless computing.

Strains, Primers, and Reagents

All strains and plasmids used in this study are listed in **Supplementary Table S1**. The primers (GENEWIZ, Suzhou, China) are listed in **Supplementary Table S2**. Plasmids were extracted using the TIANprep Mini Plasmid Kit (Tiangen, Beijing, China). DNA fragments were amplified by polymerase chain reaction (PCR) using the Q5® high-fidelity DNA polymerase purchased from NEB (Hitchin, UK). PCR products were purified using the TIANquick Midi Purification Kit (Tiangen, Beijing, China). DNA fragments were assembled using the ClonExpress II One Step Cloning Kit purchased from Vazyme (Nanjing, China). Yeast extract and tryptone were purchased from OXOID (Hants, UK). BHI broth was purchased from Hopebio (Qingdao, China). Other reagents were purchased from Solarbio (Beijing, China). Antibiotics were added to the media at the following concentrations when required: 50 μg/ ml kanamycin for *E. coli*, and 25 μg/ ml kanamycin for *C. glutamicum*.

Construction of Plasmids and Strains

E. coli DH5α was used as the host for plasmid construction, and was cultivated in Luria-Bertani (LB) medium containing (per liter) 10 g tryptone, 5 g yeast extract, and 10 g NaCl. The introduction of point mutations into the genome of *C. glutamicum* was achieved via a two-step homologous recombination procedure using the suicide vector pK18*mobsacB* (Schäfer et al., 1994). The starting strain was *C. glutamicum* ATCC 13032.

To introduce the *C568T* mutation into the endogenous gene *adhA*, the vector pK18-$adhA^{C568T}$ was constructed as follows: the flanking regions of the *adhA* gene with relevant modifications were amplified from genomic DNA of *C. glutamicum* using the primer pairs adhA-1/adhA-2 and adhA-3/adhA-4. The corresponding products were assembled into the vector pK18mob*sacB* digested with *BamH*I based on the T5 exonuclease-dependent DNA assembly method (Xia et al., 2019) using the ClonExpress II One Step Cloning Kit (Vazyme, Nanjing, China), resulting in the vector pK18-$adhA^{C568T}$. The plasmids pK18-ald^{C973T} and pK18-$ldhA^{C463T}$ were constructed analogously.

Analytical Techniques

The vectors pK18-$adhA^{C568T}$, pK18-ald^{C973T} and pK18-$ldhA^{C463T}$ were verified using Sanger sequencing at GENEWIZ (Suzhou, China). PCR products were checked by 1.5% agarose gel electrophoresis in 0.5 × Tris-acetate-EDTA (TAE), and quantified using a NanoDrop 2000 spectrophotometer (NanoDrop Technologies, Wilmington, United States).

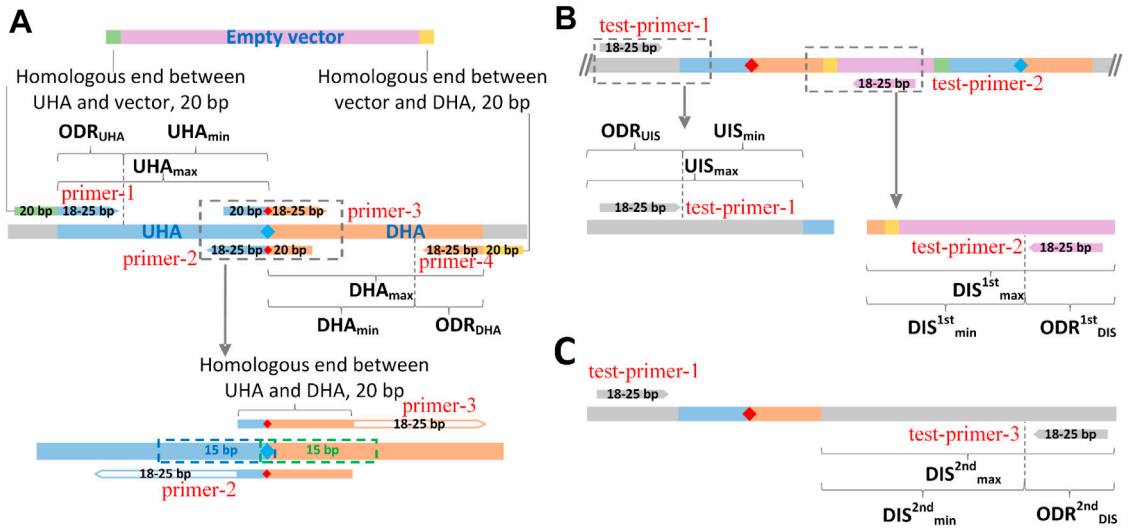

FIGURE 3 | Schematic diagram of the design principle of GEDpm-cg. Parameter settings for the design of primers and homologous arms for the vector DNA assembly **(A)**, the 1st-round of single crossover and isolation **(B)** and the 2nd-round of single crossover and isolation **(C)**. UHA, upstream homologous arm; DHA, downstream homologous arm; green band, homologous end between UHA and vector; yellow band, homologous end between DHA and vector, blue diamond, base before point mutation; red diamond, base after point mutation. $UHA_{min\text{-}max}$, length range of upstream homologous arm; ODR_{UHA}, optional design region of upstream homologous arm; $DHA_{min\text{-}max}$, length range of downstream homologous arm; ODR_{DHA}, optional design region of downstream homologous arm; $UIS_{min\text{-}max}$, length range of upstream internal sequence (sequence from 5′-end of test-primer-1 (forward primer for verification of the 2nd round of crossover) to the 5′-end of the upstream homologous arm); ODR_{UIS}, optional design region of forward primer (test-primer-1) for verification of the 2nd round of crossover; $DIS^{1st}_{min\text{-}max}$, length range of downstream internal sequence for verification of the first single crossover (sequence from the 3′-end of the downstream homologous arm to the 5′-end of test-primer-2 (reverse primer for verification of the 1st single crossover)); ODR^{1st}_{DIS}, optional design region of reverse primer (test-primer-2) for the verification of the first single crossover; $DIS^{2nd}_{min\text{-}max}$, length range of downstream internal sequence for the verification of the second single crossover (sequence from the 3′-end of the downstream homologous arm to the 5′-end of test-primer-2 (reverse primer for the verification of the 1st single crossover)); ODR^{2nd}_{DIS}, optional design region of the reverse primer (test-primer-3) for verification of the second single crossover.

RESULTS

Design Principle of the Design of Homologous Arms and Primers for Point Mutation Editing by GEDpm-cg

In order to seamlessly bridge *in-silico* design results with *in vivo* or *in vitro* experiments, DNA assembly methods should be loaded into GEDpm-cg. In comparison with the traditional restriction-ligation methods, newly developed DNA assembly methods such as Gibson Assembly and Golden Gate have been increasingly favored as streamlined assembly workflows by biologists due to their simplicity, cost effectiveness and cloning efficiency (Casini et al., 2015). In this study, overlap-based assembly methods such as Gibson Assembly and CPEC (Casini et al., 2015), in which DNA fragments are assembled based on homologous ends (usually from 15 to 40 bp), were chosen as the loading technique for GEDpm-cg. In addition to the basic two pairs of primers (primer-1/2 and 3/4) for amplifying the UHA/DHA, verification PCR using the first pair of verification primers (test-primer-1/2) is required to avoid false-positives during the 1st-round of single crossover and isolation. The correct mutants containing the point mutation are finally confirmed by sequencing using the second pair of verification primers (test-primer-1/3). Thus, a total of two homologous arms and four pairs of primers are required for the whole process of point mutation editing (**Figures 1**, **2**). The design principles of the UHA, DHA and primers are as follows.

In order to save cost, the length of primers was expected to be short. As shown in **Figure 3A**, to correctly match template sequences, the length of the 3′-end sequences was limited between 18–25 bp for any primer. To ensure the assembly efficiency among UHA, DHA and empty vector, the length of overlap regions was set to 20 bp. For the overlap between UHA/DHA and empty vector, a 20 bp sequence at the 5′-end of the linearized empty vector was added to the 5′-end of primer-1, and a 20 bp reverse complementary sequence of the 3′-end of the linearized empty vector was added to the 5′-end of primer-4. For the overlap between UHA and DHA, a 20 bp sequence covering the point mutation was added to the 5′-end of primer-3, and its reverse complementary sequence was added to the 5′-end of primer-2. For the verification of the 1st single crossover (**Figure 3B**), test-primer-1 was located upstream of the UHA in the targeted genome, and test-primer-2 was located downstream of the DHA in the pK18*mobsacB*-derived vector. Thus, if clones obtained in the 1st isolation round on kanamycin plates were unable to yield clear PCR products, they were identified as false positives that should be discarded. For the verification of the 2nd single crossover (**Figure 3C**), the verified test-primer-3 was located downstream of the DHA in the targeted

A

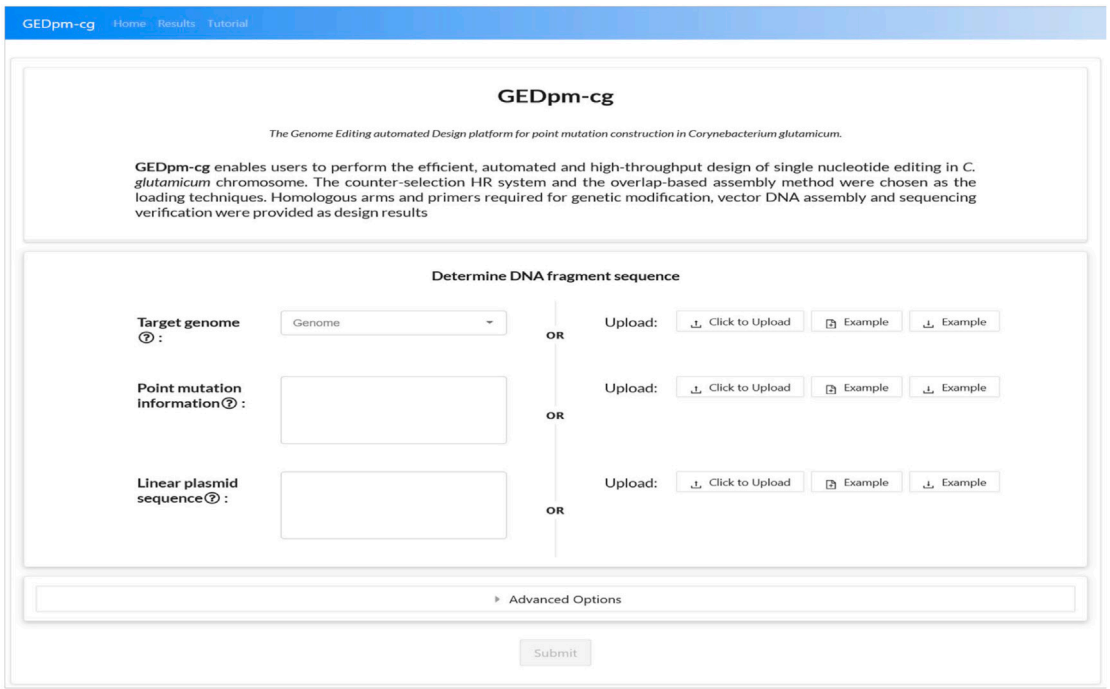

B

seq1	GGCGGCAACGGCTGGAACAGCTAGTAGTTTTCGGAAATTT	2001	A	T
seq2	GCCCATCACGATCAGACAAACAGTCAGCATGGGGCGATGG	2001	C	O
seq3	CCGAGGAAAACGCACAAAAAGTTTTGTGTGTGATCCATGA	2001	O	A
seq4	CCTCAGCGGCGGCGGCCAGGGCCAGCAGCTCACCCTCGGC	2001	C	O
seq5	AAATTTATGCCGACTTTAGCAAAAAATGAGAATGAGTTGA	2001	A	G
seq6	GATAATGCCAGTAACACCCCATTGTCCAACTGTCACCTTT	2001	C	T

C

	PRIMER_LEFT_WHOLE_SEQUENCE	PRIMER_RIGHT_WHOLE_SEQUENCE	PRODUCT_SEQUENCE	PRODUCT_WHOLE_LENGTH	PRIMER_LEFT_TM	PRIMER_RIGHT_TM	PRIMER_LEFT_TM_HOMODIMER	PRIMER_RIGHT_TM_HOMODIMER	PRIMER_PAIR_TM_HETERODIMER
seq1	GAGCTCGGTAC	TCCTAGTGAT	GAGCTCGGTA	1025	54.1714496	54.0776413	3.469743	21.719279	11.4028349
seq2	GAGCTCGGTAC	TCGAATATTC	GAGCTCGGTA	1034	54.1316824	53.1063407	-2.95695	-30.9374	10.534376
seq3	GAGCTCGGTAC	AAAATGAGGA	GAGCTCGGTA	1068	54.6556863	55.1012628	3.951485	6.7155635	5.35853939
seq5	GAGCTCGGTAC	CCAGACCAAT	GAGCTCGGTA	1066	53.872905	54.7744154	6.715564	8.7909479	12.8430702
seq6	GAGCTCGGTAC	TAACCCACAC	GAGCTCGGTA	1031	53.7868939	53.8038914	-18.5175	6.3592221	-12.708698

D

	PRIMER_INTERNAL_NUM_RETURNED	PRIMER_LEFT_EXPLAIN	PRIMER_LEFT_NUM_RETURNED	PRIMER_PAIR_EXPLAIN	PRIMER_PAIR_NUM_RETURNED	PRIMER_RIGHT_EXPLAIN	PRIMER_RIGHT_NUM_RETURNED
seq4	0	considered 664, GC content failed 17, low tm 94, high tm 203, ok 350	0	considered 0, ok 0	0	considered 664, GC content failed 132, not in any ok right region 532, ok 0	0

E

Primer_name	Sequence
seq1-1	GAGCTCGGTACCCGGGGATCGGCAATCACATCGCGCTC
seq1-2	TCCTAGTGATTGAGCAATAGGCATGGTCATGGCGATGC
seq1-3	CTATTGCTCAATCACTAGGACCGGTCGCTCAAAAGGCC
seq1-4	CAGGTCGACTCTAGAGGATCTGGCCAGCGAAATCACCA
test-seq1-1	GCGCGGGAGATGAATGAAAC
test-seq1-2	GCCAGCTGGCGAAAGGGG
test-seq1-3	GAAATCAGCTTGGTGACCGC

F

ID	Warning
seq5	The target sequence can not map to the reference genome. Please check them.
seq6	The target sequence can map to multiple positions in the reference genome. The genome editing may be mislocated.

G

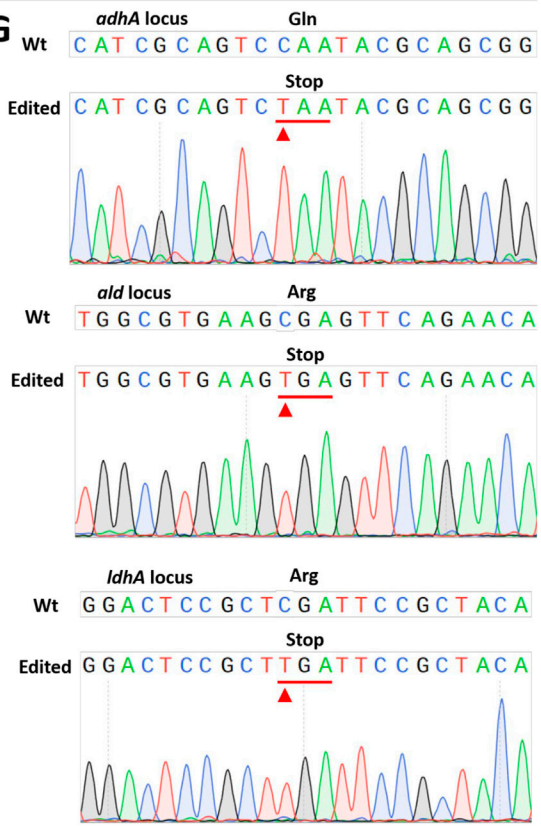

FIGURE 4 | GEDpm-cg web-based interface and examples for input, output and experimental verification. **(A)**. GEDpm-cg web-based interface. **(B)**. Example parts list CSV input file for targeted sequences. **(C)**. Example primer-1 and primer-2, list in XLSX output file. **(D)**. Example primers submitted to the sequence synthesis company, list in XLSX output file. **(E)**. Example of failed primer designs for UHA, list in XLSX output file. **(F)**. Example of possible mis-matching sequences, list in XLSX output file. **(G)**. Sanger sequencing results of point mutation genome editing for *adhA*^{C568T}, *ald*^{C973T} and *ldhA*^{C463T}. The substituted bases are marked with red arrows.

genome. The mutant strains are verified by sequencing the PCR products obtained using test-primer-1 and -3. It is worth noting that all seven primers were optimized within their respective optional design regions (ODRs, **Figure 3A**), which was determined by the user's parameter settings (**Supplementary Figure S2**), in order to reach scores as high as possible using the Primer3 algorithm.

Automated Design of Point Mutation Editing Using the GEDpm-cg Web Server

For the convenience of biologist users, GEDpm-cg is available across computer platforms via a common web-browser interface (**Figure 4A**), and as such does not require the user to install or update the software. Compared with software built at a centralized server with potential load-balancing problems when many users are submitting their requests simultaneously, GEDpm-cg, built in a serverless manner, can invoke numerous simultaneous functions in parallel, automatically scaling with the size of the workload (Enes et al., 2020). Amazon lambda (https://aws.amazon.com/lambda/) was used as the core computing service due to its quite short startup time and flexibility. An online user manual provides an overview of GEDpm-cg's functionality, step-by-step how-to examples, in-depth descriptions of input and output files, detailed documentation of GEDpm-cg, error-message explanations, and experimental protocols for the aforementioned point mutation editing.

To begin the GEDpm-cg point mutation design process, the user needs to select/upload relevant information concerning the targeted genome, point mutation information and linear vector sequence. The targeted genome can be selected among 71 offered *C. glutamicum* strains available in the NCBI database or uploaded by the user as a FASTA-format sequence file (community standard FASTA). The linear vector sequence is uploaded by the user as a TEXT (TXT) format sequence file. Because the UHA and DHA are expected to be assembled with the linear vector at the 5′-end and 3′-end, respectively, the sequence direction of the linear vector is suggested to be verified repeatedly by the user. The point mutation information is provided by uploading a CSV-format sequence file containing the sequence ID, sequence without the point mutation, index of the targeted mutation site in the sequence and the targeted nucleotide before and after the mutation is introduced (**Figure 4B**). Notably, in order to avoid repeatedly reading the large genome sequence file and reduce the design time, the length of the uploaded sequence must be larger than the sum of UHA_{max}, DHA_{max}, UIS_{max} and DIS^{2nd}_{min}, and the mutation site should be located around the middle of the uploaded sequence to satisfy the template needed for the design of the UHA, DHA and primers. In addition to the input files, the user can also alter the default DNA assembly parameters including the lengths of the UHA, DHA, UIS, DIS^{1st} and DIS^{2nd}, as well as the primer design parameters including thresholds for the melting temperature (T_m) and GC content (**Supplementary Figure S2**).

After the user submits the three inputs, GEDpm-cg will firstly evaluate whether these inputs meet the standards (see the section on 'in-depth descriptions of input and output files' in the online user manual), then utilizes BLAST (Zhang et al., 2000) to check whether the uploaded sequences for the mutation information are strictly consistent with the targeted genome (**Figure 2**). If there is any error, GEDpm-cg returns an error report (see the section on "error-message explanations" in the online user manual) to prompt the user to correct the uploaded files. Otherwise, GEDpm-cg will utilize Primer3 (Untergasser et al., 2012) to optimize the cloning primers (primer-1/2/3/4, concatenations of 20 bp overhang-generating sequences and 18–25 bp template-matching sequences) required for generating the UHA and DHA fragments, and the verification primers (test-primer-1/2/3, 18–25 bp template-matching sequences) for two rounds of single crossover (**Figure 2**). The design results will be provided in four output files. The output file, named "Design results," contains the sequence IDs, primers, lengths of targeted PCR fragment and the T_m of homodimer and heterodimer formation of primers (**Figure 4C**). Another file, named "Primer order", contains a list of primers provided to the primer synthesis company (**Figure 4D**). The output file, named "Failed task", contains the sequence IDs without accessible primers and their failure reasons judged by Primer3 (**Figure 4E**). The user can re-set the given parameters (T_m and/or GC content) for Primer3 to obtain feasible results. In addition, to avoid potential off-target events, the output file (Evaluation result) provides possible mis-matching sequences and positions for the uploaded sequences (**Figure 4F**). The user can try to lower the mis-matching possibilities by altering the lengths of the UHA/DHA. If no problems occur, batch-designs containing 10,000 tasks can be completed within 5 min. To save cloud storage resources, these output files will be stored for no more than 1 week.

Experimental Verification of Design Results for Point Mutation Editing by GEDpm-Cg

To ensure the reliability of the design results generated by GEDpm-cg, three point-mutations (**Supplementary Table S1**) in three independent genes (*adhA*, *ald* and *ldhA*) were experimentally constructed in *C. glutamicum* ATCC 13032. The related input and output files are shown in the additional files. Recently, Xia et al. (2019) developed the T5 exonuclease-mediated, overlap-based DNA assembly technique TEDA, which is relatively simple, cost-effective and highly efficient compared with currently popular overlap-based DNA assembly methods such as Gibson Assembly. The assembly of UHAs, DHAs and the linearized pK18*mobsacB* vector, and the two rounds of single crossovers and isolations were conducted according to the section "experimental protocols" in the online user manual. Agarose gel electrophoresis (**Supplementary Figure S3**) and Sanger sequencing (**Figure 4G**) confirmed that the corresponding pK18-derived vectors were successfully assembled and the three mutations had been successfully introduced into the genome. The average editing efficiency for genomic point mutation editing based on the design of GEDpm-cg can reach

45.45% (**Supplementary Table S3**), which is consistent with the theoretical 50% editing efficiency after two rounds of single crossover and isolation (Schäfer et al., 1994).

DISCUSSION

The development of microbial cell factories has been greatly facilitated by computer-aided design tools (Appleton et al., 2017b; Hillson et al., 2019; Carbonell et al., 2020), among which design tools for genome editing play an important role in liberating biologists from laborious, repetitive and error-prone design work (Montague et al., 2014; Quintin et al., 2016; Wang et al., 2019b). However, most genetic modification design tools were specifically developed to handle a specific module for a single phase of the editing process that will be more programmable, such as CHOPCHOP (Montague et al., 2014) for designing CRISPR guide RNAs, PrimeDesign (Hsu et al., 2021) for designing specifically engineered guide RNAs (pegRNAs), Merlin (Quintin et al., 2016) for designing ssDNAs, as well as j5 (Hillson et al., 2012) and Raven (Appleton et al., 2014) for designing DNA assembly primers. To further improve the automaticity of MACBETH and evaluate the off-target risk, our group previously developed an online tool (gBIG, http://gbig.ibiodesign.net/) for the high-throughput design of guide RNAs, which allowed sequence design for the base editing-mediated inactivation of over 3,000 target genes within minutes (Wang Y. et al., 2019). However, no CAD tool is currently available for one-stop design covering all the experimental steps required for genetic modification. Although laboratory biologists can employ these specific CAD tools in a stepwise manner to assist their genetic modification design, truly automated and high-throughput design is still limited by the non-standardized data exchange and input/output formats (Carbonell et al., 2020). Specifically, users have to manually extract and upload numerous templates (the optional up- and downstream homologous arms) for primer design using j5/Raven or other CAD DNA assembly tools (Hillson et al., 2012; Appleton et al., 2014), which is cumbersome in high-throughput approaches and error-prone. In this study, we developed the online tool GEDpm-cg for the automated, rapid and precise design of genomic point mutation editing in *C. glutamicum*. For the first time, the design of functional elements (homologous arms required for the counter-marker-assisted HR system), the vector DNA assembly (primers design for vector construction) and the sequencing verification are integrated in the single CAD tool GEDpm-cg (**Figure 2**). As a result, it can provide automated and high-throughput design results covering all the experimental elements required for the constructing and verification of point mutations (**Figures 4C,D**). To be biologist-friendly, GEDpm-cg provides an open and free web-service, and the step-by-step how-to examples as well as the in-depth descriptions of input and output files (see in the online user's manual) are all developed to suit the needs of our biologist colleagues. Moreover, to further ensure that the point mutation is being introduced as the user desires without off-target mutations, the alignment between the targeted sequences and targeted genome is checked in advance and the possibility of off-target events is also evaluated. Finally, a testing simulation of over 10,000 single point mutations could be completed within only 5 min, and three point-mutations in the genome of *C. glutamicum* were experimentally constructed guided by GEDpm-cg (**Figure 4G**). Thus, the *in-silico* design results were seamlessly bridged with *in-vitro* vector construction and *in-vivo C. glutamicum* point mutation editing.

Although the emerging CRISPR/Cas genome editing systems are increasingly favored for genetic manipulation in *C. glutamicum* (Wang et al., 2021), the counter-selection-based system is still a reliable genome editing technique, especially for the construction of mutations that require strictly precise nucleotide editing (Stella et al., 2019). To improve the editing efficiency of this technique, various variants were developed, for example by replacing the native promoter of *sacB* in classical pK18*mobsacB* with the 18-times stronger P_{lacM} promoter (Tan et al., 2012), replacing the negative selection marker *sacB* with the novel streptomycin-sensitive gene *rpsL* (Kim et al., 2011) or 5-fluorouracil-lethal gene *upp* (Ma et al., 2015), as well as replacing single-copy and non-replicating pK18-derived vectors with multi-copy and temperature-sensitive pCGR2-derived vectors (Okibe et al., 2011). Notably, GEDpm-cg is able to flexibly support all these counter-selection-based variants upon the uploading of specific linear vector sequences by the user. What's more, GEDpm-cg can also be used for genomic point mutation editing in other species beyond *C. glutamicum* based on this same approach if the users upload corresponding genome and vector sequences. Nevertheless, the upgrading of GEDpm-cg to support point mutation editing by other genome editing techniques such as CRISPR/Cas system and/or other editing types for fragment sequence editing is still expected to fulfil different users' preferences in our future work.

With the recent technology advances in robotic/software-assisted strain engineering system, it has become feasible to enable an ultra-efficient turnover rate of design-build-test-learn synthetic biology cycle (Chao et al., 2017; Hillson et al., 2019). The robotic system-assisted CRISPR/Cas-deaminase-mediated *C. glutamicum* genome base editing platform, MACBETH, was developed by our colleagues in 2018. The MACBETH enables a maximal editing capacity of up to 9,000 single nucleotide mutant strains within 1 month (Wang Y. et al., 2018), which obviously exceeds the ability of human labor alone to construct no more than one hundred mutant strains per month. Since the basic experimental operations will not be beyond vector construction, plating, cultivating and screening, the MACBETH platform, based on the CRISPR/Cas9 mediated base editing, can be feasibly modified to support automated point mutation editing based on the counter-marker homologous-recombination. The combination of design automation based on GEDpm-cg and experiment operation automation based on MACBETH platform will be a superior tool for high-throughput point mutation editing of *C. glutamicum*.

In conclusion, we developed GEDpm-cg with superior efficiency, user-friendliness and flexibility for the design of genomic point mutation editing in *C. glutamicum*, which can liberate biologists from laborious, repetitive and error-prone experimental design. We believe our platform can open the possibility for large-scale mutation mining via robotic/software-assisted systems and consequently lead to a better understanding/engineering of cellular metabolism in the near future.

DATA AVAILABILITY STATEMENT

The datasets presented in this study can be found in online repositories. The names of the repository/repositories and accession number(s) can be found in the article/**Supplementary Material**

AUTHOR CONTRIBUTIONS

YY and YM designed the workflow of GEDpm-cg. YM, YL, and JL performed the experiments. YY, XL, RW, and HLi wrote the codes. YM, YY, YL, and HLu performed the debugging. YM, YY, XL, MW, and HM wrote and revised the manuscript. HM, YY, and YM conceived the study. HM supervised the work.

FUNDING

This work was funded by the National Key Research and Development Program of China (2018YFA0902900, 2018YFA0900300, 2020YFA0908300, 2021YFC2100700), the International Partnership Program of Chinese Academy of Sciences (153D31KYSB20170121), the National Natural Science Foundation of China (32101186, 21908239), the Tianjin Synthetic Biotechnology Innovation Capacity Improvement Project (TSBICIP-PTJS-001), Youth Innovation Promotion Association CAS, and the China Postdoctoral Science Foundation (2018M641658).

ACKNOWLEDGMENTS

We thank Dr. Yu Wang (Tianjin Institute of Industrial Biotechnology, Chinese Academy of Sciences) for discussion on genome editing techniques.

SUPPLEMENTARY MATERIAL

The Supplementary Material for this article can be found online at: https://www.frontiersin.org/articles/10.3389/fbioe.2021.768289/full#supplementary-material

REFERENCES

Appleton, E., Madsen, C., Roehner, N., and Densmore, D. (2017b). Design Automation in Synthetic Biology. *Cold Spring Harb Perspect. Biol.* 9, a023978. doi:10.1101/cshperspect.a023978

Appleton, E., Densmore, D., Madsen, C., and Roehner, N. (2017a). Needs and Opportunities in Bio-Design Automation: Four Areas for Focus. *Curr. Opin. Chem. Biol.* 40, 111–118. doi:10.1016/j.cbpa.2017.08.005

Appleton, E., Tao, J., Haddock, T., and Densmore, D. (2014). Interactive Assembly Algorithms for Molecular Cloning. *Nat. Methods* 11, 657–662. doi:10.1038/nmeth.2939

Bailey, J. E., Sburlati, A., Hatzimanikatis, V., Lee, K., Renner, W. A., and Tsai, P. S. (2002). Inverse Metabolic Engineering: A Strategy for Directed Genetic Engineering of Useful Phenotypes. *Biotechnol. Bioeng.* 79, 568–579. doi:10.1002/bit.10441

Becker, J., Rohles, C. M., and Wittmann, C. (2018). Metabolically Engineered *Corynebacterium Glutamicum* for Bio-Based Production of Chemicals, Fuels, Materials, and Healthcare Products. *Metab. Eng.* 50, 122–141. doi:10.1016/j.ymben.2018.07.008

Binder, S., Siedler, S., Marienhagen, J., Bott, M., and Eggeling, L. (2013). Recombineering in *Corynebacterium Glutamicum* Combined with Optical Nanosensors: A General Strategy for Fast Producer Strain Generation. *Nucleic Acids Res.* 41, 6360–6369. doi:10.1093/nar/gkt312

Carbonell, P., Le Feuvre, R., Takano, E., and Scrutton, N. S. (2020). *In Silico* design and Automated Learning to Boost Next-Generation Smart Biomanufacturing. *Synth. Biol. (Oxf)* 5, ysaa020. doi:10.1093/synbio/ysaa020

Casini, A., Storch, M., Baldwin, G. S., and Ellis, T. (2015). Bricks and Blueprints: Methods and Standards for DNA Assembly. *Nat. Rev. Mol. Cel Biol* 16, 568–576. doi:10.1038/nrm4014

Chao, R., Mishra, S., Si, T., and Zhao, H. (2017). Engineering Biological Systems Using Automated Biofoundries. *Metab. Eng.* 42, 98–108. doi:10.1016/j.ymben.2017.06.003

Clomburg, J. M., Crumbley, A. M., and Gonzalez, R. (2017). Industrial Biomanufacturing: The Future of Chemical Production. *Science* 355, aag0804. doi:10.1126/science.aag0804

Ding, Q., Diao, W., Gao, C., Chen, X., and Liu, L. (2020). Microbial Cell Engineering to Improve Cellular Synthetic Capacity. *Biotechnol. Adv.* 45, 107649. doi:10.1016/j.biotechadv.2020.107649

Enes, J., Expósito, R. R., and Touriño, J. (2020). Real-time Resource Scaling Platform for Big Data Workloads on Serverless Environments. *Future Generation Comput. Syst.* 105, 361–379. doi:10.1016/j.future.2019.11.037

Hillson, N., Caddick, M., Cai, Y., Carrasco, J. A., Chang, M. W., Curach, N. C., et al. (2019). Building a Global alliance of Biofoundries. *Nat. Commun.* 10, 2040. doi:10.1038/s41467-019-10079-2

Hillson, N. J., Rosengarten, R. D., and Keasling, J. D. (2012). j5 DNA Assembly Design Automation Software. *ACS Synth. Biol.* 1, 14–21. doi:10.1021/sb2000116

Hsu, J. Y., Grünewald, J., Szalay, R., Shih, J., Anzalone, A. V., Lam, K. C., et al. (2021). PrimeDesign Software for Rapid and Simplified Design of Prime Editing Guide RNAs. *Nat. Commun.* 12, 1034. doi:10.1038/s41467-021-21337-7

Hu, J., Li, Y., Zhang, H., Tan, Y., and Wang, X. (2014). Construction of a Novel Expression System for Use in *Corynebacterium Glutamicum*. *Plasmid* 75, 18–26. doi:10.1016/j.plasmid.2014.07.005

Ikeda, M. (2003). Amino Acid Production Processes. *Adv. Biochem. engineering/biotechnology* 79, 1–35. doi:10.1007/3-540-45989-8_1

Ikeda, M., and Takeno, S. (2020). "Recent Advances in Amino Acid Production," in *Corynebacterium Glutamicum: Biology and Biotechnology*. Editors M. Inui and K. Toyoda (Cham: Springer International Publishing), 175–226. doi:10.1007/978-3-030-39267-3_7

Jiang, Y., Qian, F., Yang, J., Liu, Y., Dong, F., Xu, C., et al. (2017). CRISPR-Cpf1 Assisted Genome Editing of *Corynebacterium Glutamicum*. *Nat. Commun.* 8, 15179. doi:10.1038/ncomms15179

Kalendar, R., Khassenov, B., Ramankulov, Y., Samuilova, O., and Ivanov, K. I. (2017). FastPCR: An *In Silico* Tool for Fast Primer and Probe Design and Advanced Sequence Analysis. *Genomics* 109, 312–319. doi:10.1016/j.ygeno.2017.05.005

Kalendar, R., Lee, D., and Schulman, A. H. (2011). Java Web Tools for PCR, *In Silico* PCR, and Oligonucleotide Assembly and Analysis. *Genomics* 98, 137–144. doi:10.1016/j.ygeno.2011.04.009

Kim, I. K., Jeong, W. K., Lim, S. H., Hwang, I. K., and Kim, Y. H. (2011). The Small Ribosomal Protein S12P Gene *rpsL* as an Efficient Positive Selection Marker in Allelic Exchange Mutation Systems for *Corynebacterium Glutamicum*. *J. Microbiol. Methods* 84, 128–130. doi:10.1016/j.mimet.2010.10.007

Kvitek, D. J., and Sherlock, G. (2013). Whole Genome, Whole Population Sequencing Reveals that Loss of Signaling Networks Is the Major Adaptive Strategy in a Constant Environment. *Plos Genet.* 9, e1003972. doi:10.1371/journal.pgen.1003972

Lang, G. I., Rice, D. P., Hickman, M. J., Sodergren, E., Weinstock, G. M., Botstein, D., et al. (2013). Pervasive Genetic Hitchhiking and Clonal Interference in Forty Evolving Yeast Populations. *Nature* 500, 571–574. doi:10.1038/nature12344

Lee, J.-Y., Na, Y.-A., Kim, E., Lee, H.-S., and Kim, P. (2016). The Actinobacterium *Corynebacterium Glutamicum*, an Industrial Workhorse. *J. Microbiol. Biotechnol.* 26, 807–822. doi:10.4014/jmb.1601.01053

Lee, J. W., Na, D., Park, J. M., Lee, J., Choi, S., and Lee, S. Y. (2012). Systems Metabolic Engineering of Microorganisms for Natural and Non-natural Chemicals. *Nat. Chem. Biol.* 8, 536–546. doi:10.1038/nchembio.970

Ma, W., Wang, X., Mao, Y., Wang, Z., Chen, T., and Zhao, X. (2015). Development of a Markerless Gene Replacement System in *Corynebacterium Glutamicum* Using *Upp* as a Counter-selection Marker. *Biotechnol. Lett.* 37, 609–617. doi:10.1007/s10529-014-1718-8

Marques, F., Luzhetskyy, A., and Mendes, M. V. (2020). Engineering *Corynebacterium Glutamicum* with a Comprehensive Genomic Library and Phage-Based Vectors. *Metab. Eng.* 62, 221–234. doi:10.1016/j.ymben.2020.08.007

Montague, T. G., Cruz, J. M., Gagnon, J. A., Church, G. M., and Valen, E. (2014). CHOPCHOP: a CRISPR/Cas9 and TALEN Web Tool for Genome Editing. *Nucleic Acids Res.* 42, W401–W407. doi:10.1093/nar/gku410

Nielsen, J., and Keasling, J. D. (2016). Engineering Cellular Metabolism. *Cell* 164, 1185–1197. doi:10.1016/j.cell.2016.02.004

Okibe, N., Suzuki, N., Inui, M., and Yukawa, H. (2011). Efficient Markerless Gene Replacement in *Corynebacterium Glutamicum* Using a New Temperature-Sensitive Plasmid. *J. Microbiol. Methods* 85, 155–163. doi:10.1016/j.mimet.2011.02.012

Quintin, M., Ma, N. J., Ahmed, S., Bhatia, S., Lewis, A., Isaacs, F. J., et al. (2016). Merlin: Computer-Aided Oligonucleotide Design for Large Scale Genome Engineering with MAGE. *ACS Synth. Biol.* 5, 452–458. doi:10.1021/acssynbio.5b00219

Ruan, Y., Zhu, L., and Li, Q. (2015). Improving the Electro-Transformation Efficiency of *Corynebacterium Glutamicum* by Weakening its Cell wall and Increasing the Cytoplasmic Membrane Fluidity. *Biotechnol. Lett.* 37, 2445–2452. doi:10.1007/s10529-015-1934-x

Sandberg, T. E., Salazar, M. J., Weng, L. L., Palsson, B. O., and Feist, A. M. (2019). The Emergence of Adaptive Laboratory Evolution as an Efficient Tool for Biological Discovery and Industrial Biotechnology. *Metab. Eng.* 56, 1–16. doi:10.1016/j.ymben.2019.08.004

Schäfer, A., Tauch, A., Jäger, W., Kalinowski, J., Thierbach, G., and Pühler, A. (1994). Small Mobilizable Multi-Purpose Cloning Vectors Derived from the *Escherichia coli* Plasmids pK18 and pK19: Selection of Defined Deletions in the Chromosome of *Corynebacterium Glutamicum*. *Gene* 145, 69–73. doi:10.1016/0378-1119(94)90324-7

Stella, R. G., Wiechert, J., Noack, S., and Frunzke, J. (2019). Evolutionary Engineering of *Corynebacterium Glutamicum*. *Biotechnol. J.* 14, e1800444. doi:10.1002/biot.201800444

Tan, Y., Xu, D., Li, Y., and Wang, X. (2012). Construction of a Novel *sacB*-Based System for Marker-free Gene Deletion in *Corynebacterium Glutamicum*. *Plasmid* 67, 44–52. doi:10.1016/j.plasmid.2011.11.001

Untergasser, A., Cutcutache, I., Koressaar, T., Ye, J., Faircloth, B. C., Remm, M., et al. (2012). Primer3-new Capabilities and Interfaces. *Nucleic Acids Res.* 40, e115. doi:10.1093/nar/gks596

Wang, B., Hu, Q., Zhang, Y., Shi, R., Chai, X., Liu, Z., et al. (2018a). A RecET-Assisted CRISPR-Cas9 Genome Editing in *Corynebacterium Glutamicum*. *Microb. Cel Fact* 17, 63. doi:10.1186/s12934-018-0910-2

Wang, Q., Zhang, J., Al Makishah, N. H., Sun, X., Wen, Z., Jiang, Y., et al. (2021). Advances and Perspectives for Genome Editing Tools of *Corynebacterium Glutamicum*. *Front. Microbiol.* 12, 654058. doi:10.3389/fmicb.2021.654058

Wang, T., Li, Y., Li, J., Zhang, D., Cai, N., Zhao, G., et al. (2019a). An Update of the Suicide Plasmid-mediated Genome Editing System in Corynebacterium Glutamicum. *Microb. Biotechnol.* 12, 907–919. doi:10.1111/1751-7915.13444

Wang, Y., Liu, Y., Li, J., Yang, Y., Ni, X., Cheng, H., et al. (2019b). Expanding Targeting Scope, Editing Window, and Base Transition Capability of Base Editing in *Corynebacterium Glutamicum*. *Biotechnol. Bioeng.* 116, 3016–3029. doi:10.1002/bit.27121

Wang, Y., Liu, Y., Liu, J., Guo, Y., Fan, L., Ni, X., et al. (2018b). MACBETH: Multiplex Automated *Corynebacterium Glutamicum* Base Editing Method. *Metab. Eng.* 47, 200–210. doi:10.1016/j.ymben.2018.02.016

Xia, Y., Li, K., Li, J., Wang, T., Gu, L., and Xun, L. (2019). T5 Exonuclease-dependent Assembly Offers a Low-Cost Method for Efficient Cloning and Site-Directed Mutagenesis. *Nucleic Acids Res.* 47, e15. doi:10.1093/nar/gky1169

Zhang, X., Zhang, X., Xu, G., Zhang, X., Shi, J., and Xu, Z. (2018). Integration of ARTP Mutagenesis with Biosensor-Mediated High-Throughput Screening to Improve L-Serine Yield in *Corynebacterium Glutamicum*. *Appl. Microbiol. Biotechnol.* 102, 5939–5951. doi:10.1007/s00253-018-9025-2

Zhang, X., Zhang, X.-F., Li, H.-P., Wang, L.-Y., Zhang, C., Xing, X.-H., et al. (2014). Atmospheric and Room Temperature Plasma (ARTP) as a New Powerful Mutagenesis Tool. *Appl. Microbiol. Biotechnol.* 98, 5387–5396. doi:10.1007/s00253-014-5755-y

Zhang, Z., Schwartz, S., Wagner, L., and Miller, W. (2000). A Greedy Algorithm for Aligning DNA Sequences. *J. Comput. Biol.* 7, 203–214. doi:10.1089/10665270050081478

Conflict of Interest: The authors declare that the research was conducted in the absence of any commercial or financial relationships that could be construed as a potential conflict of interest.

Publisher's Note: All claims expressed in this article are solely those of the authors and do not necessarily represent those of their affiliated organizations, or those of the publisher, the editors and the reviewers. Any product that may be evaluated in this article, or claim that may be made by its manufacturer, is not guaranteed or endorsed by the publisher.

frontiers in Microbiology

ORIGINAL RESEARCH
published: 28 October 2021
doi: 10.3389/fmicb.2021.750150

Biosensor-Based Optimization of Cutinase Secretion by *Corynebacterium glutamicum*

Patrick J. Bakkes[1], Patrick Lenz[2], Carolin Müller[1,3], Astrid Bida[1], Doris Dohmen-Olma[1], Andreas Knapp[2†], Marco Oldiges[1,3], Karl-Erich Jaeger[2] and Roland Freudl[1]**

[1] IBG-1: Biotechnology, Institute of Bio- and Geosciences, Forschungszentrum Jülich GmbH, Jülich, Germany, [2] Institute of Molecular Enzyme Technology, Heinrich Heine University Düsseldorf, Forschungszentrum Jülich, Jülich, Germany, [3] Institute of Biotechnology, RWTH Aachen University, Aachen, Germany

OPEN ACCESS

Edited by:
Ping Zheng,
Tianjin Institute of Industrial Biotechnology, Chinese Academy of Sciences (CAS), China

Reviewed by:
Yota Tsuge,
Kanazawa University, Japan
Kambiz Morabbi Heravi,
University of Hohenheim, Germany
Dong Liu,
Nanjing Tech University, China

***Correspondence:**
Patrick J. Bakkes
p.bakkes@fz-juelich.de
Roland Freudl
r.freudl@fz-juelich.de

†Present address:
Andreas Knapp,
Castrol Germany GmbH, Mönchengladbach, Germany

Specialty section:
This article was submitted to Microbiotechnology, a section of the journal Frontiers in Microbiology

Received: *30 July 2021*
Accepted: *08 October 2021*
Published: *28 October 2021*

Citation:
Bakkes PJ, Lenz P, Müller C, Bida A, Dohmen-Olma D, Knapp A, Oldiges M, Jaeger K-E and Freudl R (2021) Biosensor-Based Optimization of Cutinase Secretion by Corynebacterium glutamicum. Front. Microbiol. 12:750150. doi: 10.3389/fmicb.2021.750150

The industrial microbe *Corynebacterium glutamicum* is gaining substantial importance as a platform host for recombinant protein secretion. We recently developed a fluorescence-based (eYFP) *C. glutamicum* reporter strain for the quantification of Sec-dependent protein secretion by monitoring the secretion-related stress response and now demonstrate its applicability in optimizing the secretion of the heterologous enzyme cutinase from *Fusarium solani pisi*. To drive secretion, either the poor-performing Pel^{SP} or the potent $NprE^{SP}$ Sec signal peptide from *Bacillus subtilis* was used. To enable easy detection and quantification of the secreted cutinase we implemented the split green fluorescent protein (GFP) assay, which relies on the GFP11-tag fused to the C-terminus of the cutinase, which can complement a truncated GFP thereby reconstituting its fluorescence. The reporter strain was transformed with different mutant libraries created by error-prone PCR, which covered the region of the signal peptide and the N-terminus of the cutinase. Fluorescence-activated cell sorting (FACS) was performed to isolate cells that show increased fluorescence in response to increased protein secretion stress. Five Pel^{SP} variants were identified that showed a 4- to 6-fold increase in the amount and activity of the secreted cutinase (up to 4,100 U/L), whereas two improved $NprE^{SP}$ variants were identified that showed a ∼35% increase in secretion, achieving ∼5,500 U/L. Most of the isolated variants carried mutations in the h-region of the signal peptide that increased its overall hydrophobicity. Using site-directed mutagenesis it was shown that the combined mutations F11I and P16S within the hydrophobic core of the Pel^{SP} are sufficient to boost cutinase secretion in batch cultivations to the same level as achieved by the $NprE^{SP}$. Screening of a Pel^{SP} mutant library in addition resulted in the identification of a cutinase variant with an increased specific activity, which was attributed to the mutation A85V located within the substrate-binding region. Taken together the biosensor-based optimization approach resulted in a substantial improvement of cutinase secretion by *C. glutamicum*, and therefore represents a valuable tool that can be applied to any secretory protein of interest.

Keywords: *Corynebacterium glutamicum*, protein secretion, Sec-dependent export, signal peptide, fluorescence-based biosensor, EYFP, FACS, split GFP

INTRODUCTION

Corynebacterium glutamicum is a well-established microbial host for industrial biotechnology that is also gaining importance as a potent platform organism for the secretory production of recombinant proteins (Lee et al., 2016; Liu et al., 2016; Freudl, 2017). Secretion of recombinant proteins into the culture medium can be a preferred strategy as it possesses several key benefits over intracellular protein production (Quax, 1997). Targeted secretion can (i) avoid the intracellular accumulation of target proteins susceptible to aggregation (e.g., inclusion body formation), (ii) bypass endogenous toxic cellular effects and (iii) evade degradation by intracellular proteases. The diderm gram-positive bacterium *C. glutamicum* is a particularly attractive secretion host, as it secretes only few innate proteins into the culture medium and lacks significant extracellular proteolytic activity (Vertès, 2013). Moreover, several interesting target proteins such as therapeutic antibodies or lipases require the formation of intramolecular disulfide bonds for complete folding, which is usually restricted in the reducing environment of the cytoplasm (Saaranen and Ruddock, 2013; Freudl, 2017). The export of such proteins into the non-reducing extra-cytoplasmic milieu thus may promote the formation of biologically active protein. Finally, the secretory production of recombinant proteins obviates the need for cell disruption, thus enabling simple protein recovery and purification, which in turn, facilitates downstream processing and reduces the overall production costs (Quax, 1997). The mechanism(s) and protein systems involved in protein translocation across the mycolic acids of the outer membrane of *C. glutamicum* are as of yet unknown.

In bacteria, the vast majority of extra-cytoplasmic proteins are exported across the cytoplasmic membrane by the general secretion (Sec) pathway (Freudl, 2017; Prabudiansyah and Driessen, 2017; Rapoport et al., 2017). Characteristically, the Sec substrate proteins carry an N-terminal signal peptide, which is crucial for targeting to the Sec translocase (Rusch and Kendall, 2007). In addition to their role in protein targeting and translocation, signal peptides can also influence the biosynthesis, the folding kinetics and the stability of the dedicated substrate protein (Deana et al., 1998; Freudl, 2018). Despite a general lack of sequence homology, Sec signal peptides share a universally conserved tripartite organization comprising a positively charged N-terminal region, a central hydrophobic core (h-region), and a polar C-terminal domain (c-region) that contains the cleavage site recognized by the signal peptidase (Izard and Kendall, 1994; Freudl, 2018). All three regions are known to effectively contribute to the export of Sec substrates (Izard and Kendall, 1994; Freudl, 2018).

The Sec system has been exploited for the secretion of a wide variety of recombinant proteins in a range of different microorganisms (Choi and Lee, 2004; Freudl, 2017; Cui et al., 2018; Hamed et al., 2018; Neef et al., 2021). However, finding a suitable signal peptide capable of driving efficient secretion remains a major bottleneck, mainly because it is still not possible to reliably predict the secretion performance of an individual signal peptide in context with the desired heterologous target protein and the applied expression host (Freudl, 2018). Hence, extensive screenings of a large variety of signal peptides seems to be the most-promising approach to identify the best-performing signal peptide. Signal peptide diversity can be achieved by the creation of multiple variants of a specific signal peptide using mutagenesis approaches (Caspers et al., 2010) or by generation of libraries from a large number of different microbial signal peptides (Brockmeier et al., 2006; Watanabe et al., 2009; Degering et al., 2010; Hemmerich et al., 2016). Besides the use of large signal peptide libraries for heterologous protein secretion in *C. glutamicum* there are many studies, too numerous to be listed in their entirety here, that report on the use of single (or a small number of different) signal peptides for the efficient secretion of a variety of different target proteins. Comprehensive overviews of the used signal peptides and the obtained amounts of the secreted target proteins, which include amongst others α-amylase, (endo)xylanase, Phospholipase C, cutinase and M18 scFv are given in Lee et al. (2016), Liu et al. (2016), and Freudl (2017).

In addition to the identification of a suitable signal peptide for secretion, efforts to improve the yield of a secreted target protein usually requires the optimization of a multitude of (co-dependent) biological and bioprocess parameters (Hemmerich et al., 2019). The monitoring of protein secretion during such optimization process however is frequently limited by the availability of an easy functional assay for the desired target protein. In addition, the multitude of potential optimization parameters requires the testing of a high number of samples, which necessitates a general assay for the monitoring of protein secretion compatible with high-throughput approaches.

For such purposes, we recently developed a fluorescent *C. glutamicum* reporter strain that is capable of quantifying Sec-dependent export of recombinant proteins by monitoring the related secretion stress, independent of an assay for the respective target protein (Jurischka et al., 2020). The mechanistic principle of this protein secretion biosensor is drawn schematically in **Figure 1**. High-level production of secretory proteins in *C. glutamicum* induces a stress response, which is triggered by the accumulation of incompletely or incorrectly folded secretory protein molecules at the cytoplasmic membrane-cell envelope interface (Kleine et al., 2017; Jurischka et al., 2020). Bacteria typically respond to such secretion stress by the upregulation of the housekeeping protease HtrA (Raivio and Silhavy, 2001; Meltzer et al., 2009; Kleine et al., 2017; Jurischka et al., 2020), which is capable of degrading the misfolded proteins at the *trans*-side of the cytoplasmic membrane. Replacement of the chromosomal *htrA* gene in *C. glutamicum* ATCC13032 (Kinoshita et al., 1957) by the gene coding for the yellow fluorescent protein eYFP, while leaving the *htrA* signal transduction pathway intact, resulted in a reporter strain that allows the monitoring of Sec-dependent export of recombinant proteins by means of its fluorescence output. The fluorescence of the reporter strain was shown to respond to the secretion of different recombinant proteins in a dose-dependent manner and allowed the differentiation between the performances of distinct signal peptides that were used to drive the secretion of cutinase from *Fusarium solani pisi* (Jurischka et al., 2020). Moreover, high-level secretory production of cutinase in the reporter strain resulted in highly fluorescent cells that can be

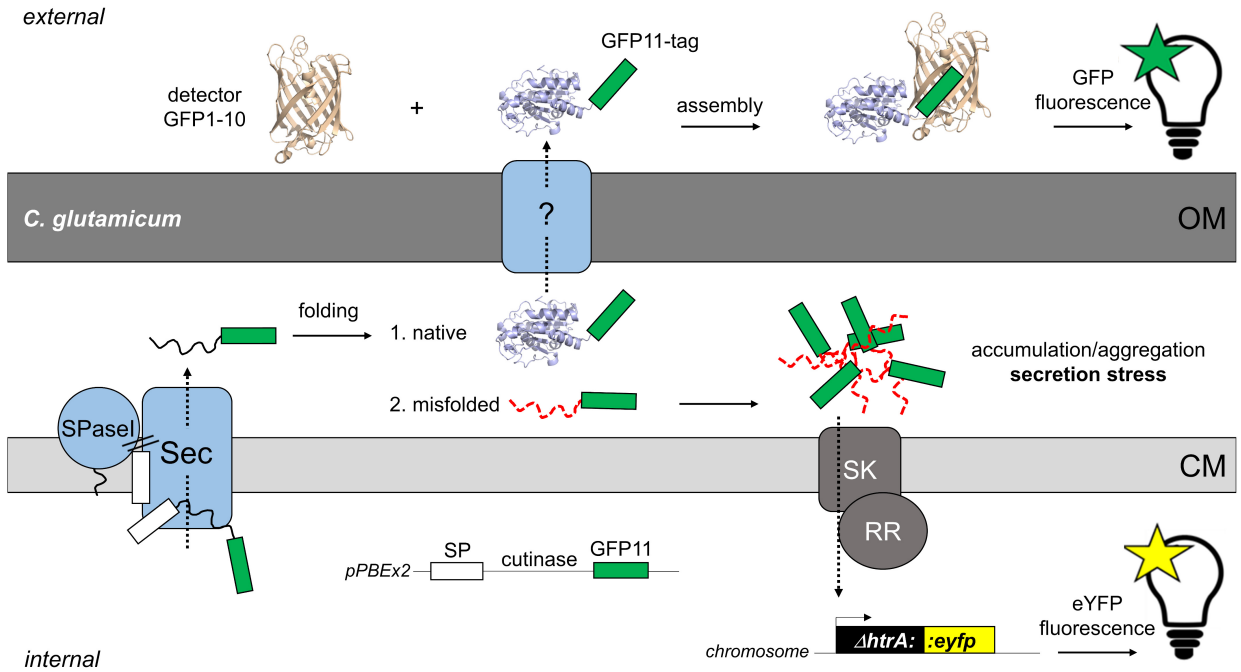

FIGURE 1 | Fluorescence-based monitoring of Sec-secretion stress in *C. glutamicum* and detection of secreted target protein by the split GFP assay. The overproduction of secretory proteins promotes accumulation of incompletely or misfolded proteins at the membrane-cell envelope interface. To alleviate this secretion stress, cells typically respond by the upregulation of the extra-cytoplasmic protease HtrA, which is able to degrade the misfolded proteins at the *trans*-side of the cytoplasmic membrane (CM). In *C. glutamicum*, a two-component system consisting of a sensory kinase (SK) and a response regulator (RR) is likely involved in regulation of expression of the adjacent *htrA* gene (Jurischka et al., 2020). In the *C. glutamicum* K9 biosensor strain, the *htrA* gene has been replaced by the *eyfp* gene, while leaving the *htrA* signal transduction pathway intact. The fluorescent reporter strain allows the monitoring of Sec-dependent secretion of recombinant proteins in a dose-dependent manner (Jurischka et al., 2020). The actual mechanism(s) and protein systems facilitating the transport of proteins across the mycolic acid outer membrane (OM) of *C. glutamicum* still remain an enigma. For detection of the target protein in the extracellular medium, we adapted the split GFP technology (Cabantous et al., 2005; Cabantous and Waldo, 2006) that previously had been adopted to monitor recombinant protein secretion *in B. subtilis* (Knapp et al., 2017). For this purpose, the eleventh β-sheet of GFP, is fused via a flexible linker to the C-terminus of the target protein (in our studies the model enzyme cutinase). The non-fluorescent detector GFP, which lacks eleventh β-sheet (GFP1-10) is produced separately in *E. coli* and purified from inclusion bodies. Combining the GFP11-tagged protein with the detector GFP1-10 enables reconstitution of functional fluorescent GFP. Subsequent measurement of the split GFP fluorescence allows detection and quantification of the secreted target protein. The white box indicates the signal peptide (SP); the green box indicates the GFP11-tag; SPase, signal peptidase.

separated from poorly secreting, low fluorescent cells using a fluorescence-activated cell sorter (Jurischka et al., 2020).

In the present study, we further investigated the applicability of the fluorescent biosensor strain in optimizing the secretion of the cutinase. Considering the fact that (large) libraries of signal peptides from different Sec proteins are not easily accessible to everyone and that reports on comparative analyses of signal peptides are rather scarce, the selection of a single signal peptide for secretion based on its performance described in literature can be a more useful approach. However, such arbitrarily selected signal peptide might not be optimal for the desired target protein and applied expression host, and thus may require optimization. Hence, a suitable alternative to testing many signal peptides of different origin is the improvement of a single signal peptide by mutagenesis approaches. We created different libraries by random mutagenesis of genes encoding signal peptide-cutinase fusions that were expressed in the reporter strain and screened by FACS to identify cells that exhibited improved cutinase secretion. For efficient Sec-dependent protein export not only the signal peptide is crucial (Izard and Kendall, 1994; Freudl, 2018), also amino acids downstream the signal peptide (N-terminus of the mature protein or "export initiation domain") have been shown to contribute to the export efficiency (Andersson and von Heijne, 1991; Musik et al., 2019). Therefore, mutagenesis was performed on the coding region for the signal peptide and a substantial part of the N-terminal domain of the mature cutinase.

To facilitate detection and quantification of the secreted cutinase, we applied the split green fluorescent protein (GFP) technology (Cabantous et al., 2005; Cabantous and Waldo, 2006) that was previously successfully adapted to monitor heterologous protein secretion in an activity-independent manner in *B. subtilis* (Knapp et al., 2017). Here, the eleventh β-sheet of GFP (GFP11) was fused to the C-terminus of the cutinase. This short GFP11-tag is able to complement a truncated, non-fluorescent GFP1-10 protein added to the culture medium after cultivation, thereby enabling reconstitution of the GFP fluorescence, which can be used as read-out for the amount of secreted cutinase (**Figure 1**). The results of our present study clearly show that secretion of the heterologous model protein cutinase by *C. glutamicum* can be

substantially improved by employing our Sec secretion biosensor as a tool for the identification of superior signal peptide variants, bypassing the need for a direct assay for the optimization of the secretion of a desired target protein.

MATERIALS AND METHODS

General Procedures

The bacterial strains and plasmids used in this study are shown in **Supplementary Table S1**. For standard cultivations, *E. coli* was grown in LB medium (Bertani, 1951) containing 50 μg/mL kanamycin at 37°C, while *C. glutamicum* was grown in BHIS medium containing 37 g/L brain heart infusion (BHI, Difco Laboratories), 91 g/L sorbitol and 25 μg/mL kanamycin at 30°C. Standard protocols were followed for DNA manipulations (Green and Sambrook, 2012). FastDigest restriction enzymes, T4 DNA ligase, FastAP thermosensitive Alkaline Phosphatase and Phusion DNA Polymerase were supplied by Thermo Fisher Scientific (Langerwehe, Germany) and used according to the manufacturer's specifications. Oligonucleotides were obtained from Eurofins (Ebersberg, Germany). For DNA amplification, appropriate PCR conditions were set for each primer pair, and PCR products were purified using the NucleoSpin gel and PCR clean up kit from Macherey-Nagel (Düren, Germany). Recombinant plasmids were isolated from *E. coli* or *C. glutamicum* using the Nucleospin plasmid purification, or NucleoSnap Plasmid Midi kit from Macherey-Nagel (Düren, Germany). DNA sequencing was carried out by Eurofins (Ebersberg, Germany). DNA concentrations were determined using a NanoDrop spectrophotometer (Thermo Fisher Scientific). Protein concentrations were determined by a BCA assay (Thermo Fisher Scientific), using BSA as a protein standard.

Plasmid Constructions

Initial plasmid constructions were carried out using the established *E. coli*/*C. glutamicum* shuttle vector pEKEx2 (Eikmanns et al., 1994). In a recent study however, we uncovered that the substantial leakiness of the *tac* promoter from pEKEx2 is caused by a reduced function of a modified plasmid-encoded *lac* repressor, while replicate DNA sequences in the pEKEx2 backbone contribute to plasmid instability (Bakkes et al., 2020). For tightly controlled secretory production of recombinant proteins, we therefore turned to the improved expression vector pPBEx2, which is a cured derivative of pEKEx2 (**Supplementary Table S1**; Bakkes et al., 2020). The plasmids, oligonucleotides and general procedures used to create the various expression constructs are shown in the **Supplementary Material** accompanying this paper.

Construction of Different Mutant Libraries

For the construction of a library of mutants of the cutinase-GFP11 fused to the Pel signal peptide (Pel^{L1}), the DNA region encompassing the Pel signal peptide (Pel^{SP}), linker and partial cutinase gene up to the internal *Kpn*I site was amplified from pPBEx2-Pel-cutinase-GFP11. For this purpose, the GeneMorph II Random Mutagenesis Kit (Agilent Technology, Santa Clara, CA, United States) and the oligonucleotide pair p07 and p08 were used (**Supplementary Table S2**). Conditions for error-prone PCR (epPCR) were set, such that approximately 3 - 5 mutations were introduced per PCR fragment. Subsequently, the epPCR products were purified, cleaved with *Pst*I and *Kpn*I, in conjunction with *Dpn*I, which eliminates the template DNA, and then ligated with gel-purified pPBEx2-Pel-cutinase-GFP11 that had been cleaved with *Pst*I and *Kpn*I. Typically, multiple ligation-transformation reactions were performed. For each ligation reaction (20 μL), 50 ng of cut vector and a 5 to 7-fold molar excess of cut insert was used. Ligation reactions were pooled and then purified. Next, multiple transformation reactions were carried out, for each using 50 μL of electrocompetent *E. coli* One Shot TOP10 cells (**Supplementary Table S1**) and 2 μL of the purified ligation mixture. Electroporation was carried out using a Gene Pulser Xcell (BioRad) and 0.1 mm electroporation cuvettes, with device settings: 1800 V, 25 μF and 200 Ω. Each batch of transformed cells was spread on a large square LB-agar plate containing 50 μg/mL kanamycin. To assess the library size, different amounts of a single batch of transformed cells were spread out. The Pel^{L1} library size was $\sim 1.8 \cdot 10^5$. All plates were incubated overnight at 37°C. The colonies were then suspended and pooled in a volume of 100 mL LB medium containing 50 μg/mL kanamycin and grown for 5 h at 37°C and 120 rpm, after which the cells were used for plasmid isolation. Next, multiple transformation reactions were carried out, using 1.3 – 2 μg of library DNA per 100 μL of electrocompetent cells of the biosensor strain *C. glutamicum* K9 (**Supplementary Table S1**; Jurischka et al., 2020). Electroporation was performed essentially as described earlier (Eggeling and Bott, 2005). The transformation reactions were spread on large square BHIS-agar plates containing 15 μg/mL kanamycin and then incubated for two days at 30°C. Hereafter, the colonies were suspended and pooled in a total volume of 100 mL BHIS medium containing 25 μg/mL kanamycin and grown for 5 h at 30°C and 120 rpm. Finally, the Pel^{L1} cells were supplemented with glycerol to a final concentration of 30% (v/v), flash-frozen using liquid nitrogen and then stored at –80°C, until use. To create the second-generation library Pel^{L2}, epPCR mutagenesis was performed on plasmid from variant V3 (P16S), which was isolated from the Pel^{L1} mutant library after FACS-based screening. For creation of the mutant library based on the NprE signal peptide ($NprE^{L}$), plasmid pPBEx2-NprE-cutinase-GFP11 was used as DNA template in epPCR reactions. For both Pel^{L2} and $NprE^{L}$, primers p07 and p08 (**Supplementary Tables S1, S2**) were used for DNA amplification. *E. coli* One Shot TOP10 electrocompetent cells were transformed with the mutant libraries Pel^{L2} and $NprE^{L}$ and then treated in the same manner as described for Pel^{L1}. Estimated library sizes were $\sim 5.8 \cdot 10^5$ and $\sim 2.4 \cdot 10^5$, respectively.

Site-Directed Mutagenesis

Site-directed mutagenesis (SDM) was performed using the Q5 Site-Directed Mutagenesis Kit from New England BioLabs

(Frankfurt am Main, Germany) according to the manufacturer's recommendations. The primers that were used to introduce the desired point mutations in the DNA region coding for the Pel^{SP} or the cutinase are listed in **Supplementary Table S2** (p09 – p18). For amplification of the nearly 9 kb plasmid fragments, 2% (v/v) DMSO was included in the reaction mixture and an extension time of 60 s per 1 kb was used. The various template and primer combinations used to create the different variants are shown in **Supplementary Table S3**. Subsequently, kinase, ligase and *Dpn*I treatment were performed according to the manufacturer's instructions. Finally, 2 μL of the reactions mixtures were used to transform chemically competent *E. coli* One Shot TOP10 cells. Recombinant plasmids were then isolated from single clones, verified by DNA sequencing and subsequently electroporated into the *C glutamicum* K9 biosensor strain as described by Eggeling and Bott (2005).

Standard Cultivation of *Corynebacterium glutamicum* K9 Biosensor Cells for Cutinase Secretion Experiments

For fluorescence-based monitoring of cutinase secretion, the *C. glutamicum* K9 biosensor cells carrying the different recombinant plasmids (**Supplementary Table S1**) were grown in BHIS medium in a 48-well flowerplate (m2p-labs, Baesweiler, Germany) in a BioLector (m2p-labs, Baesweiler, Germany) at 1,200 rpm, 85% relative humidity and 30°C for 6 h. Next, 50 μL of the BHIS precultures were transferred to a new flowerplate containing 800 μL CGXII minimal medium (Keilhauer et al., 1993) and 1% (v/v) glucose in each well and growth was continued overnight in the BioLector. Hereafter, the optical density (OD_{600}) of the cultures was determined and appropriate amounts were used to inoculate fresh CGXII minimal medium containing 1% (v/v) glucose in a new flowerplate, yielding a starting OD_{600} of ∼1 and cultivation was continued in the BioLector. Four hours after inoculation, IPTG was added to a final concentration of 250 μM and cultivation was sustained overnight. During cultivation, flowerplates were covered with a sterile gas permeable membrane to avoid evaporation. Bacterial growth was monitored online by measuring the backscatter at 620 nm (gain 20). For measuring online fluorescence of the biosensor cells, the BioLector is equipped with an eYFP filter module (λ_{ex} 508 nm, λ_{em} 532 nm). The eYFP biosensor fluorescence was measured using a signal gain of 90. The specific fluorescence of the biosensor cells was calculated by dividing the eYFP fluorescence (AU) by the corresponding backscatter (AU). The output of the biosensor cells was plotted as the specific fluorescence over time after subtraction of the corresponding specific fluorescence of the empty vector control cells (Δspecific fluorescence). The graphs thus depict the net difference in fluorescence response triggered by the secretory production of the cutinase. At the end of each cultivation, cell-free culture supernatants were prepared by centrifugation at 10,000 × *g* for 5 min and the levels of extracellular cutinase were assessed by SDS-PAGE analysis and/or complementary split GFP fluorescence and cutinase activity measurements.

Fed-Batch Cultivation of *Corynebacterium glutamicum* K9 Biosensor Cells for Cutinase Secretion

Corynebacterium glutamicum K9 biosensor cells carrying the recombinant plasmids as indicated were grown in 50 mL CGXII minimal medium containing 20 g/L glucose and 30 μg/ml kanamycin at 30°C and 300 rpm (25 mm shaking diameter). Cells were harvested in the late exponential phase and suspended in 0.9% (w/v) NaCl. The fed-batch cultivation was performed in a MTP-MF32-BOH1 flowerplate covered with F-GPRSMF32-1 sealing foil in a BioLector Pro (m2p-labs, Baesweiler, Germany), allowing for microfluidic pH control and fed-batch operation. Cultivation conditions were 30°C, 1,400 rpm, ≥30% headspace oxygen and ≥85% relative humidity. Biomass and pH were measured using a cycle time of 13 min. Per well, 800 μl CGXII minimal medium containing 22 mg/L protocatechuic acid, 30 μg/mL kanamycin and 5 g/L glucose (while urea was omitted) were inoculated with the corresponding preculture cells to an OD_{600} of 0.5. After 10 h, 400 g/L glucose were fed with 0.16 μL pump volume and a constant feed rate of 5.22 μL/h. After one hour, the pH in all wells was controlled one-sided to a set point of 6.8 with 3 M KOH, medium PI setting and 0.3 μL pump volume. Cutinase gene expression was induced with 250 μM IPTG after 8 h and cells were harvested after ∼25 h. The supernatants at the end of the cultivation were analyzed for cutinase content and activity.

Split Green Fluorescent Protein Assay

To determine the amounts of secreted cutinase-GFP11 protein, split GFP fluorescence measurements were conducted off-line at the end of the cultivations. The split GFP assay was carried out essentially as described previously (Knapp et al., 2017). In brief, the non-fluorescent detector GFP1-10 was produced in *E. coli* BL21(DE3) cells carrying pET22b-sfGFP1-10 and then purified from the inclusion bodies fraction. For reconstitution of holo-GFP, 20 μL of the *C. glutamicum* culture supernatants containing the GFP11-tagged cutinase were mixed with 180 μL of detector GFP1-10 solution in each well of a black flat-bottom 96-well microtiter plate (mtp). Culture supernatants of cells harboring the empty vector pPBEx2 served as controls. The mtp was then covered with a sterile gas permeable membrane to avoid evaporation and then incubated for 24 h at 20°C under gentle agitation to allow assembly of functional GFP. Finally, split GFP fluorescence was measured using an Infinite M1000 Pro plate reader (Tecan, Crailsheim, Germany). Excitation was performed at 485 nm (bandwidth 10 nm), while the fluorescence emission was recorded from 505 to 550 nm in 5 nm steps and using an appropriate gain factor (typically in the range of 105 – 120). The GFP-specific emission maximum at 510 nm was used for calculations. For each recombinant strain, at least two independent clones were cultivated and measurements were performed at least in duplicate.

Cutinase Activity Assays

Cutinase activity in culture supernatants was determined spectrophotometrically using *p*-nitrophenyl palmitate (*p*NPP)

as a substrate analogon, as described previously (Bakkes et al., 2020). For each recombinant strain, at least two independent clones were tested and measurements were always performed in duplicate. In addition, cutinase production was assessed by an *in situ* activity assay on agar plates. For this purpose, 3 μL of BHIS overnight cultures of *C. glutamicum* K9 biosensor cells carrying the different recombinant plasmids were spotted on BHIS-agar plates containing 400 μM IPTG, 1% (v/v), Tween-20 (substrate for cutinase) and 25 μg/mL kanamycin. The plates were incubated for at least 2 days at 30°C. The formation of optically turbid zones is indicative of production of enzymatically active cutinase (Bakkes et al., 2020).

SDS-PAGE Analysis

12.5% SDS-PAGE analysis was carried out essentially as described previously (Bakkes et al., 2020). In brief, at the end of the cultivation, the OD_{600} was determined and the cells were separated from the CGXII culture medium by centrifugation. Proteins from 500 μL culture supernatant were precipitated using a final concentration of 10% (v/v) trichloroacetic acid. Precipitated proteins were dissolved in pH-adjusted SDS-PAGE sample buffer (Laemmli, 1970). The amount of secreted protein was normalized to the cell density at the end of the cultivation and volumetric amounts corresponding to 1.5 OD_{600} cell equivalents were applied to each lane.

Flow Cytometry

Single-cell fluorescence measurements and cell sorting experiments were performed on a BD FACSAria Fusion cell sorter (BD Biosciences, Franklin Lakes, NJ, United States), using a 70 μm nozzle and a sheath pressure of 70 psi. A 488 nm blue solid laser was used for excitation. The forward-scatter characteristics (FSC) were recorded as small-angle scatter, whereas the side-scatter characteristics (SSC) were recorded as orthogonal scatter of the 488 nm laser. For measurements of the eYFP fluorescence of the *C. glutamicum* K9 biosensor cells, a 502 nm long-pass and 530/30 nm band-pass filter set was used. In all cases, prior to data acquisition, debris and electronic noise were excluded from the analysis by electronic gating in a SSC-H *vs*. FSC-H scatter plot. From the resulting population (P1) doublets were next excluded by a second gating step in a FSC-W *vs*. FSC-H scatter plot. The resulting population (P2) was then always used for fluorescence acquisition. Prior to FACS analysis/sorting, biosensor cells were appropriately diluted (typically $OD_{600} < 0.1$) in CGXII rudimentary solution pH 7.0, containing 20 g/L $(NH_4)_2SO_4$, 5 g/L urea, 1 g/L KH_2PO_4, 1 g/L K_2HPO_4, 0.25 g/L $MgSO_4 \cdot 7H_2O$, and 42 g/L MOPS. Cell samples were then passed through a 50 μm filter to remove any particulate matter and then subjected to FACS analysis. Cells were sorted into 5 mL polystyrene collection tubes (Sarstedt, Nürnbrecht, Germany) loaded with 2 mL CGXII medium containing 1% (v/v) glucose, 25 μg/mL kanamycin and appropriate amount of IPTG (typically 250 μM). For liquid sorting, precision was always set to purity, with the event rate never exceeding 16,000 events per second. Sorted cell samples were then split in half and transferred to a flowerplate for enrichment cultivation in a BioLector as described above. The cells were grown until the stationary phase was reached (24–48 h) and then subjected to FACS analysis and single cell sorting. Single cells were sorted onto OmniTrays™ (Thermo Fisher Scientific) containing BHIS-agar and 15 μg/mL kanamycin, using the single-cell sort precision mode along with an event rate of ∼6,000 – 8,000 s^{-1}. The agar plates were incubated for at least 2 days at 30°C to allow colony development. FACSDiva 8.0.2 (BD Biosciences, San Jose, United States) was used for FACS control and data analysis. A graphical workflow of the FACS analysis and sorting experiments is depicted in **Supplementary Figure S1**.

RESULTS AND DISCUSSION

Monitoring Cutinase Secretion Using the *Corynebacterium glutamicum* K9 Biosensor Strain in Combination With the Split Green Fluorescent Protein Assay

To demonstrate the applicability of the protein secretion biosensor strain, we aimed at improving the cutinase secretion driven by signal peptides showing a different secretion performance. For this purpose, the signal peptides from the *B. subtilis* enzymes pectate lyase (Pel^{SP}) and neutral protease ($NprE^{SP}$) were selected. The Pel^{SP} is known to facilitate high-level cutinase secretion in *B. subtilis* (Brockmeier et al., 2006), whereas only low levels are achieved in *C. glutamicum* (Hemmerich et al., 2016). The $NprE^{SP}$ on the other hand conveys cutinase secretion by *B. subtilis* at only low level (Brockmeier et al., 2006), whereas it is one of the best performing signal peptides for cutinase secretion in *C. glutamicum* (Hemmerich et al., 2019; Jurischka et al., 2020).

First, the performance of Pel^{SP} and $NprE^{SP}$ in facilitating the secretion of the GFP11-tagged cutinase was investigated (**Figure 2**). For this purpose, *C. glutamicum* K9 biosensor cells carrying pPBEx2-NprE-cutinase-GFP11 (**Figure 2A**) or pPBEx2-Pel-cutinase-GFP11 (**Figure 2B**) were induced with different concentrations of IPTG. K9 biosensor cells carrying the empty vector (EV) served as control. The fluorescence response of the cells to protein secretion stress over time in dependence of the IPTG concentration is shown in **Figures 2A,B** (upper panels). The secretion performance was assessed by determining the levels of the extracellular cutinase-GFP11 at the end of the cultivation by means of SDS-PAGE (**Figures 2A,B**, lower panels) and by measuring the split GFP fluorescence and the cutinase activity in the culture supernatant (**Figure 2C**).

The secretory production of NprE-cutinase-GFP11 leads to substantial secretion stress as evidenced by the eYFP fluorescence response of the biosensor cells upon induction with IPTG (**Figure 2A**, upper panel). The amount of the specific fluorescence at the end of the cultivation of the respective biosensor cells correlated with the amounts of the extracellular cutinase-GFP11 as determined by SDS-PAGE, showing a dose-dependent response (**Figure 2A**, lower panel). A similar dose-dependency was observed when NprE-cutinase without a GFP11-tag was secreted (*cf.* **Supplementary Figure S2**). However, in this case,

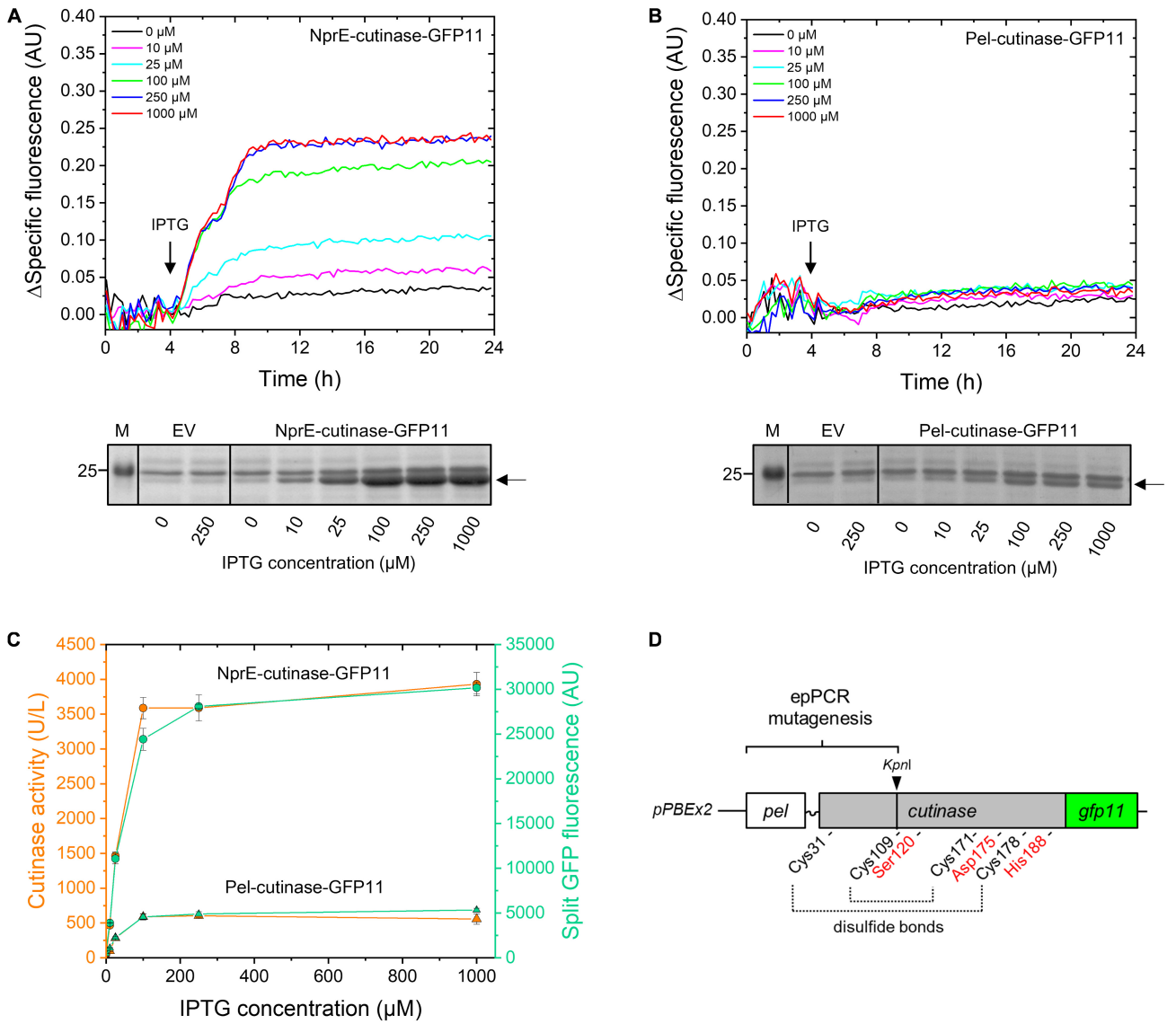

FIGURE 2 | Monitoring the secretion of GFP11-tagged cutinase using the *C. glutamicum* K9 biosensor strain and the split GFP assay. *C. glutamicum* K9 biosensor cells harboring pPBEx2 (EV), pPBEx2-NprE-cutinase-GFP11 or pPBEx2-Pel-cutinase-GFP11 were grown in CGXII medium containing 1% (v/v) glucose in a BioLector for 24 h at 30°C, 1,200 rpm and 85% relative humidity. Four hours after inoculation, IPTG was added to the cultures to indicated final concentrations. The fluorescence response of the biosensor cells during cultivation is shown in the upper panels as the Δspecific fluorescence over time for cells expressing NprE-cutinase-GFP11 **(A)** or Pel-cutinase-GFP11 **(B)**. Cutinase-GFP11 in the respective culture supernatants after 24 h of growth was analyzed by SDS-PAGE (lower panels). The proteins were visualized by Coomassie Brilliant Blue staining. EV; *C. glutamicum* K9 biosensor cells harboring pPBEx2 (empty vector). The arrows indicate the position of the processed (signal peptide-less) cutinase-GFP11 (expected size 25.1 kDa). M, marker proteins with Mw indicated in kDa. **(C)** In parallel, culture supernatants were analyzed for cutinase activity and split GFP fluorescence. **(D)** Schematic view of the epPCR mutagenesis range, which spans the Pel^{SP}, the linker region and a substantial portion of the mature N-terminal part of the cutinase gene up to the unique internal *KpnI* restriction site. Positions of amino acids important for cutinase activity are indicated; i.e., the catalytic triad Ser120-Asp175-His188 and the four cysteines involved in disulfide bond formation.

the specific fluorescence values at the end of the cultivation were slightly lower (∼0.03–0.05 AU), which may indicate that the GFP11-tag marginally contributes to increased secretion stress. The secretory production of Pel-cutinase-GFP11 on the other hand did not induce an obvious dose-dependent biosensor response (**Figure 2B**). In fact, even at saturating IPTG concentration (1 mM) the specific fluorescence at the end of the cultivation was only slightly higher than that of cells that were not exposed to IPTG. In accordance with the low fluorescence output of the biosensor cells, only low amounts of cutinase-GFP11 were present in the culture supernatants, which confirms the weak secretion performance of the Pel^{SP} (**Figure 2B**, lower panel).

In parallel, the amounts of extracellular cutinase-GFP11 were quantitatively assessed by measuring the split GFP fluorescence (**Figure 2C**). Importantly, for both Pel^{SP} and $NprE^{SP}$ a good

correlation exists between the results from the split GFP assay, the activity assay and the amounts of the secreted cutinase-GFP11 as visualized by SDS-PAGE (*cf.* **Figures 2A–C**). Thus, the split GFP assay is capable of quantification of the extracellular cutinase, which is underlined by a linear correlation between the applied amount of cutinase-GFP11 and the resultant split GFP fluorescence (**Supplementary Figure S3**). These results are in excellent agreement with cutinase-GFP11 secretion studies performed in *B. subtilis* (Knapp et al., 2017). In this respect, it is important to note that although the GFP11-tag marginally contributed to secretion stress, the tag did not have a noticeable negative effect on the amount and activity of the secreted cutinase (**Supplementary Figure S2**). However, for cutinase-GFP11 secreted by *B. subtilis* a small inhibitory effect on the lipolytic activity was noted (Knapp et al., 2017). These observations may indicate a more efficient folding of the cutinase-GFP11 in the host *C. glutamicum* after Sec-dependent export across the cytoplasmic membrane. Thus, the split GFP technology was successfully adapted to monitor recombinant protein secretion by *C. glutamicum*.

Construction and Fluorescence-Activated Cell Sorting-Based Screening of Pel^{SP}-Cutinase-GFP11 Mutant Libraries

In a first step, we aimed at improving the cutinase secretion driven by the Pel^{SP}. To identify Pel-cutinase-GFP11 variants that exhibit improved secretion, first a library of Pel-cutinase-GFP11 mutants was generated via error-prone PCR. Mutagenesis was performed on the Pel^{SP} coding region and a sizeable part of the N-terminal domain of the mature cutinase comprising amino acids 2–88 (**Figure 2D**). The signal peptide is crucial for efficient Sec-dependent protein export (Izard and Kendall, 1994; Freudl, 2018) and thus an obvious target for mutagenesis. By mutagenizing also the N-terminal part of the mature cutinase, enzyme variants with improved secretion properties and/or activity may be generated. In this respect, it is important to note that the catalytic triad Ser120-Asp175-His188, and 3 out of 4 cysteines involved in disulfide bond formation, all of which are crucial for cutinase activity, were not subject to mutagenesis (**Figure 2D**).

The Pel-cutinase-GFP11 mutant library was cloned into pPBEx2 and subsequently used to transform *E. coli*. The plasmids were then isolated from approximately $1.8 \cdot 10^5$ colonies and used to transform the *C. glutamicum* K9 biosensor strain. The resulting transformants (Pel^{L1}) were pooled for further analysis. The Pel^{L1} cells were cultivated along with the control strains Pel^{SP}, $NprE^{SP}$ and empty vector (EV) in CGXII medium containing 1% v/v glucose in a BioLector at 30°C and 1,200 rpm at 85% relative humidity. Four hours after inoculation, IPTG (250 μM final concentration) was added to the cultures to induce the secretory production of cutinase-GFP11 and growth was continued overnight. The overnight cultures were then appropriately diluted for FACS analysis. For all FACS experiments, a preselection of cells was performed to exclude cell doublets and cell debris by gating in a dot plot of FSC-H against FSC-W (**Table 1**, gate P2). The resultant gate P2 typically contained ∼93% of the total number of cells ($1.0 \cdot 10^5$) analyzed (**Table 1**).

The biosensor cells expressing Pel-cutinase-GFP11 exhibited a median fluorescence of 477 AU, which was only ∼8% higher than that of the corresponding control cells carrying the empty vector. In contrast, biosensor cells secreting cutinase-GFP11 via the $NprE^{SP}$ exhibited a median fluorescence that was 41% higher than that of the empty vector control cells (624 *vs.* 443 AU, respectively). These results are consistent with the notion that the low-level cutinase secretion facilitated by the Pel^{SP} imposes only minor stress on the cells, whereas the high-level secretion achieved by the $NprE^{SP}$ causes substantial stress to the cells. In comparison to the wild-type (WT) Pel^{SP} cells, the Pel^{L1} cells exhibited a 9% increase in median fluorescence (i.e., 521 *vs.* 477 AU), which indicates an overall increase in secretion stress. The corresponding graphs showing the eYFP fluorescence plotted against the cell size (FSC-H) are shown in **Supplementary Figure S4**.

To select for Pel^{L1} variants potentially exhibiting improved secretion, a sort gate (P3-1) was set to include as many of the highly fluorescent cells as possible, thereby excluding the cells with lower fluorescence. i.e., the less productive cells (**Table 1** and **Supplementary Figure S4**). Sort gate P3-1 contained on average 1128 Pel^{L1} cells, constituting the top 1.2% of the P2 population, while approximately six-fold fewer Pel^{SP} control cells (i.e., 186) fell into this gate (**Table 1**). The selected Pel^{L1} cells exhibited a median fluorescence of 1366 AU, which is 36% higher than that of the Pel^{SP} control cells.

Next, $2.0 \cdot 10^5$ Pel^{L1} cells were sorted from gate P3-1 and collected together in CGXII medium containing 1% (v/v) glucose and 250 μM IPTG. The pooled cells were cultivated in a BioLector until the stationary phase was reached and then analyzed by FACS. Importantly, now more than 12,000 Pel^{L1} cells fell into gate P3-1, indicating successful enrichment (>10-fold) of highly fluorescent cells (median fluorescence of 1327 AU). In addition, a control sorting experiment was carried out by performing enrichment of Pel^{L1} cells that exhibited a near average fluorescence. For this purpose, a gate (P3-M) was set to encompass the center of the P2 population (median fluorescence of 486 AU), thereby excluding the highly fluorescent cells (**Supplementary Figure S4**). Next, $2.0 \cdot 10^5$ Pel^{L1} cells were collected from gate P3-M and cultivated in a BioLector until the stationary phase was reached.

After the enrichment cultivation, individual cells were sorted from both the P3-1 culture and the P3-M control culture. For both cultures, the pre-set gate P3-1 was used to sort single cells onto BHIS-agar plates. After colony outgrowth, 88 clones each were transferred to liquid BHIS medium and cultivated overnight at 30°C and 900 rpm. To demonstrate feasibility of the sorting strategy, assessment of the cutinase secretion was carried out by performing an *in situ* activity assay. For this purpose, aliquots of the respective overnight cultures were spotted on Tween-agar plates containing IPTG to induce cutinase expression. Importantly, a substantially higher number of cutinase producing clones was obtained from

TABLE 1 | Fluorescence-activated cell sorting analysis of *C. glutamicum* K9 biosensor cells carrying the Pel^{L1} mutant library or control plasmids [a,b].

Biosensor cells carrying	Gate P2		Gate P3-1	
	Events	Median fluorescence (AU)	Events (% of P2)	Median fluorescence (AU)
Empty vector (EV)	93,149 ± 194	443 ± 13	139 ± 12 (0.1%)	994 ± 17
NprE-cutinase-GFP11 ($NprE^{SP}$)	92,683 ± 237	624 ± 10	2,326 ± 136 (2.5%)	1,140 ± 7
Pel-cutinase-GFP11 (Pel^{SP})	92,965 ± 80	477 ± 4	186 ± 18 (0.2%)	1,001 ± 6
Mutant library (Pel^{L1})	93,184 ± 353	521 ± 4	1,128 ± 93 (1.2%)	1,366 ± 11
Pel^{L1} after enrichment	93,471	810	12,112 (13%)	1,327

[a] *A detailed graphical depiction of the workflow is shown in* ***Supplementary Figure S1****.*
[b] *$1.0 \cdot 10^5$ cells of each strain were analyzed. In all cases, electronic gating (gate P2) was performed in a dot plot of FSC-H against FSC-W to exclude cell doublets and cell debris. Selection of cells with high median fluorescence was performed by appropriately setting gate P3-1 in a dot plot (****Supplementary Figure S4****), respectively. The number of cells contained within the respective gates, as well as the median fluorescence (AU) of these cells are indicated.*

the highly fluorescent cell population (P3-1) than from the control population (P3-M), i.e., ∼32% *vs.* ∼10%, respectively (**Supplementary Table S4**). The relatively low number of clones producing active cutinase present in both populations indicates that the introduction of mutations by error-prone PCR in most cases is detrimental to the secretory production and/or activity of the cutinase. When a more restrictive sort gate (P3-2) was applied, which typically collects the top 0.3% fluorescent cells (median fluorescence of ∼1800 AU) selectivity was increased to ∼43%. Thus, in all cases, sorting of the highly fluorescent Pel^{L1} cells resulted in an increased selectivity for clones producing enzymatically active cutinase, indicating a successful sorting strategy (**Supplementary Table S4**). A graphical workflow of the cultivation conditions and the FACS-based experiments is shown in **Supplementary Figure S1**.

Analysis of the Secretion Performance of Variants Isolated From the Pel^{SP}-Cutinase-GFP11 Mutant Libraries

The secretion performance of nine clones isolated by FACS from Pel^{L1} was analyzed in more detail. For this purpose, plasmid DNA was isolated from the original clones and then re-introduced in the K9 biosensor strain. The resulting recombinant strains were cultivated along with the control strains EV, Pel^{SP} and $NprE^{SP}$ in a BioLector, using 250 μM IPTG to induce expression. The secretion performance of the different strains was assessed at the end of the cultivation (24 h) by determining the amount and activity of the extracellular cutinase (**Figure 3**).

Notably, in comparison to the control strain in which cutinase-GFP11 secretion is driven by the WT Pel^{SP} (set to 100%), all nine isolated Pel^{L1} variants (V1 – V9) showed a substantial improvement of the secretion performance (**Figure 3**). Overall, the different variants showed a 2- to nearly 6-fold increase in split GFP fluorescence, while extracellular cutinase activities were 2- to 5-fold increased (**Figure 3A**). The amounts of extracellular cutinase-GFP11 as determined by SDS-PAGE were consistent with the split GFP fluorescence measurements (*cf*. **Figures 3A,B**, upper panel).

DNA sequence analysis of the plasmids isolated from the respective strains revealed 25 DNA mutations, of which 17 resulted in an amino acid substitution (**Table 2**). As might be expected, all isolated variants carried mutations within in the signal peptide region. Interestingly, several variants showed mutations at identical positions in the signal peptide, i.e., Phe11 in V1, V3, V5, and V9, and Pro16 in V7 and V8 (**Table 2**). These residues may therefore represent potential hotspots for improving the Pel^{SP}-driven cutinase secretion.

To investigate if secretion can be further improved, a second-generation mutant library (Pel^{L2}) was constructed based on one of these hotspot variants. For this purpose, V7 plasmid was selected as the template DNA for error-prone PCR, since it contains only a single DNA mutation that leads to the P16S exchange in the Pel^{SP} (**Table 2**), which increases the secretion performance by more than fourfold (**Figure 3A**). Interestingly, V8, which shows a slightly better secretion performance, contains a similar amino acid exchange at the same position, i.e., P16T, while carrying an additional five silent mutations (**Table 2**). The screening of the Pel^{L2} mutant library was carried out in an identical manner as described above for Pel^{L1}. Three novel variants (V7.1 – V7.3) were obtained that showed a substantial improvement of the secretion performance in comparison to the parental V7 (**Figure 3**). The levels of the secreted cutinase-GFP11 achieved by these variants were similar to those achieved by the initially far superior $NprE^{SP}$ (**Figures 3A,B**, lower panel). DNA sequencing revealed that V7.1 and V7.3 both carry an additional amino acid substitution besides P16S at the identical position in the signal peptide (**Table 2**). The identified mutations G13A and G13S likely contribute to the improved cutinase secretion. In case of V7.2, the additional signal peptide mutation F11I was identified. The fact that 5 of the 12 clones isolated from the mutant libraries carry a F11I/L mutation (**Table 2**), strengthens the notion that these mutations have an important contribution to the increased secretion performance (**Figure 3**).

It is of note that many of the isolated variants in addition to the signal peptide mutations also carry mutations in the cutinase region (**Table 2**), which may affect the cutinase secretion and/or activity. However, most of the isolated variants exhibited a specific activity (cutinase activity per split GFP fluorescence) close to that of the Pel^{SP} control (**Figure 3C**). Noticeable exceptions are V3 and V7.1, which show a substantial increase in specific activity, and V9, which exhibits a substantial decrease in specific activity. DNA sequence analysis identified a single amino acid substitution in the cutinase of each of these variants; A85V

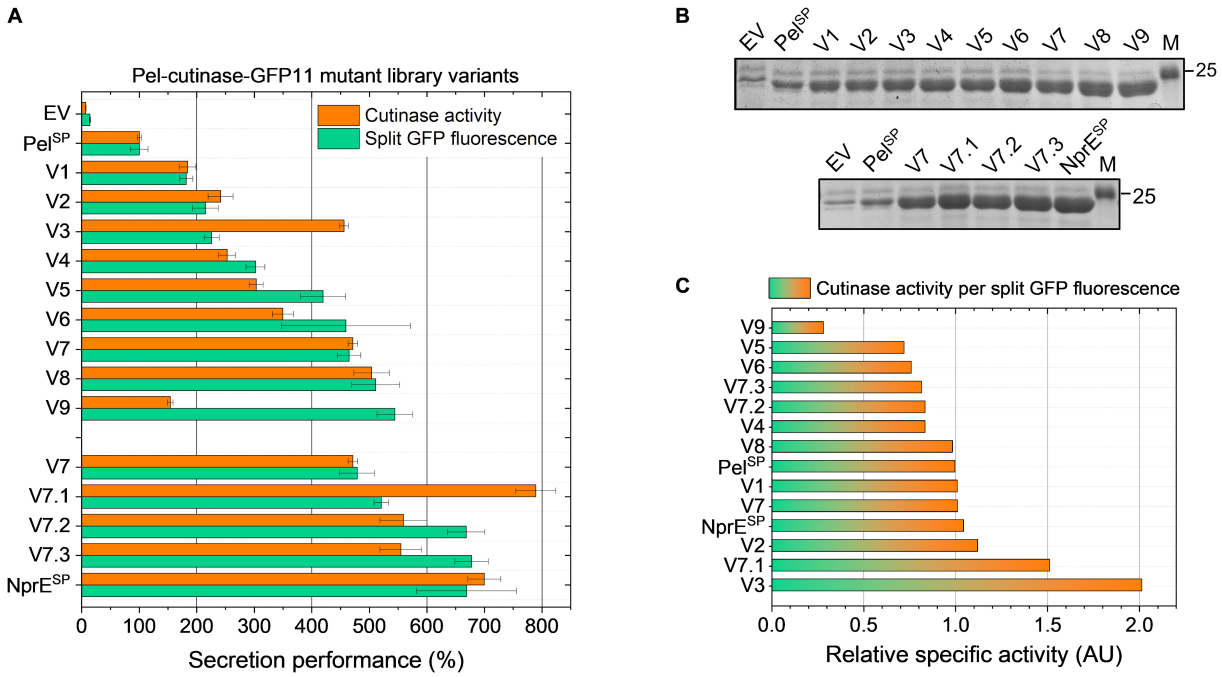

FIGURE 3 | Secretion performance of the variants isolated from the Pel^{SP}-cutinase-GFP11 mutant libraries. Plasmids were isolated from the clones isolated after FACS-based screening of the primary mutant library Pel^{L-1} (V1–V9) and the second-generation library Pel^{L-2} based on V7 (V7.1–V7.3) and then re-introduced in the *C. glutamicum* K9 biosensor strain. The recombinant strains were grown in CGXII medium containing 1% (v/v) glucose in a BioLector for 24 h at 30°C, 1,200 rpm and 85% relative humidity along with the control strains harboring pPBEx2 (EV), pPBEx2-NprE-cutinase-GFP11 (NprE^{SP}) or pPBEx2-Pel-cutinase-GFP11 (Pel^{SP}). Four hours after inoculation, IPTG was added (250 μM) to the cultures. At the end of the cultivation (24 h) the amount and activity of the extracellular cutinase-GFP11 was determined by **(A)** split GFP fluorescence and cutinase activity measurements, respectively. The secretion performance is shown relative to that of the wild-type Pel-cutinase-GFP11 (Pel^{SP}), which was set to 100%. **(B)** Complementary SDS-PAGE analysis of the extracellular levels of cutinase-GFP11 (expected size 25.1 kDa). The proteins were visualized by Coomassie Brilliant Blue staining. M, marker proteins with Mw indicated in kDa. **(C)** The relative specific activity for each variant was obtained by dividing the cutinase activity (%) by the split GFP fluorescence (%). The specific activity of the indicated variants relative to Pel^{SP} is shown in ascending order.

TABLE 2 | Overview of the variants obtained after FACS-based screening of the Pel-cutinase-GFP11 mutant libraries (Pel^{L-1} and Pel^{L-2}).

Variant	Pel^{SP} [a,b,c] **^{1}MKK VMLATALFLGLTPA GANA^{21}**	Linker [a] **^{1}AEFA^{4}**	Cutinase [a,b] **^{2}PTSNPAQELEARQLGRTTRDDLINGNSAS^{30} ^{31}CADVIFIYARGSTETGNLGTLGPSIASNLE^{60} ^{61}SAFGKDGVWIQGVGGAYRATLGDNALPR^{88}**
V1	T8S (ACG:*T*CG), F11I (TTT:*ATT*)	–	–
V2	K3T (AAA:*ACA*)	–	–
V3	F11L (TTT:TT*A*)	–	Q8 (CAG:CA*A*), L48 (TTG:CT*G*), A85V (GCT:G*TT*)
V4	T8M (ACG:A*TG*)	–	–
V5	F11L (TTT:TT*A*)	–	A7V (GCT:G*TT*), L15F (CTT:*TTT*), T18A (ACA:*GCA*), Y77F (TAC:T*TC*)
V6	T15I (ACT:A*TT*)	–	I35V (ATC:*GTC*), L81 (CTT:CT*A*))
V7	P16S (CCA:*TCA*)	–	–
V7.1	P16S + G13A (GGA:GCA)	–	T45R (ACG:A*GG*)
V7.2	P16S + F11I (TTT:*ATT*), A21 (GCA:GC*T*)	–	P87 (CCT:CC*G*)
V7.3	P16S + G13S (GGA:*AGT*)	–	P87T (CCT:*ACT*)
V8	T15 (ACT:AC*A*), P16T (CCA:*ACA*)	A4 (GCG:GC*A*)	P6 (CCT:CC*C*), R17 (AGA:CG*A*), A39 (GCC:GC*A*)
V9	F11I (TTT:*ATT*)	–	G46D (GGC:G*AC*)

[a] *The DNA coding region that was subjected to random mutagenesis included the Pel^{SP}, the small linker, and a sizeable part of the cutinase (amino acids 2–88); the corresponding amino acids of the respective parts of the wild-type fusion protein are indicated. The altered DNA triplets and the corresponding amino acid changes of the isolated variants are indicated.*
[b] *Key amino acids that were exchanged by site directed mutagenesis are indicated in bold and underlined.*
[c] *The putative h-region of the Pel^{SP} is indicated by a gray box.*

in V3, T45R in V7.1 and G46D in V9 (**Table 2**). It is reasonable to assume that these mutations are primarily responsible for the observed effects on the enzyme activity.

Impact of the Different Pel^{SP} Mutations on the Secretion Performance

The increased cutinase secretion of several of the obtained variants can be attributed to single amino acid substitutions within the Pel^{SP}, as is for instance the case for V2, V4 and V7, which carry K3T, T8M or P16S, respectively (**Table 2** and **Figure 3**). On the other hand, most isolated variants carry multiple DNA mutations within both the Pel^{SP} and the cutinase region (**Table 2**). In such cases, it is unclear what the contributions of the individual mutations are to the secretion performance. Moreover, in several variants silent mutations were identified. Although silent mutations do not alter the amino acid sequence of a protein, they can alter the mRNA folding/stability or influence the translation velocity, thus influencing the amount of protein that is produced (Brule and Grayhack, 2017) and subsequently secreted.

Based on the mutations found in the different variants (**Table 2**), potential beneficial mutations with a focus on the Pel^{SP} hotspot residues Phe11 and Pro16, were further evaluated. For this purpose, individual amino acid exchanges were introduced via site-directed mutagenesis at the designated positions into the WT Pel^{SP}-cutinase-GFP11 gene. In addition, combinatorial mutants were created with the aim to improve secretion. First, the secretion performance of the Pel^{SP} single mutants F11I, F11L, P16S (V7) and P16T was investigated (**Figure 4A**). Notably, the sole introduction of the F11L mutation resulted in a ∼2-fold improved secretion performance, whereas the amino acid exchanges F11I, P16S, and P16T each resulted in ∼4-fold increase in secretion performance (**Figure 4A**). Interestingly, by combining these beneficial mutations, variants were obtained that showed a further improvement of secretion. In comparison to the Pel^{SP} control, the Pel^{SP} variants F11L/P16S, F11I/P16T and F11I/P16S showed a 5- to 6-fold increase in secretion performance. Moreover, the secretion performance of F11I/P16S equaled that of the NprE^{SP}, which so far had proven to be a superior signal peptide for cutinase secretion in *C. glutamicum*. Thus, the replacement of only two amino acids was sufficient to convert the poor-performing Pel^{SP} into an excellent signal peptide for cutinase secretion. In an attempt to further improve secretion, two triple mutants were created. For this purpose, the G13A mutation as found in V7.1 (**Table 2**) was combined with the double mutations F11I/P16S and F11L/P16S. However, the corresponding triple mutants did however not show a significant further improvement of the secretion performance (**Figure 4A**).

The increase in the secretion performance as noted for the different Pel^{SP} variants is accompanied by an increase in the fluorescence output of the corresponding biosensor cells in all cases, indicating an increased secretion stress (**Figure 4B**). Although there is a general dose-dependent response of the specific fluorescence of the reporter strain with respect to the amounts (and activity) of the secreted cutinase, this correlation is not absolute. For instance, the biosensor fluorescence response was unable to resolve the secretion performance of the single mutants P16S/T and their derived multiple mutants that showed a better secretion performance (**Figures 4A,B**). It is important to note that the biosensor as such responds to the extent of stress associated with Sec-dependent protein export and not to the correctly folded, biologically active forms of the secreted target protein (Jurischka et al., 2020; **Figure 1**). In this respect, the introduction of the different mutations in the Pel^{SP} may have different effects on the secretion performance. The introduced mutation(s) may not only affect the number of cutinase molecules exported, by for instance altering the protein synthesis or the efficiency of export, but also the quality of the exported protein may be affected, e.g., by influencing the processing or the folding (before or after translocation). It can be envisaged that in cases where the folding is compromised, a larger proportion of incorrectly folded molecules will accumulate/aggregate in the periplasm, which triggers an increased secretion stress response (biosensor fluorescence). In cases where misfolding starts to compete with productive folding, less molecules are available for secretion, resulting in an increased biosensor fluorescence and a reduced secretion efficiency.

The hydrophobic properties of signal peptides are known to be particularly critical to the translocation process (Izard and Kendall, 1994; Freudl, 2018) and perturbations of the hydrophobic core by for instance the introduction of a charged or polar amino acid can decrease or even completely inhibit protein export (Chou and Kendall, 1990; Goldstein et al., 1991). Moreover, a minimal length and a minimum hydrophobic density of the h-region are essential for efficient protein translocation (Ryan et al., 1993; Wang et al., 2000; Duffy et al., 2010). In this regard, the Pel^{SP} (21 residues) is one of the shortest Sec signal peptides identified in *B. subtilis* (Brockmeier et al., 2006) and most of the amino acid mutations identified in the improved Pel^{SP} variants are located within the h-region (**Table 2**) and lead to an overall increase in the signal peptide hydrophobicity. The hydrophobicity profiles of the Pel^{SP} and several of its derived mutants are shown in **Figure 4C**.

The exchange of F11, which is at the center of the h-region, by the much more hydrophobic leucine or isoleucine results in a substantial increase in the overall hydrophobicity of the signal peptide (**Figure 4C**, left panel). As expected, the increase is highest for isoleucine, which is more hydrophobic. The increase in hydrophobicity of the signal peptide appears to be related to the secretion performance; showing a ∼2-fold and ∼4-fold improvement for F11L and F11I, respectively (*cf.* **Figures 4A,C**, left panel). Replacement of the hydrophilic Pro16 by the less hydrophilic serine or threonine also results in a small increase in signal peptide hydrophobicity (**Figure 4C**, left panel). In addition, the steric properties of proline also need consideration. Proline and glycine are helix breaker residues (Yaron and Naider, 1993) and substitution of Pro16 possibly eliminates a perturbation of the α-helical backbone conformation of the signal peptide, which in turn might alter the interaction of the signal peptide with (components of) the Sec-translocon. We speculate that the possible hydrophobic and steric effects associated with the P16S/T substitution contribute to the ∼4-fold improved

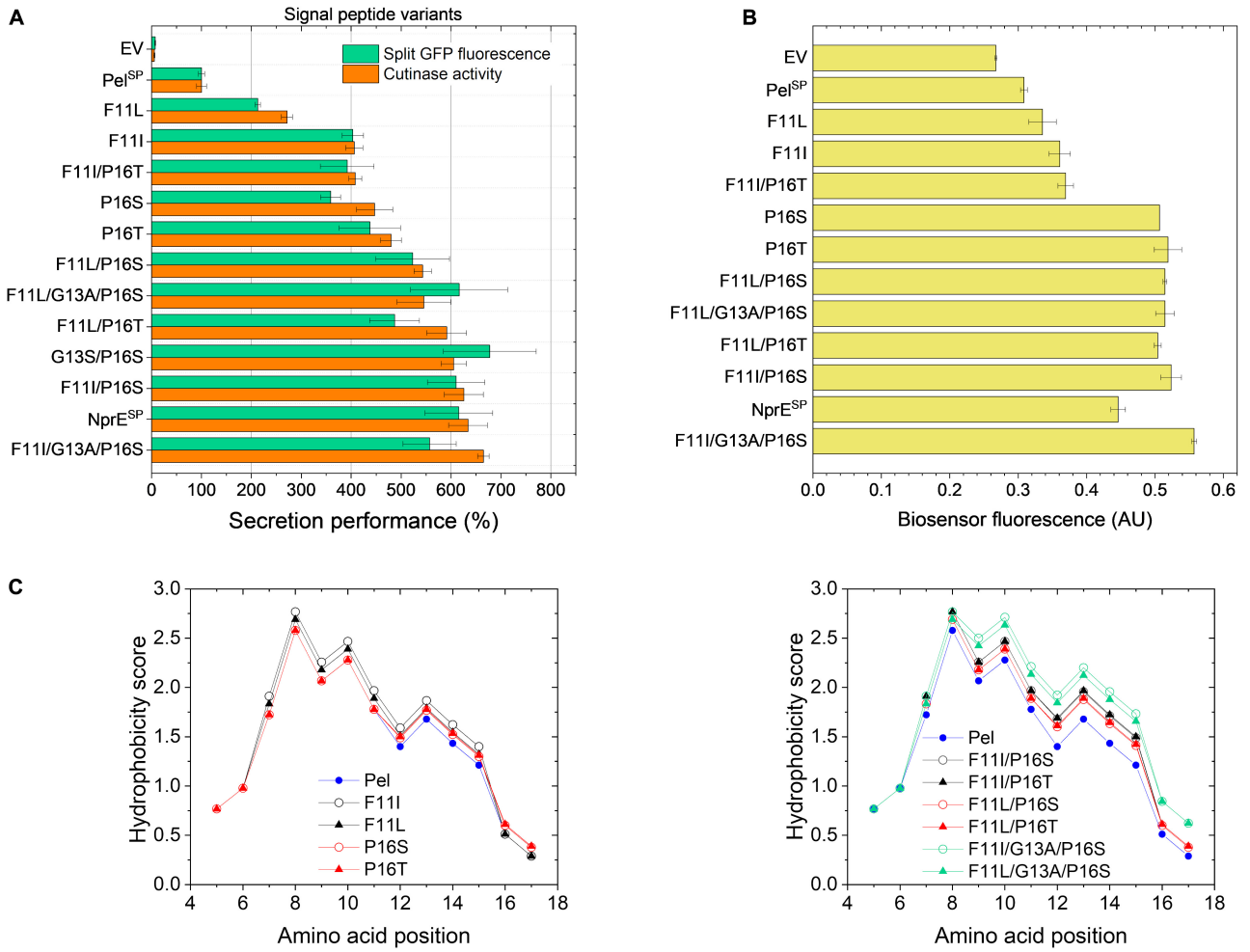

FIGURE 4 | Secretion performance and hydrophobicity of Pel^{SP} variants created by site-directed mutagenesis. *C. glutamicum* K9 biosensor cells were transformed with pPBEx2-Pel-cutinase-GFP11 mutant plasmid encoding the different Pel^{SP} variants as indicated. The recombinant strains were grown in CGXII medium containing 1% (v/v) glucose in a BioLector for 24 h at 30°C, 1,200 rpm and 85% relative humidity, along with the control strains harboring pPBEx2 (EV), pPBEx2-NprE-cutinase-GFP11 (NprE^{SP}) and pPBEx2-Pel-cutinase-GFP11 (Pel^{SP}). Four hours after inoculation, IPTG was added to the cultures to a final concentration of 250 μM. **(A)** At the end of the cultivation (24 h), the secretion performance was assessed by measuring the split GFP fluorescence (green bars) and the cutinase activity (orange bars), respectively. The secretion performance of the different variants is shown relative to that of the Pel^{SP} control (100%) and is ranked according to the cutinase activity in ascending order. **(B)** The corresponding specific fluorescence at the end of the cultivation of the biosensor cells expressing the different variants is indicated. **(C)** Hydropathy plots showing the influence of the introduced single (left panel) and multiple mutations (right panel) as indicated on the overall hydrophobicity of the Pel^{SP}. The data were obtained by ProtScale (https://web.expasy.org) and using the hydropathy scale according to Kyte and Doolittle (1982).

secretion performance. Interestingly, for the *E. coli* outer-membrane protein PhoE it has been shown that removal of a helix breaker residue (i.e., Gly^{-10}) in the h-region affected the targeting pathway, i.e., induced a switch from the post-translational (SecB-dependent) to a co-translational (SRP-dependent) export mode (Adams et al., 2002). At present, it remains unknown via which pathway(s) the cutinase is translocated across the cytoplasmic membrane of *C. glutamicum*.

In comparison to the signal peptide variants carrying the single mutations, their derived double mutants, as expected, all show a further increase in the overall hydrophobicity (**Figure 4C**, *cf.* left and right panel). For the double mutants F11I/P16S, F11L/P16S and F11L/P16T the increased hydrophobicity appears to correlate with a further increase in secretion performance, suggesting additive effects of the respective mutations. The double mutant F11I/P16T presents, however, an interesting exception. Combining the individual beneficial mutations F11I and P16T did not lead to an improvement of secretion (**Figure 4A**). In fact, the secretion performance of F11I/P16T was slightly lower than that of P16T, suggesting possible antagonistic effects of these combined mutations. The introduction of the G13A mutation in the well-secreted double mutants F11I/P16S and F11L/P16S also did not lead to a significant improvement of the secretion performance, even though the signal peptide hydrophobicity was strongly increased (**Figure 4**).

For improving recombinant protein secretion, there clearly is more to it than simply increasing the total hydrophobicity of the h-region of the signal peptide. On a protein level, the overall amino acid composition of the h-region, with different types of conformations and different degrees of side-chain hydrophobicity may contribute as well to efficient protein secretion (Izard and Kendall, 1994). Moreover, it can be envisaged that a too tight binding of the signal peptide to (one of) the Sec components might be disadvantageous in an export system that relies on a transient recognition by multiple interacting protein partners (Izard and Kendall, 1994). In addition, the various DNA mutations that were introduced for amino acid replacement can result in different mRNA transcripts that may have an altered structure and/or stability, which in turn may influence the amount of protein that is synthesized (Brule and Grayhack, 2017) and secreted.

Secretion Performance of Selected Pel^{SP} Variants in Fed-Batch Cultivations

While batch cultivation processes are predominantly used during the screening phase for novel strains or variants, fed-batch processes are state of the art for bioprocess development. However, batch conditions for screening can be error-prone, since variants with superior batch performance might underperform under fed-batch cultivation conditions in later stages (Hemmerich et al., 2019). Hence, fed-batch cultivations with selected Pel^{SP} variants were performed using micro-scale fed-batch cultivations. The obtained final data for the cutinase activity and the split GFP fluorescence measurements are shown in **Figure 5**. For comparability, the data were normalized with respect to the Pel^{SP} data. The standard error for the fed-batch data showed good reproducibility for all variants.

Importantly, the relative secretion performances of the different signal peptides under fed-batch conditions are in good agreement with those observed in batch cultivations (*cf.* **Figures 4A**, **5**). Also in fed-batch, the NprE^{SP} clearly outperforms the Pel^{SP}, showing a ∼450% higher secretion. In standard batch cultivations (250 μM IPTG/pPBEx2-based expression) the protein concentration of the extracellular cutinase-GFP11 achieved with the NprE signal peptide, as based on the split GFP fluorescence, was ∼0.5 mg/mL. For the more productive fed-batch cultivations, this would translate into a protein concentration of ∼1.5 mg/mL, which is amongst the highest concentrations reported for heterologous proteins secreted by *C. glutamicum*; i.e., endoxylanase XynA: 1.07 g/L, camelid antibody fragment (VHH): 1.57 g/L and Phospholipase C: 5.5 g/L (Ravasi et al., 2015; Yim et al., 2016).

Regarding the cutinase activities, the secretion ranking of the different signal peptides followed the order Pel^{SP} < F11I < P16S < F11I/P16S < NprE^{SP} < F11I/G13A/P16S. This confirms the observed additive effects of the Pel^{SP} mutations in the batch cultivations, although the performance of the F11I/P16S variant in batch cultivations was more similar to that of the NprE^{SP}. Importantly, the highest activity of ∼13,000 U/L in fed-batch cultivations was achieved with the Pel^{SP} variant F11I/G13A/P16S. The cutinase activity for this variant was substantially higher than that achieved with the related F11I/P16S, whereas, interestingly, the corresponding split GFP fluorescence was substantially lower. A similar effect was noted in batch cultivations, albeit less pronounced (**Figure 4A**). Apparently, the cutinase secreted via the Pel^{SP} variant F11I/G13A/P16S possesses a higher specific activity (cutinase activity per split GFP fluorescence) than the cutinase secreted via variant F11I/P16S. Moreover, the Pel^{L2} variant V7.1, which carries the same G13A/P16S mutations (**Table 2**), also showed an increased specific activity (**Figures 3A,C**). These results may indicate that amino acid mutations in the signal peptide can affect the "quality" of the exported target protein, e.g., by influencing the signal peptide processing and/or the folding after translocation.

The successful transfer of the optimized signal peptide variants from batch to fed-batch cultivation demonstrates that the signal peptide screening approach with the protein secretion biosensor strain can deliver high performing strains not only under batch screening, but also under fed-batch conditions relevant for further development stages.

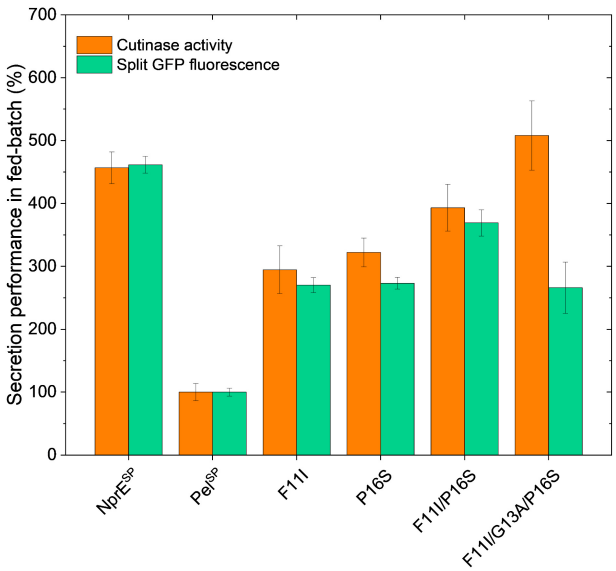

FIGURE 5 | Fed-batch of *C. glutamicum* K9 biosensor cells harboring different recombinant plasmids for secretory production of cutinase-GFP11. Biosensor cells carrying pPBEx2-NprE-cutinase-GFP11 (NprE^{SP}), pPBEx2-Pel-cutinase-GFP11 (Pel^{SP}) or the Pel^{SP} variants F11I, P16S, F11I/P16S or F11I/G13A/P16S were cultivated in a BioLector Pro at 30°C, 1,400 rpm, ≥30% headspace oxygen and ≥85% relative humidity. For the fed-batch process, CGXII medium with an initial glucose concentration of 5 g/L was inoculated to an OD_{600} of 0.5 from the respective precultures. After 10 h, glucose was fed with a constant rate of 5.22 μL/h (equals 2.09 mg/h glucose). Regulation of pH to a set point of 6.8 was performed with 3 M KOH and was initiated 1 h after the start of the cultivation. Corresponding biomass and pH profiles are shown in **Supplementary Figure S5**. After 8 h of growth, cutinase-GFP11 expression was induced by the addition of IPTG (250 μM final concentration at the time of induction) and growth was continued for ∼17 h. At the end of the cultivation, the amount and activity of the secreted cutinase-GFP11 were determined by split GFP fluorescence and cutinase activity measurements, respectively.

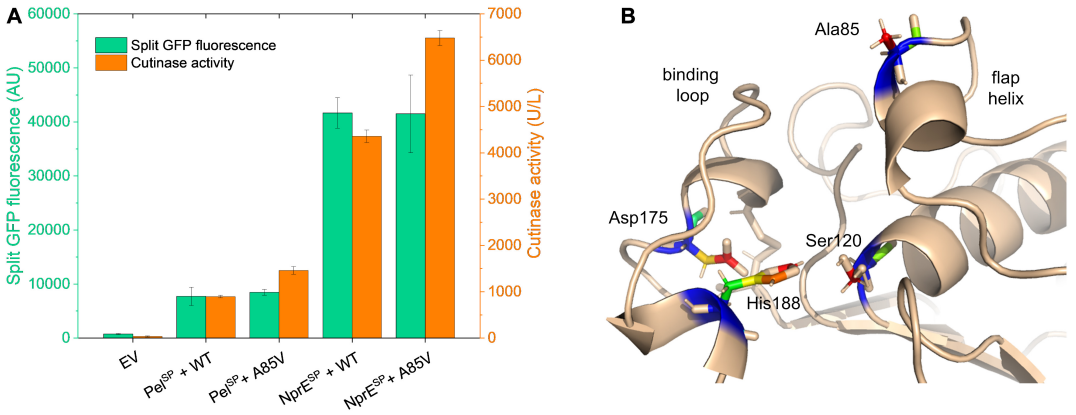

FIGURE 6 | Influence of the mutation A85V on the cutinase secretion and activity. **(A)** *C. glutamicum* K9 biosensor cells were transformed with pPBEx2-Pel-cutinase-GFP11 or pPBEx2-NprE-cutinase-GFP11 plasmid harboring either wild-type (WT) or A85V cutinase, as indicated. Biosensor cells carrying pPBEx2 (EV) served as control. The recombinant strains were grown in CGXII medium containing 1% (v/v) glucose in a BioLector for 24 h at 30°C, 1,200 rpm and 85% relative humidity. Four hours after inoculation, IPTG was added to the cultures to a final concentration of 250 μM. At the end of the cultivation (24 h), the secretion performance was assessed by measuring the split GFP fluorescence (green bars) and the cutinase activity (orange bars), respectively. **(B)** 3D-representation of the X-ray structure of *Fusarium solani pisi* cutinase (PDB: 1CEX) showing the catalytic triad Ser120-Asp175-His188 and the binding loop, which are essential for cutinase activity. The cutinase mutation A85V, which increases the enzyme activity toward *p*NPP, maps to the flap helix, which lines up with the substrate-binding pocket.

Impact of the A85V Mutation on the Cutinase Secretion and Activity

Having successfully identified several mutations in the Pel^{SP} that enhance cutinase secretion, next, the impact of potential beneficial mutations in the mature cutinase part was investigated in more detail. For this purpose, we focused on the variant V3, which exhibits the highest specific activity (**Figure 3C**). V3 carries the F11L mutation in the signal peptide, as well as two silent mutations and the A85V exchange in the cutinase (**Table 2**). It is reasonable to assume that the increased specific activity of V3 is primarily due to the A85V mutation, but contributions of the F11L or the silent mutations cannot be excluded. Therefore, a cutinase variant harboring solely the A85V mutation was created. To facilitate secretion in batch cultivations, both the WT Pel^{SP} and NprE^{SP} were used. The secretion performance of the A85V variant is shown in comparison to that of the WT cutinase (**Figure 6A**). Notably, independent of the signal peptide used, the introduction of the A85V mutation did not significantly affect the amount of the secreted cutinase, whereas the activity of the mutant enzyme in the culture supernatant was substantially increased (**Figure 6A**). The observed increase in cutinase activity was ∼60% in case of Pel^{SP} and ∼50% in case of NprE^{SP}, achieving ∼1,450 U/L and ∼6,400 U/L, respectively.

It is important to note that Ala85 lies within the substrate binding region of the enzyme, which is formed by the amino acids 40–52, 73–91, and 171–191 (Egmond and de Vlieg, 2000; Chen et al., 2013). Ala85 is part of the small flap helix (residues 81–85), which is located near the entrance of the substrate binding pocket (**Figure 6B**). Mutational analysis of cutinase from *F. solani pisi* has shown that replacement of Ala85 by a phenylalanine (or tryptophan) leads to an increase in enzyme activity on olive oil emulsions (Egmond and de Vlieg, 2000). A similar effect was observed for the cutinase CUTAB1 from *Alternaria brassicicola*. Here, replacement of the homologous Ala84 by a phenylalanine resulted in an increase in the activity of the enzyme towards longer chain substrates like *p*NPP (Koschorreck et al., 2010). It is suggested that the more hydrophobic phenylalanine in the helical flap increases the interactions with longer chain, hydrophobic substrates such as olive oil emulsions and *p*NPP (Egmond and de Vlieg, 2000; Koschorreck et al., 2010). We propose that the A85V mutation has a similar stimulatory effect on the enzyme activity of *F. solani pisi* cutinase. Although the A85V mutation did not alter the amount of the secreted cutinase, secretion of the A85V cutinase is accompanied by an increased secretion stress (**Supplementary Figure S6**). These results may indicate that the A85V mutation influences the folding of the enzyme after its translocation across the cytoplasmic membrane.

Secretion Performance of Variants Obtained From an NprE^{SP}-Cutinase-GFP11 Mutant Library

Finally, using the established biosensor-based approach, it was investigated whether the high-level cutinase secretion facilitated by the potent NprE^{SP} can be improved as well. First, an NprE^{SP} mutant library was created (in the same manner as described for Pel^{SP}) that was subsequently expressed in the *C. glutamicum* K9 biosensor strain and then screened by FACS. Initial experiments revealed two promising clones that showed a substantial increase in the cutinase secretion. The plasmids were isolated from these original clones and then re-introduced in the K9 biosensor strain. The secretion performance of the resulting recombinant strains is shown in comparison to the NprE^{SP} control (**Figure 7**). Notably, the two obtained NprE^{SP} variants showed a significant increase in the secretion performance (**Figure 7A**), which is reflected by a substantial increase in biosensor fluorescence (**Figure 7B**). The secretion performance of the two variants was very similar;

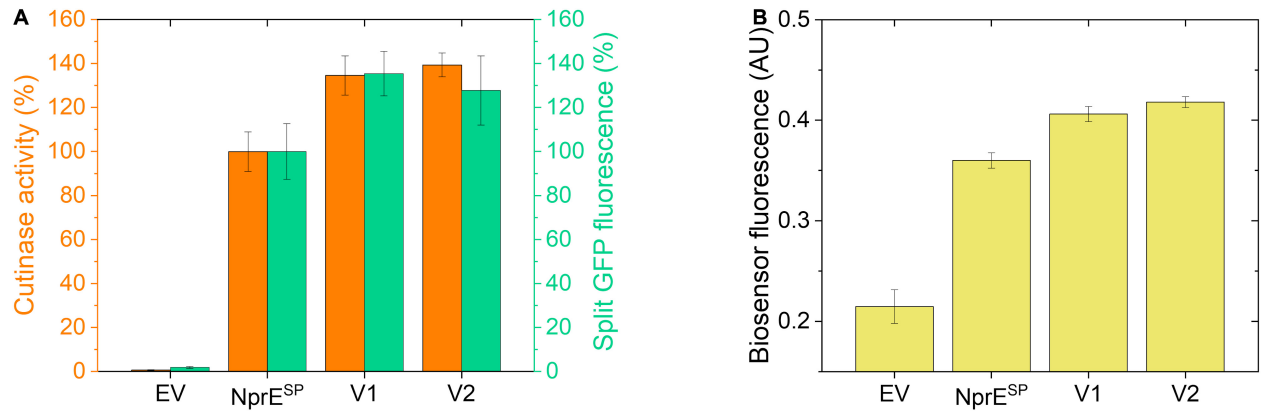

FIGURE 7 | Secretion performance of two variants obtained from the $NprE^{SP}$-cutinase-GFP11 mutant library. Random mutagenesis of pPBEx2-NprE-cutinase-GFP11 and subsequent FACS analysis and screening of biosensor cells expressing the mutant library was performed as described for the Pel^{SP}-cutinase-GFP11 mutant libraries. Plasmids were isolated from promising clones and then re-introduced in the *C. glutamicum* K9 biosensor strain. The recombinant strains were grown in CGXII medium containing 1% (v/v) glucose in a BioLector for 24 h at 30°C, 1,200 rpm and 85% relative humidity along with the control strains harboring pPBEx2 (EV) or pPBEx2-NprE-cutinase-GFP11 ($NprE^{SP}$). Four hours after inoculation, IPTG was added to the cultures to a final concentration of 250 μM. **(A)** At the end of the cultivation (24 h) the amount and activity of the extracellular cutinase-GFP11 was determined by split GFP fluorescence (green bars) and cutinase activity measurements (orange bars), respectively. **(B)** The specific fluorescence of the corresponding biosensor cells at the end of the cultivation (24 h) is indicated.

showing an approximate 35% increase in both the amount and activity of the extracellular cutinase (**Figure 7A**). DNA sequence analysis revealed that both variants carry the hydrophobic substitution S21I within the h-region of the signal peptide, whereas V2 in addition carries a silent mutation in the cutinase. These results highlight once more the importance of the signal peptide hydrophobicity in governing efficient protein secretion. The optimized variants $NprE^{SP}$-S21I and Pel^{SP}-F11I/G13A/P16S in comparison to their WT counterparts improved the secretory production of the cutinase from ∼4,000 to ∼5,500 U/L and from ∼700 to ∼4,100 U/L, respectively. These results may indicate that a well-performing signal peptide may have less room for improvement in comparison to a bad-performing signal peptide. Nevertheless, it was possible to substantially improve the secretion of the cutinase even when the excellent $NprE^{SP}$ was used as a starting point for mutagenesis, which indicates that the maximum secretion capacity of *C. glutamicum* for cutinase had not been reached.

CONCLUSION

In this study, we have successfully combined the previously developed K9 reporter strain (Jurischka et al., 2020) with the split GFP technology (Cabantous et al., 2005; Cabantous and Waldo, 2006; Knapp et al., 2017) to monitor cutinase secretion in *C. glutamicum* by means of fluorescence. Both fluorescence-based approaches allow the monitoring of Sec-dependent secretion of cutinase-GFP11 in a dose-dependent manner, independent of the usage of a direct activity assay for the target protein. The screening of the different mutant libraries using the fluorescent reporter strain in combination with high-throughput FACS proved to be a successful approach for the isolation of clones exhibiting an improved secretion performance, enabling the optimization of different signal peptides for cutinase secretion. The established biosensor-based approach is a particularly powerful tool for the optimization of an individual signal peptide for secretion, bypassing the need for the screening of large libraries of signal peptides from different Sec substrate proteins. Regarding the optimized signal peptides, it is difficult to determine the exact role of the identified mutations, as they can affect protein secretion on multiple different levels, including mRNA stability/folding, translation velocity, protein targeting and translocation as well as processing and folding. Nevertheless, many of the improved variants carry mutations in the h-region that increase the overall hydrophobicity of the signal peptide, indicating the general importance of the signal peptide hydrophobicity in governing efficient protein secretion. Therefore, targeted mutagenesis of the h-region would be a promising approach for further secretion improvement. Taken together, the biosensor-based approach for protein secretion optimization presented here offers great potential, as it can be applied to any desired signal peptide and target protein.

DATA AVAILABILITY STATEMENT

The original contributions presented in the study are included in the article/**Supplementary Material**, further inquiries can be directed to the corresponding author/s.

AUTHOR CONTRIBUTIONS

PB performed the conceptualization, investigation (implementation of split GFP assay, library construction, and screening), data analysis and visualization, and wrote the manuscript (original draft, review and editing).

PL and AK contributed to the initial study design, provided plasmids and protocols for split GFP establishment, and contributed to the writing of the manuscript. CM performed the fed-batch experiments and contributed to the writing of the manuscript. AB constructed site-directed mutants and performed the cutinase activity measurements. DD-O performed the bacterial transformations and SDS-PAGE. MO, K-EJ, and RF contributed to the study design and the writing of the manuscript (original draft, review and editing). All authors have read and approved the manuscript.

FUNDING

This project was financially supported by the CLIB-Competence Center Biotechnology (CKB) funded by the European Regional Development Fund ERDF (grant numbers 34.EFRE-0300097 and 34.EFRE-0300096).

ACKNOWLEDGMENTS

We thank Alexandra Maibaum for the cloning, expression and purification of His_6_cutinase-GFP11 and are grateful to Michael Bott for his ongoing support.

SUPPLEMENTARY MATERIAL

The Supplementary Material for this article can be found online at: https://www.frontiersin.org/articles/10.3389/fmicb.2021.750150/full#supplementary-material

REFERENCES

Adams, H., Scotti, P. A., De Cock, H., Luirink, J., and Tommassen, J. (2002). The presence of a helix breaker in the hydrophobic core of signal sequences of secretory proteins prevents recognition by the signal-recognition particle in *Escherichia coli*. *Eur. J. Biochem.* 269, 5564–5571. doi: 10.1046/j.1432-1033.2002.03262.x

Andersson, H., and von Heijne, G. (1991). A 30-residue-long "export initiation domain" adjacent to the signal sequence is critical for protein translocation across the inner membrane of *Escherichia coli*. *Proc. Natl. Acad. Sci. U. S. A.* 88, 9751–9754. doi: 10.1073/pnas.88.21.9751

Bakkes, P. J., Ramp, P., Bida, A., Dohmen-Olma, D., Bott, M., and Freudl, R. (2020). Improved pEKEx2-derived expression vectors for tightly controlled production of recombinant proteins in *Corynebacterium glutamicum*. *Plasmid* 112:102540. doi: 10.1016/j.plasmid.2020.102540

Bertani, G. (1951). Studies on lysogenesis. I. The mode of phage liberation by lysogenic *Escherichia coli*. *J. Bacteriol.* 62, 293–300.

Brockmeier, U., Caspers, M., Freudl, R., Jockwer, A., Noll, T., and Eggert, T. (2006). Systematic screening of all signal peptides from *Bacillus subtilis*: a powerful strategy in optimizing heterologous protein secretion in Gram-positive bacteria. *J. Mol. Biol.* 362, 393–402. doi: 10.1016/j.jmb.2006.07.034

Brule, C. E., and Grayhack, E. J. (2017). Synonymous Codons: choose Wisely for Expression. *Trends Genet.* 33, 283–297. doi: 10.1016/j.tig.2017.02.001

Cabantous, S., Terwilliger, T. C., and Waldo, G. S. (2005). Protein tagging and detection with engineered self-assembling fragments of green fluorescent protein. *Nat. Biotechnol.* 23, 102–107. doi: 10.1038/nbt1044

Cabantous, S., and Waldo, G. S. (2006). *In vivo* and *in vitro* protein solubility assays using split GFP. *Nat. Methods* 3, 845–854. doi: 10.1038/nmeth932

Caspers, M., Brockmeier, U., Degering, C., Eggert, T., and Freudl, R. (2010). Improvement of Sec-dependent secretion of a heterologous model protein in *Bacillus subtilis* by saturation mutagenesis of the N-domain of the AmyE signal peptide. *Appl. Microbiol. Biotechnol.* 86, 1877–1885. doi: 10.1007/s00253-009-2405-x

Chen, S., Su, L., Chen, J., and Wu, J. (2013). Cutinase: characteristics, preparation, and application. *Biotechnol. Adv.* 31, 1754–1767. doi: 10.1016/j.biotechadv.2013.09.005

Choi, J. H., and Lee, S. Y. (2004). Secretory and extracellular production of recombinant proteins using *Escherichia coli*. *Appl. Microbiol. Biotechnol.* 64, 625–635. doi: 10.1007/s00253-004-1559-9

Chou, M. M., and Kendall, D. A. (1990). Polymeric sequences reveal a functional interrelationship between hydrophobicity and length of signal peptides. *J. Biol. Chem.* 265, 2873–2880.

Cui, W., Han, L., Suo, F., Liu, Z., Zhou, L., and Zhou, Z. (2018). Exploitation of *Bacillus subtilis* as a robust workhorse for production of heterologous proteins and beyond. *World J. Microbiol. Biotechnol.* 34:145. doi: 10.1007/s11274-018-2531-7

Deana, A., Ehrlich, R., and Reiss, C. (1998). Silent mutations in the *Escherichia coli* ompA leader peptide region strongly affect transcription and translation *in vivo*. *Nucleic Acids Res.* 26, 4778–4782. doi: 10.1093/nar/26.20.4778

Degering, C., Eggert, T., Puls, M., Bongaerts, J., Evers, S., Maurer, K. H., et al. (2010). Optimization of protease secretion in *Bacillus subtilis* and *Bacillus licheniformis* by screening of homologous and heterologous signal peptides. *Appl. Environ. Microbiol.* 76, 6370–6376. doi: 10.1128/AEM.01146-10

Duffy, J., Patham, B., and Mensa-Wilmot, K. (2010). Discovery of functional motifs in h-regions of trypanosome signal sequences. *Biochem. J.* 426, 135–145. doi: 10.1042/BJ20091277

Eggeling, L., and Bott, M. (2005). *Handbook of Corynebacterium glutamicum*. Boca Raton: CRC Press, doi: 10.1201/9781420039696

Egmond, M. R., and de Vlieg, J. (2000). *Fusarium solani pisi* cutinase. *Biochimie* 82, 1015–1021.

Eikmanns, B. J., Thum-Schmitz, N., Eggeling, L., Ludtke, K. U., and Sahm, H. (1994). Nucleotide sequence, expression and transcriptional analysis of the *Corynebacterium glutamicum gltA* gene encoding citrate synthase. *Microbiology* 140, 1817–1828. doi: 10.1099/13500872-140-8-1817

Freudl, R. (2017). Beyond amino acids: use of the *Corynebacterium glutamicum* cell factory for the secretion of heterologous proteins. *J. Biotechnol.* 258, 101–109. doi: 10.1016/j.jbiotec.2017.02.023

Freudl, R. (2018). Signal peptides for recombinant protein secretion in bacterial expression systems. *Microb. Cell Fact.* 17:52. doi: 10.1186/s12934-018-0901-3

Goldstein, J., Lehnhardt, S., and Inouye, M. (1991). *In vivo* effect of asparagine in the hydrophobic region of the signal sequence. *J. Biol. Chem.* 266, 14413–14417.

Green, M. R., and Sambrook, J. (2012). *Molecular Cloning*, 4th Edn. U.S: Cold Spring Harbor Laboratory Press.

Hamed, M. B., Anne, J., Karamanou, S., and Economou, A. (2018). *Streptomyces* protein secretion and its application in biotechnology. *FEMS Microbiol. Lett.* 365:fny250. doi: 10.1093/femsle/fny1250

Hemmerich, J., Moch, M., Jurischka, S., Wiechert, W., Freudl, R., and Oldiges, M. (2019). Combinatorial impact of Sec signal peptides from *Bacillus subtilis* and bioprocess conditions on heterologous cutinase secretion by *Corynebacterium glutamicum*. *Biotechnol. Bioeng.* 116, 644–655. doi: 10.1002/bit.26873

Hemmerich, J., Rohe, P., Kleine, B., Jurischka, S., Wiechert, W., Freudl, R., et al. (2016). Use of a Sec signal peptide library from *Bacillus subtilis* for the optimization of cutinase secretion in *Corynebacterium glutamicum*. *Microb. Cell Fact.* 15:208. doi: 10.1186/s12934-016-0604-6

Izard, J. W., and Kendall, D. A. (1994). Signal peptides: exquisitely designed transport promoters. *Mol. Microbiol.* 13, 765–773. doi: 10.1111/j.1365-2958.1994.tb00469.x

Jurischka, S., Bida, A., Dohmen-Olma, D., Kleine, B., Potzkei, J., Binder, S., et al. (2020). A secretion biosensor for monitoring Sec-dependent protein export in *Corynebacterium glutamicum*. *Microb. Cell Fact.* 19:11. doi: 10.1186/s12934-019-1273-z

Keilhauer, C., Eggeling, L., and Sahm, H. (1993). Isoleucine synthesis in *Corynebacterium glutamicum*: molecular analysis of the *ilvB-ilvN-ilvC* operon. *J. Bacteriol.* 175, 5595–5603. doi: 10.1128/jb.175.17.5595-5603.1993

Kinoshita, S., Udaka, S., and Shimono, M. (1957). Studies on the amino acid fermentation - Part I. production of L-glutamic acid by various microorganisms. *J. Gen. Appl. Mirobiol.* 3, 193–205.

Kleine, B., Chattopadhyay, A., Polen, T., Pinto, D., Mascher, T., Bott, M., et al. (2017). The three-component system EsrISR regulates a cell envelope stress response in *Corynebacterium glutamicum*. *Mol. Microbiol.* 106, 719–741. doi: 10.1111/mmi.13839

Knapp, A., Ripphahn, M., Volkenborn, K., Skoczinski, P., and Jaeger, K. E. (2017). Activity-independent screening of secreted proteins using split GFP. *J. Biotechnol.* 258, 110–116. doi: 10.1016/j.jbiotec.2017.05.024

Koschorreck, K., Liu, D., Kazenwadel, C., Schmid, R. D., and Hauer, B. (2010). Heterologous expression, characterization and site-directed mutagenesis of cutinase CUTAB1 from *Alternaria brassicicola*. *Appl. Microbiol. Biotechnol.* 87, 991–997. doi: 10.1007/s00253-010-2533-3

Kyte, J., and Doolittle, R. F. (1982). A simple method for displaying the hydropathic character of a protein. *J. Mol. Biol.* 157, 105–132. doi: 10.1016/0022-2836(82)90515-0

Laemmli, U. K. (1970). Cleavage of structural proteins during the assembly of the head of bacteriophage T4. *Nature* 227, 680–685. doi: 10.1038/227680a0

Lee, J. Y., Na, Y. A., Kim, E., Lee, H. S., and Kim, P. (2016). The Actinobacterium *Corynebacterium glutamicum*, an Industrial Workhorse. *J. Microbiol. Biotechnol.* 26, 807–822. doi: 10.4014/jmb.1601.01053

Liu, X., Yang, Y., Zhang, W., Sun, Y., Peng, F., Jeffrey, L., et al. (2016). Expression of recombinant protein using *Corynebacterium Glutamicum*: progress, challenges and applications. *Crit. Rev. Biotechnol.* 36, 652–664. doi: 10.3109/07388551.2015.1004519

Meltzer, M., Hasenbein, S., Mamant, N., Merdanovic, M., Poepsel, S., Hauske, P., et al. (2009). Structure, function and regulation of the conserved serine proteases DegP and DegS of *Escherichia coli*. *Res. Microbiol.* 160, 660–666. doi: 10.1016/j.resmic.2009.07.012

Musik, J. E., Zalucki, Y. M., Day, C. J., and Jennings, M. P. (2019). Efficient function of signal peptidase 1 of *Escherichia coli* is partly determined by residues in the mature N-terminus of exported proteins. *Biochim. Biophys. Acta Biomembr.* 1861, 1018–1022. doi: 10.1016/j.bbamem.2019.03.001

Neef, J., Van Dijl, J. M., and Buist, G. (2021). Recombinant protein secretion by *Bacillus subtilis* and *Lactococcus lactis:* pathways, applications, and innovation potential. *Essays Biochem.* 65, 187–195. doi: 10.1042/EBC20200171

Prabudiansyah, I., and Driessen, A. J. M. (2017). The Canonical and Accessory Sec System of Gram-positive Bacteria. *Curr. Top. Microbiol. Immunol.* 404, 45–67. doi: 10.1007/82_2016_9

Quax, W. J. (1997). Merits of secretion of heterologous proteins from industrial microorganisms. *Folia Microbiol.* 42, 99–103. doi: 10.1007/BF02898715

Raivio, T. L., and Silhavy, T. J. (2001). Periplasmic stress and ECF sigma factors. *Annu. Rev. Microbiol.* 55, 591–624. doi: 10.1146/annurev.micro.55.1.591

Rapoport, T. A., Li, L., and Park, E. (2017). Structural and Mechanistic Insights into Protein Translocation. *Annu. Rev. Cell Dev. Biol.* 33, 369–390. doi: 10.1146/annurev-cellbio-100616-060439

Ravasi, P., Braia, M., Eberhardt, F., Elena, C., Cerminati, S., Peiru, S., et al. (2015). High-level production of Bacillus cereus phospholipase C in *Corynebacterium glutamicum*. *J. Biotechnol.* 216, 142–148. doi: 10.1016/j.jbiotec.2015.10.018

Rusch, S. L., and Kendall, D. A. (2007). Interactions that drive Sec-dependent bacterial protein transport. *Biochemistry* 46, 9665–9673. doi: 10.1021/bi7010064

Ryan, P., Robbins, A., Whealy, M., and Enquist, L. W. (1993). Overall signal sequence hydrophobicity determines the *in vivo* translocation efficiency of a herpesvirus glycoprotein. *Virus Genes* 7, 5–21. doi: 10.1007/BF01702345

Saaranen, M. J., and Ruddock, L. W. (2013). Disulfide bond formation in the cytoplasm. *Antioxid. Redox Signal.* 19, 46–53. doi: 10.1089/ars.2012.4868

Vertès, A. A. (2013). *Protein secretion systems of Corynebacterium glutamicum in: corynebacterium glutamicum. Microbiology Monographs, vol. 23*. Berlin, Heidelberg: Springer, doi: 10.1007/978-3-642-29857-8_13

Wang, L., Miller, A., and Kendall, D. A. (2000). Signal peptide determinants of SecA binding and stimulation of ATPase activity. *J. Biol. Chem.* 275, 10154–10159. doi: 10.1074/jbc.275.14.10154

Watanabe, K., Tsuchida, Y., Okibe, N., Teramoto, H., Suzuki, N., Inui, M., et al. (2009). Scanning the *Corynebacterium glutamicum* R genome for high-efficiency secretion signal sequences. *Microbiology* 155, 741–750. doi: 10.1099/mic.0.024075-0

Yaron, A., and Naider, F. (1993). Proline-dependent structural and biological properties of peptides and proteins. *Crit. Rev. Biochem. Mol. Biol.* 28, 31–81. doi: 10.3109/10409239309082572

Yim, S. S., Choi, J. W., Lee, R. J., Lee, Y. J., Lee, S. H., Kim, S. Y., et al. (2016). Development of a new platform for secretory production of recombinant proteins in *Corynebacterium glutamicum*. *Biotechnol. Bioeng.* 113, 163–172. doi: 10.1002/bit.25692

Conflict of Interest: AK is employed by Castrol Germany GmbH.

The remaining authors declare that the research was conducted in the absence of any commercial or financial relationships that could be construed as a potential conflict of interest.

Publisher's Note: All claims expressed in this article are solely those of the authors and do not necessarily represent those of their affiliated organizations, or those of the publisher, the editors and the reviewers. Any product that may be evaluated in this article, or claim that may be made by its manufacturer, is not guaranteed or endorsed by the publisher.

frontiers in Microbiology

ORIGINAL RESEARCH
published: 15 November 2021
doi: 10.3389/fmicb.2021.750206

High-Quality Genome-Scale Reconstruction of *Corynebacterium glutamicum* ATCC 13032

Martina Feierabend[1,2†], *Alina Renz*[1,2†], *Elisabeth Zelle*[3], *Katharina Nöh*[3], *Wolfgang Wiechert*[3,4] and *Andreas Dräger*[1,2*]

[1] Computational Systems Biology of Infections and Antimicrobial-Resistant Pathogens, Institute for Bioinformatics and Medical Informatics (IBMI), University of Tübingen, Tübingen, Germany, [2] Department of Computer Science, University of Tübingen, Tübingen, Germany, [3] Institute of Bio- and Geosciences, IBG-1: Biotechnology, Forschungszentrum Jülich GmbH, Jülich, Germany, [4] Computational Systems Biotechnology (AVT.CSB), RWTH Aachen University, Aachen, Germany

OPEN ACCESS

Edited by:
Yu Wang,
Tianjin Institute of Industrial Biotechnology, Chinese Academy of Sciences (CAS), China

Reviewed by:
Hongwu Ma,
Tianjin Institute of Industrial Biotechnology, Chinese Academy of Sciences (CAS), China
Ilya R. Akberdin,
Biosoft.ru, Russia

***Correspondence:**
Andreas Dräger
andreas.draeger@uni-tuebingen.de

[†]*These authors share first authorship*

Specialty section:
This article was submitted to Microbial Physiology and Metabolism, a section of the journal Frontiers in Microbiology

Received: *30 July 2021*
Accepted: *19 October 2021*
Published: *15 November 2021*

Citation:
Feierabend M, Renz A, Zelle E, Nöh K, Wiechert W and Dräger A (2021) High-Quality Genome-Scale Reconstruction of Corynebacterium glutamicum ATCC 13032. Front. Microbiol. 12:750206. doi: 10.3389/fmicb.2021.750206

Corynebacterium glutamicum belongs to the microbes of enormous biotechnological relevance. In particular, its strain ATCC 13032 is a widely used producer of L-amino acids at an industrial scale. Its apparent robustness also turns it into a favorable platform host for a wide range of further compounds, mainly because of emerging bio-based economies. A deep understanding of the biochemical processes in *C. glutamicum* is essential for a sustainable enhancement of the microbe's productivity. Computational systems biology has the potential to provide a valuable basis for driving metabolic engineering and biotechnological advances, such as increased yields of healthy producer strains based on genome-scale metabolic models (GEMs). Advanced reconstruction pipelines are now available that facilitate the reconstruction of GEMs and support their manual curation. This article presents *i*CGB21FR, an updated and unified GEM of *C. glutamicum* ATCC 13032 with high quality regarding comprehensiveness and data standards, built with the latest modeling techniques and advanced reconstruction pipelines. It comprises 1042 metabolites, 1539 reactions, and 805 genes with detailed annotations and database cross-references. The model validation took place using different media and resulted in realistic growth rate predictions under aerobic and anaerobic conditions. The new GEM produces all canonical amino acids, and its phenotypic predictions are consistent with laboratory data. The *in silico* model proved fruitful in adding knowledge to the metabolism of *C. glutamicum*: *i*CGB21FR still produces L-glutamate with the knock-out of the enzyme pyruvate carboxylase, despite the common belief to be relevant for the amino acid's production. We conclude that integrating high standards into the reconstruction of GEMs facilitates replicating validated knowledge, closing knowledge gaps, and making it a useful basis for metabolic engineering. The model is freely available from BioModels Database under identifier `MODEL2102050001`.

Keywords: *Corynebacterium glutamicum*, genome-scale metabolic model, constraint-based reconstruction, optimization, metabolic engineering, FAIR, flux balance analysis, MEMOTE

1. INTRODUCTION

The strain *Corynebacterium glutamicum* ATCC 13032 is a Gram-positive, facultatively anaerobic soil bacterium, which produces L-glutamate under particular treatments or growth conditions (Kimura, 2005). The annual production of several tons of L-glutamate (Eggeling and Bott, 2005) as well as other metabolically engineered products, such as other amino acids (Eggeling and Bott, 2015; Wendisch et al., 2016), alcohols (Inui et al., 2004a; Niimi et al., 2011; Yamamoto et al., 2013; Jojima et al., 2015), biopolymers (Liu et al., 2007), organic acids (Hüser et al., 2005; Okino et al., 2008; Takeno et al., 2013), terpenoids (Heider et al., 2014; Kang et al., 2014) or diamines (Kind et al., 2010a,b; Schneider and Wendisch, 2010), have turned *C. glutamicum* into a versatile and enormously relevant biotechnological microorganism. Despite an ongoing biotechnological application of *C. glutamicum* and the resulting knowledge on this bacterium for more than 70 years (Vertes et al., 2013), its metabolic potential not yet exhausted. Due to the prominent role of *C. glutamicum* in biotechnology, obtaining a more profound understanding of its physiology and metabolism is highly desirable.

One method of formalizing this knowledge is a genome-scale metabolic network reconstruction. Genome-scale metabolic network reconstructions represent a systematic knowledge base of bibliomic and genomic data of all known metabolic reactions of a specific target organism (Thiele and Palsson, 2010). By creating a mathematical representation of the reconstructed network, the network can be changed into a genome-scale metabolic model (GEM). GEMs enable the qualitative description of the genotype-phenotype relationship and predictions of various phenotypes (Fang et al., 2020).

GEMs can be constructed by mapping the annotated genome sequence with its genes via the encoded proteins to reactions. This step is followed by an intensive curation phase of the computational model and a subsequent analysis phase. Prevalent methods for analyzing GEMs are summarized under the therm constraint-based modeling. The main advantage of these modeling techniques over other approaches, such as dynamic modeling (Dräger et al., 2009), lies in their potential to analyze entire metabolic networks at the scale of all enzymatic capabilities of an organism without the necessity of knowing numerical values of all the kinetic parameters therein. Flux sampling can be used as an unbiased way to characterize the space of stoichiometrically feasible fluxes and solutions (Jadebeck et al., 2020). Flux balance analysis (FBA) is a biased method for steady-state analysis of GEMs. By imposing further physiologically realistic, relevant constraints and a target objective function on the computational model, the network's metabolic flux distributions can be simulated (Fang et al., 2020). Nevertheless, increasing network scale results in an increasingly complex process of reconstructing all cellular properties in the form of a coherent computer model.

In recent years, new tools and automated techniques in systems biology have emerged, such as CarveMe (Machado et al., 2018), ModelPolisher (Römer et al., 2016), MEMOTE (Lieven et al., 2020), or BOFdat (Lachance et al., 2019). These tools support the reconstruction, refinement, and validation of GEMs using Minimal Information Required In the Annotation of Models (MIRIAM) standards (Le Novère et al., 2005). Several GEMs of the *C. glutamicum* have already been published (e.g., Kjeldsen and Nielsen, 2009; Shinfuku et al., 2009, see **Figure 1**). However, these models were curated before the newly developed tools were available. Thus, these new tools were so far not applied to GEMs of *C. glutamicum*. The most recently published GEM of *C. glutamicum* is *i*CW773 (Zhang et al., 2017), which is based on Shinfuku et al. (2009). The model *i*CW773 can produce all canonical amino acids. The production rates of amino acids are generally lower than experimental results (Eggeling and Bott, 2005). Comparing these production rates to those of other published GEMs of *C. glutamicum* is difficult since neither the composition of the complete medium nor the medium used for the *in silico* experiments is reported. Based on the MEMOTE report of *i*CW773, the model seems to lack stochiometric consistency and contains no Systems Biology Ontology (SBO) terms (see below for more information on SBO terms Courtot et al., 2011). It contains 98 orphan and 116 dead-end metabolites. In the respiratory chain, the metabolites ubiquinone and its derivates are used. However, several experimental studies confirmed that the only respiratory quinones in *C. glutamicum* are menaquinone and its derivates (Kanzaki et al., 1974; Collins et al., 1977, 1979; Bott and Niebisch, 2003; Maeda et al., 2020). After conversion to Systems Biology Markup Language (SBML) Level 3 Version 1 (Hucka et al., 2018), *i*CW773 reaches a total MEMOTE score of only 29 % (Lieven et al., 2020, see below for more information on MEMOTE and this score). Newly available tools such as MEMOTE have not yet been applied to reconstruct any previous GEM of *C. glutamicum*. The goal of this model is to fill this application gap. Given its importance as a biotechnological microbe, an updated GEM reflecting the current state of knowledge about *C. glutamicum* and incorporating the scope of newly available tools is indispensable.

In this study, we present an updated GEM of high quality for *C. glutamicum* named *i*CGB21FR. It combines the knowledge about *C. glutamicum* from the previous models *i*KK446 (Kjeldsen and Nielsen, 2009) and *i*EZ482 (Zelle et al., 2015) and extends it by including a broader metabolic coverage than previous models. This GEM was reconstructed using the latest available *in silico* methods and tools and represents a model composed of the most current standards in systems biology. Furthermore, this GEM uses current community standards and follows the best-practice recommendations by Carey et al. (2020). High quality in terms of GEM reconstruction encompasses several aspects, such as a fully annotated GEM in terms of metabolites, reactions, and genes with gene-protein-reaction (GPR) associations. In addition, SBO terms (Courtot et al., 2011) are included in the model. These allow a more fine-grained description of the respective compound. With the aid of the high-quality reconstruction of the GEM, we reproduced experimentally validated findings. This model allows a more accurate *in silico* depiction of the genetic makeup of *C. glutamicum*. The new model *i*CGB21FR contributes to filling knowledge gaps in the metabolism of *C. glutamicum* by providing further information

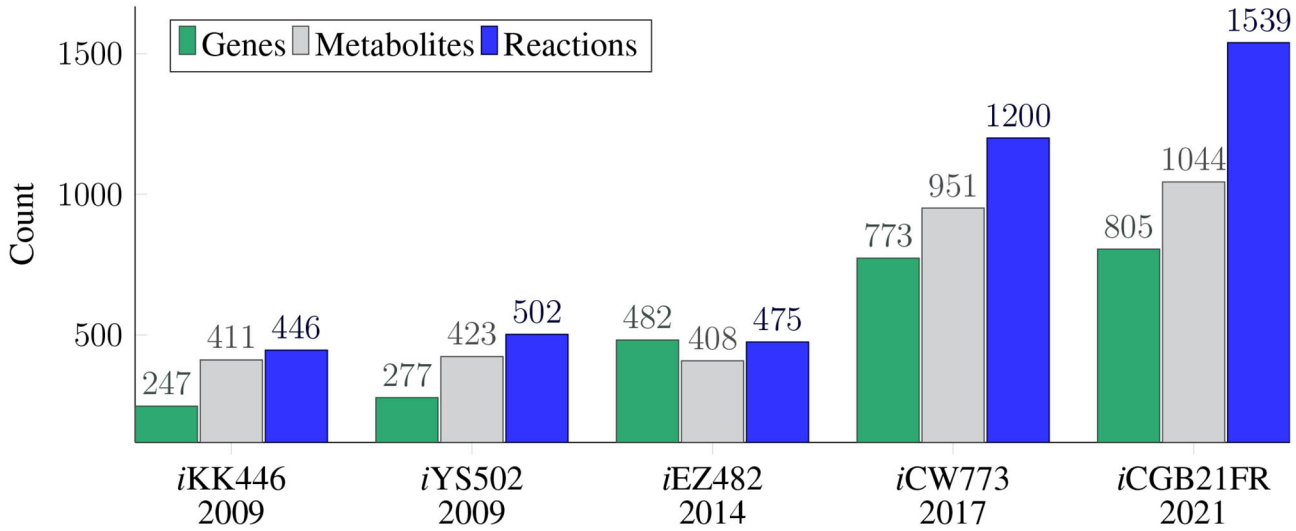

FIGURE 1 | Timeline and model history of all available *C. glutamicum* genome-scale metabolic models. The GEMs are depicted in the chronological order of their publication dates, with *i*KK446 as the first available GEM of *C. glutamicum*. The figure elucidates which GEM is based on which previous GEMs. The upper part of the timeline depicts the number of reactions (blue), metabolites (gray), and genes (green) for each of the five GEMs of *C. glutamicum*. While the number of reactions, metabolites, and genes in the first three GEMs are comparable in their magnitude, the number of metabolites and genes more than doubled in the most recent two GEMs. The number of reactions more than doubled in *i*CW773 (Zhang et al., 2017) and more than tripled in *i*CGB21FR. The model *i*CGB21FR is an updated GEM of *i*EZ482 based on the first published GEM of *C. glutamicum* *i*KK446. The model *i*CW773 is based on the shortly later published GEM *i*YS502.

on relevant pathways used in the production of L-glutamate. Finally, this model uses FAIR data standards (findable, accessible, interoperable, reusable; Wilkinson et al., 2016). Access to all data and metadata used in this model is provided. A highly detailed annotation level within the model is used, and the reconstruction process is described as transparently as possible (Carey et al., 2020).

2. MATERIALS AND METHODS

2.1. The Metabolic Network Reconstruction Process

2.1.1. Strain

The GEM of the strain *Corynebacterium glutamicum* ATCC 13032 was reconstructed using the annotated genome sequence (accession number: `NC006958.1`), which was downloaded from the National Center for Biotechnology Information (NCBI) at https://www.ncbi.nlm.nih.gov (Agarwala et al., 2018).

2.1.2. Draft Reconstruction

The reconstruction process closely followed the protocol by Thiele and Palsson (2010). In short, an automated draft reconstruction was created using CarveMe (Machado et al., 2018), version 1.2.2, and stored in the SBML Level 3 Version 1 format (Hucka et al., 2018). The SBML Level 3 extension for flux balance constraints (fbc) version 2 by Olivier and Bergmann (2018) was enabled and used under default settings for the draft reconstruction. SBML represents a machine-readable exchange format that allows manipulating computational models of biological processes (Keating et al., 2020; Renz et al., 2020). The fbc plugin enables adding structured, semantic descriptions for domain-specific model components such as charges, annotations, flux bounds, GPR rules, or chemical formulas of metabolites (Lieven et al., 2020). This initial draft contained 1496 reactions, 1030 metabolites, and 782 genes in the three compartments: extracellular, cytosol, and the periplasm.

Further automated and manual refinement of the reconstruction of *C. glutamicum* was performed using libSBML (Bornstein et al., 2008), version 5.18.0, and COBRApy (Ebrahim et al., 2013), version 0.17.1. All simulations were run using the CPLEX optimizer, version 12.10 by IBM (https://www.ibm.com/analytics/cplex-optimizer). Metabolic pathways were visualized using the Escher software (King et al., 2015). To support the display as standardized Process Description (PD) map (Rougny et al., 2019) in Systems Biology Graphical Notation (SBGN) enabled software (Touré et al., 2020), the Escher maps were converted to the SBGN Markup Language (SBGNML) format (Bergmann et al., 2020) using EscherConverter (https://github.com/draeger-lab/EscherConverter).

2.1.3. Annotations

Cross-references of the model's instances to other databases were shifted from the notes to the annotations field. Additional metadata, such as annotations and cross-references, was added using the ModelPolisher (Römer et al., 2016). The model's genes were annotated using the old and new locus tags from NCBI and the NCBI protein identifier. SBO terms (Courtot et al., 2011) further annotate the model's instances. SBO terms represent controlled vocabularies, which provide semantic information about model components. For metabolites and genes, the general SBO-terms for simple chemical (`SBO:0000247`) and genes

(SBO:0000243) were used, respectively. The SBO terms for the reactions were chosen as precisely as possible using a new curation pipeline (Fritze, 2020).

2.1.4. Refinement of Metabolite Attributes

The draft was curated to include the correct positioning of the metabolites' chemical formulas and charges. All charges were obtained, if more than one charge per compound was available, in the Biochemically, Genetically, and Genomically structured (BiGG) Models database (Norsigian et al., 2019). In the following verification step, the most appropriate charge for a given reaction in a specific compartment was manually chosen and added to the model. Dead-end metabolites and orphan metabolites were identified and, when appropriate, removed.

2.1.5. Manual Extension

Intensive manual curation was done using the databases BiGG (Norsigian et al., 2019), MetaCyc (Caspi et al., 2020), BioCyc (Karp et al., 2019), Kyoto Encyclopedia of Genes and Genomes (KEGG) (Kanehisa et al., 2019), and new bibliomic data. This draft was then revised using the *i*EZ482 model (Zelle et al., 2015) as a reference. The model *i*EZ482 is an updated version of the *i*KK446 model (Kjeldsen and Nielsen, 2009) and contains 475 reactions, 408 metabolites, and 482 genes. Reactions, metabolites, and genes present in *i*EZ482 but not in *i*CGB21FR were manually checked in MetaCyc (Caspi et al., 2020) or BioCyc (Karp et al., 2019) for their biochemical relevance in the model and, if appropriate, added. Altogether, 50 new reactions, 14 new metabolites, and 23 new genes were added to *i*CGB21FR. BiGG identifiers (IDs) and annotations were included in the model for all newly added compounds, thus enabling easier comparison with other models. If BiGG IDs were not yet existent, BioCyc IDs (Karp et al., 2019) and additional annotations such as SBO terms were added to the new instance.

2.1.6. Mass and Charge Imbalances

The chemical formulas of all participating metabolites were verified. All mass and charge imbalanced reactions were manually checked. Pseudo-reactions, including exchange, sink, or biomass reactions, were excluded from this curation step. For reactions with imbalanced charge, the charge of every participating metabolite was verified and, if necessary, adapted. Mass imbalanced reactions were checked for missing metabolites, such as protons.

2.1.7. Energy-Generating Cycles

Energy-generating cycles represent thermodynamically infeasible states. Charging of energy metabolites without any energy source causes such cycles (Fritzemeier et al., 2017). If left undetected in the model, these can result in erroneous increases in maximal yields in the biomass (Fritzemeier et al., 2017). The following 13 carrier metabolites for energy or redox equivalent were tested for their ability to form thermodynamically infeasible cycles: adenosine triphosphate (ATP), cytidine triphosphate (CTP), guanosine triphosphate (GTP), uridine triphosphate (UTP), inosine triphosphate (ITP), reduced nicotinamide adenine dinucleotide (NADH), reduced nicotinamide adenine dinucleotide phosphate (NADPH), flavin adenine mononucleotide (FMN), flavin adenine dinucleotide (FAD), menaquinol-8, 2-demethylmenaquinol 8, acetyl-CoA, and L-glutamate. All exchange reactions of the model were set to $0\,\mathrm{mmol\,gDW^{-1}\,h^{-1}}$ to investigate the presence of energy-generating cycles. Energy dissipating reactions were created for each of the 13 individual metabolites. These allow the corresponding metabolite to be removed from the system. Each reaction was added one-at-a-time to the model and then used as the objective function. If the optimization returned a result unequal to zero, an energy-generating cycle was detected and subsequently removed. Additionally, the proton exchange between cytosol and periplasm was included.

2.1.8. Biomass Objective Function

The initial biomass objective function (BOF) of *i*CGB21FR was created using CarveMe (Machado et al., 2018). It represents a universal bacterial biomass objective function (BOF). The species-specific biomass objective function (BOF) was further refined using BOFdat (Lachance et al., 2019). BOFdat allows calculating and refining a pseudo-reaction for the biomass function without using any pseudo-metabolites or macromolecules, such as deoxyribonucleic acid (DNA), ribonucleic acid (RNA), or protein. The nucleotide sequence of *C. glutamicum* ATCC 13032 was used to refine the DNA nucleotides in the BOF. Coenzymes and inorganic ions were identified and specifically adapted for *C. glutamicum* in the BOF within the second step of BOFdat. As the model initially did not simulate growth on the minimal medium CGXII (see section 2.2.2), trace elements in the BOF were compared to the elemental composition of *C. glutamicum* cells (Liebl, 2005). Based on this comparison, cobalt was removed from the BOF.

2.1.9. Subsystems and Groups Plugin

Biological pathways were obtained from the KEGG database (Kanehisa et al., 2019) using the old locus tags in the genes' annotations. Pathways associated with a reaction were added to the reaction's annotations based on genes in the GPR association. The pathways were added as a biological qualifier with the attribute OCCURS_IN. Additionally, the groups plugin was enabled, available for SBML Level 3. The groups plugin in libSBML (Bornstein et al., 2008) allows a more flexible grouping of specific connected components in the metabolic model (Hucka and Smith, 2016). The groups plugin was used to add every metabolic pathway or subsystem as a group. Participating reactions were then added to the groups as members.

2.1.10. Quality Control

The quality of the GEM was tested performing a FROG analysis (König, 2020) and using MEMOTE, version 0.11.1. MEMOTE is a platform to test standardized measures of metabolic models and outputs quality scores ranging from 0 % for poor model quality to 100 % for excellent model quality (Lieven et al., 2020). The measures that generate the MEMOTE scores evaluate the model's consistency and annotations within different categories. These categories include basic information about the model, the metabolites and reactions, the degree of annotations for metabolites, reactions, genes, and SBO terms. MEMOTE also

checks the presence of GPRs, a realistic biomass function, energy metabolism, and appropriate network topology. Apart from these individual MEMOTE scores for the different subcategories, MEMOTE also reports an overall score. This overall score represents an overall measurement of how well the model scored within all individual categories. To evaluate the consistency of the model, the stoichiometric consistency, mass and charge balances, metabolite connectivity, and unbounded fluxes in the default medium were used. Within the evaluation of the annotations, MEMOTE checks for the presence and conformity of various databases and the presence of specific SBO terms. All categories are scored individually. The overall MEMOTE quality score is calculated based on the individual category scores (Lieven et al., 2020).

2.1.11. Curation of *i*CW773

The model *i*CW773 (Zhang et al., 2017) was downloaded in Microsoft Excel format as the supplementary published and converted to Character-Separated Value (CSV) format. The application Table2Model (Dräger, 2021) was developed based on JSBML (Rodriguez et al., 2015) to parse the CSV files and convert the information to SBML Level 3 Version 1 (Hucka et al., 2018). Since the original publication did not explicitly define any units, these had to be added to the model. For consistency reasons, the units were defined in the same way as for *i*CGB21FR. The generated SBML Level 3 Version 1 file was syntactically validated using a combination of JSBML (Rodriguez et al., 2015) and libSBML (Bornstein et al., 2008), including unit consistency validation. MEMOTE version 0.11.1 (Lieven et al., 2020) was used for semantic model checking. Annotation of the model *i*CW773 was performed using the same curation pipeline described above with the help of ModelPolisher (Römer et al., 2016) and SBO term addition (Fritze, 2020). The model was wrapped in an (Bergmann et al., 2014) OMEX archive file (Neal et al., 2018) together with a metadata file and uploaded to BioModels Database (Malik-Sheriff et al., 2020), where it is available under accession `MODEL2110010001` (see Availability).

2.2. Model Validation

All model validations were performed with a physiological pH of 7.0. The growth behavior was tested in several media with access to varying carbon sources under aerobic and anaerobic conditions to validate the predictive power of the curated model *i*CGB21FR.

2.2.1. Definition of the Growth Unit

The growth rate is defined as the flux through the biomass objective function, which corresponds to the system's biomass-producing reaction. In their fundamental work from Varma and Palsson (1994) explain that "V_{gro} is the growth flux (grams of biomass produced), which with the basis of 1 g (dry weight) per h reduces to the growth rate (grams of biomass produced per gram [dry weight] per hour)." It should be noted that 1 gDW corresponds to 1 g with a semantic annotation regarding the dry weight fraction of a probe. Gottstein et al. (2016) explain that the metabolic fluxes are typically given in mmol gDW^{-1} h^{-1} and confirm (Varma and Palsson, 1994) that the growth rate μ has the unit g gDW^{-1} h^{-1}. Gottstein et al. (2016) also state that the biomass objective function describes the accumulation of biomass components per hour and relative to the amount of biomass in gDW. Consequently, all molecular species need to be expressed in the unit mmol gDW^{-1}, which corresponds to the amount of the biomass component per gram of biomass (cf. section 2.1; Gottstein et al., 2016). Since all stoichiometric coefficients have dimensionless units, the biomass forming reaction can be considered a summation of components in mmol gDW^{-1}, each times a dimensionless factor. Consequently, the rate of this reaction, which defines a change per time, results in mmol gDW^{-1} h^{-1}.

Accordingly, the SBML specification defines that the units of all reactions in a model have to be identical and are defined in units of *extent* per *time* (see Hucka et al., 2018, section 4.2.5;). According to the specification of SBML Level 3 Version 1 Release 2 (see Hucka et al., 2018, Table 9), the extent units should be substance units or a combination of units derived from those. Here, the extent of the reactions and the substance units of all compounds are defined in units of mmol gDW^{-1} (note that in contrast to Varma and Palsson (1994), we here define the biomass in units of mmol instead of in g). The time units are defined in h (or 3600 s). Hence, all reactions have the unit mmol gDW^{-1} h^{-1}. It should be noted that the upper and lower bounds of all reactions have the same unit and are therefore consistently defined with the flux through the biomass reaction. In this way, these parameters already implicitly define the flux units because the flux's upper and lower bounds must have the same unit as the flux itself.

For more information, readers may also consider the specification of the SBML extension package fbc (Olivier and Bergmann, 2018), which provides similar examples in its appendix, and the detailed analysis on this matter outlined by Gottstein et al. (2016). To improve the units' definition, *i*CGB21FR and *i*CW773 explicitly declare the attributes `extentUnits` and `timeUnits` within the `model` element in their SBML files. It also declares `substanceUnits` in mmol gDW^{-1} and the `volumeUnits` in fl so that all compounds and compartments inherit defined units from the `model` container.

Experimentally observed growth rates μ may be given in the unit 1/h. In this case, directly comparing the calculated growth rate to the experimentally obtained value is possible if the biomass consistency of a GEM approaches 1 mmol gDW^{-1} h^{-1} because then its produced biomass has a molecular weight of 1 g $mmol^{-1}$. With this, the conversion 1 g gDW^{-1} h^{-1} = 1 g g^{-1} h^{-1} = 1 h^{-1} can be performed because the biomass of the GEM is, in this case, *standardized*. A direct comparison of growth rates is then valid, because with a biomass consistency close to 1 mmol gDW^{-1} h^{-1}, the different units of the growth rate μ converge.

2.2.2. Growth in Different Media and Conditions

Following common laboratory practice in cultivating *C. glutamicum*, the complete lysogeny broth (LB) medium (Bertani, 1951) and the two minimal media M9 (Sambrook et al., 1989) and CGXII (Keilhauer et al., 1993; Eggeling and

Bott, 2005) were chosen to simulate *in silico* aerobic growth of *C. glutamicum*. Transporters for the inorganic ions nickel and calcium had to be added to allow growth on the M9 minimal medium. As protocatechuic acid is a component of the CGXII medium (Keilhauer et al., 1993), all necessary exchange and transport reactions were added to model the uptake this compound. The model *i*CGB21FR did initially not grow on the minimal medium CGXII. Literature research pointed toward cobalt in the BOF as a potential issue. Removing cobalt from the BOF allowed growth on CGXII.

D-glucose served as the predominant carbon source in the two minimal media. The composition of each medium was used to constrain the model's exchange reactions with the environment. For simulating growth in the three different media, the lower bounds of the metabolites' exchange reactions available in the respective medium were set to the default value $-10\,\mathrm{mmol\,gDW^{-1}\,h^{-1}}$ to enable the uptake. All other exchange reactions' lower bounds were set to $0\,\mathrm{mmol\,gDW^{-1}\,h^{-1}}$. While applying these medium-specific constraints, the BOF was set as the objective function. If the model did not simulate growth on one of the experimentally confirmed media, literature was queried to identify missing metabolites or reactions hampering growth. These were then added to *i*CGB21FR.

C. glutamicum is a facultative anaerobe microbe (Eggeling and Bott, 2005, 440). The growth under anaerobic conditions was evaluated to demonstrate the validity of *i*CGB21FR. The model initially created with CarveMe (Machado et al., 2018) did not simulate growth when applying anaerobic conditions by blocking the oxygen uptake. The model was evaluated using flux balance analysis (FBA) to identify relevant oxygen-carrying reactions to identify potential reasons for this. Additionally, literature was searched to find alternative or missing reactions. Furthermore, the gap-filling option of CarveMe was used for the M9 minimal medium under anaerobic conditions. To this end, a novel draft model with CarveMe was created, where the gap-filling option was enabled during the curation step. The reaction set of the gap-filled model was compared to our extended *i*CGB21FR model's reaction set, and the missing reactions were added. These six missing reactions include the catalase reaction (`CAT`), the succinate dehydrogenase (`SUCDi`), the phosphoribosylformylglycinamidine synthase (`PRFGS_1`), a different calcium transporter (`CAt4`), the fumarate reductase (`FRD7`), and the glycolate transport via proton symport (`GLYCLTt2rpp`). With the inclusion of these reactions, the model simulated anaerobic growth on all three tested media.

The *C. glutamicum*-specific CGXII minimal medium was used to test the model's growth behavior on different carbon sources. The metabolites glucose, fructose, sucrose, ribose, gluconate, pyruvate, acetate, lactate, and propionate were tested under aerobic and anaerobic conditions as sole carbon sources since experimental data confirmed their role as carbon sources (Michel et al., 2015). All tested compounds could serve as the sole carbon source under aerobic conditions. Under anaerobic conditions, however, only glucose, fructose, sucrose, and ribose could serve as carbon and energy sources (Michel et al., 2015). Therefore, all nine carbon sources were tested *in silico* under aerobic and anaerobic conditions using the CGXII minimal medium. If *i*CGB21FR did not simulate growth on one of the experimentally verified carbon sources, missing exchange and transport reactions were added based on results from a literature search. These included adding a pyruvate exchange and transport reaction and a lactate transporter for the aerobic condition. Further gap-filling steps were performed when necessary.

2.2.3. Verifying Capabilities for Amino Acid Production

The model was further validated by simulating the production of all 20 canonical amino acids in the CGXII medium and D-glucose as the predominant carbon source under aerobic conditions. The availability of D-glucose was restricted to the default uptake rate of $10\,\mathrm{mmol\,gDW^{-1}\,h^{-1}}$. The growth rate was fixed to $0.4\,\mathrm{mmol\,gDW^{-1}\,h^{-1}}$ to ensure the microbe's maintenance during the amino acid production. Subsequently, a sink reaction was created for each amino acid, set as the objective function, and optimized. The relative amino acid production was calculated by dividing the total amino acid production rate by the glucose uptake rate. The same approach was taken for the CO_2 production rate, which was set in relationship to the amino acid production rate. The efflux of the CO_2 exchange reaction (`EX_co2_e`) was taken as the CO_2 production rate. The ATP production rate was calculated by summing up the fluxes of all ATP-producing reactions. These were then correlated with the amino acid production rate, analogously to the CO_2 production rate.

2.3. Model Application: New Insights for Metabolic Engineering

As *C. glutamicum* is widely used in biotechnology, the model's capabilities can be used to yield hints for metabolic engineering. All subsequent analyses were performed using the CGXII minimal medium with D-glucose as the sole carbon source under aerobic conditions.

2.3.1. Relation Between Growth and L-glutamate Production

A sink reaction (`sink_glu__L`) was added to optimize the L-glutamate production (see **Figure 5**). This reaction was then set as the objective function. As L-glutamate is also part of the biomass objective function, a potential association between these two reactions (BOF and L-glutamate sink reaction) was evaluated by varying the BOF between 0 and the maximum growth rate $0.57\,\mathrm{mmol\,gDW^{-1}\,h^{-1}}$ while maximizing the sink reaction. $0.57\,\mathrm{mmol\,gDW^{-1}\,h^{-1}}$ is the maximum *in silico* growth rate of *i*CGB21FR under aerobic growth conditions with D-glucose as the sole carbon source on CGXII (see section 3.2).

2.3.2. Relevance of the pyruvate carboxylase (PC)

PC is a pivotal enzyme in the L-glutamate production in *C. glutamicum* (Peters-Wendisch et al., 2001). A metabolic map was drawn, which depicts the primary reactions relevant for the L-glutamate production starting at D-glucose as the predominant carbon source using the tool Escher (King et al., 2015, see **Figure 5**). The model was optimized for the sink reaction for L-glutamate (`sink_glu__L`) using FBA while fixing the growth

rate to 0.4 mmol gDW^{-1} h^{-1}. This growth rate is an intentionally chosen growth rate within the interval where the L-glutamate production is only marginally affected by growth. The resulting flux distribution is depicted in **Figure 6**. This analysis was repeated after knocking out the PC's reaction to elucidate further the PC's effect on the metabolic flux distribution.

2.3.3. Identification of Relevant Reactions for L-glutamate Production

A loopless flux variability analysis (FVA) was used to identify reactions relevant to L-glutamate production. FVA represents a standard method to evaluate the range of feasible steady-state fluxes for each reaction by sequentially minimizing and maximizing each reaction (Schellenberger et al., 2011). Loop reactions are a subset of reactions with unbounded fluxes. Loopless FVA eliminates thermodynamically infeasible loops by not allowing the model to use these loops (Schellenberger et al., 2011). After running the loopless FVA, reactions with almost identical minimal and maximal allowed flux values were extracted (relative tolerance of 10^{-5}, absolute tolerance of 10^{-8}).

3. RESULTS

3.1. The Model *i*CGB21FR Is of High Quality

The new GEM of *Corynebacterium glutamicum* constructed in this work is named *i*CGB21FR. This name follows the latest recommended naming conventions, which are part of the community standardization of metabolic models (Carey et al., 2020). The lower-case "*i*" in italics means *in silico*, followed by the species indicator "CG" for *C. glutamicum*. "B" represents the city where the particular strain ATCC 13032 was sequenced (Bielefeld, Germany, see also Kalinowski et al., 2003). The three-letter code "CGB" also serves the corresponding strain identifier in the KEGG pathway database (Kanehisa et al., 2019). It follows an iteration identifier, in this case, the year 21 of this century. The last two characters, "FR," refer to the last names of the primary model curators.

The model *i*CGB21FR is available in the SBML Level 3 Version 1 format (Hucka et al., 2019) with the fbc plugin (Olivier and Bergmann, 2018) and the groups plugin (Hucka and Smith, 2016) enabled. It contains 1042 metabolites, 1539 reactions, and 805 genes. Thus, further 42 reactions, 13 metabolites, and 25 genes were added to the model following the initial draft reconstructed with CarveMe (Machado et al., 2018). All metabolites and reactions have a human-readable, descriptive name and a chemical formula. The model comprises the cytosolic, periplasmic, and extracellular compartments.

Its overall MEMOTE score amounts to 87 %. The MEMOTE score of the initial draft model created with CarveMe was 33 %. With intensive manual curation, the number of mass and charge imbalanced reactions could be diminished from an initial 170 to 19 imbalanced reactions. These represent 1.2 % of the total number of reactions. The model has a stoichiometric consistency of 99.7 % and does not contain any energy-generating cycles, dead-end metabolites, nor orphan metabolites.

Seventeen different databases are cross-referenced in the model's instances, yielding a MEMOTE annotation score of 84 % for reactions, 84 % for metabolites, and 49 % for genes. Genes include cross-references to the three databases KEGG (Kanehisa et al., 2019), NCBI genes (Maglott et al., 2005), and NCBI proteins (Pruitt et al., 2005). Metabolites and reaction annotations contain cross-references to 13 and seven different databases, respectively. The databases BiGG (Norsigian et al., 2019), BioCyc (Karp et al., 2019), KEGG (Kanehisa et al., 2019), MetaNetX (Moretti et al., 2021), Reactome (Croft et al., 2010), and ModelSEED (Henry et al., 2010) are referenced for metabolites and reactions. Reactions also have cross-references to the RHEA database (Lombardot et al., 2019) and EC numbers. Metabolites have additional cross-references to the ChEBI database (Hastings et al., 2016), the Human Metabolome Database (HMDB) (Wishart et al., 2007), BioPath (Brandenburg et al., 2004), InChIKey (Heller et al., 2015), UniPathway (Morgat et al., 2011), lipid maps structure database (Sud et al., 2007), and the University of Minnesota Biocatalysis/Biodegradation Database (UM-BBD) (Ellis et al., 2003).

All model instances were further annotated using SBO terms (see **Figure 2**). While genes and metabolites received general SBO terms for genes and simple chemicals, the model's reactions were annotated with 23 different SBO terms. The most prominent ontology group is "biochemical reactions": 313 reactions in the model hold the general SBO term for reactions. The number of biochemical reactions is followed by the group of exchange reactions with 181 reactions. The transport reactions are described more precisely by the SBO terms for active, passive, co-, symporter-mediated, antiporter-mediated, or general transport. For all other reactions, we identified SBO terms that describe the occurring biochemical reaction more precisely. In terms of ontology, these SBO terms are child nodes of the SBO term for biochemical reactions. These terms include, for example, redox reactions, the transfer of a chemical group, hydrolysis, or phosphorylation. The SBO terms for ATP maintenance and biomass production occur only once in the model. **Figure 2** gives an overview of all 23 added reaction SBO terms and their occurrence in the model.

The plugins fbc (Olivier and Bergmann, 2018) and groups (Hucka and Smith, 2016) are enabled in *i*CGB21FR, thus allowing information such as metabolic charges, chemical formulas, or gene products to be stored. All identified KEGG pathways (Kanehisa et al., 2019) were added as a group to the model, with all reactions participating in the pathway as group members. In total, 102 groups were added to the model. The group with the most members is the "metabolic pathways" group with 563 members, followed by the "biosynthesis of secondary metabolites" group with 297 members. Other groups with more than 100 members are the "biosynthesis of amino acids" with 104 associated reactions, the "biosynthesis of cofactors" with 151 members, and the group of reactions associated with "microbial metabolism in diverse environments" with 171 members. With the help of these groups, reactions of a particular pathway can easily be extracted and analyzed.

The biomass objective function (BOF) created by CarveMe was refined in several steps to obtain realistic growth rates for the tested media. With the help of BOFdat and the nucleotide sequence of *C. glutamicum* ATCC 13032, the stoichiometric

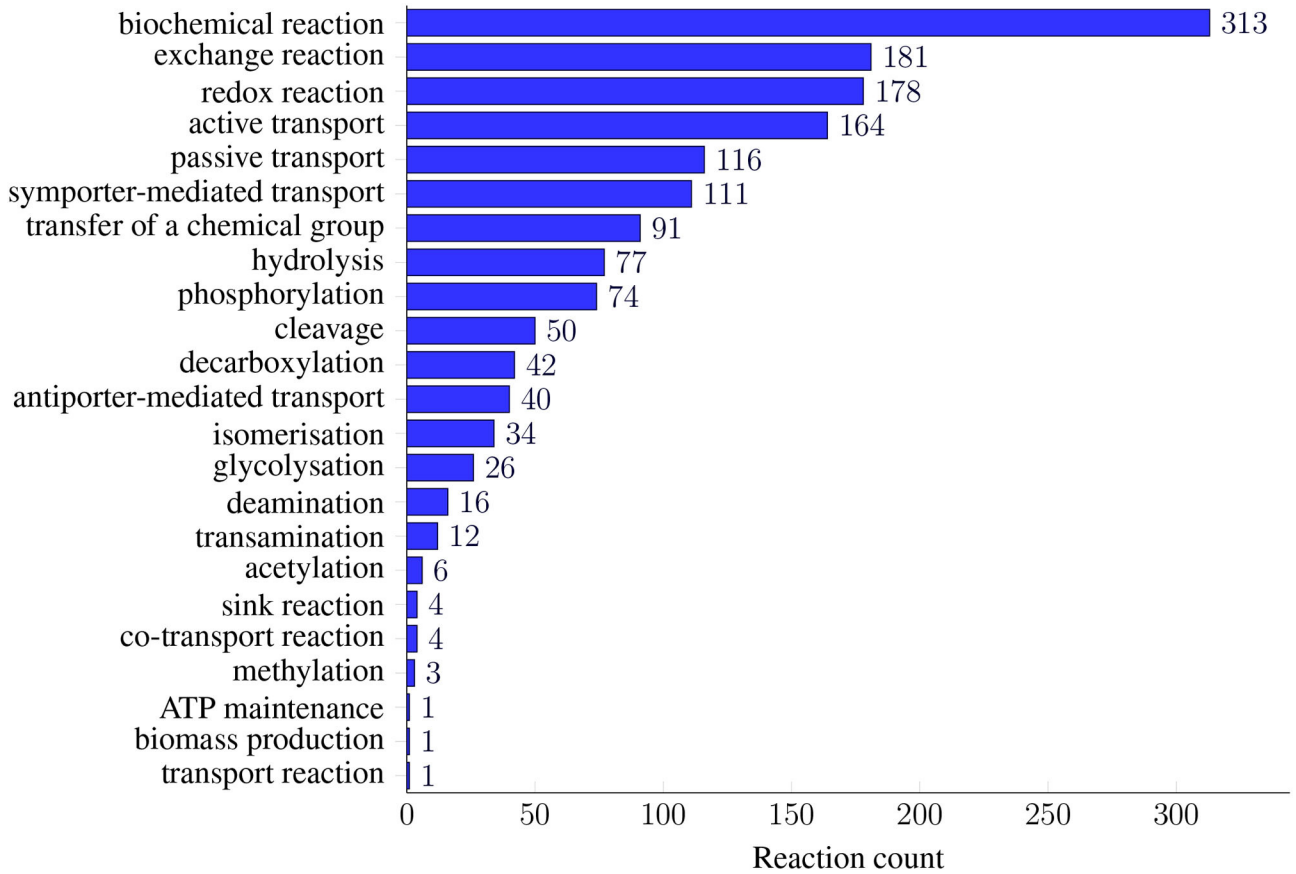

FIGURE 2 | Prevalence of SBO terms in *i*CGB21FR. SBO terms for reactions were defined as precisely and specialized as possible. As many models only annotate their metabolic reactions with the most general SBO term for biochemical reactions (`SBO:0000176`), we further refined the SBO annotations. Thus, the model's reactions were annotated with 23 different SBO terms. They ranged from different transport reactions, including active, passive, or co-transport, to specific biochemical processes, like deamination, glycosylation, or isomerization. This fine-grained reaction annotation with SBO terms easily allows for subsequent analysis regarding reaction classes.

coefficients of the DNA nucleotides were adapted. The following seven metabolites were added as coenzymes and inorganic ions to the biomass objective function: NADH, NADPH, adenosine monophosphate (AMP), pyruvate, ammonium, sodium, and nickel. The stoichiometric coefficients of 16 further coenzymes and inorganic ions were adapted using BOFdat. The inorganic ion cobalt was removed from the BOF based on the elemental composition of *C. glutamicum* ATCC 13032 cells, as described by Eggeling and Bott (2005, p.16, 18). After including these changes, the simulated biomass production is in the range of a reasonable growth rate with no blocked biomass precursors in both the default and the complete medium.

3.2. Simulations of *i*CGB21FR Are Consistent With Experimental Data

We simulated the growth of *i*CGB21FR in different media under aerobic and anaerobic conditions, and with access to different carbon sources (see **Figure 3**). Growth was tested on the two minimal media, M9 and CGXII, and the complete LB medium. The heat map in **Figure 3A** gives an overview of the growth behavior of *C. glutamicum* in the three different media under aerobic and anaerobic conditions. With 1.0266 mmol gDW^{-1} h^{-1} the biomass consistency of *i*CGB21FR is close to 1 mmol gDW^{-1} h^{-1}. Consequently, it is approximately possible to directly compare the *in-silico* growth rate to an experimentally obtained growth rate given in 1 h^{-1}. The simulated aerobic model growth on the minimal medium M9 with glucose as a single carbon source resulted in a maximal growth rate of 0.57 mmol gDW^{-1} h^{-1}. A maximal realistic aerobic growth rate of 0.57 mmol gDW^{-1} h^{-1} on CGXII was obtained using the simulation tools COBRApy (Ebrahim et al., 2013) and confirmed with the Systems Biology Simulation Core Library (SBSCL) (Panchiwala et al., 2021). The simulated value is only slightly lower than the growth rate of 0.61 h^{-1} that Unthan et al. (2014) could experimentally obtain. The model simulates growth on the complex LB medium with a growth rate of 1.0214 mmol gDW^{-1} h^{-1} under aerobic conditions without further adjustments or refinements. As expected, the growth rate

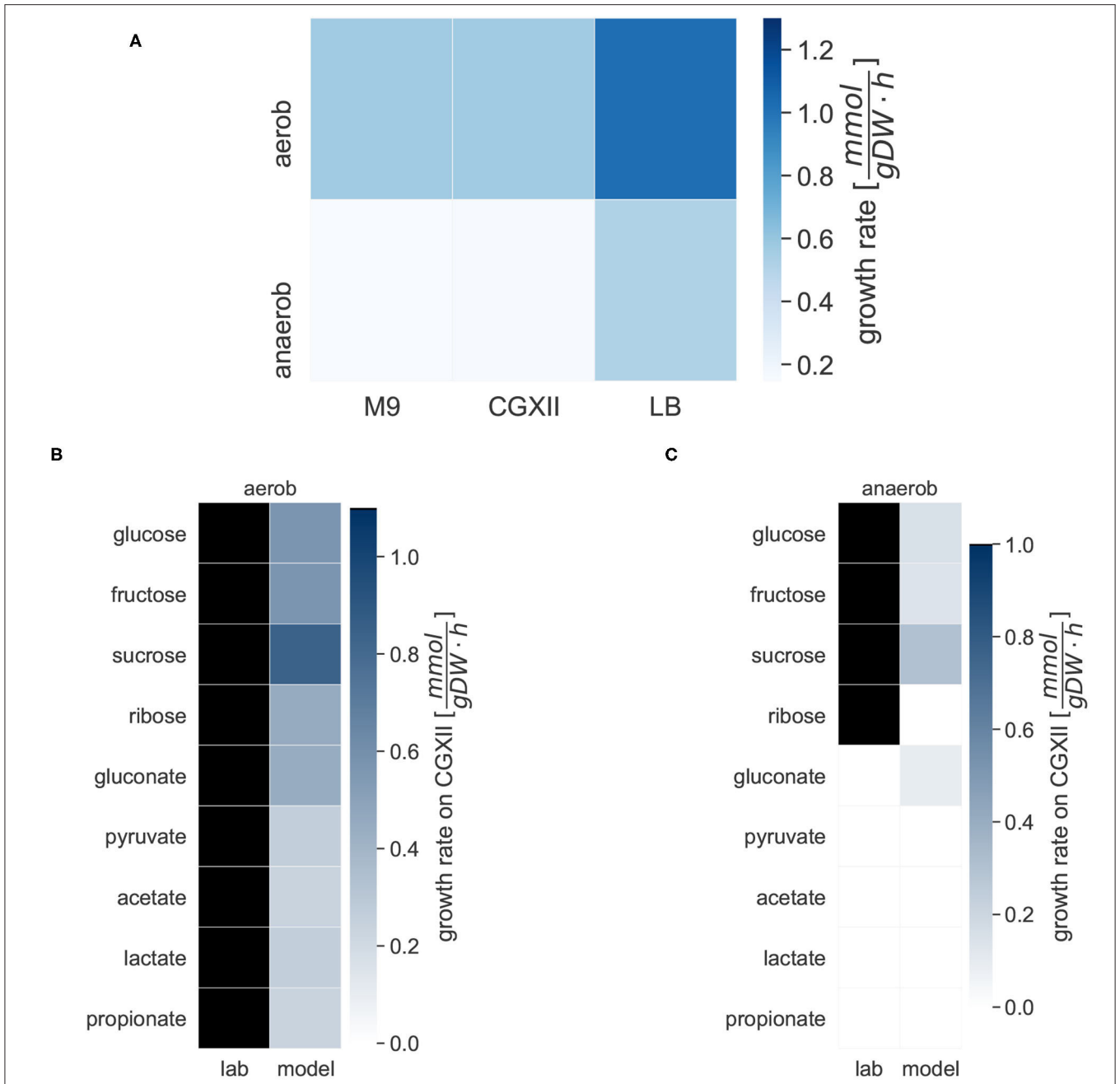

FIGURE 3 | Specific growth rates of *C. glutamicum* under different conditions. Growth rates are given in mmol gDW^{-1} h^{-1}. The darker the color, the higher the simulated growth rate under the given conditions. For the laboratory experiments, black indicates growth, and white indicates no growth on the given carbon source. **(A)** The *in silico* growth of *i*CGB21FR was simulated in the following three chemically defined media: the M9 minimal medium, the CGXII minimal medium, and the lysogeny broth (LB) complete medium. The growth was simulated under aerobic and anaerobic conditions. **(B)** Michel et al. tested the growth of *C. glutamicum* in CGXII minimal medium under aerobic conditions with different carbon sources in laboratory experiments. All tested compounds could serve as the sole carbon source under aerobic conditions (Michel et al., 2015). The different carbon sources were also evaluated with *i*CGB21FR. The model simulated growth on all given carbon sources. **(C)** The different carbon sources were also evaluated under anaerobic conditions. Michel et al. experimentally identified only glucose, pyruvate, sucrose, and ribose as carbon sources under anaerobic conditions. The model *i*CGB21FR was able to simulate growth on most of these sources as well except for ribose, but additionally showed growth on gluconate.

in the complex medium (LB) is approximately twice as high as in the two minimal media (M9 and CGXII). The aerobic growth conditions in all three media show a higher simulated growth rate compared to the anaerobic conditions, as anticipated. All growth rates are within a realistic range (Unthan et al., 2014).

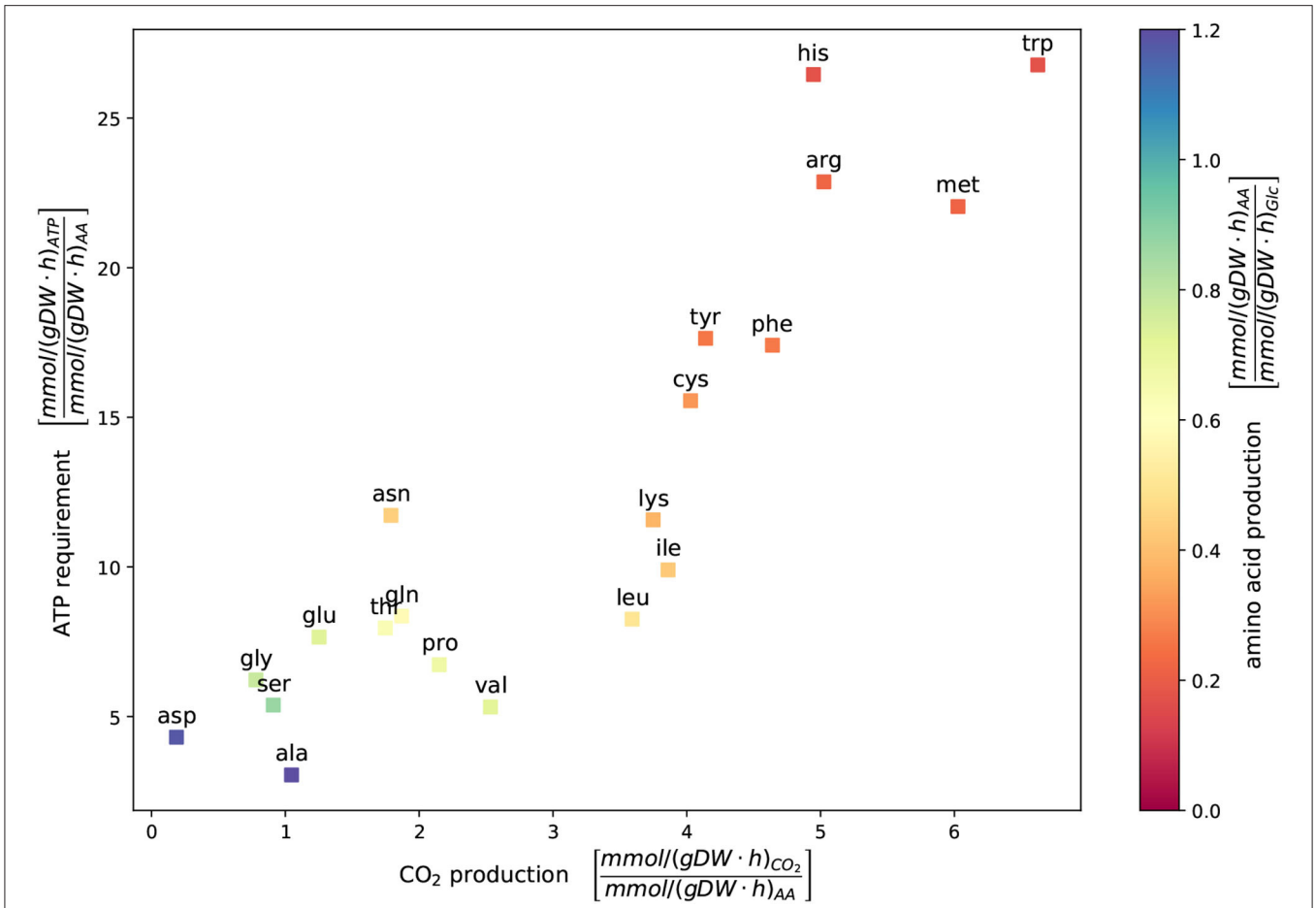

FIGURE 4 | Metabolic cost of amino acid production. The ATP requirement depicted vs. CO_2 production and the *in silico* amino acid production were determined using flux balance analysis (FBA). Glucose served as a sole carbon source under aerobic growth conditions. The availability of glucose was restricted by an uptake rate of 10 mmol gDW^{-1} h^{-1}. The growth rate was fixed to 0.4 mmol gDW^{-1} h^{-1} to ensure the organisms' viability. Each square represents the result of a single FBA with the objective to maximize the corresponding amino acid production. The color indicates the amino acid production rate in relationship to the glucose uptake rate. In this simulation, L-aspartate and L-alanine, result in the highest amino acid production rate with 11.77 mmol gDW^{-1} h^{-1} and 13.73 mmol gDW^{-1} h^{-1}, respectively. A trade-off exists between the yield of amino acid production and the energy expenditure and CO_2 production: the more ATP is required, the more CO_2 and lower amino acid production rates are yielded.

The growth of *C. glutamicum* in CGXII minimal medium under aerobic and anaerobic conditions with varying carbon sources was tested. Under aerobic conditions, the model simulated biomass production on all carbon sources. Aerobic growth was possible on all carbon sources. The growth rates varied between 0.8437 mmol gDW^{-1} h^{-1} on sucrose and 0.2401 mmol gDW^{-1} h^{-1} on acetate. In our anaerobic *in silico* experiments, biomass production was also possible on three of the experimentally validated carbon sources, but not on ribose. Additionally, gluconate can be used as carbon sources. The biomass production on gluconate yielded a rate of 0.0945 mmol gDW^{-1} h^{-1}.

The new model of *C. glutamicum* can simulate the production of all 20 canonical amino acids while growing on the CGXII medium with D-glucose as the carbon source under aerobic conditions. In **Figure 4**, each square represents the result of a single FBA with the objective to maximize the corresponding amino acid production. The color indicates the amino acid production rate with respect to the glucose uptake rate. The positioning represents the ATP requirements and CO_2 production in relation to the amino acid production rate. The two amino acids, L-aspartate (asp) and L-alanine (ala), have the highest absolute amino acid production rates with 11.77 mmol gDW^{-1} h^{-1} and 13.73 mmol gDW^{-1} h^{-1}, respectively (see also Zelle et al., 2015). In contrast, the amino acids L-histidine, L-arginine, and L-tryptophan have the lowest amino acid production rate and the highest ATP requirements. A relationship exists between the yield of amino acid production, energy expenditure, and CO_2 production: The more ATP is required, the more CO_2 produced and the lower is the amino acid production rate. L-glutamate is of particular interest for metabolic engineering in *C. glutamicum*. Its total production rate under the selected conditions yields 8.7 mmol gDW^{-1} h^{-1}.

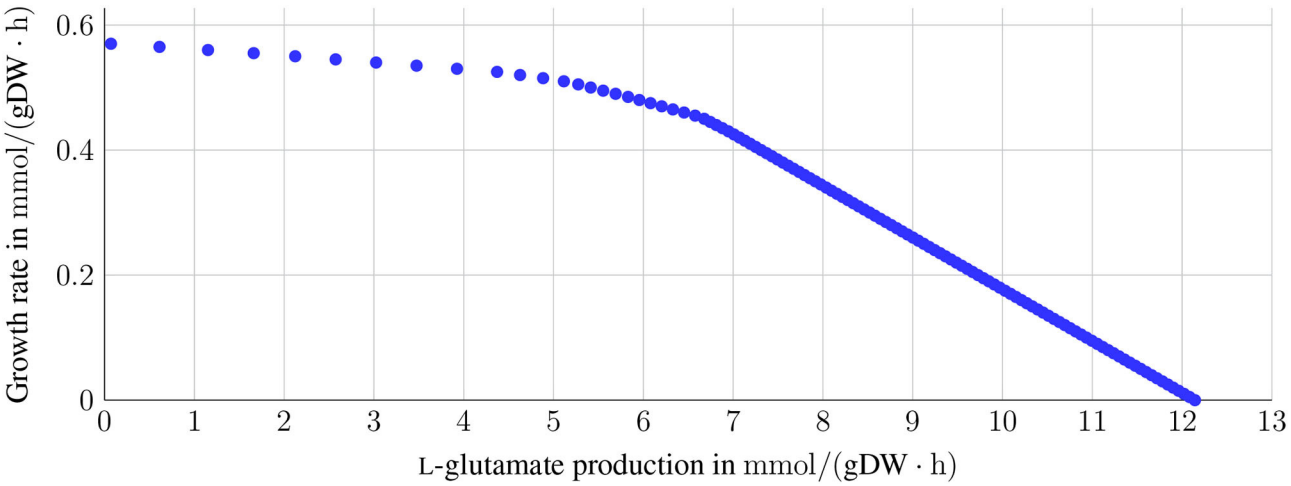

FIGURE 5 | Trade-off between L-glutamate production and growth. The sink reaction for L-glutamate was set as the objective function to investigate the relation between the production of L-glutamate and growth. The growth rate was varied between 0 and the maximum growth rate of 0.57 mmol gDW^{-1} h^{-1} with glucose as the sole carbon source on CGXII. A dependency between growth and L-glutamate production is expected, as L-glutamate is part of the growth function with a stoichiometric coefficient of 0.0149. For growth rates between 0 and up to 0.4 mmol gDW^{-1} h^{-1}, the L-glutamate production only decreases slightly (from 12 to approximately 7 mmol gDW^{-1} h^{-1}. In contrast, the production of L-glutamate decreases drastically for higher growth rates.

3.3. Pointers to Metabolic Engineering for the L-glutamate Production

C. glutamicum is a well-known L-glutamate producer. However, L-glutamate is also required for the growth or maintenance function. L-glutamate accounts for the growth function with a stoichiometric coefficient of 0.0149. Thus, a trade-off between growth requirement and the production of L-glutamate is expected. This trade-off is depicted in **Figure 5**. For growth rates between 0 mmol gDW^{-1} h^{-1} and 0.4 mmol gDW^{-1} h^{-1}, the L-glutamate production rate remains comparably high. It only decreases by 5 mmol gDW^{-1} h^{-1}. With increasing growth rates greater than 0.4 mmol gDW^{-1} h^{-1}, the L-glutamate production rate decreases rapidly.

The PC plays a pivotal role in L-glutamate production (Peters-Wendisch et al., 2001). The effect of a knock-out of the PC on the flux distribution is depicted in **Figure 6**. Knocking out the PC decreases the L-glutamate production only to a small extent (from 7.31 mmol gDW^{-1} h^{-1} to 7.26 mmol gDW^{-1} h^{-1}). The limiting factor in L-glutamate production is the availability of a carbon source (in this example, D-glucose) and, as shown above, the growth rate. The PC *in silico* knock-out experiment indicates that *C. glutamicum* can compensate for the knocked-out reaction.

Performing FVA helps to identify potential the ranges of each flux. Reactions relevant for optimizing the objective function can be identified by filtering for reactions with almost identical minimal and maximal flux values. With loopless FVA, we identified six highly relevant reactions for L-glutamate production in *C. glutamicum*. Among these six reactions were two pseudo-reactions: the exchange reaction of D-glucose and the sink reaction for L-glutamate. Glucose is the sole carbon source in the *in silico* experiment. Therefore, its strong influence on L-glutamate production is apparent. The same holds for the sink reaction that was used as the objective function in the FVA. The other four relevant reactions include the aconitate hydratase (`ACONT`), which converts citrate to isocitrate, the citrate synthase (`CS`), which converts acetyl-CoA and oxaloacetate to citrate and coenzyme A, the glucose transport via phosphoenolpyruvate, and the isocitrate dehydrogenase (`ICDHyr`), which converts isocitrate to 2-oxoglutarate (see also **Table 1**). The reactions `ACONT`, `CS`, and `ICDHyr` represent the fragile connection between glycolysis and L-glutamate biosynthesis. This connection can additionally be seen in **Figure 6**, where the three mentioned reactions are also illustrated.

4. DISCUSSION

An updated genome-scale metabolic model *i*CGB21FR of *C. glutamicum* ATCC 13032 was reconstructed and validated using newly available specialized reconstruction tools. Using recent tools, the phenotypic prediction of the model's metabolism allows a more accurate depiction of the metabolic capabilities of *C. glutamicum*. This GEM was created using current community standards for high-quality reconstructions. The new *in silico* model reproduces experimentally validated data. In addition, we also curated *i*CW773 to meet systems biology standards (see also Carey et al., 2020). Initially, the model *i*CW773 was only available as a spreadsheet in Microsoft Excel format. According to the profound debate within the systems biology community (see Ebrahim et al., 2015), using this format is no longer recommended because it does not support unambiguous interpretation and direct reuse in further model analysis, especially for non-computational scientists. Generally, models in spreadsheet files do not fully support the principles of findable, accessible, interoperable, reusable data in science (Wilkinson

TABLE 1 | Reactions of particular relevance for the production of L-glutamate in *C. glutamicum*.

Reaction ID	Reaction name	Reaction
ACONT	aconitate hydratase	Citrate ⇌ Isocitrate
CS	citrate synthase	Acetyl-CoA + H_2O + Oxaloacetate ⟶ Citrate + Coenzyme A + H^+
EX_glc__D_e	D-glucose exchange	D-Glucose ⇌ ∅
GLCpts	D-glucose transport via PEP:Pyr	D-Glucose + Phosphoenolpyruvate ⟶ D-Glucose 6-phosphate + Pyruvate
ICDHyr	isocitrate dehydrogenase (NADP)	Isocitrate + NADP ⇌ 2-Oxoglutarate + CO_2 + NADPH
sink_glu__L	sink reaction for L-glutamate	L-glutamate ⟶ ∅

Reactions identified by flux variability analysis (FVA) to be highly relevant for L-glutamate production.

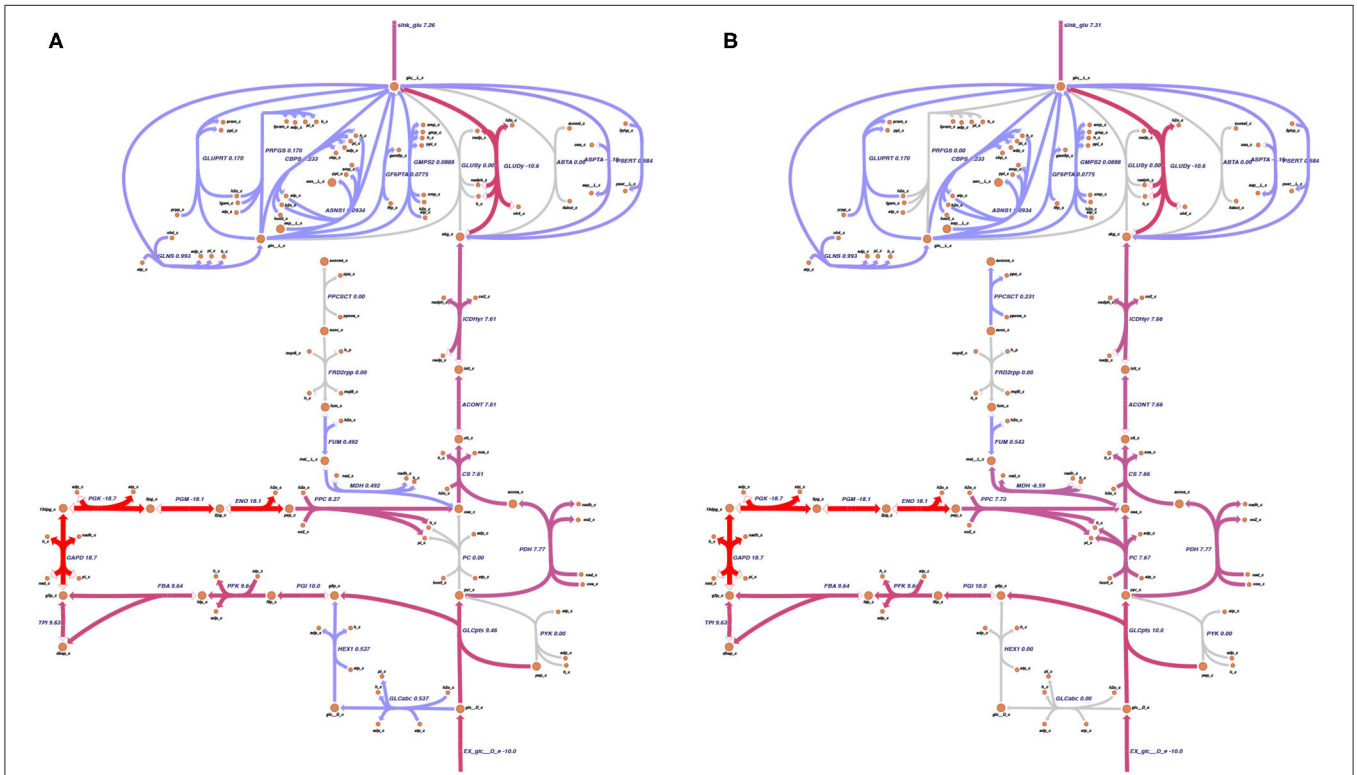

FIGURE 6 | Pyruvate carboxylase and the glutamate production. As the pyruvate carboxylase (PC) was discovered to be the bottleneck of glutamate production (Peters-Wendisch et al., 2001), its knock-out effect on the metabolic model was analyzed. For the simulation, the growth rate was fixed to 0.4 mmol gDW^{-1} h^{-1}, and the glutamate production was set as the objective function. The PC reaction was knocked out. The predicted flux distribution under maximal L-glutamate production resulting from the flux balance analysis (FBA) was plotted on the metabolic map, which was drawn using Escher (King et al., 2015). **(A)** shows the predicted flux distribution of the knock-out of the PC under maximal L-glutamate production. **(B)** depicts the predicted flux distribution of the wild-type model. In both cases, L-glutamate is produced. The maximal glutamate production rate only decreases by 0.05 mmol gDW^{-1} h^{-1} when the PC is knocked out. Thus, the model *i*CGB21FR can compensate for the loss of the PC reaction.

et al., 2016) because using them in computational analyses requires converting these files to a standardized format. After converting *i*CW773 to SBML Level 3 Version 1 and performing several curation steps, it now contains SBO terms and has a MEMOTE score that was increased from initially 29 % to 70 %. However, precaution is advised when using *i*CW773 as it contains reconstruction inconsistencies and incorrect metabolites. The curated *i*CW773 is available in SBML Level 3 Version 1 on the BioModels Database (Malik-Sheriff et al., 2020) under the accession number MODEL2110010001 (see Availability below).

4.1. Reconstruction Is of High Quality

The comprehensive annotations of all model components, including metabolites, reactions, and genes, contribute to the high quality of the reconstruction of *i*CGB21FR. Each instance is uniquely referenced to at least one database, thus providing a permanent link to clearly and uniquely identify this instance with its attributes (Juty et al., 2012). Almost all model instances are annotated with references to a minimum of one database, allowing more precise cross-referencing and interoperability between different databases. This high level of annotations is advantageous, as findable, accessible, interoperable, reusable

(FAIR) data principles allow fellow scientists to conduct research on and with this model continuously (Dräger and Palsson, 2014; Wilkinson et al., 2016). Erroneous or missing information, incompatible data formats, or missing annotations significantly hamper the reuse of GEMs (Ravikrishnan and Raman, 2015). Missing annotations can lead to identification problems of compounds and reactions. GPRs are added for different reactions, and all instances are equipped with SBO terms, facilitating FAIR data principles.

Generally, the high degree of annotations in *i*CGB21FR is confirmed by the high MEMOTE scores within the different categories. In terms of the presence of annotations, almost all MEMOTE scores of the annotation categories rank close to 100 %. This high score implies that almost all suggested standards concerning annotations are met for this GEM (see also Carey et al., 2020). The current version of MEMOTE does not include all *C. glutamicum*-specific databases, while other organism-specific databases with less relevance for our model are incorporated. One example can be found in the annotations section of the genes, where cross-references to different *Escherichia coli* databases are checked. In *i*CGB21FR, the MEMOTE score for the presence of SBO terms for biochemical reactions sticks out due to its comparatively low value. The current version of MEMOTE checks every reaction for the annotation with the most general SBO term (`SBO:0000176`), "biochemical reaction." This check implies that MEMOTE can not yet capture the fine-grained description of biochemical reactions in this model. Thus, the score of the metabolic reactions of 33.4 % diminishes the overall MEMOTE SBO term annotation score.

Two typical ways exist to calculate the biomass objective function (BOF) of an organism. These are the macromolecular-based and the sequence-based approach. A typical biomass objective function (BOF) comprises the cell's primary macromolecules, essential coenzymes, inorganic ions, and species-specific metabolites, including the cell wall components. Additionally, the energy requirements for growth and non-growth associated maintenance costs are included (Lachance et al., 2019). Using an experimentally derived biomass composition implies that its cellular composition depends on the experimental conditions under which it was obtained. For example, the availability of nutrients and the resulting growth rate influence the ratio between DNA, RNA, and proteins (Scott et al., 2010). It thus represents a biased approach to compute the biomass. When no species-specific experimental data for the sequence-based approach is available to calculate a species-specific biomass function, a universal bacterial biomass function is included. Adapted biomass composition of a highly developed and curated GEM of *E. coli* is often used (Orth et al., 2011; Xavier et al., 2017). The new model possesses a biomass function adapted specifically to *C. glutamicum*. This conceptual approach differs from previous works by Kjeldsen and Nielsen (2009) and Zelle et al. (2015). For the BOF of Kjeldsen and Nielsen (2009), a biomass equation and the corresponding energy consumption associated with each reaction were formulated for each macromolecule. No *C. glutamicum*-specific data for the energy requirement of the polymerization of macromolecules was available; thus, *E. coli* data was used instead. The BOF of *i*EZ482 is based on the BOF of Kjeldsen and Nielsen (2009). Using species-specific data forms the basis for models with high predictive value. BOFdat enables the curation and refinement of a species-specific BOF by incorporating various -omics data into its calculation. In this study, genomics data were available and applied to refine the species-specific BOF.

4.2. *i*CGB21FR Reproduces Experimentally Obtained Data

The model *i*CGB21FR was validated by simulating growth on three different media under aerobic and anaerobic conditions. *C. glutamicum* is also known to grow in the brain heart infusion (BHI) medium. Modeling requires chemically defined media for growth simulations. We could not test the growth of *i*CGB21FR in BHI as no exact composition of the chemical definition of this medium exists. Simulating aerobic growth on LB complete medium was possible without any additional refinement of the model. Aerobic growth on the two minimal media was only possible by adapting the biomass function for growth on CGXII and adding missing reactions to the model for growth on M9. Missing reactions were identified by literature research. Anaerobic growth was enabled after adding six reactions. By this, the model was refined step by step to simulate and confirm already known growth conditions.

In silico growth rates were higher on the complete medium compared to the two minimal media. The aerobic growth rates were higher than the anaerobic growth rates, with all growth rates within a realistic range (Unthan et al., 2014; Michel et al., 2015). Both findings are expected, as complete media provide more nutrients and biomass precursors than minimal media. As their name suggest, minimal media only provide minimal required nutrients for the organism to grow. *C. glutamicum* uses oxygen and the more efficient aerobic respiration. It is even often regarded as aerobe (Takeno et al., 2007). However, as *C. glutamicum* is facultatively anaerobe, it can also switch to fermentation and anaerobic respiration if oxygen is absent. Anaerobic growth by nitrate respiration is limited, as nitrate accumulates and inhibits growth. Additionally, glucose is converted to L-lactate and succinate without the growth of the organism (Inui et al., 2004b; Koch-Koerfges et al., 2013).

Two observations stick out from these growth results. First, the current tools for the reconstruction of GEMs still demand subsequent manual refinement. Even though automated tools, such as CarveMe (Machado et al., 2018), reduce the amount of time spent on the reconstruction dramatically, manual refinement remains a pivotal part of the reconstruction process. The necessity of manual curation becomes particularly apparent when comparing the growth predictions of our model for the different media. The draft model created by CarveMe enabled growth on the complete medium without further ado. However, manual refinement was essential for the simulation of growth on the two minimal media. The second interesting observation is the organism-specific gap-filling, which appears to be more fruitful when applied to media that specifically compensate for certain physiological or metabolic oddities of the organism. In our case, knowledge gap-filling was most fruitful

on the CGXII medium which, for example, compensates for the limited ability of *C. glutamicum* to synthesize and excrete siderophores (Budzikiewicz et al., 1997). This makes sense, as the minimal medium provides the microbe's bare necessities to grow. Potentially lacking compounds could be compensated by the composition of the complete medium.

We validated our model by testing the growth rate on the CGXII minimal medium under aerobic and anaerobic conditions using different experimentally validated carbon sources. Aerobic growth was possible on all experimentally validated carbon sources. In addition to the experimentally confirmed anaerobic growth on glucose, fructose, sucrose as carbon sources, our *in silico* model also grew on gluconate. We verified that all genes required to utilize gluconate as carbon sources exist in *C. glutamicum*. The rate of NADPH reoxidation could be a potential explanation for the *in silico* growth on the additional anaerobic carbon source. The enzyme 6-phosphogluconate dehydrogenase oxidizes 6-phosphogluconate to ribulose 5-phosphate. This enzyme is inhibited by NADPH, which is essential for the cellular control of the NADPH synthesis (Moritz et al., 2000). The rate of NADPH re-oxidation represents a critical element of this process. Gluconate is phosphorylated after uptake and then catabolized in the pentose phosphate pathway. If NADPH re-oxidation was too low under anaerobic conditions, NADPH could accumulate and result in complete inhibition of 6-phosphogluconate dehydrogenase activity. This accumulation would lead to a stop in growth on gluconate, as was shown by experimental data (Michel et al., 2015). If, however, NADPH re-oxidation is sufficiently fast and no NADPH accumulates, the activity of the 6-phosphogluconate dehydrogenase could remain active and allow anaerobic growth on gluconate by simulation studies with this *in silico* model.

As a final validation step of the metabolic model, its ability to produce amino acids was examined. In complex bacterial systems, amino acid production co-occurs with growth (Marx et al., 1996). The biosynthesis of amino acids requires a lot of the carbon source's total budget, usually used for bacterial growth (Neidhardt et al., 1990). The growth rate was fixed to $0.4\,\mathrm{mmol\,gDW^{-1}\,h^{-1}}$ to ensure the microbe's viability while producing amino acids. With increasing CO_2 production rate and ATP requirements, the amino acid production yield decreases. Especially smaller amino acids with only a few carbon atoms, like L-alanine with only three carbon atoms, or glycine with two carbon atoms, have a low CO_2 production and ATP requirement rate.

In contrast, amino acids with more carbon atoms, such as L-tryptophan, have a much higher ATP requirement and CO_2 production rate, while the amino acid yield is relatively low. This leads to the conclusion that building more extensive and more complex amino acids needs more energy. An increasing proportion of the consumed sugar will be used to produce more energy, is then lost as CO_2, and cannot be used for amino acid formation (Gourdon et al., 2003).

4.3. L-glutamate Production: New Insights for Metabolic Engineering

One might expect a linear correlation between the L-glutamate production and the growth rate, where the slope is related to the amino acid's stoichiometric coefficient in the biomass function. The trade-off between the production of L-glutamate and the growth rate was investigated by fixing the growth rates and maximizing the L-glutamate production (see **Figure 5**). The system moves between these two boundaries: the maximal possible growth rate and the maximal possible production of L-glutamate. The closer the values get to either maximum, the greater is the influence on the respective other value. When ceasing growth, the theoretical production of L-glutamate would reach a maximum since the available metabolic capacity is invested in the L-glutamate production. The reverse situation occurs with ceasing L-glutamate production and maximizing growth where all energetic demand is invested. L-glutamate production reaches its maximum when no growth occurs, and the available glucose is completely used to produce L-glutamate. Thus, the growth rate is the limiting factor for our *in silico* model, independent of the L-glutamate production.

The PC was first investigated to study relevant reactions for L-glutamate production (see **Figure 6**). The PC has been described as the bottleneck in the production of L-glutamate (Peters-Wendisch et al., 2001). Knocking out the PC in laboratory experiments leads to ambivalent results: Both drastic decrease (Peters-Wendisch et al., 2001) and increase (Sato et al., 2008) in L-glutamate production were reported after a disruption of the PC. Pyruvate is part of the complex network responsible for carboxylation and decarboxylation reactions, which connect the glycolysis and TCA cycle (Becker and Wittmann, 2020). In *C. glutamicum*, the PC represents one of the carboxylation enzymes, the other being the phosphoenolpyruvate carboxylase (Eikmanns, 2005). The carboxylation and decarboxylation enzymatic complex in *C. glutamicum* is a highly flexible network that enables several pathways to respond to varying metabolic circumstances (Möllney et al., 2000; Becker et al., 2008; Becker and Wittmann, 2020)—knocking out the PC in our model still allowed L-glutamate production. We also found that the amount of produced L-glutamate does not vary significantly with the PC being knocked. According to our simulation, the limiting factors in L-glutamate production are access to carbon sources and the growth rate.

Four reactions were identified that play a pivotal role in the production of L-glutamate in our model. The first is a glucose transporter, which uses the phosphoenolpyruvate (PEP)-dependent sugar phosphotransferase system. The L-glutamate yield decreased with sugar consumption rates in laboratory experiments (Gourdon et al., 2003). This seems reasonable, as glucose is the sole carbon source and starting point for glutamate production. Increasing glucose availability is only expedient if the glucose transporters' capacity is given to take up the enhanced supply of glucose. The three remaining reactions, aconitase, citrate synthase, and isocitrate dehydrogenase, are all part of the tricarboxylic acid (TCA) cycle. The TCA cycle is a complex

regulated amphibolic pathway with L-glutamate and L-lysine as derived intermediate products (Bott, 2007).

The aconitase gene is regulated by four transcriptional regulators, indicating a tight control of this enzyme. A *C. glutamicum* mutant lacking the aconitase gene was glutamate auxotrophic in the CGXII minimal medium with glucose as the carbon source (Baumgart et al., 2011). The model *i*CGB21FR could replicate the finding that aconitase is essential for L-glutamate production. It remains to be further experimentally validated how the interplay between the aconitase within the TCA cycle in terms of L-glutamate production can be optimized.

The citrate synthase catalyzes the initial reaction of the TCA cycle. Overexpression of the citrate synthase can redirect more carbon flux into the cycle and result in higher L-arginine production (Man et al., 2016). L-arginine is synthesized from the precursor L-glutamic acid (Utagawa, 2004). Thus, higher production of L-glutamate might also be dependent upon the activity of the citrate synthase. The role of the citrate synthase in L-glutamate production might be an interesting topic to investigate since it might represent a target for metabolic engineering of *C. glutamicum*'s TCA cycle. Since the citrate synthase is the initial reaction of the TCA cycle with L-glutamate and L-lysine as intermediates, its activity might prove particularly fruitful.

Isocitrate dehydrogenase catalyzes the oxidative decarboxylation of isocitrate. Becker et al. (2009) found in their investigation of the effects of the isocitrate dehydrogenase on L-lysine production that decreased activity of the isocitrate dehydrogenase improves the L-lysine production. This decrease induced a flux shift from the TCA cycle to anaplerotic carboxylation (van Ooyen et al., 2012). However, the PC functions as an anaplerotic enzyme in L-glutamate production (Peters-Wendisch et al., 1997). In other words, the isocitrate dehydrogenase has different functions in L-glutamate production than in L-lysine production. This differing function becomes more apparent when looking at the effects of isocitrate dehydrogenase inactivation in *C. glutamicum*: Inactivation of the NADP-dependent isocitrate dehydrogenase in *C. glutamicum* leads to L-glutamate auxotrophy (Eikmanns et al., 1995). This connection between the PC and the isocitrate dehydrogenase in L-glutamate production might be an interesting target for metabolic engineering.

5. CONCLUSION AND OUTLOOK

The new model *i*CGB21FR represents an GEM of high quality of the biotechnologically relevant microorganism *Corynebacterium glutamicum* ATCC 13032. We reconstructed this metabolic model with an adapted, species-specific biomass composition and realistic growth rates in different environments, which were validated using experimentally derived data. Furthermore, alternative metabolic pathways for the production of L-glutamate were shown in our *in silico* model. Particularly, these alternative pathways could be of interest for further investigation in terms of metabolic engineering. Biotin is a key player for the L-glutamate production in *C. glutamicum* since its limitation triggers L-glutamate production. Despite the inclusion of biotin in *i*CGB21FR and its participation in five biochemical reactions, its role in L-glutamate production is currently not included. The influence of biotin on the PC and the reactions involved in the alternative pathway for L-glutamate production with the pyruvate carboxylase knocked-out should be further investigated in subsequent GEMs of *C. glutamicum*.

DATA AVAILABILITY STATEMENT

The datasets presented in this study can be found in online repositories. The names of the repository/repositories and accession number(s) can be found in the article/**Supplementary Material**.

AUTHOR CONTRIBUTIONS

MF and AR curated and refined the model and conducted the study. MF, AR, and AD wrote the manuscript. EZ, KN, and WW revised the manuscript. AD supervised the study. All authors reviewed and approved the final manuscript.

FUNDING

The authors acknowledge support by the Open Access Publishing Fund of the University of Tübingen (https://uni-tuebingen.de/en/58988).

ACKNOWLEDGMENTS

We thank Elisabeth Fritze for providing access to the program she designed as part of her bachelor's requirements. Her algorithm allowed the assignment of hierarchically differentiated SBO terms to our model.

SUPPLEMENTARY MATERIAL

The Supplementary Material for this article can be found online at: https://www.frontiersin.org/articles/10.3389/fmicb.2021.750206/full#supplementary-material

REFERENCES

Agarwala, R., Barrett, T., Beck, J., Benson, D. A., Bollin, C., Bolton, E., et al. (2018). Database resources of the national center for biotechnology information. *Nucleic Acids Res.* 46, D8–D13. doi: 10.1093/nar/gkx1095

Baumgart, M., Mustafi, N., Krug, A., and Bott, M. (2011). Deletion of the aconitase gene in *Corynebacterium glutamicum* causes strong selection pressure for secondary mutations inactivating citrate synthase. *J. Bacteriol.* 193, 6864–6873. doi: 10.1128/JB.05465-11

Becker, J., Klopprogge, C., Schröder, H., and Wittmann, C. (2009). Metabolic engineering of the tricarboxylic acid cycle for improved lysine production by *Corynebacterium glutamicum*. *Appl. Environ Microbiol.* 75, 7866–7869. doi: 10.1128/AEM.01942-09

Becker, J., Klopprogge, C., and Wittmann, C. (2008). Metabolic responses to pyruvate kinase deletion in lysine producing *Corynebacterium glutamicum*. *Microb. Cell. Fact.* 7, 1–15. doi: 10.1186/1475-2859-7-8

Becker, J., and Wittmann, C. (2020). "Pathways at work: metabolic flux analysis of the industrial cell factory Corynebacterium glutamicum," in *Corynebacterium glutamicum* (Berlin; Heidelberg: Springer), 227–265.

Bergmann, F. T., Adams, R., Moodie, S., Cooper, J., Glont, M., Golebiewski, M., et al. (2014). COMBINE archive and OMEX format: one file to share all information to reproduce a modeling project. *BMC Bioinformatics* 15:369. doi: 10.1186/s12859-014-0369-z

Bergmann, F. T., Czauderna, T., Dorusoz, U., Rougny, A., Dräger, A., Touré, V., et al. (2020). Systems biology graphical notation markup language (SBGNML) version 0.3. *J. Integr. Bioinform.* 17:20200016. doi: 10.1515/jib-2020-0016

Bertani, G. (1951). Studies on lysogenesis. I. The mode of phage liberation by lysogenic *Escherichia coli*. *J. Bacteriol.* 62, 293–300. doi: 10.1128/jb.62.3.293-300.1951

Bornstein, B. J., Keating, S. M., Jouraku, A., and Hucka, M. (2008). LibSBML: an API library for SBML. *Bioinformatics* 24, 880–881. doi: 10.1093/bioinformatics/btn051

Bott, M. (2007). Offering surprises: TCA cycle regulation in *Corynebacterium glutamicum*. *Trends Microbiol.* 15, 417–425. doi: 10.1016/j.tim.2007.08.004

Bott, M., and Niebisch, A. (2003). The respiratory chain of corynebacterium glutamicum. *J. Biotechnol.* 104, 129–153. doi: 10.1016/S0168-1656(03)00144-5

Brandenburg, F. J., Forster, M., Pick, A., Raitner, M., and Schreiber, F. (2004). "BioPath" Exploration and visualization of biochemical pathways," in *Graph Drawing Software. Mathematics and Visualization*, ed M. M. P. Jünger (Berlin; Heidelberg: Springer), 215–235.

Budzikiewicz, H., Bössenkamp, A., Taraz, K., Pandey, A., and Meyer, J.-M. (1997). Corynebactin, a Cyclic Catecholate Siderophore from: *Corynebacterium glutamicum* ATCC 14067 (*Brevibacterium* sp. DSM 20411). *Zeitschrift für Naturforschung C* 52, 551–554. doi: 10.1515/znc-1997-7-820

Carey, M. A., Dräger, A., Beber, M. E., Papin, J. A., and Yurkovich, J. T. (2020). Community standards to facilitate development and address challenges in metabolic modeling. *Mol. Syst. Biol.* 16, e9235. doi: 10.15252/msb.20199235

Caspi, R., Billington, R., Keseler, I. M., Kothari, A., Krummenacker, M., Midford, P. E., et al. (2020). The MetaCyc database of metabolic pathways and enzymes - a 2019 update. *Nucleic Acids Res.* 48, D445–D453. doi: 10.1093/nar/gkz862

Collins, M., Goodfellow, M., and Minnikin, D. (1979). Isoprenoid quinones in the classification of coryneform and related bacteria. *Microbiology* 110, 127–136. doi: 10.1099/00221287-110-1-127

Collins, M., Pirouz, T., Goodfellow, M., and Minnikin, D. (1977). Distribution of menaquinones in actinomycetes and corynebacteria. *Microbiology* 100, 221–230. doi: 10.1099/00221287-100-2-221

Courtot, M., Juty, N., Knüpfer, C., Waltemath, D., Zhukova, A., Dräger, A., et al. (2011). Controlled vocabularies and semantics in systems biology. *Mol. Syst. Biol.* 7, 543. doi: 10.1038/msb.2011.77

Croft, D., OKelly, G., Wu, G., Haw, R., Gillespie, M., Matthews, L., et al. (2010). Reactome: a database of reactions, pathways and biological processes. *Nucleic Acids Res.* 39(Suppl_1):D691–97. doi: 10.1093/nar/gkq1018

Dräger, A., Kronfeld, M., Ziller, M. J., Supper, J., Planatscher, H., Magnus, J. B., et al. (2009). Modeling metabolic networks in *C. glutamicum*: a comparison of rate laws in combination with various parameter optimization strategies. *BMC Syst. Biol.* 3:5. doi: 10.1186/1752-0509-3-5

Dräger, A., and Palsson, B., Ø. (2014). Improving collaboration by standardization efforts in systems biology. *Front. Bioeng.* 2:61. doi: 10.3389/fbioe.2014.00061

Ebrahim, A., Almaas, E., Bauer, E., Bordbar, A., Burgard, A. P., Chang, R. L., et al. (2015). Do genome-scale models need exact solvers or clearer standards? *Mol. Syst. Biol.* 11, 831. doi: 10.15252/msb.20156548

Ebrahim, A., Lerman, J. A., Palsson, B. O., and Hyduke, D. R. (2013). COBRApy: constraints-based reconstruction and analysis for python. *BMC Syst. Biol.* 7:74. doi: 10.1186/1752-0509-7-74

Eggeling, L., and Bott, M. (2005). *Handbook of Corynebacterium glutamicum*. Boca Raton, FL: CRC Press.

Eggeling, L., and Bott, M. (2015). A giant market and a powerful metabolism: L-lysine provided by *Corynebacterium glutamicum*. *Appl. Microbiol. Biotechnol.* 99, 3387–3394. doi: 10.1007/s00253-015-6508-2

Eikmanns, B. (2005). "Central metabolism: tricarboxylic acid cycle and anaplerotic reactions," in *Handbook of Corynebacterium glutamicum*, eds L. Eggeling and M. Bott (Boca Raton, FL: CRC Press; Taylor & Francis Group), 241–276.

Eikmanns, B. J., Rittmann, D., and Sahm, H. (1995). Cloning, sequence analysis, expression, and inactivation of the *Corynebacterium glutatmicum* icd gene encoding isocitrate dehydrogenase and biochemical characterization of the enzyme. *J. Bacteriol.* 177, 774–782. doi: 10.1128/jb.177.3.774-782.1995

Ellis, L. B., Hou, B. K., Kang, W., and Wackett, L. P. (2003). The University of Minnesota biocatalysis/biodegradation database: post-genomic data mining. *Nucleic Acids Res.* 31, 262–265. doi: 10.1093/nar/gkg048

Fang, X., Lloyd, C. J., and Palsson, B. O. (2020). Reconstructing organisms *in silico*: genome-scale models and their emerging applications. *Nat. Rev. Microbiol.* 8, 731–743. doi: 10.1038/s41579-020-00440-4

Fritze, E. (2020). *Automating the Assignment of SBO-Terms* (Bachelor thesis). University of Tübingen.

Fritzemeier, C. J., Hartleb, D., Szappanos, B., Papp, B., and Lercher, M. J. (2017). Erroneous energy-generating cycles in published genome scale metabolic networks: Identification and removal. *PLoS Comput. Biol.* 13:e1005494. doi: 10.1371/journal.pcbi.1005494

Gottstein, W., Olivier, B. G., Bruggeman, F. J., and Teusink, B. (2016). Constraint-based stoichiometric modelling from single organisms to microbial communities. *J. R. Soc. Interface* 13, 20160627. doi: 10.1098/rsif.2016.0627

Gourdon, P., Raherimandimby, M., Dominguez, H., Cocaign-Bousquet, M., and Lindley, N. D. (2003). Osmotic stress, glucose transport capacity and consequences for glutamate overproduction in *Corynebacterium glutamicum*. *J. Biotechnol.* 104, 77–85. doi: 10.1016/S0168-1656(03)00165-2

Hastings, J., Owen, G., Dekker, A., Ennis, M., Kale, N., Muthukrishnan, V., et al. (2016). ChEBI in 2016: improved services and an expanding collection of metabolites. *Nucleic Acids Res.* 44, D1214–D1219. doi: 10.1093/nar/gkv1031

Heider, S. A., Wolf, N., Hofemeier, A., Peters-Wendisch, P., and Wendisch, V. F. (2014). Optimization of the IPP precursor supply for the production of lycopene, decaprenoxanthin and astaxanthin by *Corynebacterium glutamicum*. *Front. Bioeng. Biotechnol.* 2:28. doi: 10.3389/fbioe.2014.00028

Heller, S. R., McNaught, A., Pletnev, I., Stein, S., and Tchekhovskoi, D. (2015). InChI, the IUPAC international chemical identifier. *J. Cheminform.* 7, 23. doi: 10.1186/s13321-015-0068-4

Henry, C. S., DeJongh, M., Best, A. A., Frybarger, P. M., Linsay, B., and Stevens, R. L. (2010). High-throughput generation, optimization and analysis of genome-scale metabolic models. *Nat. Biotechnol.* 28, 977–982. doi: 10.1038/nbt.1672

Hucka, M., Bergmann, F. T., Chaouiya, C., Dräger, A., Hoops, S., Keating, S. M., et al. (2019). Systems biology markup language (SBML) level 3 version 2 core release 2. *J. Integr. Bioinform.* 16, 1. doi: 10.1515/jib-2019-0021

Hucka, M., Bergmann, F. T., Dräger, A., Hoops, S., Keating, S. M., Le Novère, N., et al. (2018). systems biology markup language (SBML) level 3 version 1 core. *J, Integr, Bioinform.* 15, 1. doi: 10.1515/jib-2017-0080

Hucka, M., and Smith, L. P. (2016). SBML Level 3 package: groups, version 1 release 1. *J. Integr. Bioinform.* 13, 1. doi: 10.1515/jib-2016-290

Hüser, A. T., Chassagnole, C., Lindley, N. D., Merkamm, M., Guyonvarch, A., Elišáková, V., et al. (2005). Rational design of a *Corynebacterium glutamicum* pantothenate production strain and its characterization by metabolic flux analysis and genome-wide transcriptional profiling. *Appl. Environ. Microbiol.* 71, 3255–3268. doi: 10.1128/AEM.71.6.3255-3268.2005

Inui, M., Kawaguchi, H., Murakami, S., Vertès, A. A., and Yukawa, H. (2004a). Metabolic engineering of *Corynebacterium glutamicum* for fuel ethanol production under oxygen-deprivation conditions. *J. Mol. Microbiol. Biotechnol.* 8, 243–254. doi: 10.1159/000086705

Inui, M., Murakami, S., Okino, S., Kawaguchi, H., Vertès, A. A., and Yukawa, H. (2004b). Metabolic analysis of *Corynebacterium glutamicum* during lactate and succinate productions under oxygen deprivation conditions. *J. Mol. Microbiol. Biotechnol.* 7, 182–196. doi: 10.1159/000079827

Jadebeck, J. F., Theorell, A., Leweke, S., and Nöh, K. (2020). Hops: high-performance library for (non-) uniform sampling of convex-constrained models. *Bioinformatics* 37, 1776–1777. doi: 10.1093/bioinformatics/btaa872

Jojima, T., Noburyu, R., Sasaki, M., Tajima, T., Suda, M., Yukawa, H., et al. (2015). Metabolic engineering for improved production of ethanol by *Corynebacterium glutamicum*. *Appl. Microbiol. Biotechnol.* 99, 1165–1172. doi: 10.1007/s00253-014-6223-4

Juty, N., Le Novère, N., and Laibe, C. (2012). Identifiers.org and MIRIAM Registry: community resources to provide persistent identification. *Nucleic Acids Res*. 40, D580–D586. doi: 10.1093/nar/gkr1097

Kalinowski, J., Bathe, B., Bartels, D., Bischoff, N., Bott, M., Burkovski, A., et al. (2003). The complete *Corynebacterium glutamicum* ATCC 13032 genome sequence and its impact on the production of L-aspartate-derived amino acids and vitamins. *J. Biotechnol*. 104, 5–25. doi: 10.1016/S0168-1656(03)00154-8

Kanehisa, M., Sato, Y., Furumichi, M., Morishima, K., and Tanabe, M. (2019). New approach for understanding genome variations in KEGG. *Nucleic Acids Res*. 47, D590–D595. doi: 10.1093/nar/gky962

Kang, M.-K., Eom, J.-H., Kim, Y., Um, Y., and Woo, H. M. (2014). Biosynthesis of pinene from glucose using metabolically-engineered *Corynebacterium glutamicum*. *Biotechnol. Lett*. 36, 2069–2077. doi: 10.1007/s10529-014-1578-2

Kanzaki, T., Sugiyama, Y., Kitano, K., Ashida, Y., and Imada, I. (1974). Quinones of brevibacterium. *Biochim. Biophys Acta* 348, 162–165. doi: 10.1016/0005-2760(74)90102-7

Karp, P. D., Billington, R., Caspi, R., Fulcher, C. A., Latendresse, M., Kothari, A., et al. (2019). The BioCyc collection of microbial genomes and metabolic pathways. *Brief. Bioinform*. 20, 1085–1093. doi: 10.1093/bib/bbx085

Keating, S. M., Waltemath, D., König, M., Zhang, F., Dräger, A., Chaouiya, C., et al. (2020). SBML Level 3: an extensible format for the exchange and reuse of biological models. *Mol. Syst. Biol*. 16, e9110. doi: 10.15252/msb.20199110

Keilhauer, C., Eggeling, L., and Sahm, H. (1993). Isoleucine synthesis in *Corynebacterium glutamicum*: molecular analysis of the ilvB-ilvN-ilvC operon. *J. Bacteriol*. 175, 5595–5603. doi: 10.1128/jb.175.17.5595-5603.1993

Kimura, E. (2005). "19 L-glutamate production," in *Handbook of Corynebacterium glutamicum* (Boca Raton, FL), 439.

Kind, S., Jeong, W. K., Schröder, H., and Wittmann, C. (2010a). Systems-wide metabolic pathway engineering in *Corynebacterium glutamicum* for bio-based production of diaminopentane. *Metab. Eng*. 12, 341–351. doi: 10.1016/j.ymben.2010.03.005

Kind, S., Jeong, W. K., Schröder, H., Zelder, O., and Wittmann, C. (2010b). Identification and elimination of the competing N-acetyldiaminopentane pathway for improved production of diaminopentane by *Corynebacterium glutamicum*. *Appl. Environ. Microbiol*. 76, 5175–5180. doi: 10.1128/AEM.00834-10

King, Z. A., Dräger, A., Ebrahim, A., Sonnenschein, N., Lewis, N. E., and Palsson, B. O. (2015). Escher: a web application for building, sharing, and embedding data-rich visualizations of biological pathways. *PLoS Comput. Biol*. 11:e1004321. doi: 10.1371/journal.pcbi.1004321

Kjeldsen, K. R., and Nielsen, J. (2009). *In silico* genome-scale reconstruction and validation of the *Corynebacterium glutamicum* metabolic network. *Biotechnol. Bioeng*. 102, 583–597. doi: 10.1002/bit.22067

Koch-Koerfges, A., Pfelzer, N., Platzen, L., Oldiges, M., and Bott, M. (2013). Conversion of *Corynebacterium glutamicum* from an aerobic respiring to an aerobic fermenting bacterium by inactivation of the respiratory chain. *Biochim. Biophys. Acta* 1827, 699–708. doi: 10.1016/j.bbabio.2013.02.004

König, M. (2020). matthiaskoenig/fbc_curation: 0.1.6. doi: 10.5281/zenodo.3708271

Lachance, J.-C., Lloyd, C. J., Monk, J. M., Yang, L., Sastry, A. V., Seif, Y., et al. (2019). BOFdat: Generating biomass objective functions for genome-scale metabolic models from experimental data. *PLoS Comput. Biol*. 15:e1006971. doi: 10.1371/journal.pcbi.1006971

Le Novè, N., Finney, A., Hucka, M., Bhalla, U. S., Campagne, F., Collado-Vides, J., et al. (2005). Minimum information requested in the annotation of biochemical models (MIRIAM). *Nat. Biotechnol*. 23, 1509–1515. doi: 10.1038/nbt1156

Liebl, W. (2005). "Corynebacterium taxonomy," in *Handbook of Corynebacterium glutamicum* (Boca Raton, FL: CRC Press), 9–34.

Lieven, C., Beber, M. E., Olivier, B. G., Bergmann, F. T., Ataman, M., Babaei, P., et al. (2020). MEMOTE for standardized genome-scale metabolic model testing. *Nat. Biotechnol*. 38, 272–276. doi: 10.1038/s41587-020-0446-y

Liu, Q., Ouyang, S.-P., Kim, J., and Chen, G.-Q. (2007). The impact of PHB accumulation on L-glutamate production by recombinant *Corynebacterium glutamicum*. *J. Biotechnol*. 132, 273–279. doi: 10.1016/j.jbiotec.2007.03.014

Lombardot, T., Morgat, A., Axelsen, K. B., Aimo, L., Hyka-Nouspikel, N., Niknejad, A., et al. (2019). Updates in Rhea: SPARQLing biochemical reaction data. *Nucleic Acids Res*. 47, D596–D600. doi: 10.1093/nar/gky876

Machado, D., Andrejev, S., Tramontano, M., and Patil, K. R. (2018). Fast automated reconstruction of genome-scale metabolic models for microbial species and communities. *Nucleic Acids Res*. 46, 7542–7553. doi: 10.1093/nar/gky537

Maeda, T., Koch-Koerfges, A., and Bott, M. (2020). Relevance of nadh dehydrogenase and alternative two-enzyme systems for growth of corynebacterium glutamicum with glucose, lactate, and acetate. *Front. Bioeng. Biotechnol*. 8:621213. doi: 10.3389/fbioe.2020.621213

Maglott, D., Ostell, J., Pruitt, K. D., and Tatusova, T. (2005). Entrez Gene: gene-centered information at NCBI. *Nucleic Acids Res*. 33(Suppl_1):D54–D58. doi: 10.1093/nar/gki031

Malik-Sheriff, R. S., Glont, M., Nguyen, T. V. N., Tiwari, K., Roberts, M. G., Xavier, A., et al. (2020). BioModels–15 years of sharing computational models in life science. *Nucleic Acids Res*. 48, D407–D415. doi: 10.1093/nar/gkz1055

Man, Z., Xu, M., Rao, Z., Guo, J., Yang, T., Zhang, X., et al. (2016). Systems pathway engineering of *Corynebacterium crenatum* for improved L-arginine production. *Sci. Rep*. 6, 1–10. doi: 10.1038/srep28629

Marx, A., de Graaf, A. A., Wiechert, W., Eggeling, L., and Sahm, H. (1996). Determination of the fluxes in the central metabolism of *Corynebacterium glutamicum* by nuclear magnetic resonance spectroscopy combined with metabolite balancing. *Biotechnol. Bioeng*. 49, 111–129. doi: 10.1002/(SICI)1097-0290(19960120)49:2andlt;111::AID-BIT1andgt;3.0.CO;2-T

Michel, A., Koch-Koerfges, A., Krumbach, K., Brocker, M., and Bott, M. (2015). Anaerobic growth of *Corynebacterium glutamicum* via mixed-acid fermentation. *Appl. Environ. Microbiol*. 81, 7496–7508. doi: 10.1128/AEM.02413-15

Dräger, A. (2021). Table2model: 1.0.1.

Moretti, S., Tran, V. D. T., Mehl, F., Ibberson, M., and Pagni, M. (2021). MetaNetX/MNXref: unified namespace for metabolites and biochemical reactions in the context of metabolic models. *Nucleic Acids Res*. 49, D570–D574. doi: 10.1093/nar/gkaa992

Morgat, A., Coissac, E., Coudert, E., Axelsen, K. B., Keller, G., Bairoch, A., et al. (2011). UniPathway: a resource for the exploration and annotation of metabolic pathways. *Nucleic Acids Res*. 40, D761–D769. doi: 10.1093/nar/gkr1023

Moritz, B., Striegel, K., de Graaf, A. A., and Sahm, H. (2000). Kinetic properties of the glucose-6-phosphate and 6 phosphogluconate dehydrogenases from *Corynebacterium glutamicum* and their application for predicting pentose phosphate pathway flux *in vivo*. *Eur. J. Biochem*. 267, 3442–3452. doi: 10.1046/j.1432-1327.2000.01354.x

Neal, M. L., König, M., Nickerson, D., Mısırlı, G., Kalbasi, R., Dräger, A., et al. (2018). Harmonizing semantic annotations for computational models in biology. *Brief. Bioinform*. 20, 540–550. doi: 10.1101/246470

Neidhardt, F. C., Ingraham, J. L., and Schaechter, M. (1990). *Physiology of the Bacterial Cell: A Molecular Approach, Vol. 20*. Sunderland, MA: Sinauer Associates.

Niimi, S., Suzuki, N., Inui, M., and Yukawa, H. (2011). Metabolic engineering of 1,2-propanediol pathways in *Corynebacterium glutamicum*. *Appl. Microbiol. Biotechnol*. 90, 1721–1729. doi: 10.1007/s00253-011-3190-x

Norsigian, C. J., Pusarla, N., McConn, J. L., Yurkovich, J. T., Dräger, A., Palsson, B. O., et al. (2019). BiGG Models 2020: multi-strain genome-scale models and expansion across the phylogenetic tree. *Nucleic Acids Res*. 48:gkz1054. doi: 10.1093/nar/gkz1054

Okino, S., Suda, M., Fujikura, K., Inui, M., and Yukawa, H. (2008). Production of L-lactic acid by *Corynebacterium glutamicum* under oxygen deprivation. *Appl. Microbiol. Biotechnol*. 78, 449–454. doi: 10.1007/s00253-007-1336-7

Olivier, B. G., and Bergmann, F. T. (2018). SBML level 3 package: flux balance constraints version 2. *J. Integr. Bioinform*. 15:20170082. doi: 10.1515/jib-2017-0082

Orth, J. D., Conrad, T. M., Na, J., Lerman, J. A., Nam, H., Feist, A. M., et al. (2011). A comprehensive genome-scale reconstruction of *Escherichia coli* metabolism" 2011. *Mol. Syst. Biol*. 7, 535. doi: 10.1038/msb.2011.65

Panchiwala, H., Shah, S., Planatscher, H., Zakharchuk, M., König, M., and Dräger, A. (2021). The systems biology simulation core library. *Bioinformatics* doi: 10.1093/bioinformatics/btab669. [Epub ahead of print].

Petersen S, de Graaf AA, Eggeling L, Möllney M, Wiechert W, Sahm H. *In vivo* quantification of parallel and bidirectional fluxes in the

anaplerosis of Corynebacterium glutamicum. *J Biol Chem*. (2000) 275:35932–41. doi: 10.1074/jbc.M908728199

Peters-Wendisch, P. G., Schiel, B., Wendisch, V. F., Katsoulidis, E., Möckel, B., Sahm, H., et al. (2001). Pyruvate carboxylase is a major bottleneck for glutamate and lysine production by *Corynebacterium glutamicum*. *J. Mol. Microbiol. Biotechnol*. 3, 295–300.

Peters-Wendisch, P. G., Wendisch, V. F., Paul, S., Eikmanns, B. J., and Sahm, H. (1997). Pyruvate carboxylase as an anaplerotic enzyme in *Corynebacterium glutamicum*. *Microbiology* 143, 1095–1103. doi: 10.1099/00221287-143-4-1095

Pruitt, K. D., Tatusova, T., and Maglott, D. R. (2005). NCBI Reference Sequence (RefSeq): a curated non-redundant sequence database of genomes, transcripts and proteins. *Nucleic Acids Res*. 33(Suppl_1):D501–D504. doi: 10.1093/nar/gki025

Ravikrishnan, A., and Raman, K. (2015). Critical assessment of genome-scale metabolic networks: the need for a unified standard. *Brief. Bioinform*. 16, 1057–1068. doi: 10.1093/bib/bbv003

Renz, A., Mostolizadeh, R., and Dräger, A. (2020). "Clinical applications of metabolic models in SBML format," in *Systems Medicine, Vol. 3*, ed O. Wolkenhauer (Oxford: Academic Press), 362–371.

Rodriguez, N., Thomas, A., Watanabe, L., Vazirabad, I. Y., Kofia, V., Gómez, H. F., et al. (2015). JSBML 1.0: providing a smorgasbord of options to encode systems biology models. *Bioinformatics* 31, 3383–3386. doi: 10.1093/bioinformatics/btv341

Römer, M., Eichner, J., Dräger, A., Wrzodek, C., Wrzodek, F., and Zell, A. (2016). ZBIT bioinformatics toolbox: a web-platform for systems biology and expression data analysis. *PLoS ONE* 11:e0149263. doi: 10.1371/journal.pone.0149263

Rougny, A., Touré, V., Moodie, S., Balaur, I., Czauderna, T., Borlinghaus, H., et al. (2019). Systems biology graphical notation: process description language level 1 version 2.0. *J. Integr. Bioinform*. 16:20190022. doi: 10.1515/jib-2019-0022

Sambrook, J., Fritsch, E. F., and Maniatis, T. (1989). *Molecular Cloning: A Laboratory Manual, 2nd Edn*. Cold Spring Harbor, NY: Cold Spring Harbor Laboratory Press.

Sato, H., Orishimo, K., Shirai, T., Hirasawa, T., Nagahisa, K., Shimizu, H., et al. (2008). Distinct roles of two anaplerotic pathways in glutamate production induced by biotin limitation in *Corynebacterium glutamicum*. *J. Biosci. Bioeng*. 106, 51–58. doi: 10.1263/jbb.106.51

Schellenberger, J., Lewis, N. E., and Palsson, B., Ø. (2011). Elimination of thermodynamically infeasible loops in steady-state metabolic models. *Biophys. J*. 100, 544–553. doi: 10.1016/j.bpj.2010.12.3707

Schneider, J., and Wendisch, V. F. (2010). Putrescine production by engineered *Corynebacterium glutamicum*. *Appl. Microbiol. Biotechnol*. 88, 859–868. doi: 10.1007/s00253-010-2778-x

Scott, M., Gunderson, C. W., Mateescu, E. M., Zhang, Z., and Hwa, T. (2010). Interdependence of cell growth and gene expression: origins and consequences. *Science* 330, 1099–1102. doi: 10.1126/science.1192588

Shinfuku, Y., Sorpitiporn, N., Sono, M., Furusawa, C., Hirasawa, T., and Shimizu, H. (2009). Development and experimental verification of a genome-scale metabolic model for *Corynebacterium glutamicum*. *Microb. Cell Fact*. 8, 1–15. doi: 10.1186/1475-2859-8-43

Sud, M., Fahy, E., Cotter, D., Brown, A., Dennis, E. A., Glass, C. K., et al. (2007). Lmsd: Lipid maps structure database. *Nucleic Acids Res*. 35(Suppl_1):D527–D532. doi: 10.1093/nar/gkl838

Takeno, S., Ohnishi, J., Komatsu, T., Masaki, T., Sen, K., and Ikeda, M. (2007). Anaerobic growth and potential for amino acid production by nitrate respiration in *Corynebacterium glutamicum*. *Appl. Microbiol. Biotechnol*. 75, 1173–1182. doi: 10.1007/s00253-007-0926-8

Takeno, S., Takasaki, M., Urabayashi, A., Mimura, A., Muramatsu, T., Mitsuhashi, S., et al. (2013). Development of fatty acid-producing *Corynebacterium glutamicum* strains. *Appl. Environ. Microbiol*. 79, 6776–6783. doi: 10.1128/AEM.02003-13

Thiele, I., and Palsson, B., Ø. (2010). A protocol for generating a high-quality genome-scale metabolic reconstruction. *Nat. Protoc*. 5, 93. doi: 10.1038/nprot.2009.203

Touré, V., Dräger, A., Luna, A., Dogrusoz, U., and Rougny, A. (2020). The "Systems biology graphical notation: current status and applications in systems medicine," in *Systems Medicine, Vol. 3*, ed O. Wolkenhauer (Oxford: Academic Press), 372–381.

Unthan, S., Grünberger, A., van Ooyen, J., Gätgens, J., Heinrich, J., Paczia, N., et al. (2014). Beyond growth rate 0.6: What drives *Corynebacterium glutamicum* to higher growth rates in defined medium. *Biotechnol. Bioeng*. 111, 359–371. doi: 10.1002/bit.25103

Utagawa, T. (2004). Production of arginine by fermentation. *J. Nutr*. 134, 2854S–2857S. doi: 10.1093/jn/134.10.2854S

van Ooyen, J., Noack, S., Bott, M., Reth, A., and Eggeling, L. (2012). Improved L-lysine production with *Corynebacterium glutamicum* and systemic insight into citrate synthase flux and activity. *Biotechnol. Bioeng*. 109, 2070–2081. doi: 10.1002/bit.24486

Varma, A., and Palsson, B. O. (1994). Stoichiometric flux balance models quantitatively predict growth and metabolic by-product secretion in wild-type *Escherichia coli* W3110. *Appl. Environ. Microbiol*. 60, 3724–3731. doi: 10.1128/aem.60.10.3724-3731.1994

Vertes, A. A., Inui, M., and Yukawa, H. (2013). "The biotechnological potential of Corynebacterium glutamicum, from Umami to Chemurgy," in *Corynebacterium glutamicum* (Berlin; Heidelberg: Springer), 1–49. doi: 10.1007/978-3-642-29857-8_1

Wendisch, V. F., Jorge, J. M., Pérez-García, F., and Sgobba, E. (2016). Updates on industrial production of amino acids using *Corynebacterium glutamicum*. *World J. Microbiol. Biotechnol*. 32, 105. doi: 10.1007/s11274-016-2060-1

Wilkinson, M. D., Dumontier, M., Aalbersberg, I. J., Appleton, G., Axton, M., Baak, A., et al. (2016). The FAIR Guiding Principles for scientific data management and stewardship. *Sci. Data* 3, 1–9. doi: 10.1038/sdata.2016.18

Wishart, D. S., Tzur, D., Knox, C., Eisner, R., Guo, A. C., Young, N., et al. (2007). HMDB: the human metabolome database. *Nucleic Acids Res*. 35(Suppl_1):D521–D526. doi: 10.1093/nar/gkl923

Xavier, J. C., Patil, K. R., and Rocha, I. (2017). Integration of biomass formulations of genome-scale metabolic models with experimental data reveals universally essential cofactors in prokaryotes. *Metab. Eng*. 39, 200–208. doi: 10.1016/j.ymben.2016.12.002

Yamamoto, S., Suda, M., Niimi, S., Inui, M., and Yukawa, H. (2013). Strain optimization for efficient isobutanol production using *Corynebacterium glutamicum* under oxygen deprivation. *Biotechnol. Bioeng*. 110, 2938–2948. doi: 10.1002/bit.24961

Zelle, E., NÖh, K., and Wiechert, W. (2015). "Growth and production capabilities of Corynebacterium glutamicum: interrogating a genome-scale metabolic network model," in *Corynebacterium glutamicum: From Systems Biology to Biotechnological Applications*, ed A. Burkovski (Poole: Caister Academic Press), 39–54. doi: 10.21775/9781910190050.04

Zhang, Y., Cai, J., Shang, X., Wang, B., Liu, S., Chai, X., et al. (2017). A new genome-scale metabolic model of *Corynebacterium glutamicum* and its application. *Biotechnol, Biofuels* 10:169. doi: 10.1186/s13068-017-0856-3

Conflict of Interest: The authors declare that the research was conducted in the absence of any commercial or financial relationships that could be construed as a potential conflict of interest.

Publisher's Note: All claims expressed in this article are solely those of the authors and do not necessarily represent those of their affiliated organizations, or those of the publisher, the editors and the reviewers. Any product that may be evaluated in this article, or claim that may be made by its manufacturer, is not guaranteed or endorsed by the publisher.

frontiers in Bioengineering and Biotechnology

ORIGINAL RESEARCH
published: 15 November 2021
doi: 10.3389/fbioe.2021.746322

A Myo-Inositol-Inducible Expression System for *Corynebacterium glutamicum* and Its Application

Nan Lu†, Chenglin Zhang†, Wenjie Zhang, Haoran Xu, Yuhong Li, Minhua Wei, Jing Meng, Yan Meng, Junzhe Wang and Ning Chen**

College of Biotechnology, Tianjin University of Science and Technology, Tianjin, China

Corynebacterium glutamicum is one of the important industrial microorganisms for production of amino acids and other value-added compounds. Most expression vectors used in *C. glutamicum* are based on inducible promoter (P_{tac} or P_{trc}) activated by isopropyl-β-D-thiogalactopyranoside (IPTG). However, these vectors seem unsuitable for large-scale industrial production due to the high cost and toxicity of IPTG. Myo-inositol is an ideal inducer because of its non-toxicity and lower price. In this study, a myo-inositol-inducible expression vector pMI-4, derived from the expression vector pXMJ19, was constructed. Besides the original chloramphenicol resistance gene *cat*, multiple cloning sites, and *rrnB* terminator, the pMI-4 (6,643 bp) contains the $iolR^q$ cassette and the myo-inositol-inducible promoter P_{iolT1}. The pMI-4 could stably replicate in the *C. glutamicum* host. Meanwhile, the non-myo-inositol degradation host strain *C. glutamicumΔiolGΔoxiCΔoxiDΔoxiE* for maintaining the pMI-4 was developed. Overexpression of $hemA^M$ and *hemL* using pMI-4 resulted in a significant accumulation of 5-aminolevulinic acid, indicating its potential application in metabolic engineering and industrial fermentation.

Keywords: *Corynebacterium glutamicum*, expression vector, IolR, iolT1, myo-inositol, 5-aminolevulinic acid

OPEN ACCESS

Edited by:
Yu Wang,
Tianjin Institute of Industrial Biotechnology (CAS), China

Reviewed by:
Guoqiang Xu,
Jiangnan University, China
Suiping Zheng,
South China University of Technology, China

***Correspondence:**
Chenglin Zhang
zcl@tust.edu.cn
Ning Chen
ningch@tust.edu.cn

†These authors have contributed equally to this work

Specialty section:
This article was submitted to Synthetic Biology, a section of the journal Frontiers in Bioengineering and Biotechnology

Received: *23 July 2021*
Accepted: *05 October 2021*
Published: *15 November 2021*

Citation:
Lu N, Zhang C, Zhang W, Xu H, Li Y, Wei M, Meng J, Meng Y, Wang J and Chen N (2021) A Myo-Inositol-Inducible Expression System for Corynebacterium glutamicum *and Its Application. Front. Bioeng. Biotechnol. 9:746322. doi: 10.3389/fbioe.2021.746322*

INTRODUCTION

As a non-pathogenic Gram-positive bacterium, *Corynebacterium glutamicum* has been widely used in industrial biotechnology for the production of several million tons of amino acids annually, especially L-glutamate, L-lysine, and L-valine (Hasegawa et al., 2012; Eggeling and Bott, 2015; Wendisch, 2020). Besides amino acids, the current product spectrum that is accessible with *C. glutamicum* comprises organic acids, diamines, vitamins, aromates, and alcohols (Chen et al., 2016; Chung et al., 2017; Becker et al., 2018; Kogure and Inui, 2018; Sato et al., 2020). Benefiting from the genome annotation of *C. glutamicum* and the availability of molecular biology techniques and tools, significant progress has been made in designing production strains by metabolic engineering *via* rational approaches (Ikeda and Nakagawa, 2003; Nesvera and Patek, 2011; Suzuki and Inui, 2013; Wang et al., 2021).

Overexpression of genes encoding the rate-limiting enzymes involved in pathways is one of the most efficient strategies (Nesvera and Patek, 2011; Suzuki and Inui, 2013). Several vectors for gene overexpression in *C. glutamicum* have been developed, such as pXMJ19, pEC-XK-99E, and pDXW-8. Most of these expression vectors are based on inducible promoters (P_{tac} or P_{trc}) regulated by isopropyl-β-D-thiogalactopyranoside (IPTG) (Jakoby et al., 1999; Kirchner and Tauch, 2003; Xu

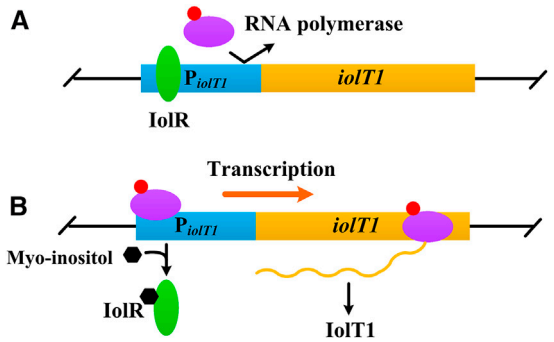

FIGURE 1 | Negative control of *iolT1* transcription. **(A)** No myo-inositol. The repressor IolR binds to the promoter of *iolT1* (P_{iolT1}) and blocks RNA polymerase from transcribing the *iolT1*. **(B)** With presence of myo-inositol. Myo-inositol as an inducer binds to the repressor IolR, resulting in its dissociation and allowing RNA polymerase to transcribe the *iolT1*.

et al., 2010; Li et al., 2020). However, IPTG is toxic to cell growth and expensive, which makes it unsuitable for industrial production (Li et al., 2020).

Myo-inositol, a water-soluble vitamin B group compound, is found to induce transcription of several genes involved in its transport and catabolism (**Figure 1**), such as *iolT1* (encoding myo-inositol transporter), *iolG* (encoding myo-inositol dehydrogenase), and *iolH* (encoding myo-inositol isomerases/epimerase) (Krings et al., 2006; You et al., 2020). Furthermore, this induction works regardless of whether the glucose is present or not (Krings et al., 2006; Klaffl et al., 2013). Besides, compared with IPTG, myo-inositol is much cheaper and non-toxic to cells (Krings et al., 2006; Takeno et al., 2016). Above all, myo-inositol seems an alternative inducer for gene expression in *C. glutamicum*.

In this study, a myo-inositol-inducible expression vector pMI-4 for *C. glutamicum* was constructed. Meanwhile, the chassis strain that is suitable for maintaining pMI-4 and unable to consume myo-inositol, *C. glutamicum*Δ*iolG*Δ*oxiC*Δ*oxiD*Δ*oxiE*, was developed. This constructed expression system was successfully applied to express $hemA^M$ (encoding glutamyl-tRNA reductase) and *hemL* (encoding glutamate-1-semialdehyde aminotransferase) for production of 5-aminolevulinic acid (5-ALA).

TABLE 1 | Strains and plasmids used in this study.

Strains/plasmids	Characteristics	Source
Strains		
Escherichia coli DH5α	F-, Δ(*lacZYA-argF*)U169 *recA1endA1 hsdR17*	Purchased from Invitrogen
Corynebacterium glutamicum ATCC 13032	Wild type	Laboratory stock
C. glutamicum/pMI-1-*gfp*	*C. glutamicum* ATCC 13032 harboring pMI-1-*gfp*	This work
C. glutamicum/pMI-3-*gfp*	*C. glutamicum* ATCC 13032 harboring pMI-3-*gfp*	This work
C. glutamicum/pMI-4-*gfp*	*C. glutamicum* ATCC 13032 harboring pMI-4-*gfp*	This work
*C. glutamicum*Δ*iolG* Δ*oxiC*Δ*oxiD*Δ*oxiE*	*C. glutamicum* ATCC 13032 in which Δ*iolG* and Δ*oxiC*-Δ*oxiD*-Δ*oxiE* cluster were deleted	This work
*C. glutamicum*Δ*iolG*Δ*oxiC*Δ*oxiD*Δ*oxiE*/pMI-4-*gfp*	*C. glutamicum*Δ*iolG*Δ*oxiC*Δ*oxiD*Δ*oxiE* harboring pMI-4-*gfp*	This work
AL-1	Native promoters of *ppc* and *gltA* were replaced by P_{tuf} in *C. glutamicum*Δ*iolG*Δ*oxiC*Δ*oxiD*Δ*oxiE*	This work
AL-CK1	AL-1 harboring pMI-4	This work
AL-2	AL-1 harboring pMI-4-$hemA^M$-*hemL*	This work
AL-CK2	AL-1 harboring pAL1	This work
AL-3	AL-2 with a copy of *pntAB* driven by P_{iolT1} in genome (*cgl 2000*:P_{iolT1}-*pntAB*)	This work
Plasmids		
pXMJ19	Cm^r, P_{tac}-MCS	Jakoby et al. (1999)
pEGFP-N1	Kan^r, *gfp*	Laboratory stock
pK18*mobsacB*	Integration vector, Kan^r, *sacB*	Schäfer, et al. (1994)
pMI-1	pXMJ19Δ*lacI*ΔP_{tac}	This work
pMI-2	pMI-1 with P_{iolT1}	This work
pMI-3	pMI-2 with *iolR* cassette	This work
pMI-4	pMI-2 with *iolR* cassette driven by P_{tuf}	This work
pMI-3-*gfp*	pMI-3 harboring *gfp*	This work
pMI-4-*gfp*	pMI-4 harboring *gfp*	This work
pAL1	pXMJ19 harboring $hemA^M$ and *hemL* located tandemly in one operon	Zhang et al. (2020)
pMI-4-$hemA^M$-*hemL*	pMI-4 harboring $hemA^M$ and *hemL* located tandemly in one operon	This work
pK18*mobsacB*Δ*iolG*	pK18*mobsacB* harboring upstream homologous arm (UHA) and downstream homologous arm (DHA) of *iolG*	This work
pK18*mobsacB*Δ*oxiII*	pK18*mobsacB* harboring UHA and DHA of Δ*oxiC*-Δ*oxiD*-Δ*oxiE* cluster	This work
pK18*mobsacB*P_{tuf}:P_{ppc}	pK18*mobsacB* harboring P_{ppc} UHA, P_{tuf}, and P_{ppc} DHA	Zhang et al. (2018)
pK18*mobsacB*P_{tuf}:P_{gltA}	pK18*mobsacB* harboring P_{gltA} UHA, P_{tuf}, and P_{gltA} DHA	Zhang et al. (2018)
pK18*mobsacB*cgl *2000*:P_{iolT1}-*pntAB*	pK18*mobsacB* harboring UHA and DHA of *cgl 2000* and P_{iolT1}-*pntAB*	This work

MATERIALS AND METHODS

Bacterial Strains, Media, and Cultivation Conditions

The strains and plasmids used are listed in **Table 1**. *Escherichia coli*, used for recombinant DNA experiments, was cultured in lysogeny broth medium at 37°C. *C. glutamicum* ATCC 13032 and its recombinants were cultured at 30°C in Brain Heart Infusion (BHI) medium or CGXII medium. Modified CGXII medium [50 g/l glucose, 15 g/L $(NH_4)_2SO_4$, 2 g/l yeast extract, 4 g/l tryptone, 1 g/l KH_2PO_4, 0.25 g/l $MgSO_4{\cdot}7H_2O$, 42 g/l 3-morpholinopropanesulfonic acid, 10 mg/l $CaCl_2$, 0.1 mg/l $FeSO_4{\cdot}7H_2O$, 0.1 mg/l $MnSO_4{\cdot}7H_2O$, 1 mg/l $ZnSO_4{\cdot}7H_2O$, 0.2 mg/l $CuSO_4$, 0.02 mg/l $NiCl_2{\cdot}6H_2O$, and 0.2 mg/l biotin] was used for production of 5-ALA. When necessary, media were supplemented with 20 μg/ml chloramphenicol or 40 μg/ml kanamycin.

To investigate the effect of myo-inositol on cell growth, *C. glutamicum* ATCC 13032 cells were cultivated in CGXII containing 0.1–100 mM of myo-inositol, and the optical density at 600 nm (OD_{600}) was determined after cultivation of 48 h at 30°C with shaking at 200 rpm. To investigate the effect of myo-inositol on glucose utilization, *C. glutamicum*Δ*iolG*Δ*oxiC*Δ*oxiD*Δ*oxiE* cells were cultivated in CGXII medium containing 5 mM of myo-inositol or not at 30°C with shaking at 200 rpm. The final concentration of glucose was determined after cultivation of 48 h.

Construction of Strains and Plasmids

All the primers used in this study are listed in **Supplementary Table S1**. *E. coli* DH5α was used for vector construction experiments. *C. glutamicum* ATCC 13032 was used as a base strain for investigating the characteristics of plasmids and for construction of the non-myo-inositol-degrading host. Preparation of competent cells and transformation were performed according to the standard protocols (Sambrook and Russell, 2001; Eggeling and Bott, 2005). Strains and plasmids were constructed as follows.

The plasmid pXMJ19 was used as the backbone. The fragments amplified from pXMJ19 with primers PX-1 and PX-2 were digested by *Hpa* I and were subsequently self-ligated to obtain pMI-1. P_{iolT1} was amplified with primers PX-3 and PX-4 from genomic DNA of *C. glutamicum* ATCC 13032, and the resulting fragments were ligated to *Hpa* I-digested pMI-1 using a ClonExpress II One Step Cloning Kit, generating pMI-2. Similarly, fragments of *iolR* cassette amplified with primers PX-5 and PX-6 were ligated to pMI-2, resulting in pMI-3. Primers PX-7/tuf-iolR-1 and tuf-iolR-2/PX-6 were used to amplify *iolR* cassette (without the native promoter) and the constitutive promoter P_{tuf}. The fragments were fused using overlap PCR and then were ligated to pMI-2 to obtain pMI-4. Primers gfp-1 and gfp-2 were used to amplify *gfp* from vector pEGFP-N1, which was ligated into *Hind* III-digested pMI-3 and pMI-4, resulting in pMI-3-*gfp* and pMI-4-*gfp*, respectively. The fused $hemA^M$-*hemL* was amplified with primers PAL-1 and PAL-2 from pAL1 (Zhang et al., 2020) and was ligated into *Hind* III-digested pMI-4, resulting in pMI-4-$hemA^M$-*hemL*.

Primers iolG-1/iolG-2 and iolG-3/iolG-4 were used to amplify the upstream homologous arm and downstream homologous arm of *iolG* from *C. glutamicum* ATCC 13032. The fragments were fused using overlap PCR, and the resulting fragments were ligated to *Xba* I/*Eco*R I-digested pK18mob*sacB*, generating pK18*mobsacB*Δ*iolG*; similarly, pK18*mobsacB*Δ*oxiII* for deleting *oxiC-oxiD-oxiE* cluster as well as pK18*mobsacBcgl 2000*: P_{iolT1}-*pntAB* for *pntAB* integration were constructed. Knockout of *iolG* and *oxiC-oxiD-oxiE* cluster occurred *via* two successive recombination events using pK18*mobsacB*Δ*iolG* and pK18*mobsacB*Δ*oxiII* to generate *C. glutamicum*Δ*iolG*Δ*oxiC*Δ*oxiD*Δ*oxiE*. AL-1 and AL-3 were constructed using the same approach.

The plasmids pMI-3-*gfp* and pMI-4-*gfp* were transformed into *C. glutamicum* ATCC 13032, and pMI-4-$hemA^M$-*hemL* was transformed into AL-1, obtaining *C. glutamicum*/pMI-3-*gfp*, *C. glutamicum*/pMI-4-*gfp*, and AL-2, respectively.

Stability Analysis of pMI-4

*C. glutamicum*Δ*iolG*Δ*oxiC*Δ*oxiD*Δ*oxiE*/pMI-4 and *C. glutamicum*Δ*iolG*Δ*oxiC*Δ*oxiD*Δ*oxiE*/pXMJ19 were respectively inoculated in BHI medium containing chloramphenicol and were cultivated overnight at 30°C with shaking at 200 rpm as the seed. The seed was then inoculated into BHI medium without chloramphenicol and was cultivated at 30°C for 30 generations. Samples were taken every five generations. After appropriate dilution, they were spread on BHI plates with or without chloramphenicol, followed by incubation for 24 h. The ratio of colonies on BHI with chloramphenicol/colonies on BHI without chloramphenicol was used to determine the stability.

Conditions for 5-ALA Production

A single colony was transferred to 5 ml BHI medium and was cultivated overnight at 30°C with shaking at 200 rpm. Next, the culture was inoculated into a 500-ml shake flask containing 45 ml of modified CGXII medium for a 64-h incubation at 30°C, 200 rpm. To induce gene expression, myo-inositol was added at a final concentration of 0.1–5 mM when the OD_{600} of cell reached approximately 0.8.

Detection of GFP Activity

C. glutamicum/pMI-1-*gfp*, *C. glutamicum*/pMI-3-*gfp*, and *C. glutamicum*/pMI-4-*gfp* were respectively grown overnight in 24-deep-well plates containing 2 ml/well CGXII medium. Then, 20 μl of each culture were inoculated into 2 ml fresh CGXII medium and grown for 24 h. Fluorescence intensities normalized against culture OD_{600} (determined using a Synergy H4 Microplate Reader, BioTek, United States) were used to indicate the expression level of GFP (Peng et al., 2017).

Real-Time Quantitative PCR

The transcriptional level of *gfp*, $hemA^M$, and *pntAB* was quantified using real-time quantitative PCR. Total RNA was extracted after 4 h of induction by myo-inositol using RNAiso

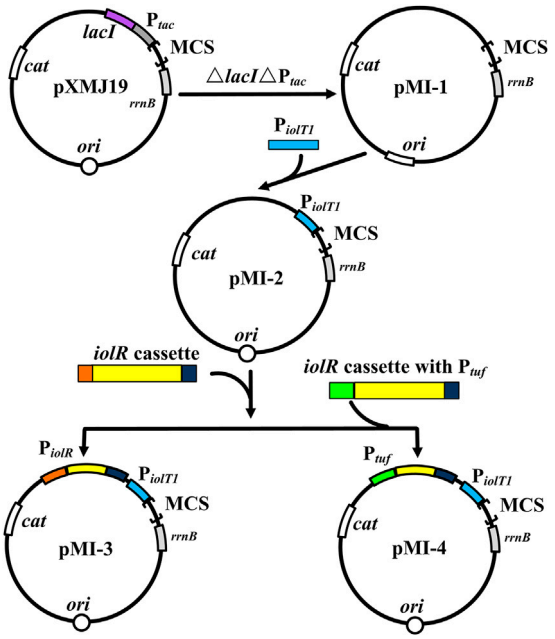

FIGURE 2 | Construction of pMI-4. MCS, multiple cloning sites; *cat*, chloramphenicol resistance gene; *rrnB*, the transcriptional terminator; P_{tac}, *tac* promoter; *lacI*, repressor LacI of P_{tac}-encoding gene; *ori*, the origin of replication for *C. glutamicum*; P_{iolT1}, *iolT1* promoter; *iolR* cassette, fragment comprises promoter, encoding sequence, and terminator of *iolR*; P_{tuf}, promoter of the gene encoding elongation factor TU.

Plus (Takara Bio Inc., Dalian, China), and cDNA was obtained by reverse transcription with a PrimeScript RT Reagent Kit (Takara Bio Inc., Dalian, China). Gene transcription levels were measured using SYBR Premix Ex TaqTM II (Takara Bio Inc., Dalian, China), and 16S rDNA was used as an internal control. Data were analyzed using the $2^{-\Delta\Delta CT}$ method (Livak and Schmittgen, 2001).

Analytical Procedure

Cell growth was monitored by measuring the OD_{600}. Concentrations of 5-ALA were measured with modified Ehrlich's reagent (Mauzerall and Granick, 1956). Briefly, the supernatants of cultures were reacted with acetylacetone (in sodium acetate buffer, pH 4.8, 1.0 M) at 80°C for 20 min. The absorbance at 553 nm was measured 30 min after adding of the modified Ehrlich's reagent. *C. glutamicum* cells grown in CGXII medium for 24 h were harvested by centrifugation at 4°C and 13,000×*g* for 10 min. The intracellular NADPH was quantified using an Enzychrom $NADP^+$/NADPH assay kit, following the manufacturer's instruction. The myo-inositol concentrations were determined by HPLC (Bio-Rad Aminex HPX-87H column) with 5 mM H_2SO_4 as the mobile phase and a refractive index detector (Lu et al., 2018).

Statistical Analysis

Statistical significance was determined by one-way analysis of variance, followed by Dunnett's multiple comparison test. The data are average of three biological replicates with error bars representing standard deviation. Results with *p* values of less than or equal to 0.05 were considered significant.

RESULTS AND DISCUSSION

Construction of Myo-Inositol-Inducing Expression Vector pMI-4

To verify the non-toxicity of myo-inositol to cell growth, *C. glutamicum* ATCC 13032 cells were cultivated in a medium containing different concentrations of myo-inositol (0.1–100 mM). The biomass of the cells under each concentration of myo-inositol exhibited no difference and was similar with those in the medium without myo-inositol (**Supplementary Figure S1**), indicating the non-toxicity of myo-inositol to cell growth. The myo-inositol-inducing vector pMI-4 was constructed for use in *C. glutamicum* as shown in **Figure 2**. The plasmid pXMJ19, carrying the chloramphenicol resistance gene *cat* and the inducible promoter P_{tac}, was used as the backbone (Jakoby et al., 1999). Herein, P_{iolT1} of *C. glutamicum*, the promoter of myo-inositol transport protein encoding gene *iolT1*, was used. P_{iolT1} is a myo-inositol-inducing promoter, which is repressed by the repressor IolR (encoded by *iolR*) in the absence of myo-inositol, but was active in the presence of myo-inositol (**Figure 1**). Initially, the P_{tac} and $lacI^q$ cassette were removed from pXMJ19, generating pMI-1 (5,281 bp). Subsequently, the P_{iolT1} was introduced to the upstream of multi-cloning sites in pMI-1, resulting in pMI-2 (5,488 bp). Finally, the *iolR* cassette from *C. glutamicum* ATCC 13032 was introduced to the upstream of P_{iolT1} in pMI-2, resulting in pMI-3 (6,750 bp).

In order to investigate whether pMI-3 was induced by myo-inositol, the *gfp* gene encoding green fluorescent protein was introduced to pMI-1 and pMI-3, resulting in pMI-1-*gfp* (as a control) and pMI-3-*gfp*, respectively. These two plasmids were respectively transformed into *C. glutamicum* ATCC 13032 to generate *C. glutamicum*/pMI-1-*gfp* and *C. glutamicum*/pMI-3-*gfp*. The GFP activities in *C. glutamicum*/pMI-1-*gfp* and *C. glutamicum*/pMI-3-*gfp* were determined. As shown in **Figure 3A**, GFP activity was hardly detected in the control strain *C. glutamicum*/pMI-1-*gfp* neither in the presence nor the absence of myo-inositol. In contrast, *C. glutamicum*/pMI-3-*gfp* exhibited significant GFP fluorescence (fluorescence/OD_{600}, 167.1) in the presence of myo-inositol, indicating that pMI-3 was myo-inositol inducible.

Notably, considerable GFP fluorescence of *C. glutamicum*/pMI-3-*gfp* was also observed in the absence of myo-inositol (fluorescence/OD_{600}, 50.3), indicating the leaky expression of GFP. It was probably due to the negative auto-regulation of *iolR* gene (Krings et al., 2006; Klaffl et al., 2013). To verify our hypothesis, the native promoter in *iolR* cassette was replaced with the constitutive promoter *tuf* to generate $iolR^q$ cassette, which was then inserted into pMI-2 (resulting in pMI-4, 6,643 bp). The *gfp* gene was introduced to pMI-4, generating pMI-4-*gfp*, and was subsequently transformed into *C. glutamicum* ATCC 13032 to generate *C. glutamicum*/pMI-4-*gfp*. As shown in **Figure 3A**, GFP of *C. glutamicum*/pMI-4-*gfp*

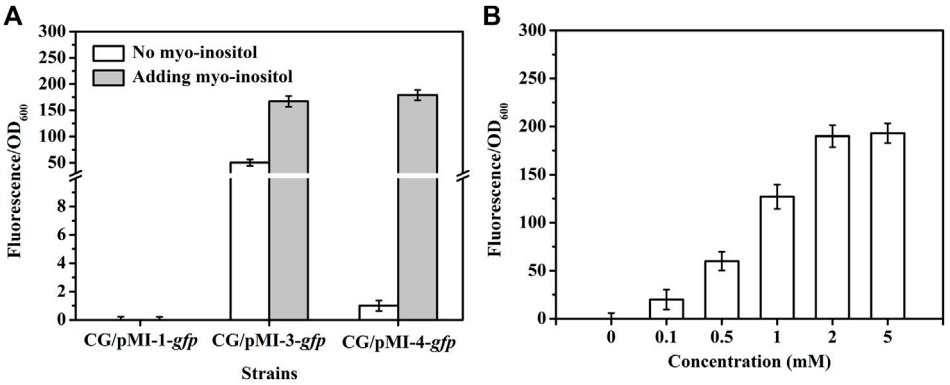

FIGURE 3 | GFP fluorescence intensities in *C. glutamicum* strains. **(A)** GFP fluorescence intensities in *C. glutamicum* strains harboring different vectors in the absence (white) or presence of myo-inositol (gray). CG/pMI-1-*gfp*, CG/pMI-3-*gfp*, and CG/pMI-4-*gfp* indicate *C. glutamicum*/pMI-1-*gfp*, *C. glutamicum*/pMI-3-*gfp*, and *C. glutamicum*/pMI-4-*gfp*, respectively. *C. glutamicum*/pMI-1-*gfp* was used as a control. In this strain, GFP was not expressed because pMI-1-*gfp* lacks a promoter. The vector pMI-3-*gfp* contains P_{iolT1} and *iolR* cassette with its native promoter P_{iolR}, and the vector pMI-4-*gfp* contains P_{iolT1} and $iolR^q$ cassette with the constitutive P_{tuf}. **(B)** The effect of myo-inositol concentrations on GFP expression in *C. glutamicum*/pMI-4-*gfp*. *C. glutamicum*/pMI-4-*gfp* was induced by myo-inositol at different concentrations.

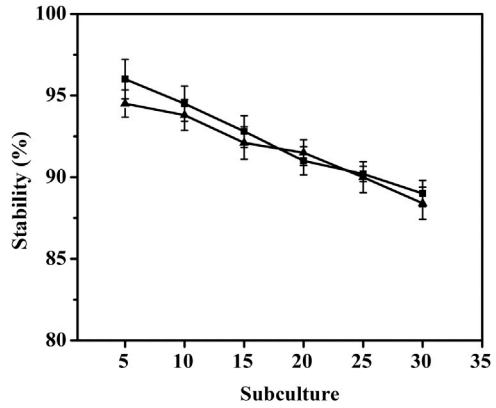

FIGURE 4 | Stability of the vector pMI-4. Filled square (■) represents *C. glutamicum*/pMI-4, and filled triangle (▲) represents *C. glutamicum*/pXMJ19.

was only active in the presence of myo-inositol (fluorescence/OD_{600}, 179.3). This result indicated the non-leaky expression of GFP in the pMI-4-*gfp* with $iolR^q$.

To further investigate the characteristics of pMI-4, the effect of myo-inositol concentration on GFP expression in *C. glutamicum*/pMI-4-*gfp* was determined. As shown in**Figure 3B**, the GFP fluorescence intensities were reinforced with the increase of myo-inositol concentration and then reached a constant level (approximately 190), indicating the dose-dependent effects of myo-inositol on GFP expression when the myo-inositol concentration was below 2 mM.

To investigate the stability of pMI-4 in *C. glutamicum*, it was transformed into *C. glutamicum* ATCC 13032 to generate *C. glutamicum*/pMI-4, and *C. glutamicum*/pXMJ19 was used a control. As shown in **Figure 4**, no significant difference in the stability of the vectors pMI-4 (approximately 96%–88%) and pXMJ19 was observed after 30 generations without chloramphenicol.

Blocking Myo-Inositol Degradation Pathway in *C. glutamicum*

To further test the applicability of pMI-4, the transcriptional level of *gfp* in *C. glutamicum*/pMI-4-*gfp* was detected during the fermentation. As shown in **Figure 5A**, the transcriptional level of *gfp* was gradually increased during the first 16 h of fermentation, but sharply declined after then. It was supposed that myo-inositol was utilized by cells, and the lowered concentration resulted in the recovery of IolR depression (Krings et al., 2006). Then, the concentration of myo-inositol was detected, and its consumption was found to start at 8 h (**Figure 5A**). Therefore, it was essential to block the degradation of myo-inositol to maintain its concentration at a constant level.

Myo-inositol dehydrogenase is the first enzyme responsible for degradation of myo-inositol (Krings et al., 2006). There are four myo-inositol dehydrogenase isozymes (encoded by *iolG*, *oxiC*, *oxiD*, and *oxiE*, respectively) in *C. glutamicum*. These four genes were deleted in *C. glutamicum* ATCC 13032. The generated *C. glutamicum*Δ*iolG*Δ*oxiC*Δ*oxiD*Δ*oxiE* was cultivated on CGXII containing myo-inositol (20 g/l) as carbon source to investigate its ability of myo-inositol utilization. As shown in **Figure 6**, unlike the wild-type *C. glutamicum* ATCC13032, *C. glutamicum*Δ*iolG*Δ*oxiC*Δ*oxiD*Δ*oxiE* was not able to grow on myo-inositol. Whereas, its growth on glucose was hardly affected compared with *C. glutamicum* ATCC13032, indicating that deleting the myo-inositol dehydrogenase isozymes resulted in the disability of myo-inositol degradation but did not affect the growth on glucose. To investigate the effect of myo-inositol on glucose utilization by *C. glutamicum*Δ*iolG*Δ*oxiC*Δ*oxiD*Δ*oxiE*, the cells were cultivated in CGXII medium containing 5 mM of myo-inositol (the maximum dose for induction). No significant differences in cell growth and glucose consumption were

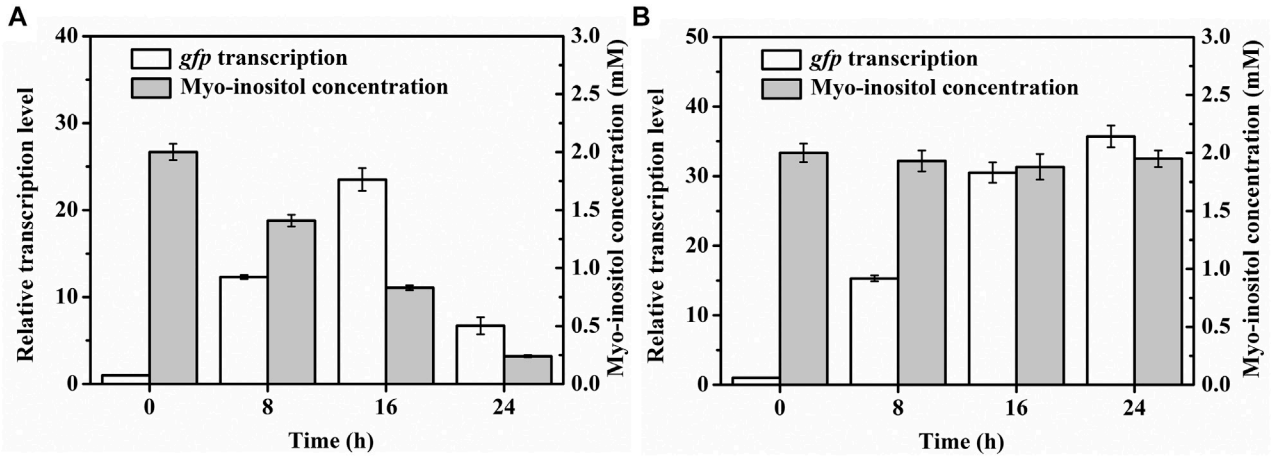

FIGURE 5 | Transcriptional levels of *gfp* in *C. glutamicum* strains during the cultivation process. **(A)** Transcriptional levels of *gfp* in *C. glutamicum*/pMI-4-*gfp* and the myo-inositol concentrations during the cultivation process. **(B)** Transcriptional levels of *gfp* in *C. glutamicumΔiolGΔoxiCΔoxiDΔoxiE*/pMI-4-*gfp* and the myo-inositol concentrations during the cultivation process.

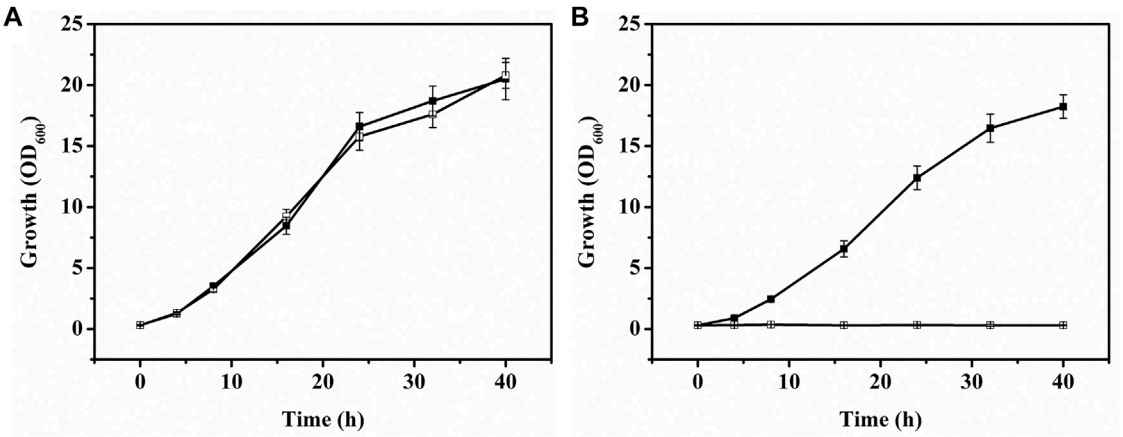

FIGURE 6 | Growth of *C. glutamicum* strains on glucose or myo-inositol. **(A)** Growth of *C. glutamicum* ATCC 13032 [filled square (■)] and *C. glutamicumΔiolGΔoxiCΔoxiDΔoxiE* [white square (□)] on glucose. **(B)** Growth of *C. glutamicum* ATCC 13032 [filled square (■)] and *C. glutamicumΔiolGΔoxiCΔoxiDΔoxiE* [white square (□)] on myo-inositol.

observed between the cells cultivated with and without myo-inositol (**Supplementary Figure S2**). So, it was inferred that glucose metabolism may not be negatively affected under the myo-inositol concentration for induction.

The plasmid pMI-4-*gfp* was transformed into the *C. glutamicumΔiolGΔoxiCΔoxiDΔoxiE*, and the consumption of myo-inositol as well as the transcription level of *gfp* was determined. As shown in **Figure 5B**, no consumption of myo-inositol by *C. glutamicumΔiolGΔoxiCΔoxiDΔoxiE*/pMI-4-*gfp* was detected during the cultivation process. Meanwhile, a continuous increase in transcriptional levels of *gfp* was observed in this strain. These results further indicated that the degradation of myo-inositol was successfully blocked by deleting the myo-inositol dehydrogenase-encoding genes, and this resulted in constantly reinforced transcriptional level of *gfp*.

Application of the Myo-Inositol-Inducing Expression System for Producing 5-ALA

To investigate the application of the myo-inositol-inducing expression system, it was used to overexpress the key genes for production of 5-ALA. Initially, to enhance the α-ketoglutarate supply for the synthesis of 5-ALA, the *ppc* (encoding phosphoenolpyruvate carboxylase) and *gltA* (encoding citrate synthase) in *C. glutamicumΔiolGΔoxiCΔoxiDΔoxiE* was overexpressed by replacing the native promoters with the constitutive promoter *tuf*, resulting in AL-1. The glutamyl-tRNA reductase (encoded by *hemA*) and glutamate-1-semialdehyde aminotransferase (encoded by *hemL*) are rate-limiting enzymes for 5-ALA synthesis (Yu et al., 2015). The mutant $hemA^{M}$ (two Lys residues inserted between Thr-2 and Leu-3) from *Salmonella*

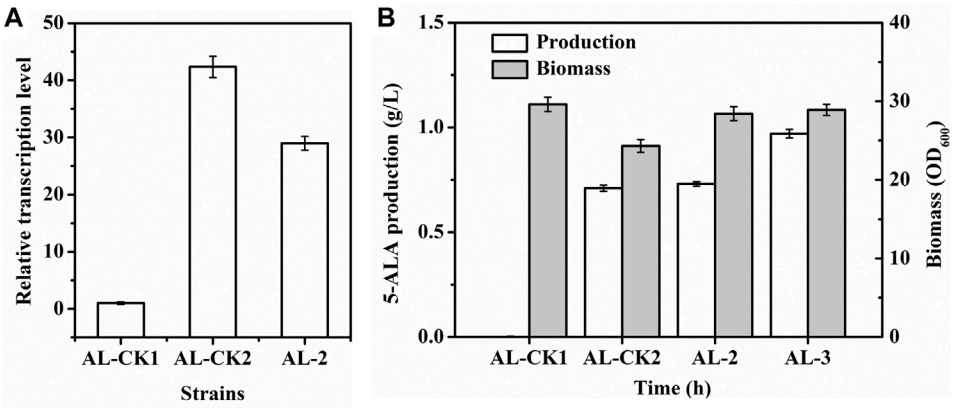

FIGURE 7 | 5-ALA production, biomass, and $hemA^M$ transcription of strains. **(A)** $hemA^M$ transcription; **(B)** 5-ALA production (white) and biomass (gray). AL-CK1 was used as a control. AL-CK1, AL-1 (*C. glutamicumΔiolGΔoxiCΔoxiDΔoxiE*P_{ppc}:$P_{tuf}$$P_{gltA}$:$P_{tuf}$) harboring pMI-4; AL-CK2, AL-1 harboring pAL1; AL-2, AL-1 harboring pMI-4-$hemA^M$-*hemL*; AL-3, *C. glutamicumΔiolGΔoxiCΔoxiDΔoxiE*P_{ppc}:$P_{tuf}$$P_{gltA}$:$P_{tuf}$ *cgl 2000*:P_{iolT1}-*pntAB* harboring pMI-4-$hemA^M$-*hemL*.

arizona (Yu et al., 2015) and *hemL* from *E. coli* were proven conducive for efficient production of 5-ALA. Therefore, these two genes were introduced into pMI-4. The generated pMI-4-$hemA^M$-*hemL* was subsequently transformed into AL-1, resulting in AL-2. At the same time, pMI-4 and pAL1 (pXMJ19 harboring $hemA^M$ and *hemL*) was transformed into AL-1 to obtain AL-CK1 and AL-CK2, which were used as controls.

Fermentation was performed in flasks to evaluate the characteristics of AL-2 and then the performance of this myo-inositol-inducing expression system. Compared with the transcriptional level of $hemA^M$ (approximately 42-fold) in AL-CK2 induced by IPTG (1 mM), the transcriptional level of $hemA^M$ in AL-2 induced by the same dose of myo-inositol was lower (approximately 29-fold, **Figure 7A**). Nevertheless, the biomass of AL-2 (OD_{600} = 28.4) was significantly higher than that of AL-CK2 (OD_{600} = 24.3, **Figure 7B**). Furthermore, the final production of 5-ALA by AL-2 reached 0.73 g/l, slightly higher (4.2%) than that by AL-CK2 (0.71 g/l, **Figure 7B**). These results indicated that a stronger expression of genes sometimes was not essential for efficient production. Notably, the glucose consumption by AL-2 (30.1 g/l) was 5.6% lower than that by AL-CK2 (31.9 g/l), and this generated an increase of 9.0% in the yield of 5-ALA (24.3 VS 22.3 mg/g glucose). It was supposed that the increased cell growth and decreased glucose consumption were due to the following reasons: unlike IPTG, myo-inositol was not toxic to cell, and thus, cell growth and metabolism were not inhibited; furthermore, the constructed myo-inositol-inducible vector relieved the metabolic burden in some degree since the transcription intensity of P_{iolT1} was lower than that of P_{tac} in pXMJ19 under the same dose of inducer, which resulted in relatively lower glucose requirement and improved cell growth.

The glutamyl-tRNA reductase is NADPH dependent, and enhancing NADPH regeneration has been proven to facilitate increased 5-ALA production (Zhang et al., 2020). Previous reports showed that overexpressing the *pntAB* gene (encoding pyridine nucleotide transhydrogenase) could improve NADPH regeneration (Kabus et al., 2007; Hao et al., 2020). To test the applicability of P_{iolT1}, a copy of *pntAB* driven by P_{iolT1} was integrated into the genome of AL-2 (generating AL-3) so that transcription of *pntAB* was induced by myo-inositol. As a result, the transcription level of *pntAB* in AL-3 was detected to be gradually enhanced after the addition of myo-inositol and maintained constant after 16 h (**Supplementary Figure S3**). Moreover, the intracellular NADPH in AL-3 was significantly improved by 27.7% (from 0.65 to 0.83 μmol/g DCW). As shown in **Figure 7A**, the production of 5-ALA by AL-3 was increased by 32.9% (0.97 g/l) compared with AL-2. This result indicated the potential application of P_{iolT1} in metabolic engineering.

Besides *iolT1*, transcription of several genes, such as *iolA* (encoding aldehyde dehydrogenase) and *iolC* (encoding carbohydrate kinase), was detected up-regulated to different levels when *C. glutamicum* cells were grown on myo-inositol. These results indicated that the promoters of these genes are probably inducible by myo-inositol, and strengths of these promoters are diverse. Therefore, these promoters will be exploited for gene overexpression in the future work.

CONCLUSION

A myo-inositol-inducible expression vector pMI-4, containing the $iolR^q$ cassette and P_{iolT1}, was constructed in this study. The pMI-4 was proven to stably replicate in *C. glutamicum* cells without antibiotic selection pressure. Furthermore, the chassis *C. glutamicumΔiolGΔoxiCΔoxiDΔoxiE*, which was not able to degrade myo-inositol and suitable for maintaining pMI-4, was developed as the host strain. Through overexpression of $hemA^M$ and *hemL* using the vector pMI-4 in the engineered chassis *C. glutamicumΔiolGΔoxiCΔoxiDΔoxiE*, the production of 5-ALA achieved 0.73 g/l, which indicated the potential application of this expression system in metabolic engineering and industrial production. Furthermore, the P_{iolT1} was proved to be applicable for overexpressing genes by integrating to genome.

DATA AVAILABILITY STATEMENT

The original contributions presented in the study are included in the article/**Supplementary Material**, and further inquiries can be directed to the corresponding authors.

AUTHOR CONTRIBUTIONS

CZ and NL designed the research, performed data analysis, and wrote the manuscript. NL, WZ, and HX constructed the expression vectors and the host strain and investigated the characteristic of the vectors. YL, MW, and JM constructed the 5-ALA producing strains. YM and JW performed the fermentation assays. CZ and NC supervised the research. All authors contributed to the article and approved the submitted version.

FUNDING

This research was financially supported by the National Key Research and Development Program of China (2021YFC2101802), the Natural Science Foundation of China (32170049, 31300069, and 31770053), the Tianjin Synthetic Biotechnology Innovation Capacity Improvement Project (TSBICIP-KJGG-009), the Training program of innovation and entrepreneurship for undergraduates (202110057132 and 202110057314), and the China Postdoctoral Science Foundation Funded Project (2017M611170 and 2018T110662).

SUPPLEMENTARY MATERIAL

The Supplementary Material for this article can be found online at: https://www.frontiersin.org/articles/10.3389/fbioe.2021.746322/full#supplementary-material

REFERENCES

Becker, J., Rohles, C. M., and Wittmann, C. (2018). Metabolically Engineered Corynebacterium Glutamicum for Bio-Based Production of Chemicals, Fuels, Materials, and Healthcare Products. *Metab. Eng.* 50, 122–141. doi:10.1016/j.ymben.2018.07.008

Chen, Z., Huang, J., Wu, Y., Wu, W., Zhang, Y., and Liu, D. (2016). Metabolic Engineering of Corynebacterium Glutamicum for the Production of 3-Hydroxypropionic Acid from Glucose and Xylose. *Metab. Eng.* 39, 151–158. doi:10.1016/j.ymben.2016.11.009

Chung, S.-C., Park, J.-S., Yun, J., and Park, J. H. (2017). Improvement of Succinate Production by Release of End-Product Inhibition in Corynebacterium Glutamicum. *Metab. Eng.* 40, 157–164. doi:10.1016/j.ymben.2017.02.004

Eggeling, L., and Bott, M. (2015). A Giant Market and a Powerful Metabolism: L-Lysine provided by Corynebacterium Glutamicum. *Appl. Microbiol. Biotechnol.* 99, 3387–3394. doi:10.1007/s00253-015-6508-2

Eggeling, L., and Bott, M. (2005). *Handbook of Corynebacterium Glutamicum*. Boca Raton: CRC Press.

Hao, Y., Ma, Q., Liu, X., Fan, X., Men, J., Wu, H., et al. (2020). High-Yield Production of L-Valine in Engineered *Escherichia C* by a Novel Two-Stage Fermentation. *Metab. Eng.* 62, 198–206. doi:10.1016/j.ymben.2020.09.007

Hasegawa, S., Uematsu, K., Natsuma, Y., Suda, M., Hiraga, K., Jojima, T., et al. (2012). Improvement of the Redox Balance Increases L-Valine Production by Corynebacterium Glutamicum under Oxygen Deprivation Conditions. *Appl. Environ. Microbiol.* 78, 865–875. doi:10.1128/AEM.07056-11

Ikeda, M., and Nakagawa, S. (2003). The Corynebacterium Glutamicum Genome: Features and Impacts on Biotechnological Processes. *Appl. Microbiol. Biotechnol.* 62, 99–109. doi:10.1007/s00253-003-1328-1

Jakoby, M., Ngouoto-Nkili, C.-E., and Burkovski, A. (1999). Construction and Application of New Corynebacterium Glutamicum Vectors. *Biotechnol. Tech.* 13, 437–441. doi:10.1023/A:1008968419217

Kabus, A., Georgi, T., Wendisch, V. F., and Bott, M. (2007). Expression of the *Escherichia C* pntAB Genes Encoding a Membrane-Bound Transhydrogenase in Corynebacterium Glutamicum Improves L-Lysine Formation. *Appl. Microbiol. Biotechnol.* 75, 47–53. doi:10.1007/s00253-006-0804-9

Kirchner, O., and Tauch, A. (2003). Tools for Genetic Engineering in the Amino Acid-Producing Bacterium Corynebacterium Glutamicum. *J. Biotechnol.* 104, 287–299. doi:10.1016/S0168-1656(03)00148-2

Klaffl, S., Brocker, M., Kalinowski, J., Eikmanns, B. J., and Bott, M. (2013). Complex Regulation of the Phosphoenolpyruvate Carboxykinase Gene Pck and Characterization of its GntR-Type Regulator IolR as a Repressor of Myo-Inositol Utilization Genes in Corynebacterium Glutamicum. *J. Bacteriol.* 195, 4283–4296. doi:10.1128/JB.00265-13

Kogure, T., and Inui, M. (2018). Recent Advances in Metabolic Engineering of Corynebacterium Glutamicum for Bioproduction of Value-Added Aromatic Chemicals and Natural Products. *Appl. Microbiol. Biotechnol.* 102, 8685–8705. doi:10.1007/s00253-018-9289-6

Krings, E., Krumbach, K., Bathe, B., Kelle, R., Wendisch, V. F., Sahm, H., et al. (2006). Characterization of Myo -Inositol Utilization by Corynebacterium Glutamicum : the Stimulon, Identification of Transporters, and Influence on L -Lysine Formation. *J. Bacteriol.* 188, 8054–8061. doi:10.1128/JB.00935-06

Li, Y., Ai, Y., Zhang, J., Fei, J., Liu, B., Wang, J., et al. (2020). A Novel Expression Vector for Corynebacterium Glutamicum with an Auxotrophy Complementation System. *Plasmid* 107, 102476. doi:10.1016/j.plasmid.2019.102476

Livak, K. J., and Schmittgen, T. D. (2001). Analysis of Relative Gene Expression Data Using Real-Time Quantitative PCR and the 2−ΔΔCT Method. *Methods* 25, 402–408. doi:10.1006/meth.2001.1262

Lu, Y., Wang, L., Teng, F., Zhang, J., Hu, M., and Tao, Y. (2018). Production of Myo-Inositol from Glucose by a Novel Trienzymatic cascade of Polyphosphate Glucokinase, Inositol 1-Phosphate Synthase and Inositol Monophosphatase. *Enzyme Microb. Technol.* 112, 1–5. doi:10.1016/j.enzmictec.2018.01.006

Mauzerall, D., and Granick, S. (1956). The Occurrence and Determination of Delta-Amino-Levulinic Acid and Porphobilinogen in Urine. *J. Biol. Chem.* 219, 435–446. doi:10.1016/s0021-9258(18)65809-0

Nešvera, J., and Pátek, M. (2011). Tools for Genetic Manipulations in Corynebacterium Glutamicum and Their Applications. *Appl. Microbiol. Biotechnol.* 90, 1641–1654. doi:10.1007/s00253-011-3272-9

Peng, F., Wang, X., Sun, Y., Dong, G., Yang, Y., Liu, X., et al. (2017). Efficient Gene Editing in Corynebacterium Glutamicum Using the CRISPR/Cas9 System. *Microb. .Cell .Fact.* 16, 201. doi:10.1186/s12934-017-0814-6

Sambrook, J., and Russell, D. W. (2001). *Molecular Cloning: A Laboratory Manual*. Cold Spring Harbor. NY: Cold Spring Harbor Laboratory Press.

Sato, N., Kishida, M., Nakano, M., Hirata, Y., and Tanaka, T. (2020). Metabolic Engineering of Shikimic Acid-Producing Corynebacterium Glutamicum from Glucose and Cellobiose Retaining its Phosphotransferase System Function and Pyruvate Kinase Activities. *Front. Bioeng. Biotechnol.* 8, 569406. doi:10.3389/fbioe.2020.569406

Schäfer, A., Tauch, A., Jäger, W., Kalinowski, J., Thierbach, G., and Pühler, A. (1994). Small Mobilizable Multi-Purpose Cloning Vectors Derived from the *Escherichia C* Plasmids pK18 and pK19: Selection of Defined Deletions in the Chromosome of Corynebacterium Glutamicum. *Gene* 145, 69–73. doi:10.1016/0378-1119(94)90324-7

Suzuki, N., and Inui, M. (2013). *Genome Engineering of Corynebacterium Glutamicum*. Berlin: Springer.

Takeno, S., Hori, K., Ohtani, S., Mimura, A., Mitsuhashi, S., and Ikeda, M. (2016). l -Lysine Production Independent of the Oxidative Pentose Phosphate Pathway by Corynebacterium Glutamicum with the Streptococcus Mutans gapN Gene. *Metab. Eng.* 37, 1–10. doi:10.1016/j.ymben.2016.03.007

Wang, Q., Zhang, J., Al Makishah, N. H., Sun, X., Wen, Z., Jiang, Y., et al. (2021). Advances and Perspectives for Genome Editing Tools of Corynebacterium Glutamicum. *Front. Microbiol.* 12, 654058. doi:10.3389/fmicb.2021.654058

Wendisch, V. F. (2020). Metabolic Engineering Advances and Prospects for Amino Acid Production. *Metab. Eng.* 58, 17–34. doi:10.1016/j.ymben.2019.03.008

Xu, D., Tan, Y., Huan, X., Hu, X., and Wang, X. (2010). Construction of a Novel Shuttle Vector for Use in Brevibacterium Flavum, an Industrial Amino Acid Producer. *J. Microbiol. Methods* 80, 86–92. doi:10.1016/j.mimet.2009.11.003

You, R., Wang, L., Shi, C., Chen, H., Zhang, S., Hu, M., et al. (2020). Efficient Production of Myo-Inositol in *Escherichia C* through Metabolic Engineering. *Microb. Cel. Fact.* 19, 109. doi:10.1186/s12934-020-01366-5

Yu, X., Jin, H., Liu, W., Wang, Q., and Qi, Q. (2015). Engineering Corynebacterium Glutamicum to Produce 5-Aminolevulinic Acid from Glucose. *Microb. Cel. Fact.* 14, 183. doi:10.1186/s12934-015-0364-8

Zhang, C., Li, Y., Ma, J., Liu, Y., He, J., Li, Y., et al. (2018). High Production of 4-Hydroxyisoleucine in Corynebacterium glutamicum by Multistep Metabolic Engineering. *Metab. Eng.* 49, 287–298. doi:10.1016/j.ymben.2018.09.008

Zhang, C., Li, Y., Zhu, F., Li, Z., Lu, N., Li, Y., et al. (2020). Metabolic Engineering of an Auto-Regulated Corynebacterium Glutamicum Chassis for Biosynthesis of 5-Aminolevulinic Acid. *Bioresour. Technol.* 318, 124064. doi:10.1016/j.biortech.2020.124064

Conflict of Interest: The authors declare that the research was conducted in the absence of any commercial or financial relationships that could be construed as a potential conflict of interest.

Publisher's Note: All claims expressed in this article are solely those of the authors and do not necessarily represent those of their affiliated organizations or those of the publisher, the editors, and the reviewers. Any product that may be evaluated in this article, or claim that may be made by its manufacturer, is not guaranteed or endorsed by the publisher.

frontiers in Bioengineering and Biotechnology

ORIGINAL RESEARCH
published: 18 November 2021
doi: 10.3389/fbioe.2021.766674

Genomics Characterization of an Engineered *Corynebacterium glutamicum* in Bioreactor Cultivation Under Ionic Liquid Stress

*Deepanwita Banerjee[1,2†], Thomas Eng[1,2†], Yusuke Sasaki[1,2], Aparajitha Srinivasan[1,2], Asun Oka[2,3], Robin A. Herbert[1,2], Jessica Trinh[1,2], Vasanth R. Singan[2,4], Ning Sun[2,3], Dan Putnam[5], Corinne D. Scown[1,6], Blake Simmons[1,2] and Aindrila Mukhopadhyay[1,2]**

[1]Joint BioEnergy Institute, Lawrence Berkeley National Laboratory, Emeryville, CA, United States, [2]Biological Systems and Engineering Division, Lawrence Berkeley National Laboratory, Berkeley, CA, United States, [3]Advanced Biofuels and Bioproducts Process Development Unit, Lawrence Berkeley National Laboratory, Emeryville, CA, United States, [4]Joint Genome Institute, Lawrence Berkeley National Laboratory, Berkeley, CA, United States, [5]Department of Plant Sciences, University of California, Davis, Davis, CA, United States, [6]Energy Analysis and Environmental Impacts Division, Lawrence Berkeley National Laboratory, Berkeley, CA, United States

OPEN ACCESS

Edited by:
Yu Wang,
Tianjin Institute of Industrial Biotechnology (CAS), China

Reviewed by:
Xinqing Zhao,
Shanghai Jiao Tong University, China
Julio Augusto Freyre-Gonzalez,
National Autonomous University of Mexico, Mexico

***Correspondence:**
Aindrila Mukhopadhyay
amukhopadhyay@lbl.gov

†These authors have contributed equally to this work and share first authorship

Specialty section:
This article was submitted to Synthetic Biology, a section of the journal Frontiers in Bioengineering and Biotechnology

Received: *29 August 2021*
Accepted: *27 October 2021*
Published: *18 November 2021*

Citation:
Banerjee D, Eng T, Sasaki Y, Srinivasan A, Oka A, Herbert RA, Trinh J, Singan VR, Sun N, Putnam D, Scown CD, Simmons B and Mukhopadhyay A (2021) Genomics Characterization of an Engineered Corynebacterium glutamicum *in Bioreactor Cultivation Under Ionic Liquid Stress. Front. Bioeng. Biotechnol. 9:766674. doi: 10.3389/fbioe.2021.766674*

Corynebacterium glutamicum is an ideal microbial chassis for production of valuable bioproducts including amino acids and next generation biofuels. Here we resequence engineered isopentenol (IP) producing *C. glutamicum* BRC-JBEI 1.1.2 strain and assess differential transcriptional profiles using RNA sequencing under industrially relevant conditions including scale transition and compare the presence *vs* absence of an ionic liquid, cholinium lysinate ([Ch][Lys]). Analysis of the scale transition from shake flask to bioreactor with transcriptomics identified a distinct pattern of metabolic and regulatory responses needed for growth in this industrial format. These differential changes in gene expression corroborate altered accumulation of organic acids and bioproducts, including succinate, acetate, and acetoin that occur when cells are grown in the presence of 50 mM [Ch][Lys] in the stirred-tank reactor. This new genome assembly and differential expression analysis of cells grown in a stirred tank bioreactor clarify the cell response of an *C. glutamicum* strain engineered to produce IP.

Keywords: *Corynebacterium glutamicum*, RNAseq, fed-batch, bioreactor, ionic Liquid, isopentenol, acetoin, lignin hydrolysate

INTRODUCTION

Due to process advantages, biological methods for the production of amino acids over chemical synthesis methods fostered the identification of natural glutamine overproducing microbes (Kinoshita et al., 1958). Since then, *Corynebacterium glutamicum* has been used successfully to produce specialty glutamine and specialty amino acids to meet global demand. The advent of accessible whole-genome sequencing and mutagenesis methods have enabled a clearer understanding of how specific isolates can overproduce these desired molecules, as well as how they maintain productivity across volumetrically-larger scales (Becker et al., 2018; Pérez-García and Wendisch, 2018; Wolf et al., 2021). Using *C. glutamicum* to produce non-native metabolites as next-generation biofuels is an attractive large-volume market with the potential to reduce global carbon emissions. Potential biofuels can be produced from terpenes, which use different metabolic

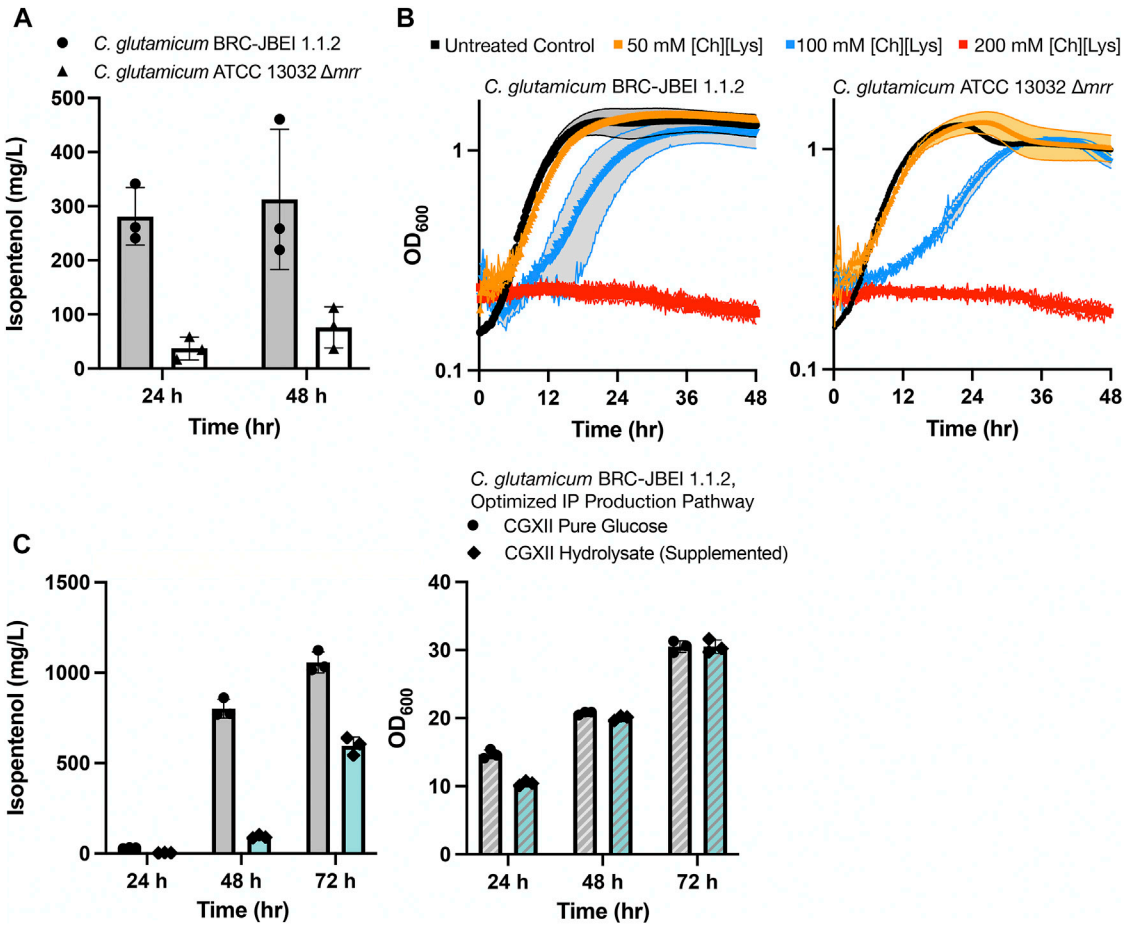

FIGURE 1 | Growth and isopentenol production characterization of two genetically distinct engineered *C. glutamicum* strains, **(A)** Isopentenol (IP) production in *C. glutamicum* strains of the genotypes indicated harboring an IP production plasmid. Cells were cultivated in 24-well deep well plates. IP titers reported at 48-h time points are corrected for evaporation in this plate format (Materials and Methods), **(B)** Growth curves for *C. glutamicum* strains of the indicated strain backgrounds cultivated in CGXII media in the presence or absence of the IL, cholinium lysinate ([Ch][Lys]), [Ch][Lys] was exogenously added to the culture media at the start of the time course, **(C)** Production of IP from *C. glutamium* grown in CGXII minimal media with pure glucose (4% w/v) or ensiled [Ch][Lys] pretreated sorghum hydrolysate. An optimized IP production plasmid carrying a *hmgR* variant from *Silicibacter pomeroyi* was used. The optical density of cultures as a proxy for cell density is noted on the right-hand panel.

precursors (reviewed in (Pérez-García and Wendisch, 2018)). We have previously described the heterologous expression of the terpenoid isopentenol (IP; also known as 3-methyl-3-buten-1-ol or isoprenol) pathway in *C. glutamicum* (Sasaki et al., 2019). IP can be used directly as a drop-in biogasoline (Reninger and McPhee, 2008; Chou and Keasling, 2012) or as a precursor to a jet fuel, DMCO (Baral et al., 2021). Producing IP was improved using optimal pathway homologs, specific media formulation and aeration conditions and an empirically determined carbon/nitrogen ratio (Sasaki et al., 2019).

In this study we build upon this established system to analyze the behavior of *C. glutamicum* strains engineered to produce IP in a bioreactor. The bioreactor cultivation and process conditions can provide key diagnostic information essential to build robust production platform strains (Wehrs et al., 2019). In addition, it is also valuable to understand microbial response to the carbon feedstock that is anticipated for actual production. Here, we explore the use of plant-based lignocellulosic hydrolysate generated using ionic liquid (IL) as a pretreatment reagent. Toxicity from residual pretreatment reagents such as ILs is a known source of growth impediment (Hou et al., 2013; Santos et al., 2014). *C. glutamicum* is tolerant to many ILs, another attribute that makes it an ideal host for biomass conversion (Sasaki et al., 2019). In this study, we characterize an IP-producing engineered *C. glutamicum* strain with long-read Pacific Biosciences (PacBio) whole-genome sequencing. This high-quality assembly allowed accurate mapping for differential RNA expression analysis from a diagnostic fed-batch *C. glutamicum* IP production run. These side-by-side experiments characterize the cellular response to the IL, cholinium lysinate ([Ch][Lys]), when grown in a fed-batch stirred tank bioreactor.

RESULTS

Characterization of Isopentenol Production and Ionic Liquid Tolerance in *C. glutamicum* Strains

We established that the strain reported in Sasaki et al., 2019, *C. glutamicum* (previously referred to as ATCC 13032 NHRI 1.1.2) outperformed another isolate, ATCC 13032 Δ*cglIM* Δ*cgLIR* Δ*cgLIIR* (referred to as "Δ*mrr*") (**Figure 1A**). *C. glutamicum* Δ*mrr* was first described in Baumgart et al., 2013 and is a methylation-deficient strain widely used due to its improved plasmid transformation and genomic integration rate (Schäfer et al., 1997; Baumgart et al., 2013). When *C. glutamicum* BRC-JBEI 1.1.2 is used in conjunction with an IP production pathway, it can produce 300 mg/L IP from pure glucose, but the product titers are near the lower detection limit by GC-FID in the *C. glutamicum* ATCC 13032 Δ*mrr* strain. While only *C. glutamicum* BRC-JBEI 1.1.2 produced IP, both the type strain and this specific isolate tolerate high concentrations of exogenous ILs (**Figure 1B**), suggesting that IL tolerance was a shared feature between these two isolates despite differences in IP production.

We also confirmed the ability of *C. glutamicum* BRC-JBEI 1.1.2 to handle renewable carbon streams from sorghum biomass using an improved carbon extraction protocol enhanced by the use of ensiled biomass (Magurudeniya et al., 2021). The ensiling process enables naturally occurring lactic-acid secreting bacteria to partially decompose the hemicellulose in sorghum while stored in a silo before downstream processing. After ensiling, the biomass was pretreated with [Ch][Lys] followed by enzymatic saccharification (Materials and Methods). This hydrolysate contained 48.7 g/L glucose, 17.9 g/L xylose, and trace concentrations of aromatic compounds. Our optimized *C. glutamicum* BRC-JBEI 1.1.2 with an optimized IP production system had no detected growth defects when grown with 58% (v/v) hydrolysate supplemented media and produced 1 g/L IP from pure glucose or ~600 mg/L IP from sorghum hydrolysate (**Figure 1C**). These results showcase its versatility with handling actual plant biomass derived carbon streams. For the remainder of this study, we focus on characterizing the genetic differences present in *C. glutamicum* BRC-JBEI 1.1.2 relative to other closely related *C. glutamicum* strains that might explain the IP production values between these two strains.

Genomic Characterization of *C. glutamicum* BRC-JBEI 1.1.2

While 16S rRNA sequencing suggested that *C. glutamicum* Δ*mrr* strain as in the *C. glutamicum* ATCC 13032 strain background, this same method indicated that *C. glutamicum* BRC-JBEI 1.1.2 is related to *C. glutamicum* CICC10112 or SCgG1/SCgG2. To overcome the limitation inherent to 16S rRNA-based identification, we turned to using whole genome sequencing. Only SCgG1 and SCgG2 have been characterized with whole-genome sequencing, and to our knowledge there was no additional information about *C. glutamicum* CICC10112 beyond the partial 16S ribosomal sequence. As 16S rRNA is inconclusive for isolate-level identification (Sabat et al., 2017; Hahne et al., 2018; Johnson et al., 2019), we reasoned that the whole-genome sequencing in this IP producing strain would ensure an accurate reference genome in downstream RNAseq analysis if the improved performance observed in this strain was due to variations in the strain background. One of the major limitations in short-read sequencing is the difficulty in assembling overlapping contigs to generate a high-quality *de novo* assembly of a single contiguous read. Therefore, we chose PacBio long-read sequencing (Koren and Phillippy, 2015) for optimal coverage over short read sequencing as a potential solution. However, routine methods for lysing and isolating *C. glutamicum* genomic DNA were insufficient for building high-quality genome assemblies since the physical lysis method we employed (Eng et al., 2018) shears DNA to fragments ranging from 2 to 8 kb in size. Detergent-based lysis methods failed to extract genomic DNA, even with prolonged incubation times. We developed a method to isolate larger DNA fragments approximately 20 kb in size for the PacBio Sequel (Pacific Biosciences) assembly pipeline using a zymolyase protease treatment for cell lysis (see Materials and Methods). This modified DNA extraction protocol enabled us to use PacBio long read sequencing to generate a high-quality *de novo* genome assembly.

We now report a new genome assembly of a single contiguous scaffold of 3,352,276 bases with 53.83% GC content (**Figure 2**). Genome-wide average nucleotide identity (ANI) confirmed this isolate was 99.9987% identical to *C. glutamicum* SCgG1 and SCgG2 as well as another sequenced *C. glutamicum* isolate, Z188. The average nucleotide identity alignment for the 28 sequenced *C. glutamicum* isolates has been deposited at the database of the Joint Genome Institute (https://genome.jgi.doe.gov/portal/), Project ID 1203597 and is also included in **Supplementary Table S1**. *C. glutamicum* BRC-JBEI 1.1.2 differs from SCgG1 only by a few single nucleotide polymorphisms (~10) and two additional genes that are absent from SCgG1, a putative transposase and a hypothetical protein coding sequence that is 414 bp in length. When *C. glutamicum* BRC-JBEI 1.1.2 was compared with more commonly used reference strains, *C. glutamicum* R and 13032 (Bielefeld), we identified genomic islands encoding genes unique to BRC-JBEI 1.1.2. Genome topology analysis also identified a 140 kb inversion in the genome of BRC-JBEI 1.1.2 isolate (**Figure 2A**). Out of 3,097 genes, homology mapping indicated that 85% (2,641 genes) were at least 80% identical to known genes in *C. glutamicum* ATCC 13032. With a less restrictive % identity threshold of 50%, the identical ratio could account for 89% (2,777 genes). Nonetheless, 320 genes did not meet the minimum % identity threshold and could not be annotated with this reference genome (**Supplementary Figure S1**).

Some of these unknown genes that were unique to BRC-JBEI 1.1.2 might be related to the catabolism of IL. Intriguingly, a putative choline dehydrogenase, *Ga0373873_2846*, showed only 40% identity to other known choline dehydrogenases primarily found in Gram-negative microbes such as *Burkholderia phytofirmans* PsJN and *Cupriavidus basilensis* FW507-4G11. Meta-COG analysis of these four *C. glutamicum* genomes

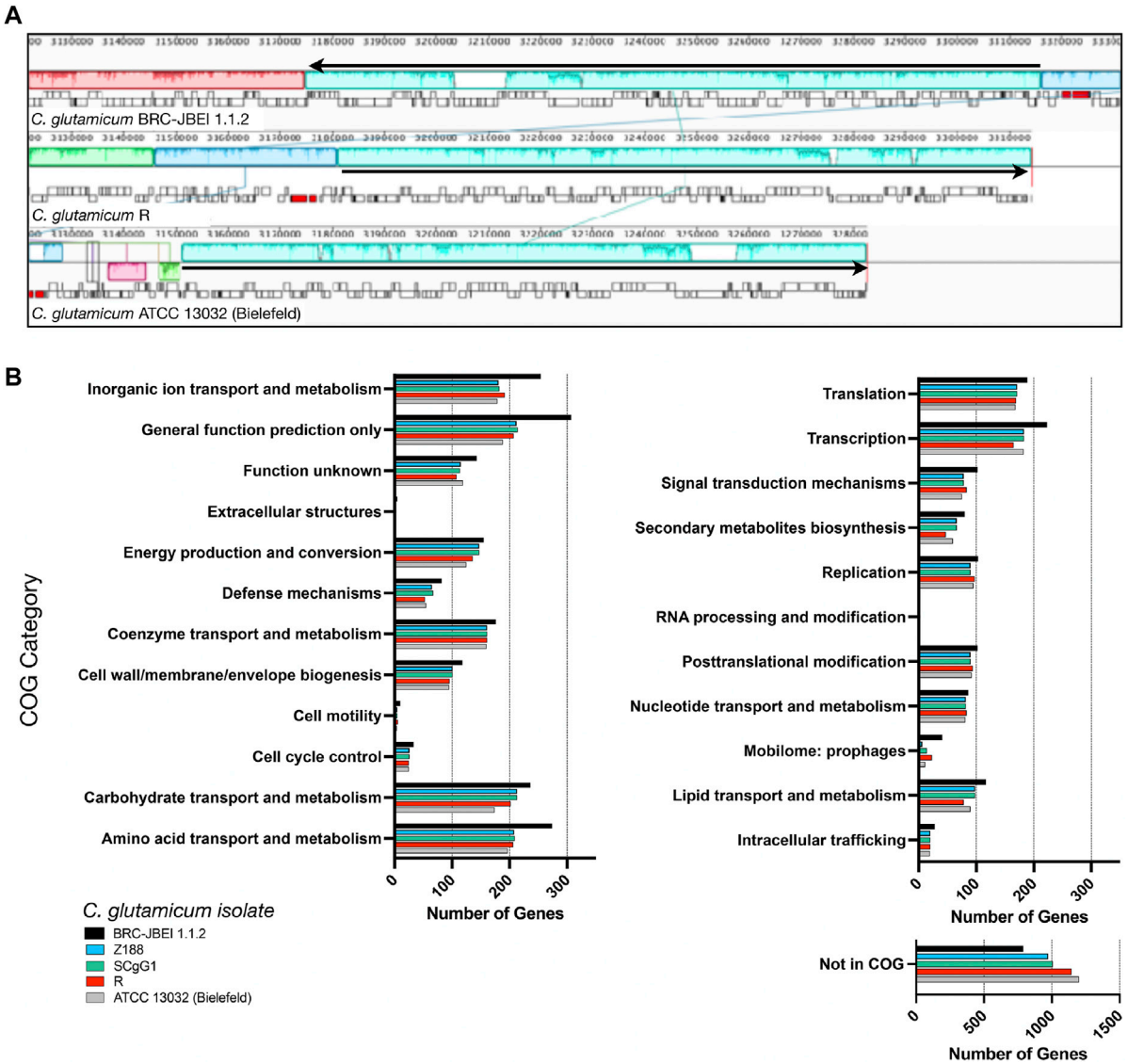

FIGURE 2 | Comparison of the *C. glutamicum* BRC-JBEI 1.1.2 strain with closely related *C. glutamicum* strains, **(A)** A meta-analysis of gene function using clusters of orthologous genes (COGs) analysis. The total number of genes in each category for each strain is represented with colored bars as indicated, **(B)** Mauve genome alignment of *C. glutamicum* BRC-JBEI 1.1.2 with *C. glutamicum* R and 13032 (Bielefeld). Similar genomic regions share the same color across the three different genomes compared. A 140 kb chromosomal inversion is highlighted in light blue, and the relative direction of the inversion in each strain is indicated with a black arrow. Individual genes are indicated with open rectangles underneath the colored area.

revealed that *C. glutamicum* BRC-JBEI 1.1.2 contains over 100 additional genes related to the transport or metabolism of inorganic ions, carbohydrates, and amino acids, suggesting a broader metabolic capacity to utilize a more significant number of substrates than the type strain (**Figure 2**). In summary, this genome sequencing analysis was valuable for characterizing differences between *C. glutamicum* BRC-JBEI 1. 1.2 and the more routinely studied type strain ATCC 13032. Due to its similarity with SCgG1 and SCgG2, *C. glutamicum* BRC-JBEI 1.1.2 is likely an industrial glutamate overproducing isolate but has more annotations in the inorganic ion and amino acid transport and metabolism COG categories than its nearest neighbors, SCgG1, SCgG2, and Z188 that need further characterization.

Transcriptome Analysis Identifies Changes in *C. glutamicum* Beyond Metabolism During Scale-Up

Next, we sought to build a systems-level understanding of *C. glutamicum* gene expression changes in bioreactors upon exogenous IL treatment. This data could be useful for subsequent Design-Build-Test-Learn (DBTL) cycles in providing the diagnostic information for future strain optimization strategies

(Opgenorth et al., 2019). We prepared samples from sequential time points during a scaleup campaign to analyze shifts in gene expression as a proxy for changes in metabolic and regulatory behavior in both [Ch][Lys] treated and untreated runs. First, we determined if the failure to produce IP was due to loss of the production pathway, possibly due to loss of the plasmid-borne IP pathway genes. The IP production pathway is composed of 5 genes in 2 adjacent operons under the *trc* and *lacUV5* promoters, namely *mk, pmd* and *atoB, hmgS, hmgR* respectively. Using the transcripts per million (TPM) metrics, we examined absolute gene expression levels as well as changes over the course of the production campaign. The IP pathway started off high for both *hmgR* and *hmgS* in the shake flask (200,000 TPM), but expression of these two genes decreased between 10-16x over the duration of the 65-h fed batch. Expression amounts of *atoB* in the shake flask were comparatively lower (1,500 TPM) but decreased 4x at the shake flask to bioreactor transition. *atoB* TPM counts remained low for the duration of the subsequent time points. Since the pathway genes were still expressed during this run, we then focused on analyzing gene expression changes in the native *C. glutamicum* genome.

To interpret the differential gene expression results with genes identified in the new assembly for *C. glutamicum* BRC-JBEI 1.1.2, we mapped gene names and identifiers from *C. glutamicum* ATCC 13032 back onto the open reading frames (ORFs) in *C. glutamicum* BRC-JBEI 1.1.2 as genes in the type strain genome have been broadly characterized. We used a medium confidence cutoff of 70% identity to capture most homologs when analyzing this dataset. First, we characterised gene expression upon inoculating cells from the seed culture in a shake flask to the bioreactor. This differential gene expression (DEG) was calculated as the ratio of an early time point in the bioreactor (6.5 h post inoculation in the stirred tank) divided by values from the seed culture immediately before transfer. This time point was chosen to give cells approximately three doublings to ensure the cells were rapidly growing under these new conditions. The result showed differential expression of 258 genes after 6.5 h (**Figure 3**, and **Supplementary Dataset S1**).

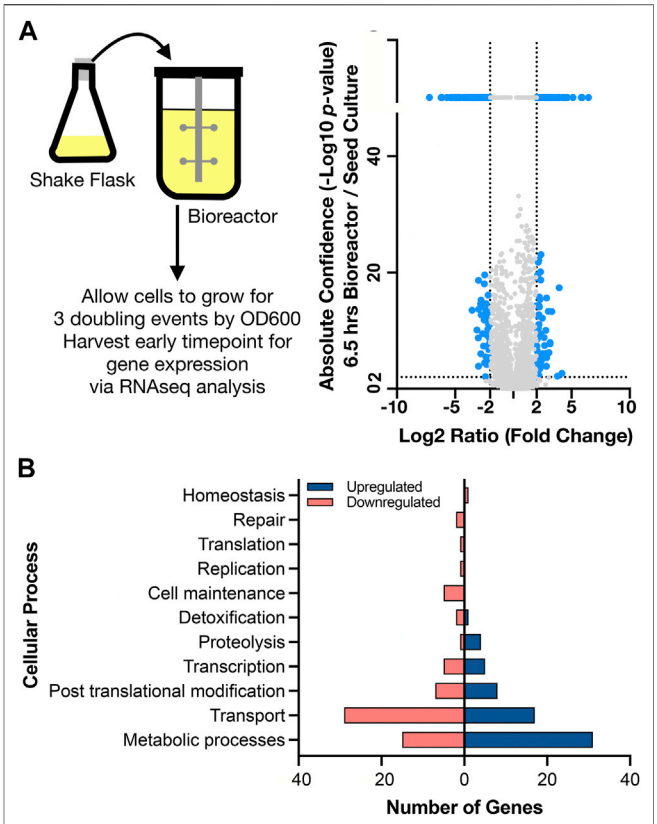

FIGURE 3 | Genome wide expression differences in diverse cellular processes upon shifting to a stirred tank bioreactor, **(A)** *Left side.* Schematic showing scale transition from 25 ml seed culture of IP producing *C. glutamicum* in CGXII media to a stirred tank bioreactor. *Right side.* Volcano plot comparing differential gene expression (6.5 h post inoculation /shake flask) via RNAseq analysis to absolute confidence (*p* value) of the same time points. Fold changes greater than 4 ($\log_2 = 2$) and absolute confidence values > 2 ($p < 0.001$) are considered significant. The threshold for significance is demarcated with dotted lines and the corresponding genes are colored blue. Genes with insignificant differential expression are indicated in grey. Genes with confidence values > 40 are placed above the break on the *y* axis, **(B)** Analysis of gene classes enriched in the scale transition. Differentially expressed genes from a) were binned into functional categories based on COG annotations and putative function by BLAST alignment. Upregulated genes are indicated in dark blue; downregulated genes are indicated in light red.

Overexpressed Metabolic Genes

Many genes encoding metabolic functions were differentially expressed in the transition from shake flask to stirred tank format. We used a fold change cutoff of 4 ($\log_2 > 2$) and a *p* value < 0.001 to identify both large and statistically significant changes (**Figure 3A**). Gene ontology (GO) (Ashburner et al., 2000) enrichment annotations identified the highest number of DEGs belonging to metabolism and transport processes (**Figure 3B**). The strongest fold changes (16-fold increase or higher) were in metabolism; Cgl2807 (*adhA*, zinc dependent alcohol dehydrogenase), Cgl1396 (acetylglutamate kinase), Cgl2886 and Cgl2887 (two FAD-dependent oxidoreductases) and Cgl3007 (*mez,* malic enzyme). Of these genes, Cgl2807/*adhA* encodes for a Zn-dependent alcohol dehydrogenase that together with Cgl2796 has been reported to maintain redox balance (Zhang et al., 2018). While the cells had been previously adapted in CGXII medium for the seed culture, we observed differentially increased gene expression of several amino acid biosynthesis pathways. Increased gene expression for nearly complete pathways needed for methionine, leucine, and arginine biosynthesis were detected, as well as the gene responsible for glutamate synthesis, *gdh*. Three genes responsible for the conversion of propionate to succinate and pyruvate through the methylcitrate cycle were also upregulated. Upregulated DEGs encoding for myo-inositol metabolism directing flux towards acetyl-CoA and DHAP included Cgl0163/*iolE,* Cgl0161/*iolB,* Cgl0158/*iolC*, Cgl0160/*iolA*/*msmA*, and Cgl0157/*iolR*. Of the myo-inositol pathway genes, *iolR* was reported to regulate PTS-independent glucose uptake by repressing the expression of glucokinases in *C. glutamicum* (Zhou et al., 2015). The upregulation of myo-inositol catabolic pathways could be attributed to supplemental yeast extract amended to the CGXII medium in the bioreactor. Yeast extract was added to the bioreactors as it was found to improve IP production in

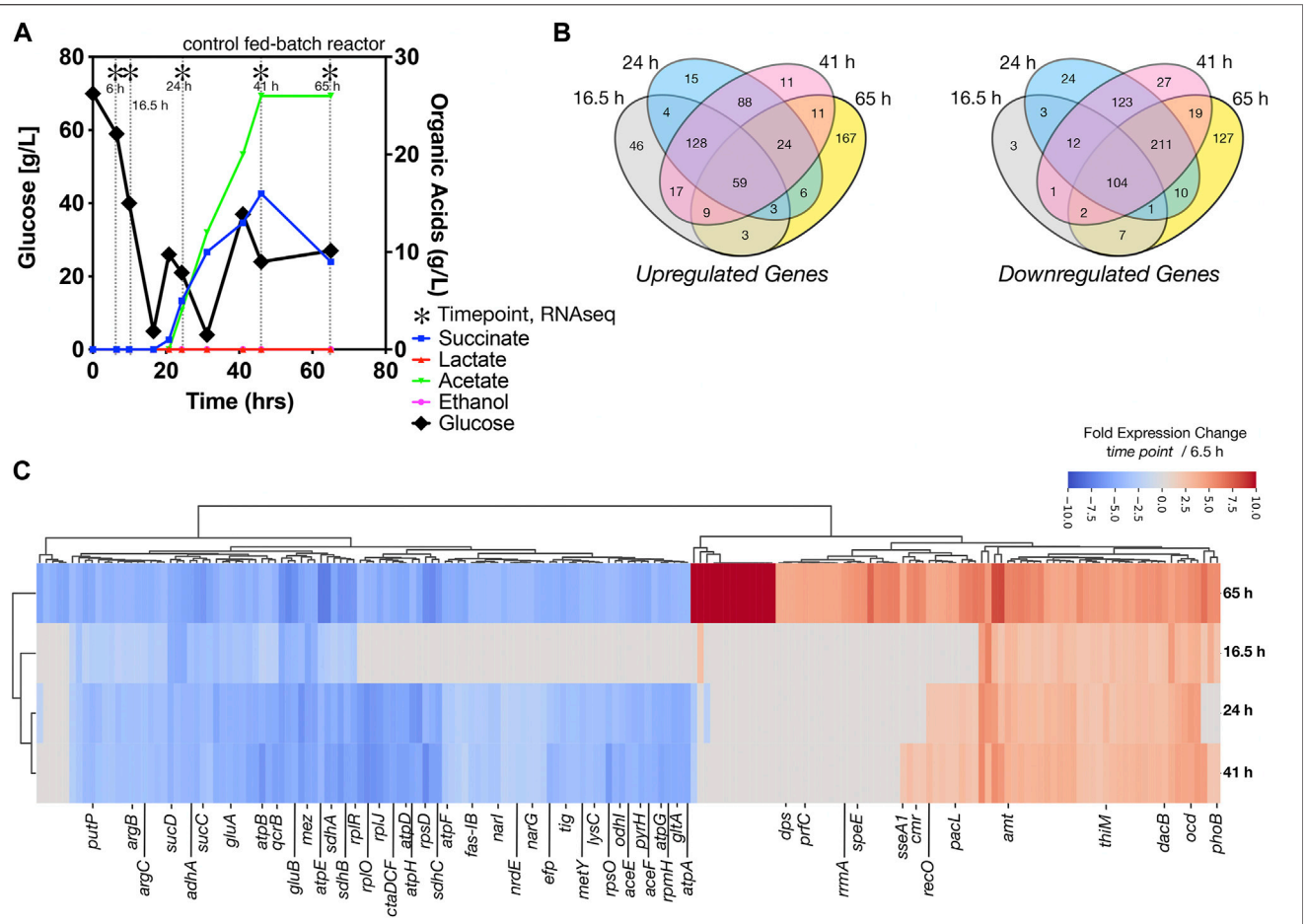

FIGURE 4 | Growth of engineered *C. glutamicum* for IP in a control stir tank bioreactor, **(A)** HPLC analysis of glucose and organic acids detected in the 2 L stirred tank bioreactor. Cells were harvested from the indicated time points with (*). Refer to **Figure 5A** for the [Ch][Lys] treated bioreactor. **(B)** Shared and unique differentially expressed genes. Venn diagrams indicate the number of Upregulated *(left)* and downregulated *(right)* genes at the indicated time points, **(C)** Hierarchical cluster analysis of the top 181 differentially expressed genes at the 65-h time point vs. the 6.5 h time point for both up or down regulation. A number of genes that are highly expressed only in stationary phase *vs* constitutively expressed are observed.

Escherichia coli (Kang et al., 2019). Inositol is found in the yeast extract (>160 mg/g range) for many commercial preparations.

Overexpressed Regulatory and Stress Responsive Genes

A wide range of regulatory factors and stress responsive genes were also upregulated at the shake flask to bioreactor transition time point. Cgl2988/*malR*, which encodes for a MarR type transcriptional regulator and Cgl3007/*mez* were both highly upregulated. MalR represses expression of the malic enzyme gene, *mez* (Krause et al., 2012) and is a global regulator of stress-responsive cell envelope remodeling in *C. glutamicum* (Hünnefeld et al., 2019). Cgl2996/*ino-1* (myo-inositol-1-phosphate synthase) is the first enzyme in mycothiol biosynthesis and plays a major role in the detoxification of stress-inducing factors, maintaining the redox balance and protection against oxidative stress (Chen et al., 2019). The universal stress response protein Cgl1407/*uspA2* and HSP 60 family chaperonin, Cgl2716/*groEL* were also upregulated.

Underexpressed Metabolic, Transporter and Regulatory Genes

A similar number of genes were downregulated during the transition from shake flask to bioreactor (**Figure 3B**). Of the genes uniquely downregulated at 6.5 h, included Cgl1427/*cmk,* cytidyl kinase, Cgl2605/*bioD,* thioredoxin reductase. Cgl1427 has been reported to be crucial for maintaining triphosphate pools (ATP, CTP) under oxygen-limiting environments (Takeno et al., 2013) but it's downregulation implies these early time points are not oxygen-limited. Several genes involved in transport were also significantly downregulated with a cutoff threshold $\log_2$ ratio less than −4. These included ABC transporter ATPase proteins Cgl1351, Cgl1546/*pacL* (cation specific) and Cgl1567 along with Cgl2222, a major facilitator superfamily (MFS) transporter. Downregulated genes Cgl0026-Cgl0029 have been reported to be Zur-binding sites that are involved in zinc homeostasis in *C. glutamicum* (Schröder et al., 2010). Other downregulated transporters included the lysine exporter Cgl1262/*lysE,* exporter systems for branched chain amino acid

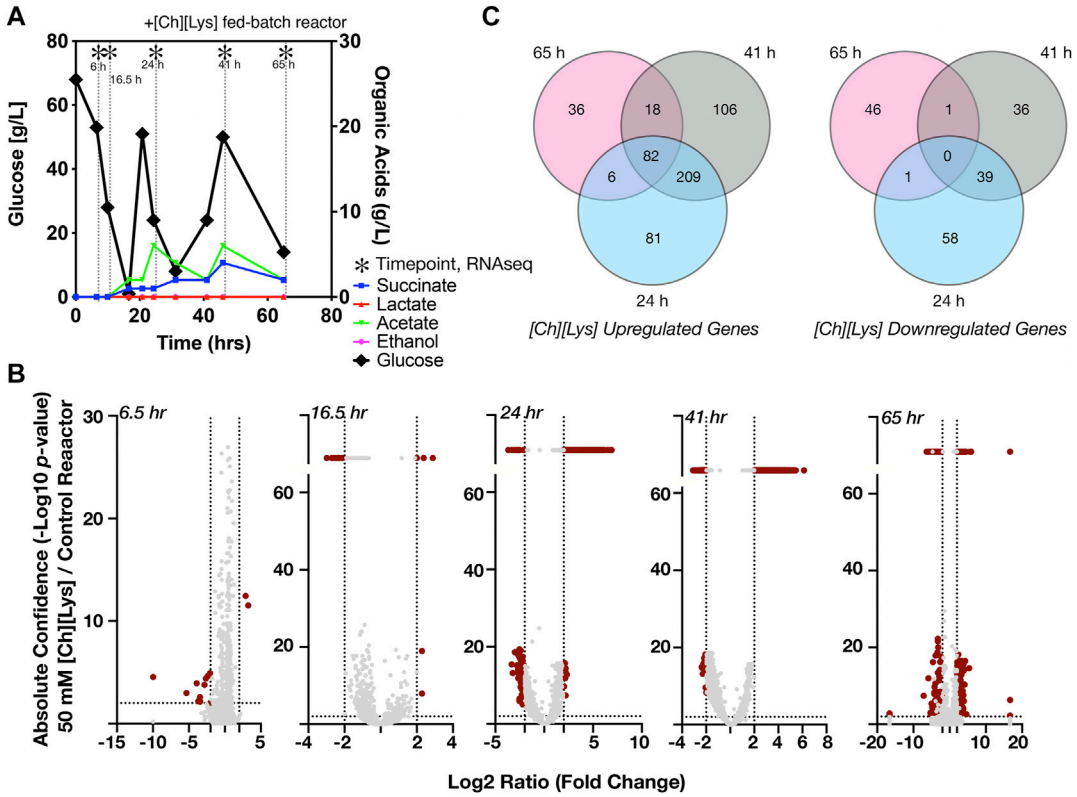

FIGURE 5 | Differential expression of genes in response to 50 mM of [Ch][Lys], **(A)** HPLC analysis of glucose and organic acids detected in the 2-L stirred tank bioreactor of cells grown in the presence of an initial concentration of 50 mM [Ch][Lys]. Cells were harvested from the indicated time points with (*). Refer to **Figure 4A** for the control bioreactor. The glucose and organic acid values for the time course in this figure panel have been previously described in Eng et al., 2020, **(B)** Volcano plots of differentially expressed genes for each time point. Genes which have confidence values or $\log_2$ ratios greater than the maximum value on each axis are plotted on a discontinuous portion of the axis as indicated with a line break. c) Shared and unique differentially expressed genes in response to [Ch][Lys]. Very few differences were detected in the 6 and 16.5 h time points and are not included in the Venn diagram. DEG was calculated as the ratio between the treated reactor and its corresponding time-matched sample in the other control reactor. Venn diagrams indicate the number of upregulated *(left)* and downregulated *(right)* genes at the indicated time points.

and methionine (*brnE/brnF*) along with several MFS transporters (Cgl1065, Cgl1076/*pcaK*, Cgl0380, Cgl0381, Cgl2685/*lmrB*) and the ABC type phosphate uptake system (*pstSCAB*). Several other ABC transporter subunits (permease or substrate-binding domain or the ATPase) responsible for transport of iron, calcium, cobalt, cadmium, copper, sn-glycerol-3-phosphate were also downregulated. Downregulated transcriptional regulators during this scale transition phase belong to the GntR family (Cgl2316), ArsR family (Cgl2279), PadR family (Cgl2979) and CopY family (Cgl0385). A complete list of DEGs can be found in **Supplementary Dataset S1 through S6** and at the JGI Genome Portal (https://genome.jgi.doe.gov/portal/) under Project ID 1203597.

Metabolic Pathway Alterations During Fed-Batch Cultivation Indicated by Differentially Expressed Genes

After inoculation into the bioreactors, we benchmarked the bioreactor run with online and offline measurements including growth, glucose consumption, and organic acid secretion, with and without [Ch][Lys]. We noted several differences between cells grown in the control reactor and the [Ch][Lys] treated reactor. While cells were pulse-fed the same feed solution to restore glucose levels back to 60 g/L, the [Ch][Lys] treated engineered strain produced much less acetate and succinate than the control (**Figures 4A**, **5A**). Overall OD_{600} measurements indicated similar initial growth patterns before the first feeding, but after feeding, OD_{600} measurements did not appreciably increase further and instead we detected overflow metabolite accumulation above 10 g/L of succinate and acetate (**Figure 4A**). The control reactor decreased in OD_{600} from a high of 49 to a 21 OD_{600}. The [Ch][Lys] reactor also decreased in OD_{600}, but from a similar high of 50 to 36 OD_{600} (**Supplementary Figure S2**). We correlated gene expression changes during this campaign for both reactors using RNAseq analysis to understand how glucose was redirected from growth to the generation of these overflow metabolites (**Supplementary Dataset S2**).

Differentially Expressed Metabolic Genes

We observed several genes encoding metabolic processes related to succinate and acetate metabolism were downregulated in the time course, such as *ptaA*, *ackA* and *sucC*. Decreasing their gene expression suggests a decrease in activity, enabling greater succinate or acetate accumulation due to fewer competing reactions for these metabolites as precursors. Cgl2211, a putative

succinate exporter (Huhn et al., 2011; Litsanov et al., 2012; Prell et al., 2020) was upregulated at 65 h, that might explain higher succinate excretion profile for the fed-batch cultivation in the absence of the IL (**Figure 4A**). The higher acetate secretion in this bioreactor correlated with upregulated Cgl2066 transcripts at 24 and 41 h, which encodes a putative acyl phosphatase that converts acetyl phosphate to acetate. At the last phase of cultivation Cgl2380/*mdh* was upregulated (log_2 ratio of 3.14) with 12-fold over expression. Malate dehydrogenase, *mdh*, is involved in a NADH based reversible reaction in TCA and is responsible for NADH balance maintenance and succinate formation. The malic enzyme, Cgl3007/*mez,* was downregulated across all later time points (log_2 ratio of −3.1 to −7.65), with 10-fold decrease in expression in the last time point alone. Malic enzyme, upregulated during transition from shake flask to a bioreactor scale (log_2 ratio of 5.11 at 6.5 h), is involved in gluconeogenesis important for NADPH regeneration for anabolic processes and pyruvate flux at the cost of carbon loss as 1 mole of CO_2. The later time points (24 h and later) had many shared downregulated genes (211 genes), indicating a phenotypic similarity (**Figure 4B**). We also observed significant downregulation of *adhA*, *ald*, *sucCD*, *malE/mez* (**Figure 4C**, blue colored genes), which were previously reported during microaerobic aeration in a bioreactor cultivation of *C. glutamicum* (Lange et al., 2018).

Differentially Expressed Transporter Genes

A more comprehensive analysis of differential gene expression indicated that many transporters were upregulated in these bioreactor time points (**Figure 4C**, red colored genes). These included ABC transporters for phosphonate (*pctABCD*); sn-glycerol-3-phosphate (*ugpABCE*) and phosphate (*pstSCAB),* a branched chain amino acid and methionine exporter (Cgl0258/*brnF*); Cgl0968/*lysI*, which encodes a protein involved in lysine uptake (Seep-Feldhaus et al., 1991). Cgl1502, a putative MFS transporter (PTS based sugar importer) was upregulated in all later bioreactor cultivation time points. A different complement of transport-related genes were also downregulated across all the later time points that included genes encoding for maltose and trehalose ABC transporter subunits (Cgl2460 and Cgl0727) and the entire glutamate ABC transporter operon *gluABCD*.

Overexpressed Regulatory Genes

Transcriptional regulators that were upregulated across all the later time points of the bioreactor cultivation and were associated with putative functions included Cgl2496/PucR family, Cgl0962/TetR family, Cgl2934/MarR family, Cgl1367/LacI family and Cgl2616/LysR family. Cgl2776 which is a putative XRE family transcriptional regulator MsrR was found to be upregulated from 24 to 65 h. *msrR* is located downstream of the *cmr* gene that encodes for a MFS multidrug efflux protein and upstream of Cgl2775/*sseA1*, a sulfurtransferase and Cgl2774. These late-phase upregulated genes have been previously reported to be regulated by MsrR and overexpressed in response to oxidative stress response in *C. glutamicum* (Si et al., 2020). Genes under the control of DtxR, a master regulator of iron homeostasis at late exponential phase (Küberl et al., 2020), and AmtR, a master regulator of nitrogen metabolism (Beckers et al., 2005) were also upregulated at later time points compared to 6.5 h. The iron homeostasis genes included Cgl0387 (putative membrane protein) and Cgl2035, an ABC-type cobalamin/Fe^{3+}-siderophores transporter. The nitrogen metabolism regulon included genes encoding for ammonium permease, *amt*; a predicted ornithine decarboxylase (*ocd*) and the ABC transporter for urea UrtABCDE. Ammonium is a critical precursor for growth and tetramethylpyrazine (TMP) production (Xiao et al., 2014). A regulator involved in diverting acetyl CoA flux towards fatty acid biosynthesis, Cgl2490/*fasR* was constitutively expressed up until the last time point during bioreactor cultivation in absence of IL. This TetR type transcriptional regulator controls fatty acid biosynthesis and malonyl CoA formation from acetyl CoA and has been deleted for improving malonyl CoA production (Milke et al., 2019). Our analysis correlated this repression by *fasR* with down regulated Cgl2495/*fas-IA* as well as downregulation of Cgl0700/*accBC*, Cgl0708/*dtsR1* and Cgl0707/*dtsR2* during later time points in absence of IL.

Underexpressed Cell Division Genes

Genes encoding cell division proteins including *mraZ, ftsX, ftsW, ftsE, sepF,* were downregulated for later stage cultivation time points (24 h and later) correlating with the lack of increased OD_{600} after glucose was fed at the 24-h time point.

Differentially Expressed Genes at Endpoint Bioreactor Cultivation

We observed a unique class of genes that were only expressed after high accumulation of succinate and acetate at the 65-h time point. At this time point, glucose consumption has stalled, and the overflow organic acids have plateaued at the ~10 g/L concentration. Genes encoding for ROS detoxification including catalase gene Cgl0255/*katA*, superoxide dismutase gene Cgl2927/*sod* along with Cgl2003/*gor,* a mycothione reductase involved in arsenate detoxification were upregulated. DEGs that were downregulated included genes encoding for *catA2, catC, nagI*, *qsuB, benC and benD.* These are enzymes involved in aromatic compound degradation through beta-ketoadipate pathway that would reroute flux into TCA through succinate and acetyl CoA.

Together the differential gene expression profile suggests that at the cell density reached by 20 h, there was a general cell stress response and the activation of microaerobic-specific genes. The growth conditions did not promote additional cell growth due to the downregulation of cell division genes; glucose uptake genes were still highly active, enabling a significant conversion of glucose to organic acids but not biomass accumulation. We interpret the expression of these genes as indicative of the unfavorable growth conditions.

C. glutamicum Exhibits a Complex Response to the IL, Cholinium Lysinate Under Fed-Batch Cultivation in the Bioreactor

Next we analyzed differential gene expression when cells were grown in the presence of 50 mM [Ch][Lys], simulating

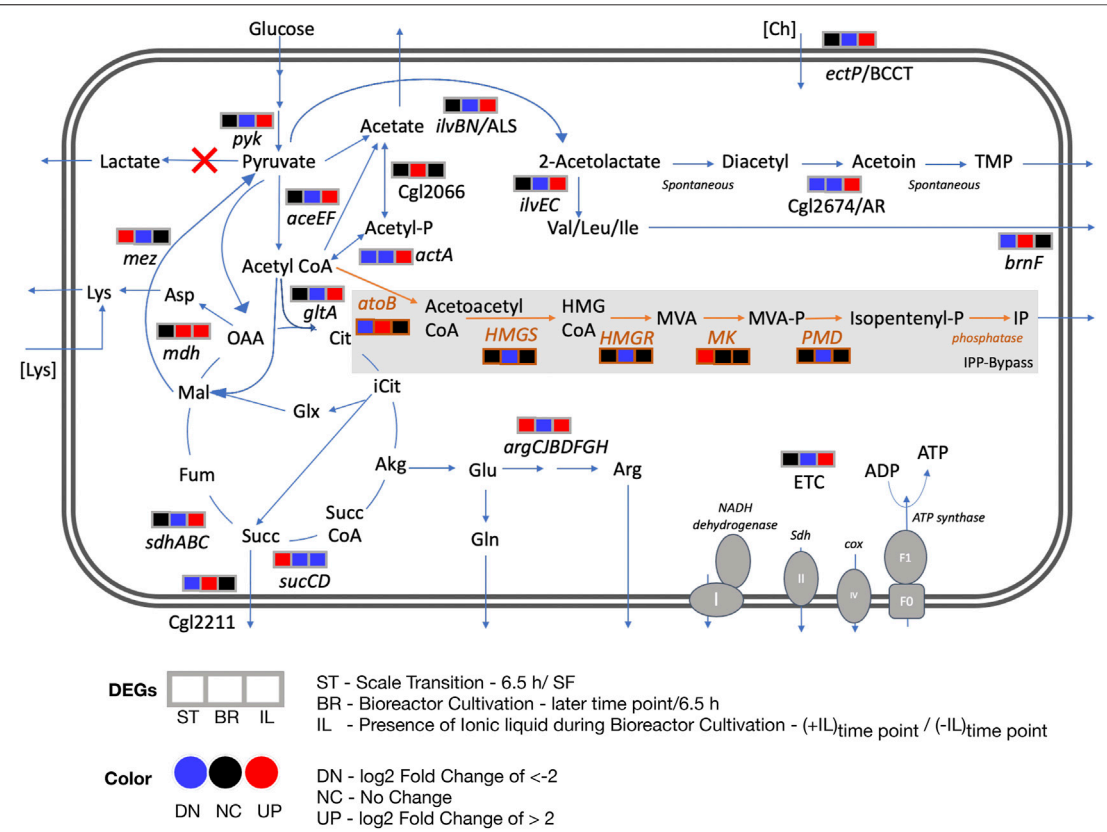

FIGURE 6 | Differential transcript profiles of engineered *C. glutamicum* under fed-batch cultivation. Three DEGs corresponding to three discrete conditions that were analyzed are represented here: ST - scale transition from shake flask (SF) to early bioreactor cultivation (6.5 h), BR - bioreactor later stage cultivation in the absence of IL and IL - bioreactor cultivation in the presence of IL compared to in the absence of IL. The heterologous pathway for IP production is shown in orange. Red crosses show the gene deletions in the *C. glutamicum* strain used in this study. Abbreviations: Acetyl-P, acetyl phosphate; Akg, alpha ketoglutarate; Arg, arginine; Asp, aspartate; *atoB*, acetyl-CoA acetyltransferase; Cit, citrate; Ch, cholinium; Cox, cytochrome oxidase; ETC, Electron transport chain; Fum, fumarate; Glx, glyoxylate; Glu, glutamate; Gln, glutamine; *HMGS*, hydroxymethylglutaryl-CoA synthase; *HMGR*, 3-hydroxy-3-methylglutaryl-CoA reductase; HMG CoA, 3-hydroxy-3-methyl-glutaryl-coenzyme A; Icit, isocitrate; IP, Isopentenol; Lys, lysine; Mal, malate; *MK*, mevalonate kinase; MVA, mevalonate; MVA-P, mevalonate; OAA, oxaloacetate; PMD, phosphomevalonate decarboxylase; Succ, succinate; Succ CoA, succinyl-CoA; Sdh, succinate dehydrogenase; TMP, tetramethylpyrazine.

hydrolysate prepared under a water-conservation regimen (Neupane et al., 2017). ILs have been reported to increase osmotic pressure, interact with lipid structures and consequently disrupt microbial membranes (Thuy Pham et al., 2010; Khudyakov et al., 2012; Yu et al., 2016). *C. glutamicum* exhibited differential expression of 727 genes (**Supplementary Dataset S3**), during the [Ch][Lys] treated fed-batch bioreactor cultivation in comparison to the untreated culture at the time-matched samples (**Figure 5A**). While both bioreactors consumed the initial glucose in the reactor at similar rates, their response to the first feeding at 24 h differed. The [Ch][Lys] reactor showed maximum accumulation of 4 g/L succinate and 6 g/L acetate over the duration of this time course, a 4-fold decrease for both organic acids in the absence of [Ch][Lys] (compare **Figures 4A**, **5A**). In the presence of [Ch][Lys], genes encoding for succinate utilization such as *sdhA*, *sdhB* and *sdhC* were all upregulated at 24 and 41 h in contrast to the control reactor. Similarly, genes encoding for pyruvate decarboxylation to acetyl CoA (instead of acetate) via *aceE* and *aceF* were also highly upregulated at later time points.

During the early cultivation time points (6.5–16.5 h), only 1.5% of the total pool of differentially expressed genes changed in response specifically to [Ch][Lys], but the datasets diverged after the first feeding at 24 h as biomass formation reached its maximum (**Figure 5B**). Only two genes were upregulated at the 6.5 h time point: a MFS transporter (Cgl2611) and its transcriptional regulator (Cgl2612) (**Supplementary Dataset S3**). The BRC-JBEI 1.1.2 homolog is 97.37% identical to Cgl2611 which exports cadaverine, a L-lysine derived product (Kind et al., 2011; Adkins et al., 2012; Jones et al., 2015; Tsuge et al., 2016). Cgl2611 expression was not detected at the control 6.5 h time point, but both genes are highly upregulated with or without [Ch][Lys] treatment in the remaining time points. Cgl1203, which encodes a phospho-N-acetylmuramoyl-pentapeptide-transferase associated with cell wall biosynthesis, was only upregulated at 16.5 h.

Early transcriptome changes in *C. glutamicum* during bioreactor cultivation post [Chl][Lys] exposure included overexpression of MFS transporters along with repression of mechanosensitive channels that were consistent with IL

tolerance mechanisms reported in other microbes (Khudyakov et al., 2012; Martins et al., 2013; Yu et al., 2016). Many genes were downregulated in response to exogenous [Ch][Lys] in the bioreactor and represented 25% of DEGs. Cgl0879/*mscL*, a large-conductance mechanosensitive channel, that is related to osmotic regulation (Krämer, 2009), was uniquely downregulated at 16.5 h.

A comprehensive analysis of upregulated DEGs at more than one time point represented around 59% of the total upregulated genes in the presence of IL (**Figure 5B**). Nearly 15% of those genes showed consistent overexpression from 24 h through 65 h (**Figure 5C**). This differential transcript profile reflects the metabolic perturbation over the course of the fed-batch cultivation after the initial glucose exhaustion followed by glucose pulse feeding and is depicted in **Figure 6**. Prominent DEGs include those encoding for energy metabolism, amino acids biosynthesis, response to oxidative and other environmental stress conditions (**Supplementary Dataset S4**).

Overexpressed Metabolic Genes

Genes involved in energy metabolism were highly upregulated during the later phase of fed-batch cultivation in the presence of IL compared to its absence. These included NADH dehydrogenase (Cgl1465), succinate dehydrogenase, *sdhABC* genes at 24 and 41 h; cytochrome oxidase, *ctaDCEF*, cytochrome reductase, *qcrCAB* and the ATP synthase complex (Cgl1206 to Cgl1213) genes at 24, 41 and 65 h. Amino acid biosynthetic genes upregulated at the later time points included the arginine biosynthetic genes *argC, argJ, argB* and *argH* at 65 h and *argG* and *argD* at mid cultivation phase (41 h). ArgJ protein was also enriched in the acetoin/TMP producing *C. glutamicum* strain (Eng et al., 2020). Genes encoding for other amino acid biosynthesis included Cgl1139/*metE*, Cgl2446/*metB* and Cgl0653/*metY* at 24 and 41 h from the methionine/homocysteine pathway; Cgl2204/*ilvE* at 24 h and Cgl1273/*ilvC* at 24 and 41 h in the branched amino acid pathway.

Overexpressed Genes Encoding Ribosomal Proteins

Several ribosomal proteins were significantly upregulated during the same cultivation phase (24 and 41 h) including 30S ribosomal proteins S15 (Cgl1976/*rpsO*) and S18 (Cgl0866/*rpsR*); 50S ribosomal proteins L28 (Cgl0869/*rpmB*) and L15 (Cgl0542/*rplO*) along with the ribosome recycling factor Cgl2023/*frr*.

Overexpressed Transporter Genes

We also observed the upregulation of an ABC transporter (Cgl0946 and Cgl0947), a multidrug transport system (MTS) operon, in part regulated by its adjacent two-component system (TCS) (Cgl0948-Cgl0949, also upregulated). MTS offers a natural defense against toxic compounds and is reported to be upregulated in response to the non-ionic surfactant Tween 40 (Jiang et al., 2020). Also, Cgl2312/*ectP*, a putative BCCT family transporter was overexpressed in the bioreactor with IL at 24 h time point. This gene, an orthologue for *betT* gene in *E. coli* and *P. putida*, was under-expressed in the bioreactor without IL at later time points (24 h, 41 h). Betaine/carnitine/choline (BCCT) family transporters could enable cholinium uptake and catabolism. An array of other transporters and transcriptional regulators were also downregulated in the presence of IL (**Supplementary Dataset S3**).

While the analysis above compared matched time points with or without [Ch][Lys] treatment, we also included one additional analysis to examine DEGs from samples in the same reactor but as they progressed from the 41 to 65 h time point (**Supplementary Figure S3**, and **Supplementary Dataset S6**). As observed from our earlier analysis in **Figure 4C** a set of DEGs in the control bioreactor were detected, consistent with entry into the stationary phase. Significantly downregulated genes also included genes encoding for a stationary phase repressor protein/redox responsive transcription factor, *whiB*/Cgl0599 (Walter et al., 2020) and a branched chain amino acid transporter (Cgl2250) (Graf et al., 2019). Cgl2250 has been reported to be downregulated during the transition from exponential to stationary phase in *C. glutamicum* (Larisch et al., 2007).

Indication of Flux Rerouting in the Presence of IL Stress During Fed-Batch Bioreactor Cultivation

Our transcriptome analysis identified differential profiles for energy metabolism, amino acid biosynthesis and redox related genes as discussed in the previous section (**Figure 6**). Several genes encoding for metabolic reactions related to acetoin and TMP accumulation were specifically upregulated in the presence of 50 mM of [Ch][Lys] at the 24 h or 41 h time points (**Supplementary Dataset S3**, **Supplementary Figure S4**) when compared to the control samples at the same time points. Of the two subunits of the acetolactate synthase (ALS) *ilvB and ilvN,* the smaller regulatory subunit, Cgl1272/*ilvN* was upregulated in the presence of IL fed-batch cultivation when compared to the absence of IL at 24 h. Acetolactate synthase in *C. glutamicum* takes part in diverting pyruvate flux towards branched chain amino acids biosynthesis and acetoin biosynthesis and could be a precursor to TMP (Eng et al., 2020) (**Figure 5**). Although branched chain amino acid biosynthesis has been extensively researched for engineering branched chain alcohol (e.g. isobutanol) producing *C. glutamicum* strains (Hasegawa et al., 2020) the branched chain amino acid degradation towards isopentenol biosynthesis (through HMG-CoA) and TCA through acetyl CoA still remains to be fully investigated. The other proposed enzyme in TMP accumulation is the NADH consuming acetoin reductase (AR, Cgl2674) and was also significantly upregulated ($\log_2 > 4$) at 41 h in presence of 50 mM of [Ch][Lys] compared to fed-batch cultivation in the absence of IL at similar time points. Genes encoding mechanisms that divert pyruvate flux towards acetyl CoA (Cgl2248/*aceE* and Cgl2207/*aceF*) were also upregulated along with genes for pyruvate kinase (Cgl2089/*pyk*) and citrate synthase (Cgl0829/*gltA*).

DISCUSSION

C. glutamicum is a strong contender as a microbial chassis for IP production and is already used at commercial scales. To test IP production in stirred-tank bioreactors, we used process

optimizations empirically identified for high IP titers in *E. coli* (Kang et al., 2019). In *E. coli*, Kang et al. reported IP titers > 3 g/L in fed-batch mode production; in contrast, these process parameters led to much lower IP titers in *C. glutamicum*. It is possible that these optimizations were specific to *E. coli;* the impact of this IP production pathway in *C. glutamicum* upon shifting from batch mode to fed-batch mode in a stirred tank bioreactor may have resulted in a different host-specific metabolic response.

What parameters are important in selecting one microbial host over another? From a genetic tractability perspective, *C. glutamicum*'s biggest drawback *vs.* model microbes such as *E. coli* could arise from its reduced transformation efficiency, which was lower by 3–5 orders of magnitude (Chung et al., 1989; Inoue et al., 1990; Ruan et al., 2015). However, Baumgart and coworkers made an astute observation; by using a methylation deficient strain of *C. glutamicum*, one could both improve transformation efficiency as well as plasmid copy number (Baumgart et al., 2013). Improved pathway copy number (both genomically integrated or plasmid-borne) in *E. coli* had already been shown to dramatically improve heterologous isoprenoid titers (Goyal et al., 2018; Chatzivasileiou et al., 2019). With this premise we initially used a methylation deficient strain as our starting host. However, the methylation deficient strain only produced trace titers of IP, but a related strain produced both improved IP titers 20x or a co-product, tetra-methylpyrazine. Understanding the genetic differences in this isolate BRC-JBEI 1.1.2 was the major thrust of this study.

Leveraging strain isolate differences is already commonplace when analyzing natively expressed products, such as natural products from *Streptomyces* spp. or wine, beer, and baking in *Saccharomyces* spp. (Nepal and Wang, 2019; Gallone et al., 2016). In *E. coli*, the Hanahan cloning strain DH1 is the preferred strain for the production of many terpenes, but experimentally identified modifications are needed to translate port pathways to other *E. coli* isolates as with the case for limonene production in *E. coli* BL21 (DE3) (Tsuruta et al., 2009; Rolf et al., 2020). A potential explanation for DH1 being a more robust host may be due to its elevated number of ribosomes compared to strains DH10, BL21, or BW25113 (Cardinale et al., 2013), which may indirectly help with heterologous pathway protein expression. Our whole-genome sequencing analysis identified a large number of genetic differences in our engineered isopentenol producing *C. glutamicum* BRC-JBEI 1.1.2 isolate (many associated with metabolic functions) that are unaccounted for when using the reference *C. glutamicum* genome. Previously we used computationally driven maximum theoretical yields calculations for a product across several microbes to evaluate microbial potential for a specific product/substrate pair (Banerjee et al., 2020). However, the accuracy of such predictions relies on the metabolic reactions curated for the reference strain and are challenging to apply in isolates used with differences at the genomic or metabolic level (refer to IP titers in **Figure 1A**). Pan-genome assemblies and metabolic models can be applied to this situation (both for BRC-JBEI 1.1.2 and DH1) to more accurately account for these metabolic features (Monk et al., 2013; Norsigian et al., 2018).

For emerging processes using IL pretreated lignocellulosic biomass, *C. glutamicum* as the microbial IP producer for this process is compelling. To the best of our knowledge, this is the first transcriptomics analysis of an engineered isopentenol producing *C. glutamicum* strain in fed-batch conditions. Due to the relative similarity between this isolate to the type strain, we were able to use existing gene annotations with a fairly low homology cutoff (> 70%) for the majority of detected transcripts in this study. A large number of significant DEGs identified in this analysis encode hypothetical proteins that lack functional information. These genes can be further characterized using functional genomics tools such as parallelized transposon mutant libraries (Lim et al., 2019; Cain et al., 2020) or high throughput transcription factor characterization (Rajeev et al., 2011; Rajeev et al., 2014) to improve our understanding of these useful *C. glutamicum* isolates.

Our analysis here indicated a number of actionable targets for future studies to improve isopentenol titers under stirred tank fed-batch conditions. Deleting *mdh* could limit accumulation of succinate, a highly overexpressed gene. Deleting or down regulating *gltA,* Cgl2211, *brnF* and arginine biosynthesis genes that were also highly upregulated (**Figure 6**); could enlarge the acetyl-CoA pool, in turn improving IP titers. Additional gene targets should include *pta-ackA, poxB, actA* and Cgl2066 to block acetate formation. These proposed targets are specific to *C. glutamicum* host engineering for isopentenol production. Our transcriptomics analysis also implicated *ectP*, a BCCT family transporter similar to *E. coli betT* and *P. putida betT-III,* as a transporter for [Ch][Lys]; *ectP* was overexpressed in the presence of ILs. A BCCT transporter has been proposed to be involved in uptake and catabolism of the cholinium ion from [Ch][Lys] in both *E. coli* and *P. putida* (Park et al., 2020). Characterizing IL tolerance is an active research thrust in our laboratory.

In summary, our transcriptomic analysis under industrially relevant process conditions provides a toehold for future DBTL cycles. Future learn steps can leverage the information gleaned here to target the critical features implicated for improved *C. glutamicum* strain performance when producing desirable products, like isopentenol. Even accounting for potential increased cell heterogeneity in the bioreactor (Wehrs et al., 2019), important features both common and unique to conditions allow a closer look into cell physiology.

MATERIALS AND METHODS

Reagents and Experimental Conditions

In a previous report (Sasaki et al., 2019), we referred to the IP producing *C. glutamicum* strain as ATCC 13032 NHRI 1.1.2, as indicated in our archival notes. As we cannot confirm the provenance of *C. glutamicum* BRC-JBEI 1.1.2 and how it may have been derived from its closest relatives *C. glutamicum* SCgG1 or SCgG2, we opted to give this strain a unique identifier to avoid further confusion.

Unless indicated elsewhere, all reagents used were molecular biology grade or higher. Primers were synthesized by IDT DNA Technologies (Coralville, IA). CGXII media was prepared as previously described (Sasaki et al., 2019; Keilhauer et al., 1993). All strains and plasmids used in this study are described in **Supplementary Table S2**. *C. glutamicum* strains were struck to single colonies from glycerol stock on LB plates containing the appropriate antibiotic and prepared for production runs as previously described (Eng et al., 2020). The fed-batch cultivation

with 50 mM of [Ch][Lys] supplementation was previously described in (Eng et al., 2020). The control bioreactor without [Ch][Lys] was conducted at the same time and the glucose feeding regime was identical to that of the ionic liquid (IL) supplemented reactor. For RNAseq extraction, 5 ml culture samples were harvested in 1 ml aliquots, collected by centrifugation at 14,000 × *g* for 3 min, and stored at −80°C until subsequent RNA extraction. The supernatant from one of the appropriate time point aliquots was processed for organic acid analysis as described previously (Eng et al., 2020). Lab-scale IP production in deep well plates or 5 ml culture tubes were conducted as previously described (Eng et al., 2020). Isopentenol titers reported for the deep well plate format were corrected for evaporation at the 48 h time point as conducted previously (Sasaki et al., 2019). Exogenous [Ch][Lys] toxicity against *C. glutamicum* ATCC13032 and BRC-JBEI 1.1.2 was analyzed in a 48-well microtiter dish format. Cells were first adapted two times in CGXII minimal media with 4% (w/v) D-glucose. When cells were back diluted into fresh media in the microtiter dish, the starting Optical Density (OD) was set to 0.1 with a fill volume of 200 µl. The plate was incubated with shaking at 30°C and exogenous [Ch][Lys] added at the start of the time course. OD was monitored at 600 nm on a Synergy 4 plate reader (BioTek Instruments, Winooski VT) with the continuous shaking setting.

Production Run With Ensiled Sorghum Hydrolysate

CGXII minimal media was supplemented with ensiled sorghum biomass hydrolysate to test the ability of *C. glutamicum* BRC-JBEI 1.1.2 to utilize carbon sources from renewable feedstock pretreated with IL. Briefly, the forage sorghum (NK300 type, grown in Fresno, CA) was planted in Spring 2020 and harvested in Fall 2020. A forage harvester was used to both harvest and chop the sorghum biomass, which was then loaded in a silage pit, inoculated, and covered to maintain anaerobic conditions. The pit was opened in November 2020 and a sample of the ensiled material was collected, packed with dry ice while in transit, and stored at 4°C. A 210 L scale Andritz Hastelloy C276 pressure reactor (AG, Graz, Austria) with a helical impeller was utilized to process ensiled sorghum for the pretreatment and saccharification processes. Ensiled sorghum biomass was pretreated at 20% w/w solid loading with 10% w/w [Ch][Lys] at 140°C for 3 h with a mixing speed of 30 rpm. Solid loading was calculated based on the dry matter content determined using a Binder VDL115 vacuum oven. After 3 h at the target temperature, the reactor was cooled to room temperature before proceeding with the next steps. The Andritz reactor is sealed during this process, preventing contamination until further processing. Following pretreatment, the pretreated materials were adjusted to pH 5.1 using 50% v/v sulfuric acid and an enzyme cocktail of Novozyme, Inc. Cellic Ctec3 and Cellic Htec3 commercial enzymes in a ratio of 9:1 was added. Concentration of the commercial stocks were determined using Bradford assays and bovine serum albumin as a reference. Enzyme load was conducted at a ratio of 10 mg enzyme per 1 g of dry weight biomass. Following pH adjustment and enzyme addition, RODI water was added to obtain a final solid loading of 18.70%. Saccharification by enzymatic hydrolysis was operated at 50°C, 30 rpm for 70 h (Barcelos et al., 2021). The hydrolysate was then sequentially filtered using a filter press through 5, 1, and 0.25 µm filters. Final filter sterilization was completed with a 0.2 µm filter and stored at −80°C until further use. This hydrolysate was thawed and added in place of water in CGXII media (amounting to 2.8 % (w/v) glucose), pH was adjusted to 7.4 and filter sterilized one additional time before use. We make the assumption the hydrolysate contained no biologically available nitrogen. To maintain a C/N ratio of glucose/ammonium sulfate + urea of 2.8, pure glucose powder was supplemented to the hydrolysate CGXII cultivation medium composition (Sasaki et al., 2019).

DNA and RNA Isolation

Genomic DNA from *C. glutamicum* BRC-JBEI 1.1.2 was isolated with the following protocol. In brief, strains from glycerol stocks were struck to single colonies on LB plates grown at 30°C overnight. A single colony was then inoculated into a 250 ml shake flask with 25 ml LB media and grown overnight to saturation. Cells were collected by centrifugation at 4,000 × *g* for 5 min. The cell pellet was then resuspended in 2 ml lysis buffer (2 mM EDTA, 250 mM NaCl, 2% (w/v) SDS, 2% (v/v) Triton-X 100, 2% (v/v) Tween-80, 5 mM DTT, 30 units Zymolase 100T, 1 mg/ml RNaseA). Zymolyase was supplied by US Biological (Salem, MA). The cells were initially incubated at 50°C for 30 min to promote protease activity and then incubated for an additional 3 h at 37°C with occasional mixing, at which point the lysate became noticeably viscous. DNA was extracted following standard protocols for isolation of DNA using phenol chloroform: isoamyl alcohol and subsequent isopropanol precipitation (Sambrook and Russell, 2001).

RNA was extracted from *C. glutamicum* samples using a Direct-Zol RNA Kit (Zymo Research, Irvine, CA) following the manufacturer's protocol. *C. glutamicum* cells were lysed after initially resuspending the cell pellet in 500 µl TRI reagent and mixed with glass beads. This mixture was then subject to cell disruption using a bead-beater (Biospec Inc., Bartlesville, OK) with a 3-min homogenization time at maximum intensity. After bead beating, samples were collected following the manufacturer's protocol without any additional modifications. RNA quality was assessed using a BioAnalyzer (Agilent Technologies, Santa Clara, CA) before RNA library preparation and downstream analysis.

For 16S ribosomal sequencing, *C. glutamicum* ATCC 13032 Δ*mrr* and *C. glutamicum* JBEI-BRC 1.1.2 were struck from glycerol stocks to single colonies on LB plates and incubated overnight at 30°C. A single colony was isolated and boiled in 50 µl dH_20 for 10 min. 1 µl of the boiled colony was used for PCR with primer pair (JGI_27F: 5′-AGAGTTTGATCCTGGCTCAG-3′ and JGI_1391R: 5′-GACGGGCRGTGWGTRCA-3′) with NEB Q5 Polymerase (New England Biolabs, Ipswitch, MA). The PCR amplicon was confirmed by agarose gel electrophoresis and the sequence was determined using conventional Sanger Sequencing (Genewiz LLC, Chelmsford, MA).

PacBio Genome Assembly

DNA sequencing was generated at the DOE Joint Genome Institute (JGI) using the Pacific Biosciences (PacBio) sequencing technology. A Pacbio SMRTbell(tm) library was constructed and sequenced on the PacBio Sequel and PacBio RS II platforms, which generated 397,096 filtered subreads (1,418,602,725 subread bases) totaling

3,352,276 bp. The mean coverage for this genome was 432.21x. All general aspects of library construction and sequencing performed at the JGI can be found at http://www.jgi.doe.gov.

RNAseq Library Generation and Processing for Illumina NGS

Stranded RNAseq library(s) were created and quantified by qPCR. Sequencing was performed using an Illumina instrument (refer to **Supplementary Table S3** for specifics per library). Raw fastq file reads were filtered and trimmed using the JGI QC pipeline resulting in the filtered fastq file (*.filter-RNA.gz files). Using BBDuk (https://sourceforge.net/projects/bbmap/), raw reads were evaluated for artifact sequence by kmer matching (kmer = 25), allowing for 1 mismatch and detected artifacts which were trimmed from the 3′ end of the reads. RNA spike-in reads, PhiX reads and reads containing any Ns were removed. Quality trimming was performed using the phred trimming method set at Q6. Following trimming, reads that did not meet the length threshold of at least 50 bases were removed.

Filtered reads from each library were aligned to the reference genome using HISAT2 version 2.2.0 (Kim et al., 2015). Strand-specific coverage bigWig files were generated using deepTools v3.1 (Ramírez et al., 2014). Next, featureCounts (Liao et al., 2014) was used to generate the raw gene counts (counts.txt) file using gff3 annotations. Only primary hits assigned to the reverse strand were included in the raw gene counts (-s 2 -p --primary options). Raw gene counts were used to evaluate the level of correlation between biological replicates using Pearson's correlation and determine which replicates would be used in the DEG analysis (**Supplementary Figure S5**). In the heatmap view, the libraries were ordered as groups of replicates. The cells containing the correlations between replicates have a purple (or white) border around them. For fragments per kilobase of transcript per million fragments mapped (FPKM) and TPM, normalized gene counts refer to SRA reads (Data availability section). A sample legend and description of RNAseq libraries used in this paper is described in **Supplementary Table S3**.

Transcriptome Analysis

Global transcriptome response under various experiment conditions were measured using Geneious Prime 2021 (https://www.geneious.com). The normalized expression was calculated and the differentially expressed genes (DEGs) were filtered for absolute $\log_2$ ratio >2 (i.e. a 4-fold up or down regulation), absolute confidence >3 ($p < 0.001$) and >90% sequence identity. The DEGs at various conditions were functionally annotated using Blast2GO suite (Götz et al., 2008) to assign GO annotations (Galperin et al., 2015). Each DEG was subjected to pathway analysis using the KEGG (Kyoto Encyclopedia of Genes and Genomes) database (http://www.kegg.jp/kegg/pathway.html) to explore the biological implications. Biocyc (https://biocyc.org/) was used to calculate pathway enrichment for the last 65 h/41 h time point and for additional gene orthologs identification. Pathways were considered significant if $p < 0.05$. Hierarchically clustered heat maps were generated with average linkage method and euclidean distance metric in Jupyter notebook using Python library Seaborn 0.11.1 (Waskom et al., 2020).

DATA AVAILABILITY STATEMENT

The datasets presented in this study can be found in online repositories. The names of the repository/repositories and accession number(s) can be found below: https://www.ncbi.nlm.nih.gov/, PRJNA533344 https://www.ncbi.nlm.nih.gov/, GCA_011761195.1 https://www.ncbi.nlm.nih.gov/, SRP23996 https://www.ncbi.nlm.nih.gov/, SRP239973 https://www.ncbi.nlm.nih.gov/, SRP239963 https://www.ncbi.nlm.nih.gov/, SRP239971 https://www.ncbi.nlm.nih.gov/, SRP239972 https://www.ncbi.nlm.nih.gov/, SRP239970 https://www.ncbi.nlm.nih.gov/, SRP2399a68 https://www.ncbi.nlm.nih.gov/, SRP239969 https://www.ncbi.nlm.nih.gov/, SRP239966 https://www.ncbi.nlm.nih.gov/, SRP239967 https://www.ncbi.nlm.nih.gov/, SRP239964 https://www.ncbi.nlm.nih.gov/, SRP239965.

AUTHOR CONTRIBUTIONS

Raised Funds: AM and BS. Conceptualization of the project: AM and TE. Strain construction, molecular biology, bioreactor sample collection and processing: YS, TE, RH, and JT. Analytical Chemistry, IP Production Assays, IL toxicity assays: YS, TE, and AS. Interpreted results: YS, DB, TE, and AM. Contributed critical reagents: NS, AO, CS, DP, TE, YS, JT, and BS. RNAseq library generation, data collection, validation: VS, YS, and TE. Drafted the manuscript: DB, TE, and AM. All authors read, contributed feedback, and approved the final manuscript for publication.

FUNDING

A portion of this work was conducted by the United States Department of Energy Joint Genome Institute, a DOE Office of Science User Facility, supported by the Office of Science of the United States Department of Energy under Contract No. DE-AC02-05CH11231. Other portions of this work were part of the Joint Bioenergy Institute project, funded by the United States Department of Energy, Office of Science, through contract DE-AC02-05CH11231 between Lawrence Berkeley National Laboratory and the United States Department of Energy.

ACKNOWLEDGMENTS

We thank Andrew Lau for feedback on the figures. We also thank Venkata Ramana Reddy Pidatala and Alex Codik for technical assistance.

SUPPLEMENTARY MATERIAL

The Supplementary Material for this article can be found online at: https://www.frontiersin.org/articles/10.3389/fbioe.2021.766674/full#supplementary-material

REFERENCES

Adkins, J., Pugh, S., McKenna, R., and Nielsen, D. R. (2012). Engineering Microbial Chemical Factories to Produce Renewable "Biomonomers". *Front. Microbio.* 3, 313. doi:10.3389/fmicb.2012.00313

Ashburner, M., Ball, C. A., Blake, J. A., Botstein, D., Butler, H., Cherry, J. M., et al. (2000). Gene Ontology: Tool for the Unification of Biology. *Nat. Genet.* 25, 25–29. doi:10.1038/75556

Banerjee, D., Eng, T., Lau, A. K., Sasaki, Y., Wang, B., Chen, Y., et al. (2020). Genome-scale Metabolic Rewiring Improves Titers Rates and Yields of the Non-native Product Indigoidine at Scale. *Nat. Commun.* 11, 5385. doi:10.1038/s41467-020-19171-4

Baral, N. R., Yang, M., Harvey, B. G., Simmons, B. A., Mukhopadhyay, A., Lee, T. S., et al. (2021). Production Cost and Carbon Footprint of Biomass-Derived Dimethylcyclooctane as a High Performance Jet Fuel Blendstock. *ACS Sustainable Chem. Eng.* 9, 11872–11882. doi:10.1021/acssuschemeng.1c03772

Barcelos, C. A., Oka, A. M., Yan, J., Das, L., Achinivu, E. C., Magurudeniya, H., et al. (2021). High-Efficiency Conversion of Ionic Liquid-Pretreated Woody Biomass to Ethanol at the Pilot Scale. *ACS Sustain. Chem. Eng.* 9, 4042–4053. doi:10.1021/acssuschemeng.0c07920

Baumgart, M., Unthan, S., Rückert, C., Sivalingam, J., Grünberger, A., Kalinowski, J., et al. (2013). Construction of a Prophage-free Variant of *Corynebacterium glutamicum* ATCC 13032 for Use as a Platform Strain for Basic Research and Industrial Biotechnology. *Appl. Environ. Microbiol.* 79, 6006–6015. doi:10.1128/AEM.01634-13

Becker, J., Rohles, C. M., and Wittmann, C. (2018). Metabolically Engineered *Corynebacterium glutamicum* for Bio-Based Production of Chemicals, Fuels, Materials, and Healthcare Products. *Metab. Eng.* 50, 122–141. doi:10.1016/j.ymben.2018.07.008

Beckers, G., Strösser, J., Hildebrandt, U., Kalinowski, J., Farwick, M., Krämer, R., et al. (2005). Regulation of AmtR-Controlled Gene Expression in *Corynebacterium glutamicum*: Mechanism and Characterization of the AmtR Regulon. *Mol. Microbiol.* 58, 580–595. doi:10.1111/j.1365-2958.2005.04855.x

Cain, A. K., Barquist, L., Goodman, A. L., Paulsen, I. T., Parkhill, J., and van Opijnen, T. (2020). A Decade of Advances in Transposon-Insertion Sequencing. *Nat. Rev. Genet.* 21, 526–540. doi:10.1038/s41576-020-0244-x

Cardinale, S., Joachimiak, M. P., and Arkin, A. P. (2013). Effects of Genetic Variation on the *E. coli* Host-Circuit Interface. *Cel Rep.* 4, 231–237. doi:10.1016/j.celrep.2013.06.023

Chatzivasileiou, A. O., Ward, V., Edgar, S. M., and Stephanopoulos, G. (2019). Two-step Pathway for Isoprenoid Synthesis. *Proc. Natl. Acad. Sci. USA.* 116, 506–511. doi:10.1073/pnas.1812935116

Chen, C., Chen, K., Su, T., Zhang, B., Li, G., and Pan, J. (2019). Myo-inositol-1-phosphate Synthase (Ino-1) Functions as a Protection Mechanism in *Corynebacterium glutamicum* Under Oxidative Stress. *Microbiologyopen.* 8, e00721. doi:10.1002/mbo3.721

Chou, H. H., and Keasling, J. D. (2012). Synthetic Pathway for Production of Five-Carbon Alcohols from Isopentenyl Diphosphate. *Appl. Environ. Microbiol.* 78, 7849–7855. doi:10.1128/AEM.01175-12

Chung, C. T., Niemela, S. L., and Miller, R. H. (1989). One-step Preparation of Competent *Escherichia coli*: Transformation and Storage of Bacterial Cells in the Same Solution. *Proc. Natl. Acad. Sci.* 86, 2172–2175. doi:10.1073/pnas.86.7.2172

Eng, T., Demling, P., Herbert, R. A., Chen, Y., Benites, V., Martin, J., et al. (2018). Restoration of Biofuel Production Levels and Increased Tolerance under Ionic Liquid Stress Is Enabled by a Mutation in the Essential *Escherichia coli* Gene cydC. *Microb. Cel Fact.* 17, 159. doi:10.1186/s12934-018-1006-8

Eng, T., Sasaki, Y., Herbert, R. A., Lau, A., Trinh, J., Chen, Y., et al. (2020). Production of Tetra-Methylpyrazine Using Engineered *Corynebacterium glutamicum*. *Metab. Eng. Commun.* 10, e00115. doi:10.1016/j.mec.2019.e00115

Gallone, B., Steensels, J., Prahl, T., Soriaga, L., Saels, V., Herrera-Malaver, B., et al. (2016). Domestication and Divergence of *Saccharomyces cerevisiae* Beer Yeasts. *Cell* 166, 1397–1410. doi:10.1016/j.cell.2016.08.020

Galperin, M. Y., Makarova, K. S., Wolf, Y. I., and Koonin, E. V. (2015). Expanded Microbial Genome Coverage and Improved Protein Family Annotation in the COG Database. *Nucleic Acids Res.* 43, D261–D269. doi:10.1093/nar/gku1223

Götz, S., García-Gómez, J. M., Terol, J., Williams, T. D., Nagaraj, S. H., Nueda, M. J., et al. (2008). High-throughput Functional Annotation and Data Mining with the Blast2GO Suite. *Nucleic Acids Res.* 36, 3420–3435. doi:10.1093/nar/gkn176

Goyal, G., Costello, Z., Alonso-Gutierrez, J., Kang, A., Lee, T. S., Garcia Martin, H., et al. (2018). Parallel Integration and Chromosomal Expansion of Metabolic Pathways. *ACS Synth. Biol.* 7, 2566–2576. doi:10.1021/acssynbio.8b00243

Graf, M., Haas, T., Müller, F., Buchmann, A., Harm-Bekbenbetova, J., Freund, A., et al. (2019). Continuous Adaptive Evolution of a Fast-Growing *Corynebacterium glutamicum* Strain Independent of Protocatechuate. *Front. Microbiol.* 10, 1648. doi:10.3389/fmicb.2019.01648

Hahne, J., Kloster, T., Rathmann, S., Weber, M., and Lipski, A. (2018). Isolation and Characterization of Corynebacterium Spp. From Bulk Tank Raw Cow's Milk of Different Dairy Farms in Germany. *PLoS ONE* 13, e0194365. doi:10.1371/journal.pone.0194365

Hasegawa, S., Jojima, T., Suda, M., and Inui, M. (2020). Isobutanol Production in *Corynebacterium glutamicum*: Suppressed Succinate By-Production by pckA Inactivation and Enhanced Productivity via the Entner-Doudoroff Pathway. *Metab. Eng.* 59, 24–35. doi:10.1016/j.ymben.2020.01.004

Hou, X.-D., Liu, Q.-P., Smith, T. J., Li, N., and Zong, M.-H. (2013). Evaluation of Toxicity and Biodegradability of Cholinium Amino Acids Ionic Liquids. *PLoS ONE* 8, e59145. doi:10.1371/journal.pone.0059145

Huhn, S., Jolkver, E., Krämer, R., and Marin, K. (2011). Identification of the Membrane Protein SucE and its Role in Succinate Transport in *Corynebacterium glutamicum*. *Appl. Microbiol. Biotechnol.* 89, 327–335. doi:10.1007/s00253-010-2855-1

Hünnefeld, M., Persicke, M., Kalinowski, J., and Frunzke, J. (2019). The MarR-type Regulator MalR Is Involved in Stress-Responsive Cell Envelope Remodeling in *Corynebacterium glutamicum*. *Front. Microbiol.* 10, 1039. doi:10.3389/fmicb.2019.01039

Inoue, H., Nojima, H., and Okayama, H. (1990). High Efficiency Transformation of *Escherichia coli* with Plasmids. *Gene* 96, 23–28. doi:10.1016/0378-1119(90)90336-P

Jiang, Y., Huang, M.-Z., Chen, X.-L., and Zhang, B. (2020). Proteome Analysis Guided Genetic Engineering of *Corynebacterium glutamicum* S9114 for Tween 40-triggered Improvement in L-Ornithine Production. *Microb. Cel Fact.* 19, 2. doi:10.1186/s12934-019-1272-0

Johnson, J. S., Spakowicz, D. J., Hong, B.-Y., Petersen, L. M., Demkowicz, P., Chen, L., et al. (2019). Evaluation of 16S rRNA Gene Sequencing for Species and Strain-Level Microbiome Analysis. *Nat. Commun.* 10, 5029. doi:10.1038/s41467-019-13036-1

Jones, C. M., Hernández Lozada, N. J., and Pfleger, B. F. (2015). Efflux Systems in Bacteria and Their Metabolic Engineering Applications. *Appl. Microbiol. Biotechnol.* 99, 9381–9393. doi:10.1007/s00253-015-6963-9

Kang, A., Mendez-Perez, D., Goh, E.-B., Baidoo, E. E. K., Benites, V. T., Beller, H. R., et al. (2019). Optimization of the IPP-Bypass Mevalonate Pathway and Fed-Batch Fermentation for the Production of Isoprenol in *Escherichia coli*. *Metab. Eng.* 56, 85–96. doi:10.1016/j.ymben.2019.09.003

Keilhauer, C., Eggeling, L., and Sahm, H. (1993). Isoleucine Synthesis in *Corynebacterium glutamicum*: Molecular Analysis of the ilvB-ilvN-ilvC Operon. *J. Bacteriol.* 175, 5595–5603. doi:10.1128/jb.175.17.5595-5603.1993

Khudyakov, J. I., D'haeseleer, P., Borglin, S. E., Deangelis, K. M., Woo, H., Lindquist, E. A., et al. (2012). Global Transcriptome Response to Ionic Liquid by a Tropical Rain forest Soil Bacterium, Enterobacter Lignolyticus. *Proc. Natl. Acad. Sci.* 109, E2173–E2182. doi:10.1073/pnas.1112750109

Kim, D., Langmead, B., and Salzberg, S. L. (2015). HISAT: a Fast Spliced Aligner with Low Memory Requirements. *Nat. Methods* 12, 357–360. doi:10.1038/nmeth.3317

Kind, S., Kreye, S., and Wittmann, C. (2011). Metabolic Engineering of Cellular Transport for Overproduction of the Platform Chemical 1,5-diaminopentane in *Corynebacterium glutamicum*. *Metab. Eng.* 13, 617–627. doi:10.1016/j.ymben.2011.07.006

Kinoshita, S., Nakayama, K., and Akita, S. (1958). Taxonomical Study of Glutamic Acid Accumulating Bacteria, Micrococcus Glutamicus Nov. Sp. *Bull. Agric. Chem. Soc. Jpn.* 22, 176–185. doi:10.1271/bbb1924.22.176

Koren, S., and Phillippy, A. M. (2015). One Chromosome, One Contig: Complete Microbial Genomes from Long-Read Sequencing and Assembly. *Curr. Opin. Microbiol.* 23, 110–120. doi:10.1016/j.mib.2014.11.014

Krämer, R. (2009). Osmosensing and Osmosignaling in *Corynebacterium glutamicum*. *Amino Acids* 37, 487–497. doi:10.1007/s00726-009-0271-6

Krause, J. P., Polen, T., Youn, J.-W., Emer, D., Eikmanns, B. J., and Wendisch, V. F. (2012). Regulation of the Malic Enzyme Gene malE by the Transcriptional Regulator MalR in *Corynebacterium glutamicum*. *J. Biotechnol.* 159, 204–215. doi:10.1016/j.jbiotec.2012.01.003

Küberl, A., Mengus-Kaya, A., Polen, T., and Bott, M. (2020). The Iron Deficiency Response of *Corynebacterium glutamicum* and a Link to Thiamine Biosynthesis. *Appl. Environ. Microbiol.* 86, 1–16. doi:10.1128/AEM.00065-20

Lange, J., Münch, E., Müller, J., Busche, T., Kalinowski, J., Takors, R., et al. (2018). Deciphering the Adaptation of *Corynebacterium glutamicum* in Transition from Aerobiosis via Microaerobiosis to Anaerobiosis. *Genes* 9, 297. doi:10.3390/genes9060297

Larisch, C., Nakunst, D., Hüser, A. T., Tauch, A., and Kalinowski, J. (2007). The Alternative Sigma Factor SigB of *Corynebacterium glutamicum* Modulates Global Gene Expression during Transition from Exponential Growth to Stationary Phase. *BMC Genomics* 8, 4. doi:10.1186/1471-2164-8-4

Liao, Y., Smyth, G. K., and Shi, W. (2014). featureCounts: an Efficient General Purpose Program for Assigning Sequence Reads to Genomic Features. *Bioinformatics* 30, 923–930. doi:10.1093/bioinformatics/btt656

Lim, H. C., Sher, J. W., Rodriguez-Rivera, F. P., Fumeaux, C., Bertozzi, C. R., and Bernhardt, T. G. (2019). Identification of New Components of the RipC-FtsEX Cell Separation Pathway of Corynebacterineae. *Plos Genet.* 15, e1008284. doi:10.1371/journal.pgen.1008284

Litsanov, B., Brocker, M., and Bott, M. (2012). Toward Homosuccinate Fermentation: Metabolic Engineering of *Corynebacterium glutamicum* for Anaerobic Production of Succinate from Glucose and Formate. *Appl. Environ. Microbiol.* 78, 3325–3337. doi:10.1128/AEM.07790-11

Magurudeniya, H. D., Baral, N. R., Rodriguez, A., Scown, C. D., Dahlberg, J., Putnam, D., et al. (2021). Use of Ensiled Biomass Sorghum Increases Ionic Liquid Pretreatment Efficiency and Reduces Biofuel Production Cost and Carbon Footprint. *Green. Chem.* 23, 3127–3140. doi:10.1039/D0GC03260C

Martins, I., Hartmann, D. O., Alves, P. C., Planchon, S., Renaut, J., Leitão, M. C., et al. (2013). Proteomic Alterations Induced by Ionic Liquids in Aspergillus nidulans and Neurospora Crassa. *J. Proteomics* 94, 262–278. doi:10.1016/j.jprot.2013.09.015

Milke, L., Kallscheuer, N., Kappelmann, J., and Marienhagen, J. (2019). Tailoring *Corynebacterium glutamicum* towards Increased Malonyl-CoA Availability for Efficient Synthesis of the Plant Pentaketide Noreugenin. *Microb. Cel Fact.* 18, 71. doi:10.1186/s12934-019-1117-x

Monk, J. M., Charusanti, P., Aziz, R. K., Lerman, J. A., Premyodhin, N., Orth, J. D., et al. (2013). Genome-scale Metabolic Reconstructions of Multiple *Escherichia coli* Strains Highlight Strain-specific Adaptations to Nutritional Environments. *Proc. Natl. Acad. Sci.* 110, 20338–20343. doi:10.1073/pnas.1307797110

Nepal, K. K., and Wang, G. (2019). Streptomycetes: Surrogate Hosts for the Genetic Manipulation of Biosynthetic Gene Clusters and Production of Natural Products. *Biotechnol. Adv.* 37, 1–20. doi:10.1016/j.biotechadv.2018.10.003

Neupane, B., Murthy Konda, N. V. S. N., Singh, S., Simmons, B. A., and Scown, C. D. (2017). Life-Cycle Greenhouse Gas and Water Intensity of Cellulosic Biofuel Production Using Cholinium Lysinate Ionic Liquid Pretreatment. *ACS Sustain. Chem. Eng.* 5, 10176–10185. doi:10.1021/acssuschemeng.7b02116

Norsigian, C. J., Kavvas, E., Seif, Y., Palsson, B. O., and Monk, J. M. (2018). iCN718, an Updated and Improved Genome-Scale Metabolic Network Reconstruction of Acinetobacter Baumannii AYE. *Front. Genet.* 9, 121. doi:10.3389/fgene.2018.00121

Opgenorth, P., Costello, Z., Okada, T., Goyal, G., Chen, Y., Gin, J., et al. (2019). Lessons from Two Design-Build-Test-Learn Cycles of Dodecanol Production in *Escherichia coli* Aided by Machine Learning. *ACS Synth. Biol.* 8, 1337–1351. doi:10.1021/acssynbio.9b00020

Park, M. R., Chen, Y., Thompson, M., Benites, V. T., Fong, B., Petzold, C. J., et al. (2020). Response of Pseudomonas Putida to Complex, Aromatic-Rich Fractions from Biomass. *ChemSusChem* 13, 4455–4467. doi:10.1002/cssc.202000268

Pérez-García, F., and Wendisch, V. F. (2018). Transport and Metabolic Engineering of the Cell Factory *Corynebacterium glutamicum*. *FEMS Microbiol. Lett.* 365, 1–11. doi:10.1093/femsle/fny166

Prell, C., Burgardt, A., Meyer, F., and Wendisch, V. F. (2020). Fermentative Production of L-2-Hydroxyglutarate by Engineered *Corynebacterium glutamicum* via Pathway Extension of L-Lysine Biosynthesis. *Front. Bioeng. Biotechnol.* 8, 630476. doi:10.3389/fbioe.2020.630476

Rajeev, L., Luning, E. G., Dehal, P. S., Price, M. N., Arkin, A. P., and Mukhopadhyay, A. (2011). Systematic Mapping of Two Component Response Regulators to Gene Targets in a Model Sulfate Reducing Bacterium. *Genome Biol.* 12, R99. doi:10.1186/gb-2011-12-10-r99

Rajeev, L., Luning, E. G., and Mukhopadhyay, A. (2014). DNA-affinity-purified Chip (DAP-Chip) Method to Determine Gene Targets for Bacterial Two Component Regulatory Systems. *J. Vis. Exp.* (89), 1–12. doi:10.3791/51715

Ramírez, F., Dündar, F., Diehl, S., Grüning, B. A., and Manke, T. (2014). deepTools: a Flexible Platform for Exploring Deep-Sequencing Data. *Nucleic Acids Res.* 42, W187–W191. doi:10.1093/nar/gku365

Reninger, N. S., and McPhee, D. J. (2008). Fuel Compositions Comprising Farnesane and Farnesane Derivatives and Method of Making and Using Same. Available at: https://patents.google.com/patent/US20080083158A1/en (Accessed August 14, 2021).

Rolf, J., Julsing, M. K., Rosenthal, K., and Lütz, S. (2020). A Gram-Scale Limonene Production Process with Engineered *Escherichia coli*. *Molecules* 25, 1881. doi:10.3390/molecules25081881

Ruan, Y., Zhu, L., and Li, Q. (2015). Improving the Electro-Transformation Efficiency of *Corynebacterium glutamicum* by Weakening its Cell wall and Increasing the Cytoplasmic Membrane Fluidity. *Biotechnol. Lett.* 37, 2445–2452. doi:10.1007/s10529-015-1934-x

Sabat, A. J., van Zanten, E., Akkerboom, V., Wisselink, G., van Slochteren, K., de Boer, R. F., et al. (2017). Targeted Next-Generation Sequencing of the 16S-23S rRNA Region for Culture-independent Bacterial Identification - Increased Discrimination of Closely Related Species. *Sci. Rep.* 7, 3434. doi:10.1038/s41598-017-03458-6

Sambrook, J., and Russell, D. Wi. (2001). *Molecular Cloning: A Laboratory Manual3 Volume Set)Cold Spring Harbor*. Third Edition (N.Y: Cold Spring Harbor Laboratory Press).

Santos, A. G., Ribeiro, B. D., Alviano, D. S., and Coelho, M. A. Z. (2014). Toxicity of Ionic Liquids toward Microorganisms Interesting to the Food Industry. *RSC Adv.* 4, 37157–37163. doi:10.1039/C4RA05295A

Sasaki, Y., Eng, T., Herbert, R. A., Trinh, J., Chen, Y., Rodriguez, A., et al. (2019). Engineering *Corynebacterium glutamicum* to Produce the Biogasoline Isopentenol from Plant Biomass Hydrolysates. *Biotechnol. Biofuels* 12, 41. doi:10.1186/s13068-019-1381-3

Schäfer, A., Tauch, A., Droste, N., Pühler, A., and Kalinowski, J. (1997). The *Corynebacterium glutamicum* cglIM Gene Encoding a 5-cytosine Methyltransferase Enzyme Confers a Specific DNA Methylation Pattern in an McrBC-Deficient *Escherichia coli* Strain. *Gene* 203, 95–101. doi:10.1016/S0378-1119(97)00519-2

Schröder, J., Jochmann, N., Rodionov, D. A., and Tauch, A. (2010). The Zur Regulon of *Corynebacterium glutamicum* ATCC 13032. *BMC Genomics* 11, 12. doi:10.1186/1471-2164-11-12

Seep-Feldhaus, A. H., Kalinowski, J., and Pühler, A. (1991). Molecular Analysis of the *Corynebacterium glutamicum* Gene Involved in Lysine Uptake. *Mol. Microbiol.* 5, 2995–3005. doi:10.1111/j.1365-2958.1991.tb01859.x

Si, M., Chen, C., Zhong, J., Li, X., Liu, Y., Su, T., et al. (2020). MsrR Is a Thiol-Based Oxidation-Sensing Regulator of the XRE Family that Modulates C. Glutamicum Oxidative Stress Resistance. *Microb. Cel Fact.* 19, 189. doi:10.1186/s12934-020-01444-8

Takeno, S., Shirakura, D., Tsukamoto, N., Mitsuhashi, S., and Ikeda, M. (2013). Significance of the Cgl1427 Gene Encoding Cytidylate Kinase in Microaerobic Growth of *Corynebacterium glutamicum*. *Appl. Microbiol. Biotechnol.* 97, 1259–1267. doi:10.1007/s00253-012-4275-x

Thuy Pham, T. P., Cho, C.-W., and Yun, Y.-S. (2010). Environmental Fate and Toxicity of Ionic Liquids: a Review. *Water Res.* 44, 352–372. doi:10.1016/j.watres.2009.09.030

Tsuge, Y., Kawaguchi, H., Sasaki, K., and Kondo, A. (2016). Engineering Cell Factories for Producing Building Block Chemicals for Bio-Polymer Synthesis. *Microb. Cel Fact.* 15, 19. doi:10.1186/s12934-016-0411-0

Tsuruta, H., Paddon, C. J., Eng, D., Lenihan, J. R., Horning, T., Anthony, L. C., et al. (2009). High-level Production of Amorpha-4,11-Diene, a Precursor of the Antimalarial Agent Artemisinin, in *Escherichia coli*. *PLoS ONE* 4, e4489. doi:10.1371/journal.pone.0004489

Walter, T., Veldmann, K. H., Götker, S., Busche, T., Rückert, C., Kashkooli, A. B., et al. (2020). Physiological Response of *Corynebacterium glutamicum* to Indole. *Microorganisms* 8, 1945. doi:10.3390/microorganisms8121945

Waskom, M., Gelbart, M., Botvinnik, O., Ostblom, J., Hobson, P., Lukauskas, S., et al. (2020). Seaborn: Statistical Data Visualization. *J. Open Source Softw.* 6 (60), 3021. doi:10.21105/joss.03021

Wehrs, M., Tanjore, D., Eng, T., Lievense, J., Pray, T. R., and Mukhopadhyay, A. (2019). Engineering Robust Production Microbes for Large-Scale Cultivation. *Trends Microbiol.* 27, 524–537. doi:10.1016/j.tim.2019.01.006

Wolf, S., Becker, J., Tsuge, Y., Kawaguchi, H., Kondo, A., Marienhagen, J., et al. (2021). Advances in Metabolic Engineering of *Corynebacterium glutamicum* to Produce High-Value Active Ingredients for Food, Feed, Human Health, and Well-Being. *Essays Biochem.* 65, 197–212. doi:10.1042/EBC20200134

Xiao, Z., Hou, X., Lyu, X., Xi, L., and Zhao, J.-y. (2014). Accelerated green Process of Tetramethylpyrazine Production from Glucose and Diammonium Phosphate. *Biotechnol. Biofuels* 7, 106. doi:10.1186/1754-6834-7-106

Yu, C., Simmons, B. A., Singer, S. W., Thelen, M. P., and VanderGheynst, J. S. (2016). Ionic Liquid-Tolerant Microorganisms and Microbial Communities for Lignocellulose Conversion to Bioproducts. *Appl. Microbiol. Biotechnol.* 100, 10237–10249. doi:10.1007/s00253-016-7955-0

Zhang, H., Li, Y., Wang, C., and Wang, X. (2018). Understanding the High L-valine Production in *Corynebacterium glutamicum* VWB-1 Using Transcriptomics and Proteomics. *Sci. Rep.* 8, 3632. doi:10.1038/s41598-018-21926-5

Zhou, Z., Wang, C., Xu, H., Chen, Z., and Cai, H. (2015). Increasing Succinic Acid Production Using the PTS-independent Glucose Transport System in a *Corynebacterium glutamicum* PTS-Defective Mutant. *J. Ind. Microbiol. Biotechnol.* 42, 1073–1082. doi:10.1007/s10295-015-1630-9

Conflict of Interest: The authors declare that the research was conducted in the absence of any commercial or financial relationships that could be construed as a potential conflict of interest.

Publisher's Note: All claims expressed in this article are solely those of the authors and do not necessarily represent those of their affiliated organizations, or those of the publisher, the editors and the reviewers. Any product that may be evaluated in this article, or claim that may be made by its manufacturer, is not guaranteed or endorsed by the publisher.

frontiers in Bioengineering and Biotechnology

ORIGINAL RESEARCH
published: 15 December 2021
doi: 10.3389/fbioe.2021.751334

Construction of an IS-Free *Corynebacterium glutamicum* ATCC 13 032 Chassis Strain and Random Mutagenesis Using the Endogenous IS*Cg1* Transposase

*Marten Linder [1], Markus Haak [1], Angela Botes [2,3], Jörn Kalinowski [1] and Christian Rückert [1,2]**

[1]CeBiTec Bielefeld, Technology Platform Genomics, Bielefeld University, Bielefeld, Germany, [2]Department of Biology, Massachusetts Institute of Technology, Cambridge, MA, United States, [3]School of Molecular and Cell Biology, University of the Witwatersrand, Johannesburg, South Africa

OPEN ACCESS

Edited by:
Yu Wang,
Tianjin Institute of Industrial Biotechnology (CAS), China

Reviewed by:
Lorenzo Pasotti,
University of Pavia, Italy
Qiuqiang Gao,
Columbia University, United States

***Correspondence:**
Christian Rückert
christian.rueckert@cebitec.uni-bielefeld.de

Specialty section:
This article was submitted to Synthetic Biology, a section of the journal Frontiers in Bioengineering and Biotechnology

Received: *31 July 2021*
Accepted: *02 November 2021*
Published: *15 December 2021*

Citation:
Linder M, Haak M, Botes A, Kalinowski J and Rückert C (2021) Construction of an IS-Free Corynebacterium glutamicum *ATCC 13 032 Chassis Strain and Random Mutagenesis Using the Endogenous ISCg1 Transposase. Front. Bioeng. Biotechnol. 9:751334. doi: 10.3389/fbioe.2021.751334*

Mobile genetic elements (MGEs) contribute to instability of the host genome and plasmids. Previously, removal of the prophages in the industrial amino acid producer *Corynebacterium glutamicum* ATCC 13 032 resulted in strain MB001 which showed better survival under stress conditions and increased transformability. Still, eight families of Insertion Sequence (IS) elements with 27 potentially active members remain in MB001, two of which were demonstrated to be detrimental in biotechnological processes. In this study, systematical deletion of all complete IS elements in MB001 resulted in the MGE-free strain CR101. CR101 shows growth characteristics identical to the wildtype and the increased transformability of MB001. Due to its improved genome stability, we consider this strain to be an optimal host for basic research and biotechnology. As a "zero-background" host, it is also an ideal basis to study *C. glutamicum* IS elements. Re-sequencing of CR101 revealed that only five spontaneous point mutations had occurred during the construction process, highlighting the low mutation rate of *C. glutamicum* on the nucleotide level. In a second step, we developed an easily applicable IS*Cg1*-based transposon mutagenesis system to randomly transpose a selectable marker. For optimal plasmid stability during cloning in *Escherichia coli*, the system utilizes a genetic switch based on the phage integrase Bxb1. Use of this integrase revealed the presence of a functional *attB* site in the *C. glutamicum* genome. To avoid cross-talk with our system and increase ease-of-use, we removed the *attB* site and also inserted the Bxb1 encoding gene into the chromosome of CR101. Successful insertion of single markers was verified by sequencing randomly selected mutants. Sequencing pooled mutant libraries revealed only a weak target site specificity, seemingly random distribution of insertion sites and no general strand bias. The resulting strain, ML103, together with plasmid pML10 provides a easily customizable system for random mutagenesis in an otherwise genomically stable *C. glutamicum*. Taken together, the MGE-free *C. glutamicum* strain CR101, the derivative ML103, and the plasmid pML10 provide a useful set of tools to study *C. glutamicum* in the future.

Keywords: corynebacterium glutamcium, IS elements, prophages, genetic switch, "genome healing", mutagenesis, ISCg1

1 INTRODUCTION

Corynebacterium glutamicum is a GRAS-classified (Generally Recognized as Safe), Gram-positive bacterium which is known to be non-pathogenic, non-motile, and non-sporulating. Due to its safety of use, its easy genetic accessibility, and good performance parameters (fast growth on cheap carbon sources, resistance to changes in pO2, etc.), it is widely used in fermentation processes today (Becker and Wittmann, 2012). Besides production of amino acids and other bulk chemicals (Wendisch, 2020, 2016), it is also applied for production of high-value compounds (Wolf et al., 2021). While many *C. glutamicum* strains have been isolated, to our knowledge just two are widely used in basic research and biotechnology: strain ATCC 13 032 and strain R. This might in part be due to the presence of the paracrystalline protein surface (S) layer in many other *C. glutamicum* strains (Hansmeier et al., 2004) that was shown to interfere with DNA transfer by electroporation in *Caulobatcer* species (Gilchrist and Smit, 1991) and in part due to the early availability of complete genome sequences for the two strains (Ikeda and Nakagawa, 2003; Kalinowski et al., 2003; Yukawa et al., 2007). Of those two, strain ATCC 13 032 not only constitutes the type strain of the species, but is used by most researchers, while strain R is apparently used exclusively by researchers at the Research Institute of Innovative Technology for the Earth (Kyoto, Japan).

While *C. glutamicum* has many beneficial properties that make it well suited for industrial applications and basic research, it still suffers from the problem of all living systems, i.e., the spontaneous occurrence of mutations. Fortunately, the genomes of *Corynebacterium* species are known to be very stable on the large scale, with even distant species sharing a high degree of chromosomal synteny (Ikeda and Nakagawa, 2003; Yukawa et al., 2007) which is attributed to the lack of a complete recombination system (Nakamura et al., 2003). In contrast to this stability on the large scale, the genome of *C. glutamicum* contains a large number of mobile genetic elements (MGEs) (Kalinowski et al., 2003; Yukawa et al., 2007) which might cause instability on the gene level. Indeed, removal of MGEs and prophages was shown to greatly enhance the stability of the genome (Umenhoffer et al., 2010; Renda et al., 2014). This has been demonstrated conclusively for the model and production organisms *Bacillus subtilis* (Ozaki et al., 2007) and *Escherichia coli* (Pósfai et al., 2006; Umenhoffer et al., 2010). For *C. glutamicum*, there is good evidence that at least some of the prophages and IS elements present are active and can affect the behaviour of the bacteria. For example, Frunzke et al. (2008) showed that the prophage CPG3 found in strain ATCC 13 032 can excise from the genome, replicate as an episome and cause cell lysis when present in high copy numbers. Furthermore, the available genome sequences for *C. glutamicum* ATCC 13 032 differ in the the number of prophages and IS elements present (Kalinowski, 2005), another indication of at least some of them being active.

Concerning the creation of an MGE-free *C. glutamicum* strain, some prior work exists, but no rigorous effort to remove all potentially active MGEs has been reported so far. For example, Suzuki et al. (2005) removed a total of eight regions in strain R, comprising 190 kbp (188 genes) which contained, among others, one prophage and 17 IS elements, and demonstrated that the resulting strain displayed wildtype-like growth. Regarding the removal of IS elements, Choi et al. (2015) created two strains, one lacking all four copies of IS*Cg1* (WJ004) and one lacking all four copies of IS*Cg2* (WJ008). Interestingly, they found that their version of strain ATCC 13 032 contained only four copies of IS*Cg2* instead of the five reported by Ikeda and Nakagawa (2003) and Kalinowski et al. (2003) and that one copy of IS*Cg1*, IS*Cg1c*, was absent and replaced by a copy at a different position. For both strains, they observed improvements in heterologous protein expression as well as transformability. Last but not least, Baumgart et al. (2013) removed the three prophages CGP1-CPG3 present in their version of strain ATCC 13 032. The resulting strain, MB001, also displayed wildtype-like growth but increased transformability and improved expression of a heterologous protein due to an increased copy-number of the used vector. Based on these findings, we therefore build upon previous works (Baumgart et al., 2013) to establish an MGE-free strain by removing all potentially active IS elements in the prophage-free strain MB001. The version of strain ATCC 13 032 sequenced in Bielefeld contains a total of 38 potential IS elements (27 considered to be complete, 11 partials) belonging to eight families (Kalinowski et al., 2003). While the IS*L3* and IS*30* families have only one member each in this strain, IS*Cg1* (4 copies) and IS*Cg2* (5 copies), the IS*3* family is by far the most abundant and diverse (9 instances from five members). With one of its members, IS*Cg14*, being located on the deleted prophage CGP3, this leaves 26 elements to be removed in strain MB001.

Besides being an optimal host for basic research and biotechnology due to its improved stability, an MGE-free strain also provides an ideal basis to study native IS elements as well as to establish and test random mutagenesis systems based on these. In combination with high-throughput sequencing such IS-based systems have a wide range of applications (Cain et al., 2020). For example, Suzuki et al. (2006) used IS*Cg1* in strain R which naturally lacks this IS element to identify essential genes in *C. glutamicum*. Likewise, mutagenesis by larger elements can be helpful in adaptive laboratory evolution experiments, as this allows not only for gene disruption but also for gene activation (Hennig et al., 2020). Therefore, we endeavored to build an IS*Cg1*-based random mutagenesis system that allows for, among others, controllable random insertion of a selectable marker. To facilitate cloning and replication of transposition constructs in a host such as *E. coli*, we used a genetic switch based on a genomically integrated Bxb1 phage integrase (Bonnet et al., 2012), activating expression only after transfer to *C. glutamicum*.

TABLE 1 | Bacterial strains.

Name	Relevant genotype/information[a]	Source/References
E. coli DH5αMCR	F⁻ *endA1 supE44 mcrA thi-1 hsdR17 λ⁻ recA1 relA1* Δ(*lacZYA-argF*) *U169* (Φ80d*lacZ*Δ *M15*) *gyrA96 deoR* Δ(*mrr-hsdRMS-mcrBC*)	Grant et al. (1990)
C. glutamicum		
ATCC 13 032	Wild type, Nx[r]	ATCC[b]
ATCC 13 869	"*Brevibacterium lactofermentum*", Nx[r]	ATCC
ATCC 14 067	"*Brevibacterium flavum*", Nx[r]	ATCC
AS 1.542	"*Corynebacterium crenatum*", Nx[r]	Chen et al. (2012)
MB001	*C. glutamicum* ATCC 13 032 with deleted prophages: ΔCGP1, ΔCGP2, and ΔCGP3	Baumgart et al. (2013)
CR099	*C. glutamicum* MB001 with deleted IS elements Δ*ISCg1a*, Δ*ISCg1b*, Δ*ISCg1c*, Δ*ISCg1d*, Δ*ISCg1e*, Δ*ISCg2b*, Δ*ISCg2c*, Δ*ISCg2d*, Δ*ISCg2e*, and Δ*ISCg2f*	Baumgart et al. (2018), this study
CR100	*C. glutamicum* CR099 with deleted IS elements Δ*ISCg5a*, Δ*ISCg5b*, Δ*ISCg5c*, Δ*ISCg8*, Δ*ISCg12*, Δ*ISCg13a*-Δ*ISCg21a*, Δ*ISCg13b*, Δ*ISCg16a* and Δ*ISCg16b*	this study
CR101	*C. glutamicum* CR100 with deleted IS elements Δ*ISCg3a*, Δ*ISCg3b*, Δ*ISCg4*, Δ*ISCg6a*-Δ*ISCg7*, Δ*ISCg6c*, Δ*ISCg9*, and Δ*ISCg15a-b*	this study
ML102	CR101 with *bxbI* inserted at Δ*ISCg3a*	this study
ML103	ML102 with Δ*groEL*	this study

[a] *r superscript indicates resistance. Nx, Nalidixic acid; Km, Kanamycin*
[b] *ATCC; American Type Culture Collection, Rockville, MD*

The strains created in this study should not only aid basic research by combining generally wildtype-like behaviour with reduced random mutation events, but also industrial applications as IS elements contribute to the degeneration of bacterial production strains (Peng and Liang, 2020). Furthermore, IS*Cg1*-based random mutagenesis allows for multi-copy insertion of genes of interest, a method that was shown to significantly increase, e.g., heterologous protein expression (Yomantas et al., 2011).

2 MATERIALS AND METHODS

2.1 Bacterial Strains, Plasmids and Culture Media

The bacterial strains and plasmids used in this study are listed in **Table 1** and **Supplementary. Table S2**, respectively. Plasmids pCRn100 days to pCRn125 days, pMLi002 and pMLd009 are based on the pK18 *mobsacB* vector (Schäfer et al., 1994a). pCRn100 days to pCRn125 days were used for successive genomic deletion of IS*Cg* elements in MB001. pMLi002 allows for genomic integration of the coding sequence of the Bxb1 phage integrase at the former locus of IS*Cg3a* deleted by pCRn110 days pMLd009 is used to remove *groEL*1 in the genome. The plasmid pML10 was build using pUC19 as backbone. It is used for cloning and replication in *E. coli* and as a transposition construct in *C. glutamicum*. It carries a kanamycin resistance cassette flanked by the IS*Cg1* inverted repeats as transposable element as well as the transposase encoded by *tnp1*. Expression of this gene in turn depends on a Bxb1 integrase-based switch (Bonnet et al., 2012). *E. coli* strains carrying plasmids were routinely grown on solid Antibiotic Medium No. 3 (PA) (Oxoid, Wesel, Germany) at 37°C. *C. glutamicum* strains were grown on solid brain-heart broth (BH) (VWR International, Darmstadt, Germany) at 30°C. Antibiotics used for selection of plasmids and strains were nalidixic acid (50 μg/ml for corynebacteria) and kanamycin (50 μg/ml for *E. coli*, 25 μg/ml for corynebacteria).

2.2 DNA Isolation, Transfer and Manipulation

Standard procedures were employed for molecular cloning and transformation of *E. coli* DH5α, as well as for electrophoresis (Sambrook et al., 1989). Transformation of *C. glutamicum* was performed by electroporation using the methods of Tauch et al. (2002).

Sequence similarity-based searches with nucleotide sequences were performed using the basic local alignment search tool (BLAST, Altschul et al., 1990).

2.3 Construction of Plasmids

Plasmids pCRn100 days to pCR125 days as well as pMLi002, pMLd009 and pML10 were constructed using Gibson assembly (Gibson et al., 2009). The primers used are listed in **Supplementary. Table S1**. In case of "genome healing" constructs, the final insert was amplified directly from either "*Brevibacterium lactofermentum*" ATCC 13 869, "*Brevibacterium flavum*" ATCC 14 067, or "*Corynebacterium crenatum*" AS 1.451 gDNA using the respective primers _d1 and _d4. In all other cases, two products (primer pairs _d1 and _d2 respectively _d3 and _d4) were amplified from *C. glutamicum* MB001 gDNA. The insert(s) were then assembled with linearized pK18 *mobsacB* amplified via the primers pK18_ga1 and pK18_ga2. Primers pk18_dgroel1 and pk18_dgroel2 were used to linearize pK18 *mobsacB* for *groEL*1 deletion. The homologous flanks were amplified with the primers d1_groel1-d4_groel1 from ATCC 13 032. Linearization of pCRn110 days for insertion of the Bxb1 integrase coding sequence was achieved with the primer pair pK18_bxbI_1 and pK18_bxbI_2 and the sequence of the Bxb1 integrase was amplified with the primer pair bxbI_ins1 and bxbI_ins2 from *Mycobacterium smegmatis*. The backbone for pML10 was linearized with the primer pair switch_ga1 and switch_ga2 from pUC19. The switch, consisting of the Bxb1 integrase *attB* and *attP* flanking the original constitutive Anderson promoter (Anderson, 2013) was amplified via the

overlapping primers *attP*_Pcons and Pcons_*attB*. *Kan*^{r} originates form pK18 *mobsacB* and the imperfect inverted repeats for IS*Cg1* are from ATCC 13 032. All PCRs were performed using Phusion High–Fidelity DNA polymerase, the assembly was done using Gibson Assembly Master Mix (both Thermo Fisher Scientific, Germany). The assembly mixture was used to transform *E. coli* DH5*α*MCR, the transformants were selected on PA plates containing 50 *μ*g/ml kanamycin and 40 mg/L X-Gal (5-bromo-4-chloro-3-indolyl-*β*-D-galactopyranoside) and verified by Sanger sequencing.

2.4 Site-specific Gene Disruption/ Replacement

Site-specific gene disruption was performed using the non-replicable integration vector pK18mobsacB which allows for marker-free deletion of the target gene (Schäfer et al., 1994c). The resulting plasmids pCR100 days to pCR124 days and pMLi002and pMLd009 were transformed into *C. glutamicum* MB001 respectively subsequent deletion mutants by electroporation (Tauch et al., 2002). Integration of the introduced plasmids into the chromosome by single-crossover was tested by selection on BH plates containing 25 *μ*g/ml kanamycin. For the deletion of the target gene, the kanamycin-resistant (Km^r) cells were grown overnight in liquid BH and spread on BH plates containing 10% sucrose. Cells growing on this plate were tested for kanamycin sensitivity (Km^s) by parallel picking on BH plates containing either kanamycin or sucrose. Sucrose-resistant and kanamycin-sensitive cells were then tested for the deletion by PCR and checked for IS activity using Southern blotting and hybridization (Evans et al., 1994) if deemed appropriate.

2.5 Transposon Mutant Sequencing

Genomic DNA was isolated using the NucleoSpin Microbial DNA Mini kit (Macherey-Nagel, Germany). Single mutant colonies were sequenced using the Rapid Barcoding Kit SQK-RBK004 (Oxford Nanopore Technologies, UK) on R9.4.1 flowcells on a GridION.

For sequencing of complete mutant libraries, all colonies were pooled before genomic DNA was isolated. Subsequently, the gDNA was fragmented to approximately 10,000 bp fragments using a Covaris g-TUBE. The ends of the fragments blunted and an A-overhang was added with the NEBNext Ultra II End Repair/dA-Tailing Module. The A-overhang is then used for ligation of dsDNA adapters derived from annealing the oligos D7 and D7_top carrying part of the TruSeq D7 sequence. In a first round of PCR using Phusion High–Fidelity DNA polymerase, fragments are amplified between a biotinylated primer tnp_o, binding in the kanamycin resistance marker about 500 nt upstream of the inverted repeat, and the TruSeq D7 primer. After amplification, fragments were purified with Dynabeads M-270 Streptavidin binding the biotinylated fragment ends. During washing of the trapped DNA on a magnet rack, 0.1 mM NaOH was applied to retain ssDNA of the amplified region. This is followed by a half-nested second round of PCR with LongAmp Taq DNA Polymerase. Here, primer D7 is paired with a phosphorylated nested primer tnp_i, located 150 bp from the 3′-end of the kanamycin resistance cassette.

After purification, the DNA was used in the adapter ligation step of the Ligation Sequencing Kit SQK-LSK109 (Oxford Nanopore Technologies) and sequenced on an R9.4.1 flowcell on a GridION. The sequencing reads where mapped to pML10 and *C. glutamicum* CR101 respectively using minimap2 (Li, 2018) with options-cx map-ont–eqx–secondary = no. Reads mapping to both references were processed using custom Python scripts to identify transposition sites based on the local alignments. These were visualized in a polar genome plot using the Python library Matplotlib (Hunter, 2007). Sites with at least two mapped reads were subjected to an analysis of the target site of IS*Cg1* by creating a sequence logo with WebLogo3 (Crooks, 2004) based on the strand-specific 8 bp of genomic sequence downstream the inverted repeat at each transposition site.

2.6 Determination of Growth Rates and Transformation Efficiency

Cultivations to check for differences in growth behaviour of MB001, CR101, ML102 and ML103 were performed using a BioLector I (m2p-labs). Four biological replicates of each strain were cultivated in four technical replicates. Samples were cultivated in 1 ml BHI at 30°C, 1,100 rpm, and at 85% humidity. Measurements were taken every 15 min and the growth rates were calculated for each sample with the BioLection software using a sliding window of eight data points (i.e. 2 h). Afterwards, for each strain first the average growth rate for each biological replicate was calculated, followed by calculation of the mean and standard deviation from those averages.

The transformation efficiency was determined as described by Baumgart et al. (2013) with one modification: In case of the integrative plasmid, 1,000 ng instead of 500 ng were used. For each strain, three independent cultivations, i.e. biological replicates, were performed to create competent cells as described by Tauch et al. (2002). From each batch prepared in that manner, four aliquots were used for electroporation with the respective plasmid, serving as technical replicates.

2.7 Genome Sequencing, Assembly, and Accession Numbers

The complete genome sequence of *C. glutamicum* CR101 was determined using a hybrid assembly approach as described by Ballas et al. (2020). All sequences from other *C. glutamicum* strains were obtained from GenBank (Agarwala et al., 2017): BX927147 (*C. glutamicum* ATCC 13 032), CP005959 (*C. glutamicum* MB001), CP016335 ("*B. lactofermentum*" ATCC 13 869), CP022614 ("*B. flavum*" ATCC 14 067), and LOQT01 ("*C. crenatum*" AS1.452). All data generated during this project is available *via* BioProject PRJNA750341.

3 RESULTS

3.1 Construction of Strain CR101

To construct strain CR101, containing no potentially active IS elements (Kalinowski et al., 2003; Pfeifer-Sancar et al., 2013), strain MB001 lacking all prophages (Baumgart et al., 2013) was used as a basis. Interestingly, the genome of this strain contains five copies of IS*Cg1*, named IS*Cg1e*, which is located at position 541,217 to 542,527 (CP005959) and disrupts gene *cgp_0611*. To determine the boundaries of the necessary deletions as well as to amplify the inserts used for double-crossovers, we applied a "genome healing" approach: First, using BLAST we searched for the sequence of the IS*Cg* elements with 2,500 bp flanks in the genome sequences of 3 *C. glutamicum* strains available at our lab ("*Brevibacterium lactofermentum*" ATCC 13 869, "*Brevibacterium flavum*" ATCC 14 067, and "*Corynebacterium crenatum*" AS1.452) to identify the orthologous regions in the three genomes. In those cases where 1) there was a syntenous region present, but 2) without the IS*Cg* element found in MB001, we then compared the number of differences between the target sequence and that of MB001 in the 750 bp directly up- and downstream of the missing region. If these showed >99% identity, primers were designed to amplify a deletion construct with 500–600 bp flanking sequences. In case of more than one potential candidate, i.e., a region satisfying the rules present in more than one genome, the candidate with the highest similarity to the region in MB001 was selected. Using this approach, 12 regions were identified in ATCC 13 869, three in ATCC 14 067, and two in AS1.452 (see **Supplementary Table S2**). For IS*Cg1e*, a fifth copy of IS*Cg1* that was absent in the ATCC 13 032 wildtype (Kalinowski et al., 2003, Table two), the region was compared to the wildtype genome and genomic DNA of the wildtype was used to amplify the construct for "genome healing". For the remaining eight regions, deletion constructs were build conventionally, based on RNAseq data (Pfeifer-Sancar et al., 2013) to remove the CDS as well as the corresponding promoter.

These constructs were then used to sequentially remove the IS elements, starting with IS*Cg1* and IS*Cg2* as the supposedly most active. This resulted in strain CR099 (see **Supplementary Figure S2**) which was already successfully used as the basis in other genome reduction projects (Baumgart et al., 2018). To ensure that no further jumps of IS elements still remaining in the respective strain had occurred, the presence of the various IS elements was checked by Southern blotting and hybridization at key points, usually at least after removal of all instances of an element present in several copies or after deletion of three to four copies of elements present only once. Thereby, we were able to detect a total of seven jumps of IS*Cg1* (see **Supplementary Figure S1** for an example), two jumps of IS*Cg2*, one of IS*Cg5*, one of IS*Cg13* and one of IS*Cg16* (data not shown). The strain with those active as well as several other elements removed was dubbed CR100 (see **Supplementary Figure S2**). Removal of the remaining seven elements progressed without further complications, resulting in the final, prophage- and IS-free strain CR101.

To ensure the complete removal as well as to detect all other mutations introduced during the 26 rounds of genetic manipulation, the complete genome sequence of *C. glutamicum* CR101 was established using a hybrid assembly approach based on Illumina short read and Oxford Nanopore Technologies (ONT) long read data. The final genome sequence has a size of 3,034,563 bp, compared to 3,079,25 bp for MB001. Comparison of the annotated genomes revealed that 11 genes were "healed" through the removal of the various IS elements. While a large number of synonymous and missense mutations was introduced in the flanking regions, they all corresponded to the sequences found in the donor genomes and are thus unlikely to change the function of genes encoded in these regions. On the other hand, only four missense mutations and one frameshift were detected in the remainder of the genome, indicating an overall low rate of spontaneous mutations in *C. glutamicum*. The final strains were also checked for changes in growth rate and transformability. Strains CR101, ML102, and ML103 showed no significant difference in growth rate compared to the progenitor *C. glutamicum* MB001 (**Supplementary Table S3**). In case of transformability, a slight increase in the number of transformants per μg DNA could be observed (**Supplementary Figure S3**), but analysis via two-way ANOVA with replication indicates that this is not significant in case of the replicative plasmid ($p = 0.44$ for an alpha of 0.05) as the variance between biological replicates far exceeds that among the four strains. In case of the integrative plasmid, the observed change is statistically significant ($p = 0.023$), but again the variability between batches of competent cells is extremely high.

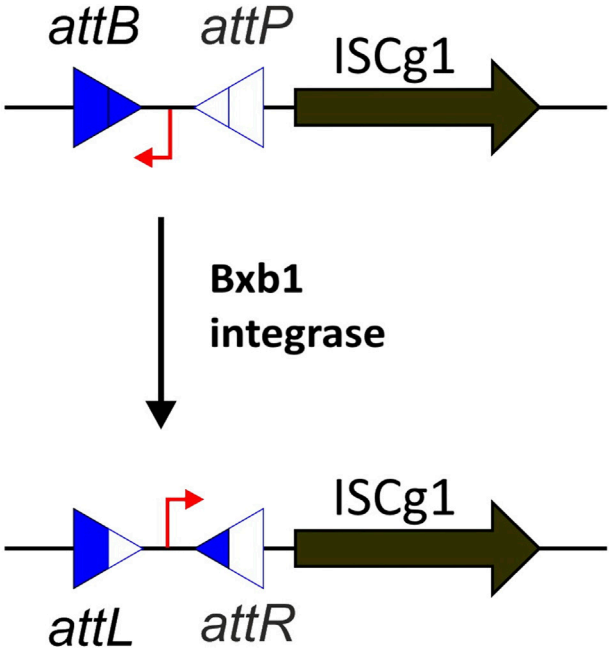

FIGURE 1 | Principle of the Bxb1 phage integrase genetic switch. In its default state, the promoter (in red) is in opposite orientation to the IS*Cg1* transposase and therefore no expression takes place. As soon as the integrase is abundant, the bacterial and phage attachment sites *attB* and *attP* are targeted by the integrase, transitioning the switch into the active state by recombination, forming the hybrid attachment sites *attL* and *attR*.

FIGURE 2 | Alignment of the minimal required bacterial attachment site sequences of the phage Bxb1 in its natural host *M. smegmatis* and the observed attachment site in *C. glutamicum*. Base pairs coloured in red are specific for *attB* identity in *M. smegmatis*. The green central GT is the essential dinucleotide for recombination and the dashed arrows indicate palindromic base pairs.

3.2 Development of a Genetic Switch Based System for Random Insertion Mutagenesis

As random insertion mutagenesis is of use in some experimental contexts, e.g., adaptive laboratory evolution Hennig et al. (ALE 2020), we decided to re-purpose IS*Cg1*, using a system similar to that developed by Suzuki et al. (2006).

In most scenarios, only a single transposition event per mutant is desired. Therefore, pUC19 was used as a transposition construct, as it is a non-replicating vector in *C. glutamicum* and allows for easy replication and isolation in *E. coli* (Yanisch-Perron et al., 1985). We then used the regular IS*Cg1* sequence from ATCC 13 032 as transposase and a kanamycin resistance cassette flanked by the 24 bp imperfect terminal inverted repeats as transposon. This way, only a successful transposition into the genome provides resistance to kanamycin. However, problems occurred when we tried to isolate the plasmid from *E. coli* because IS*Cg1* transposition turned out to be highly active in *E. coli* already. This resulted in mostly "empty" plasmids, i.e., plasmids from which the transposon cassette had jumped into the *E. coli* chromosome. To acquire sufficient quantities of active plasmid for large-scale transposon mutagenesis, the plasmid pML10 was designed using a Bxb1 phage integrase genetic switch inserted upstream of IS*Cg1* (**Figure 1**). The switch consists of a constitutive promoter flanked by the bacterial and phage attachment sites targeted by the Bxb1 integrase (Bonnet et al., 2012). By default, the promoter is in opposing orientation to IS*Cg1* such that no expression is occurring and subsequently no transposition takes place. To invert the switch and enable expression of IS*Cg1*, the coding sequence for the Bxb1 integrase has been inserted into the genome of CR101 at the former locus of IS*Cg3a* creating ML102. As soon as pML10 is transformed into ML102 the Bxb1 integrase targets the *attB* and *attP* attachment sites flanking the promoter, forming the hybrid attachment sites *attL* and *attR* by recombination. In the process, the orientation of the promoter is inverted and drives the expression of IS*Cg1*.

During sequencing of the first mutants, we noticed the occurrence of integration of the whole transposition construct pML10 into *groEL*1 with high frequency (data not shown). Examination of the sequences of several mutants revealed that all these insertions occurred at the same site and with the same directionality. The subsequent comparison of the bacterial attachment site in *M. smegmatis* to the integration site of our mutants showed a significant degree of similarity, indicating a partially conserved *attB* site in *groEL*1. Recognition of this site by the Bxb1 integrase then results in integration of the plasmid via the *attP* site of the genetic switch. Interestingly, many nucleotides defining *attB* functionality as well as the central GT dinucleotide thought to be essential (Singh et al., 2013) are not well conserved in the site present in *C. glutamicum groEL*1 (**Figure 2**).

To circumvent the genomic integration via the Bxb1 integrase as a competing event to transposition via IS*Cg1*, we deleted *groEL*1. While this gene is essential in many organisms, there are two copies present in *C. glutamicum* ATCC 13 032 and *groEL*1 was actually disrupted by IS*Cg1c* prior to its removal in CR099 and thus CR101. In subsequent mutant libraries of the strain ML103 no further display of integration via Bxb1 integrase was observed.

3.3 Sequencing of ML103 Transposon Mutants

To test our genetic-switch-based system for random insertion mutagenesis, 200 transformations via electroporation of 800 ng pML10 each into ML103 were performed. On most agar plates less than $0.5 \cdot 10^2$ colonies were observed, but several cases with hundreds of colonies were also detected. From the resulting transposon mutants generated in ML103, we selected 12 single colonies for whole genome sequencing. One mutant colony was picked because of its noticeably intense yellow phenotype (**Supplementary Figure S4**), the others were selected randomly. In each of these mutants, only one transposition took place, each located at a different genomic position. The complete genome sequence of the phenotypically distinct mutant revealed a transposition into *crtR* which has been characterized as encoding a MarR-type repressor. CrtR represses the *crt* operon which is involved in decaprenoxanthin synthesis, a yellow carotenoid. Deletion of *crtR* increases transcription of the *crt* operon by 10 to 30-fold (Henke et al., 2017), probably explaining the striking phenotype of our mutant.

To further determine the suitability of IS*Cg1* in terms of target site bias, all mutants were pooled and ligation-based ONT sequencing libraries were constructed by targeted enrichment of the region downstream of the selection marker. Sequencing resulted in 3,207 independent transposition sites indicating no obvious target site preference on a genomic scale (**Figure 3**). Allocation of transposition sites with respect to strand directionality is evenly distributed with 1,582 sites on the leading strand and 1,625 sites on the lagging strand. Weblogo analysis of the eight bp target site of IS*Cg1* (**Figure 4**) suggests a bias towards loci with high AT content in the central four base pairs with strong discrimination against G and C at position four and 5. Frequency analysis of the central tetranucleotide (**Supplementary Table S4**) shows that no specific single sequence appears to be predominant which is in line with previous analyses (Inui et al., 2005).

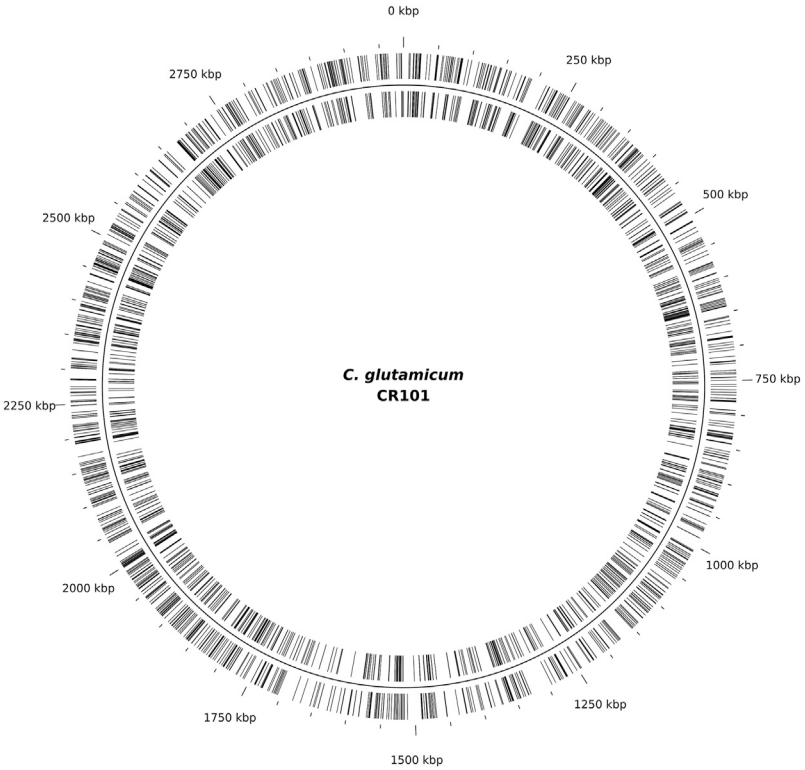

FIGURE 3 | Transposition sites mapped to the genome of CR101. A total of 3,207 transposition sites were identified by mapping sequencing reads of the random mutagenesis experiment performed with *C. glutamicum* ML103 to *C. glutamicum* CR101, with 1,582 sites on the leading strand (outer lines) and 1,625 sites on the lagging strand (inner lines).

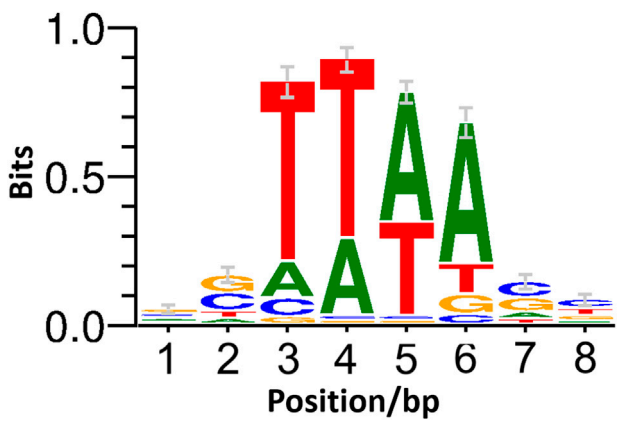

FIGURE 4 | Weblogo of the IS*Cg1* target site. WebLogo (Crooks, 2004) of the IS*Cg1* target site based on the strand-specific 8 bp of genomic sequence downstream of the inverted repeat at transposition sites with at least two mapped reads.

4 DISCUSSION

The first goal of this work, the construction of a prophage- and IS-free *C. glutamicum* strain derived from the industrially relevant type strain ATCC 13 032, was successfully achieved. While no obvious differences compared to the progenitor strain MB001 could be observed, this result was predictable and is actually the favored outcome. Like Choi et al. (2015) who reported a significant increase in transformability in strains lacking all copies of either IS*Cg1* or IS*Cg2*, we also observed a slight increase, albeit not significant in our case. This is unsurprising as there is no molecular basis for this behaviour: none of the genes restored is known or suspected to play a role in DNA uptake or any other associated function. The most likely explanation for this discrepancy is the progenitor strain used for the removal of the IS elements (see **Supplementry Figure S3**): Choi et al. (2015) used the wildtype ATCC 13 032 while we used the derivative MB001, already lacking the prophages (Baumgart et al., 2013). Interestingly, MB001 shows properties akin to those reported by Choi et al. (2015). As at least one of the prophages, CGP3 which also carries a restriction-modification system known to be detrimental to plasmid uptake in *C. glutamicum* (Schäfer et al., 1994b), was shown to be unstable and prone to spontaneous excision and maybe loss (Frunzke et al., 2008), it stands to argue that such an event happened during the works of Choi et al. (2015). Since various rounds of plasmid-dependent deletions were used, this would actually be positively selected for. Likewise, the unchanged growth rate was expected, as again this was the intended outcome. Indeed, even when combining 11 large scale deletions in strain CR099, totaling about 240 kbp, Baumgart

et al. (2018) observed no detrimental effect on the growth rate of the mutant when compared to the wildtype.

Meanwhile, the work of Choi et al. (2015) as well as ours showed that at least some IS elements in *C. glutamicum* are highly active, especially IS*Cg1*. For example, the heterogeneity of TAG-producing cells (Fig. 6 Plassmeier et al., 2016) was later found to be caused by IS*Cg1* jumping into the production plasmid (C. Rückert, personal observation, 2017). Thus, *C. glutamicum* CR101 should be an ideal host to profit from increased stability while retaining wildtype behaviour in almost all other aspects.

Yet, while genome stability is preferable in most situations in basic research and industrial biotechnology, the availability of an reliable mutagenesis system with one transposition event per mutant is also a valuable tool. Therefore, we decided to use IS*Cg1* due to its proven activity in *C. glutamicum* and demonstrated value for whole genome analysis (Suzuki et al., 2006). Surprisingly, this approach initially resulted in a failure caused by IS*Cg1* activity during plasmid propagation in *E. coli*. While again delivering proof of high transposition activity mediated by IS*Cg1* transposase, this made direct use of our system difficult. It is interesting to note that, to the best of our knowledge, these problems have not been reported before as this problem should occur with any transposon that is active in *E. coli*. To solve this problem, we considered using a repressor-based system, but such circuits are often challenging due to minimal expression leakage (Kato, 2020) and often require inducer substances to be effective. Therefore, we turned to the Bxb1 integrase which is highly directional with no need for additional cofactors or proteins (Kim et al., 2003) to create a system that is silent in *E. coli* and only becomes active when transferred to the proper *C. glutamicum* strain expressing Bxb1. Indeed we observed no activity of pML10 in *E. coli*. Sequencing of randomly selected single transposon mutants in ML103 revealed only single transposition events, validating the design concept.

In the scope of this work we also observed an intense yellow-coloured mutant colony which sequencing identified as an integration of the transposon into *crtR*, characterized by Henke et al., 2017 as repressor of the *crt* operon. In their work, deletion of *crtR* increased decaprenoxanthin synthesis by 10–30 fold compared to the wildtype (Henke et al., 2017). This indicates the potential of the system to also screen for phenotypically striking mutations.

Also of potential interest is the integration of pML10 into a partially conserved *attB* site in *groEL*1. The GroEL gene is the target for Bxb1 prophage integration in its natural host *M. smegmatis* (Kim et al., 2003). Using *C. glutamicum* ML102, this allows for targeted integration of any vector carrying the proper *attP* site.

One problem that needs to be addressed is the fairly low efficiency of our system. The observation of several electroporation events giving rise to more than a thousand colonies demonstrates that the system works in principle but is constrained by one or more factors that need to be determined. The obvious explanation, i.e. a low transformation efficiency, can be ruled out, as the transformability of ML103 is comparable to MB001 and thus increased compared to the wildtype. Instead, this might be caused by an imbalanced Bxb1 activity, resulting in either not enough switching activity in *C. glutamicum* ML103, or, more likely, in too much Bxb1 being present. In the latter case, excess Bxb1 might bind to *attL* and *attR* and thereby act as an repressor of the switched promoter. This might be solved by modulating Bxb1 expression and will be addressed in the future.

IS*Cg1* in general was shown to be useable for the purpose of random mutagenesis. Analysis of the eight bp target site suggest a bias towards T for position three and four and towards A for the position five and six at the central four bp stretch with strong discrimination against G and C at positions four and 5 (**Figure 4**). While cursory inspection of the WebLogo implies that TTAA might be the predominant target motif, the list of tetranucleotide frequencies (**Supplementary Table S4**) reveals that this is not the case: neither is it the most common one nor is there any one sequence exceeding 20% of total transpositions with TTTA at 19.5% being the most prominent tetramer. In contrast to positions three to six, positions 1 and 2 as well as Position seven and eight show a slight tendency towards G and C. A distinct consensus for the target site preference however can not be derived. This strongly suggest that IS*Cg1* is applicable to target at such a random rate to potentially hit every feature in the genome of *C. glutamicum*. Indeed, the 3,207 independent sites hit in this work seem to be randomly distributed across the genome and displayed no general strand bias (**Figure 3**).

Thus, the transposon system using ML103 provides a useful, modular tool for random transposon mutagenesis with an easily applicable library generation protocol for ONT sequencing and IS*Cg1* as a randomly integrating transposase. The system can be adapted with little effort, e.g., by integration of an outward facing promoter on pML10 to allow for random gene activation/overexpression or by using a replicative vector to allow for multiple transpositions in a single mutant. For this purpose and to further facilitate industrial application, removal of the integrated kanamycin resistance cassette would be beneficial. This could be addressed by, e.g., combining our system with a Cre/*loxP*-mediated self-removal as described by Huang et al. (2017) by integrating two *lox* sites and an inducible Cre recombinase into the payload of pML10.

Taken together, the three strains *C. glutamicum* CR101, ML102, and ML103 in combination with plasmid ML103 provide a useful toolbox in basic research and industrial biotechnology.

DATA AVAILABILITY STATEMENT

The datasets presented in this study can be found in online repositories. The names of the repository/repositories and accession number(s) can be found in the article/**Supplementary Material**.

AUTHOR CONTRIBUTIONS

ML, MH, and CR drafted the manuscript and performed ONT sequencing. MH developed the python scripts and ran bioinformatic

analyses. CR performed data processing and assembled the genome sequence. AB and CR designed deletion constructs and performed serial deletions to construct strain CR101. ML constructed the switch strain and plasmid. JK and CR designed, planned, and interpreted the experimental work, coordinated the study and performed final editing of the manuscript.

ACKNOWLEDGMENTS

We acknowledge the financial support of the German Research Foundation (DFG) and the Open Access Publication Fund of Bielefeld University for the article processing charge. We thank Saskia Dymek for her help in performing the electroporation experiments. Furthermore we thank Lucas Jacob and Carina Prell for instruction and support in the execution of BioLector cultivations.

SUPPLEMENTARY MATERIAL

The Supplementary Material for this article can be found online at: https://www.frontiersin.org/articles/10.3389/fbioe.2021.751334/full#supplementary-material

REFERENCES

Agarwala, R., Barrett, T., Beck, J., Benson, D. A., Bollin, C., Bolton, E., et al. (2017). Database Resources of the National center for Biotechnology Information. *Nucleic Acids Res.* 46, D8–D13. doi:10.1093/nar/gkx1095

Altschul, S. F., Gish, W., Miller, W., Myers, E. W., and Lipman, D. J. (1990). Basic Local Alignment Search Tool. *J. Mol. Biol.* 215, 403–410. doi:10.1016/s0022-2836(05)80360-2

Anderson, J. C. (2013). Anderson Promoter Collection. Available: http://parts.igem.org/promoters/catalog/anderson [Dataset].

Ballas, P., Rückert, C., Wagener, K., Drillich, M., Kämpfer, P., Busse, H.-J., et al. (2020). *Corynebacterium Urogenitale* Sp. Nov. Isolated from the Genital Tract of a Cow. *Int. J. Syst. Evol. Microbiol.* 70, 3625–3632. doi:10.1099/ijsem.0.004198

Baumgart, M., Unthan, S., Kloß, R., Radek, A., Polen, T., Tenhaef, N., et al. (2018). *Corynebacterium Glutamicum* Chassis C1*: Building and Testing a Novel Platform Host for Synthetic Biology and Industrial Biotechnology. *ACS Synth. Biol.* 7, 132–144. doi:10.1021/acssynbio.7b00261

Baumgart, M., Unthan, S., Rückert, C., Sivalingam, J., Grünberger, A., Kalinowski, J., et al. (2013). Construction of a Prophage-free Variant of *Corynebacterium Glutamicum* ATCC 13032 for Use as a Platform Strain for Basic Research and Industrial Biotechnology. *Appl. Environ. Microbiol.* 79, 6006–6015. doi:10.1128/aem.01634-13

Becker, J., and Wittmann, C. (2012). Bio-based Production of Chemicals, Materials and Fuels - Corynebacterium Glutamicum as Versatile Cell Factory. *Curr. Opin. Biotechnol.* 23, 631–640. doi:10.1016/j.copbio.2011.11.012

Bonnet, J., Subsoontorn, P., and Endy, D. (2012). Rewritable Digital Data Storage in Live Cells via Engineered Control of Recombination Directionality. *Proc. Natl. Acad. Sci.* 109, 8884–8889. doi:10.1073/pnas.1202344109

Cain, A. K., Barquist, L., Goodman, A. L., Paulsen, I. T., Parkhill, J., and van Opijnen, T. (2020). A Decade of Advances in Transposon-Insertion Sequencing. *Nat. Rev. Genet.* 21, 526–540. doi:10.1038/s41576-020-0244-x

Chen, X., Kohl, T. A., Rückert, C., Rodionov, D. A., Li, L.-H., Ding, J.-Y., et al. (2012). Phenylacetic Acid Catabolism and its Transcriptional Regulation in *Corynebacterium Glutamicum*. *Appl. Environ. Microbiol.* 78, 5796–5804. doi:10.1128/AEM.01588-12

Choi, J. W., Yim, S. S., Kim, M. J., and Jeong, K. J. (2015). Enhanced Production of Recombinant Proteins with *Corynebacterium Glutamicum* by Deletion of Insertion Sequences (IS Elements). *Microb. Cel Fact* 14. doi:10.1186/s12934-015-0401-7

Crooks, G. E., Hon, G., Chandonia, J.-M., and Brenner, S. E. (2004). WebLogo: A Sequence Logo Generator: Figure 1. *Genome Res.* 14, 1188–1190. doi:10.1101/gr.849004

Evans, M. R., Bertera, A. L., and Harris, D. W. (1994). The Southern Blot. *Mol. Biotechnol.* 1, 1–12. doi:10.1007/bf02821507

Frunzke, J., Bramkamp, M., Schweitzer, J.-E., and Bott, M. (2008). Population Heterogeneity in *Corynebacterium Glutamicum* ATCC 13032 Caused by Prophage CGP3. *J. Bacteriol.* 190, 5111–5119. doi:10.1128/jb.00310-08

Gibson, D. G., Young, L., Chuang, R.-Y., Venter, J. C., Hutchison, C. A., and Smith, H. O. (2009). Enzymatic Assembly of DNA Molecules up to Several Hundred Kilobases. *Nat. Methods* 6, 343–345. doi:10.1038/nmeth.1318

Gilchrist, A., and Smit, J. (1991). Transformation of Freshwater and marine Caulobacters by Electroporation. *J. Bacteriol.* 173, 921–925. doi:10.1128/jb.173.2.921-925.1991

Grant, S. G., Jessee, J., Bloom, F. R., and Hanahan, D. (1990). Differential Plasmid rescue from Transgenic Mouse DNAs into *Escherichia coli* Methylation-Restriction Mutants. *Proc. Natl. Acad. Sci.* 87, 4645–4649. doi:10.1073/pnas.87.12.4645

Hansmeier, N., Bartels, F. W., Ros, R., Anselmetti, D., Tauch, A., Pühler, A., et al. (2004). Classification of Hyper-Variable *Corynebacterium Glutamicum* Surface-Layer Proteins by Sequence Analyses and Atomic Force Microscopy. *J. Biotechnol.* 112, 177–193. doi:10.1016/j.jbiotec.2004.03.020

Henke, N. A., Heider, S. A. E., Hannibal, S., Wendisch, V. F., and Peters-Wendisch, P. (2017). Isoprenoid Pyrophosphate-dependent Transcriptional Regulation of Carotenogenesis in *Corynebacterium Glutamicum*. *Front. Microbiol.* 8. doi:10.3389/fmicb.2017.00633

Hennig, G., Haupka, C., Brito, L. F., Rückert, C., Cahoreau, E., Heux, S., et al. (2020). Methanol-essential Growth of *Corynebacterium Glutamicum*: Adaptive Laboratory Evolution Overcomes Limitation Due to Methanethiol Assimilation Pathway. *Ijms* 21, 3617. doi:10.3390/ijms21103617

Huang, Y., Li, L., Xie, S., Zhao, N., Han, S., Lin, Y., et al. (2017). Recombineering Using RecET in *Corynebacterium Glutamicum* ATCC14067 via a Self-Excisable Cassette. *Sci. Rep.* 7. doi:10.1038/s41598-017-08352-9

Hunter, J. D. (2007). Matplotlib: A 2d Graphics Environment. *Comput. Sci. Eng.* 9, 90–95. doi:10.1109/MCSE.2007.55

Ikeda, M., and Nakagawa, S. (2003). The *Corynebacterium Glutamicum* Genome: Features and Impacts on Biotechnological Processes. *Appl. Microbiol. Biotechnol.* 62, 99–109. doi:10.1007/s00253-003-1328-1

Inui, M., Tsuge, Y., Suzuki, N., Vertès, A. A., and Yukawa, H. (2005). Isolation and Characterization of a Native Composite Transposon, Tn 14751 , Carrying 17.4 Kilobases of *Corynebacterium Glutamicum* Chromosomal DNA. *Appl. Environ. Microbiol.* 71, 407–416. doi:10.1128/aem.71.1.407-416.2005

J. Sambrook, E. Fritsch, and T. Maniatis (Editors) (1989). *Molecular Cloning. A Laboratory Manual*. 2 edn (Cold Spring Harbor, NY, United States: Cold Spring Harbour Laboratory Press).

Kalinowski, J., Bathe, B., Bartels, D., Bischoff, N., Bott, M., Burkovski, A., et al. (2003). The Complete *Corynebacterium Glutamicum* ATCC 13032 Genome Sequence and its Impact on the Production of L-Aspartate-Derived Amino Acids and Vitamins. *J. Biotechnol.* 104, 5–25. doi:10.1016/s0168-1656(03)00154-8

Kalinowski, J. (2005). "The Genomes of Amino Acid-Producing Corynebacteria," in *Handbook of Corynebacterium Glutamicum*. Editors L. Eggeling and M. Bott. 1 edn. (Boca Raton, FL: CRC Press), 37–56. doi:10.1201/9781420039696.pt3

Kato, Y. (2020). Extremely Low Leakage Expression Systems Using Dual Transcriptional-Translational Control for Toxic Protein Production. *Ijms* 21, 705. doi:10.3390/ijms21030705

Kim, A. I., Ghosh, P., Aaron, M. A., Bibb, L. A., Jain, S., and Hatfull, G. F. (2003). Mycobacteriophage Bxb1 Integrates into the *Mycobacterium Smegmatis groEL*1 Gene. *Mol. Microbiol.* 50, 463–473. doi:10.1046/j.1365-2958.2003.03723.x

Li, H. (2018). Minimap2: Pairwise Alignment for Nucleotide Sequences. *Bioinformatics* 34, 3094–3100. doi:10.1093/bioinformatics/bty191

Nakamura, Y., Nishio, Y., Ikeo, K., and Gojobori, T. (2003). The Genome Stability in *Corynebacterium* Species Due to Lack of the Recombinational Repair System. *Gene* 317, 149–155. doi:10.1016/s0378-1119(03)00653-x

Ozaki, K., Ara, K., Nakamura, K., Yamane, K., Sekiguchi, J., and Ogasawara, N. (2007). *Bacillus* Minimum Genome Factory: Effective Utilization of Microbial Genome Information. *Biotechnol. Appl. Biochem.* 46, 169. doi:10.1042/ba20060111

Peng, M., and Liang, Z. (2020). Degeneration of Industrial Bacteria Caused by Genetic Instability. *World J. Microbiol. Biotechnol.* 36. doi:10.1007/s11274-020-02901-7

Pfeifer-Sancar, K., Mentz, A., Rückert, C., and Kalinowski, J. (2013). Comprehensive Analysis of the *Corynebacterium Glutamicum* Transcriptome Using an Improved RNAseq Technique. *BMC Genomics* 14, 888. doi:10.1186/1471-2164-14-888

Plassmeier, J., Li, Y., Rueckert, C., and Sinskey, A. J. (2016). Metabolic Engineering *Corynebacterium Glutamicum* to Produce Triacylglycerols. *Metab. Eng.* 33, 86–97. doi:10.1016/j.ymben.2015.11.002

Po´sfai, G., Plunkett, G., Fehe´r, T., Frisch, D., Keil, G. M., Umenhoffer, K., et al. (2006). Emergent Properties of Reduced-Genome *Escherichia coli*. *Science* 312, 1044–1046. doi:10.1126/science.1126439

Renda, B. A., Hammerling, M. J., and Barrick, J. E. (2014). Engineering Reduced Evolutionary Potential for Synthetic Biology. *Mol. Biosyst.* 10, 1668–1678. doi:10.1039/c3mb70606k

Schäfer, A., Kalinowski, J., and Pühler, A. (1994a). Increased Fertility of *Corynebacterium Glutamicum* Recipients in Intergeneric Matings with *Escherichia coli* after Stress Exposure. *Appl. Environ. Microbiol.* 60, 756–759. doi:10.1128/aem.60.2.756-759.1994

Schäfer, A., Schwarzer, A., Kalinowski, J., and Pühler, A. (1994b). Cloning and Characterization of a DNA Region Encoding a Stress-Sensitive Restriction System from *Corynebacterium Glutamicum* ATCC 13032 and Analysis of its Role in Intergeneric Conjugation with *Escherichia coli*. *J. Bacteriol.* 176, 7309–7319. doi:10.1128/jb.176.23.7309-7319.1994

Schäfer, A., Tauch, A., Jäger, W., Kalinowski, J., Thierbach, G., and Pühler, A. (1994c). Small Mobilizable Multi-Purpose Cloning Vectors Derived from the *Escherichia coli* Plasmids pK18 and pK19: Selection of Defined Deletions in the Chromosome of *Corynebacterium Glutamicum*. *Gene* 145, 69–73. doi:10.1016/0378-1119(94)90324-7

Singh, S., Ghosh, P., and Hatfull, G. F. (2013). Attachment Site Selection and Identity in Bxb1 Serine Integrase-Mediated Site-specific Recombination. *Plos Genet.* 9, e1003490–14. doi:10.1371/journal.pgen.1003490

Suzuki, N., Nonaka, H., Tsuge, Y., Inui, M., and Yukawa, H. (2005). New Multiple-Deletion Method for the *Corynebacterium Glutamicum* Genome, Using a Mutant *Lox* Sequence. *Appl. Environ. Microbiol.* 71, 8472–8480. doi:10.1128/aem.71.12.8472-8480.2005

Suzuki, N., Okai, N., Nonaka, H., Tsuge, Y., Inui, M., and Yukawa, H. (2006). High-throughput Transposon Mutagenesis of *Corynebacterium Glutamicum* and Construction of a Single-Gene Disruptant Mutant Library. *Appl. Environ. Microbiol.* 72, 3750–3755. doi:10.1128/aem.72.5.3750-3755.2006

Tauch, A., Kirchner, O., Löffler, B., Götker, S., Pühler, A., and Kalinowski, J. (2002). Efficient Electrotransformation of *Corynebacterium Diphtheriae* with a Mini-Replicon Derived from the *Corynebacterium Glutamicum* Plasmid pGA1. *Curr. Microbiol.* 45, 362–367. doi:10.1007/s00284-002-3728-3

Umenhoffer, K., Fehér, T., Balikó, G., Ayaydin, F., Pósfai, J., Blattner, F. R., et al. (2010). Reduced Evolvability of *Escherichia coli* MDS42, an IS-Less Cellular Chassis for Molecular and Synthetic Biology Applications. *Microb. Cel Fact* 9, 38. doi:10.1186/1475-2859-9-38

Wendisch, V. F. (2020). Metabolic Engineering Advances and Prospects for Amino Acid Production. *Metab. Eng.* 58, 17–34. doi:10.1016/j.ymben.2019.03.008

Wendisch, V. F. (2016). "Microbial Production of Amino Acid-Related Compounds," in *Amino Acid Fermentation* (Springer Japan), 255–269. doi:10.1007/10_2016_34

Wolf, S., Becker, J., Tsuge, Y., Kawaguchi, H., Kondo, A., Marienhagen, J., et al. (2021). Advances in Metabolic Engineering of *Corynebacterium Glutamicum* to Produce High-Value Active Ingredients for Food, Feed, Human Health, and Well-Being. *Essays Biochem.* 65, 197–212. doi:10.1042/ebc20200134

Yanisch-Perron, C., Vieira, J., and Messing, J. (1985). Improved M13 Phage Cloning Vectors and Host Strains: Nucleotide Sequences of the M13mpl8 and pUC19 Vectors. *Gene* 33, 103–119. doi:10.1016/0378-1119(85)90120-9

Yomantas, Y. A., Abalakina, E. G., Golubeva, L. I., Gorbacheva, L. Y., and Mashko, S. V. (2011). Overproduction of *Bacillus Amyloliquefaciens* Extracellular Glutamyl-Endopeptidase as a Result of Ectopic Multi-Copy Insertion of an Efficiently-Expressed *Mpr* Gene into the *Bacillus Subtilis* Chromosome. *Microb. Cel Fact* 10. doi:10.1186/1475-2859-10-64

Yukawa, H., Omumasaba, C. A., Nonaka, H., Kós, P., Okai, N., Suzuki, N., et al. (2007). Comparative Analysis of the *Corynebacterium Glutamicum* Group and Complete Genome Sequence of Strain R. *Microbiology* 153, 1042–1058. doi:10.1099/mic.0.2006/003657-0

Conflict of Interest: The authors declare that the research was conducted in the absence of any commercial or financial relationships that could be construed as a potential conflict of interest.

frontiers in Bioengineering and Biotechnology

ORIGINAL RESEARCH
published: 20 December 2021
doi: 10.3389/fbioe.2021.768490

Indirect Pathway Metabolic Engineering Strategies for Enhanced Biosynthesis of Hyaluronic Acid in Engineered *Corynebacterium glutamicum*

Yan Du[1], *Fangyu Cheng*[1], *Miaomiao Wang*[1], *Chunmeng Xu*[1] *and Huimin Yu*[1,2]*

[1]*Key Laboratory for Industrial Biocatalysis of the Ministry of Education, Department of Chemical Engineering, Tsinghua University, Beijing, China,* [2]*Center for Synthetic and Systems Biology, Tsinghua University, Beijing, China*

Hyaluronic acid (HA) is composed of alternating D-glucuronic acid and *N*-acetyl-D-glucosamine, with excellent biocompatibility and water retention capacity. To achieve heterologous biosynthesis of HA, *Corynebacterium glutamicum*, a safe GRAS (generally recognized as safe) host, was utilized and metabolically engineered previously. In this work, to achieve further enhancement of HA yield, four strategies were proposed and performed separately first, i.e., (1) improvement of glucose uptake via *iolR* gene knockout, releasing the inhibition of transporter IolT1/IolT2 and glucokinases; (2) intensification of cardiolipin synthesis through overexpression of genes *pgsA1/pgsA2/cls* involved in cardiolipin synthesis; (3) duly expressed *Vitreoscilla* hemoglobin in genome, enhancing HA titer coupled with more ATP and improved NAD^+/NADH (>7.5) ratio; and (4) identification of the importance of glutamine for HA synthesis through transcriptome analyses and then enhancement of the HA titer via its supplement. After that, we combined different strategies together to further increase the HA titer. As a result, one of the optimal recombinant strains, Cg-dR-CLS, yielded 32 g/L of HA at 60 h in a fed-batch culture, which was increased by 30% compared with that of the starting strain. This high value of HA titer will enable the industrial production of HA via the engineered *C. glutamicum*.

Keywords: hyaluronic acid, engineered *Corynebacterium glutamicum*, IolR deletion, cardiolipin (CL), *Vitreoscilla* hemoglobin (VHb), glutamine

OPEN ACCESS

Edited by:
Yu Wang,
Tianjin Institute of Industrial Biotechnology (CAS), China

Reviewed by:
Yu-Sin Jang,
Gyeongsang National University, South Korea
Yota Tsuge,
Kanazawa University, Japan

***Correspondence:**
Huimin Yu
yuhm@tsinghua.edu.cn

Specialty section:
This article was submitted to Synthetic Biology, a section of the journal Frontiers in Bioengineering and Biotechnology

Received: *31 August 2021*
Accepted: *22 November 2021*
Published: *20 December 2021*

Citation:
Du Y, Cheng F, Wang M, Xu C and Yu H (2021) Indirect Pathway Metabolic Engineering Strategies for Enhanced Biosynthesis of Hyaluronic Acid in Engineered Corynebacterium glutamicum. *Front. Bioeng. Biotechnol. 9:768490. doi: 10.3389/fbioe.2021.768490*

INTRODUCTION

Hyaluronic acid (HA), composed of alternating β-1,3-*N*-acetyl-D-glucosamine (GlcNAc) and β-1,4-D-glucuronic acid (GlcUA), belongs to the glycosaminoglycan family (Westbrook et al., 2018; Cheng et al., 2019b; Wang et al., 2020) and mainly exists in animal tissues such as chicken crowns. HA has already been applied in the clinical, cosmetic, pharmaceutical, and food industry due to its excellent biocompatibility and extraordinary water-retaining properties (Stecco et al., 2011; Graca et al., 2020; Yu et al., 2020). Generally, HAs with different molecular weights (M_Ws) have different applications (Qiu et al., 2021). High-molecular-weight HA (HMW-HA, $M_W \geq 1 \times 10^6$ Da) is mainly used for joint cavity injection and cartilage degeneration repair, owing to its good viscoelasticity, moisture

retention, and lubrication properties. Low-molecular-weight HA (LMW-HA, 1×10^4–1×10^6 Da) usually plays an important role in the cosmetics field (Qiu et al., 2021), since it can improve skin elasticity and reduce wrinkles (Pavicic et al., 2011), as well as regulate skin metabolism and delay aging (Camacho et al., 2016). In addition, HA oligosaccharides ($M_W \leq 1 \times 10^4$ Da) may have significant application prospects in the food health field (Boltje et al., 2009), as they have been widely used in fruit juice, soy milk, jelly, and other food. In the future, HAs with different M_Ws will have more and better development prospects in different fields (Qiu et al., 2021).

Nowadays, industrial HA production has already been achieved through fermentation of group C *Streptococcus* (*Streptococcus equisimilis* and *Streptococcus zooepidemicus*) (Liu et al., 2011) and has gradually replaced the traditional animal issue extraction methods. However, *Streptococcus* sp. may produce some exotoxins and immunogens during HA production (Cheng et al., 2019b; Wang et al., 2020). Considering the potential hazards, adoption of GRAS (generally recognized as safe) strains to produce HA is required urgently. Up to now, HA has been biosynthesized successfully in *Escherichia coli* (Yu and Stephanopoulos 2008; Mao et al., 2009; Woo et al., 2019), *Lactococcus lactis* (Prasad et al., 2010; Sunguroglu et al., 2018; Jeeva et al., 2019), *Bacillus subtilis* (Westbrook et al., 2018a; Westbrook et al., 2018b; Li et al., 2019), *Agrobacterium* sp. (Mao and Chen 2007), and *Corynebacterium glutamicum* (Hoffmann and Altenbuchner 2014; Cheng et al., 2016; Cheng et al., 2017; Cheng et al., 2019b; Wang et al., 2020; Zheng et al., 2020). Even though the HA titers obtained from heterologous hosts are in general still lower than those achieved by natural, pathogenic producers. In the biosynthesis of HA, HA polymer is synthesized by an enzyme called HA synthase (HAS), which is grouped into two classes (Agarwal et al., 2019). Class I HAS is a kind of integral membrane protein containing a single domain, while Class II HAS is a soluble/membrane anchored protein with two domains (Weigel 2015). Most of the HAS found so far belong to Class I, such as HAS from *S. equisimilis* (seHAS) and *Streptococcus pyogenes* (spHAS); however, Class II enzyme is found only in *Pasteurella multocida* (pmHAS). It was reported that seHAS and spHAS contained a single HAS protein associated with an additional component with a mass of about 23 kDa, which was identified as cardiolipin (CL), one of the common bacterial membrane phospholipids (Weigel 2002). Thus, the active HAS enzyme contains a HAS protein monomer and about 14–18 CL molecules as a complex, in which CL is essential for enzymatic activity. It has not been studied whether enhanced CL synthesis would have an impact on HA production.

In order to meet the requirements of industrial production, researchers have made lots of efforts to increase the yield of HA in recombinant strains. Some hosts naturally harbor an almost complete metabolic route for HA synthesis, just lacking the HAS gene (hasA), such as *B. subtilis*, *E. coli*, and *C. glutamicum* (Manfrao-Netto et al., 2021). Based on the heterologous expression of *hasA*, different artificial *has* operons containing a combination of different genes have been constructed in various hosts to increase HA titer. Examples are *sp*ABC and *sse*AB in *E. coli* (Yu and Stephanopoulos 2008), *pmhasA-tuaD-gtaB* (operon *has*ABC) in *B. subtilis* 168 (Jia et al., 2013), and *ssehasA-hasB* operon in *C. glutamicum* (Cheng et al., 2016), which in general obtained about 1–7 g/L of HA. Besides, engineering metabolic pathways promoted the yield of HA as well in different strains (Jin et al., 2016; Westbrook et al., 2018a). Wang et al. (2020) coupled HA degradation with HA production through adding leech hyaluronidase, which led to 74.1 g/L of HA accumulation with super-low M_W (~53 kDa). In addition, some researchers also found that the cell-morphology engineering strategies, for example, downregulating or overexpressing the cell division initiator protein FtsZ in *B. subtilis* or *C. glutamicum*, can further enhance the HA titer (Westbrook et al., 2016; Zheng et al., 2020). For the overexpression of *Vitreoscilla* sp. hemoglobin (VHb), however, contrary results were reported in different strains: in *B. subtilis*, expression of VHb improved the HA titer from 0.9 to 1.8 g/L (Chien and Lee 2007); but in *C. glutamicum*, co-expression of the VHb gene (*vgb*) with *hasA* lowered HA yield by about 1.5-fold (Hoffmann and Altenbuchner 2014). In view of this, the effect of VHb varies case by case, which needs to be further investigated. Except for the genetic strategies, some researchers also enhanced the HA yield through optimization of the culture medium. Important functions of trace element and different kinds of carbon and nitrogen sources such as corn syrup powder and glucose were highlighted (Cheng et al., 2016; Chahuki et al., 2019).

Herein, we proposed four indirect pathway metabolic strategies to further enhance the HA titer in engineered *C. glutamicum*, i.e., enhancing the carbon substrate uptake via genetically activating the PTS-independent uptake system; regulating HA synthesis through the intensified synthesis of CL (an auxiliary molecule of HAS); duly expressing VHb via integration of the gene *vgb* into the genome of *C. glutamicum*, thereby promoting cell oxygen transfer, energy metabolism, and finally HA synthesis; and lastly finding the key inorganic nitrogen source (glutamine) through transcriptome analyses and then enhancing the HA titer via its supplementation. Combination strategies were further evaluated, and HA titer was significantly enhanced by optimal combinations.

MATERIALS AND METHODS

Kits, Strains, Media, Plasmids, and Growth Conditions

DNA amplification was performed using 2× Phanta Max Master Mix, purchased from Vazyme (Nanjing, China). A DNA Gel Extraction Kit and Plasmid Miniprep Kit were purchased from Omega (Norcross, GA, United States). Gibson Assembly Reaction Kits were used, purchased from Clonesmarter Technologies (Scottsdale, AZ, United States). An ATP Assay Kit was obtained from Solarbio (Beijing, China), and a NAD^+/NADH Assay Kit (WST-8 method) was purchased from Beyotime (Shanghai, China).

All the strains and plasmids used in this study were listed in **Table 1**, and the primers used for gene amplifications were listed

TABLE 1 | Plasmids and strains in this study.

Plasmids and strains	Description	Reference
Plasmids		
pEC-XK99E	Kana^r, P_{trc}-MCS, *rep* from native plasmid pGA1 (GenBank: X90817.2) of *C. glutamicum*	Yang et al. (2016)
pEC-AB	pEC-XK99E derivate, P_{tac}-*hasA*-*hasB*	Cheng et al. (2019b)
AP_{dapB}BaF	pEC-XK99E derivate, P_{tac}-*hasA*-P_{dapB}-*hasB*-Ter, P_{tac}-as-F-Ter	Cheng et al. (2019b)
AP_{dapB}B-*pgs*A1-aF	AP_{dapB}BaF derivate, P_{dapB}-*pgs*A1	This work
AP_{dapB}B-*pgs*A2-aF	AP_{dapB}BaF derivate, P_{dapB}-*pgs*A2	This work
AP_{dapB}B-*cls*-aF	AP_{dapB}BaF derivate, P_{dapB}-*cls*	This work
pK18mobsacB	Kana^r, *sacB* from *B. subtilis*	Cheng et al. (2019a)
pK18mobsacB-Δ*iolR*	pK18mobsacB derivate, harboring upstream and downstream homologous arms of *iolR*	This work
pK18mobsacB-Δ*ldh*::*vgb*	pK18mobsacB derivate, harboring upstream and downstream homologous arms of *ldh*, and *vgb* gene	This work
Strains		
E. coli Trans10	F-*mcr*A Δ(*mrr-hsd*RMS-*mcr*BC) φ80 *lac*ZΔM15Δ*lac*X74 *rec*A1 *ara*Δ139 Δ(*ara-leu*) 7697 *gal*U *gal*K *rps*L (Str^R) *end*A1 *nup*G	TransGen
C. glutamicum ATCC13032	Wild type	Cheng et al. (2016)
Cg-ΔLACPZ	Wild-type derivate, Δ*ldh*, Δ*ackA-pta*, Δ*cat*, Δ*poxB*, Δ*zwf*	Cheng et al. (2019b)
Cg-0-half	Wild-type derivate, containing the plasmid pEC-AB, with half HA titer of Cg-0	Cheng et al. (2019b)
Cg-0	Wild-type derivate, Δ*ldh*, Δ*ackA-pta*, Δ*cat*, Δ*poxB*, Δ*zwf*, containing the plasmid AP_{dapB}BaF	Cheng et al. (2019b)
Cg-dR	Cg-0 derivate, containing the plasmid AP_{dapB}BaF, Δ*iolR*	This work
Cg-VHb	Cg-0 derivate, containing the plasmid AP_{dapB}BaF, Δ*ldh*::*vgb*	This work
Cg-pgsA1	Cg-0 derivate, containing the plasmid AP_{dapB}B-*pgs*A1-aF	This work
Cg-pgsA2	Cg-0 derivate, containing the plasmid AP_{dapB}B-*pgs*A2-aF	This work
Cg-CLS	Cg-0 derivate, containing the plasmid AP_{dapB}B-*cls*-aF	This work
Cg-dR-VHb	Cg-0 derivate, containing the plasmid AP_{dapB}BaF, Δ*iolR*, Δ*ldh*::*vgb*	This work
Cg-dR-CLS	Cg-0 derivate, containing the plasmid AP_{dapB}B-*cls*-aF, Δ*iolR*	This work
Cg-VHb-CLS	Cg-0 derivate, containing the plasmid AP_{dapB}B-*cls*-aF, Δ*ldh*::*vgb*	This work
Cg-dR VHb-VLS	Cg-0 derivate, containing the plasmid AP_{dapB}B-*cls*-aF, Δ*iolR*, Δ*ldh*::*vgb*	This work

in **Supplementary Table S1**. *E. coli* trans10 (TransGen Biotech Co., LTD) was used to construct and amplify the recombinant plasmids. Luria-Bertani broth (LB) medium (tryptone 10 g/L, yeast extract 5 g/L, and NaCl 10 g/L) was used for culturing *E. coli* strains. If necessary, 50 μg/ml kanamycin was added. *C. glutamicum* ATCC13032 was the starting host strain for subsequent *C. glutamicum* engineered strains. Cg-0 was constructed previously in our laboratory, and its genotype was shown in **Table 1** (Cheng et al., 2019b). For flask culture, all of the engineered *C. glutamicum* strains were cultured in a 500 ml flask containing 50 ml fermentation medium (40 g/L glucose, 20 g/L $(NH_4)_2SO_4$, 1 g/L K_2HPO_3, 0.5 g/L KH_2PO_3, 5 g/L $MgSO_4{\cdot}7H_2O$, 0.01 g/L $FeSO_4{\cdot}7H_2O$, and 0.01 g/L $MnSO_4$, pH = 7.2) at 28°C, 200 rpm. The pH of the medium was adjusted to 7.2 every 12 h, and glucose was supplemented every 24 h.

Plasmid pK18mobsacB containing the *sacB* gene was used to conduct genome editing (such as *iolR* gene deletion) via double-crossover homologous recombination driven by sucrose selection (Schafer et al., 1994). Gene *vgb* was cloned from a plasmid in a previous study (Wang et al., 2018). The recombinant plasmid pK18mobsacB-Δ*ldh*::*vgb* was constructed and used for *vgb* integration into the genome. The genes relating to synthesis of CL (*pgsA1*, *pgsA2*, and *cls*) were amplified from the *C. glutamicum* genome and were fused into the plasmid AP_{dapB}BaF, resulting in the plasmid AP_{dapB}B-*pgs*A1/*pgs*A2/*cls*-aF. Competent cells of Cg-ΔLACPZ were used for construction of strain Cg-dR and Cg-VHb by homologous recombination via pK18mobsacB. Engineered strains Cg-dR, Cg-VHb, Cg-pgsA1, Cg-pgsA2, Cg-CLS, Cg-dR-VHb, Cg-dR-CLS, Cg-VHb-CLS and Cg-dR-VHb-CLS were constructed and utilized for studies in this work.

Cell Growth Measurement (OD_{600}) and HA Titer Assay

During flask cultivation, 1.5 ml broth sample was withdrawn at 24, 48, and 72 h, to determine the OD_{600} and HA titer of different recombinant strains. The HA titer was determined as follows: 3 ml ethanol was added into 1 ml fermentation broth, stored at 4°C for 2 h. The precipitation was collected by centrifugation (10,000 rpm, 3 min). Then 1 ml distilled water was added, and the HA yield was measured by the modified CTAB method, as previously described.

Transcriptome Analysis of *C. glutamicum*

Cells of the two recombinant *C. glutamicum* strains (Cg-0 and Cg-0-half) cultured for 24 h were collected and centrifuged at room temperature for 10 min at 10,000 rpm and then stored at −70°C. The frozen cells were sent to Beijing Novogene to determine the transcriptome data.

VHb Expression Verification Through Matrix-Assisted Laser Desorption/Ionization Time-of-Flight Mass Spectrometry

The broth samples of Cg-0 and Cg-VHb were collected at 24 h in parallel culture. After centrifugation at 13,000 rpm for 5 min, cell pellets were harvested and washed twice with phosphate buffer solution (PBS, 20 mM, pH = 7.2). Then the cell suspensions in PBS were sent for MALDI-TOF-MS analyses, using an ABI 4800 Plus analyzer (Applied Biosystems, Foster City, CA, United States).

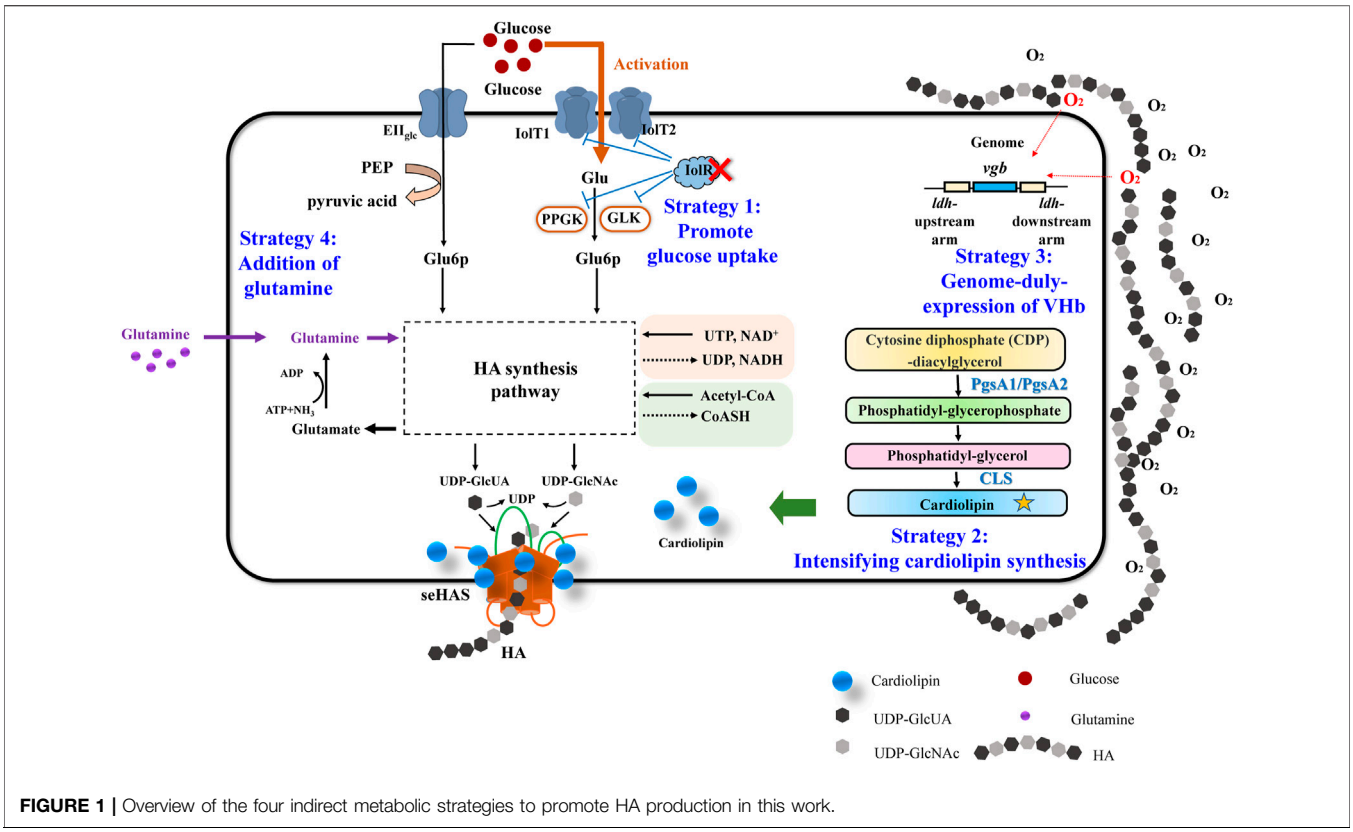

FIGURE 1 | Overview of the four indirect metabolic strategies to promote HA production in this work.

ATP and NAD$^+$/NADH Measurement

ATP and NAD$^+$/NADH results of Cg-0 or Cg-VHb were measured by an ATP Assay Kit (Solarbio) and NAD$^+$/NADH Assay Kit (Beyotime), respectively. For both assays, 1 ml broth sample at 24 or 48 h with a cell concentration of 1 OD was withdrawn and centrifuged at 13,000 rpm for 5 min. The pellet was washed twice and resuspended with 1 ml PBS (pH = 7.2, 20 mM) and then used for ATP assay and NAD$^+$/NADH measurement with the standard protocol of the kit.

Fed-Batch Culture in a 10 L Fermenter

The fed-batch culture was conducted in a 10 L fermenter (Sartorius), containing 4 L fermentation medium as described above supplemented with 2 g/L glutamine. The aeration was set as 1 vvm, and agitation was set as 600 rpm, at 28°C. After 48 h of fermentation, the agitation was set as 800 rpm. The pH of the medium was retained at 7.2 by 8 M NaOH and 6 M HCl. The concentration of glucose was measured every 2 h after 8 h of fermentation. And 800 g/L glucose was added when its concentration dropped below 10 g/L, ensuring that the residual glucose concentration remained between 8 and 15 g/L.

RESULTS

As mentioned above, various efforts have been made to promote HA production in recombinant *C. glutamicum*, for example, optimization of *has* operon, knocking out competitive metabolic pathways, membrane engineering to enlarge the availability of cell membrane, and coupling HA synthesis with HA hydrolysis. Besides these, here, we tried to find out some strategies, indirect, non-regular, but effective as well, to further improve the HA titer in engineered *C. glutamicum*. **Figure 1** showed the overview of the indirect metabolic strategies to promote HA production in this work.

Enhancing HA Synthesis via Improvement of Glucose Uptake by IolR Deletion

As illustrated in **Figure 1**, Strategy 1 highlighted the promotion of glucose uptake via transport regulation. Carbon sources are essential factors for cell growth and target product synthesis. For most industrial fermentation processes, glucose is always the main carbon source due to its low price and high utilization efficiency. There are two glucose transport systems in *C. glutamicum*: phosphoenolpyruvate-dependent glucose phosphorylation via the phosphotransferase system (PTS^{Glc}) and PTS-independent glucose uptake system (non-PTS^{Glc}), such as the coupling system of myo-inositol permease and glucokinase (IPGS), and the coupling system of beta-glucoside-PTS permease and glucokinase (GPGS) (Ruan et al., 2020). For the IPGS pathway, glucoses are firstly transported into cells by myo-inositol permeases (IolT1/IolT2) and then phosphorylated by glucokinases (Glk and PpgK). The transcription of *iolT1/iolT2/glk/ppkg*, however, is repressed by a GntT-type regulator IolR in *C. glutamicum* (Klaffl et al., 2013).

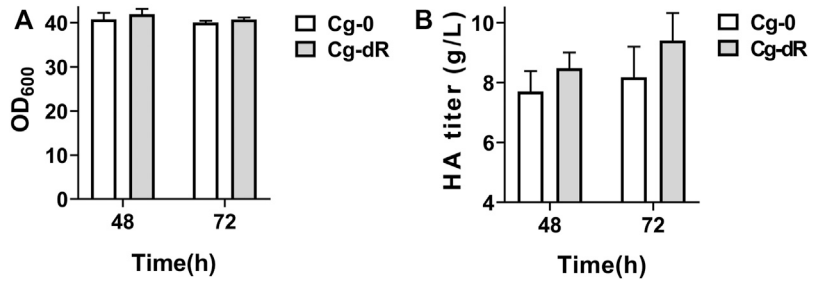

FIGURE 2 | Cell growth and HA titer comparison of Cg-dR and control Cg-0. **(A)** OD_{600}; **(B)** HA titer. Experiments were performed in triplicate.

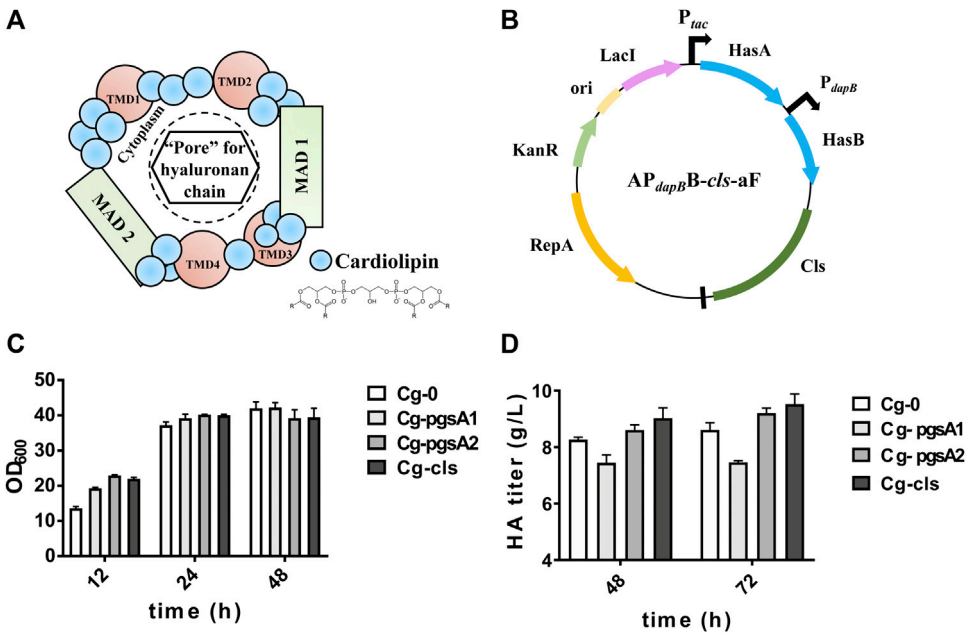

FIGURE 3 | Cell growth and HA titer results after intensification of CL synthesis. **(A)** Hypothetical model of the active CLS–HAS complex: the scheme depicts the close association of CL molecules (blue dots) with one HAS protein to create an active enzyme. The growing HA chain would be transferred through this pore-like opening. The membrane domains of the HAS are labeled as transmembrane domains (TMDs) or membrane-associated domains (MADs) (Tlapak-Simmons et al., 1999). **(B)** Plasmid map of $AP_{dapB}B$-*cls*-aF. **(C)** OD_{600} of the engineered strains Cg-pgsA1, Cg-pgsA2, and Cg-CLS. **(D)** HA titer of the same engineered strains. Strain Cg-0 was the control. Experiments were performed in triplicate.

Deletion of the regulator IolR can strongly activate the non-PTS system and enhance the glucose uptake rate (Zhang B. et al., 2019). Therefore, deleting the IolR gene, thereby improving the glucose uptake efficiency, was proposed to be the first strategy to enhance HA titer.

As described in **Table 1**, the HA producer Cg-0 was utilized as the starting strain for subsequent studies, which could yield 6.2 g/L of HA in flask culture and 24.5 g/L of HA in fed-batch culture (Cheng et al., 2019b). The engineered Cg-dR was obtained after successful deletion of the gene *iolR* (**Supplementary Figure S2**). Effects of IolR deletion on cell growth and HA synthesis were evaluated via parallel flask culture of Cg-0 and Cg-dR. As shown in **Figure 2**, the OD_{600} of Cg-dR showed a litter difference with that of Cg-0, while the HA titer of Cg-dR was 6.9% higher than that of Cg-0 at 48 h, reaching 8.48 g/L.

Enhancing HA Synthesis via Intensification of CL Synthesis—Auxiliary Factor of HAS

Strategy 2 focused on the auxiliary factor for maintaining the high activity of HAS, which is of great importance for HA biosynthesis. It was reported that CL was the activator for seHAS (Tlapak-Simmons et al., 1998; Tlapak-Simmons et al., 1999). The active *Streptococcal* HAS contains a single HAS monomer and multiple CL molecules (14–18 molecules of CL) (Tlapak-Simmons et al., 1998); and the exogenous CL could rescue the HAS activity (Kakizaki et al., 2002). CL, also known as diphospholipin, is synthesized from the intermediate metabolite cytosine diphosphate-diacylglycerol (CDP-DAG) by phosphatidylglycerophosphate synthase (PGS), phosphatidylglycerophosphate phosphatase (PTPMT), and CL synthase (CLS). Among them, the key enzyme

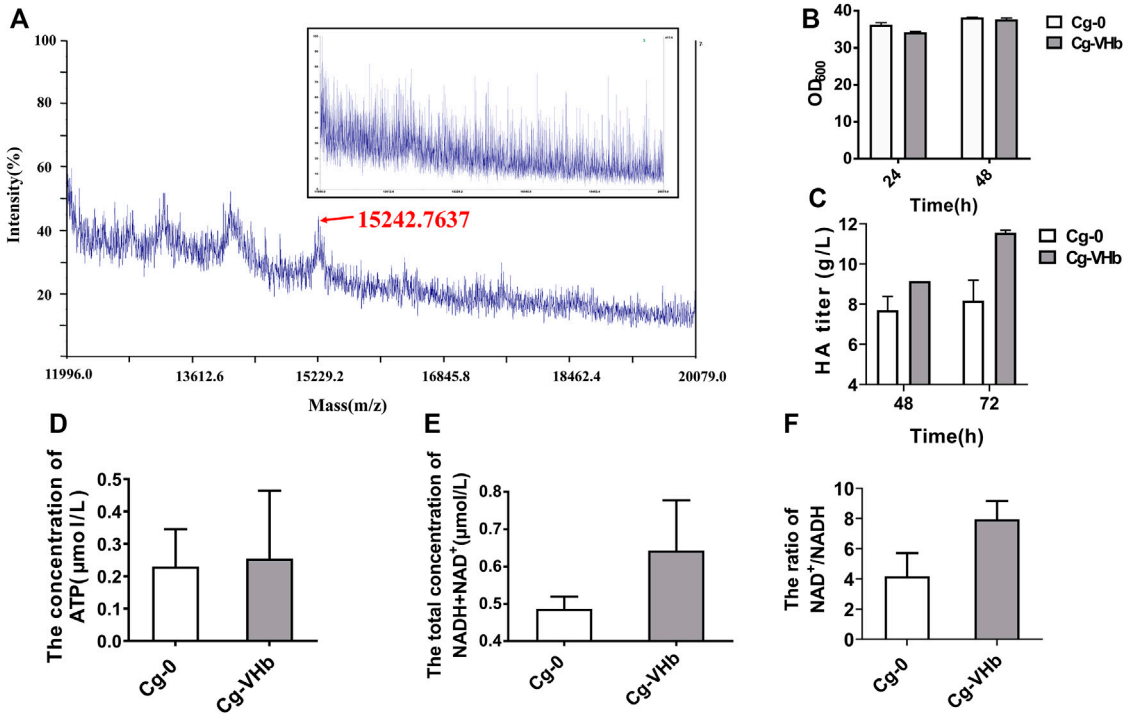

FIGURE 4 | Enhancing HA synthesis via duly expressed VHb in genome. **(A)** MALDI-TOF-MS. **(B)** OD_{600}. **(C)** HA titer. **(D)** ATP concentration. **(E)** Total concentration of NAD^+ and NADH. **(F)** The ratio of NAD^+ to NADH. In **(D)**, Cg-VHb and Cg-0 were cultured in a flask for 24 h, and in **(E,F)**, Cg-VHb and Cg-0 were cultured in a flask for 48 h. All of the measurements were performed in triplicate.

phosphatidylglycerol phosphate synthase has two copies in the *C. glutamicum* genome, which are annotated as *pgsA1* and *pgsA2*, and the CLS is annotated as *cls*. In this study, the CL metabolic pathway was intensified via overexpression of *pgsA1*/*pgsA2*/*cls* genes, thereby indirectly enhancing the HAS activity and HA production.

The hypothetical "HAS–CL" complex model is shown in **Figure 3A**, in which CL molecules bind with different domains of HAS to form a "pore" for HA transportation. Three key enzymes for CL synthesis were figured out and labeled in **Figure 1**. Three engineered strains, Cg-pgsA1, Cg-pgsA2, and Cg-CLS overexpressing the above enzymes separately, were constructed and were evaluated in flask culture for 72 h (**Figures 3C,D**). For HA titer, *pgsA2* and *cls* both enhanced the HA synthesis by ~10% (reaching 9.2 and 9.5 g/L, respectively) with respect to that of the control Cg-0 (8.6 g/L), although *pgsA1* reduced the HA titer by 14%.

Enhancing HA Synthesis via the Duly Expressed VHb in Genome

HA synthesis is a high-energy-demand process, in which many reactions need UTP and NAD^+. Besides, acetyl-CoA is also required. For example, 1 mol of glucose-1-P is transformed to UDP-glucose, consuming 1 mol of UTP; after that, 1 mol of UDP-glucose is converted into 1 mol of UDP-glucuronic acid, consuming 2 mol of NAD^+ and releasing 2 mol of NADH. The metabolism or recycle of these co-factors and also cell growth all need oxygen. To meet the high-oxygen and high-energy requirements of HA production, increasing dissolved oxygen (DO) is regarded as an effective strategy for both native producers and recombinant strains. Traditional stirring or aeration-rate optimization usually causes high energy consumption and physical damage to the cells (Galaction et al., 2004). VHb, found in the obligate aerobic bacteria *Vitreoscilla*, can improve respiration and energy metabolism under oxygen-limited conditions (Orii and Webster 1986; Zhao et al., 2017). To duly express VHb via a genome-integrated way to enhance oxygen transfer and cell intake was proposed as Strategy 3 for enhanced HA production.

Engineered Cg-VHb was constructed by inserting the gene *vgb* into the site of the lactate dehydrogenase gene (*ldh*) (**Supplementary Figure S3**). MALDI-TOF-MS was adopted to verify expression of VHb, as shown in **Figure 4A**. In comparison with Cg-0, a new peak occurred in Cg-VHb at around 15 kDa, which was the expressed VHb. Flask culture results showed that although cell growth was not obviously changed (**Figure 4B**), the HA titer of Cg-VHb was highly increased by 26% at 72 h (11.56 g/L) compared with that of Cg-0 (**Figure 4C**).

The ATP content was further assayed for both Cg-0 and Cg-VHb. As shown in **Figure 4D**, intracellular ATP concentration of Cg-VHb was higher than that of Cg-0 by 10.7%. At the same time, the intracellular NAD^+/NADH ratio was investigated as well. It could be seen that the total concentration of NAD^+ and NADH in Cg-VHb was higher than that of Cg-0 by 32.3% and that Cg-VHb generated more NAD^+, resulting in a higher NAD^+/NADH (>7.5) ratio of Cg-VHb than that of Cg-0. These results indicated that introduction of VHb indeed intensified uptake

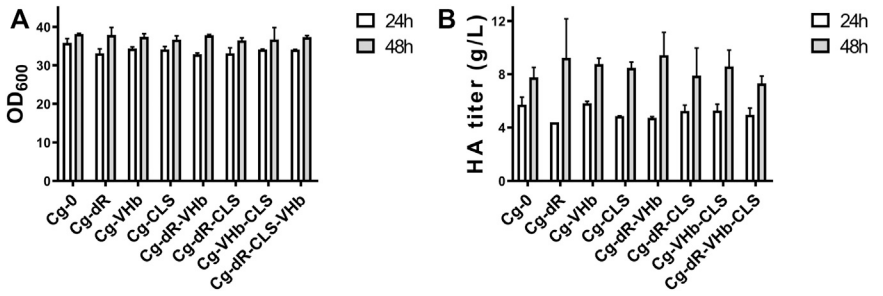

FIGURE 5 | Combination of different indirect genetic strategies on cell growth and HA synthesis. **(A)** OD_{600} of different strains. **(B)** The HA titer of different strains. Strain Cg-0 was the control. Experiments were performed in triplicate.

of oxygen, especially in the late stage of fermentation, thereby leading to more ATP and promoting the energy metabolism.

Combination of the Indirect Genetic Strategies

With combination of the above genetic strategies, we further constructed four engineered strains, i.e., Cg-dR-VHb, Cg-dR-CLS, Cg-VHb-CLS, and Cg-dR-CLS-VHb. We assayed the cell concentrations (**Figure 5A**) and HA titers (**Figure 5B**) at 24 and 48 h in flask culture for different strains. At 48 h, Cg-dR-VHb showed the highest HA yield, reaching 9.43 g/L. But surprisingly, the triple-strategy strain Cg-dR-VHb-CLS behaved even worse than the control, which should be further investigated.

Effect of Glutamine and Combination of Four Strategies on Cell Growth and HA Synthesis

According to the synthesis pathway of HA in recombinant *C. glutamicum* (**Supplementary Figure S1**), one molecule of glutamine is required together with UTP, NAD^+, and acetyl-CoA (**Figure 1**). Glutamine provides an amino group for fructose 6-phosphate (F6P), which is converted into GlcN-6P by glutamine-fructose-6-phosphate aminotransferase, GlmS. Obviously, lots of glutamines will be consumed during HA synthesis. Thereby, we investigated the importance of glutamine for HA synthesis via both transcriptional analysis and glutamine supplementation, which was regarded as the fourth strategy.

To ensure the significance of glutamine on HA synthesis, transcriptome analysis was specifically performed with two controls, Cg-0 and Cg-0-half (the HA titer was only half of Cg-0). In total, 242 upregulated genes were identified. Not considering the putative protein genes, artificially expressed genes, and structural protein genes, five genes, *cgl2910*, *proB*, *cgl0453*, *hisH*, and *cgl0448*, were found to be related with glutamate/glutamine metabolism, as listed in **Table 2**.

It can be found that the products of these five genes are just the enzymes involved in the metabolism of glutamic acid and glutamine, as shown in **Figure 6A**. So next, we added 2 g/L of glutamine into the medium and conducted flask culture for 48 h to test the cell growth and HA accumulation characteristics. As shown in **Figures 6B,C**, both OD_{600} and HA synthesis were significantly affected by glutamine addition, especially for Cg-dR-CLS and Cg-VHb-CLS. The highest HA titer, 10.66 g/L, was achieved by Cg-dR-CLS with glutamine, while the control Cg-0 only accumulated 8.26 g/L HA under the same conditions. Further, we performed fed-batch culture in a 10 L fermenter by Cg-dR-CLS, and the time profiles were shown in **Figure 7**. It can be seen that the HA titer of Cg-dR-CLS at 60 h reached 32 g/L, HA yield on glucose was 0.28 g/g, and HA productivity was 0.53 g/L/h. These results were higher than those of the superior strain CgHA25 we previously reported (Cheng et al., 2019b). This indicated that the strategies in this work performed well during the scale-up process.

DISCUSSION

In this study, we strengthened the biosynthesis of HA in recombinant *C. glutamicum* through four indirect, non-regular metabolic strategies. We assumed the HA-producing strain as a "whole block factory" and enhanced the product synthesis via intensified bioprocesses, such as substrate uptake, HAS activity improvement, and oxygen transfer.

Firstly, glucose uptake was intensified by IolR knockout, leading to a 6.9% increase of HA titer. This is a common effective strategy for enhancing the titer of different products synthetized by *C. glutamicum*. For example, deletion of IolR and overexpression of IolT1 also increased the yield of L-ornithine by 10% (Zhang B. et al., 2019). Similarly, Zhang X. et al. (2019) found enhanced cell growth and L-serine production of 3.9-fold and 5.9-fold, respectively, via inactivation of IolR. Based on the same metabolic regulation strategy, some other alternative strategies can also be tried to strengthen carbon utilization and thereby enhance the product yield, such as overexpression of the glucose transporters IolT1/T2 and EII_{glc}.

CLs can bind HAS to form complexes and play an essential role in maintaining the biological activity of HAS. In a cell-free system, Weigel et al. reported that addition of CL into purified HAS increased the K_m for UDP-GlcUA and decreased the K_m for UDP-GlcNAc, finally giving an overall stimulation of V_{max}. Both the seHAS and spHAS could maintain ~60% initial activity by addition of bovine CL after being stored at −80°C for 2 months (Tlapak-Simmons et al., 1999). Based on the literature, we analyzed the CL synthesis pathway in *C. glutamicum* and focused on three key enzymes, PgsA1, PgsA2, and Cls.

TABLE 2 | Identified key proteins with significant transcription difference in Cg-0 and Cg-0-half transcriptome.

Genes	Gene description	Readcount Cg-0	Readcount Cg-0-half
cgl2910	Pyruvate kinase	1,426.7924	641.107
proB	Glutamate 5-kinase Catalyzing the formation of L-glutamate 5-semialdehyde from L-glutamate which is the precursor of L-proline	934.6316	403.2274
cgl0453	Catalyzing the formation of 2,5-dioxopentanoate, which is the precursor of glutamate	146.2368	60.8088
hisH	Glutamine amidotransferase class I	516.5292	228.2846
cgl0448	Type 1 glutamine amidotransferase-like domain-containing protein	245.6064	170.6814

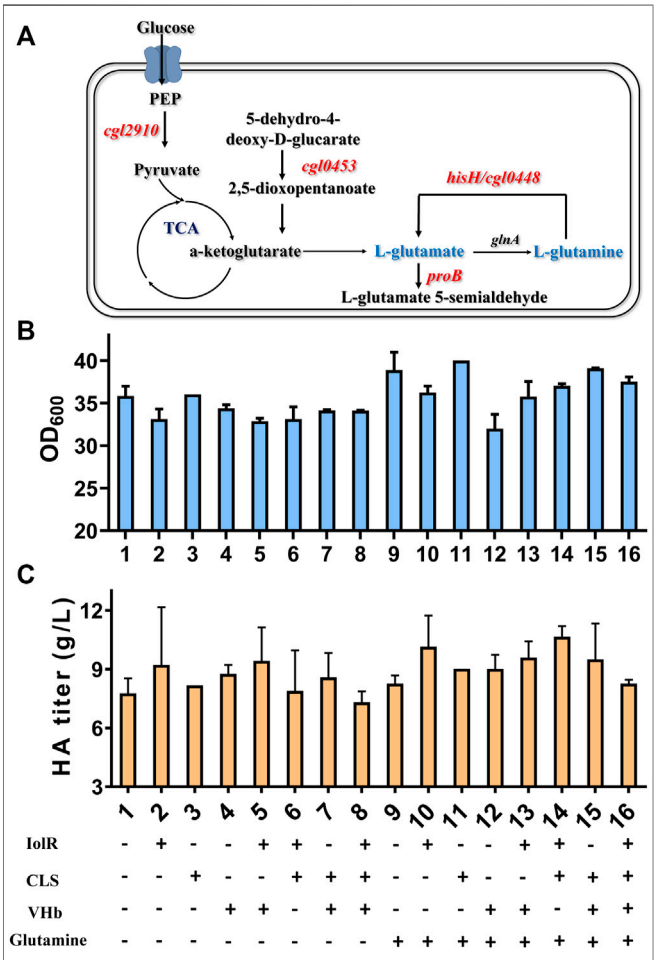

FIGURE 6 | Glutamine metabolic pathway and effects of combined four strategies on cell growth and HA synthesis. **(A)** The key enzymes identified by transcriptome analysis are involved in glutamate or glutamine synthesis. **(B)** OD_{600} results of eight engineered strains under 16 different conditions. **(C)** HA titer of eight engineered strains under 16 different conditions.

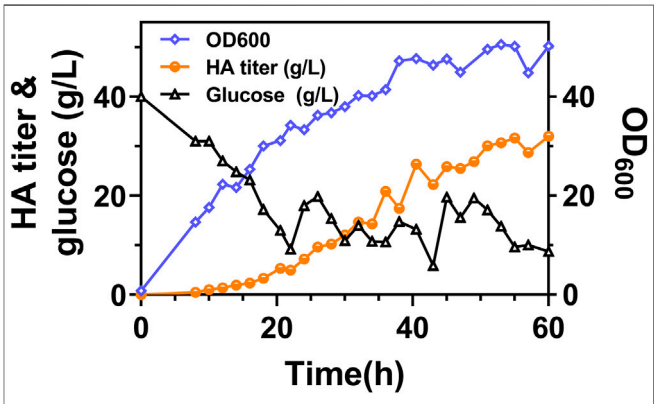

FIGURE 7 | The time profiles of fed-batch fermentation by Cg-dR-CLS. Glucose feeding started at 22 h.

We found that overexpression of *pgsA1/pgsA2/cls* can all accelerate cell growth to some degree, especially in the first 24 h. As reported previously, the *pgsA* gene codes for phosphatidylglycerophosphate synthase, which catalyzes the committed step of biosynthesis of phosphatidylglycerol (Dowhan 1997). And the *cls* gene codes for CLS, which condenses two molecules of phosphatidylglycerol to form CL in the prokaryote. As the major acidic phospholipids of the organism, phosphatidylglycerol and CL play important roles in bacterial cell structure and diverse physiological processes, such as DNA replication, cell division, respiration, and osmotic stress response (Wood 2018). Yasuhiro Shiba et al. (2004) reported that a *pgsA*-null mutation is lethal for *E. coli*. Xia et al. confirmed that *E. coli* are dependent on phosphatidylglycerol for cell growth, which cannot be substituted with phosphatidylinositol (Xia and Dowhan 1995). It can be seen that phosphatidylglycerol is essential for cell growth. As for CL, Kazuhisa Sekimizu et al. found that CL could activate the dnaA protein, which serves as the initiation of the protein of replication (Sekimizu and Kornberg 1988). Amer H. Asseri et al. (2021) reported that CL can also enhance the enzymatic activity of cytochrome *bd* for *C. glutamicum*, which is a terminal oxidase of respiratory pathways and can also enhance the oxygen consumption activity by twofold. Satomi Nishijima et al. (1988) came to the conclusion that the *cls* gene may confer growth or survival advantages for *E. coli*. In summary, *pgsA1/pgsA2/cls* genes are vital for cell growth and other physiological processes, and overexpression of these genes may promote cell growth to a certain degree.

In addition, we also found that *pgsA1* overexpression had a negative effect on HA titer, while *pgsA2* and *cls* could significantly promote the HA synthesis. We measured the concentration of free CLs in Cg-0 and Cg-CLS (**Supplementary Table S2**) and found that overexpression of *cls* led to an obvious increase of intracellular CLs. As for the negative effect of *pgsA1* on the HA titer, we assumed that *pgsA1* and *pgsA2* might have different activities towards conversion of CDP-DAG, thus leading to different concentrations of CL. In addition, Triscott and

Vanderijn (1986) reported that the optimal activity of HAS occurred at a CL/protein ratio (μg/μg) of 5:1. In the future, we can clone *pgsA1*/*pgsA2*/*cls* and HAS under different inducible promoters and then accurately adjust the ratio of CL/HAS, thereby further enhancing the HA synthesis.

The HA synthesis process requires high-oxygen and high-energy conditions. It was observed that a higher HA titer was achieved in aerobic conditions than in anaerobic conditions (Huang et al., 2006; Prasad et al., 2010). According to our previous study, the recombinant *C. glutamicum* can produce HA with M_w ranging from 0.2 to 0.3 MDa (Cheng et al., 2019b). It was reported that when the M_w of HA was above 5.7×10^4 Da, the broth viscosity increased with the HA concentration increasing, which would result in a great obstacle for nutrient and oxygen transfer. Nowadays, the industrialized HA titer was 6–10 g/L with a M_w of 2 MDa in *Streptococcus* (Cheng et al., 2019b). The high viscosity of fermentation media made the elevation of the HA titer in *Streptococcus* much more difficult. Therefore, to duly express VHb is probably an effective solution for this. Zhao et al. (2017) found that expression of VHb in *E. coli* resulted in a 94.4% increase of *trans*-4-hydroxy-L-proline production in a 100 ml shaking flask culture compared to the same strain without VHb expression. Wang et al. (2018) cloned and expressed VHb in a surfactin-producing strain *B. subtilis* THY-15, leading to a 24% increase in flask. But surprisingly, in *C. glutamicum*, co-expression of the VHb gene (*vgb*) with *hasA* based on plasmids lowered HA yield by 1.5-fold (Hoffmann and Altenbuchner 2014). Therefore, we deduced that duly expressing VHb is important for its positive function. We introduced VHb into the host via a genome-integrated strategy. After introduction of VHb, intracellular ATP and NAD^+ increased dramatically, indicating that the energy metabolism was improved during fermentation. And it was assumed that more oxygen strengthened the oxidative phosphorylation process, thus improving NAD^+ replenishment as well as the ratio of NAD^+/NADH (Garrigues et al., 1997; Lan et al., 2006; Guez et al., 2008).

Besides, expression of the *vgb* gene increased the total concentration of NADH and NAD^+. This could be attributed to the increased activity of the tricarboxylic acid (TCA) cycle (Pablos et al., 2014). It was reported that VHb can capture oxygen and transfer it to the terminal oxidases, and the dissociation rate constant of VHb is significantly higher than other hemoglobins. *E. coli*-expressing *vgb* would direct a higher fraction of glucose through the pentose phosphate pathway (ppp) and channel less acetyl-CoA through TCA than the wild-type strain, which generated an excess amount of NADPH, and resulted in a transhydrogenation reaction, leading to an H^+-flux from NADPH to NAD^+. To sum up, the effective delivery of oxygen to the cytochromes would regenerate NAD^+ faster, activating the TCA cycle as well. During the dynamic balance of NADH and NAD^+, the generation rate of NAD^+ got faster, which probably led to the increase of the total concentration of NAD^+ and NADH. As for the HA titer, we found that the HA titer of Cg-VHb was highly increased by 26%. Therefore, we supposed that integration of the VHb gene into the host genome is a promising strategy for industrialized HA bioproduction.

Finally, we investigated the influence of another important factor, amino group carrier (glutamine), on HA synthesis. We analyzed the transcriptome differences between HA high-producing strain and HA low-producing strain and identified that five genes relating to the metabolism of glutamate or glutamine were upregulated significantly. This indicated that when producing HA, the bacteria would enhance their native glutamic acid and glutamine synthesis to enhance the supplement of inorganic nitrogen for HA synthesis. To confirm this deduction, we tested the effectiveness of the exogenous addition of glutamine. Correspondingly, we found that the titer of HA was increased significantly. These results also implied that deficient supplement of glutamine will limit HA bioproduction to some degree. Aside from addition of glutamate/glutamine into the medium, we can also strengthen the synthesis of glutamine or glutamic acid in the engineered strains, for example, by overexpression of glutamine or glutamate synthase.

To conclude, four indirect metabolic engineering strategies for HA titer enhancement in engineered *C. glutamicum* were proposed and investigated in this work. In general, the enhancement of carbon uptake efficiency (specifically glucose), the auxiliary factor titer of HAS (CL), oxygen-transfer efficiency via duly expressing VHb, and supplement of glutamine all played positive and significant roles for enhanced HA synthesis. Combination strategies further elevated the HA titer, and the optimal strains showed a 30% increase in HA production under present conditions. It can be expected that after overall optimization and accurate regulation of different strategies next, the HA titer will be further increased significantly and thereby enable the scaled-up production of HA via the engineered *C. glutamicum*.

DATA AVAILABILITY STATEMENT

The original contributions presented in the study are included in the article/**Supplementary Material**, further inquiries can be directed to the corresponding author.

AUTHOR CONTRIBUTIONS

YD, FC, MW, and CX performed the experiments and processed the data; YD wrote the paper; and HY planned and supervised the project.

FUNDING

This work was supported by the National Key R&D Program of China (2018YFA0902200), Natural Science Foundation of China (Nos. 21776157 and 22078173) and Shandong Province Key R&D Program of China (2020CXGC010602).

SUPPLEMENTARY MATERIAL

The Supplementary Material for this article can be found online at: https://www.frontiersin.org/articles/10.3389/fbioe.2021.768490/full#supplementary-material

REFERENCES

Agarwal, G., K V, K., Prasad, S. B., Bhaduri, A., and Jayaraman, G. (2019). Biosynthesis of Hyaluronic Acid Polymer: Dissecting the Role of Sub Structural Elements of Hyaluronan Synthase. *Sci. Rep.* 9, 12510. doi:10.1038/s41598-019-48878-8

Asseri, A. H., Godoy-Hernandez, A., Goojani, H. G., Lill, H., Sakamoto, J., McMillan, D. G. G., et al. (2021). Cardiolipin Enhances the Enzymatic Activity of Cytochrome Bd and Cytochrome Bo3 Solubilized in Dodecyl-Maltoside. *Sci. Rep.* 11 (1), 8006. doi:10.1038/s41598-021-87354-0

Boltje, T. J., Buskas, T., and Boons, G. J. (2006). Opportunities and Challenges in Synthetic Oligosaccharide and Glycoconjugate Research. *Nat. Chem.* 1 (8), 611–622. doi:10.1038/nchem.399

Camacho, K. M., Menegatti, S., and Mitragotri, S. (2016). Low-molecular-weight Polymer-Drug Conjugates for Synergistic Anticancer Activity of Camptothecin and Doxorubicin Combinations. *Nanomedicine* 11 (9), 1139–1151. doi:10.2217/nnm.16.33

Chahuki, F. F., Aminzadeh, S., Jafarian, V., Tabandeh, F., and Khodabandeh, M. (2019). Hyaluronic Acid Production Enhancement via Genetically Modification and Culture Medium Optimization in *Lactobacillus Acidophilus*. *Int. J. Biol. Macromolecules* 121, 870–881. doi:10.1016/j.ijbiomac.2018.10.112

Cheng, F., Luozhong, S., Guo, Z., Yu, H., and Stephanopoulos, G. (2017). Enhanced Biosynthesis of Hyaluronic Acid Using Engineered *Corynebacterium Glutamicum* via Metabolic Pathway Regulation. *Biotechnol. J.* 12 (10), 1–8. doi:10.1002/biot.201700191

Cheng, F., Gong, Q., Yu, H., and Stephanopoulos, G. (2016). High-titer Biosynthesis of Hyaluronic Acid by recombinantCorynebacterium Glutamicum. *Biotechnol. J.* 11 (4), 574–584. doi:10.1002/biot.201500404

Cheng, F., Luozhong, S., Yu, H., and Guo, Z. (2019a). Biosynthesis of Chondroitin in Engineered *Corynebacterium Glutamicum*. *J. Microbiol. Biotechnol.* 29 (3), 392–400. doi:10.4014/jmb.1810.10062

Cheng, F., Yu, H., and Stephanopoulos, G. (2019b). Engineering *Corynebacterium Glutamicum* for High-Titer Biosynthesis of Hyaluronic Acid. *Metab. Eng.* 55, 276–289. doi:10.1016/j.ymben.2019.07.003

Chien, L. J., and Lee, C. K. (2007). Enhanced Hyaluronic Acid Production in *Bacillus Subtilis* by Coexpressing Bacterial Hemoglobin. *Biotechnol. Prog.* 23 (5), 1017–1022. doi:10.1021/bp070036w

Dowhan, W. (1997). Molecular Basis for Membrane Phospholipid Diversity: Why Are There So many Lipids? *Annu. Rev. Biochem.* 66, 199–232. doi:10.1146/annurev.biochem.66.1.199

Galaction, A. I., Cascaval, D., Oniscu, C., and Turnea, M. (2004). Enhancement of Oxygen Mass Transfer in Stirred Bioreactors Using Oxygen-Vectors. 1. Simulated Fermentation Broths. *Bioproc. Biosyst Eng.* 26 (4), 231–238. doi:10.1007/s00449-004-0353-5

Garrigues, C., Loubiere, P., Lindley, N. D., and Cocaign-Bousquet, M. (1997). Control of the Shift from Homolactic Acid to Mixed-Acid Fermentation in Lactococcus Lactis: Predominant Role of the NADH/NAD+ Ratio. *J. Bacteriol.* 179 (17), 5282–5287. doi:10.1128/jb.179.17.5282-5287.1997

Graça, M. F. P., Miguel, S. P., Cabral, C. S. D., and Correia, I. J. (2020). Hyaluronic Acid-Based Wound Dressings: A Review. *Carbohydr. Polym.* 241, 116364. doi:10.1016/j.carbpol.2020.116364

Guez, J. S., Müller, C. H., Danze, P. M., Büchs, J. P., and Jacques, P. (2008). Respiration Activity Monitoring System (RAMOS), an Efficient Tool to Study the Influence of the Oxygen Transfer Rate on the Synthesis of Lipopeptide by *Bacillus Subtilis* ATCC6633. *J. Biotechnol.* 134 (1-2), 121–126. doi:10.1016/j.jbiotec.2008.01.003

Hoffmann, J., and Altenbuchner, J. (2014). Hyaluronic Acid Production with Corynebacterium Glutamicum : Effect of media Composition on Yield and Molecular Weight. *J. Appl. Microbiol.* 117 (3), 663–678. doi:10.1111/jam.12553

Huang, W.-C., Chen, S.-J., and Chen, T.-L. (2006). The Role of Dissolved Oxygen and Function of Agitation in Hyaluronic Acid Fermentation. *Biochem. Eng. J.* 32 (3), 239–243. doi:10.1016/j.bej.2006.10.011

Jeeva, P., Shanmuga Doss, S., Sundaram, V., and Jayaraman, G. (2019). Production of Controlled Molecular Weight Hyaluronic Acid by Glucostat Strategy Using Recombinant *Lactococcus Lactis* Cultures. *Appl. Microbiol. Biotechnol.* 103 (11), 4363–4375. doi:10.1007/s00253-019-09769-0

Jia, Y., Zhu, J., Chen, X., Tang, D., Su, D., Yao, W., et al. (2013). Metabolic Engineering of *Bacillus Subtilis* for the Efficient Biosynthesis of Uniform Hyaluronic Acid with Controlled Molecular Weights. *Bioresour. Tech.* 132, 427–431. doi:10.1016/j.biortech.2012.12.150

Jin, P., Kang, Z., Yuan, P., Du, G., and Chen, J. (2016). Production of Specific-Molecular-Weight Hyaluronan by Metabolically Engineered *Bacillus Subtilis* 168. *Metab. Eng.* 35, 21–30. doi:10.1016/j.ymben.2016.01.008

Kakizaki, I., Takagaki, K., Endo, Y., Kudo, D., Ikeya, H., Miyoshi, T., et al. (2002). Inhibition of Hyaluronan Synthesis inStreptococcus equiFM100 by 4-methylumbelliferone. *Eur. J. Biochem.* 269 (20), 5066–5075. doi:10.1046/j.1432-1033.2002.03217.x

Klaffl, S., Brocker, M., Kalinowski, J., Eikmanns, B. J., and Bott, M. (2013). Complex Regulation of the Phosphoenolpyruvate Carboxykinase Gene *Pck* and Characterization of its Gntr-type Regulator Iolr as a Repressor of Myo-Inositol Utilization Genes in *Corynebacterium Glutamicum*. *J. Bacteriol.* 195 (18), 4283–4296. doi:10.1128/jb.00265-13

Lan, C. Q., Oddone, G., Mills, D. A., and Block, D. E. (2006). Kinetics ofLactococcus Lactis Growth and Metabolite Formation under Aerobic and Anaerobic Conditions in the Presence or Absence of Hemin. *Biotechnol. Bioeng.* 95 (6), 1070–1080. doi:10.1002/bit.21070

Li, Y., Li, G., Zhao, X., Shao, Y., Wu, M., and Ma, T. (2019). Regulation of Hyaluronic Acid Molecular Weight and Titer by Temperature in Engineered *Bacillus Subtilis*. *3 Biotech.* 9 (6), 225. doi:10.1007/s13205-019-1749-x

Liu, L., Liu, Y., Li, J., Du, G., and Chen, J. (2011). Microbial Production of Hyaluronic Acid: Current State, Challenges, and Perspectives. *Microb. Cel Fact* 10, 99. doi:10.1186/1475-2859-10-99

Manfrao-Netto, J. H. C., Queiroz, E. B., de Oliveira Junqueira, A. C., Gomes, A. M. V., de Morais, D. G., Paes, H. C., et al. (2021). Genetic Strategies for Improving Hyaluronic Acid Production in Recombinant Bacterial Culture. *J. Appl. Microbiol* 00, 1–19.

Mao, Z., and Chen, R. R. (2007). Recombinant Synthesis of Hyaluronan by *Agrobacterium* Sp. *Biotechnol. Prog.* 23 (5), 1038–1042. doi:10.1021/bp070113n

Mao, Z., Shin, H.-D., and Chen, R. (2009). A Recombinant *E. coli* Bioprocess for Hyaluronan Synthesis. *Appl. Microbiol. Biotechnol.* 84 (1), 63–69. doi:10.1007/s00253-009-1963-2

Nishijima, S., Asami, Y., Uetake, N., Yamagoe, S., Ohta, A., and Shibuya, I. (1988). Disruption of the *Escherichia coli Cls* Gene Responsible for Cardiolipin Synthesis. *J. Bacteriol.* 170 (2), 775–780. doi:10.1128/jb.170.2.775-780.1988

Orii, Y., and Webster, D. A. (1986). Photodissociation of Oxygenated Cytochrome O(s) (Vitreoscilla) and Kinetic Studies of Reassociation. *J. Biol. Chem.* 261 (8), 3544–3547. doi:10.1016/s0021-9258(17)35680-6

Pablos, T. E., Sigala, J. C., Le Borgne, S., and Lara, A. R. (2014). Aerobic Expression ofVitreoscillahemoglobin Efficiently Reduces Overflow Metabolism inEscherichia Coli. *Biotechnol. J.* 9 (6), 791–799. doi:10.1002/biot.201300388

Pavicic, T., Gauglitz, G. G., Lersch, P., Schwach-Abdellaoui, K., Malle, B., Korting, H. C., et al. (2011). Efficacy of Cream-Based Novel Formulations of Hyaluronic Acid of Different Molecular Weights in Anti-wrinkle Treatment. *J. Drugs Dermatol.* 10 (9), 990–1000.

Prasad, S. B., Jayaraman, G., and Ramachandran, K. B. (2010). Hyaluronic Acid Production Is Enhanced by the Additional Co-expression of UDP-Glucose Pyrophosphorylase in *Lactococcus Lactis*. *Appl. Microbiol. Biotechnol.* 86 (1), 273–283. doi:10.1007/s00253-009-2293-0

Qiu, Y., Ma, Y., Huang, Y., Li, S., Xu, H., and Su, E. (2021). Current Advances in the Biosynthesis of Hyaluronic Acid with Variable Molecular Weights. *Carbohydr. Polym.* 269, 118320. doi:10.1016/j.carbpol.2021.118320

Ruan, H., Yu, H., and Xu, J. (2020). The Glucose Uptake Systems in *Corynebacterium Glutamicum*: a Review. *World J. Microbiol. Biotechnol.* 36 (9), 126. doi:10.1007/s11274-020-02898-z

Schäfer, A., Tauch, A., Jäger, W., Kalinowski, J., Thierbach, G., and Pühler, A. (1994). Small Mobilizable Multi-Purpose Cloning Vectors Derived from the *Escherichia coli* Plasmids pK18 and pK19: Selection of Defined Deletions in the Chromosome of Corynebacterium Glutamicum. *Gene* 145 (1), 69–73. doi:10.1016/0378-1119(94)90324-7

Sekimizu, K., and Kornberg, A. (1988). Cardiolipin Activation of dnaA Protein, the Initiation Protein of Replication in *Escherichia coli*. *J. Biol. Chem.* 263 (15), 7131–7135. doi:10.1016/s0021-9258(18)68615-6

Shiba, Y., Yokoyama, Y., Aono, Y., Kiuchi, T., Kusaka, J., Matsumoto, K., et al. (2004). Activation of the *Rcs* Signal Transduction System Is Responsible for the Thermosensitive Growth Defect of an *Escherichia coli* Mutant Lacking Phosphatidylglycerol and Cardiolipin. *J. Bacteriol.* 186 (19), 6526–6535. doi:10.1128/jb.186.19.6526-6535.2004

Stecco, C., Stern, R., Porzionato, A., Macchi, V., Masiero, S., Stecco, A., et al. (2011). Hyaluronan within Fascia in the Etiology of Myofascial Pain. *Surg. Radiol. Anat.* 33 (10), 891–896. doi:10.1007/s00276-011-0876-9

Sunguroglu, C., Sezgin, D. E., Celik, P. A., and Cabuk, A. (2018). Higher Titer Hyaluronic Acid Production in Recombinant *Lactococcus Lactis*. *Prep. Biochem. Biotechnol.* 48 (8), 734–742. doi:10.1080/10826068.2018.1508036

Tlapak-Simmons, V. L., Baggenstoss, B. A., Clyne, T., and Weigel, P. H. (1999). Purification and Lipid Dependence of the Recombinant Hyaluronan Synthases from Streptococcus Pyogenes andStreptococcus Equisimilis. *J. Biol. Chem.* 274 (7), 4239–4245. doi:10.1074/jbc.274.7.4239

Tlapak-Simmons, V. L., Kempner, E. S., Baggenstoss, B. A., and Weigel, P. H. (1998). The Active *Streptococcal* Hyaluronan Synthases (HASs) Contain a Single HAS Monomer and Multiple Cardiolipin Molecules. *J. Biol. Chem.* 273 (40), 26100–26109. doi:10.1074/jbc.273.40.26100

Triscott, M. X., and van de Rijn, I. (1986). Solubilization of Hyaluronic Acid Synthetic Activity from Streptococci and its Activation with Phospholipids. *J. Biol. Chem.* 261 (13), 6004–6009. doi:10.1016/s0021-9258(17)38485-5

Wang, Q., Yu, H., Wang, M., Yang, H., and Shen, Z. (2018). Enhanced Biosynthesis and Characterization of Surfactin Isoforms with Engineered *Bacillus Subtilis* through Promoter Replacement and *Vitreoscilla* Hemoglobin Co-expression. *Process Biochem.* 70, 36–44. doi:10.1016/j.procbio.2018.04.003

Wang, Y., Hu, L., Huang, H., Wang, H., Zhang, T., Chen, J., et al. (2020). Eliminating the Capsule-like Layer to Promote Glucose Uptake for Hyaluronan Production by Engineered *Corynebacterium Glutamicum*. *Nat. Commun.* 11 (1), 3120. doi:10.1038/s41467-020-16962-7

Weigel, P. H. (2015). Hyaluronan Synthase: The Mechanism of Initiation at the Reducing End and a Pendulum Model for Polysaccharide Translocation to the Cell Exterior. *Int. J. Cel Biol* 2015, 367579. doi:10.1155/2015/367579

Weigel, P. H. (2002). Functional Characteristics and Catalytic Mechanisms of the Bacterial Hyaluronan Synthases. *IUBMB Life (International Union Biochem. Mol. Biol. Life)* 54 (4), 201–211. doi:10.1080/15216540214931

Westbrook, A. W., Moo-Young, M., and Chou, C. P. (2016). Development of a CRISPR-Cas9 Tool Kit for Comprehensive Engineering of *Bacillus Subtilis*. *Appl. Environ. Microbiol.* 82 (16), 4876–4895. doi:10.1128/aem.01159-16

Westbrook, A. W., Ren, X., Moo-Young, M., and Chou, C. P. (2018a). Engineering of Cell Membrane to Enhance Heterologous Production of Hyaluronic Acid in *Bacillus Subtilis*. *Biotechnol. Bioeng.* 115 (1), 216–231. doi:10.1002/bit.26459

Westbrook, A. W., Ren, X., Oh, J., Moo-Young, M., and Chou, C. P. (2018b). Metabolic Engineering to Enhance Heterologous Production of Hyaluronic Acid in *Bacillus Subtilis*. *Metab. Eng.* 47, 401–413. doi:10.1016/j.ymben.2018.04.016

Woo, J. E., Seong, H. J., Lee, S. Y., and Jang, Y. S. (2019). Metabolic Engineering of *Escherichia coli* for the Production of Hyaluronic Acid from Glucose and Galactose. *Front. Bioeng. Biotechnol.* 7, 351. doi:10.3389/fbioe.2019.00351

Wood, J. M. (2018). Perspective: Challenges and Opportunities for the Study of Cardiolipin, a Key Player in Bacterial Cell Structure and Function. *Curr. Genet.* 64 (4), 795–798. doi:10.1007/s00294-018-0811-2

Xia, W., and Dowhan, W. (1995). Phosphatidylinositol Cannot Substitute for Phosphatidylglycerol in Supporting Cell Growth of *Escherichia coli*. *J. Bacteriol.* 177 (10), 2926–2928. doi:10.1128/jb.177.10.2926-2928.1995

Yang, P., Liu, W., Cheng, X., Wang, J., Wang, Q., and Qi, Q. (2016). A New Strategy for Production of 5-aminolevulinic Acid in Recombinant *Corynebacterium Glutamicum* with High Yield. *Appl. Environ. Microbiol.* 82 (9), 2709–2717. doi:10.1128/aem.00224-16

Yu, H., and Stephanopoulos, G. (2008). Metabolic Engineering of *Escherichia coli* for Biosynthesis of Hyaluronic Acid. *Metab. Eng.* 10 (1), 24–32. doi:10.1016/j.ymben.2007.09.001

Yu, L.-M., Liu, T., Ma, Y.-L., Zhang, F., Huang, Y.-C., and Fan, Z.-H. (2020). Fabrication of Silk-Hyaluronan Composite as a Potential Scaffold for Tissue Repair. *Front. Bioeng. Biotechnol.* 8, 1–9. doi:10.3389/fbioe.2020.578988

Zhang, B., Gao, G., Chu, X.-H., and Ye, B.-C. (2019a). Metabolic Engineering of *Corynebacterium Glutamicum* S9114 to Enhance the Production of L-Ornithine Driven by Glucose and Xylose. *Bioresour. Tech.* 284, 204–213. doi:10.1016/j.biortech.2019.03.122

Zhang, X., Lai, L., Xu, G., Zhang, X., Shi, J., Koffas, M. A. G., et al. (2019b). Rewiring the central Metabolic Pathway for High-Yield L-Serine Production in *Corynebacterium Glutamicum* by Using Glucose. *Biotechnol. J.* 14 (6), e1800497. doi:10.1002/biot.201800497

Zhao, T.-X., Li, M., Zheng, X., Wang, C.-H., Zhao, H.-X., Zhang, C., et al. (2017). Improved Production of Trans-4-hydroxy-L-proline by Chromosomal Integration of the *Vitreoscilla* Hemoglobin Gene into Recombinant *Escherichia coli* with Expression of Proline-4-Hydroxylase. *J. Biosci. Bioeng.* 123 (1), 109–115. doi:10.1016/j.jbiosc.2016.07.018

Zheng, Y., Cheng, F., Zheng, B., and Yu, H. (2020). Enhancing Single-Cell Hyaluronic Acid Biosynthesis by Microbial Morphology Engineering. *Synth. Syst. Biotechnol.* 5 (4), 316–323. doi:10.1016/j.synbio.2020.09.002

Conflict of Interest: The authors declare that the research was conducted in the absence of any commercial or financial relationships that could be construed as a potential conflict of interest.

Publisher's Note: All claims expressed in this article are solely those of the authors and do not necessarily represent those of their affiliated organizations, or those of the publisher, the editors and the reviewers. Any product that may be evaluated in this article, or claim that may be made by its manufacturer, is not guaranteed or endorsed by the publisher.

frontiers in Microbiology

ORIGINAL RESEARCH
published: 04 February 2022
doi: 10.3389/fmicb.2021.677702

Genome-Scale Mining of Novel Anchor Proteins of *Corynebacterium glutamicum*

Kerui Lin[1,2], Nannan Zhao[1,2], Youhua Cai[3], Ying Lin[1,2], Shuangyan Han[1,2] and Suiping Zheng[1,2]**

[1] Guangdong Key Laboratory of Fermentation and Enzyme Engineering, School of Biology and Biological Engineering, South China University of Technology, Guangzhou, China, [2] Guangdong Research Center of Industrial Enzyme and Green Manufacturing Technology, School of Biology and Biological Engineering, South China University of Technology, Guangzhou, China, [3] Star Lake Bioscience Co. Inc., Zhaoqing Guangdong, Zhaoqing, China

The display of recombinant proteins on the surfaces of bacteria is a research topic with many possible biotechnology applications—among which, the choice of host cell and anchoring motif is the key for efficient display. *Corynebacterium glutamicum* is a promising host for surface display due to its natural advantages, while single screening methods and fewer anchor proteins restrict its application. In this study, the subcellular localization (SCL) predictor LocateP and tied-mixture hidden Markov models were used to analyze all five known endogenous anchor proteins of *C. glutamicum* and test the accuracy of the predictions. Using these two tools, the SCLs of all proteins encoded by the genome of *C. glutamicum 13032* were predicted, and 14 potential anchor proteins were screened. Compared with the positive controls NCgl1221 and NCgl1337, three anchoring proteins—NCgl1307, NCgl2775, and NCgl0717—performed better. This study also discussed the applicability of the anchor protein screening method used in this experiment to other bacteria.

Keywords: *Corynebacterium glutamicum*, genome-scale mining, surface display, anchor protein, gram-positive bacteria

OPEN ACCESS

Edited by:
Christoph Wittmann, Saarland University, Germany

Reviewed by:
Gerd M. Seibold, Technical University of Denmark, Denmark
Thomas T. Eng, Lawrence Berkeley National Laboratory, United States

***Correspondence:**
Suiping Zheng
spzheng@scut.edu.cn
Shuangyan Han
syhan@scut.edu.cn

Specialty section:
This article was submitted to Microbial Physiology and Metabolism, a section of the journal Frontiers in Microbiology

Received: *09 March 2021*
Accepted: *17 December 2021*
Published: *04 February 2022*

Citation:
Lin K, Zhao N, Cai Y, Lin Y, Han S and Zheng S (2022) Genome-Scale Mining of Novel Anchor Proteins of Corynebacterium glutamicum. Front. Microbiol. 12:677702. doi: 10.3389/fmicb.2021.677702

BACKGROUND

Bacteria that display recombinant proteins on their surfaces play an important role in many biotechnology applications. The choice of host cells and anchoring motifs is essential for the effective display of passenger proteins on cell surfaces. As a host for surface display, *Corynebacterium glutamicum* possesses many useful characteristics, and some successful platforms have been reported. Firstly, *C. glutamicum* exhibits low extracellular protease activity, which is conducive to protein display on its surface (Liu et al., 2013, 2016). Secondly, it is robust and has a wide spectrum of natural carbon source substrates, including pentose, hexose, monosaccharides, and toxic aromatic compounds (Qi et al., 2007; Sasaki et al., 2009; Choi et al., 2019). In addition, *C. glutamicum* has strong tolerance to a variety of inhibitors and weak carbon catabolite repression. Surface display can endow engineered *C. glutamicum* with new functions, expanding their substrate spectra and strengthening the impact of degradation and

utilization on renewable biomass (Choi et al., 2019; Zhang et al., 2020).

In order to display proteins on the surface of *C. glutamicum*, several anchoring motifs have been used. At present, the display system of *C. glutamicum* only has three types of anchor proteins: foreign protein (PgsA), mycoloylated proteins [NCgl1337, NCgl0933 (PorB), NCgl0932 (PorC), PorH (NCgl number of PorH have not been assigned)], and membrane protein (NCgl1221, mechanosensitive channel, MscCG) (Tateno et al., 2007b, 2009; Choi et al., 2018; Inui and Toyoda, 2020). These recombinant strains with anchor proteins have been modified to display carbohydrate-active enzymes (CAZy), such as amylase (Tateno et al., 2007a), glucanase (Ryu and Karim, 2011), glucosidase (Muñoz-Gutiérrez et al., 2012), cellulase complex (Kim et al., 2014) etc., which enable the engineered strains to degrade and utilize cheap biomass. However, similar to most other bacterial hosts, the choice of anchoring motif is critical to the display efficiency of *C. glutamicum*. In order to increase the versatility of the *C. glutamicum* cell surface display technology, it is necessary to develop new and efficient anchoring motifs.

In recent years, the screening of the anchoring proteins of *C. glutamicum* has been based mainly on partial screening rather than direct genome-wide screening of the characteristics of anchor proteins—for example, the process of screening Ncgl1337 as the anchor protein was to identify and analyze the mycolic acid layer protein by SignalP and tied-mixture hidden Markov models (TMHMM) and then display the reporter for further analysis and verification (Choi et al., 2018). The process of screening porin anchor proteins was similar to that (Tateno et al., 2009; Choi et al., 2018). It is worth mentioning that the mining of anchor proteins in other Gram-positive bacteria is generally based on a certain subcellular level or anchoring domain, such as membrane-associated protein (has a transmembrane domain or lipoprotein) or cell wall-associated protein [has a C-terminal Leu-Pro-X-Thr-Gly (LPXTG) motif or cell wall-binding domain] (Desvaux et al., 2006; Fischetti, 2019). These research methods are also used in *Staphylococcus aureus* (Foster, 2019), *Lactococcus lactis* (Plavec et al., 2019), and *Bacillus subtilis* (Guoyan et al., 2019), which are currently the most studied Gram-positive bacteria for anchor proteins.

With recent advancements in bioinformatics technology and the accumulation of a large volume of genome sequencing data as well as the demand for new and efficient anchor proteins, it is necessary to develop new and high-throughput anchor protein mining methods. The optimal properties of anchor proteins should have effective signal peptides or transport signals to allow the fusion protein to pass through the inner membrane. They should have a strong anchoring structure and be compatible with the foreign sequence to be inserted or fused, and they also should resist the attack of the protease present in the periplasmic space or the medium (Lee et al., 2003). In order to identify secreted proteins on the genome scale, numerous subcellular proteomics studies have been carried out (Bumann et al., 2002; Wu et al., 2008; Sharma and Bisht, 2017). In comparison, computational prediction is a relatively fast, auxiliary alternative to microbiological experimental methods that helps to determine SCL and analyze protein function. In recent decades, computational methods and machine learning methods have also become more prominent. Various SCL predictors have been developed, such as SignalP (Almagro Armenteros et al., 2019), PSORTm (Peabody et al., 2020), and LocateP (Zhou et al., 2008). These predictors are designed to identify and classify SCLs based on the Swiss-Prot database or metagenomic sequences. Among them, LocateP can distinguish seven different SCLs within bacteria on the genome scale: intracellular, multi-transmembrane, N-terminally membrane anchored, C-terminally membrane anchored, lipid-anchored, LPXTG-type cell wall-anchored, and secreted/released proteins. Moreover, LocateP can distinguish pathways of general secretion (Sec)- or twin-arginine translocation (Tat)-dependent secretion. LocateP was tested on data sets extracted from the literature, and its accuracy has always been greater than 90%. In addition, researchers have used LocateP to predict the SCLs of all proteins encoded by the genomes of Gram-positive bacteria (Zhou et al., 2008). On the other hand, TMHMM, based on a hidden Markov model approach, can predict the full topology of a protein and visualize its transmembrane structure (Krogh et al., 2001). The application of these tools can greatly facilitate the prediction and mining of anchor proteins.

In this study, we reported a novel method for screening anchor proteins of *C. glutamicum* ATCC13032 based on genome-scale mining. This method attempts to use the SCL prediction tools LocateP and TMHMM to screen the anchor proteins in the genome of *C. glutamicum*. First, we analyzed the five known endogenous anchor proteins of *C. glutamicum* to test the accuracy of prediction of the software packages. Based on the results obtained, the anchor proteins on the genome of *C. glutamicum* ATCC13032 were predicted and analyzed. We screened 25 possible anchor proteins and used enhanced green fluorescent protein (EGFP) and mCherry as reporters to verify the potential anchor proteins and then compared the performance of these two reporters. Then, through the display of α-amylase, the practicality of displaying three highly effective anchor proteins on the surface of *C. glutamicum* was examined. Finally, we discussed the general applicability of this screening method for use with Gram-positive bacteria.

MATERIALS AND METHODS

Reagents, Primers, and Growth Conditions

The reagents and primers used in this study are listed in **Supplementary Tables 1**, **2**. *Escherichia coli* Top10 was used as cloning host for plasmid construction, and *C. glutamicum* ATCC 13032 was used for gene editing. *E. coli* was cultured in LB medium (10 g L^{-1} peptone, 5 g L^{-1} yeast extract, and 10 g L^{-1} NaCl) at 37°C, and *C. glutamicum* ATCC 13032 was cultured in BHISG medium (37 g L^{-1} brain heart infusion, 9.1 g L^{-1} sorbitol, and 10 g L^{-1} glucose) at 30°C. For resistant strains, antibiotics were added as follows: final concentration of 50 μg L^{-1} kanamycin for *E. coli* and 25 μg L^{-1} kanamycin for *C. glutamicum*. In addition, the concentration

of isopropyl-βd-thiogalactoside (IPTG) used to induce the expression of α-amylase was 0.5 mM.

Application of Bioinformatics Technology in the Screening of Anchor Proteins

As mentioned earlier, several endogenous anchor proteins of *C. glutamicum* have been described, namely, NCgl1337, NCgl1221, PorB, PorC, and PorH. In this study, we downloaded the protein sequences of these known endogenous anchor proteins of *C. glutamicum* in FASTA format from the National Center for Biotechnology Information website[1] and subjected them to LocateP and TMHMM for SCL prediction analysis and transmembrane structure prediction (**Table 1**, **Supplementary Figure 1**, and **Supplementary Table 3**). Next, we analyzed and studied whether the predicted results met the screening requirements of anchor proteins and then used these two tools to predict and screen potential anchor proteins in the genome of *C. glutamicum*.

In the next experiment, we downloaded the protein sequence of the *C. glutamicum* ATCC13032 (GCF_000011325.1, from NCBI bioproject PRJNA307, reference sequence: NC_003450) genome in FASTA format[2] and then subjected the protein sequence to LocateP and TMHMM for prediction and analysis. Then, based on the characteristics of the anchor proteins, the parameter standards for anchor protein screening were formulated (**Table 2**), and these two tools were then used to predict and screen potential anchor proteins.

Construction of the Surface Display System of Recombinant *C. glutamicum*

The amplification and identification of gene fragments were performed by KOD DNA polymerase (TOYOBO, Japan) and Taq DNA polymerase (Thermo Fisher Scientific, Waltham, MA, United States). The Seamless Assembly Cloning Kit (Clone Smarter, United States) was used to assemble the plasmids using the principle of homologous recombination. In all expression vectors, the ribosome binding site (AAAGGAGGCCCTTCAG) is added before the open reading frame of the fusion protein. The constructed plasmids were verified by DNA sequencing (Shanghai Generay, Shanghai, China). All primers were synthesized by Shanghai Generay Biotech Co., Ltd. (Shanghai, China).

The construction of the *C. glutamicum* surface display system used pEC-XK99e as the carrier and EGFP, mCherry, and α-amylase as the reporters, respectively. The gene (*amyE*) of α-amylase (BSU_03040) was derived from *B. subtilis* 168. The N-terminal fusion or C-terminal fusion was determined according to the characteristics of the anchor proteins screened. Among these 25 anchor proteins, NCgl0550, NCgl0633, and NCgl2291 are C-terminal fusions, and the rest are N-terminal fusions (the term C-terminal or N-terminal fusion here refers to the way the anchor protein anchors on the cell surface, not the way the anchor protein anchors the passenger protein). The N-terminal/C-terminal of the anchor protein has a FLAG (DYKDDDDK, where D = aspartic acid, Y = tyrosine, and K = lysine) tag.

The construction of all the expression vectors was constructed using the same cloning strategy with a different PCR primer set. For the expression vector of passenger protein EGFP, here is the construction of Ncgl1307-EGFP as an example (**Figure 1A**). Using the genomic DNA of *C. glutamicum* ATCC13032 as a template and using 5am F and 5am R as primers, the Ncgl1307 gene sequence fragment 1 was amplified by PCR; using the EGFP gene as the template and using EGFP F-N site and EGFP R-N site as primers, the target protein EGFP gene fragment 2 was amplified; using pEC-XK99e as a template and pEC F and pEC R as primers, the gene sequence linearized vector of pEC-XK99e was amplified. Finally, these three fragments were assembled into a plasmid by Seamless Assembly Cloning Kit. For the expression vector where the passenger protein is mCherry, here is the construction of Ncgl1307-mCherry as an example (**Figure 2A**). Using mCherry gene as template and mCherry-pEC F and mCherry-pEC R as primers, mCherry gene fragment 3 was amplified. Then, Seamless Assembly Cloning Kit was used to assemble fragment 1, fragment 3, and linearized vector. For the expression vector where the passenger protein is amylase, here is the construction of Ncgl1307-amylase as an example (**Figure 3A**). Using the amylase gene as a template and Amy F and Amy R as primers, the target protein amylase gene fragment 4 was amplified. Then, Seamless Assembly Cloning Kit was used to assemble fragment 1, fragment 4, and linearized vector.

Flow Cytometry and Laser Confocal Microscopy of the Recombinant *C. glutamicum* Surface Display System

The recombinant *C. glutamicum* cells were induced and cultured in BHISG medium supplemented with 25 μg/ml kanamycin and 0.5 mM IPTG (final concentration) for 24 h, centrifuged at 6,000 rpm for 10 min, and then resuspended in 1 ml phosphate-buffered saline (PBS), and the optical density at 600 nm ($OD_{600\ nm}$) was adjusted to 1. The cells were centrifuged at 6,000 rpm for 10 min and resuspended in 0.2 ml PBS containing 1% bovine serum albumin (BSA). Then, 1 μl of anti-FLAG monoclonal antibodies (1 μg/ml; Sigma, United States) was added, and the mixture was incubated at room temperature for 2 h, with gentle shaking to avoid precipitation. Subsequently, the cells were washed twice with PBS and resuspended with 0.2 ml PBS containing 1% BSA. For the strain whose reporter was EGFP, 1 μl of 2 μg/μl Alexa Fluor 647-labeled goat anti-mouse IgG antibody [AF647, Alexa Fluor 647-labeled Goat Anti-Mouse IgG (H + L), Beyotime, China] was added, incubated at room temperature for 1 h, and then shaken continuously to suspend it. Finally, a BD Accuri™ C6 Plus Flow Cytometer (BD Biosciences, San Jose, CA, United States) was used to measure the fluorescence intensity. A total of 50,000 cells per sample was collected. Subsequently, the sample was centrifuged and resuspended, then coated on a microscope slide, and finally observed through a confocal microscope (Leica TCS SP8, Wetzlar, Germany). The image was acquired at an excitation wavelength of 488 nm and

[1] https://www.ncbi.nlm.nih.gov

[2] https://ftp.ncbi.nlm.nih.gov/genomes/refseq/bacteria/Corynebacterium_glutamicum/latest_assembly_versions

TABLE 1 | The prediction results of the known endogenous anchor proteins of *C. glutamicum* made by LocateP: (1) Intracellular probability score: range −1 to +1, threshold: 0.5.

Anchor protein	Protein ID	Product	Pathway	Cellular destination	Subcellular localization	Intracellular possibility	Signal peptide possibility	N-anchored possibility	Cleavage site
NCgl1337	WP_003858702.1	SGNH/GDSL hydrolase family protein	Sec-(SPI)	Extracellular	@Secretory (released) (with CS)	0.17	1	−2	PATAQSSG
NCgl1221	WP_011014245.1	Mechano sensitive ion channel	Sec-(SPI)	Membrane	@Multi-transmembrane	0.17	−1	1	No cleavage site
NCgl0933	WP_003856752.1	PorB	Sec-(SPI)	Extracellular	@Secretory (released) (with CS)	−0.17	1	−1	FAAPASAS
NCgl0932	WP_003856749.1	PorC	Sec-(SPI)	Extracellular	@Secretory (released) (with CS)	−0.17	1	−1	PSASAQDF
PorH	WP_011265995.1	PorH	No pathway	Cytoplasmic	@Intracellular	1	−1	−1	No cleavage Site

Values higher than 0.5 increase the probability of the protein occurring in the cell; (2) Extracellular probability score: range −1 to +1, threshold: 0.5. The higher the score, the more likely the protein will be transported to the non-cytoplasmic compartment; (3) N-anchor probability score: no range, threshold: 0. The higher the score, the higher the probability that the protein is retained on the membrane by its N-terminus. A negative score indicates that the protein is very likely to be secreted or released from the membrane (Zhou et al., 2008).

TABLE 2 | Screening criteria for potential anchor proteins in this experiment.

Subcellular localization	Length	Signal peptide probability (LocateP parameter)	TMHMM parameter	N-anchored probability (LocateP parameter)	Total probability of N-in (TMHMM parameter)
@C-terminally anchored (with CS)	<600	Choose larger parameters	Outside probability of first 20 AA on C-side >0.5; outside probability <0.5		
@Multi-transmembrane (lipid-modified N-termini)	<600		Outside probability of first 20 AA of C-terminal or N-terminal >0.5; outside probability <0.5	Choose larger parameters	
@Lipid-anchored	<600		Outside probability of first 20 AA of C-terminal or N-terminal >0.5; outside probability <0.5	Choose larger parameters	
@Multi-transmembrane	<600		Outside probability of first 20 AA of C-terminal or N-terminal >0.5; outside probability <0.5		
@N-terminally anchored (no CS)	<600		Outside probability of first 20 AA at N-terminal end >0.5; outside probability <0.5	Choose larger parameters	>0.8
@Secretory (released) (with CS)	<600		Outside probability of first 20 AA of C-terminal or N-terminal >0.5; outside probability <0.5	Choose larger parameters	>0.8

These screening criteria are applicable to anchor proteins anchored at the N-terminus, and the opposite is true for anchor proteins anchored at the C-terminus.

an emission wavelength of 520 nm. For strains whose reporter was mCherry, an Alexa Fluor 488-labeled goat anti-mouse IgG antibody [AF 488, Alexa Fluor 488-labeled Goat Anti-Mouse IgG (H + L), Beyotime, China] was used. A confocal microscope was used at the excitation wavelength of 667 nm and the emission wavelength of 651 nm to acquire the images. For flow cytometry analysis, Comp-FL1-A:APC-A was used to detect AF647, and Comp-FL1-A:FITC-A was used to detect AF 488. The data of flow cytometry and confocal microscopy were analyzed and processed by GraphPad Prism 8 and LAS X software, respectively.

Protein Fractionation and Analysis

Corynebacterium glutamicum harboring NCgl1307-Amy or NCgl2775-Amy or NCgl0717-Amy was selected and induced by 0.5 mM IPTG. The induced cells grew at 30°C with continuous shaking for 24 h before the cells were harvested. The cell surface fraction was prepared as described by Tateno et al. (2007b). The supernatant samples containing only cell wall-associated proteins were analyzed by sodium dodecyl sulfate-polyacrylamide gel electrophoresis (SDS-PAGE) using 8% gel. Then, the proteins were electroblotted onto a nitrocellulose

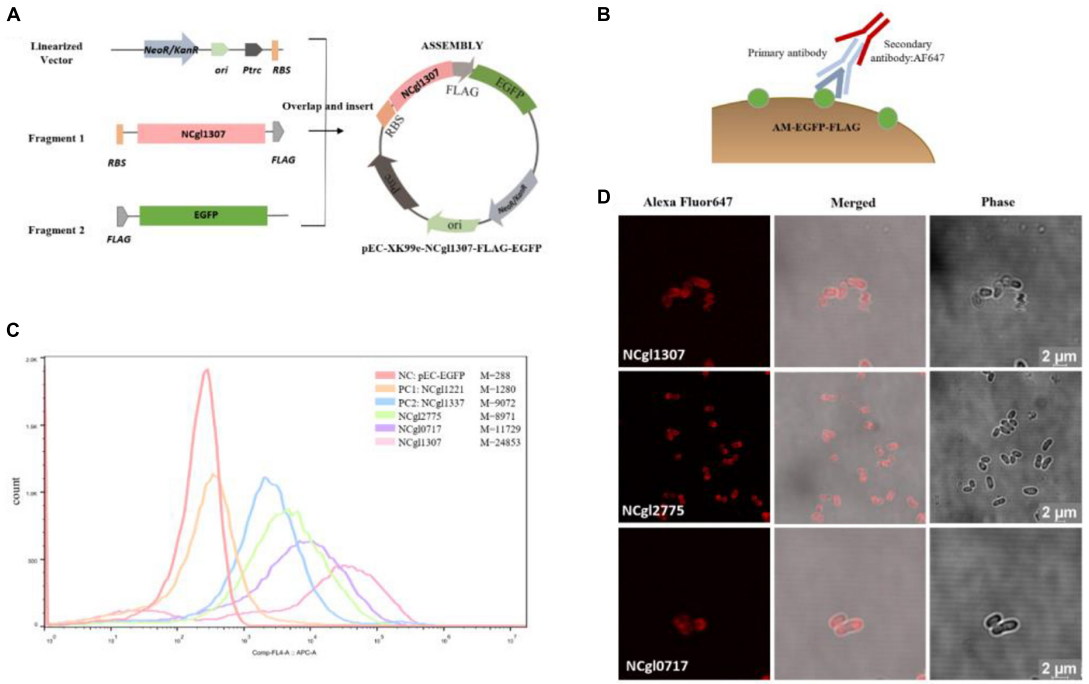

FIGURE 1 | Screen and confirmation of anchoring protein display on the cell surface by displaying EGFP. **(A)** Construction of recombinant *Corynebacterium glutamicum* surface display plasmid with EGFP as passenger protein. The construction of all the expression vectors of passenger protein EGFP was constructed using the same cloning strategy with a different PCR primer set. Take the construction of Ncgl1307-EGFP as an example. Using the genomic DNA of *C. glutamicum* ATCC13032 as a template and using 5am F and 5am R as primers, the Ncgl1307 gene sequence fragment 1 was amplified by PCR; using the EGFP gene as a template and using EGFP F-N site and EGFP R-N site as primers, the target protein EGFP gene fragment 2 was amplified; using pEC-XK99e as a template and pEC F and pEC R as primers, the gene sequence linearized vector of pEC-XK99e was amplified. Finally, this three fragments were assembled into a plasmid by Seamless Assembly Cloning Kit. **(B)** Schematic diagram of the immunofluorescence reaction. Anti-flag monoclonal antibody and Alexa Fluor 647-labeled antibody were added to the EGFP-FLAG. **(C)** Flow cytometry analysis. The peak figures of different colors from left to right represent the fluorescent signal intensities of cells harboring pEC-EGFP, Ncgl1221-EGFP, Ncgl1337-EGFP, NCgl2775-EGFP, NCgl0717-EGFP, or NCgl1307-EGFP, respectively. Of these, cells harboring pEC-EGFP were the negative control (NC_{-EGFP}), and cells harboring Ncgl1221-EGFP and Ncgl1337-EGFP were the positive control 1 ($PC1_{-EGFP}$) and the positive control 2 ($PC2_{-EGFP}$), respectively. M is mean value of Comp-FL-A:APC-A_Area. **(D)** Image observed on a confocal microscope based on immunofluorescence reaction. The red fluorescence comes from the fluorescence of the Alexa Fluor 647-labeled antibody on the flag label (667 nm—excitation, 651 nm—emission).

membrane (Immobilon-P Membrane, PVDF, 0.45 mm; EMD Millipore Corporation, Billerica, MA, United States). As the molecular weight marker, prestained protein standards (26616; Thermo Fisher Scientific, United States) were used. The membrane was blocked for 1 h at 37°C with Tris-buffered saline (TBS) with Tween-20 containing 5% BSA. After washing for five times with TBS, the membrane was incubated with the anti-FLAG monoclonal antibody (Sigma, United States) at a dilution of 1:5,000 and the secondary Goat Anti-mouse IgG (H&L) (HRP) antibody (Aksomics, China) at a dilution of 1:5,000. The membrane was then stained with ultra-sensitive ECL chemiluminescence substrate (BL520A, Biosharp, China) according to the protocol of the manufacturer. Finally, ChemiScope 3300 mini integrated chemiluminescence imaging system (Clinx, China) was used for detection.

Determination of Amylase Activity and Growth Curve

The amylase activity is determined by using the EnzChek® Ultra Amylase Assay Kit (Invitrogen, United States), and the specific steps used relate to the method used by Choi et al. (2018). The reaction mixture was added on a black 96-well plate (100 μl/well) (Corning, United States). Fluorescence was measured by a TECAN Infinite M200 ELISA plate reader (Tecan, Switzerland), using excitation at 485 nm and fluorescence detection at 520 nm. One unit (U) of α-amylase activity was defined as the amount of enzyme required to liberate 1.0 mg of glucose from starch in 3 min, at pH 6.9 and 20°C. The data was analyzed by GraphPad Prism 8 software. Each incubation was conducted in triplicate, and the results are presented as mean ± standard error from at least three independent experiments.

The strains picked from the plate were inoculated into BHISG and cultured overnight at 30°C and 280 rpm. CGXII medium (**Supplementary Table 1**) was used to determine the growth curve, and glucose (4%; Damao, China) or soluble starch (4%; Damao, China) was used as the only carbon source. The initial OD_{600nm} of cell density was 0.1–0.3, and the strain was cultured at 30°C and 280 rpm in 12-well plates. The OD_{600} optical density was measured every 4 h for 32 h. During the cultivation process, final concentrations of 25 μg/ml kanamycin and 0.5 mM IPTG were added to the resistant strains of

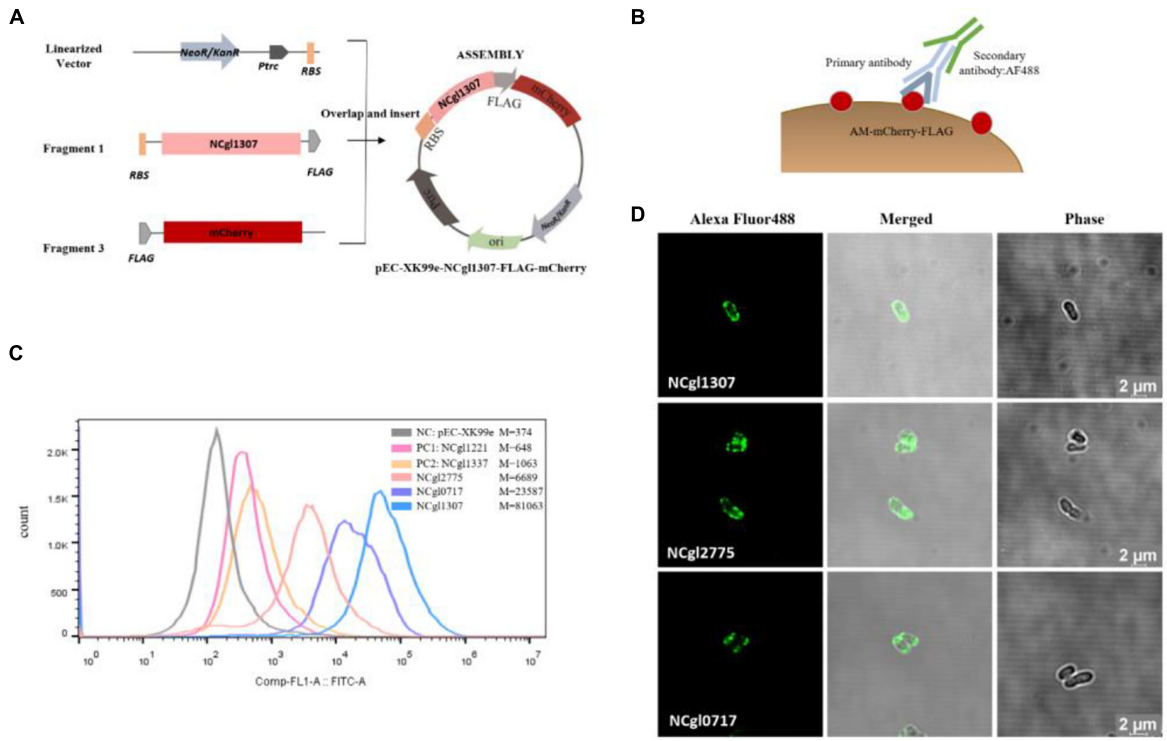

FIGURE 2 | Screening and confirmation of anchoring protein display on the cell surface by displaying mCherry. **(A)** Construction of recombinant *Corynebacterium glutamicum* surface display system with mCherry as passenger protein. Take the construction of Ncgl1307-mCherry as an example. Using mCherry gene as template and mCherry-pEC F and mCherry-pEC R as primers, mCherry gene fragment 3 was amplified. Then, Seamless Assembly Cloning Kit was used to assemble fragment 1, fragment 3, and linearized vector (**Figure 1A**). **(B)** Schematic diagram of the immunofluorescence reaction. Anti-flag monoclonal antibody and Alexa Fluor 488-labeled antibody were added to the mCherry-FLAG. **(C)** Flow cytometry analysis. The peak figures of different colors from left to right represent the fluorescent signal intensities of cells harboring pEC-XK99e, Ncgl1221-mCherry, Ncgl1337-mCherry, NCgl2775-mCherry, NCgl0717-mCherry, or NCgl1307-mCherry, respectively. Of these, cells harboring pEC-XK99e were the negative control ($NC_{-mCherry}$), and cells harboring Ncgl1221-mCherry and Ncgl1337-mCherry were the positive control 1 ($PC1_{-mCherry}$) and the positive control 2 ($PC2_{-mCherry}$), respectively. *M* is the mean value of Comp-FL-A:FITC-A_Area. **(D)** Image observed on a confocal microscope. The green fluorescence comes from the fluorescence of the Alexa Fluor 488-labeled antibody on the flag label (488 nm—excitation, 520 nm—emission).

C. glutamicum. The data was analyzed by GraphPad Prism 8 software. Each incubation was conducted in triplicate, and the results are presented as mean ± standard error from at least three independent experiments.

RESULTS AND DISCUSSION

Predictions of the Known Endogenous Anchor Proteins

Previously, several anchor proteins of *C. glutamicum* have been described, including NCgl1337, NCgl1221, PorB, PorC, and PorH. All except NCgl1221 are located in the mycolic acid layer. Of these five proteins, PorB, PorC, and PorH are porins, and they function as channels for transporting small molecules in the mycolic acid layer. NCgl1221 is a mechanosensitive channel and the main glutamate exporter of *C. glutamicum*, which is located on the cell membrane (Issa et al., 2017; Nakayama et al., 2019). To test the accuracy of the predictions made by LocateP and TMHMM, we analyzed the five known endogenous anchor proteins mentioned above by these two software packages. The prediction of LocateP showed that these proteins all belong to Sec-(SPI) secretion pathways and locate in the extracellular or cell membrane, except PorH (**Table 1**). The analysis of TMHMM also indicated that the parameters of these proteins are suitable for anchor proteins, including signal peptides and transmembrane structures (**Supplementary Figure 1** and **Supplementary Table 3**). Therefore, the predictions of the known anchor proteins made by LocateP and TMHMM of *C. glutamicum* are quite reliable.

In order to screen the anchor proteins in *C. glutamicum* ATCC13032, the amino acid (AA) sequence of the predicted proteins of *C. glutamicum* ATCC13032 were subjected in the FASTA format to LocateP and TMHMM. Then, based on the characteristics of these subcellular compartments and the requirements for screening anchor proteins in this experiment, we developed several screening criteria (**Table 2**). In view of the metabolic burden caused by the excessive molecular weight of the anchoring protein, proteins below 600 AA were selected. As for the signal peptide, those parameters of a larger signal peptide were selected in order to increase the possibility of forming an anchor protein. For N-terminal anchor proteins,

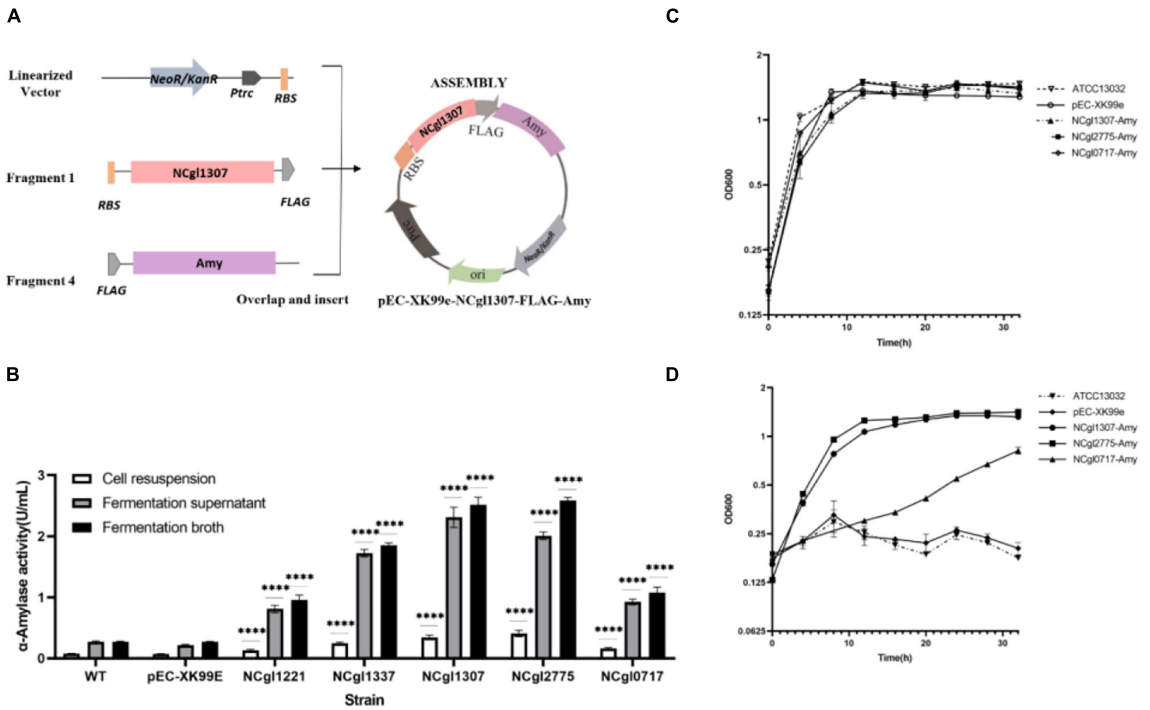

FIGURE 3 | Display of α-amylase on the cell surface using NCgl1307, NCgl2775, or NCgl0717 as anchoring motifs. **(A)** Construction and identification of a recombinant *Corynebacterium glutamicum* surface display system with α-amylase as passenger protein. Take the construction of Ncgl1307-amylase as an example. Using the amylase gene as a template and Amy F and Amy R as primers, the target protein amylase gene fragment 4 was amplified. Then, Seamless Assembly Cloning Kit was used to assemble fragment 1, fragment 4, and linearized vector (**Figure 1A**). **(B)** α-Amylase activity assay with WT, NC (cells harboring pEC-XK99e), cells harboring NCgl1307-Amy, NCgl2775-Amy, and NCgl0717-Amy, respectively. The data represent the mean value and standard deviation of biological triplicates. Statistical significance, $^{****}P < 0.0001$. **(C)** Growth curve of *C. glutamicum* with glucose as the sole carbon source, including WT, pEC-XK99e, NCgl1307-Amy, NCgl2775-Amy, and NCgl0717-Amy (representing cells harboring pEC-XK99e, NCgl1307-Amy, NCgl2775-Amy, or NCgl0717-Amy, respectively). **(D)** Growth curve of *C. glutamicum* with starch as the sole carbon source, including WT, pEC-XK99e, NCgl1307-Amy, NCgl2775-Amy, and NCgl0717-Amy (representing cells harboring pEC-XK99e, NCgl1307-Amy, NCgl2775-Amy, or NCgl0717-Amy, respectively). The data represent the mean value and standard deviation of biological triplicates.

to ensure that the reporter or other functional proteins fused to the anchor protein can extend outside the cell, the inside probability parameter of the first 20 AA at the N-terminal end should be >0.5, and the outside probability should be <0.5. For @N-terminally anchored (no CS) and @Secretory (released) (with CS) N-anchored probability (LocateP parameter) and total probability of N-in (TMHMM2.0 parameter), larger parameters should be chosen to increase the probability of N-terminal anchoring. These screening rules are reversed for C-terminally anchor proteins. Based on these screening criteria, we screened 25 potential anchor proteins with high scores from the *C. glutamicum* ATCC13032 genome (**Table 3** and **Supplementary File 1**).

Construction of the Surface Display System Using EGFP as the Passenger Protein

In the cells of organisms of the three-domain system (archaea, bacteria, and eukaryotes), secretory proteins are usually synthesized in the form of a precursor protein, carrying a split N-terminal signal peptide, which is used to locate the protein in a membrane-embedded export device (Rapoport et al., 1996; Eichler, 2000). *C. glutamicum* has two main protein secretion pathways: Sec-dependent pathway to secrete unfolded proteins and Tat-dependent pathway to secrete folded proteins (Vertès, 2013; Freudl, 2017). Fluorescent proteins are the main cell biology tool for analyzing the subcellular topology of protein, of which EGFP and mCherry are commonly used. EGFP is an excellent reporter of the Tat system in *Streptomyces listeri* (Hamed et al., 2018) and *E. coli* (Lee et al., 2006) because active EGFP can only be secreted after cytoplasmic folding and subsequent translocation through the Tat pathway. Fusion of GFP to a Sec-specific signal peptide resulted in the periplasmic localization of GFP, but in an inactive form (Albiniak et al., 2013). However, the monomeric red fluorescent protein mCherry is functional regardless of the translocation pathway (Speck et al., 2011). In order to eliminate interference by the reporter due to its own secretion pathway and compare the differences between the two commonly used reporters EGFP and mCherry, we used these two reporters to screen the anchor proteins sequentially.

First, we used EGFP as the passenger protein to test the display effect of the 25 potential anchor proteins (**Table 3**). The potential anchored protein predicted was amplified by PCR and

TABLE 3 | The 25 potential anchor proteins screened in this experiment based on the predicted results of LocateP and tied-mixture hidden Markov models.

	Identifier	Locus tag	Pathway	Cellular destination	Subcellular localization	Intracellular possibility	Signal peptide possibility	N-anchored possibility	Cleavage site	Potential anchored site
1	WP_011013799.1 hypothetical protein	NCgl0550	Sec-(SPI)	Membrane	@C-terminally anchored (with CS)	0	1	−2	PTASAATL	C site
2	WP_011013739.1 type VII secretion-associated serine protease mycosin	NCgl0633	Sec-(SPI)	Membrane	@C-terminally anchored (with CS)	0	1	−2	TRAQEVEA	C site
3	WP_011014951.1 cytochrome c oxidase subunit II	NCgl2115	Sec-(SPII)	Membrane	@Multi-transmembrane (lipid-modified N-termini)	0	1	1	LAMAGCE	N site
4	WP_011265759.1 gi|62390400| ref|YP_225802.1| hypothetical protein cg1712	NCgl1460	Sec-(SPII)	Extracellular	@Lipid-anchored	0.17	1	1	LLLSACT	N site
5	WP_011014306.1 hypothetical protein	NCgl1307	Sec-(SPII)	Extracellular	@Lipid-anchored	−0.33	1	1	FVLSGCG	N site
6	WP_011014779.1 glutamate ABC transporter substrate-binding protein	NCgl1876	Sec-(SPII)	Extracellular	@Lipid-anchored	−0.33	1	1	VTLTACG	N site
7	WP_011265985.1 twin-arginine translocation signal domain-containing protein	NCgl2562	Possibly Tat/Sec-(SPII)	Extracellular	@Lipid-anchored	−0.33	1	1	ATLAACA	N site
8	WP_011013364.1 sensor histidine kinase	NCgl0067	Sec-(SPI)	Membrane	@Multi-transmembrane	0.17	−1	2	No Cleavage Site	N site
9	WP_004567665.1 MULTISPECIES: DUF4233 domain-containing protein	NCgl2291	Sec-(SPI)	Membrane	@Multi-transmembrane	0.17	−1	1	No cleavage site	C site
10	WP_01101483.1 family transporter	NCgl1147	Sec-(SPI)	Membrane	@Multi-transmembrane	0.17	−1	1	No cleavage site	N site
11	WP_011014865.1 ABC transporter ATP-binding protein	NCgl1998	Sec-(SPI)	Membrane	@Multi-transmembrane	0.17	−0.5	1	No cleavage site	N site
12	WP_003859459.1 MULTISPECIES: HlyC/CorC family transporter	NCgl2206	Sec-(SPI)	Membrane	@Multi-transmembrane	0.17	0	0	No cleavage site	N site
13	WP_003863539.1 MULTISPECIES: potassium channel family protein	NCgl0743	Sec-(SPI)	Membrane	@Multi-transmembrane	0.17	−1	−1	No cleavage site	N site
14	WP_011013342.1 penicillin-binding protein 2	NCgl0042	Sec-(SPI)	Membrane	@N-terminally anchored (no CS)	0.17	1	7	No cleavage site	N site
15	WP_011013540.1 TlpA family protein disulfide reductase	NCgl0289	Sec-(SPI)	Membrane	@N-terminally anchored (no CS)	0.17	1	7	No cleavage site	N site
16	WP_011014270.1 SRPBCC family protein	NCgl1250	Sec-(SPI)	Membrane	@N-terminally anchored (no CS)	0.17	1	7	No cleavage site	N site

(Continued)

TABLE 3 | (Continued)

	Identifier	Locus tag	Pathway	Cellular destination	Subcellular localization	Intracellular possibility	Signal peptide possibility	N-anchored possibility	Cleavage site	Potential anchored site
17	WP_011015453.1 cutinase family protein	NCgl2775	Sec-(SPI)	Membrane	@N-terminally anchored (no CS)	0.17	1	7	No cleavage site	N site
18	WP_003853779.1 MULTISPECIES: DUF4247 domain-containing protein	NCgl2610	Sec-(SPI)	Membrane	@N-terminally anchored (no CS)	0.17	1	5	No cleavage site	N site
19	WP_011013420.1 hypothetical protein	NCgl0136	Sec-(SPI)	Extracellular	@Secretory (released) (with CS)	0.17	1	−1	IAATPATA	N site
20	WP_011013818.1 CAP domain-containing protein	NCgl0661	Sec-(SPI)	Extracellular	@Secretory (released) (with CS)	0.17	1	−1	PSAHAFTA	N site
21	WP_011013866.1 hypothetical protein	NCgl0717	Sec-(SPI)	Extracellular	@Secretory (released) (with CS)	0.17	1	−1	DIATSTTT	N site
22	WP_011014348.1 copper transporter	NCgl1361	Sec-(SPI)	Extracellular	@Secretory (released) (with CS)	0.17	1	−1	GIAFGTYV	N site
23	WP_011014599.1 LysM peptidoglycan-binding domain-containing protein	NCgl1682	Sec-(SPI)	Extracellular	@Secretory (released) (with CS)	0.17	1	−1	GGSGVTFL	N site
24	WP_042383306.1 hypothetical protein	NCgl2577	Sec-(SPI)	Extracellular	@Secretory (released) (with CS)	0.17	1	−1	VVALRGGS	N site
25	WP_003858490.1 resuscitation-promoting factor	NCgl0872	Sec-(SPI)	Extracellular	@Secretory (released) (with CS)	0.17	1	−2	VTAAATKK	N site

connected to pEC-XK99e through homologous recombination. In order to reduce the impact of space barrier on the screening process, the membrane protein NCgl1221 and the mycolic acid protein NCgl1337 were selected as two positive control of anchor proteins. The strain harboring pEC-EGFP was the negative control.

Flow Cytometry and Laser Confocal Scanning Microscopy of the Recombinant *C. glutamicum* Surface Display System Based on Immunofluorescence

In the initial experiment, the strain displaying EGFP was resuspended for laser confocal analysis without immunofluorescence reaction. The results showed that most samples could not determine whether EGFP was displayed on the surface due to strong intracellular fluorescence interference (**Supplementary Figure 2**). Therefore, immunofluorescence reaction was used before fluorescence-activated cell sorting (FACS) and confocal microscopy analysis (**Figures 1B**, **2B**).

The 25 anchor proteins were fused with the EGFP-FLAG, and Ncgl1221 ($PC1_{-EGFP}$) and Ncgl1337 ($PC2_{-EGFP}$) were used as the two positive controls. In order to evaluate the fluorescence localization, we used FACS and confocal fluorescence microscopy based on the immunofluorescence reaction. In FACS analysis, the 14 cells harboring FLAG-tagged fusion-anchored proteins showed a significant drift compared to the negative control (cells harboring pEC-EGFP) (**Supplementary Figure 3**). In addition, among the 14 recombinant strains, the cells harboring NCgl1307-EGFP, NCgl2775-EGFP, and NCgl0717-EGFP showed a more significant drift than the two positive controls ($PC1_{-EGFP}$ and $PC2_{-EGFP}$) (**Figure 1C**).

In order to further confirm the localization of fluorescence, we observed these 25 recombinant strains with immunofluorescence under a confocal microscope. The results showed that these 14 recombinant strains mentioned above all showed the red fluorescent signal of the secondary antibody under a laser confocal microscope, including cells harboring NCgl1307, NCgl2775, and NCgl0717 (**Figure 1D**), which performed well in flow cytometry. The results showed that these 14 proteins could be used as anchor proteins to display EGFP on the surface of *C. glutamicum*.

Using the Mined Anchor Protein to Display mCherry

The active fluorescent EGFP needs to be secreted through the Tat pathway, while the monomeric red fluorescent protein mCherry is functional regardless of the translocation pathway (Speck et al., 2011). Almost all the 25 potential anchor proteins screened above are secreted through the Sec pathway (**Table 3**). In order to eliminate the interference from its own secretory pathway when EGFP acts as a reporter, we selected several anchor proteins to display mCherry.

In this experiment, NCgl1307, NCgl2775, NCgl0717, NCgl0743, NCgl1361, and NCgl2610 were fused with mCherry-FLAG. Ncgl1221 ($PC1_{-mCherry}$) and Ncgl1337 ($PC2_{-mCherry}$) were used as the two positive controls of anchor protein. In order to evaluate the fluorescence localization, we used FACS and confocal fluorescence microscopy. In FACS analysis, the protein-anchored cells showed a more significant drift than the negative control (NC, cells harboring pEC-XK99e) (**Supplementary Figure 4**). In addition, the cells harboring NCgl2775-mCherry, NCgl0717-mCherry, and NCgl1307-mCherry showed a higher fluorescence intensity than the positive controls (cells harboring Ncgl1221-mCherry or Ncgl1337-mCherry) (**Figure 2C**); these results were similar to those of EGFP. At the same time, when comparing the strain with the reporter as EGFP (**Figure 1C**), the peak pattern of the recombinant strain harboring NCgl0717-mCherry and NCgl1307-mCherry shifted more obviously (**Figure 2D**).

Expression of Anchor Protein—Amy Fusion Protein—on the Cell Surface

In order to explore the potential practical applications of the mined anchor proteins, we used α-amylase (AmyE) of *B. subtilis* 168 as the passenger protein. The expression of the anchor protein—Amy fusion proteins—in *C. glutamicum* was analyzed by SDS-PAGE and Western blot analysis of the cell wall fraction. The molecular size of the individual NCgl1307, NCgl2775, NCgl0717, and Amy proteins is approximately 38, 40 (Meniche et al., 2009), 27, and 73 kDa, respectively. The molecular size of the fusion proteins NCgl1307-Amy, NCgl2775-Amy, and NCgl0717-Amy was therefore predicted to be approximately 111, 113, and 100 kDa, respectively. Bands at the predicted molecular size were observed on Western blot, indicating the successful expression of the fusion proteins in the cell wall fraction (**Supplementary Figure 5**). However, the sample of the fusion proteins used on Western blot was easily degraded.

Next, the amylase activity and cell growth of display platforms with NCgl1307-Amy, NCgl2775-Amy, and NCgl0717-Amy were analyzed (**Figure 3**). Compared with the positive controls NCgl1221 and NCgl1337, the enzyme activity of the strain containing NCgl1307 and NCgl2775 was higher than that of the two positive control strains. The enzyme activity of the strain containing NCgl0717 is higher than that of the positive control strain containing NCgl1221 and lower than that of the positive control strain containing NCgl 1337 (**Figure 3B**). Their enzyme activities of cell resuspension reached 0.34 (52), 0.41 (62), and 0.16 U/ml (25 U/g dry cells), respectively.

In addition, WT and strains harboring pEC-XK99e, NCgl1307-Amy, NCgl2775-Amy, and NCgl0717-Amy have similar growth curves in the glucose medium. Of these, WT has the highest OD_{600} value in the stable phase (**Figure 3C**). This may be caused by the heavy metabolic burden of recombinant strains affected by plasmids and antibiotics. As negative controls, WT and cells harboring pEC-XK99e did not grow well in the starch medium because of their inability to utilize starch (**Figure 3D**). In contrast, strains harboring NCgl1307-Amy, NCgl2775-Amy, and NCgl0717-Amy grew much better in the starch medium. Of these, the growth trends of the strains with NCgl1307-Amy and NCgl2775-Amy were similar in both the starch and the glucose media, including the time point for entering the stable phase and the maximum OD_{600} value, which suggested that the strains harboring NCgl1307-Amy and NCgl2775-Amy are well able to utilize starch.

However, the protein sequence of the α-amylase gene (*amyE*, BSU_03040) used in this experiment includes signal peptide (1–27 AA) and propeptide (28–41 AA)[3]. The signal peptide and propeptide sequences will be cleaved off after guiding the transport of the amylase protein across the membrane. This should be the main reason why most amylases are present in the supernatant in this experiment. In subsequent experiments, we plan to remove the gene sequences of the signal peptide and propeptide and further explore the application of the 14 anchored proteins to the display of this α-amylase or other functional proteins.

Moreover, using the protein basic local alignment search tool (BLASTP) and protein functional region analysis, it was found that, among the three anchor proteins screened, NCgl2775 is a membrane protein and possesses comparable esterase and thioesterase activities *in vitro* (Meniche et al., 2009), which means that these enzyme activities may work synergistically with the displayed enzymes. Therefore, the characteristic of this anchor protein may have a more useful application value in the future. NCgl1307 and NCgl0717 are hypothetical proteins, and their functions need to be studied further. The results in BLASTP also showed that these three anchor proteins are also present in many other *C. glutamicum* species, and it is expected that they may have more extensive uses in the future.

CONCLUSION AND PROSPECTS

In this study, we used the subcellular localization and parameter prediction of LocateP and the transmembrane structure prediction and visualization of TMHMM to screen the anchor proteins in the protein sequence of the *C. glutamicum* genome. A total of 14 potential anchor proteins were screened. Among them, three had a higher rivet efficiency than the previously mined NCgl1221 and NCgl1337 and showed enzyme

[3]https://www.uniprot.org/uniprot/P00691

activities with amylase. These results confirmed the effectiveness of the screening method. At the same time, any protein that can rivet the protein of interest to the cell surface could be used as a potential anchor protein. Therefore, our screening method is likely to be applicable to other Gram-positive bacteria. Moreover, the operations during the screening by LocateP and TMHMM can be carried out according to specific parameters. LocateP has completed the prediction of SCLs of all of the proteins encoded by the Gram-positive bacterial genome (Zhou et al., 2008). Those laid a good foundation for further high-throughput screening of anchor proteins. With advancements in information technology, it is expected that researchers will be able to combine these two tools to develop open-source software specifically for screening the anchor proteins of Gram-positive bacteria. This could help develop more efficient anchor proteins for basic theoretical research and practical industrial applications.

On the other hand, in the screening process of anchor proteins, the reporters EGFP and mCherry have their own characteristics. The different preferences in secretion pathway of these two reporters may have few effects on secretion and anchoring. Meanwhile, the secretion pathway of the signal peptide may play a major role in the secretion and transport of the anchor protein–reporter. It is worth mentioning that, no matter which fluorescent protein is selected, the ideal anchoring effect cannot be directly observed under the confocal laser microscope without immunofluorescence reactions because of the interference from intracellular fluorescence. In summary, functional proteins with FLAG tags against secondary antibodies AF488 might be a good choice in the screening process for anchor proteins. This combination can achieve better results in both FACS and confocal microscopy and directly verify the practicality of anchor proteins.

DATA AVAILABILITY STATEMENT

The original contributions presented in the study are included in the article/**Supplementary Material**, further inquiries can be directed to the corresponding author/s.

AUTHOR CONTRIBUTIONS

KL and SZ designed and carried out the main studies. SH, NZ, YC, and YL have made a lot of contributions in the experiment design, experiment execution, and manuscript revision. All authors read and approved the final manuscript.

FUNDING

This work was supported by the Tianjin Synthetic Biotechnology Innovation Capacity Improvement Project (TSBICIP-KJGG-005) and National Natural Science Foundation of China (grant no. 31671840).

SUPPLEMENTARY MATERIAL

The Supplementary Material for this article can be found online at: https://www.frontiersin.org/articles/10.3389/fmicb.2021.677702/full#supplementary-material

Supplementary Figure 1 | Tied-mixture hidden Markov models predicted the results for the transmembrane structure of the known endogenous anchor proteins of *Corynebacterium glutamicum*. **(A)** NCgl1337, **(B)** NCgl1221, **(C)** PorB, **(D)** PorC, and **(E)** PorH.

Supplementary Figure 2 | Laser confocal scanning microscopy analysis of the recombinant *Corynebacterium glutamicum* surface display system without immunofluorescence reaction.

Supplementary Figure 3 | Flow cytometric analysis of recombinant *Corynebacterium glutamicum* with surface-displayed EGFP based on immunofluorescence reaction (single-comparison chart). The peak image without color filling on the left is the peak image of the negative control strain (NC, cells harboring pEC-EGFP, M = 288). The NCgl number indicates the corresponding strain displaying NCgl protein-EGFP. Cells harboring Ncgl1221-EGFP and Ncgl1337-EGFP were the positive control 1 ($PC1_{\_EGFP}$) and the positive control 2 ($PC2_{\_EGFP}$), respectively. M is the mean value of Comp-FL-A:APC-A _Area.

Supplementary Figure 4 | Flow cytometry analysis of recombinant *Corynebacterium glutamicum* with surface-displayed mCherry based on immunofluorescence reaction (single-comparison chart). The peak image without color filling on the left is the peak image of the negative control strain (NC, cells harboring pEC-XK99e, M = 374). The NCgl number indicates the corresponding strain displaying NCgl protein-mCherry. Cells harboring Ncgl1221-mCherry and Ncgl1337-mCherry were the positive control 1 ($PC1_{\_mCherry}$) and the positive control 2 ($PC2_{\_mCherry}$), respectively. M is the mean value of Comp-FL-A:FITC-A_Area.

Supplementary Figure 5 | Western blot analysis of protein production in *Corynebacterium glutamicum*. **(A)** Lanes 8 and 9 represent the cell wall fraction protein of cells harboring NCgl0717-Amy and NCgl1307-Amy, respectively. **(B)** Lane 3 represents the cell wall fraction protein of cells harboring NCgl2775-Amy.

Supplementary Table 1 | Reagent used in this study.

Supplementary Table 2 | Primers used in this study.

Supplementary Table 3 | The prediction results of the known endogenous anchor proteins of *C. glutamicum* made by TMHMM.

Supplementary File 1 | Tied-mixture hidden Markov models predicted the results for the 25 possible anchor proteins of *Corynebacterium glutamicum*.

REFERENCES

Albiniak, A. M., Matos, C. F. R. O., Branston, S. D., Freedman, R. B., Keshavarz-Moore, E., and Robinson, C. (2013). High-level secretion of a recombinant protein to the culture medium with a *Bacillus subtilis* twin-arginine translocation system in *Escherichia coli*. *FEBS J.* 280, 3810–3821. doi: 10.1111/febs.12376

Almagro Armenteros, J. J., Tsirigos, K. D., Sønderby, C. K., Petersen, T. N., Winther, O., Brunak, S., et al. (2019). SignalP 5.0 improves signal peptide predictions using deep neural networks. *Nat. Biotechnol.* 37, 420–423. doi: 10.1038/s41587-019-0036-z

Bumann, D., Aksu, S., Wendland, M., Janek, K., Zimny-Arndt, U., Sabarth, N., et al. (2002). Proteome analysis of secreted proteins of the gastric pathogen *Helicobacter pylori*. *Infect. Immun.* 70, 3396–3403. doi: 10.1128/IAI.70.7.3396-3403.2002

Choi, J. W., Jeon, E. J., and Jeong, K. J. (2019). Recent advances in engineering *Corynebacterium glutamicum* for utilization of hemicellulosic biomass. *Curr. Opin. Biotechnol.* 57, 17–24. doi: 10.1016/j.copbio.2018.11.004

Choi, J. W., Yim, S. S., and Jeong, K. J. (2018). Development of a potential protein display platform in *Corynebacterium glutamicum* using mycolic acid layer protein, NCgl1337, as an anchoring motif. *Biotechnol. J.* 13:1700509. doi: 10.1002/biot.201700509

Desvaux, M., Dumas, E., Chafsey, I., and Hébraud, M. (2006). Protein cell surface display in Gram-positive bacteria: from single protein to macromolecular protein structure. *FEMS Microbiol. Lett.* 256, 1–15. doi: 10.1111/j.1574-6968.2006.00122.x

Eichler, J. (2000). Archaeal protein translocation crossing membranes in the third domain of life. *Eur. J. Biochem.* 267, 3402–3412. doi: 10.1046/j.1432-1327.2000.01396.x

Fischetti, V. A. (2019). Surface proteins on Gram-Positive bacteria. *Microbiol. Spectr.* 7:GPP3-0012-2018. doi: 10.1128/microbiolspec.GPP3-0012-2018

Foster, T. J. (2019). "Surface proteins of *Staphylococcus aureus*," in *Gram-positive pathogens*, eds V. A. Fischetti, R. P. Novick, J. J. Ferretti, D. A. Portnoy, M. Braunstein, and J. I. Rood (Washington, DC: American Society for Microbiology), 599–617.

Freudl, R. (2017). Beyond amino acids: use of the *Corynebacterium glutamicum* cell factory for the secretion of heterologous proteins. *J. Biotechnol.* 258, 101–109. doi: 10.1016/j.jbiotec.2017.02.023

Guoyan, Z., Yingfeng, A., Zabed, H. M., Qi, G., Yang, M., Jiao, Y., et al. (2019). *Bacillus subtilis* spore surface display technology: a review of its development and applications. *J. Microbiol. Biotechnol.* 29, 179–190. doi: 10.4014/jmb.1807.06066

Hamed, M. B., Vrancken, K., Bilyk, B., Koepff, J., Novakova, R., van Mellaert, L., et al. (2018). Monitoring protein secretion in *Streptomyces* using fluorescent proteins. *Front. Microbiol.* 9:3019. doi: 10.3389/fmicb.2018.03019

Inui, M., and Toyoda, K. (2020). *Corynebacterium glutamicum: biology and biotechnology*. Cham: Springer.

Issa, H., Huc-Claustre, E., Reddad, T., Bonadé Bottino, N., Tropis, M., Houssin, C., et al. (2017). Click-chemistry approach to study mycoloylated proteins: evidence for PorB and PorC porins mycoloylation in *Corynebacterium glutamicum*. *PLoS One* 12:e0171955. doi: 10.1371/journal.pone.0171955

Kim, S. J., Hyeon, J. E., Jeon, S. D., Choi, G., and Han, S. O. (2014). Bi-functional cellulases complexes displayed on the cell surface of *Corynebacterium glutamicum* increase hydrolysis of lignocelluloses at elevated temperature. *Enzyme Microb. Technol.* 66, 67–73. doi: 10.1016/j.enzmictec.2014.08.010

Krogh, A., Larsson, B., von Heijne, G., and Sonnhammer, E. L. (2001). Predicting transmembrane protein topology with a hidden Markov model: application to complete genomes. *J. Mol. Biol.* 305, 567–580. doi: 10.1006/jmbi.2000.4315

Lee, P. A., Tullman-Ercek, D., and Georgiou, G. (2006). The bacterial twin-arginine translocation pathway. *Annu. Rev. Microbiol.* 60, 373–395. doi: 10.1146/annurev.micro.60.080805.142212

Lee, S. Y., Choi, J. H., and Xu, Z. (2003). Microbial cell-surface display. *Trends Biotechnol.* 21, 45–52. doi: 10.1016/S0167-7799(02)00006-9

Liu, L., Yang, H., Shin, H.-D., Li, J., Du, G., and Chen, J. (2013). Recent advances in recombinant protein expression by *Corynebacterium*, *Brevibacterium*, and *Streptomyces*: from transcription and translation regulation to secretion pathway selection. *Appl. Microbiol. Biotechnol.* 97, 9597–9608. doi: 10.1007/s00253-013-5250-x

Liu, X., Yang, Y., Zhang, W., Sun, Y., Peng, F., Jeffrey, L., et al. (2016). Expression of recombinant protein using *Corynebacterium glutamicum*: progress, challenges and applications. *Crit. Rev. Biotechnol.* 36, 652–664. doi: 10.3109/07388551.2015.1004519

Meniche, X., Labarre, C., de Sousa-D'Auria, C., Huc, E., Laval, F., Tropis, M., et al. (2009). Identification of a stress-induced factor of *Corynebacterineae* that is involved in the regulation of the outer membrane lipid composition$^{\nabla}$. *J. Bacteriol.* 191, 7323–7332. doi: 10.1128/JB.01042-09

Muñoz-Gutiérrez, I., Oropeza, R., Gosset, G., and Martinez, A. (2012). Cell surface display of a β-glucosidase employing the type V secretion system on ethanologenic *Escherichia coli* for the fermentation of cellobiose to ethanol. *J. Ind. Microbiol. Biotechnol.* 39, 1141–1152. doi: 10.1007/s10295-012-1122-0

Nakayama, Y., Hashimoto, K.-I., Kawasaki, H., and Martinac, B. (2019). "Force-From-Lipids" mechanosensation in *Corynebacterium glutamicum*. *Biophys. Rev.* 11, 327–333. doi: 10.1007/s12551-019-00524-3

Peabody, M. A., Lau, W. Y. V., Hoad, G. R., Jia, B., Maguire, F., Gray, K. L., et al. (2020). PSORTm: a bacterial and archaeal protein subcellular localization prediction tool for metagenomics data. *Bioinformatics* 36, 3043–3048. doi: 10.1093/bioinformatics/btaa136

Plavec, T. V., Štrukelj, B., and Berlec, A. (2019). Screening for new surface anchoring domains for *Lactococcus lactis*. *Front. Microbiol.* 10:1879. doi: 10.3389/fmicb.2019.01879

Qi, S.-W., Chaudhry, M. T., Zhang, Y., Meng, B., Huang, Y., Zhao, K.-X., et al. (2007). Comparative proteomes of *Corynebacterium glutamicum* grown on aromatic compounds revealed novel proteins involved in aromatic degradation and a clear link between aromatic catabolism and gluconeogenesis via fructose-1,6-bisphosphatase. *Proteomics* 7, 3775–3787. doi: 10.1002/pmic.200700481

Rapoport, T. A., Jungnickel, B., and Kutay, U. (1996). Protein transport across the eukaryotic endoplasmic reticulum and bacterial inner membranes. *Annu. Rev. Biochem.* 65, 271–303. doi: 10.1146/annurev.bi.65.070196.001415

Ryu, S., and Karim, M. N. (2011). A whole cell biocatalyst for cellulosic ethanol production from dilute acid-pretreated corn stover hydrolyzates. *Appl. Microbiol. Biotechnol.* 91, 529–542. doi: 10.1007/s00253-011-3261-z

Sasaki, M., Jojima, T., Kawaguchi, H., Inui, M., and Yukawa, H. (2009). Engineering of pentose transport in *Corynebacterium glutamicum* to improve simultaneous utilization of mixed sugars. *Appl. Microbiol. Biotechnol.* 85, 105–115. doi: 10.1007/s00253-009-2065-x

Sharma, D., and Bisht, D. (2017). Secretory proteome analysis of streptomycin-resistant *Mycobacterium tuberculosis* clinical isolates. *SLAS Discov.* 22, 1229–1238. doi: 10.1177/2472555217698428

Speck, J., Arndt, K. M., and Müller, K. M. (2011). Efficient phage display of intracellularly folded proteins mediated by the TAT pathway. *Protein Eng. Des. Sel.* 24, 473–484. doi: 10.1093/protein/gzr001

Tateno, T., Fukuda, H., and Kondo, A. (2007b). Production of L-Lysine from starch by *Corynebacterium glutamicum* displaying alpha-amylase on its cell surface. *Appl. Microbiol. Biotechnol.* 74, 1213–1220. doi: 10.1007/s00253-006-0766-y

Tateno, T., Fukuda, H., and Kondo, A. (2007a). Direct production of L-lysine from raw corn starch by *Corynebacterium glutamicum* secreting *Streptococcus bovis* alpha-amylase using cspB promoter and signal sequence. *Appl. Microbiol. Biotechnol.* 77, 533–541. doi: 10.1007/s00253-007-1191-6

Tateno, T., Hatada, K., Tanaka, T., Fukuda, H., and Kondo, A. (2009). Development of novel cell surface display in *Corynebacterium glutamicum* using porin. *Appl. Microbiol. Biotechnol.* 84, 733–739. doi: 10.1007/s00253-009-2021-9

Vertès, A. A. (2013). "Protein Secretion Systems of *Corynebacterium glutamicum*," in *Corynebacterium glutamicum*, eds H. Yukawa and M. Inui (Berlin: Springer).

Wu, Z., Zhang, W., and Lu, C. (2008). Comparative proteome analysis of secreted proteins of *Streptococcus suis* serotype 9 isolates from diseased and healthy pigs. *Microb. Pathog.* 45, 159–166. doi: 10.1016/j.micpath.2008.04.009

Zhang, B., Jiang, Y., Li, Z., Wang, F., and Wu, X.-Y. (2020). Recent progress on chemical production from non-food renewable feedstocks using *Corynebacterium glutamicum*. *Front. Bioeng. Biotechnol.* 8:606047. doi: 10.3389/fbioe.2020.606047

Zhou, M., Boekhorst, J., Francke, C., and Siezen, R. J. (2008). LocateP: genome-scale subcellular-location predictor for bacterial proteins. *BMC Bioinformatics* 9:173. doi: 10.1186/1471-2105-9-173

Conflict of Interest: YC was employed by Star Lake Bioscience Co. Inc.

The remaining authors declare that the research was conducted in the absence of any commercial or financial relationships that could be construed as a potential conflict of interest.

Publisher's Note: All claims expressed in this article are solely those of the authors and do not necessarily represent those of their affiliated organizations, or those of the publisher, the editors and the reviewers. Any product that may be evaluated in this article, or claim that may be made by its manufacturer, is not guaranteed or endorsed by the publisher.

Advantages of publishing in Frontiers

OPEN ACCESS
Articles are free to read for greatest visibility and readership

FAST PUBLICATION
Around 90 days from submission to decision

HIGH QUALITY PEER-REVIEW
Rigorous, collaborative, and constructive peer-review

TRANSPARENT PEER-REVIEW
Editors and reviewers acknowledged by name on published articles

Frontiers
Avenue du Tribunal-Fédéral 34
1005 Lausanne | Switzerland

Visit us: www.frontiersin.org
Contact us: frontiersin.org/about/contact

REPRODUCIBILITY OF RESEARCH
Support open data and methods to enhance research reproducibility

DIGITAL PUBLISHING
Articles designed for optimal readership across devices

FOLLOW US
@frontiersin

IMPACT METRICS
Advanced article metrics track visibility across digital media

EXTENSIVE PROMOTION
Marketing and promotion of impactful research

LOOP RESEARCH NETWORK
Our network increases your article's readership